IAEA TECDOC SERIES

IAEA-TECDOC-1733

Evaluation of Advanced Thermohydraulic System Codes for Design and Safety Analysis of Integral Type Reactors

IAEA
International Atomic Energy Agency

EVALUATION OF ADVANCED THERMOHYDRAULIC SYSTEM CODES FOR DESIGN AND SAFETY ANALYSIS OF INTEGRAL TYPE REACTORS

The following States are Members of the International Atomic Energy Agency:

AFGHANISTAN
ALBANIA
ALGERIA
ANGOLA
ARGENTINA
ARMENIA
AUSTRALIA
AUSTRIA
AZERBAIJAN
BAHAMAS
BAHRAIN
BANGLADESH
BELARUS
BELGIUM
BELIZE
BENIN
BOLIVIA
BOSNIA AND HERZEGOVINA
BOTSWANA
BRAZIL
BULGARIA
BURKINA FASO
BURUNDI
CAMBODIA
CAMEROON
CANADA
CENTRAL AFRICAN REPUBLIC
CHAD
CHILE
CHINA
COLOMBIA
CONGO
COSTA RICA
CÔTE D'IVOIRE
CROATIA
CUBA
CYPRUS
CZECH REPUBLIC
DEMOCRATIC REPUBLIC OF THE CONGO
DENMARK
DOMINICA
DOMINICAN REPUBLIC
ECUADOR
EGYPT
EL SALVADOR
ERITREA
ESTONIA
ETHIOPIA
FIJI
FINLAND
FRANCE
GABON
GEORGIA
GERMANY
GHANA
GREECE
GUATEMALA
HAITI
HOLY SEE
HONDURAS
HUNGARY
ICELAND
INDIA
INDONESIA
IRAN, ISLAMIC REPUBLIC OF
IRAQ
IRELAND
ISRAEL
ITALY
JAMAICA
JAPAN
JORDAN
KAZAKHSTAN
KENYA
KOREA, REPUBLIC OF
KUWAIT
KYRGYZSTAN
LAO PEOPLE'S DEMOCRATIC REPUBLIC
LATVIA
LEBANON
LESOTHO
LIBERIA
LIBYA
LIECHTENSTEIN
LITHUANIA
LUXEMBOURG
MADAGASCAR
MALAWI
MALAYSIA
MALI
MALTA
MARSHALL ISLANDS
MAURITANIA
MAURITIUS
MEXICO
MONACO
MONGOLIA
MONTENEGRO
MOROCCO
MOZAMBIQUE
MYANMAR
NAMIBIA
NEPAL
NETHERLANDS
NEW ZEALAND
NICARAGUA
NIGER
NIGERIA
NORWAY
OMAN
PAKISTAN
PALAU
PANAMA
PAPUA NEW GUINEA
PARAGUAY
PERU
PHILIPPINES
POLAND
PORTUGAL
QATAR
REPUBLIC OF MOLDOVA
ROMANIA
RUSSIAN FEDERATION
RWANDA
SAN MARINO
SAUDI ARABIA
SENEGAL
SERBIA
SEYCHELLES
SIERRA LEONE
SINGAPORE
SLOVAKIA
SLOVENIA
SOUTH AFRICA
SPAIN
SRI LANKA
SUDAN
SWAZILAND
SWEDEN
SWITZERLAND
SYRIAN ARAB REPUBLIC
TAJIKISTAN
THAILAND
THE FORMER YUGOSLAV REPUBLIC OF MACEDONIA
TOGO
TRINIDAD AND TOBAGO
TUNISIA
TURKEY
UGANDA
UKRAINE
UNITED ARAB EMIRATES
UNITED KINGDOM OF GREAT BRITAIN AND NORTHERN IRELAND
UNITED REPUBLIC OF TANZANIA
UNITED STATES OF AMERICA
URUGUAY
UZBEKISTAN
VENEZUELA
VIET NAM
YEMEN
ZAMBIA
ZIMBABWE

The Agency's Statute was approved on 23 October 1956 by the Conference on the Statute of the IAEA held at United Nations Headquarters, New York; it entered into force on 29 July 1957. The Headquarters of the Agency are situated in Vienna. Its principal objective is "to accelerate and enlarge the contribution of atomic energy to peace, health and prosperity throughout the world''.

IAEA-TECDOC-1733

EVALUATION OF ADVANCED THERMOHYDRAULIC SYSTEM CODES FOR DESIGN AND SAFETY ANALYSIS OF INTEGRAL TYPE REACTORS

INTERNATIONAL ATOMIC ENERGY AGENCY
VIENNA, 2014

COPYRIGHT NOTICE

For further information on this publication, please contact:

Nuclear Power Technology Development Section
International Atomic Energy Agency
Vienna International Centre
PO Box 100
1400 Vienna, Austria
Email: Official.Mail@iaea.org

Printed by the IAEA in Austria
February 2014

IAEA Library Cataloguing in Publication Data

Evaluation of advanced thermohydraulic system codes for design and safety analysis of integral type reactors. — Vienna : International Atomic Energy Agency, 2014.
p. ; 30 cm. — (IAEA-TECDOC series, ISSN 1011–4289 ; no. 1733)
ISBN 978–92–0–100314–0
Includes bibliographical references.

1. Light water reactors — Technological innovations. 2. Nuclear reactors — Computer programs. 3. Nuclear reactors — Containment — Safety measures. I. International Atomic Energy Agency. II. Series.

IAEAL 14–00872

FOREWORD

The integral pressurized water reactor (PWR) concept, which incorporates the nuclear steam supply systems within the reactor vessel, is one of the innovative reactor types with high potential for near term deployment. An International Collaborative Standard Problem (ICSP) on Integral PWR Design, Natural Circulation Flow Stability and Thermohydraulic Coupling of Primary System and Containment during Accidents was established in 2010. Oregon State University, which made available the use of its experimental facility built to demonstrate the feasibility of the Multi-application Small Light Water Reactor (MASLWR) design, and sixteen institutes from seven Member States participated in this ICSP. The objective of the ICSP is to assess computer codes for reactor system design and safety analysis. This objective is achieved through the production of experimental data and computer code simulation of experiments. A loss of feedwater transient with subsequent automatic depressurization system blowdown and long term cooling was selected as the reference event since many different modes of natural circulation phenomena, including the coupling of primary system, high pressure containment and cooling pool are expected to occur during this transient. The power maneuvering transient is also tested to examine the stability of natural circulation during the single and two phase conditions.

The ICSP was conducted in three phases: pre-test (with designed initial and boundary conditions established before the experiment was conducted), blind (with real initial and boundary conditions after the experiment was conducted) and open simulation (after the observation of real experimental data). Most advanced thermohydraulic system analysis codes such as TRACE, RELAPS and MARS have been assessed against experiments conducted at the MASLWR test facility. The ICSP has provided all participants with the opportunity to evaluate the strengths and weaknesses of their system codes in the transient analysis. This publication provides a brief summary of the ICSP tests and results from all participants, a comparison of blind calculation results, lessons learned, and conclusions drawn from the ICSP.

The IAEA expresses its appreciation to B. Woods, Oregon State University, for leading this ICSP as chairperson and for conducting ICSP tests at the MASLWR test facility. The IAEA officer responsible for this publication was J.H. Choi of the Division of Nuclear Power.

EDITORIAL NOTE

This publication has been prepared from the original material as submitted by the contributors and has not been edited by the editorial staff of the IAEA. The views expressed remain the responsibility of the contributors and do not necessarily represent the views of the IAEA or its Member States.

Neither the IAEA nor its Member States assume any responsibility for consequences which may arise from the use of this publication. This publication does not address questions of responsibility, legal or otherwise, for acts or omissions on the part of any person.

The use of particular designations of countries or territories does not imply any judgement by the publisher, the IAEA, as to the legal status of such countries or territories, of their authorities and institutions or of the delimitation of their boundaries.

The mention of names of specific companies or products (whether or not indicated as registered) does not imply any intention to infringe proprietary rights, nor should it be construed as an endorsement or recommendation on the part of the IAEA.

The IAEA has no responsibility for the persistence or accuracy of URLs for external or third party Internet web sites referred to in this publication and does not guarantee that any content on such web sites is, or will remain, accurate or appropriate.

CONTENTS

1. INTRODUCTION 1

1.1. BACKGROUND 1

1.2. MASLWR CONCEPTUAL DESIGN 1

1.3. ICSP OBJECTIVE 2

1.4. STRUCTURE 2

2. OSU MASLWR TEST FACILITY DESCRIPTION 3

2.1. OSU MASLWR TEST FACILITY OVERVIEW 3

2.1.1. Primary circuit 3
2.1.2. Secondary circuit 4
2.1.3. Containment 5
2.1.4. Data acquisition, instrumentation and control 5

2.2. PRIMARY SYSTEMS 5

2.2.1. Reactor pressure vessel shell 6
2.2.2. Core 6
2.2.3. Hot leg riser 7
2.2.4. Upper plenum 8
2.2.5. Pressurizer 8
2.2.6. Steam generator — primary side 9
2.2.7. Cold leg downcomer 9
2.2.8. Geometric data summary 9

2.3. SECONDARY SYSTEMS 12

2.3.1. Main feed water system 12
2.3.2. Steam generator — secondary side 13
2.3.3. Main steam system 14

2.4. CONTAINMENT AND COOLING POOL 14

2.4.1. High pressure containment vessel 14
2.4.2. Cooling pool vessel 15
2.4.3. Heat transfer plate 15

2.5. AUTOMATIC DEPRESSURIZATION SYSTEM 16

2.5.1. Automatic depressurization system blowdown lines 16
2.5.2. Automatic depressurization system vent lines 16
2.5.3. Automatic depressurization system sump return lines 17

2.6. DATA ACQUISITION, INSTRUMENTATION AND CONTROL SYSTEM 17

3. ICSP TESTS 20

3.1. SP-2: LOSS OF FEEDWATER TRANSIENT 20

3.2. SP-3: POWER MANEUVERING 27

4. PARTICIPANT'S MODELS AND RESULTS 33

4.1. AERB — INDIA 33

4.1.1. Computer codes 33
4.1.2. System idealization 33
4.1.3. Analysis results for loss of feedwater transients 34

4.1.4. Analysis results for power maneuvering 44
4.2. BARC (RELAP5) — INDIA 47
4.2.1. Computer code 47
4.2.2. System idealization 47
4.2.3. Analysis results for loss of feedwater transient 49
4.2.4. Analysis results for power manoeuvring (SP3) 62
4.3. CIAE — CHINA 68
4.3.1. Computer code 68
4.3.2. System idealization 68
4.3.3. Analysis results for loss of feedwater transient 70
4.3.4. Analysis results for power maneuvering 79
4.4. ENEA — ITALY 84
4.4.1. Computer codes 84
4.4.2. System idealization 85
4.4.3. Analysis results for loss of feedwater transient 87
4.4.4. Analysis results for power maneuvering 94
4.5. GIDROPRESS — RUSSIAN FEDERATION 99
4.5.1. Computer codes 99
4.5.2. System idealization 99
4.5.3. Analysis results for loss of feedwater transient 102
4.5.4. Analysis results for power maneuvering 112
4.5.5. Summary 112
4.6. IBRAE — RUSSIAN FEDERATION 118
4.6.1. Computer codes 118
4.6.2. System idealization 118
4.6.3. Analysis results for loss of feedwater transient 121
4.6.4. Analysis results for power maneuvering 134
4.7. KAERI — REPUBLIC OF KOREA 141
4.7.1. Computer Codes 141
4.7.2. System idealization 141
4.7.3. Analysis results for loss of feedwater transient 142
4.7.4. Analysis results for power maneuvering 154
4.8. KINS — REPUBLIC OF KOREA 161
4.8.1. Computer codes 161
4.8.2. System idealization 161
4.8.3. Analysis results for loss of feedwater transient 164
4.8.4. Analysis results for power manoeuvring 174
4.9. NPCIL — INDIA 182
4.9.1. Computer code 182
4.9.2. System idealization 183
4.9.3. Analysis results for loss of feedwater transient 185
4.9.4. Analysis results for power manoeuvring 193
4.10. NRC — USA 199
4.10.1. Computer codes 199
4.10.2. System idealization 201
4.10.3. Analysis results for loss of feedwater transient 202
4.10.4. Analysis results for power manoeuvring 219

4.11. NUSCALE – USA 229
4.11.1. Computer codes 229
4.11.2. System idealization 229
4.11.3. Analysis results for loss of feedwater transient 231
4.11.4. Analysis results for power maneuvering 243
4.12. BARC (CATHARE) — INDIA 248
4.12.1. Computer code 248
4.12.2. System idealization 248
4.12.3. Analysis results for loss of feedwater transient 250
4.12.4. Analysis results for power maneuvering 250
4.13. SJTU — CHINA 257
4.13.1. Computer codes 257
4.13.2. System idealization 257
4.13.3. Analysis results for loss of feedwater transient 259
4.13.4. Analysis results for power maneuvering 265
4.14. SNPTRD — CHINA 270
4.14.1. Computer codes 270
4.14.2. System idealization 270
4.14.3. Analysis results for loss of feedwater transient 271
4.14.4. Analysis results for power maneuvering 276
4.15. UNIPA — ITALY 283
4.15.1. Computer codes 283
4.15.2. System idealization 283
4.15.3. Analysis results for loss of feedwater transient 285
4.15.4. Analysis results for power maneuvering 297
4.16. UNIPI — ITALY 304
4.16.1. Computer codes 304
4.16.2. System idealization 305
4.16.3. Analysis results for loss of feedwater transient 308
4.16.4. Analysis results for power maneuvering 317
5. COMPARISON OF BLIND CALCULATION RESULTS 324
5.1. LOSS OF FEEDWATER TRANSIENT 324
5.1.1. RPV thermal hydraulic behaviour 324
5.1.2. SG thermal hydraulic behaviour 325
5.1.3. HPC thermal hydraulic behaviour 325
5.1.4. CPV thermal hydraulic behaviour 325
5.2. POWER MANEUVERING 342
5.2.1. RPV thermal hydraulic behaviour 342
5.2.2. SG thermal hydraulic behaviour 343
6. LESSONS LEARNED 355
6.1. PROCEDURAL CHALLENGES 355
6.2. TECHNICAL LESSONS 356
7. CONCLUSIONS 360
APPENDIX I: TEST PROCEDURES 363

APPENDIX II: SUMMARY ON HEAT TRANSFER AND PRESSURE DROP IN HELICAL COIL STEAM GENERATOR 373
REFERENCES 376
ABBREVIATIONS 378
CONTRIBUTORS TO DRAFTING AND REVIEW 380

1. INTRODUCTION

1.1. BACKGROUND

Oregon State University (OSU) has constructed a system-level test facility to examine natural circulation phenomena of importance to integral reactors. The test facility simulates the Multi-application Small Light Water Reactor (MASLWR) integral reactor concept design developed by Idaho National Engineering and Environmental Laboratory, OSU and NEXANT–Bechtel [1]. The MASLWR is a small modular pressurized light water reactor relying on natural circulation during both normal operation and transient/accident conditions. Its small size makes the prototypical MASLWR relatively portable and thus well suited for employment in smaller electricity grids. These smaller electricity grids may be found in developing or remote regions. In addition to generating electricity, the prototypical MASLWR can be used to produce process steam for industrial applications. The MASLWR module is also scalable and a number of modules could be used in a "field" concept to generate electricity for larger electricity grids.

A series of three tests have been conducted from 2002 to 2003 at the OSU MASLWR test facility in order to assess the behavior of this reactor concept in both normal and transient operation. After the completion of this preliminary test series, through a grant from the International Atomic Energy Agency (IAEA), the OSU MASLWR Test Facility core was reconfigured to eliminate a recurring grounding problem and improve facility reliability in anticipation of conducting an IAEA International Collaborative Standard Problem (ICSP). Although a relatively minor modification to a complex and highly capable facility, both the availability for high power and rapid transient natural circulation phenomenology testing as well as the spectrum of operating transients that can be investigated using the test facility have been greatly improved.

1.2. MASLWR CONCEPTUAL DESIGN

As conceived, the MASLWR is an integral pressurized light water reactor relying on natural circulation during both normal operation and transient/accident conditions. The layout of the MASLWR conceptual design is shown in Figure 1-1. The MASLWR nuclear steam supply system (NSSS) is contained within the reactor vessel and the core flow is driven by natural circulation. The steam generators are located in the upper region of the vessel outside of the hot leg chimney and consist of banks of vertical helical tubes. Primary coolant flows outside the steam generator tubes, and the feedwater is fully vaporized inside the tubes after traveling approximately 60% of the tube length resulting in superheated steam at the steam generator exit.

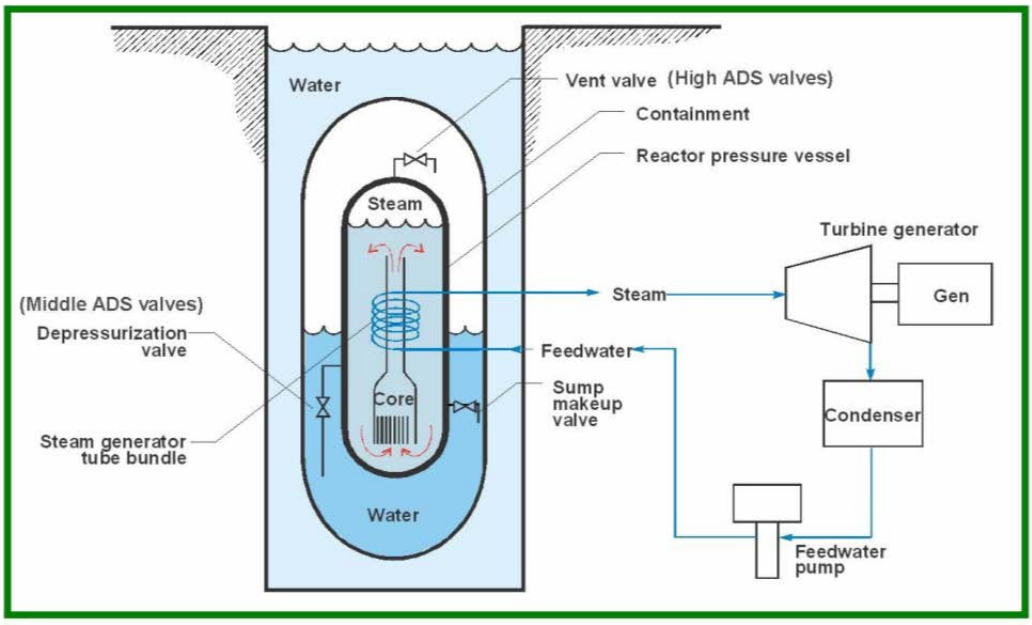

FIG. 1-1. MASLWR conceptual design layout [1].

MASLWR's safety systems are designed to operate passively. There are no emergency cooling pumps and offsite power is not required for safety system operation. The reactor pressure vessel (RPV) is surrounded by a cylindrical containment partially filled with water. This containment provides pressure suppression and liquid makeup capabilities. The reactor pressure vessel can be depressurized using the automatic depressurization system (ADS), which consists of six valves discharging into various locations within the containment. The entire containment vessel is submerged in a pool of water that acts as the ultimate heat sink.

1.3. ICSP OBJECTIVE

The purpose of this IAEA ICSP is to provide experimental data on flow instability phenomena under natural circulation conditions and coupled containment/reactor vessel behavior in integral-type reactors. This data can be used to assess computer codes for reactor system design and analysis. The objective of these tests is to provide data for the following phenomena:

- Natural circulation flow instability: Conduct stepwise increase in primary core power in order to determine the effect of core power and feedwater flow rates on natural circulation flow rates in small integral PWRs.
- Coupled Containment Pressurization: Conduct a loss of feedwater transient with subsequent ADS blowdown and long term cooling to determine the progression of a loss of feedwater transient in small integral natural circulation PWRs. These tests would examine the blowdown phase as well as the coupling of the primary to containment systems and the long term cooling using sump natural circulation. This data could be used for the analysis of system codes to determine if they model specific phenomena in an accurate manner.

1.4. STRUCTURE

Following this introduction, Sections 2 and 3 will focus on a detailed description of the OSU MASLWR test facility, its instrumentation and the tests conducted under this IAEA ICSP. Section 4 will discuss the models and key analysis results prepared by each of the ICSP participants. This discussion will include a brief description of the computer codes used and the models developed. It will also include some discussion by each participant concerning the results that were achieved during blind and open phases of the calculation for their individual models.

Section 5 will focus on a comparison of blind calculations from all the participants for the important test variables. Section 6 will cover lessons learned, and conclusions and recommendations made in Section 7.

2. OSU MASLWR TEST FACILITY DESCRIPTION

2.1. OSU MASLWR TEST FACILITY OVERVIEW

This section provides a brief overview of the Oregon State University (OSU) Multi-Application Small Light Water Reactor (MASLWR) test facility [1]. Figure 2-1 shows the photograph of MASLWR test facility. Detailed descriptions of relevant test facility components, geometric data, and instrumentation locations necessary for modeling the facility and interpreting experimental test results are provided in subsequent sections.

FIG.2-1. MASLWR test facility.

2.1.1. Primary circuit

The primary circuit of the test facility models the self-contained integrated reactor core and steam generator system. The core is comprised of electric heaters. The steam generator is comprised of helical coils that are located in the vessel, above the core and outside of the hot leg chimney. This relative placement of core and steam generator allows for sufficient natural circulation flow under normal steady state and transient operating conditions. The primary circuit of the test facility has been designed with limits for operation at a primary side pressure of 11.4 MPa(g) and a primary side temperature of 590°K.

Primary coolant flows up through the core and hot leg riser. The steam generator in the upper portion of the vessel then cools this hot fluid. The cooler fluid flows downward around the outside of the hot leg riser into the lower plenum. From the lower plenum the fluid is drawn back into the core and heated once more. Figure 2-2 shows a schematic of the significant test facility primary circuit components.

The test facility core consists of 56 electric heaters distributed in a square array with a maximum core power of 398 kW. The core geometry and thermal characteristics (flow areas, hydraulic diameters and local heat flux) have been preserved on a scaled basis.

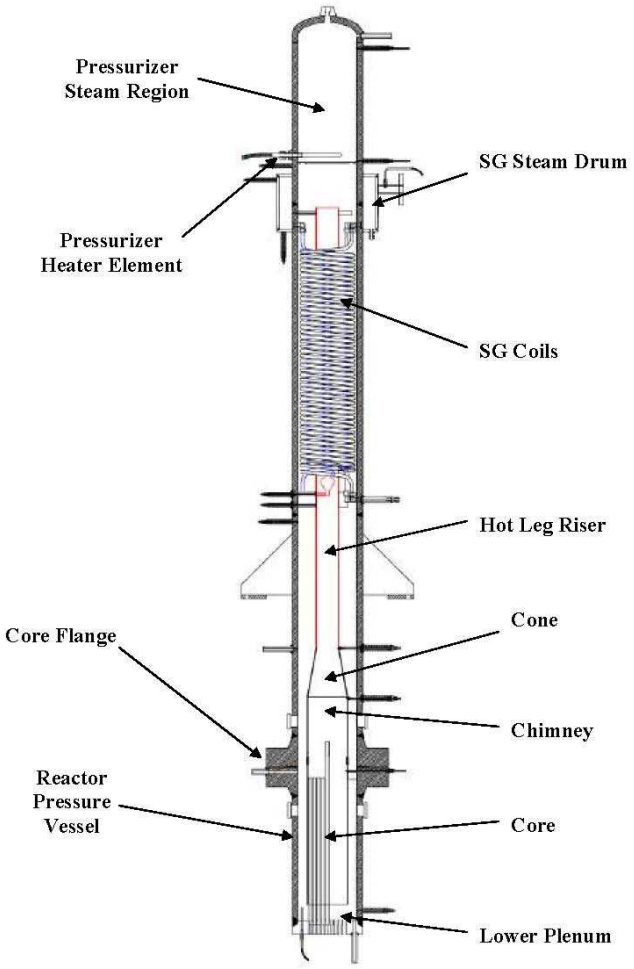

FIG. 2-2. Reactor pressure vessel key areas.

2.1.2. Secondary circuit

The steam generator (SG) is a helical coil, once through heat exchanger located within the pressure vessel in the annular space between the hot leg riser and the inside surface of the pressure vessel shell. Feed water is provided from the city water supply and, after de-ionization and chemical treatment, is pumped into the SG from a feedwater storage tank by a positive displacement pump. This pump uses a variable speed controller to allow for precise control of the main feed water (MFW) mass flow rate. The steam produced is vented to atmosphere.

The SG consists of three vertical parallel helical coil tube sections. The outer and middle coils consist of five tubes each while the inner coil consists of four tubes. Each coil is separate from the others but the tubes within a coil are joined at a common inlet header to ensure pressure equilibrium. Cold feedwater enters at the bottom of the SG and boils off after traveling a certain length in the SG tubes. This boil off length is a function of both core power and MFW flow rate. Nominally, this boil off length is approximately 60% of the length of the steam generator tubes so the steam will leave the SG at superheated. Each SG coil exhausts the superheated steam into a common steam drum from where it is subsequently exhausted to atmosphere.

2.1.3. Containment

The MASLWR containment vessel and the surrounding containment cooling pool are modeled in the OSU MASLWR test facility as two separate vessels. One vessel models the suppression pool volume, vapor bubble volume and the condensation surface inside of the containment vessel. The second vessel models the heat capacity of the water pool within which the containment vessel is held. A stainless steel plate separates the two vessels. This plate models the scaled heat transfer surface between the containment vessel and the surrounding vessel pool.

The containment vessel is connected to the reactor pressure vessel (RPV) by six independent automatic depressurization system (ADS) lines. There are two blowdown lines, two vent lines and two sump recirculation (core makeup) lines. Flow through each of these lines is via an independent automatically operated valve controlled through the test facility control system. The containment vessel is capable of prolonged operation at 2.07 MPa(g) and 477.6°K.

2.1.4. Data acquisition, instrumentation and control

The test facility is instrumented to capture the behavior of the facility during steady-state and transient operation. The following information can be obtained by the test facility data acquisition system:

- Feed water—mass flow rate and temperature;
- Feed water through each SG coil—mass flow rate, temperature and pressure;
- Main steam—volumetric flow rate and pressure;
- Differential pressure—across core, hot leg chimney, SG, and annulus below SG;
- Pressurizer—coolant level, pressure and temperature;
- Temperatures—core inlet, core exit, primary loop at SG.

The test facility control system accomplishes two tasks. The first is to process input signals from the various facility instrumentation (thermocouples, pressure meters, flow meters, valve and relay positions). The second is to generate control signals determined by the system logic (valve and relay control signals, heater and pump control signals). The following systems can be regulated by the test facility control system:

- Core heaters (including decay power modeling);
- Main feed water pump;
- Pressurizer heaters;
- Feedwater storage tank level;
- Pressurizer water level (draining during system heatup only);
- Containment heaters (used to maintain an adiabatic boundary condition on all walls of containment except for the prescribed condensation wall ensuring that heat transfer only takes place between the cooling pool vessel and the high pressure containment vessel).

2.2. PRIMARY SYSTEMS

This section provides a detailed description of the relevant OSU MASLWR test facility primary circuit components, geometric data, and instrumentation locations. The integral reactor components include the reactor pressure vessel (RPV) shell, core, hot leg riser, upper plenum, steam generator (SG), cold leg downcomer, lower plenum, and pressurizer (PZR). Due to the many components contained in the RPV, the flow area varies with the height of the vessel. The water level within the RPV is normally above the pressurizer heaters, which are located above the upper plenum. The atmosphere above the water level normally consists of a saturated steam bubble, created and maintained by the pressurizer heaters.

Throughout this section and the remainder of the document, elevation measurements are referenced to the core seal ring at the joint between the lower shell and the exchanger section and azimuthal measurements are referenced to building north.

2.2.1. Reactor pressure vessel shell

The reactor pressure vessel (RPV) shell consists of four sections: lower shell, exchanger section (including external support flange), coil section, and pressurizer section. The lower surface of the cylindrical lower shell is planar, the exchanger and coil sections are right circular cylinders, and the upper head of the cylindrical pressurizer section is hemispherical. All sections are constructed from nominal 14" SA312 TP304 Schedule 140 stainless steel (SS) pipe and have an outside diameter (OD) of 35.56 cm, an inside diameter (ID) of 29.21 cm, and a wall thickness of 3.175 cm. The RPV shell is surrounded by 10.2 cm of Thermo-12 hydrous calcium silicate insulation.

The flanges that join the lower shell to the exchanger section are SA184 F304 SS raised face weld neck fittings that are fillet welded to the RPV shell. A 0.3175 cm spiral wound metallic gasket is used to seal the gap between the flanges. The core seal ring at the joint between the lower shell and the exchanger section defines the zero reference level for elevation measurements, and this reference location is 167.3 cm above the facility floor.

The RPV shell has penetrations for the steam generator feedwater header, steam drum, pressurizer heaters, over-pressure safety valve, automatic depressurization system (ADS) vent lines, ADS blowdown lines, ADS sump recirculation lines, vessel fill and drain lines, core heater elements, and instrumentation.

2.2.2. Core

The RPV houses the core, which is modeled by 57 cylindrical rods distributed in a 1.86 cm pitch square array with a 1.08 pitch to diameter ratio. The core rods are SA312 TP304 SS water-tight penetrations via the lower (heater) plate of the RPV lower shell, into which either an electric heater (one of 56) or a thermocouple array (center rod only) is inserted.

Each core heater rod is 73.7 cm long with an external diameter of 1.25 cm and a heated length of 59.7 cm. The nominal power of each heater rod is 7.1 kW resulting in a maximum core power of 398 kW. As previously noted, the core geometry and thermal characteristics (flow areas, hydraulic diameters and local heat flux) have been preserved on a scaled basis.

The core is shrouded to separate the downcomer region from the core region and ensure all flow enters the core via the bottom and travels the entire heated length (i.e., there is no core bypass flow). The cold return flow exits the un-rodded lower plenum region below the downcomer radially inward into the rodded (but unheated) lower plenum region, then upward into the bottom of the core via the 20.3 cm diameter SA240 TP304 SS lower core flow plate. The rodded lower core flow plate holes are oversized at 1.72 cm diameter to create a flow annulus between the flow plate and the 1.59 cm diameter core rod. In addition to the 57 core rod flow holes, the lower flow plate contains 76 auxiliary flow holes with a 0.635 cm diameter each and arranged at the same 1.86 cm square pitch (Figure 2-3).

To ensure that each heated rod receives approximately equal axial coolant flow, the core shroud is shaped to partially block the primary coolant flow through the outermost auxiliary flow holes. The amount of blockage is dependent on the number and location of heated rods adjacent to each auxiliary flow hole. The total flow area of each auxiliary flow hole is divided into four equal sized quadrants, and flow is permitted through the quadrant only if there is a core rod flow hole adjacent to that quadrant.

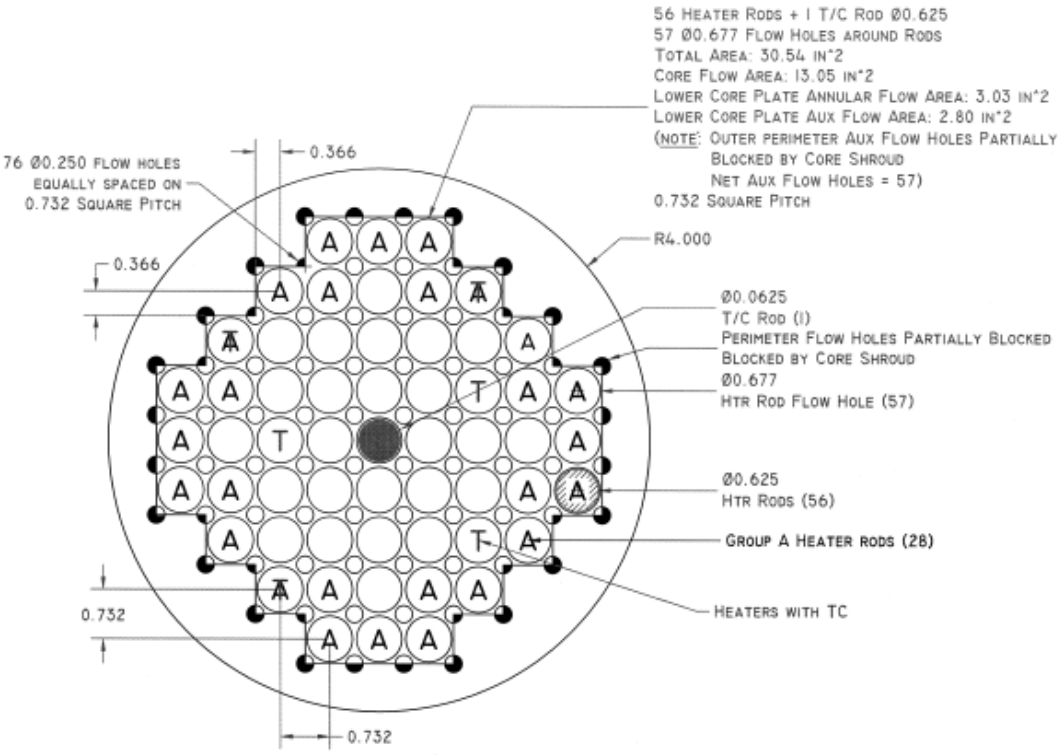

FIG. 2-3. Lower core flow plate.

The core region is instrumented as follows:

- One thermocouple rod (six thermocouples, TF-101 through TF-106) at the center of the core. The thermocouples are vertically spaced every 15.24 cm, with TF-101 at the lower plane of the heated region of the core (lower edge of thermocouple at 60.96 cm below reference) and TF-106 approximately 15.24 cm above the active heated core region (upper edge of thermocouple at 17.78 cm above reference).
- Four thermocouples, TF-121 through TF-124, penetrate the planar lower shell head into the unrodded lower plenum region, equally spaced azimuthally (at 45°, 135°, 225°, and 315° for TF-121 through TF-124, respectively) at a radius 12.7 cm from the center of the core and an elevation of 75.18 cm below reference. These thermocouples measure the temperature of the cold leg entering the core.
- One penetration at 64.82 cm below reference, 0° azimuth, for the high pressure side of DP-101, DP-106, and LDP-106. DP-101 measures the pressure loss across the core, DP-106 measures the cold leg downcomer pressure loss from the steam generator bundle outlet to the core inlet, and LDP-106 measures the water level in the RPV up to the upper plenum baffle plate.

In addition to the instrumentation penetrations, there are non-interfering RPV penetrations for filling and draining the RPV. These lines are used for facility startup, shutdown, and maintenance and are not relevant to facility steady state and/ or transient experimentation.

2.2.3. Hot leg riser

After leaving the core, the flow enters the chimney of the hot leg riser. The hot leg riser, extending above the core shroud from the chimney to the upper plenum, creates a riser/downcomer configuration to enable natural circulation.

The lower region (chimney) of the hot leg riser is constructed from 8” Schedule 40 SS304 pipe with an OD of 20.32 cm, an ID of 19.71 cm, and a wall thickness of 0.305 cm. The upper region of the hot leg riser is constructed from 4” Schedule 40 SA312 TP304 SS pipe with an OD of 11.43 cm, an ID of 10.23 cm, and a wall thickness of 0.602 cm. The transition from the lower to upper hot leg riser

regions is accomplished with a 0.305 cm thickness SA240 TP304 SS cone. The cone has a half angle of 20.61° and spans an elevation change of 24.46 cm. The upper hot leg riser exits into the upper plenum region at the bottom of the pressurizer section below the upper baffle plate.

There are instrumentation penetrations inward from the RPV shell, through the cold leg, to the hot leg riser region:

- at 40.0 cm above reference for DP-102 (low pressure side) and DP-103 (high pressure side);
- at 69.5 cm above reference for DP-103 (low pressure side) and DP-104 (high pressure side);
- at 299.1 cm above reference for DP-104 (low pressure side) and DP-105 (low pressure side);
- at 148.6 cm and 154.0 cm above reference for FDP-131.

DP-102 measures the hot leg pressure loss from the core outlet to the inlet of the transition cone, DP-103 measures the hot leg pressure loss across the transition cone, DP-104 measures the hot leg chimney pressure loss from the exit of the transition cone to the upper plenum, and DP-105 measures the cold leg pressure loss across the steam generator bundle from the outlet plenum to the top of the downcomer.

FDP-131 measures the differential pressure created by the v-cone flowmeter within the chimney. The vcone flowmeter utilizes a centrally-located cone inside the hot leg riser that interacts with the primary coolant flow, flattening the coolant velocity profile and creating a low pressure region immediately downstream of the cone. This optimizes the velocity profile of the primary coolant flow at the point of measurement, assuring accurate, reliable, and consistent differential pressure readings resulting in a highly accurate primary coolant flow measurement.

2.2.4. Upper plenum

After leaving the top of the hot leg riser, the flow enters the upper plenum. The upper plenum directs the flow radially outward and then down into the steam generator coil bundle of the steam generator section. The upper plenum is separated from the heated upper pressurizer section by a 1.27 cm thick SA240 TP304 SS baffle plate, at 308.6 cm above reference. The baffle plate has eight 2.54 cm diameter holes, radially located at 12.7 cm and spaced uniformly around the baffle plate periphery which allow free communication of the pressurizer pressure to the remainder of the RPV during normal operation and for volume surges into and/ or out of the pressurizer due to transients.

2.2.5. Pressurizer

The pressurizer (PZR), located above and in thermal hydraulic communication with the upper plenum via the baffle plate holes, maintains primary system static pressure during normal steady state and transient conditions. There are three heater elements, each 4 kW, that are modulated by the test facility control system to maintain nominal primary system static pressure at the desired pressure level (nominally 11.4 MPa(g)). The heater elements are 1.59 cm OD SS SA249 TP316L cartridge heaters with a heated length of 20.32 cm.

The significant RPV penetrations into the pressurizer are:

- at 311.5 cm above reference, 180°, for LDP-301 (high pressure side) and LDP-106 (low pressure side),
- at 314.3 cm above reference, centered at 270°, for the three pressurizer heaters,
- at 374.5 cm above reference, 180°, for LDP-301 (low pressure side) and PT-301,
- at 374.5 cm above reference, 315°, for TF-301, and
- at 374.5 cm above reference, 270°, for ADS vent lines.

LDP-301 measures the water level in the pressurizer above a reference approximately 2.8 cm below the pressurizer heaters. LDP-106 measures the water level in the RPV above the bottom of the RPV to the LDP-301 reference level. PT-301 measures the steam media pressure in the pressurizer, and TF-301 measures the steam media temperature in the pressurizer.

In addition to the penetrations described above, there are vent valve and safety valve penetrations in the pressurizer section hemispherical head. The vent line is used for startup, shutdown, and maintenance operations. The safety valve provides RPV overpressure protection. Both exhaust to atmosphere outside the test facility building.

2.2.6. Steam generator - primary side

In the MASLWR concept design, the primary coolant is circulated around the outside of the steam generator tubes. The test facility tube bundle is a helical coil consisting of fourteen SA249 TP316L SS 1.59 cm OD tubes with a total heated length of 86.0 m. Steam generator details are provided in Section 2.3.2.

2.2.7. Cold leg downcomer

After leaving the upper plenum, the flow continues downward through the steam generator section and into the cold leg downcomer region. The cold leg downcomer region is an annular region bounded by the RPV wall ID on the outside and the hot leg riser OD on the inside, and the flow area reduces at the hot leg riser cone. The flow exits the cold leg downcomer region into the lower plenum to complete the primary flow circuit.

Significant penetrations into the cold leg downcomer region are:

- four 1.27 cm thermocouple penetrations at 154.0 cm above reference for TF-131 through TF-134, equally spaced azimuthally (at 45°, 135°, 225°, and 315° for TF-131 through TF-134, respectively);
- one 1.27 cm penetration at 154.0 cm above reference, 270° azimuth, for FDP-131 (low pressure side);
- one 1.27 cm penetration at 148.6 cm above reference, 270° azimuth, that penetrates radially inward through the cold leg downcomer into the hot leg riser region for FDP-131 (high pressure side);
- one 1.91 cm penetration at 66.68 cm above reference, 270° azimuth, for the ADS blowdown line;
- one 1.91 cm penetration at 5.08 cm above reference, 270° azimuth, for the ADS sump return (RPV reflood) line.

Thermocouples TF-131 through TF-134 measure the steam generator tube bundle exit cold leg temperature. FDP-131 measures the differential pressure created by the v-cone flowmeter within the chimney.

2.2.8. Geometric data summary

The relevant geometric data for the primary system is given in Table 2-1 with the reference elevation as the center of the upper core plate which also corresponds to the center of the core seal ring. Figure 2-4 shows the elevation data for the primary loop, and the location numbers on Figure 2-4 cross-reference to the location numbers in Table 2-1. In Table 2-1, there are a few additional notes which are explained here:

- The lower plenum has an axial length of 6.20 cm outside of the core barrel and an axial length of 4.93 cm beneath the core in the rodded region. The RPV shell has an inner diameter of 29.21 cm and the core barrel has an outer diameter of 20.32 cm with a wall thickness of 0.305 cm.
- In the upper plenum, flow exits the hot leg (4.026 cm ID, 4.5 cm OD) and enters the 29.21 cm ID of the pressurizer shell.
- The dimensions of the hemispherical portion of the pressurizer cap are not known.
- The coil outlet and inlet shown in Figure 2-4 do not depict the actual coil turns.

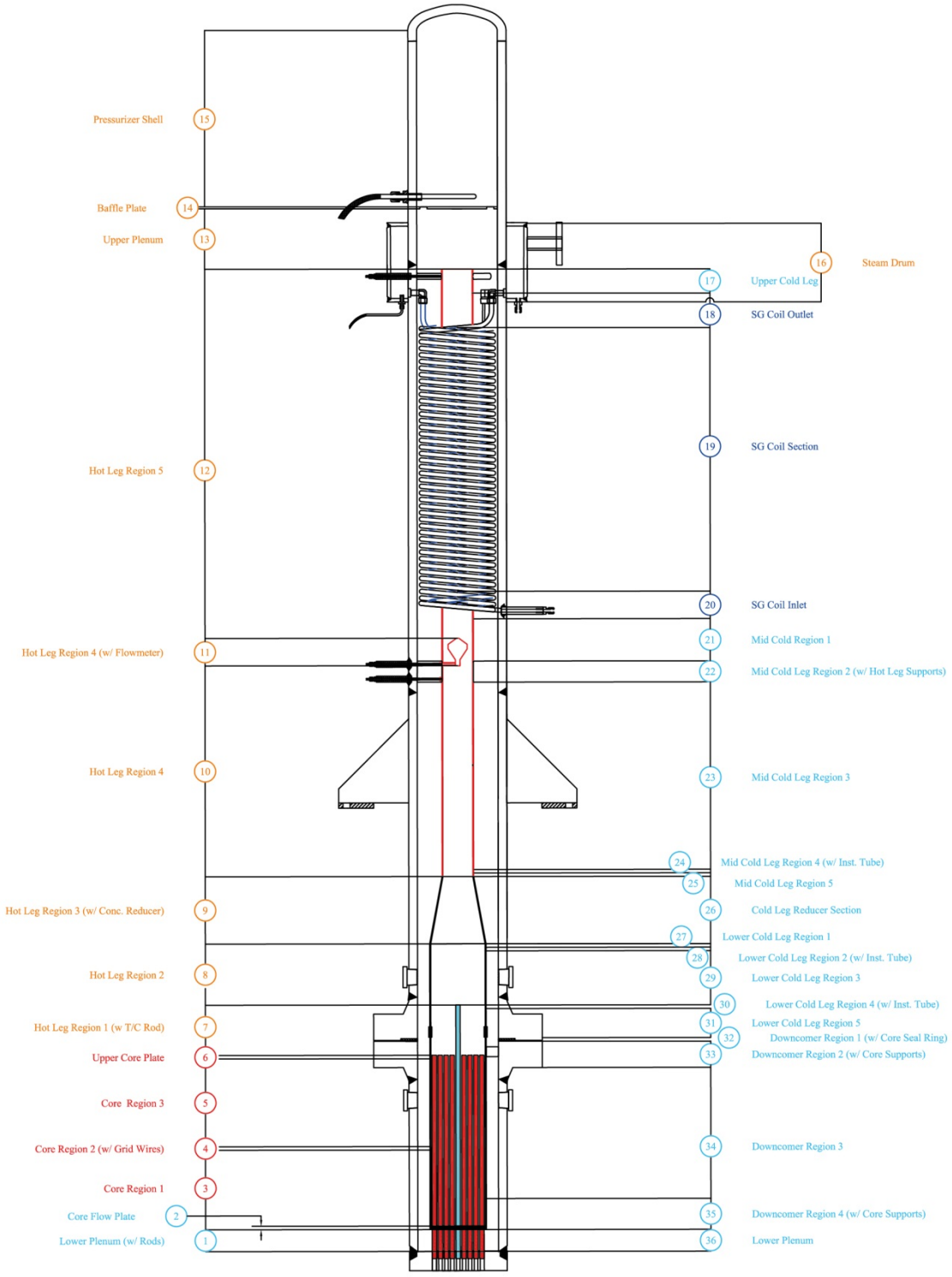

FIG. 2-4. OSU MASLWR test facility primary system elevation reference points.

TABLE 2-1. OSU MASLWR PRIMARY SYSTEM GEOMETRIC DATA

No.	Region	Elevation (cm)	Axial Length (cm)	Flow Area (cm^2)	Wetted Perimeter (cm)	Heated Perimeter (cm)	Heat Transfer Area (cm^2)
1	Lower Plenum (w/ rods)	-68.58 -62.38	6.20	NA	NA	NA	NA
2	Core Flow Plate	-62.38 -61.11	1.27	37.61	705.91	NA	NA
3	Core Region 1	-61.11 -29.96	31.15	84.22	351.21	279.73	8480.52
4	Core Region 2 (w/ grid wires)	-29.96 -29.73	0.23	43.10	703.5831	279.29	64.34
5	Core Region 3	-29.73 -0.64	29.09	84.22	351.21	279.29	8215.82
6	Upper Core Plate	-0.64 0.63	1.27	95.62	391.11	NA	NA
7	Hot Leg Region 1 (w/ TC rod)	0.63 16.51	15.88	304.81	63.92	NA	NA
8	Hot Leg Region 2	16.51 42.55	26.04	305.13	61.92	NA	NA
9	Hot Leg Region 3 (w/ conc. red.)	42.55 67.01	24.46	193.63	47.02	NA	NA
10	Hot Leg Region 4	67.01 154.0	86.99	82.13	32.13	NA	NA
11	Hot Leg Region 4 (w/ flowmeter)	154.0 165.11	11.11	65.65	49.85	NA	NA
12	Hot Leg Region 5	165.11 287.05	121.94	82.13	32.13	NA	NA
13	Upper Plenum	287.05 307.98	20.93	NA	NA	NA	NA
14	Baffle Plate	307.98 309.25	1.27	40.54	63.84	NA	NA
15	Pressurizer Shell	309.25 373.39	64.135	670.12	91.77	NA	NA
16	Steam Drum	293.52 263.04	30.48	1698.74	297.24	NA	NA
17	Upper Cold Leg	287.05 272.72	14.33	567.51	127.67	NA	NA
18	SG Coil Outlet	272.72 262.61	10.11	456.39	408.01	280.34	2834.70
19	SG Coil Section	262.61 167.95	94.66	411.43	521.49	393.82	37280.60
20	SG Coil Inlet	167.95 157.84	10.11	456.39	408.01	280.34	2834.70
21	Mid Cold Leg Region 1	157.84 154.0	3.84	567.51	127.67	NA	NA
22	Mid Cold Leg Region 2 (w/ HL supports)	154.0 146.38	7.62	533.64	173.39	NA	NA

TABLE 2-1. OSU MASLWR PRIMARY SYSTEM GEOMETRIC DATA (CONTINUED)

No.	Region	Elevation (cm)	Axial Length (cm)	Flow Area (cm^2)	Wetted Perimeter (cm)	Heated Perimeter (cm)	Heat Transfer Area (cm^2)
23	Mid Cold Leg Region 3	146.38 69.86	76.52	567.51	127.67	NA	NA
24	Mid Cold Leg Region 4 (w/ inst. tube)	69.86 69.22	0.64	558.64	144.18	NA	NA
25	Mid Cold Leg Region 5	69.22 67.01	2.21	567.51	127.67	NA	NA
26	Cold Leg Reducer Section	67.01 42.55	24.46	456.52	141.64	NA	NA
27	Lower Cold Leg Region 1	42.55 40.32	2.23	345.83	155.60	NA	NA
28	Lower Cold Leg Region 2 (w/ inst. tube)	40.32 39.68	0.64	339.78	163.22	NA	NA
29	Lower Cold Leg Region 3	39.68 5.40	34.28	345.83	155.60	NA	NA
30	Lower Cold Leg Region 4 (w/ inst. tube)	5.40 4.76	0.64	339.78	163.22	NA	NA
31	Lower Cold Leg Region 5	4.76 0.95	3.81	345.83	155.60	NA	NA
32	Downcomer Region 1 (w/ core seal ring)	0.95 -0.95	1.91	325.25	157.60	NA	NA
33	Downcomer Region 2 (w/ core supports)	-0.95 -11.11	10.16	323.25	181.0	NA	NA
34	Downcomer Region 3	-11.11 -52.22	41.11	345.83	155.60	NA	NA
35	Downcomer Region 4 (w/ core supports)	-52.22 -62.38	10.16	323.25	181.0	NA	NA
36	Lower Plenum	-62.38 -68.58	6.20	NA	NA	NA	NA

2.3. SECONDARY SYSTEMS

This section provides a detailed description of the relevant OSU MASLWR test facility main feed water and main steam system components, geometric data, and instrumentation locations.

2.3.1. Main feed water system

2.3.1.1. Feed water treatment and storage

The main feed water (MFW) system supplies high purity (deionized and demineralized) water to the steam generator (SG) for heat removal by generation of superheated steam. Potable water from the city water supply passes through a mechanical filter and a resin bed to remove impurities and flows to the feed water storage tank via solenoid operated valve MF-504. The test facility control system cycles MF-504 open and closed to maintain water level in the feed water storage tank within the desired level band. Feed water storage tank water height is measured by level differential pressure instrument LDP-

501. As necessary, water treatment chemicals can be batch added to the feed water storage tank from a chemical treatment tank using an installed positive displacement pump.

2.3.1.2. Main feed water pump

The main feed pump (MFP) is a 3 phase, 480 VAC, 5 hp positive displacement pump with a maximum rated flow of 15.9 liters per minute at 1750 shaft revolutions per minute. The maximum discharge pressure is 1500 psig. The MFP speed is controlled by a variable speed controller that is continuously adjustable from 0 - 100% rated flow.

The MFP can be isolated from the downstream main feed water system supply lines by pneumatic motor operated globe valve MF-508. Air flow to the MFP discharge isolation valve MF-508 actuator is controlled via solenoid operated valve AS-508. Operation of AS-508 is determined by the test facility control system logic programming for the test being conducted.

The MFP controller is interlocked with MFP discharge isolation valve MF-508 position, to ensure that the MFP is not energized unless MF-508 is fully open.

2.3.1.3. Main feed water system supply lines

Immediately downstream of the MFP discharge isolation valve is a thermocouple, TF-501, to measure the feed water temperature, and a magnetic flow meter, FMM-501, for measuring the total feed water mass flow. The single MFW line splits into three supply lines, one for each coil bank of SG tubes. Each coil bank supply line has a Coriolis flow meter (FCM-511, FCM-521, and FCM-531 for the outer, mid, and inner banks respectively) and a pressure transducer (PT-511, PT-521, and PT-531 for the outer, mid, and inner banks respectively). Each coil bank supply line has a check valve to prevent backflow from the SG into the main feed water system.

2.3.2. Steam generator - secondary side

The steam generator (SG) consists of a helical coil, once through heat exchanger located within the pressure vessel in the annular space between the hot leg riser and the inside surface of the reactor pressure vessel (RPV). There are three separate parallel sections (coils) of stainless steel (SS) tubes. The outer and middle coils consist of five tubes each while the inner coil consists of four tubes. Each coil is separate from the others but joined at a common inlet header to ensure pressure equilibrium within the coil. The SG geometric data is given in Table 2-2.

Cold MFW enters at the bottom of the SG and boils off after traveling a certain length in the SG. This boil off length is a function of both core power and MFW flow rate. Nominally, this boil off length is approximately 60% of the actual length of the SG tubes so the steam will leave the SG at superheated.

TABLE 2-2. STEAM GENERATOR BUNDLE GEOMETRIC DATA

Bank	Inner	Mid	Outer
Tube wrap direction (inlet to outlet, viewed from above)	cw	ccw	cw
Number of tubes in bank	4	5	5
Number of rotations from feed inlet to steam outlet	13	9.5	7.5
Tube spacing (tube center to tube center)	1.98 cm	2.11 cm	2.62 cm
Average tube length of bank	6.05 m	6.15 m	6.21 m
Tube lead length outside of RPV	0.152 m	0.152 m	0.152 m
Total average tube length	6.21 m	6.30 m	6.36 m
Total tube bank surface area	1.209 m^2	1.535 m^2	1.551 m^2
Individual tube outside diameter	1.59 cm	1.59 cm	1.59 cm
Individual tube wall thickness	0.165 cm	0.165 cm	0.165 cm

Each SG coil exhausts the superheated steam into a common steam drum from where it is subsequently exhausted to atmosphere via the main steam system. At the exit plane of each SG tube is a thermocouple for measuring the steam temperature; TF-611 through TF-615 for the outer coil, TF-621 through TF-625 for the mid coil, and TF-631 through TF-634 for the inner coil.

2.3.3. Main steam system

The main steam (MS) system receives superheated steam from the SG steam drum and exhausts the steam to atmosphere. Immediately downstream of the SG steam drum is pneumatic motor operated globe valve MS-502. Air flow to MS header isolation valve MS-502 actuator is controlled via solenoid operated valve AS-502. Operation of AS-502 is determined by the test facility control system logic programming for the test being conducted.

Pneumatic motor operated globe valve MS-503 isolates the MS header from the steam header drain line, and is mechanically and functionally similar to MS-502. MS-502 and MS-503 are interlocked to prevent them both from being simultaneously commanded shut, which would isolate both SG discharge paths, removing the primary coolant system heat sink.

Pressure transducer PT-602 measures Main steam header pressure upstream of MS-502. Downstream of MS-502 is vortex flow meter FVM-602. FVM-602 measures the steam mass flowrate, steam pressure, and steam temperature prior to the steam being discharged to atmosphere outside the test facility building.

2.4. CONTAINMENT AND COOLING POOL

The containment and cooling system of the OSU MASLWR test facility models the containment structure in which the MASLWR pressure vessel sits as well as the cavity within which the containment structure is located. This modeling is accomplished by using two vessels, a high-pressure containment (HPC) vessel and a cooling pool vessel (CPV), with a heat transfer surface between them to establish the proper heat transfer area. The HPC, CPV, and heat transfer plate are described below.

2.4.1. High pressure containment vessel

The SS304 high-pressure containment (HPC) vessel is a 5.75 m tall vessel consisting of three sections: a lower cylindrical section, an upper cylindrical section, and an eccentric cone section that joins the two. The lower cylindrical section measures 27.0 cm outside diameter (OD), 0.419 cm wall thickness, and 3.87 m long. The lower end is closed with a 2.54 cm thickness plate. The upper cylindrical section measures 50.8 cm OD, 0.476 cm wall thickness, and 1.21 m long. The upper end is closed with a 16.5 cm high, 0.635 cm wall thickness, hemispherical head. The 0.794 cm wall thickness eccentric cone section is flared from the 27.0 cm OD lower section to the 50.8 cm upper section OD over an elevation of 50.8 cm.

A 3.81 cm thick, 16.8 cm wide, SA240 TP304 stainless steel (SS) heat transfer plate runs the entire 5.59 m vertical length (less hemispherical upper head) of the HPC and physically joins the HPC to the CPV. The entire HPC (less heat transfer plate) is covered by 10.2 cm of Thermo-12 hydrous calcium silicate insulation.

There are six penetrations into the HPC from the reactor pressure vessel (RPV) automatic depressurization system (ADS): two blowdown lines (66.68 cm above reference), two vent lines (374.5 cm above reference), and two sump return (RPV reflood) lines (5.08 cm above reference). The blowdown and sump return lines penetrate the lower cylindrical section and the vent line penetrates the upper cylindrical section. Other HPC penetrations include a HPC safety valve, an equalization line between the HPC and CPV fitted with a blowout plug (to provide cooling pool vessel overpressure protection), pressure and differential pressure instrument tees, and maintenance connections for fill and drain.

The HPC shell is electrically heated by four groups of heaters to eliminate heat transfer from the HPC to its surroundings, except for heat transfer to the CPV through the heat transfer plate. The four 3

phase, 208 VAC, heater groups are located on the exterior surface of the HPC (i.e., under the insulation blanket) and above the containment water level.

Adjacent to each heater group are two thermocouples, one measuring wall temperature (TW-891 through TW-894) and one measuring heater temperature (TH-891 through TH-894). The test facility control system energizes the heater groups to establish and maintain the HPC wall temperature at the level specified by the test plan being conducted. Water level in the HPC is sensed by differential pressure gauge LDP-801. Pressure in the HPC is sensed by PT-801. The temperature inside the HPC is measured by the five thermocouples adjacent to the heat transfer plate (TF-821, TF-831, TF-841, TF-851, TF-861).

Geometric data for the HPC is given in Table 2-3.

2.4.2. Cooling pool vessel

The SA516 Grade 70 SS cooling pool vessel (CPV) is a 7.37 m tall right cylindrical tank made from 76.2 cm OD, 0.635 cm wall thickness pipe. The CPV is covered by 5.08 cm of Thermo-12 hydrous calcium silicate insulation. Geometric data for the CPV is given in Table 2-3.

The temperature inside the CPV is measured by the five thermocouples adjacent to the heat transfer plate (TF-825, TF-835, TF-845, TF-855, TF-865), and by one thermocouple (TH-892) at the top of the CPV. Differential pressure transducer LDP-901 measures the level inside the CPV. The CPV also has penetrations for maintenance activities.

2.4.3. Heat transfer plate

The SA240 TP304 SS heat transfer plate provides the heat conduction surface between the HPC and the CPV. It is the same height as the HPC without the hemispherical head (5.59 m), 16.8 cm wide and 3.81 cm thick. The heat transfer plate models the heat transfer area between the MASLWR conceptual design high pressure containment vessel and the cooling pool in which it sits. Geometric data for the heat transfer plate is given in Table 2-3.

The heat transfer plate has six sets of five thermocouples measuring the temperature distribution from the HPC to the CPV. Two of the five thermocouples measure the fluid temperature (air, water, or steam) adjacent to the heat transfer plate surface (one each inside the HPC and CPV), two are embedded in the heat transfer plate near each surface (one each near the HPC and CPV) and the other is embedded in the heat transfer plate at the midpoint of the plate thickness. The holes drilled in the heat transfer plate for the thermocouples are filled with boron nitride heat conducting spray to minimize the difference between the actual heat transfer plate temperature and the temperature sensed by the embedded thermocouples.

TABLE 2-3. CONTAINMENT AND COOLING GEOMETRIC DATA

Component	Length (m)	Diameter (m)	Notes
HPC vessel	5.75	-	
HPC lower cylinder	3.87	0.27	
HPC eccentric cone	0.51	0.27	Lower end
HPC eccentric cone	0.51	0.51	Upper end
HPC upper cylinder	1.21	0.51	
HPC upper head hemisphere	0.17	0.51	
CPV	7.37	0.76	Nominal water level 2.23 m
Heat transfer plate	5.59	n/a	3.81 cm thick, 16.8 cm wide

2.5. AUTOMATIC DEPRESSURIZATION SYSTEM

This section describes the OSU MASLWR test facility automatic depressurization system (ADS) vent and blowdown lines, and sump recirculation lines.

2.5.1. Automatic depressurization system blowdown lines

The automatic depressurization system (ADS) blowdown lines connect the reactor pressure vessel (RPV) cold leg to the high-pressure containment (HPC). They are horizontally oriented (i.e., there is no elevation change) at 66.68 cm above reference and they are geometrically similar from the RPV to the HPC. The ADS blowdown lines are constructed with SS304 and all external surfaces are covered with 5.1 cm of Thermo-12 hydrous calcium silicate insulation.

The ADS blowdown connection to the RPV is via a fillet welded 10 cm long, 1.91 cm nominal diameter schedule 80 pipe. The single ADS blowdown line leaving the RPV tees into two 1.27 cm diameter, 0.1651 cm wall thickness lines which lead to 1.27 cm fast-acting pneumatic motor operated globe valves PCS-107A and PCS-107B. Air flow to the PCS-107A and PCS-107B actuators is controlled via solenoid operated valves AS-107A and AS-107B, respectively. Operation of the solenoid control valves is determined by the test facility control system logic programming for the test being conducted.

Downstream from each isolation valve is a transition piece with an internal 0.636 cm square-edge orifice. The transition piece serves two purposes: it transitions the line back from the 1.27 cm pipe to 1.57 cm inside diameter (ID) tubing which is the size to the HPC, and it presents the proper scaled flow area for the ADS blowdown line valve.

The two ADS blowdown lines enter the HPC via a fillet welded stub, penetrate 22.2 cm, then turn downward for 73.4 cm before terminating below the HPC waterline at a sparger.

The sparger consists of two 5.72 cm diameter, 0.635 cm thick, stainless steel plates welded to a 0.635 cm thick stainless steel spacer ring between them. Into each plate is drilled five 0.7938 cm holes at 2.223 cm radius, equally spaced around the plate periphery. The two plates are aligned such that their drilled holes are rotated 45 degrees relative to each other (i.e., maximum hole misalignment). A 2.54 cm hole is drilled into the center of one plate face, and a pipe coupler is welded to that face to allow joining the sparger to the incoming ADS blowdown line.

Each ADS blowdown line is instrumented with a thermocouple (TF-872A, TF-872B) downstream of its associated orifice and external to the HPC.

2.5.2. Automatic depressurization system vent lines

The ADS vent lines connect the RPV pressurizer (PZR) steam space to the HPC. They are horizontally oriented (i.e., there is no elevation change) at 374.5 cm above reference and they are geometrically similar from the RPV to the HPC. The ADS vent lines are constructed with SS304 and all external surfaces are covered with 5.1 cm of Thermo-12 hydrous calcium silicate insulation. Aside from their geometric layout, the ADS vent lines are otherwise similar to the ADS blowdown lines.

The ADS vent connection to the RPV is via a fillet welded 10 cm long, 1.91 cm nominal diameter schedule 80 pipe. The single ADS vent line leaving the RPV tees into two 1.27 cm diameter, 0.1651 cm wall thickness lines which lead to 1.27 cm fast-acting pneumatic motor operated globe valves PCS-106A and PCS-106B. Air flow to the PCS-106A and PCS-106B actuators is controlled via solenoid operated valves AS-106A and AS-106B, respectively. Operation of the solenoid control valves is determined by the test facility control system logic programming for the test being conducted.

Downstream from each isolation valve is a transition piece with an internal 0.636 cm square-edge orifice. The transition piece serves two purposes: it transitions the line back from the 1.27 cm pipe to 1.57 cm ID tubing which is the size to the HPC, and it presents the proper scaled flow area for the ADS vent line valve.

The two ADS vent lines enter the HPC via a fillet welded stub well above the waterline, penetrate 22.0 cm, and terminate in a sparger. Each ADS vent line is instrumented with a thermocouple (TF-873A, TF-873B) downstream of its associated orifice and external to the HPC.

2.5.3. Automatic depressurization system sump return lines

The ADS sump return (reactor pressure vessel reflood) lines connect the RPV lower cold leg to the HPC. They are horizontally oriented (i.e., there is no elevation change) at 5.08 cm above reference and they are geometrically similar from the RPV to the HPC. The ADS sump return lines are constructed with SS304 and all external surfaces are covered with 5.1 cm of Thermo-12 hydrous calcium silicate insulation. Aside from their geometric layout, the ADS vent lines are otherwise similar to the ADS blowdown and vent lines.

The ADS sump return connection to the RPV is via a fillet welded 10 cm long, 1.91 cm nominal diameter schedule 80 pipe. The single ADS sump return line leaving the RPV tees into two 1.27 cm diameter, 0.1651 cm wall thickness lines which lead to 1.27 cm fast-acting pneumatic motor operated globe valves PCS-108A and PCS-108B. Air flow to the PCS-108A and PCS-108B actuators is controlled via solenoid operated valves AS-108A and AS-108B, respectively. Operation of the solenoid control valves is determined by the test facility control system logic programming for the test being conducted.

Downstream from each isolation valve is a transition piece with an internal 0.636 cm square-edge orifice. The transition piece serves two purposes: it transitions the line back from the 1.27 cm pipe to 1.57 cm ID tubing which is the size to the HPC, and it presents the proper scaled flow area for the ADS sump return line valve.

The two ADS sump return lines enter the HPC via a fillet welded stub, penetrate 22.0 cm, then turn downward for 21.0 cm before terminating well below the HPC waterline. There is no sparger on the end of this part of the ADS.

Each ADS sump return line is instrumented with a thermocouple (TF-871A, TF-871B) downstream of its associated orifice and external to the HPC.

2.6. DATA ACQUISITION, INSTRUMENTATION AND CONTROL SYSTEM

The OSU MASLWR test facility instrumentation and control system measures key system parameters, performs logic operations in accordance with user provided instructions, and issues control commands to change the system configuration based on those instructions.

In addition to executing user input test profiles, the data acquisition and control system monitors vital safety related parameters for unsafe operating conditions and issues safety commands to place the MASLWR test facility in a safe shutdown condition if necessary.

The OSU MASLWR test facility is instrumented for capturing the behavior of the system during both steady state and transient operating conditions. The following instrument types are utilized in the test facility:

- Thermocouples to measure fluid, heater, and wall temperatures. Controlled purity wire connects the premium grade thermocouples to the data acquisition and control system input module.
- Pressure transducers to measure the static pressure within tanks and piping.
- Differential pressure transducers to measure liquid levels in tanks, vessels, and piping. They are also used to determine the pressure drop across various components and flow rates.
- Electric power measurement devices to monitor the core power and provide feedback for closed loop core power control.
- Magnetic flowmeters to measure single-phase liquid flow rates.
- Coriolus flowmeters to measure mass flow rates.
- A vortex flowmeter to measure steam mass flow rate. This device also measures local pressure and temperature.

An instrumentation diagram is shown in Figure 2-5. The instrument uncertainty associated with the installed instrumentation is given in Table 2-4. The number, type, and uncertainty of installed instrumentation is sufficient for most test profiles run on the test facility but additional or higher accuracy temporary instrumentation can be installed if necessary to collect unique or currently unmonitored parameters, often with little or no permanent facility modification necessary.

TABLE 2-4. INSTALLED INSTRUMENTATION MEASUREMENT UNCERTAINTY

Instrument Type	Tag Number	Uncertainty
Vortex flow meter	FVM-602	1.5% of indicated value
Coriolis flow meter	FCM-511, -521, -531	0.5% of indicated value
Magnetic flow meter	FMM-501	0.5% of indicated value
Thermocouple	Various; TW-xxx, TF-xxx, TH-xxx	±1.1˚C (Type 4) or ±2.2˚C
Pressure meter	PT-511, -521, -531	±0.45psig[a]
Pressure meter	PT-301	±1.2psig[a]
Pressure meter	PT-602	±0.375psig[a]
Pressure meter	PT-801	±0.45psig[a]
Differential pressure meter	DP-101, -103, -105	±0.0175 inches H_2O[a]
Differential pressure meter	DP-102	±0.00185 inches H_2O[a]
Differential pressure meter	DP-104	±0.025 inches H_2O[a]
Differential pressure meter	DP-106	±0.05 inches H_2O[a]
Differential pressure meter	DP-107	±0.02 inches H_2O[a]
Differential pressure meter	DP-108	±0.03 inches H_2O[a]
Flow differential pressure meter	FDP-131	±0.025 inches H_2O[a]
Level differential pressure meter	LDP-106	±0.1125 inches H_2O[a]
Level differential pressure meter	LDP-301	±0.02 inches H_2O[a]
Level differential pressure meter	LDP-501, -801	±0.1875 inches H_2O[a]
Level differential pressure meter	LDP-901	±0.0625 inches H_2O[a]
Level differential pressure meter	LDP-601	±0.016 inches H_2O[a]
Power meter	KW-101, -102	0.6% of indicated value

[a] Uncertainty is reference accuracy provided by the manufacturer.

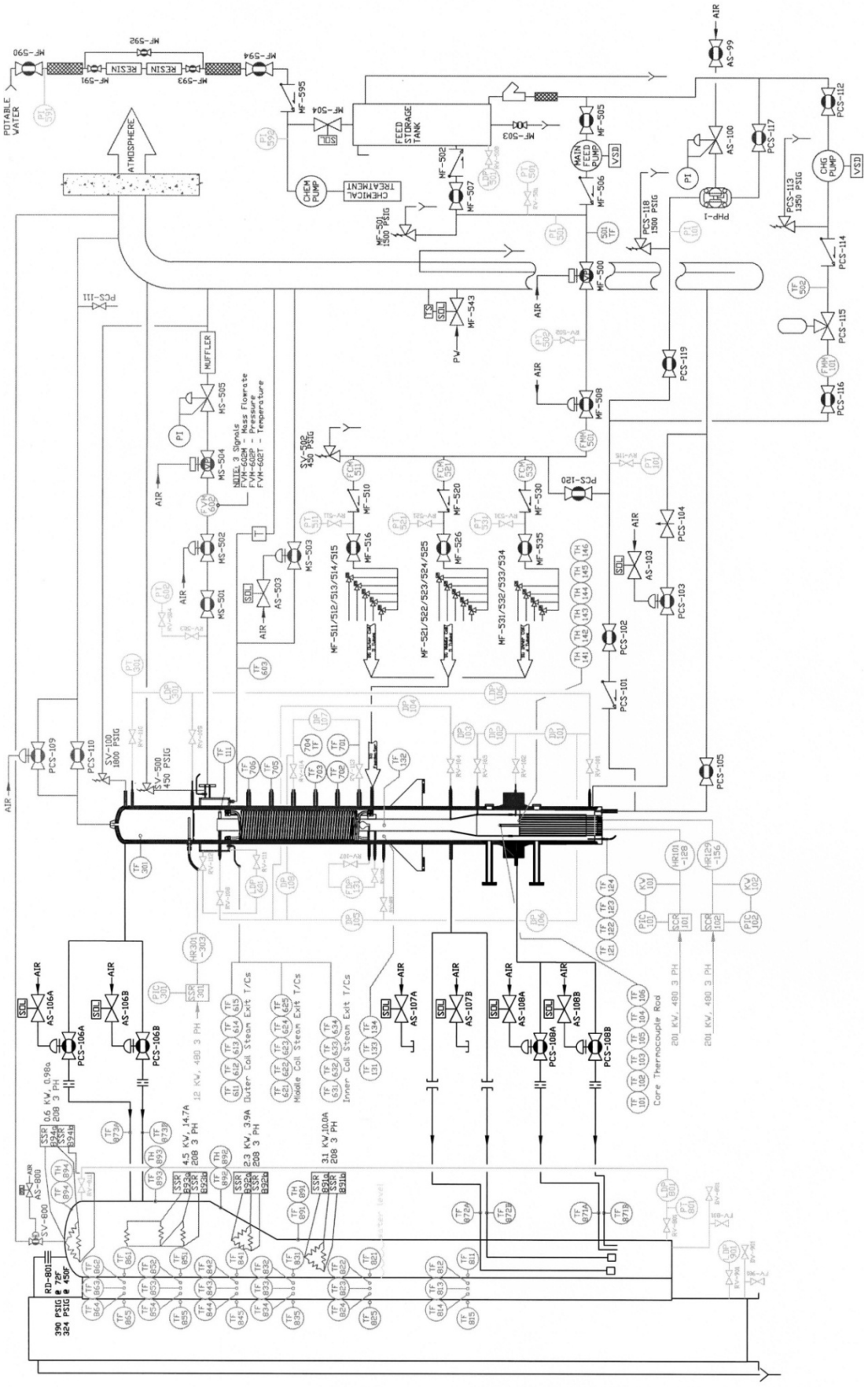

FIG. 2-5. MASLWR instrumentation diagram.

3. ICSP TESTS

Two tests were conducted at the OSU MASLWR Test facility in support of the current ICSP.

- SP-2: loss of feedwater transient with subsequent ADS operation and long term cooling. The purpose of this test was to conduct a loss of feedwater transient with subsequent automatic depressurization system (ADS) actuation and long term cooling to observe the thermalhydraulic behavior in primary, secondary and containment systems including natural circulation phenomena between primary and containment systems.
- SP-3: power maneuvering (normal operating conditions at different power levels). The test was a substitute for the original test planned under this ICSP, "stepwise reduction in primary system volume at decay power". The substitution was made over concerns about the ability of the test facility to safely handle the reduction in primary system volume while at power.

3.1. SP-2: LOSS OF FEEDWATER TRANSIENT

SP-2 was conducted to simulate a loss of feedwater, activation of safety systems, and the long term cooling of the OSU MASLWR test facility to determine the progression of a loss of feedwater transient. Initially, the test facility was brought to steady state at 75% power with a primary pressure of 8.618 MPa(g) and the main feed pump running on the secondary side.

By the original procedures, once the initial conditions are reached the test is initiated by stopping the main feed pump thus cutting off flow to the steam generators. With the subsequent loss of the reactor heat sink the primary pressure will begin to rise. When the pressurizer pressure reaches 9.064 MPa(a) the MASLWR core heaters will be set to decay power and valve PCS-106A will be placed in "Auto" mode to allow ADS-106A to open on high pressure (9.409 MPa(a)) venting into the high-pressure containment. PCS-106A and SV-800 will be operated in automatic mode to vent the primary system to the high-pressure containment while at the same time preventing the high pressure containment from exceeding its maximum operating pressure of 2.169 MPa(a). Table 3-1 highlights the opening and closing logic for these two valves as outlined in procedure SP-2 (Appendix I).

TABLE 3-1. MASLSWR PRIMARY SYSTEM VENTING LOGIC

PT-801 HPC Pressure	PCS-106A	SV-800
1.825 MPa(a) and rising	SHUT	SHUT
1.997 MPa(a) and rising	SHUT	OPEN
1.480 MPa(a) and lowering	OPEN	SHUT

When the difference between RPV and HPC pressures is less than 0.034 MPa, vent valves PCS-106A, PCS-106B, PCS-108A and PCS-108B open. The test continues until the pressurizer pressure drops below 0.618 MPa(a) or 5 hours have elapsed since commencing the procedure.

There were several deviations from the original procedures during the actual conduct of the test. The first change was to the MASLWR primary system venting logic outlined in Table 3-1. No flow measurement devices are installed at the MASLWR test facility that will track the mass lost through SV-800. It was determined that the pressure in the high-pressure containment would be controlled solely using PCS-106A. Thus SV-800 was closed for the duration of the transient while PCS-106A was opened at or below an HPC pressure of 1.480 MPa(a) and closed at or above an HPC pressure of 1.825 MPa(a). Table 3-2 shows the opening and closing times for PCS-106A. Note that all times are given in seconds from the time that the main feed pump is stopped.

The second major procedural change involved the initiation of the blowdown. During the actual test, the blowdown was initiated 18 seconds after decay power was initiated when the primary pressure reached 9.064 MPa(a), instead of waiting until the primary system pressure reached 9.409 MPa(a). Table 3-3 shows the core heater power during the transient. Completed test procedures for SP-2 are included in Appendix I.

TABLE 3-2. PCS-106A OPENING AND CLOSING TIME FOR SP-2

Event Number	Open (s)	Close (s)	Event Number	Open (s)	Close (s)
1	48.00	131.00	25	1999.00	2008.00
2	165.00	175.00	26	2085.00	2094.00
3	222.00	231.00	27	2171.00	2181.00
4	287.00	295.00	28	2259.00	2268.00
5	359.00	367.00	29	2345.00	2355.00
6	434.00	443.00	30	2433.00	2443.00
7	512.00	520.00	31	2521.00	1531.00
8	591.00	599.00	32	2609.00	2619.00
9	670.00	678.00	33	2697.00	2707.00
10	750.00	758.00	34	2786.00	2796.00
11	830.00	838.00	35	2876.00	2886.00
12	911.00	919.00	36	2966.00	2977.00
13	993.00	1000.00	37	3056.00	3068.00
14	1074.00	1082.00	38	3148.00	3160.00
15	1156.00	1164.00	39	3240.00	3252.00
16	1240.00	1248.00	40	3332.00	3345.00
17	1323.00	1331.00	41	3426.00	3439.00
18	1406.00	1414.00	42	3521.00	3535.00
19	1490.00	1498.00	43	3617.00	3632.00
20	1574.00	1582.00	44	3715.00	3731.00
21	1658.00	1666.00	45	3814.00	3832.00
22	1743.00	1751.00	46	3917.00	3938.00
23	1828.00	1836.00	47	4024.00	null
24	1913.00	1922.00			

TABLE 3-3. SP-2 DECAY POWER

Time (s)	Core Bundle #1 (kW)	Core Bundle #2 (kW)	Time (s)	Core Bundle #1 (kW)	Core Bundle #2 (kW)
0	149.5	147.9	4000.0	3.7	2.8
100.0	14.5	14.1	5000.0	3.3	2.3
200.0	12.1	11.5	6000.0	3.0	2.0
300.0	10.7	10.0	7000.0	2.7	1.8
400.0	9.7	9.0	8000.0	2.5	1.6
500.0	9.0	8.3	9000.0	2.3	1.5
600.0	8.4	7.6	10000.0	2.2	1.3
700.0	7.9	7.1	11000.0	2.1	1.2
800.0	7.5	6.7	12000.0	1.9	1.1
900.0	7.1	6.4	13000.0	1.9	0.9
1000.0	6.8	6.1	14000.0	1.7	0.9
2000.0	5.2	4.3	15000.0	1.6	0.8
3000.0	4.2	3.4			

Table 3-4 shows the initial conditions for blind calculation of SP-2. The values presented in the table represent the last measurement before the main feed pump was stopped which effectively begins the transient. Table 3-4 also shows the initial conditions used by all of the ICSP participants in their computer models to allow for a comparison between modelers and the actual initial conditions. Table 3-5 outlines the sequence of the major events that occurred while running test SP-2. Table 3-6 shows the ambient temperature measurements taken during the test. Tables 3-2, 3-3 and 3-6 represent the boundary conditions for the transient at the experimental facility.

No anomalies that would affect the quality of the test data were observed during the tests. However, some initial observations can be made. The core power indicators, kW-101 and kW-102, indicated a power into the core heaters that was somewhat less than anticipated by the facility control logic. There is confidence that the decay power indications shown in Table 3-3 are accurate, but these values were different than anticipated by procedure.

LDP-106, showing the level inside of the RPV, oscillated significantly during the blowdown due to boiling of water inside of the RPV. After the blowdown was finished the level indication settled down and then steadily decreased due to the cooling of the system.

PT-301 indicates the pressurizer pressure and is a good indicator of the pressure throughout the RPV. It shows a spike when the main feed water is turned off and then a sharp decline as the blowdown commences. Small oscillations are seen during the blowdown and then the system pressure stabilizes. Ultimately, the system pressure begins to decrease steadily as the system cools.

The temperature indications for instruments inside the RPV vary greatly depending on their position with respect to the core and the steam generator. Those that lie after the core but before the steam generator, TF-106 and TF-111, saw a sharp drop when the blowdown began and then oscillated while PCS-106A was being actuated. After blowdown the temperature gradually decreased as the system cooled.

For those instruments that lie after the steam generator, TF-131/133/134 and TF-121 through 124, there was a rise in temperature when the blowdown commenced. This was because these instruments had been below the average temperature of the system so when the flow by natural circulation stopped the temperatures all settled closer to the average, and then began decreasing.

TF-121 through 124 also notably have a sharp decrease in temperature after all the ADS lines are opened that none of the other temperature graphs show any sign of. This is because TF-121 through 124 are below the ADS lines and when they were opened the cold water from the HPC entered the primary system only affecting these thermocouples. As time progressed these thermocouples rose in temperature as the water became more similar to the rest of the system.

The thermocouples in the HPC (those in the 800 s) all show relatively similar trends. There is a sharp increase when the blowdown starts then as PCS-106A actuates the temperature increase slows. As the ADS lines are all opened there is a small bump in temperature and then a gradual decrease. None of these vary by much more than 10°C after the blowdown. The thermocouples that are placed higher in the HPC (those with higher numbers) have a higher temperature than those below them [2].

Although a single test, there are a number of phases during the tests, with a host of different phenomena occurring in each. Table 3-7 provides a summary of the various phenomena that occur during SP-2 along with an indication of which of these phenomena have been addressed by the individual participants. For each participant, “+” indicates that phenomenon was occurred/predicted clearly, “o” indicates that phenomenon was occurred/predicted partially/indirectly, “–” indicates that phenomenon was not occurred/predicted, and “NA” indicates that model is not appropriate to predict the phenomenon (no measurement in experiment).

TABLE 3-4. SP-2 INITIAL CONDITIONS FOR BLIND CALCULATION

Parameter	MASLWR	Unit	Experimental Value	AERB	BARC (RELAP)	CIAE	ENEA	GPRESS	IBRAE	KAERI	KINS
Pressurizer pressure	PT-301	MPa(a)	8.718	8.687	8.719	8.72	8.64	8.718	8.718	8.702	8.720
Pressurizer level	LDP-301	m	0.3606	0.365	0.28	0.364	0.33	0.3615	0.346	0.361	0.400
Power to core heater rods	KW-101/102	kW	297.4	298.0	298.0	297.0	297.3	297.0	297.3	297.5	299.0
Feedwater temperature	TF-501	ºC	21.2	21.0	25.0	31.5	20.0	21.4	21.4	21.4	21.39
Steam temperature	FVM-602-T	ºC	205.4	202.0	205.0	211.0	202.0	199.3	231.2	203.9	205.1
Steam temperature	Avg. of TF-611 to TF-634	ºC	203.1	202.0	205.0	211.0	202.0	200.3	231.2	203.9	210.1
Steam pressure	FVM-602-P	MPa(a)	1.411	1.401	1.421	1.5	1.45	1.482	1.411	1.411	1.411
Ambient air temperature		ºC	25.0		27.0	26.9	24.0	25.0	25.0		
HPC pressure	PT-801	MPa(a)	0.127	0.124	0.121	0.126	0.135	0.129	0.132	0.127	0.128
HPC water temperature	TF-811	ºC	26.7	27.0	30.0	27.7	23.1	26.9	26.7	27.0	27.7
HPC water level	LDP-801	m	2.820	2.79	2.9	2.821	2.88	2.800	2.822	2.820	2.810
Primary flow at core outlet	FDP-131	kg/s	1.82	1.76	1.36	1.66	1.48	1.77	1.68	1.72	1.85
Primary coolant temperature at core inlet	TF- 121/122/ 123/124	ºC	215.1	214.5	223.0	216.0	210.0	218.8	215.6	215.8	215.7
Primary coolant temperature at core outlet	TF-106	ºC	251.5	250.5	268.0	254.0	250.0	253.3	252.4	251.5	250.5
Feedwater flow	FMM-501	kg/s	0.106	0.13	0.111	0.107	0.1256	0.108	0.110	0.094	0.109
Steam flow		kg/s		0.115	~0.111	0.107	0.1256	0.102	0.106	0.094	0.109
Primary coolant subcooling at core outlet		ºC		50.0	33.7	47.0	50.0	47.7	48.3	49.4	50.8
Total heat loss through primary system		kW		0.57	1.3	0.68	10.0	2.38	2.0	41.71	
Heat transfer through SG		kW		297.5	296.7	284.0	278.0	290.0	296.5	255.8	299.0
Maximum surface temperature of core heater rods		ºC		303.7	309.0	304.0	303.0	301.8	302.6	NA	290.0
Location from the SG secondary inlet to reach - saturation - superheat		m		 1.228 2.456	 0.2 2.65		 1.7 5.2	 2.0 5.7	 1.5 5.0	 1.58 5.99	 1.815 5.445
CPV water level	LDP-901	m	6.35	6.6	6.35	6.35	6.37	6.2	6.35	6.35	6.41
CPV water temperature	TF-815	ºC	25.95	26.5	27.0	26.0	20.1	27.0	25.0	27.1	27.1

TABLE 3-4. SP-2 INITIAL CONDITIONS FOR BLIND CALCULATION (CONTINUED)

Parameter	MASLWR	Unit	Experimental Value	NPCIL	NUSCALE	SJTU	SNPTRD	UNIPA	UNIPI	USNRC
Pressurizer pressure	PT-301	MPa(a)	8.718	8.718	8.805	8.719	8.718	8.72	8.70	8.72
Pressurizer level	LDP-301	m	0.3606	0.358	0.303	0.35	0.35	0.34	0.357	0.361
Power to core heater rods	KW-101/102	kW	297.4	298.0	297.5	299.0	299.0	298.0	297.4	299.0
Feedwater temperature	TF-501	ºC	21.2	21.0	21.4	20.0	21.4	21.3	21.39	21.4
Steam temperature	FVM-602-T	ºC	205.4	204.0	205.4	193.0	200.0	200.0	202.2	204.5
Steam temperature	Avg. of TF-611 to TF-634	ºC	203.1	204.0	205.4	193.0	261.3	199.7	202.2	215.5
Steam pressure	FVM-602-P	MPa(a)	1.411	1.427	1.411	1.32	1.411	1.414	1.429	1.481
Ambient air temperature		ºC	25.0	25.0	25.0	19.9	27.0	24.9	20.0	25.0
HPC pressure	PT-801	MPa(a)	0.127	0.128	0.142	0.11	0.101	0.128	0.141	0.127
HPC water temperature	TF-811	ºC	26.7	27.0	27.1	26.9	27.0	26.9	26.6	20.5
HPC water level	LDP-801	m	2.820	2.827	2.806	2.82	2.794	2.81	2.86	2.85
Primary flow at core outlet	FDP-131	kg/s	1.82	1.79	1.34	1.76	1.6985	1.62	1.69	1.61
Primary coolant temperature at core inlet	TF- 121/122/ 123/124	ºC	215.1	222.6	197.6	214.4	216.5	211.0	217.3	231.0/229.6
Primary coolant temperature at core outlet	TF-106	ºC	251.5	257.9	244.7	250.7	250.9	250.3	254.5	267.6
Feedwater flow	FMM-501	kg/s	0.106	0.112	0.1065	0.128	0.41	0.1108	0.125	0.0-0.1114
Steam flow		kg/s		0.112	0.0920	0.128	0.41	0.1093	0.125	0.1101
Primary coolant subcooling at core outlet		ºC		43.2	57.0	49.9	51.0	53.0	46.8	33.5
Total heat loss through primary system		kW		0.68	4.66		5.0	~1.0	3.2	8.75
Heat transfer through SG		kW		297.9	292.6		293.60	296.2	297.4	299.0
Maximum surface temperature of core heater rods		ºC		316.7	303.1		306.9	298.8	295.7	303.2
Location from the SG secondary inlet to reach - saturation - superheat		m		 1.1 5.06	 0.818 2.45		 1.08 -	 1.63 5.35	 2.2 5.5	 1.784 3.306
CPV water level	LDP-901	m	6.35	6.35	6.35	6.5	6.35	6.30	6.37	6.35
CPV water temperature	TF-815	ºC	25.95	27.0	25.0	20.9	27	26.9	24.85	20.0

TABLE 3-5. SP-2 SEQUENCE OF EVENTS

Event	SP-2 Test (s)
Start of simulation – steady state (start of data collection)	0
Stop MFP Close HPC vent valve SV-800	0
PZR pressure (PT-301) reaches 9.064 MPa(a) Enter decay power mode	30[(1)]
PZR pressure (PT-301) reaches 9.409 MPa(a) De-energize PZR heaters Open ADS vent valve (PCS-106A)	48[(2)]
Start long-term cooling when pressure difference between primary system and HPC (PT-301 minus PT-801) becomes less than 5 psi (0.034 MPa) Open and remain open of PCS-106A and PCS-106B Open and remain open of PCS-108A and PCS-108B	4114-4117
End of test when one of the following conditions is reached: - PZR pressure ≤ 0.135 MPa(a) - Primary coolant temperature (TF-132) ≤ 35 ºC - 24 hours have elapsed	15822

(1) 30s does not match exactly with PT-301 data due to error/delay in measurement.

(2) Operator de-energized PZR heaters and opened PCS-106A manually after 18 s from decay power mode before PT-301 reaching setpoint (9.409 MPa(a)).

TABLE 3-6. SP-2 AMBIENT TEMPERATURE

Time (hours:minutes)	Ambient Temperature (°C)
0:00 (MFP Stop)	25.0
0:29	25.2
1:16	25.2
1:34	25.4
1:45	25.8
2:05	25.8
2:32	24.5
2:48	23.7
3:12	24.7
3:40	24.3
4:01	24.2
4:21	24.9

TABLE 3-7. SP-2 PHENOMENA CHECK

Phenomena	Experiment		AERB	BARC (RELAP5)	CIAE	ENEA	GIDROPRESS	IBRAE	KAERI	KINS	NPCIL	NuScale	SJTU	SNPTRD	UNIPA	UNIPI	USNRC
	Phenomena	Measurement															
HPC Pool: Thermal stratification	+	+	+	NA	+	+	o	o	o	+	NA	NA	o	+	o	o	+
HPC Pool: Natural convection	+	NA	+	NA	+	NA	o	o	o	+	+	NA	+	NA	NA	o	o
HPC Pool: Steam condensation	+	NA	o	+	+	+	o	+	+	+	+	-	+	o	o	+	+
HPC: Effect of non-condensable gases on condensation heat transfer	+	NA	-	+	+	+	+	o	+	o	+	o	o	+	+	+	o
HPC: Condensation on containment structures	+	o	o	+	+	+	+	+	NA	-	+	+	o	+	+	+	o
Distribution of pressure drop through primary system	+	+	+	+	+	+	+	+	+	+	+	+	o	+	+	+	+
Break flow	+	o	+	+	o	+	+	+	+	+	+	+	+	+	+	+	+
Single phase NC	+	+	+	+	+	+	+	+	+	+	+	+	+	-	+	+	+
Two phase NC	+	NA	+	+	+	+	+	+	+	+	+	+	o	+	+	+	o
Intermittent two phase NC	o	NA	+	+	NA	+	+	o	o	+	o	+	-	+	+	o	-
Heat transfer in core	+	+	+	+	+	+	+	+	+	+	+	+	+	+	+	+	+
Heat transfer in SG	+	-	o	+	+	+	o	+	+	+	+	+	+	+	+	+	+
Primary-containment coupling during blowdown and long-term cooling	+	o	+	+	+	+	o	+	+	+	+	+	+	+	+	+	+

+ Phenomenon occurred/predicted clearly

o Phenomenon occurred/predicted partially/indirectly

- Phenomenon not occurred/predicted

NA Model is not appropriate to predict the phenomenon. No measurement in experiment.

3.2. SP-3: POWER MANEUVERING

SP-3 was conducted to characterize the steady-state natural circulation in the primary side during various core power inputs at the MASLWR test facility. By the original procedure, this was accomplished by configuring the MASLWR facility in a natural circulation state and varying the power inputs of the core heaters. Power inputs of the core heaters were increased step by step from 10 percent of full power to 80 percent of full power, with a 10 percent increment at each step. For each power input, the primary side flow rate, hot leg and cold leg temperatures were monitored to determine whether the flow stabilization achieved. The primary side and steam generator pressures were maintained at 8.618 MPa(g) and 1.379 MPa(g), respectively, for all power inputs.

Several procedural problems were encountered during the performance of SP-3. Firstly, by procedure, the MASLWR test facility should be allowed to reach steady state prior to increasing the core power and moving on to the next step. The following three parameters were used to determine whether the MASLWR test facility had reached steady state conditions or not:

- Constant hot leg temperature as indicated by TF-106 (±2.8°C),
- Constant cold leg temperature as indicated by TF-131 (±2.8°C), and
- Constant primary mass flow rate as indicated by FDP-131 (±5%).

Following the completion of the test, during the data analysis phase, it became clear that although these three parameters may be steady state within the bounds of the procedure, many other parameters within the test facility might not be. Thus, steady state conditions were not reached between steps during the completion of SP-3 as required by procedure.

The second procedural problem was the result of inadequate adherence to the procedures by the test operators. Between each step, the test procedure calls for the operators to adjust the position of MF-500 (feed water control) to achieve saturated conditions at the secondary side outlet. This step was not completed between each power increase during SP-3. Changes to the feed water control were not made during the test to control the secondary side outlet conditions.

Another deviation from the original procedure was a charging flow to RPV during SP-3 experiment. OSU provided the information on this so that ICSP participants could use this as a boundary condition.

Table 3-8 shows the initial conditions for blind calculation of SP-3. The values presented in the table represent the average of the specified instruments over the two-minute data collection time for the initial power level (40 kW) for the test. Table 3-8 also shows the initial conditions used by all of the ICSP participants in their computer models to allow for a comparison between participants and the actual initial conditions. Table 3-9 outlines the sequence of the major events that occurred while running test SP-3. Table 3-10 shows the boundary conditions for the test; core power, feedwater flow rate, feedwater temperature, and secondary side pressure. Note that the ambient temperature during SP-3 was not measured but is estimated between 20 - 24°C.

The defining characteristic of the data from SP-3 is the gradual step-up of the volumetric flow rate of the primary circuit. There are a few instruments that definitively illustrate this ramp-up and plateau. FDP-131, the differential pressure transmitter across the V Cone flow meter, illustrates the ramp-up and gradual increase in pressure due to the increase in volumetric flow rate. The differential pressure reading across the chimney in the riser from DP-104 also illustrates the gradual increase in pressure, as does the differential pressure reading across the core.

The outer coil steam exit temperatures measured by TF-611 through TF-615 showed the temperature transients at each power level. The same trend was seen for the middle and inner coil steam exit temperatures (TF-621 through TF-625 and TF-631 through TF-634). The trends for these thermocouples were expected since the pressure experienced similar transients for each power levels. The thermocouple at the chimney exit, TF-111, also showed a temperature transient at each power level.

The water temperature of the downcomer section with the steam generator bundles is measured by TF-701 through 706. TF-701 was noted to be out of service in the critical parameter list and configuration

status due to an incorrect display of digital signals and measurement of temperatures. These thermocouples are at different elevations but showed similar trends with each other.

TF-131, TF-133 and TF-134 are located at the downcomer below the steam generators. They also showed the similar trend with each other. The trend is different from TF-301. The main feedwater temperature, TF-501, does not vary greatly since the main feedwater pump was not powered on during the test. On the other hand, the charging pump exit temperature, TF-502, does show a slight increase and then drop in temperature.

The heater core temperature is measured by TH-141 through 146. The core heater rods were energized for this procedure. The temperature readings have similar transients throughout the test. TH-144 has the highest temperature reading that approaches the heater rod trip setpoint, however, it is still well below the rating of the heater rods. The core thermocouple rod located just above the core (TF-101 through 106) and the lower plenum thermocouples (TF-121 through 124) located below the core have a slight drop in temperature and show the same trends.

The pressure transmitter on the inlet line of the steam generator (PT-511, 521 and 531) read approximately the same value throughout the test. The steam vent line, FVM-602, shows an increasing flow rate as power increases. The reading by DP-102 and DP-103 showed a very small pressure loss across the riser section and riser cone. The pressure loss in the chimney and across the steam generator in the downcomer is measured by DP-104 and DP-105. Higher pressure loss is observed in these two differential pressure readings [3].

As with SP-2, during SP-3 there are a number of different phenomena occurring during the test. Table 3-11 provides a summary of the various phenomena that occur during SP-3 along with an indication of which of these phenomena have been addressed by the individual participants. For each participant, “+” indicates that phenomenon was occurred/predicted clearly, “o” indicates that phenomenon was occurred/predicted partially/indirectly, “-” indicates that phenomenon was not occurred/predicted, and “NA” indicates that model is not appropriate to predict the phenomenon (no measurement in experiment).

TABLE 3-8. SP-3 INITIAL CONDITIONS FOR BLIND CALCULATION

Parameter	MASLWR	Unit	Experimental Value	AERB	BARC (CATHARE)	BARC (RELAP)	CIAE	ENEA	GPRESS	IBRAE	KAERI
Pressurizer pressure	PT-301	MPa(a)	8.718	8.699	8.723	8.719	8.72	8.70	8.718	8.718	8.719
Pressurizer level	LDP-301	m	0.357	0.325	0.51	0.330	0.35	0.35	0.376	0.34	0.357
Power to core heater rods	KW-101/102	kW	42.1	40.0	40.0	40.0	40.0	40.0	42.0	42.2	40.0
Feedwater temperature	TF-501	ºC	31.5	31.0	31.5	30.5	31.5	31.5	31.5	31.5	31.5
Steam temperature	FVM-602-T	ºC	205.4	255.0	255.0-257.0	261.9	261.0	262.0	208.5	259.7	260.7
Steam temperature	Avg. of TF-611 to TF-634	ºC	256.4	255.0	256.0	261.9	261.0	262.0	262.6	259.7	260.7
Steam pressure	FVM-602-P	MPa(a)	1.446	1.42	1.464	1.446	1.44	1.45	1.48	1.44	1.446
Ambient air temperature		ºC		27.0	30.0	27.0	26.9	24.0	27.0	25.0	
Primary flow at core outlet	FDP-131	kg/s	0.68[(1)]	0.85	0.60	0.63	0.71	0.68	0.74	0.78	0.66
Primary coolant temperature at core inlet	TF- 121/122/ 123/124	ºC	250.3	250.5	256.6	258.9	251.0	253.0	253.5	251.3	251.2
Primary coolant temperature at core outlet	TF-106	ºC	262.8	260.5	269.5	270.8	262.0	264.8	264.3	261.7	262.8
Feedwater flow	FMM-501	kg/s	0.010	0.010	0.013	0.014	0.010	0.010	0.011	0.012	0.010
Steam flow		kg/s		0.010	0.013	0.134	0.010	0.010	0.010	0.012	0.010
Primary coolant subcooling at core outlet		ºC		30.0	31.6	30.3	40.0	36.5	36.8	39.6	38.3
Total heat loss through primary system		kW		0.6	1.0	1.6	0.9	6.7	3.2	4.7	11.8
Heat transfer through SG		kW		32.0	37.7	38.0	28.7	29.0	31.14	33.7	28.1
Maximum surface temperature of core heater rods		ºC		270.0	286.9	320.0	277.0	264.9	278.1	273.4	NA
Location from the SG secondary inlet to reach		m									
- saturation				0.307	0.38	0.4		0.38	0.2	0.2	0.32
- superheat				0.921	2.448	2.45		0.96	0.6	0.7	1.58

(1) Initial primary core flow in experiment was oscillating. The primary core flow (0.68 kg/s) in this table is not a steady-state value. The average initial core flow in the experiment was 0.48 kg/s.

TABLE 3-8. SP-3 INITIAL CONDITIONS FOR BLIND CALCULATION (CONTINUED)

Parameter	MASLWR	Unit	Experimental Value	KINS	NPCIL	NUSCALE	SJTU	SNPTRD	UNIPA	UNIPI	USNRC
Pressurizer pressure	PT-301	MPa(a)	8.718	8.719	8.718	8.603	8.719	8.718	8.72	8.714	8.721
Pressurizer level	LDP-301	m	0.357	0.383	0.359	0.359	0.360	0.3616	0.360	0.348	0.359
Power to core heater rods	KW-101/102	kW	42.1	40.0	40.0	42.1	40.0	40.0	40.0	42.0	42.1
Feedwater temperature	TF-501	ºC	31.5	31.5	31.6	31.5	31.5	31.0	31.5	31.5	31.5
Steam temperature	FVM-602-T	ºC	205.4	205.4	263.9	259.4	260.0	263.0	238.0	260.5	256.7
Steam temperature	Avg. of TF-611 to TF-634	ºC	256.4	259.3	263.9		260.0	224.2	261.7	260.5	259.0
Steam pressure	FVM-602-P	MPa(a)	1.446	1.446	1.465	1.740	1.445	1.48	1.446	1.465	1.447
Ambient air temperature		ºC		22.0	25.0		19.9	30.0	22.0	20.0	24.9
Primary flow at core outlet	FDP-131	kg/s	0.68[(1)]	0.88	0.85	0.69	0.68	0.6	0.80	0.83	0.75
Primary coolant temperature at core inlet	TF-121/122/ 123/124	ºC	250.3	250.4	255.1	251.3	251.1	257.0	253.0	251.9	249.7
Primary coolant temperature at core outlet	TF-106	ºC	262.8	259.8	264.6	262.9	263.2	269.0	263.0	262.1	260.2
Feedwater flow	FMM-501	kg/s	0.010	0.010	0.013	0.015	0.014	0.014	0.013	0.014	0.010
Steam flow		kg/s		0.010	0.013	0.015	0.014	0.014	0.013	0.014	0.012
Primary coolant subcooling at core outlet		ºC		41.4	38.0	37.5	38.0	32.0	39.4	39.0	41.1
Total heat loss through primary system		kW		11.4	5.1	0	0.0	0.5	~5.0	2.1	12.1
Heat transfer through SG		kW		28.6	36.5	42.1		39.5	35.9	40.3	30.1
Maximum surface temperature of core heater rods		ºC		269.3	278.8	276.4		275.0	273.9	275.7	270.1
Location from the SG secondary inlet to reach		m									
- saturation				0	0.2	0.41		0.04	0.70	0.5	0.154
- superheat				0.908	0.4	0.0		0.24	0.93	0.5	0.615

(1) Initial primary core flow in experiment was oscillating. The primary core flow (0.68 kg/s) in this table is not a steady-state value. The average initial core flow in the experiment was 0.48 kg/s.

TABLE 3-9. SP-3 SEQUENCE OF EVENTS

Event	SP-3 Test (s)
Start of simulation – steady state (start of data collection)	0
Initiate core power increase to 80 kW	0
Initiate core power increase to 120 kW	870
Initiate core power increase to 160 kW	1642
Initiate core power increase to 200 kW	2177
Initiate core power increase to 240 kW	4004
Initiate core power increase to 280 kW	4498
Initiate core power increase to 320 kW	5096

TABLE 3-10. SP-3 BOUNDARY CONDITIONS

Time (s)	KW-101 (kW)	KW-102 (kW)	FCM-511 (kg/s)	FCM-521 (kg/s)	FCM-531 (kg/s)	TF-501 (˚C)	FVM-602-P (MPa (a))	FVM-602-T (˚C)
0	21.1	21.0	0.0034	0.0032	0.0036	31.5	1.44	205.8
870	39.6	40.4	0.0134	0.0157	0.0144	26.9	1.44	241.7
1642	59.1	60.3	0.0128	0.0148	0.0131	26.1	1.43	249.3
2177	79.2	79.9	0.0182	0.0195	0.0177	25.4	1.43	253.8
4004	98.9	99.2	0.0240	0.0268	0.0224	23.1	1.44	208.8
4498	119.5	119.6	0.0291	0.0327	0.0271	22.2	1.44	205.3
5096	140.4	139.2	0.0332	0.0375	0.0310	21.6	1.43	206.3

TABLE 3-11. SP-3 PHENOMENA CHECK

Phenomena	Experiment		AERB	BARC (RELAP5)	BARC (CATHARE)	CIAE	ENEA	GIDROPRESS	IBRAE	KAERI	KINS	NPCIL	NuScale	SJTU	SNPTRD	UNIPA	UNIPI	USNRC
	Phenomena	Measurement																
Distribution of pressure drop through primary system	+	+	+	+	+	+	+	+	+	+	+	+	+	o	+	+	+	+
NC: stability	+	+	+	+	+	+	NA	+	+	o	-	+	+	o	+	+	+	o
Bypass heat transfer from chimney to downcomer	+	+	+	+	+	+	+	+	+	+	-	+	+	+	+	+	+	+
Single phase NC	+	+	+	+	+	+	+	+	+	+	+	+	+	+	+	+	+	+
Two phase NC	NA		+	+	NA	+	NA	NA	-	-	-	-	-	o	-	-		NA
Intermittent two phase NC	NA		+	-	NA	NA	NA	NA	-	-	-	-	-	-	-	-		NA
Heat transfer in core	+	+	+	+	+	+	-	+	+	+	+	+	+	+	+	+	+	+
Heat transfer in SG	+	+	o	+	+	+	-	+	+	+	+	+	+	+	+	+	+	+
SG: superheating in secondary	+	+	+	+	+	+	-	+	o	+	+	+	+	+	+	+	+	+

\+ Phenomenon occurred/predicted clearly

o Phenomenon occurred/predicted partially/indirectly

\- Phenomenon not occurred/predicted

NA Model is not appropriate to predict the phenomenon. No measurement in experiment.

4. PARTICIPANT'S MODELS AND RESULTS

4.1. AERB – INDIA

4.1.1. Computer codes

RELAP5/SCDAP/MOD3.4 [5] was used. RELAP5 is a light water reactor (LWR) transient analysis code, developed at the Idaho National Engineering Laboratory (INEL). Its specific applications include simulations of transients in LWR systems such as loss of coolant, anticipated transients without scram, and operational transients such as loss of feed water, loss of off-site power, station blackout and turbine trip. It can also be used for simulations of a wide variety of hydraulic and thermal transients in both nuclear and non-nuclear systems involving mixtures of steam, water, noncondensable, and solute. The RELAP5 hydrodynamic model is a one-dimensional, transient, two-fluid model for flow of a two-phase steam-water mixture that can contain noncondensable components in the steam phase and/or a soluble component in the water phase. The RELAP5/SCDAP/MOD3.4 thermal-hydraulic model solves field equations for eight primary dependent variables.

4.1.2. System idealization

In the interest of studying the flow instability phenomena in an integral type reactor, Oregon State University (OSU) has constructed a system-level test facility. The test facility simulates the Multi-application Small Light Water Reactor (MASLWR) concept developed by Idaho National Engineering and Environmental Laboratory, OSU and NEXANT–Bechtel. The test facility is designed for full pressure and full temperatures of the prototype with one third scale in length. In this section, the modeling approach to predict the transient response of the MASLWR using thermal-hydraulic code RELAP5/SCDAP/MOD3.4 is described.

4.1.2.1. System idealization for blind calculation

In the RELAP5 nodalization, the primary side heater, riser and the downcomer sections were modeled as pipe and annulus components. The nodal discretizations of each RELAP components are as shown in Figure 4-1. The core section (component 120) has 6 axial nodes with 5 heat structures connected with 5 axial nodes. The riser section (130) with 13 axial nodes is connected to the top of the core with a single junction. The SG section of the cold leg is modeled as component 150, and the lower cold leg and downcomer sections are modeled as 9 axial nodes of an annulus component (160). The lower plenum is modeled as a single volume (170) communicating with the hot and cold leg through single junctions. The lower part of pressurizer is modeled as pipe component (140) and the steam portion of the pressurizer is modeled using a branch component (180). A servo valve was used for modeling the steam control valve and motor valve is used to model the ADS valves. The high pressure containment (505) and cooling pool vessel (605) are modeled using a pipe component with 10 axial nodes. In the secondary side, helical coils of the steam generator (SG) are modeled as an equivalent vertical tube using a pipe component. For the blind calculations, the coils are modeled as a single equivalent pipe. Constant feed flow is maintained using a time dependent junction component. To account for the effect of heat losses and thermal capacitance, heat structures are applied for all the components of the system. The geometrical data and RELAP component number for the respective regions of the facility are listed in Table 2-1. For SP-2 simulations, the vent lines (523 & 524), blowdown lines (518 & 519), and sump return lines (512 & 513) are modeled using pipe and motor valve components connecting the downcomer section and HPC.

In simulating SP-3, the core power is raised to 20% for every 1000 s to a maximum of 80% of full power. Stratification model is enables for modeling of pressurizer and chocked floe model is not used for the simulation.

4.1.2.2. Modeling change for open calculation

The nodalization scheme of blind calculation is adopted for the open calculation with few modifications. The SG secondary volume is modeled in as PIPE component of 10 volumes against 5

volumes in the blind calculation. Additional water charging into the primary during the SP-3 transients as done in the experiment is also simulated in the open calculation.

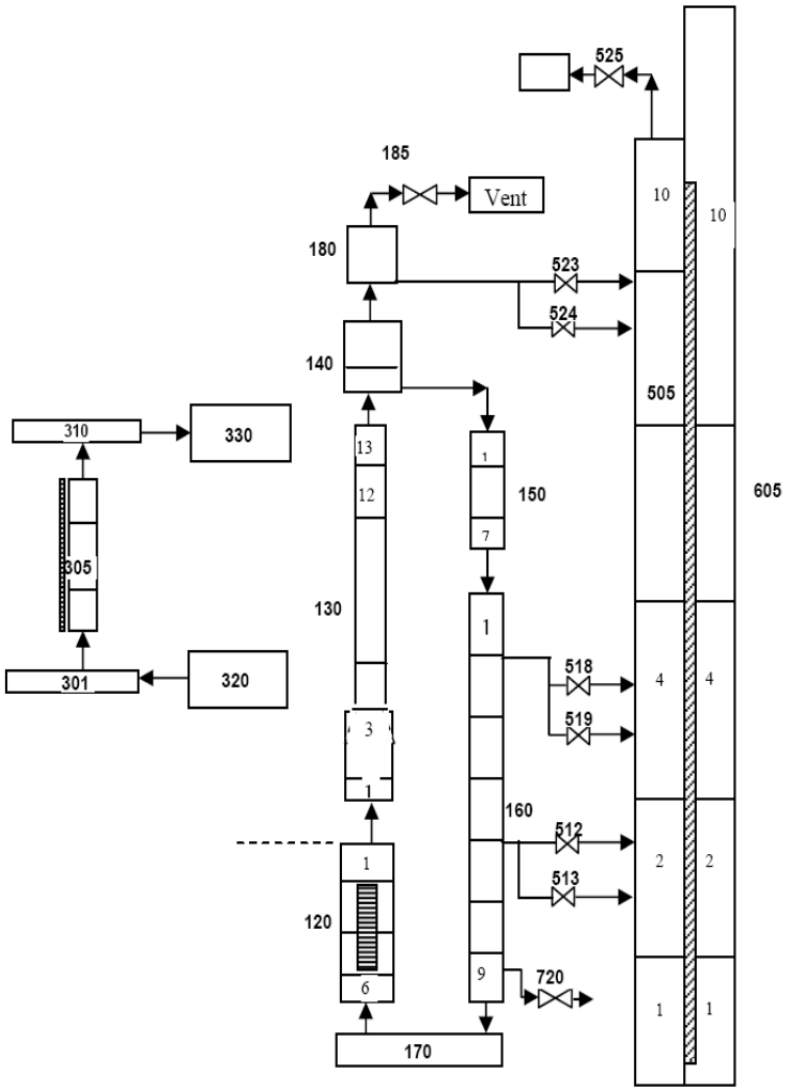

FIG. 4-1. Nodalization scheme for MASLWR.

4.1.3. Analysis results for loss of feed-water transients

Transient simulations for loss of feed-water transients (SP-2) have been carried out to understand the phenomena like natural circulation flow instability and loss of feed water transients with ADS operation in small integral natural circulation reactors. Initial conditions for the transient simulations were obtained by performing steady state. The predicted transients results carried out according to the operator procedure outlined in ICSP specification are presented in this section [4].

4.1.3.1. RPV thermal-hydraulic behavior

Figure 4-2 shows the temporal traces of the system parameters predicted during loss of feed water and opening of ADS lines. The transient simulation is initiated by stopping the feed water flow and the closure of HPC vent valve. This results in increase of RPV pressure and when it reaches 8.9 MP(a), the core power is put in decay mode. The system falls into a transient mode as the ADS vent valve is opened after 18s of reaching 8.9 MPa(a), and the RPV communicates with the HPC. ADS valve is opened and closed for an HPC pressure at 1.8 MPa(a) and 1.45 MPa(a) respectively. A sudden drop in RPV pressure and level is observed in the initial stage and later, the level sets up to 3.0 m. As a result of the sudden pressure drop, boiling in the core is initiated, and the primary flow starts to oscillate and

the flow remain to oscillate for the most part of the transients as it approches zero. At arround 4000 s the pressure difference between the RPV and HPC falls below 0.034 MPa which signals the opening of PCS-108 valves and thus the lower part of the PRV and HPC starts communicating.

A comparison of major RPV parameters like pressure, temperature and level observed in the experiment, blind and open calculation are presented in the Figures 4-3, 4-4 and 4-5 respectively. It was observed that the depressurization time of primary as predicted in the open calculation matches well with the experimental observation (Fig. 4-3). The difference in the prediction of open and blind calculation is due to the different in K-loss factors applied for the ADS valve (PCS-106A). The open calculation prediction of primary depressurization time can be appropriated towards the experimental values by changing the heat transfer surface area of the heat transfer plate between HPC and CPV which affects the condensation rate of the steam hitting the HPC wall.

As natural circulation is established between the RPV and HPC, an increase in primary flow is observed during 8000 – 13,000 s (Fig. 4-6). Later, a significant increase in the amplitude of flow oscillation is observed when the net void generation in core increases, resulting in an incresed riser temperature (Fig. 4-7). This in turn causes onset of vapour generation (flashing) in the adiabatic riser section where the void fraction at riser exit is found to be higher than the core exit, resulting in further increase in amplitude of flow oscillation (Fig. 4-8). The system remains to be in an oscillatory mode for the remaining period.

The mass flow through the ADS valves are ploted in Figure 4-9. It is observed that the natural circualtion flow between the HPC and the RPV is established at around 4000 s when both the ADS valves (106 & 108) are kept open. It is observed that the flow in the ADS valve (108) is oscillatory with reverse flow owing to the void generation in the core and riser section of the primary. At the instant of opening (108 valves), liquid flows into the RPV from HPC and it results in increased RPV level and decreased void in core and riser. The flow is seen to be negative due to the connection of the valves from RPV side to HPC.

The cummulative discharge in the ADS-106A valve for both the blind and open calculation is shown in Figure 4-10. The cummulative discharge in the blind case is found to be higher as the K-loss in the valve is much lower, and hence the discharge for every opening is higher.

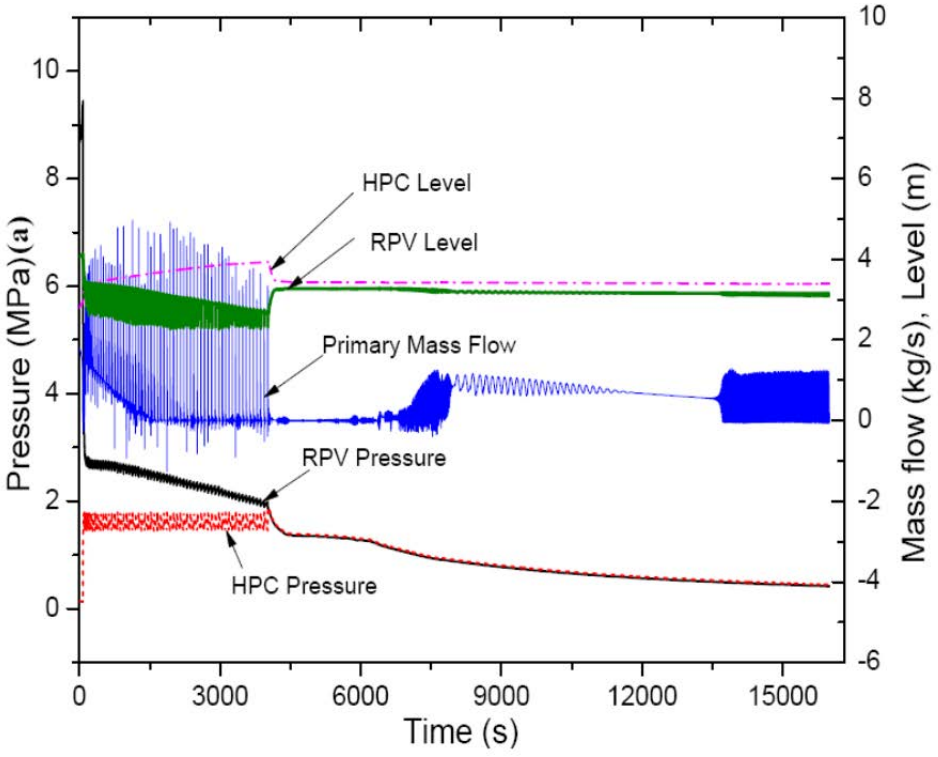

FIG. 4-2. System parameters during loss of feed water with ADS operation (open calculation).

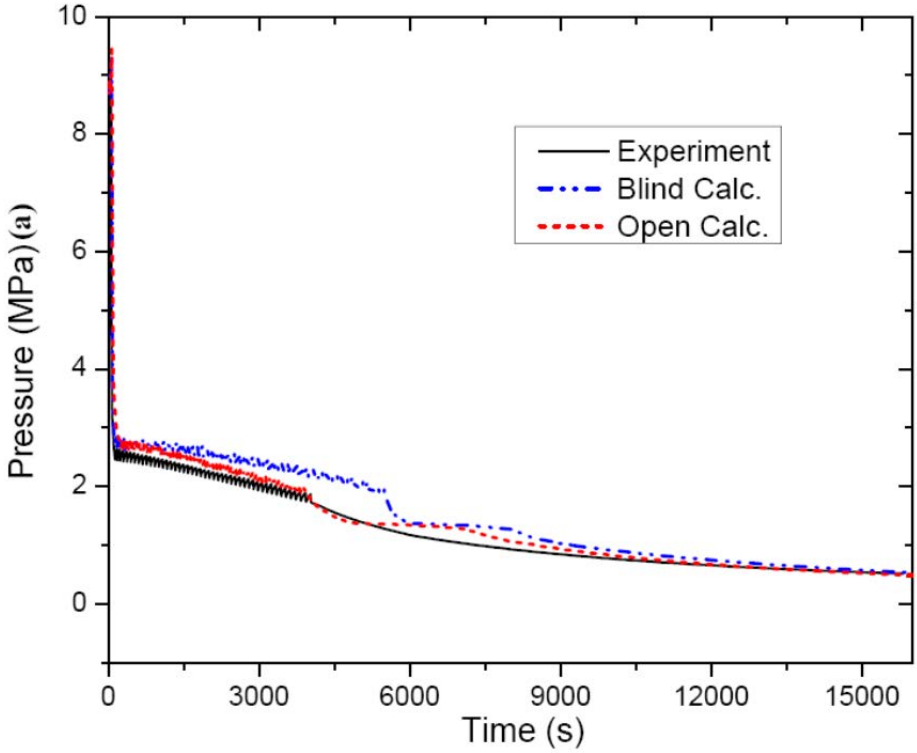

FIG. 4-3. RPV pressure.

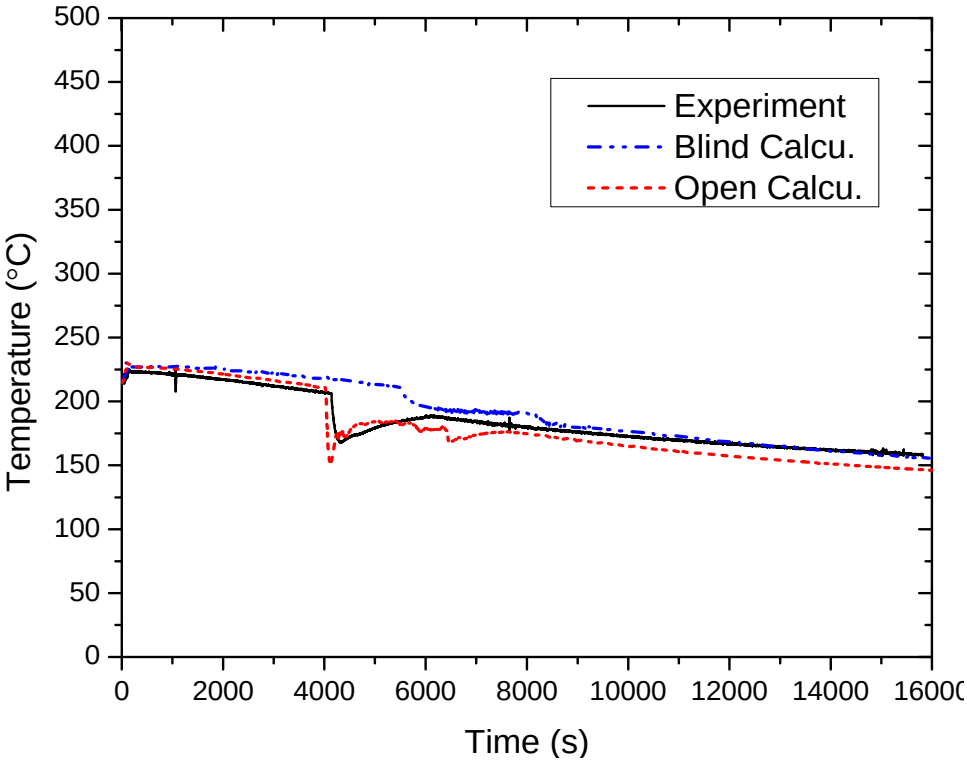

FIG. 4-4. Core inlet temperature.

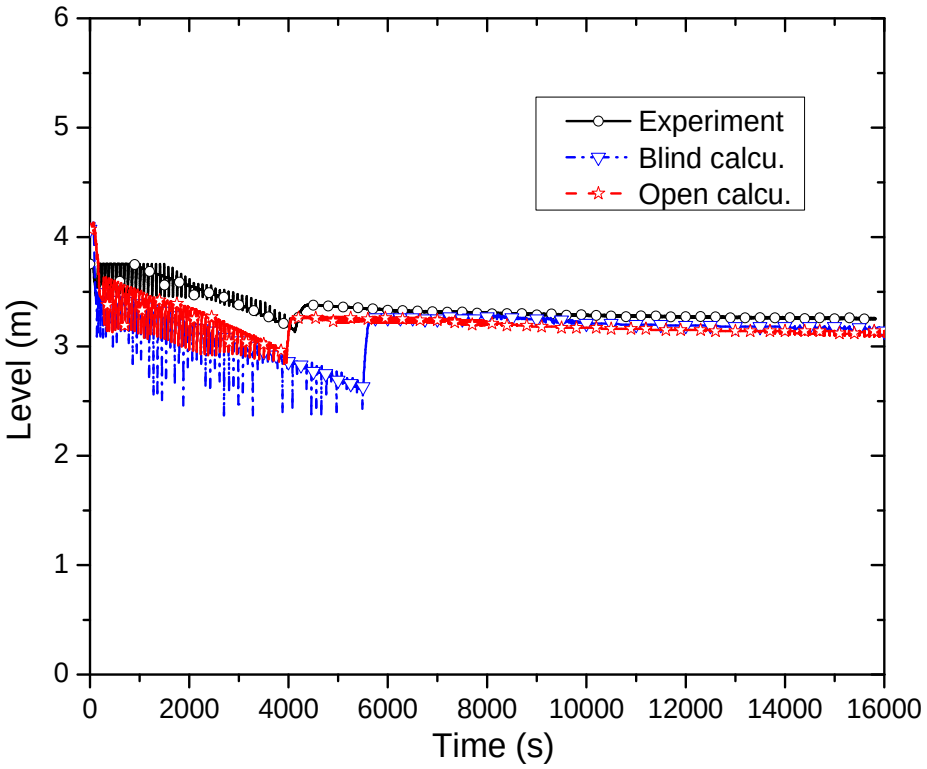

FIG. 4-5. RPV level.

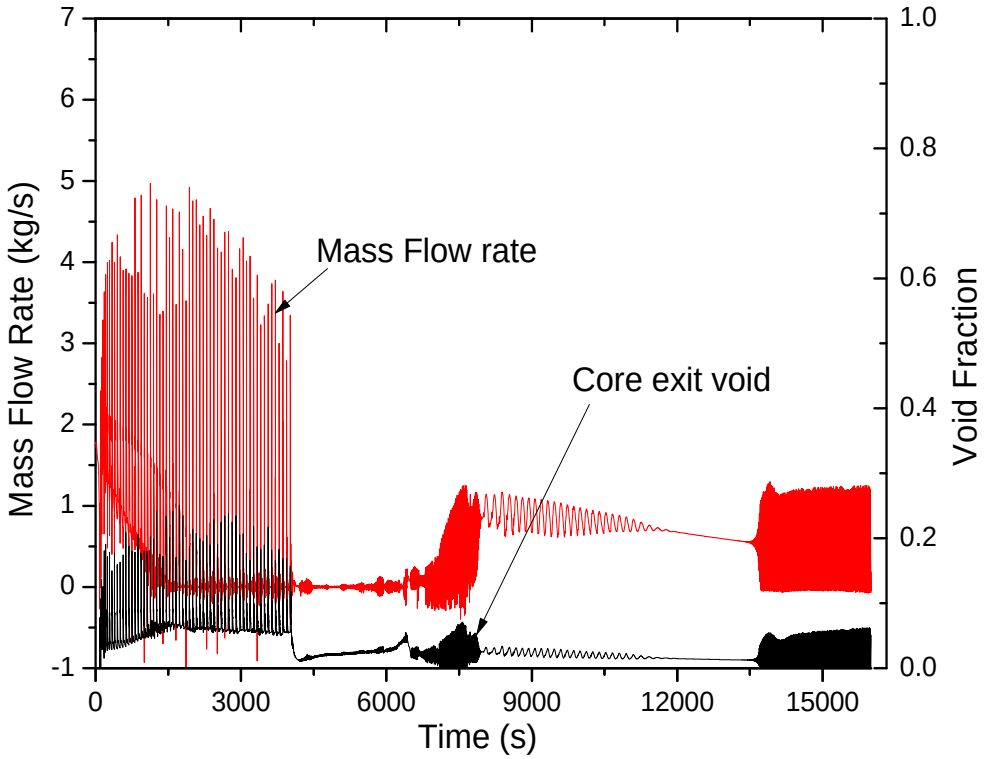

FIG. 4-6. Core exit void and mass flow rate (open calculation).

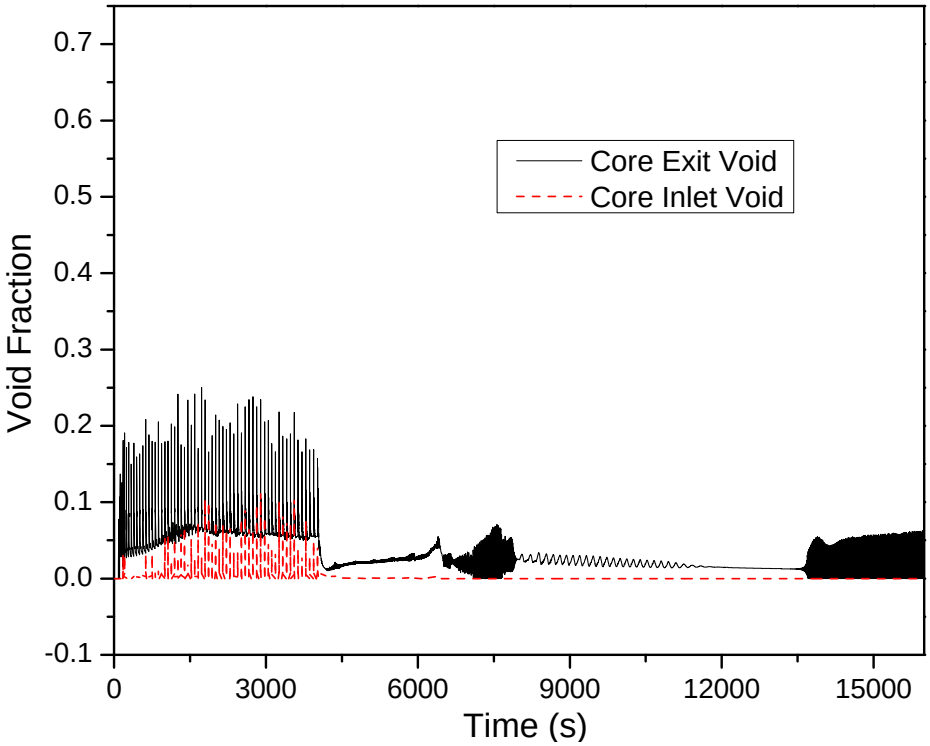

FIG. 4-7. Core void fraction (open calculation).

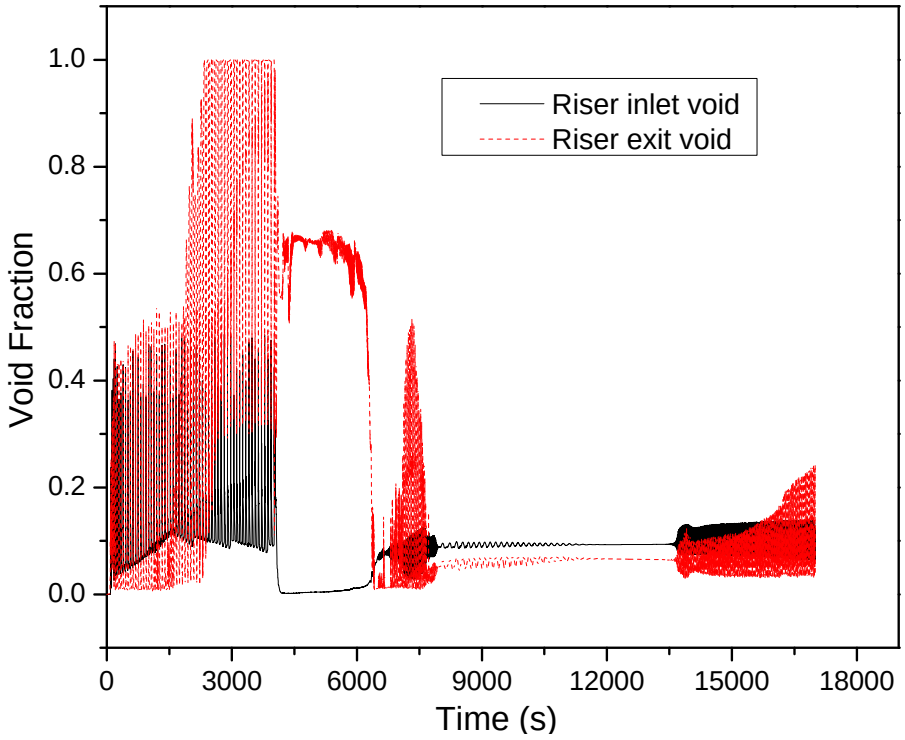

FIG. 4-8. Riser void fraction (open calculation).

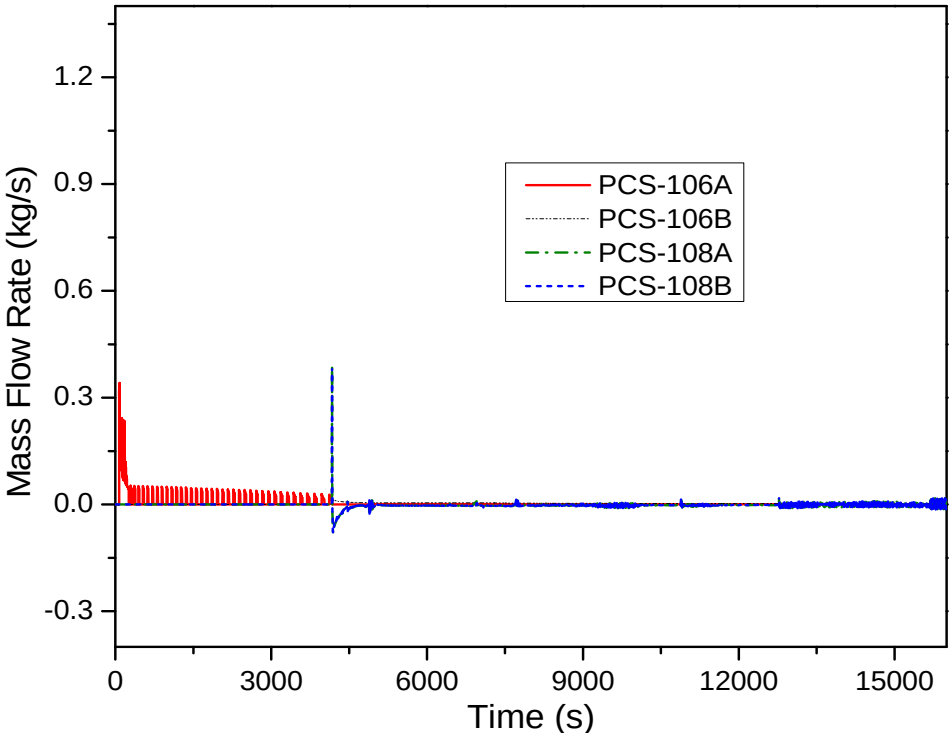

FIG. 4-9. Mass flow rate through ADS valves in open calculation(open calculation).

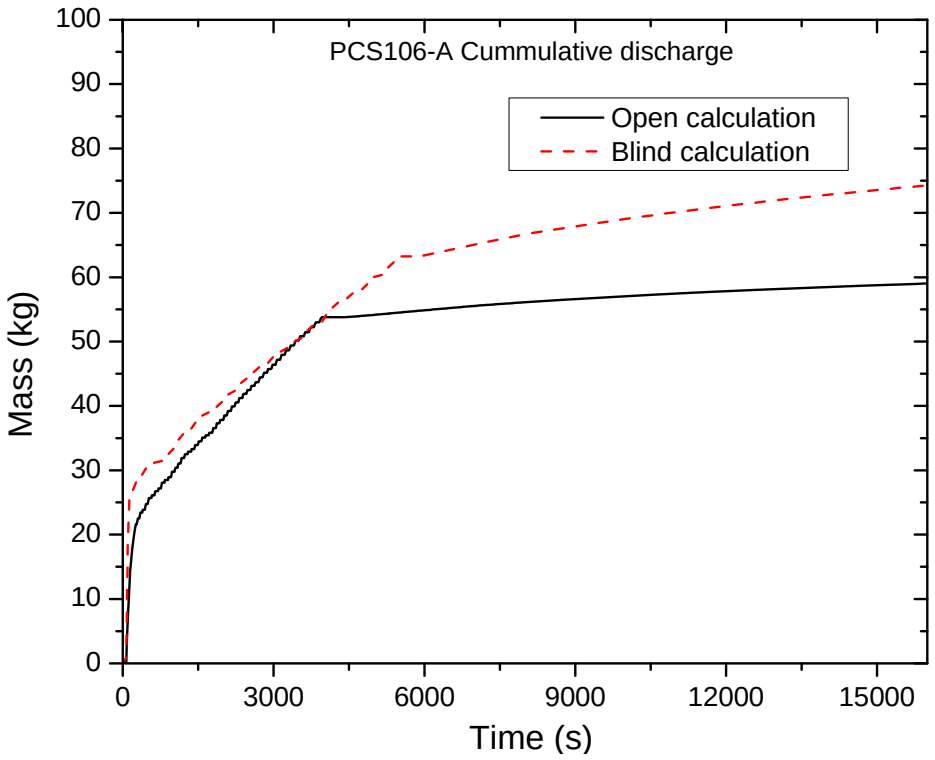

FIG. 4-10. Cummulative discharge through PCS 106-A valve.

4.1.3.2. SG thermal-hydraulic behavior

The heat removed in the SG, and the inlet and exit temperature of the cooling fluid is plotted in Figures 4-11 and 4-12 respectively. Figure 4-11 shows that the SG which is idle during the transients, participates in the heat transfer (4500 – 5500 s) when the primary level drops and fills up again by the cooler HPC water. Figure 4-12 shows that the steam exit is at superheated condition during the PCS valve operat
primary side

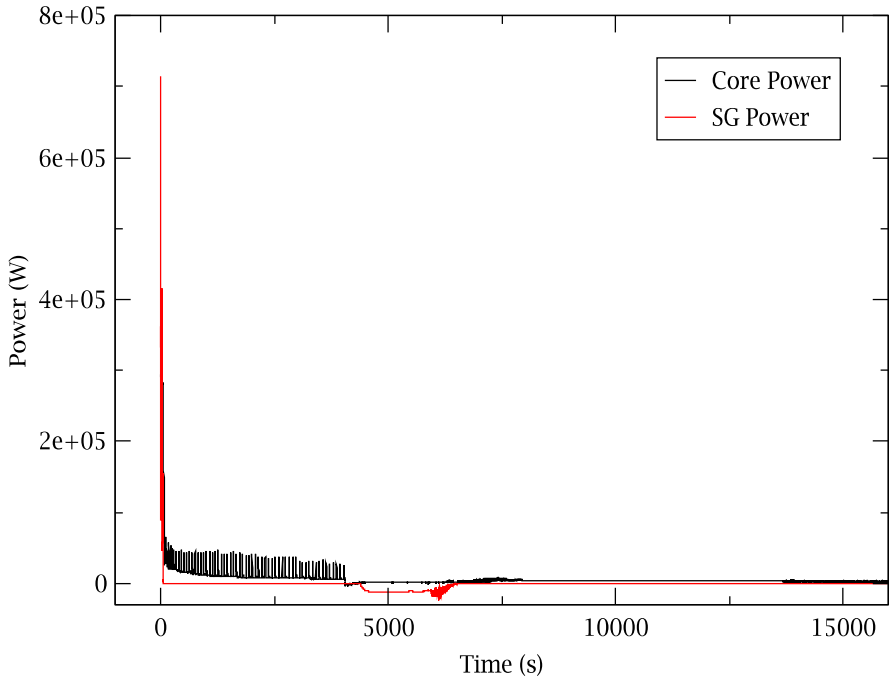

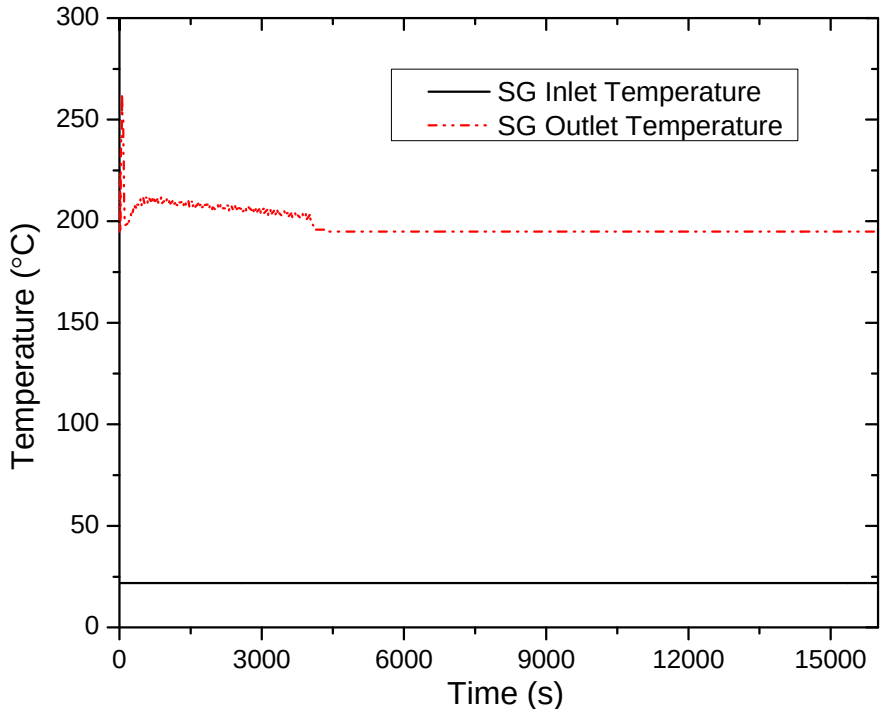

FIG. 4-12. Steam generator inlet and exit temperature.

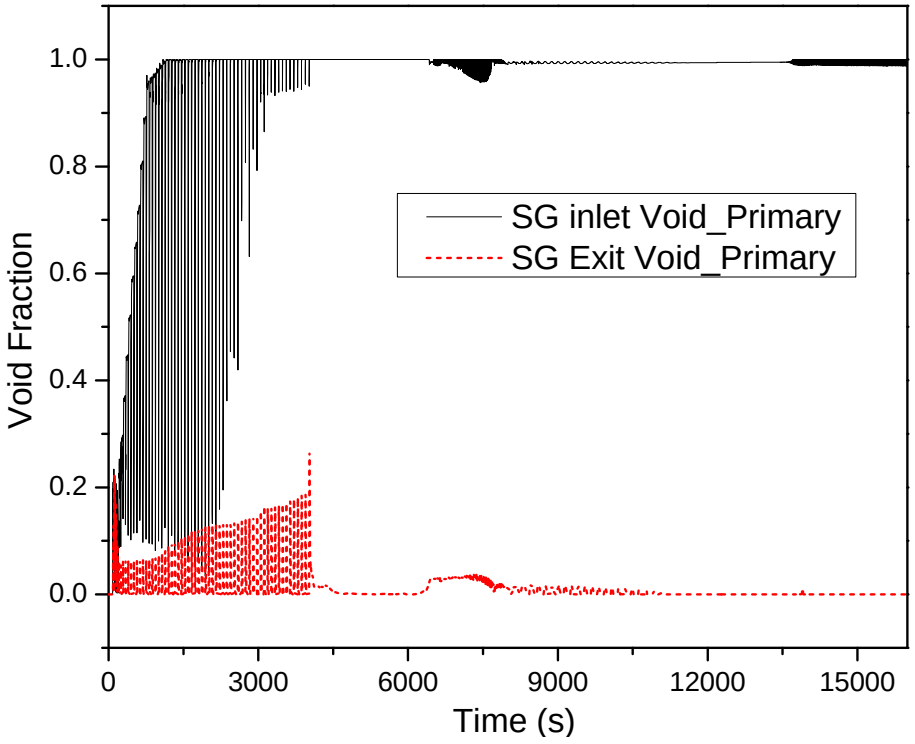

FIG. 4-13. Void fraction in SG primary region.

4.1.3.3. HPC thermal-hydraulic behavior

The pressurization of HPC due to the steam discharge from RPV through PCS-106A valve is shown in Figure 4-14 in comparison with the blind predication and experimental observation. The open calculation results agree well with the experimental observation. In the blind case, due to the lower condensation rate in the HPC walls, the PCS-106A operation is prolonged, and hence the time taken for pressure equalization between HPC and RPV. The liquid level in the HPC from the open and blind calculation along with and experimental observation is shown in Figure 4-15.

Figure 4-16 shows the temperature profile in the HPC. For convenience, only open calculation predictions in the CPV is compared with experiment since the prediction of HPC temperature is similar for open and blind cases. It is observed that the upper nodes (50506 – 50509) are at a higher temperature and the lower nodes are relatively at a lower temperature establishing thermal stratification in HPC. The numerical predications show an underestimate of temperature in the lower HPC region and an over estimate in the upper region. This can be explained with the context of temperature measurement (thermocouple mountings) in the actual and numerical scenario. In case of the numerical model the temperature is measured in the cell center (i.e. in the volume center on the HPC), but in the test facility the thermocouple is placed close by the HPC wall that is in contact with CPV. In the upper HPC region, when steam is discharged from the PCS valve into the containment, it passes through the central volume bearing a higher temperature and later condenses at the wall closer to CPV which is at a lower temperature. In the lower HPC region, where the heat transfer is from the hotter wall to the water, the temperature is expected to be higher near the wall (experimental measurement) than the central volume (numerical model prediction). The sudden increase in lower HPC temperature observed in the experiment is due to the axial conduction of the HPC walls, which is not modeled in the RELAP5 model.

The drop in void fraction in certain nodes of the HPC indicate the condensation of the steam coming from PRV when the ADS valve is under operation, and later increases when the HPC level drops due to the opening of ADS 108 valves (Fig 4-17).

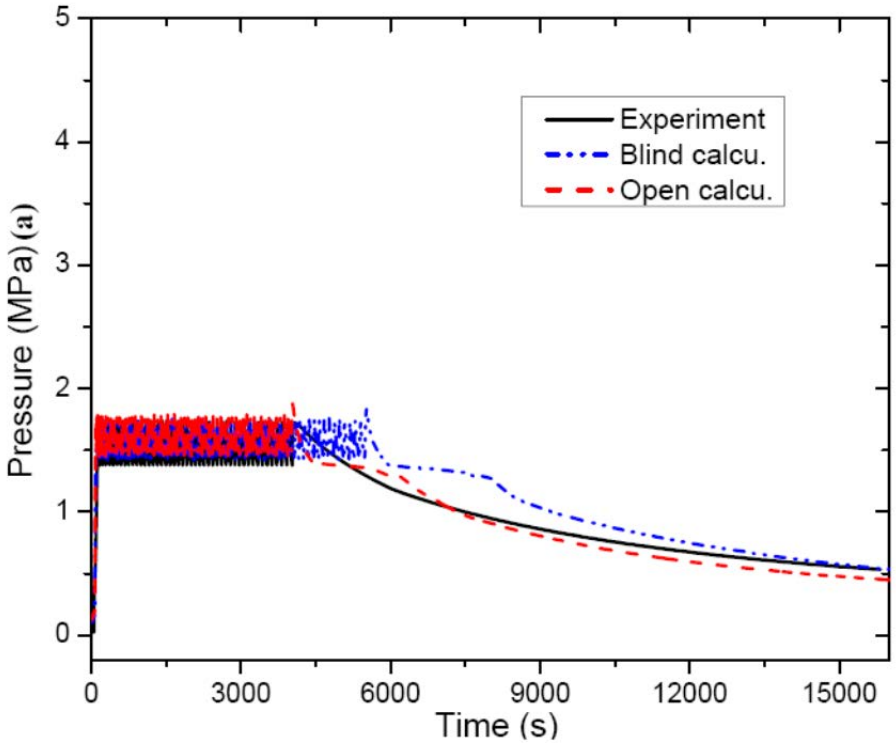

FIG. 4-14. HPC pressure.

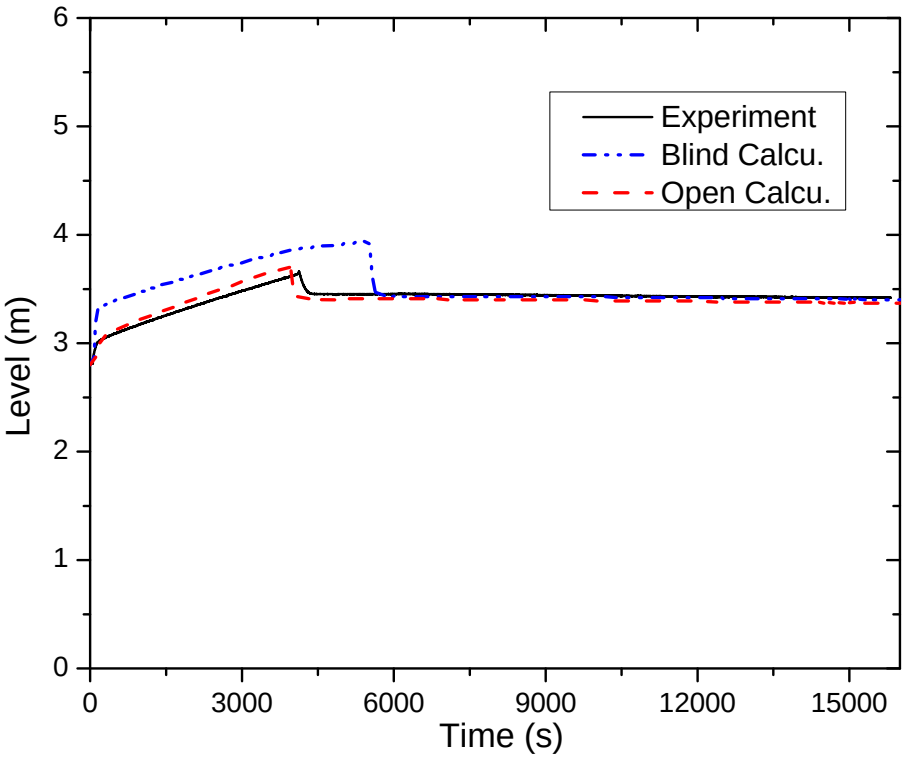

FIG. 4-15. HPC level.

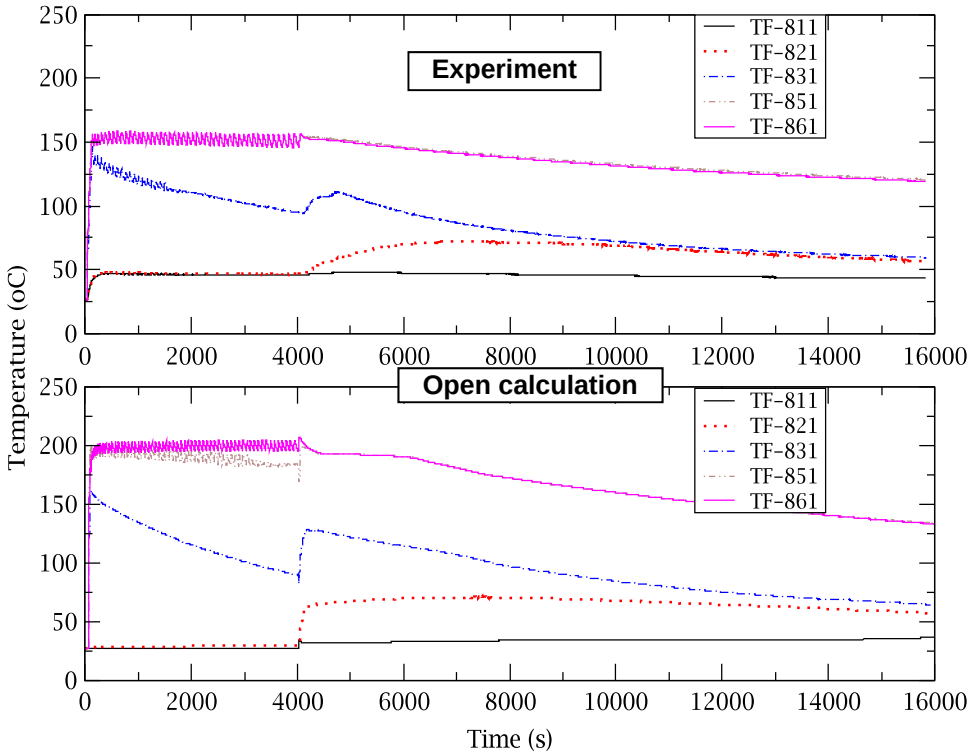

FIG. 4-16. Temperature at different heights of HPC.

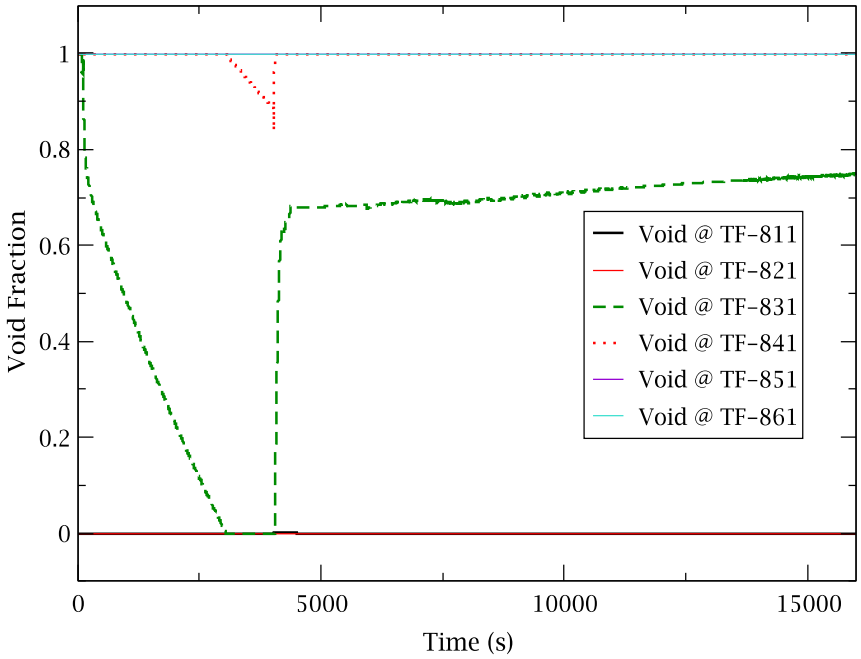

FIG. 4-17. Void fraction at different heights of HPC (open calculation).

4.1.3.4. CPV thermal-hydraulic behavior

In open calculation, the temperature in the cooling pool as shown in Figure 4-18 is found to increase upto a maximum of 65°C (upper CPV) in comparison to 70°C observed in the experiment. For convenience, only open calculation predictions in the CPV is compared with experiment since the prediction of CPV parameters are similar for open and blind cases. In the numerical prediction, the raise in CPV temperature is found to be gradual showing thermal stratification along the axial length. However in the experiment, the temperature even in the lower CPV region which is expected to have a very low thermal gradient is found to increase sharply during the start of the transients. This difference is again owing to the placement on the thermocouple closer to the CPV wall where the wall gets heated-up (axial conduction) due to the steam condensation in the upper part.

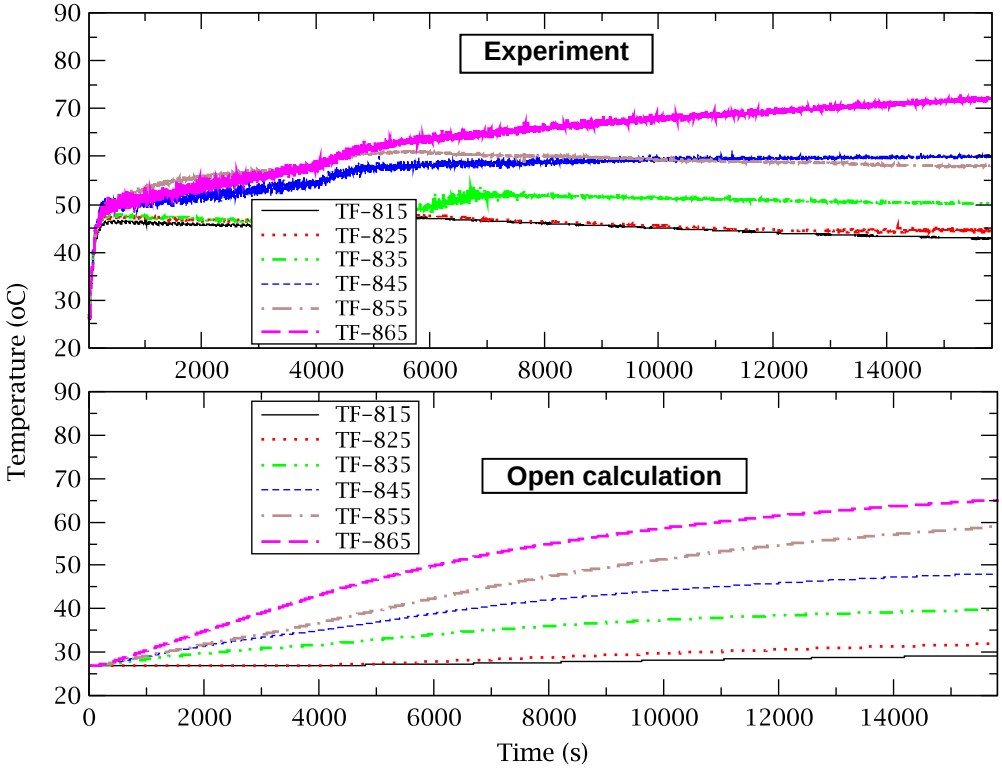

FIG. 4-18. CPV temperature.

4.1.4. Analysis results for power maneuvering

4.1.4.1. RPV thermal-hydraulic phenomena

The primary flow rate predicted by open and blind calculation along with the experimental observation is shown in Figure 4-19. Steady state power simulation is done with 10% (40 kW) of full power (400 kW), and the observation are used as initial condition for the transient simulation. Further, transient simulation is done by increasing the core power by 10% in steps. During the transients, additional water charging into the primary is also simulated in the open calculation. The primary mass flow is found to be rising from 0.8 kg/s at 10% power to 1.7 kg/s at 80% of full power.

The core inlet temperature is plotted in Figure 4-20. It is observed that a steady state condition is not established at each step increase in power. The deviation is blind calculation results as the external water charging was not modeled in the blind calculation phase. Throughout the transients, the core inlet subcooling is seen to be always more than 20°C (Fig. 4-22) as required by the procedure mentioned by OSU.

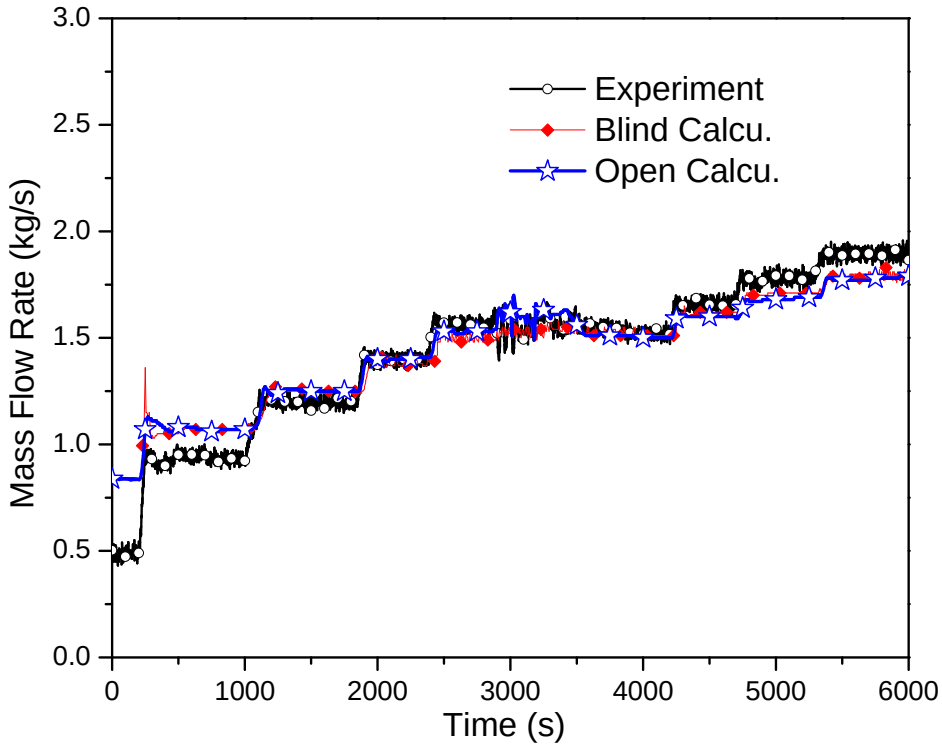

FIG. 4-19. System parameters during normal operating conditions at different power levels.

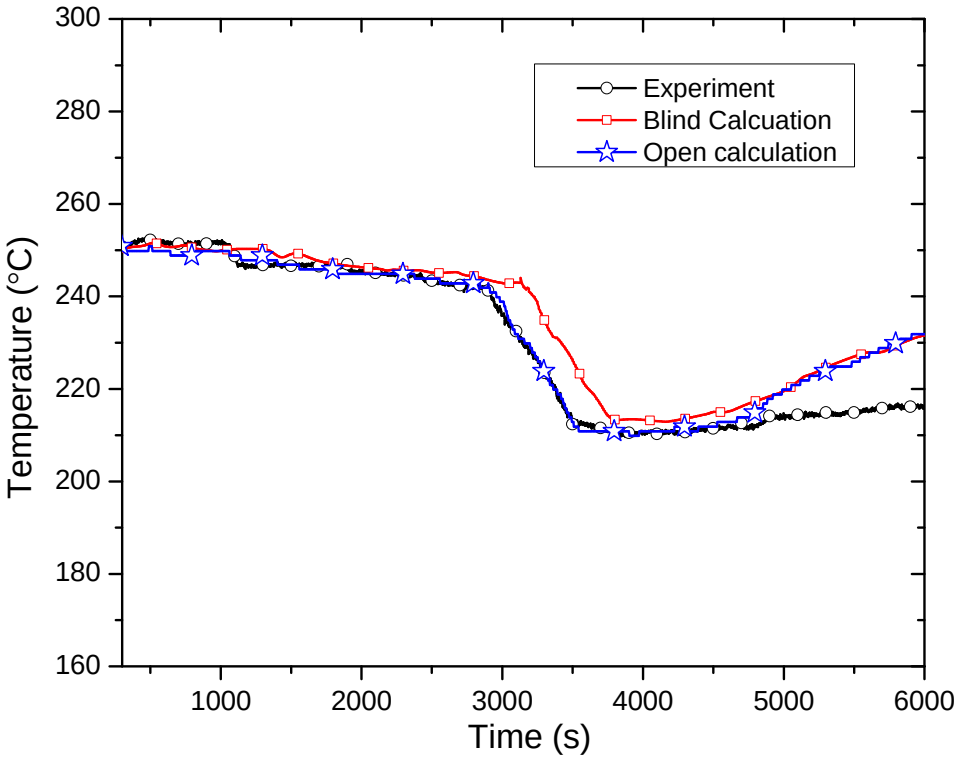

FIG. 4-20. Core inlet Temperature.

4.1.4.2. SG thermal-hydraulic phenomena

The temporal trace of the secondary flow is plotted in Figure 4-21. The steam quality at SG exit is more than unity because of the superheated condition during the initial phase and drops after the external charging of water in the primary (Fig. 4-22).

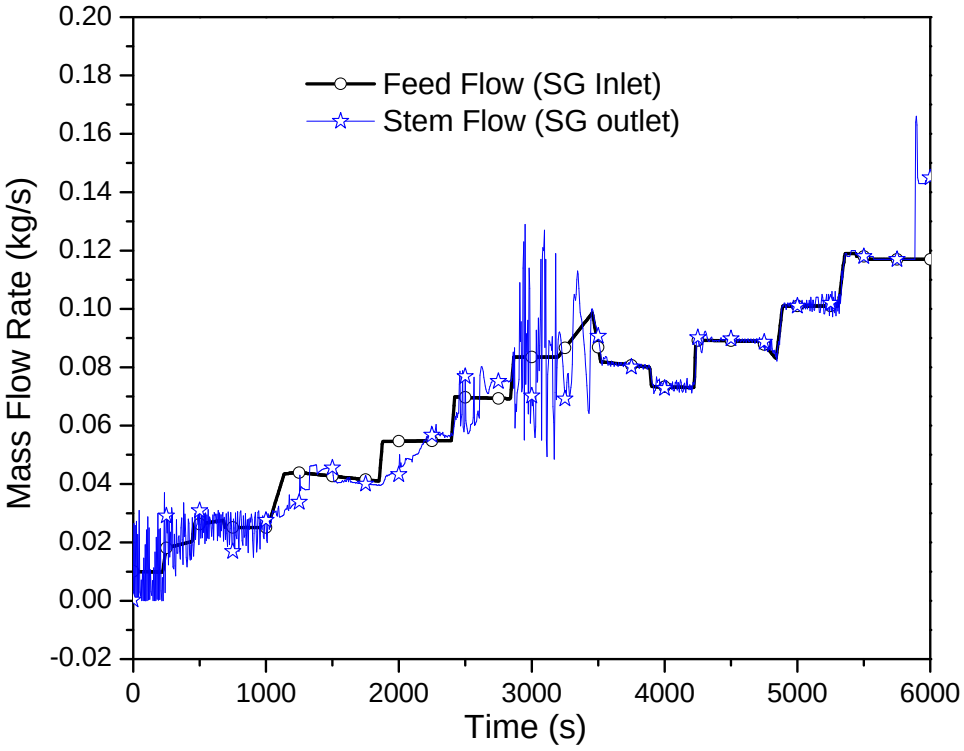

FIG. 4-21. SG feed and steam flow (open calculation).

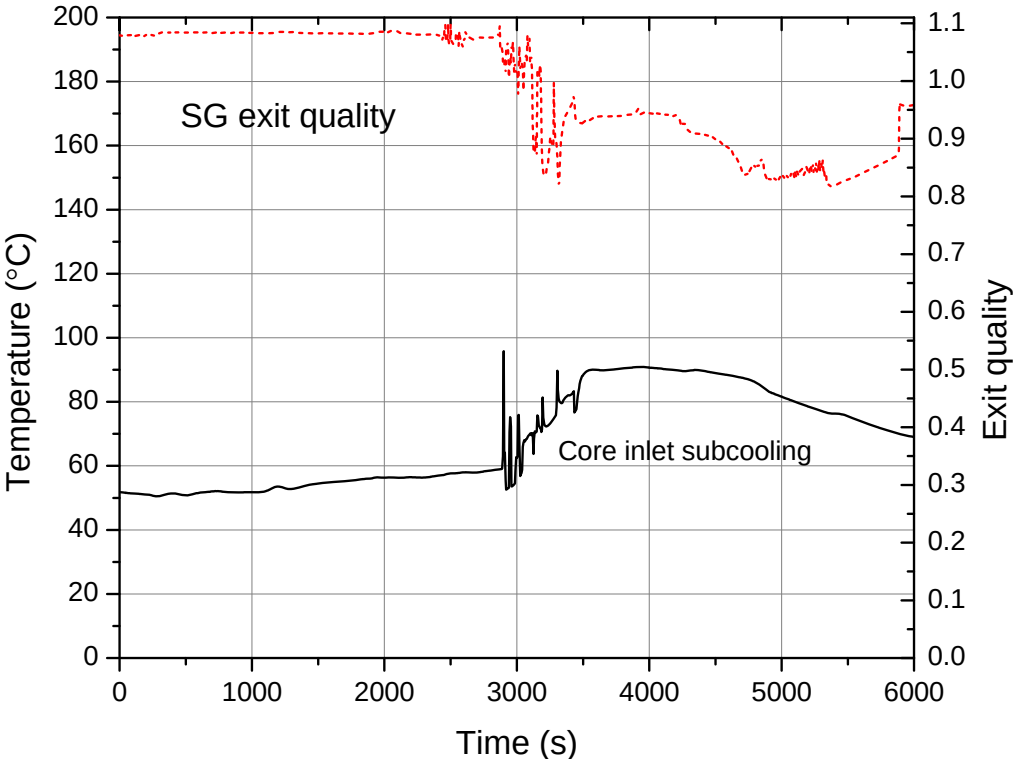

FIG. 4-22. SG exit quality and core inlet subcooling (open calculation).

4.2. BARC (RELAP5) - INDIA

4.2.1. Computer code

RELAP5/MOD3.2 code is used for simulating the natural circulation behavior in MASLWR test facility for Loss of Feed-water Transient and power maneuvering. RELAP5/MOD3.2 utilizes the one-dimensional, transient, two-fluid model for the two-phases like steam and water. The code can also deal with noncondensable components in the steam phase and/or a soluble component in the water phase. RELAP5/MOD3.2 is a thermal-hydraulic system code that solves six field equations viz two mass, two momentum and two energy conservation equations, for the two phases.

RELAP5/MOD3.2 is based on a non-homogeneous and non-equilibrium model for the two phase system that is solved by a fast, partially implicit numerical scheme to permit economical calculation of system transients. The objective of RELAP5 development was to produce a code that includes important first-order effects necessary for accurate prediction of system transients but that was sufficiently simple and cost effective so that parametric or sensitivity studies are possible. The code includes many generic component models using which any thermal hydraulic system can be simulated. The component models include pumps, valves, pipes, heat releasing or absorbing structures, reactor point kinetics, electric heaters, jet pumps, turbines, separators, accumulators, and control system components. In addition, special process models are included for effects such as form loss, flow at an abrupt area change, branching, choked flow, boron tracking, and noncondensable gas transport.

4.2.2. System idealization

4.2.2.1. System idealization for blind calculation

Figure 4-23 shows the system nodalisation for the MASLWR test facility. The whole facility is divided into five hydraulic components, RPV hot leg (core and chimney part), RPV cold leg (downcomer part), RPV pressuriser part, HPC and CPV volumes. The various components of the facility viz. heater, riser and the downcomer sections are modeled as pipe components of the RELAP5 code.

Lower plenum is modeled as single volume, which is connected to the hot leg side of the facility. Hot leg side of the facility is modeled as pipe volume (101 and 102), which comprises of heater section (core flow plate, core region and upper core plate) and chimney. The upper plenum, baffle plate, and pressuriser are also modeled as pipe components. The pressuriser comprises of 20 volumes and pressuriser heater is associated with 5 volumes. Pressuriser heaters are kept in automatic mode so that it maintains the RPV pressure. When RPV pressure falls below 8.719 MPa(a), pressurizer heaters switches on; otherwise remains switched off. The cold leg of the facility is modeled as pipe component 108 and 109. The components 108 and 109 are divided axially in same manner as 101 and 102. Volume 108 corresponds to downcomer and is parallel to 102 while volume 109 corresponds to lower part of downcomer and is parallel to 101. This scheme is adopted for having the same length of heat structures between the two volumes while simulating the heat transfer between hot leg and cold leg of the RPV.

The three coils of SG are modeled as a single lumped coil having lumped flow area (pipe component 135 having 20 volumes). Hydraulic diameter is kept same for simulating the resistance in the coils. The heat structures are modeled for all the RPV volumes for heat loss to the ambient. The heat transfer coefficient at the boundaries is taken as 5 W/m^2-K. HPC is modeled as a pipe component having 78 volumes with 2.8 m water level while CPV is modeled with 80 volumes and 6.35 m water level. CPV pressure is maintained with the TDV (Time Dependent Volume) of air at ambient pressure and temperature, connected at the top of the CPV. The two components, HPC and CPV, are connected with a SS heat transfer plate. The plate is modeled as heat structure component associated with HPC on the left boundary and CPV on the right boundary. The noncondensable air is modeled in the space above water level in HPC and CPV.

The vent valves (PCS-106A and PCS-106B) and sump return valves (PCS-108A and PCS-108B) are modeled as motorized valve and trip valve component of RELAP5/MOD3.2 code. The motorized

valve is used for PCS-106A vent valve for opening and closing at a specified HPC pressure. The time delay is assumed to be 2 s for this valve. The same nodalisation scheme is used for both SP2 and SP3 tests.

The various special models in RELAP5/MOD3.2 are choked flow model, abrupt area change model and stratification model. Abrupt area change model is enabled at the junctions of sudden area change like conical reduction in chimney of RPV. Abrupt area change model is also applied to all the valves between the RPV and HPC. Stratification model is enabled for modeling of pressurizer. Choked flow model is used for the simulation of the vent valves PCS-106A and PCS-106B and the sump return valves PCS-108A and PCS-108B.

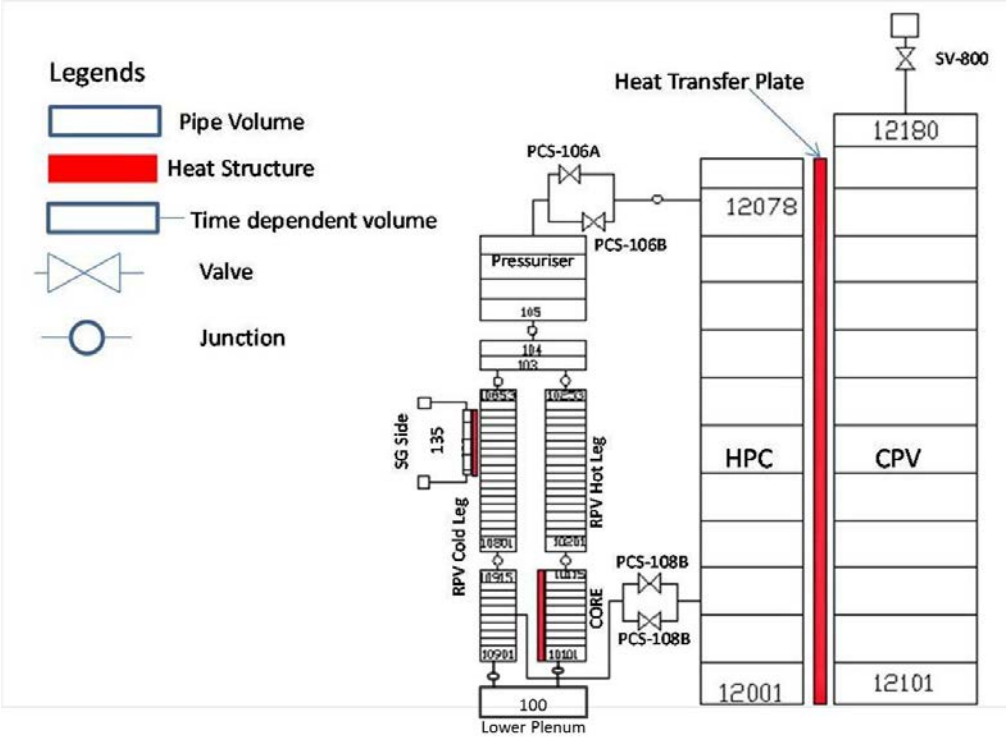

FIG. 4-23. System nodalisation for SP2 and SP3 tests

4.2.2.1. Modelling changes for open calculation

For performing open calculations changes are made in the nodalisation scheme as well as in the models used. The changes made are different for SP2 and SP3 tests.

Changes for SP2 Test: For SP2 test, major changes are made in the nodalisation scheme. For blind calculations, HPC was assumed to be adiabatic along with the lines connecting RPV to HPC; while for open calculations the heat losses of HPC and lines connecting the RPV and HPC are considered. In blind calculations, PCS-106A valve, opening and closing was simulated as per the timings specified in the boundary and initial conditions document provided by OSU [4]. Open calculations are carried out with the logic of opening and closing of the valves. However, the valve open and close timings were not matching with that of experiment. Hence PCS-106A valve timings are matched by adjusting the loss coefficient and heat transfer area between HPC and RPV. Heat transfer plate surface area is increased by 5% for open calculations for matching the transient results of open calculations with that of experiment.

Changes for SP3 Test: Open calculations are performed with changes made in the loss coefficients at various junctions. The loss coefficient and abrupt area change is removed from all the junctions except a few i.e. junction connecting lower plenum to the heater inlet, at the baffle plate and at the primary side SG coil inlet and outlet. The heat transfer area from primary to secondary had to be increased by 6 times for open calculations for simulating the temperature variation in open calculations as that of experiments.

4.2.3. Analysis results for loss of feed-water transient

The steady state calculation for open and blind cases are carried out assuming initial conditions with RPV level of 4.35 m, pressurizer level of 0.39 m, RPV pressure of 8.72 MPa(a) and Core heater power of 298 kW. The heat loss to ambient was calculated by the code and is found to be ~1.3 kW for blind calculation while it is assumed to be 2.5 kW for open calculations. The secondary side inlet mass flow rate was calculated to obtain steam superheat of 13.9°C. The secondary side mass flow rate was kept as 0.110997 kg/s. Initial temperature in RPV was considered to be 292°C. PZR heaters were considered to operate under automatic mode. It was observed that the RPV temperatures start dropping and following steady state conditions are obtained after calculating the transient for over 600 s. Table 4-1 shows the steady state values of various important parameters. Table 4-2 shows the important vent time sequence for the SP2 transient in the initial phase.

TABLE 4-1. STEADY STATE PARAMETERS FOR LOSS OF FEED-WATER TRANSIENT (SP2)

Parameter	Experimental data	Blind calculation	Open calculation
RPV Pressure (MPa(a))	8.72	8.7	8.72
Power (kW)	297.4	298	298
Heater Inlet Temperature (°C)	215	223	220
Heater Outlet Temperature (°C)	251.5	268	265
Primary Mass Flow rate (kg/s)	Not Given	1.38	1.34
Steam Outlet Temperature (°C)	205.3	208	204.8

TABLE 4-2. IMPORTANT EVENT TIME FOR LOSS OF FEED-WATER TRANSIENT (SP2)

Event	Experiment (s)	Blind Cal. (s)	Open Cal. (s)
Start of simulation – steady state (start of data collection)	Not Given	- 600	- 600
Stop MFP Close HPC vent valve SV-800	0	0	0
PZR pressure (PT-301) reaches 9.064 MPa(a) (1300 psig) Enter decay power mode	30	34	32
PZR pressure (PT-301) reaches 9.409 MPa(a) (1350 psig) De-energize PZR heaters Open ADS vent valve (PCS-106A)	48	51	50
Start long-term cooling when pressure difference between primary system and HPC (PT-301 minus PT-801) becomes less than 5 psi (0.034 MPa): Open and remain open of PCS-106A and PCS-106B Open and remain open of PCS-108A and PCS-108B	4114 - 4117	4114 4117	3980 4110
End of test when one of the following conditions is reached: - PZR pressure ≤ 0.135 MPa(a) - Primary coolant temperature (TF-132) ≤ 35 °C - 24 hours have elapsed	15822	18000	18000

4.2.3.1. RPV thermal-hydraulic behaviour

Figure 4-24 to 4-31 show the various RPV parameters for the SP2 test. Figure 4-24 shows the RPV pressure during the transient. RPV pressure starts rising soon after the Main Feed Pump (MFP) is tripped. The RPV pressure rises to 9.064 MPa(a) in 32 s for open calculations while it reached 9.064

MPa(a) in 34 s for blind calculations. The reason for delay in pressure rise of RPV may be attributed to the increased heat loss. Further the delay of 18 s is considered for switching the power into the decay power mode. In this way the decay power mode starts at 50 s for open calculations. At the time t = 50 s the valve PCS-106A also opens and RPV depressurizes into the HPC. As soon as the PCS-106A opens, RPV pressure starts falling. The valve PCS-106A closes on its set point and RPV pressure increases due to boxing up of RPV. The valve PCS-106A opens and closes depending upon its setting based on HPC pressure. Blind calculation results are matching with the experiment since blind calculations are performed with the valve opening and closing time same as that of experiment whereas open calculations are performed with the logic of opening and closing of valve PCS-106A. It is observed from the results that RPV pressure decreases to 1.865 MPa(a) within 4000 s during experiment and blind calculations both. RPV pressure decreases to 1.865 MPa(a) at a time t = 3980 s for open calculations. There is a gap of 20 s between experiment and open calculations, for establishing equal pressures in the two vessels i.e. RPV and HPC. Subsequently, the RPV pressure decreases more rapidly for open calculations than that of experiment performed. It is due to the more heat transfer area (5% more) taken in the open calculation. If the heat transfer area is kept as taken in blind calculations, the HPC and RPV pressures do not fall up to 0.5 MPa(a) within 16,000 s as observed in experiment.

Figure 4-25 shows the flow rate variation of RPV, the steady state flow rate (1.35 kg/s) increases suddenly as the ADS valves open. The bi-directional oscillations are observed during the initial part of transient upto 4000 s. Experimental data is not available for primary mass flow. Sump recirculation valves open at 3980 s for open calculations and at 4000 s for experiment and blind calculations both. The sump recirculation valves PCS-108A and PCS-108B open, when the pressure difference between the RPV and HPC remains 0.137 MPa(a). During the time period 4000 – 6000 s the RPV flow again increases due to opening of sump recirculation valves. The relatively cold water entering RPV through sump recirculation valves leads to drop in the heater inlet temperature as seen in Figure 4-26. An oscillatory natural circulation flow is observed in open calculation. The dip is also observed in heater outlet temperatures (Fig. 4-27), which is due to the flow of low temperature water from HPC to RPV on the opening of sump recirculation valves. This dip is observed in the experiment only in heater inlet temperature, while there is no dip in the heater outlet temperature for experiment. Besides this dip, experiment and open calculation results are found to be in good agreement.

Figure 4-28 shows the fluid temperature inside the pressurizer which is slightly high in open calculation and qualitative trend matches for open calculation and experiment. Figure 4-29 shows the RPV water level, which decreases initially due to flow of steam-water mixture from RPV to HPC and increases after opening of sump recirculation valves i.e. PCS-108A and PCS-108B. Figures 4-30 and 4-31 show the measured and predicted pressure drops in the heated section and the downcomer section respectively. The predicted pressure drops are found to be in good agreement with experimental values.

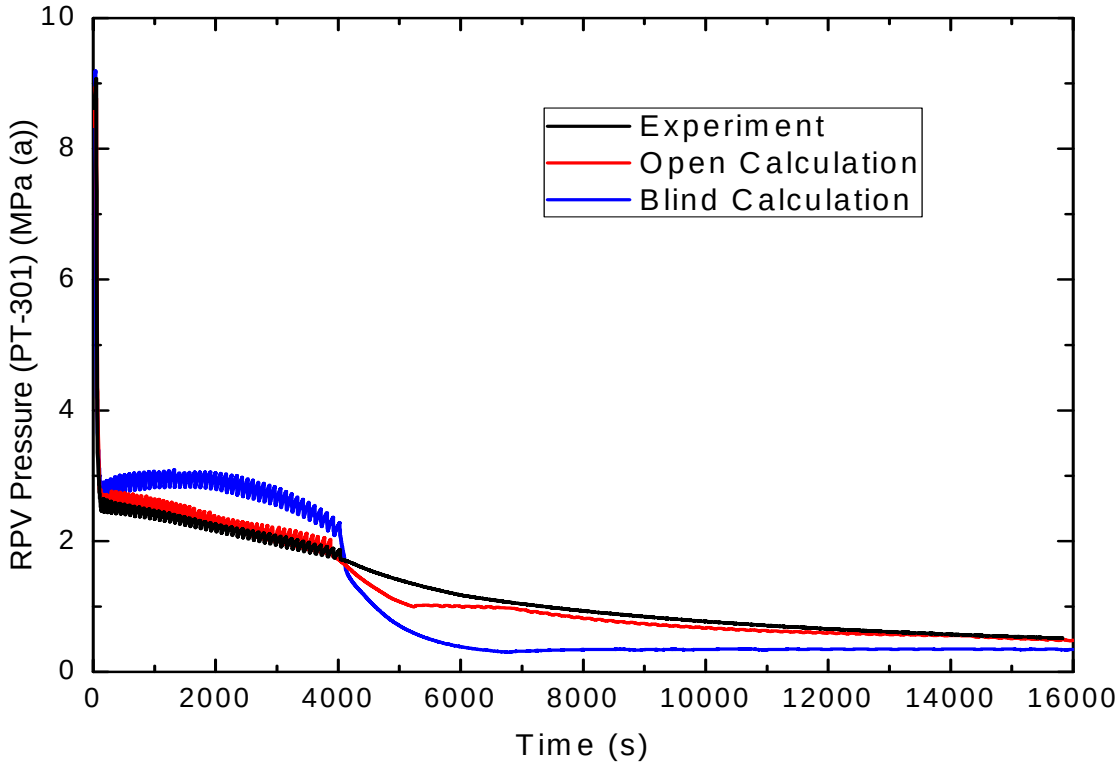

FIG. 4-24. RPV pressure.

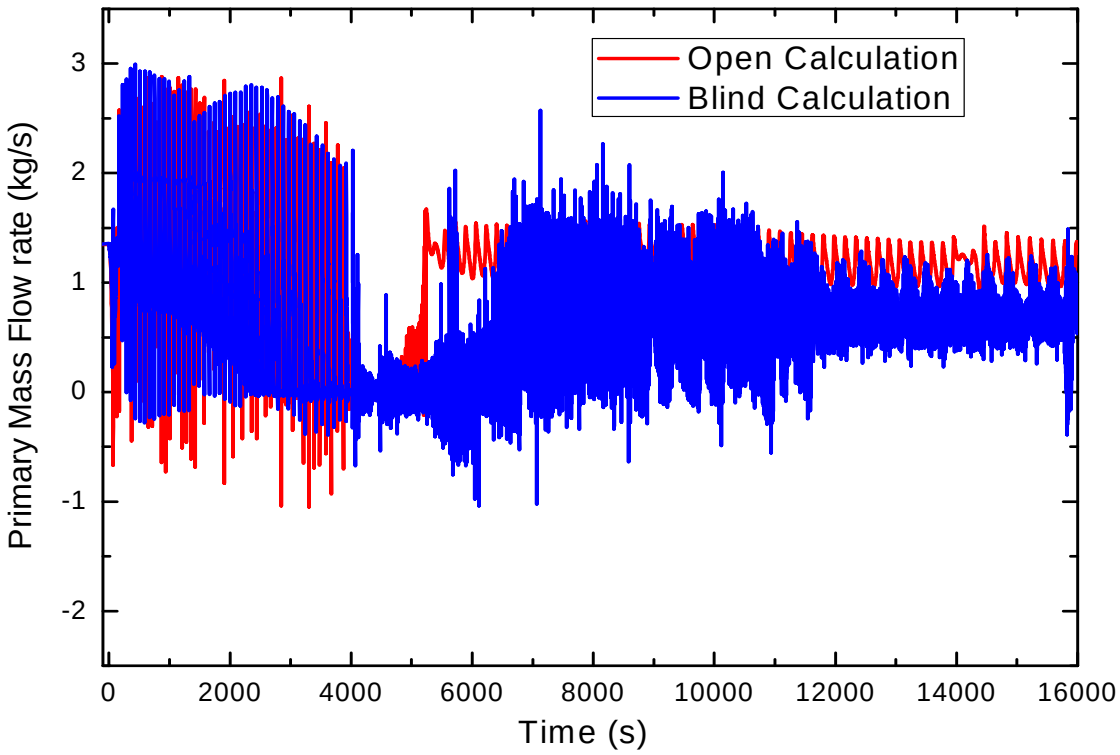

FIG. 4-25. Primary mass flow.

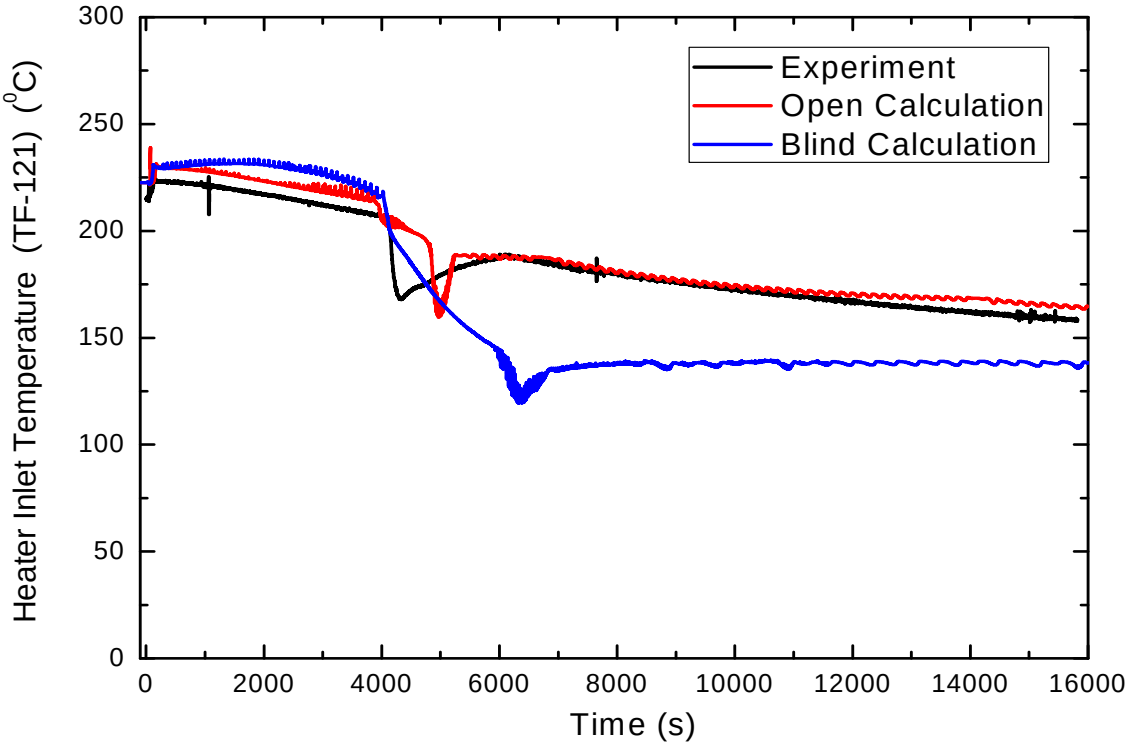

FIG. 4-26. Heater (core) inlet temperature.

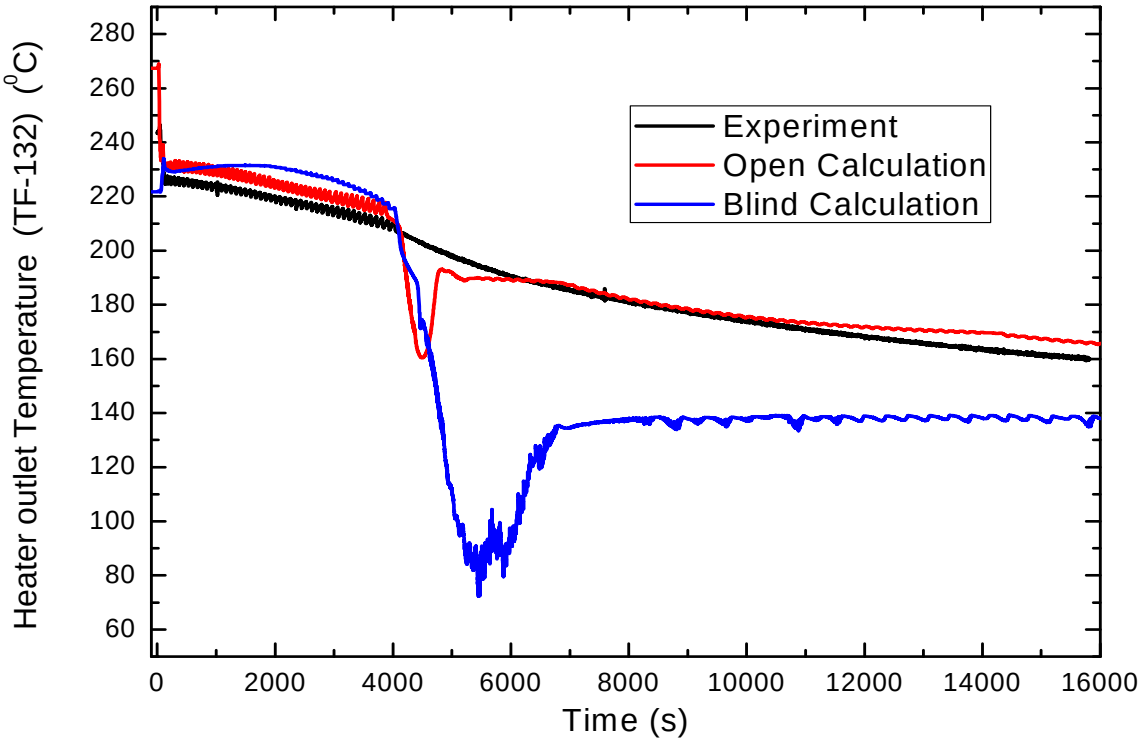

FIG. 4-27. Heater (core) outlet temperature.

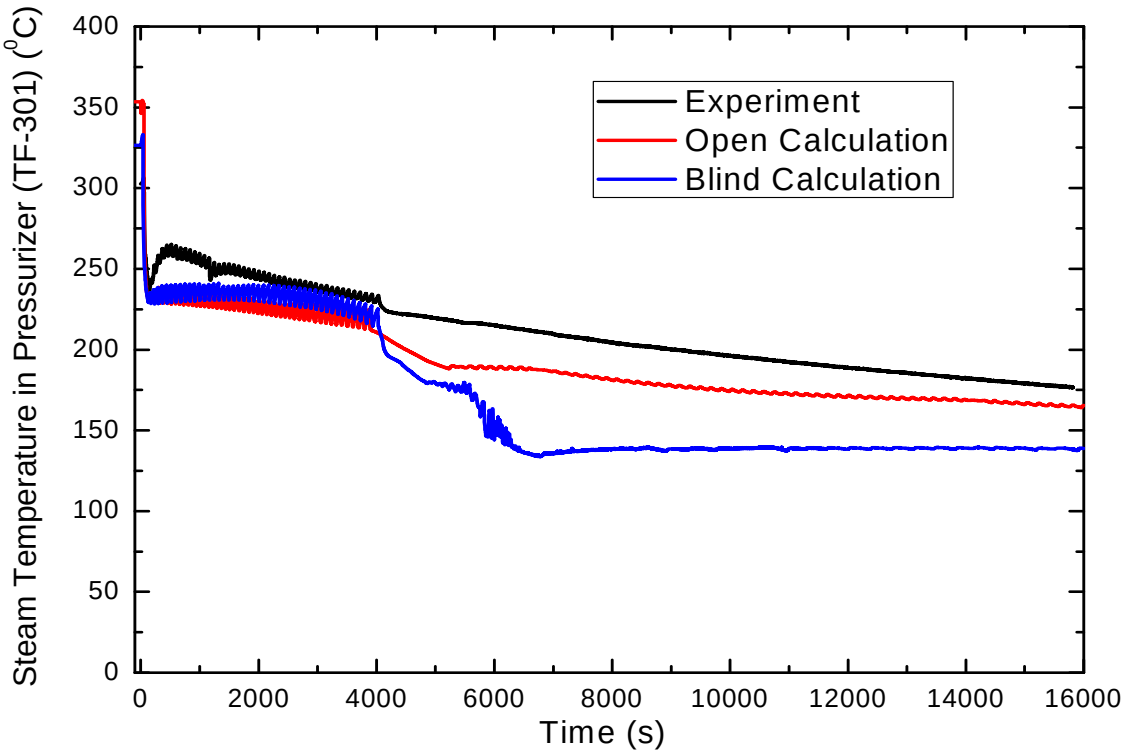

FIG. 4-28. Pressurizer fluid temperature.

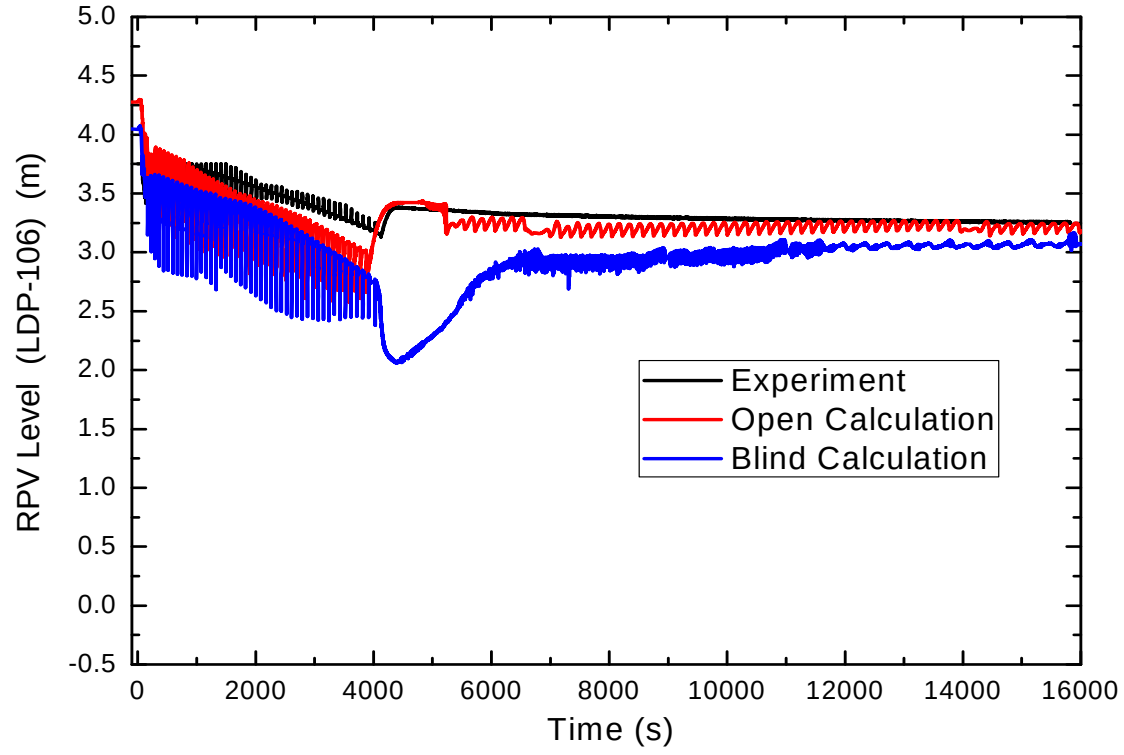

FIG. 4-29. RPV level (LDP-106).

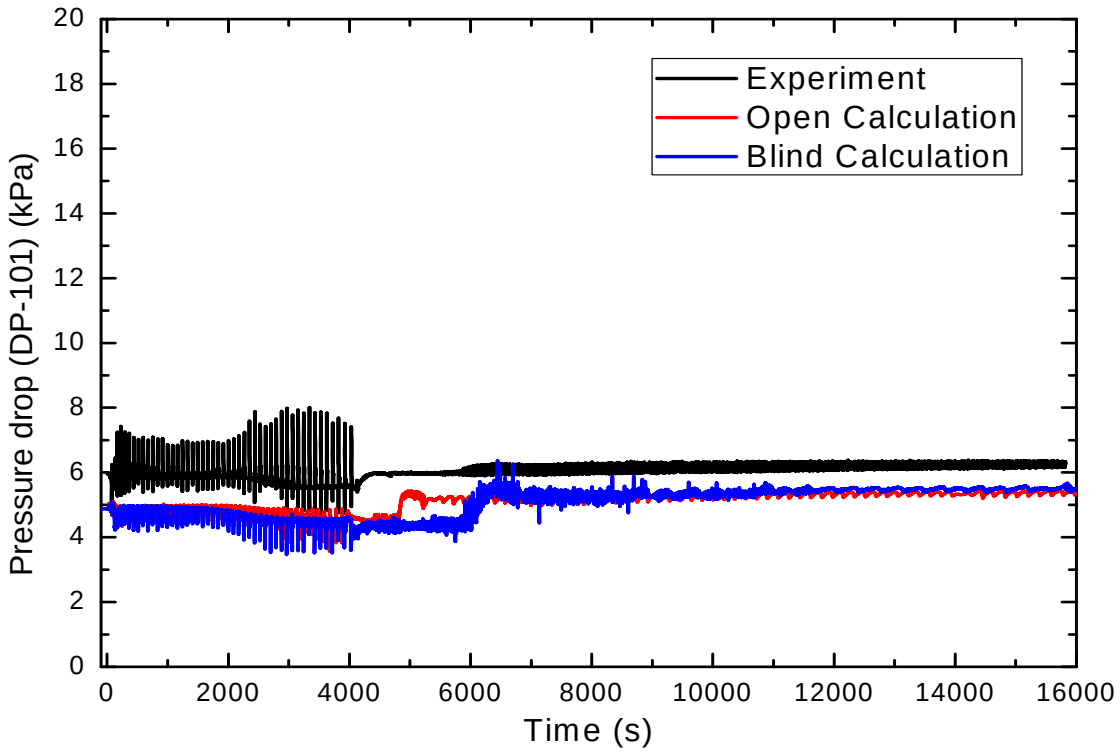

FIG. 4-30. Core pressure drop (DP-101).

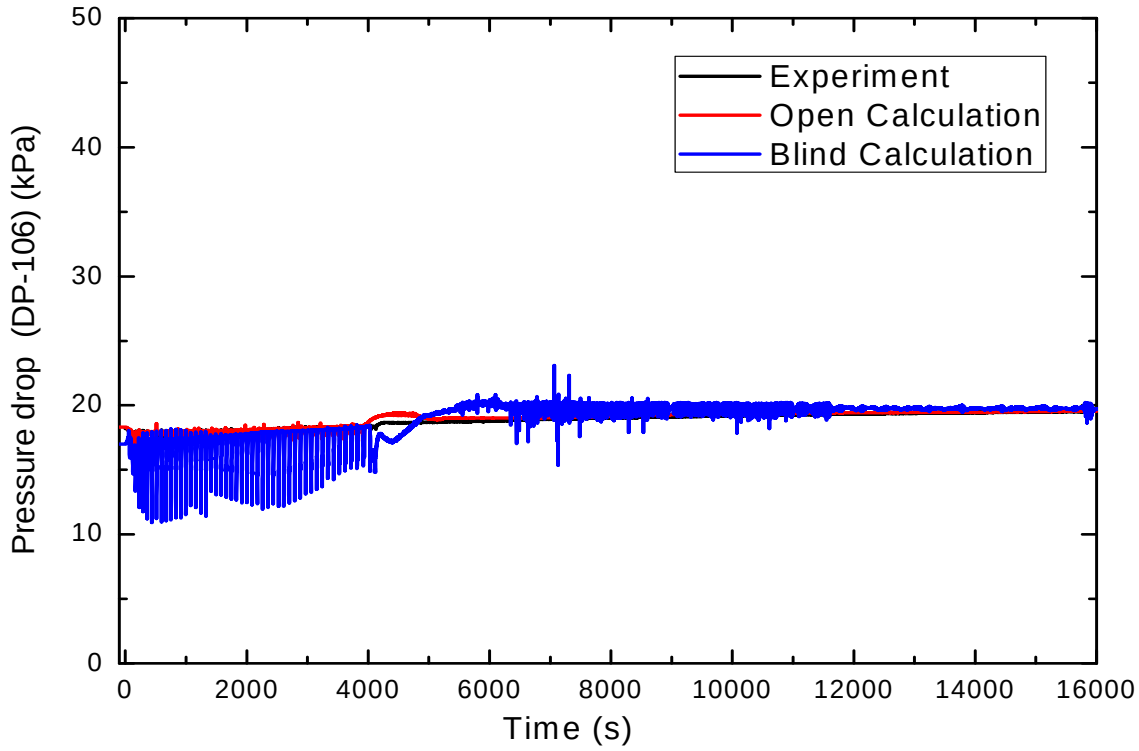

FIG. 4-31. Downcomer side pressure drop (DP-106).

4.2.3.2. SG thermal-hydraulic behaviour

The SP2 test transient starts with stopping of the main feed pump (MFP) and isolation of the secondary side SG circuit. The secondary side flow becomes zero instantly. Figure 4-32 shows the feed water flow, which is zero.

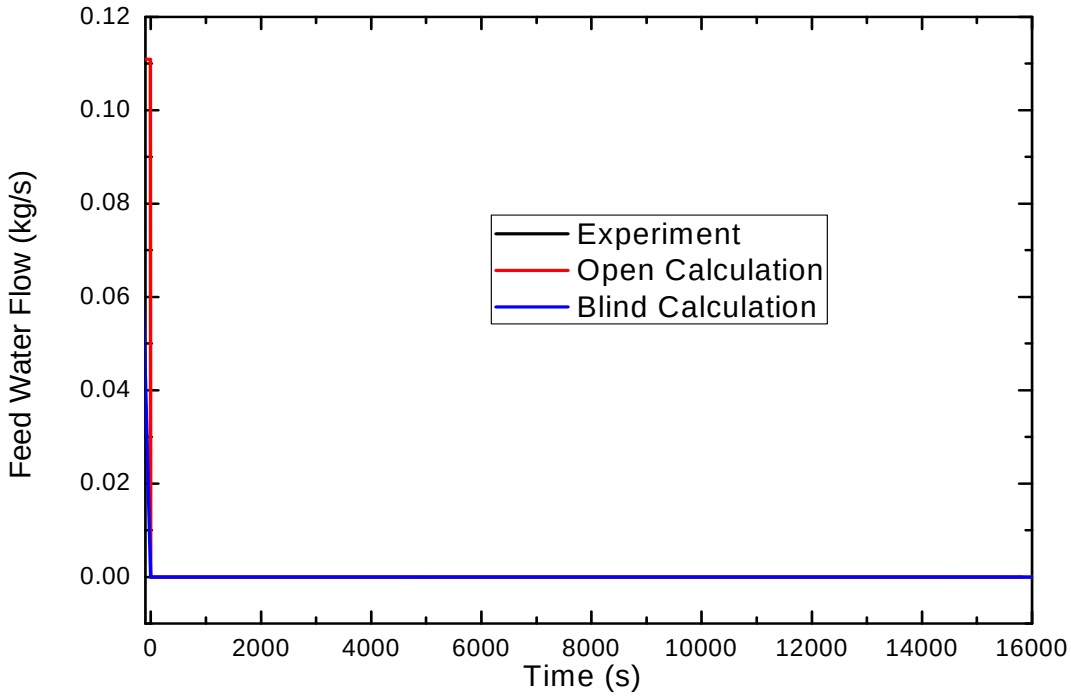

FIG. 4-32. Feed Water Flow (FMM-501.)

4.2.3.3. HPC thermal-hydraulic behaviour

Figure 4-33 shows mass flow rate of vent valve PCS-106A which opens and closes on HPC pressure signal. Initially a high flow is observed through the valve (0.325 kg/s for open calculation and 0.29 kg/s for blind calculation). Subsequently the mass flow rate is less for open calculation in comparison with blind calculation.

Figures 4-34 to 4-39 show the various important HPC parameters. HPC pressure (Fig. 4-34) fluctuates between 1.48 to 1.86 MPa(a) as the vent line PCS-106A opens and closes on these pressure settings. HPC pressure achieves a maximum of 1.9 MPa(a) at 3980 s when all the ADS vent valves and sump recirculation valves open as observed in open calculations. Figure 4-35 shows HPC level variation during the test, which depicts that HPC level increases up to 4000 s and then decreases, while reverse behavior is observed in RPV level (Fig. 4-29). The water from HPC goes into the RPV after 3980 s (open calculations) as sump recirculation valves open, leading to fall in HPC level and corresponding rise is observed in RPV level; eventually both RPV and HPC level stabilizes to an equilibrium level of ~3.4 m.

The fluid temperatures inside the HPC at different axial locations are shown in Figures 4-36 to 4-39. At 4.67 m axial location of HPC, fluid temperature fluctuates between 190 to 210°C (Fig. 4-36), due to fluctuation in the HPC pressure. In open calculations, the HPC top volume temperature is observed to be the saturation temperature corresponding to the HPC pressure, since the steam condenses at that temperature. A relatively less temperature (less than saturation temperature) is observed during the experiment in the steam space of HPC. Figure 4-37 shows the HPC fluid temperature at 4.16 m axial location. At 4.16 m location also the steam condenses so the temperature of the fluid remains at the saturation temperature. At an axial location of 3.17 m inside HPC, initially there is a steam space, so temperature is fluctuating around the saturation temperature but as the condensation progresses the temperature starts falling as shown in Figure 4-38. The temperature at 3.17 m axial location again increases after 4000 s because of the opening of the sump recirculation valves PCS-108A and PCS-

108B. As the PCS-108A and PCS-108B open, the high temperature fluid from the top of HPC moves towards the sump recirculation valves (bottom of HPC), mixes with the relatively cold water at bottom of HPC and leading to increase in fluid temperature at lower axial location at 3.17 m. Figure 4-39 shows the HPC fluid temperature at 1.57 m axial location.

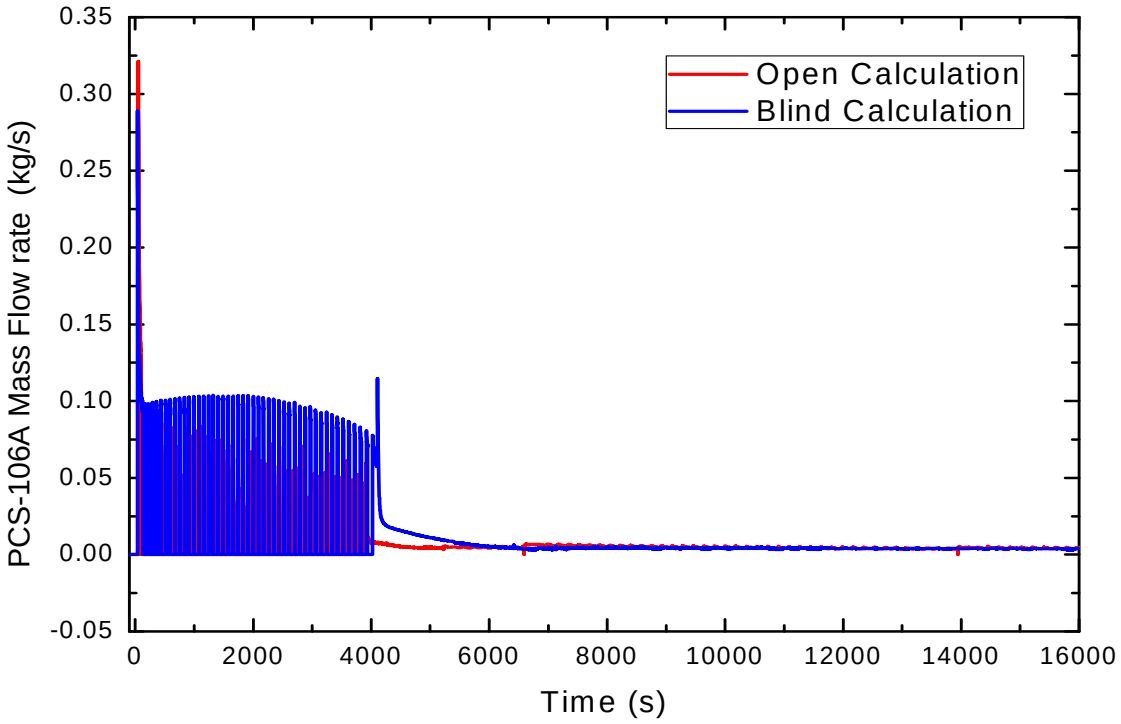

FIG. 4-33. Vent mass flow rate.

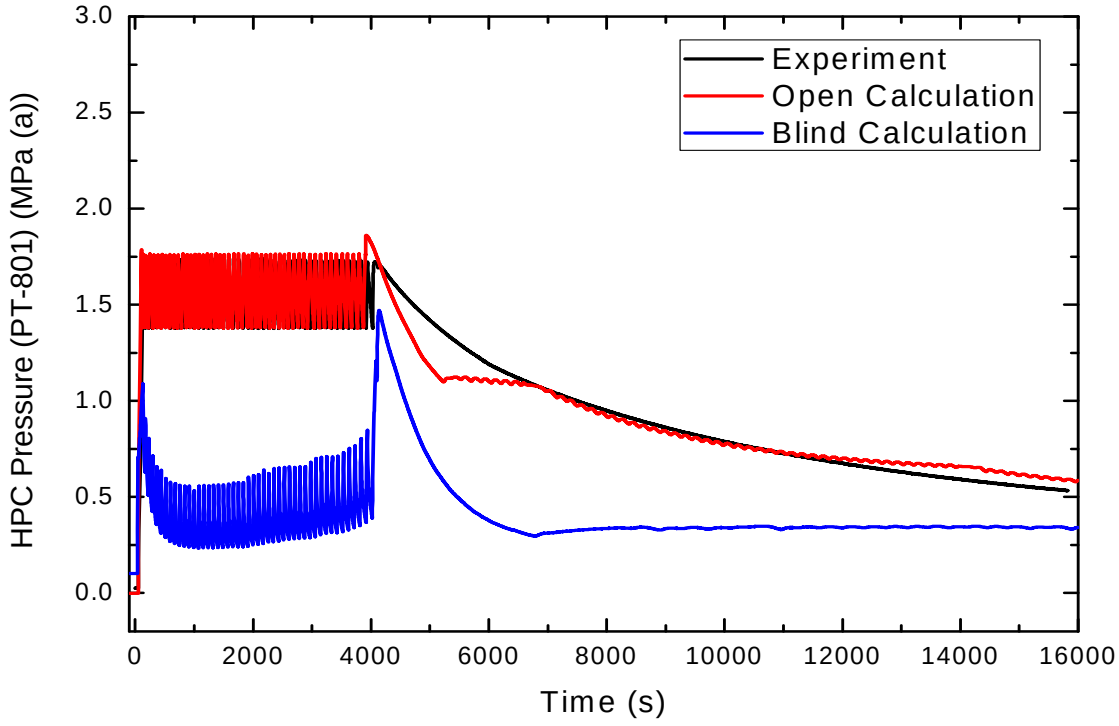

FIG. 4-34. HPC pressure.

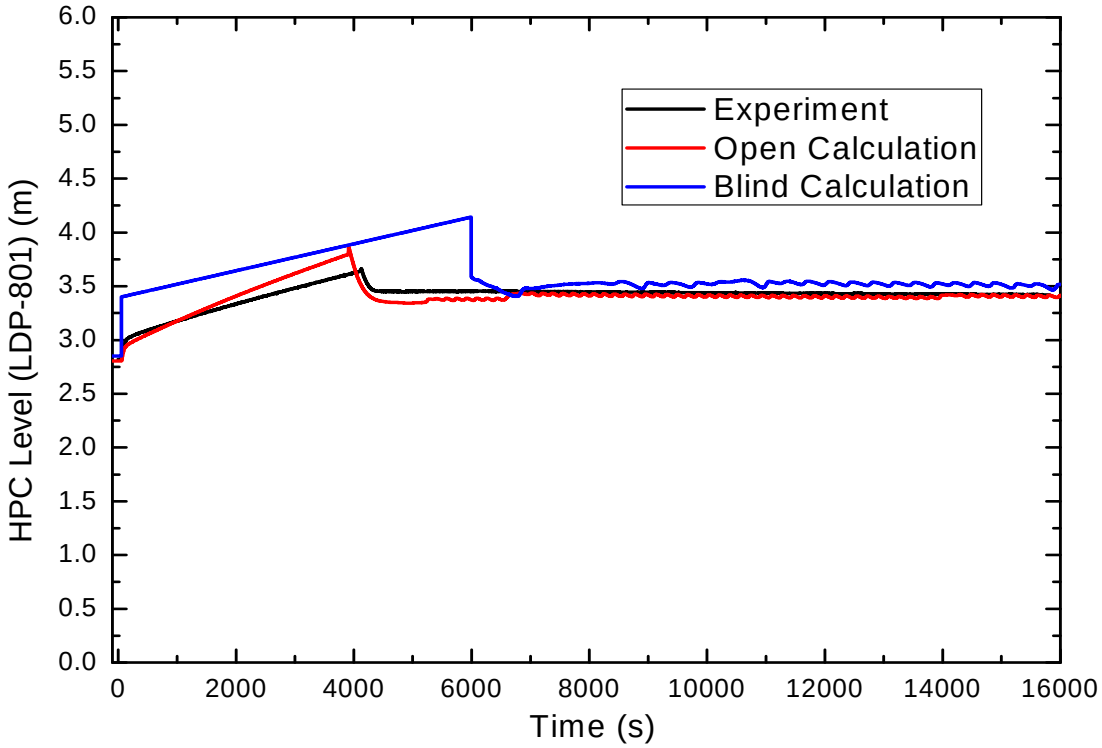

FIG. 4-35. HPC level.

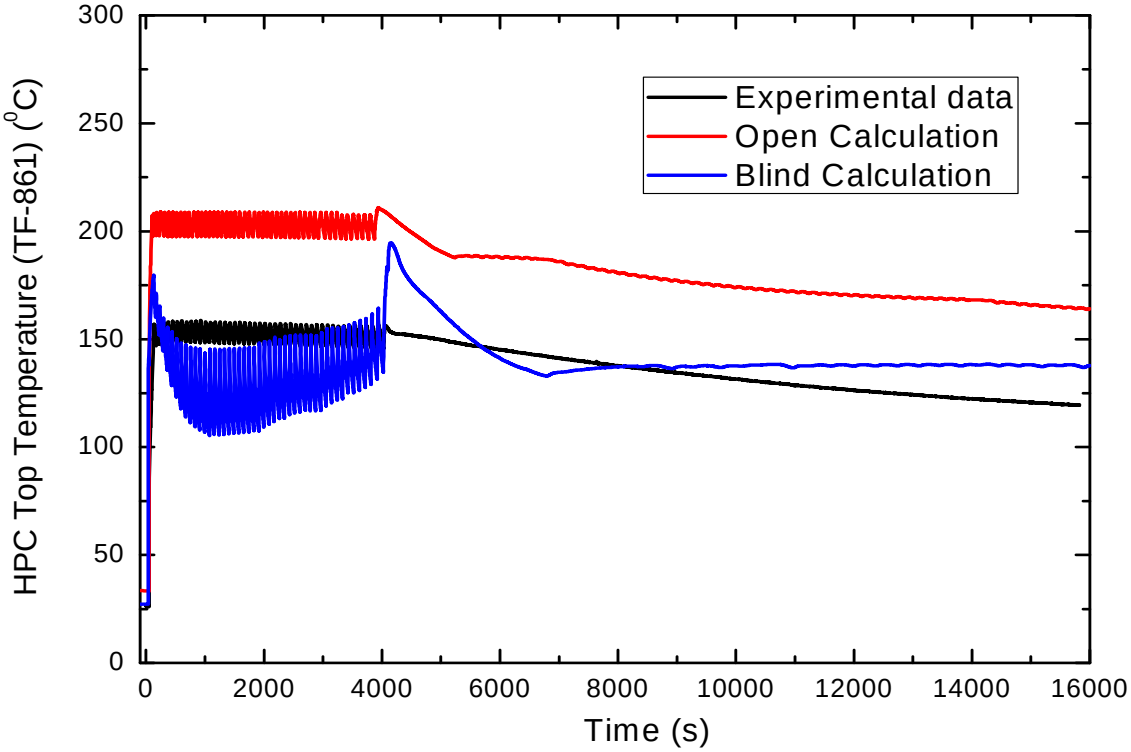

FIG. 4-36. HPC Temperature at 4.67 m axial location.

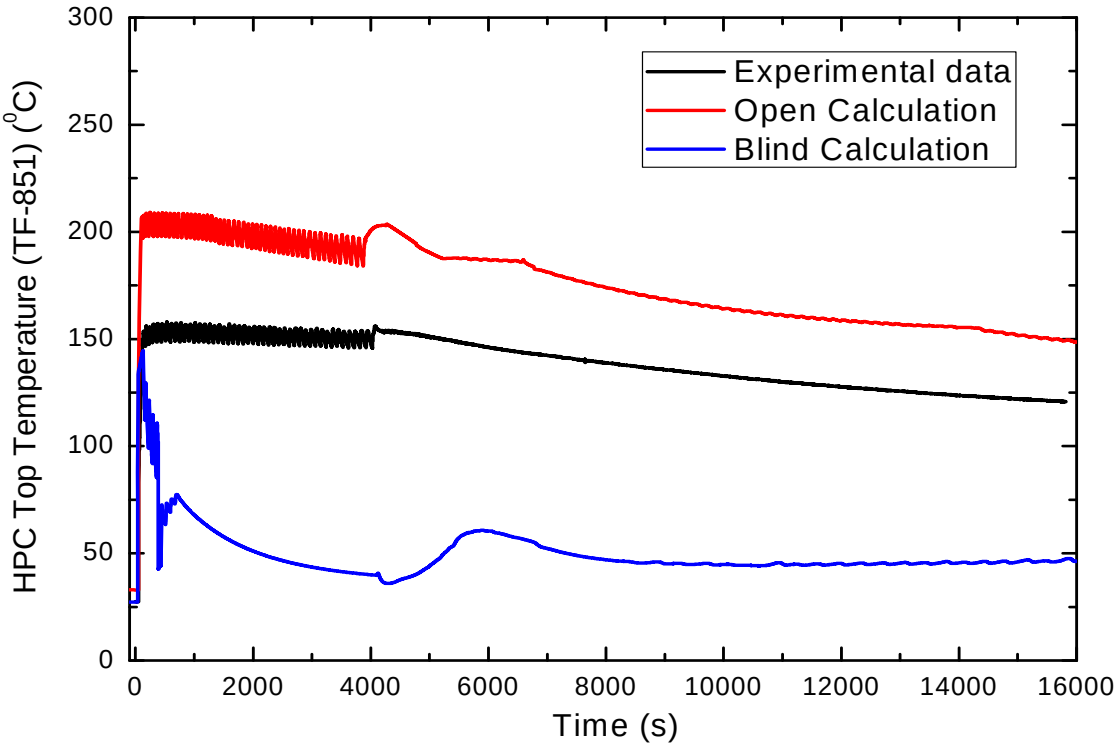

FIG. 4-37. HPC Temperature at 4.16 m axial location.

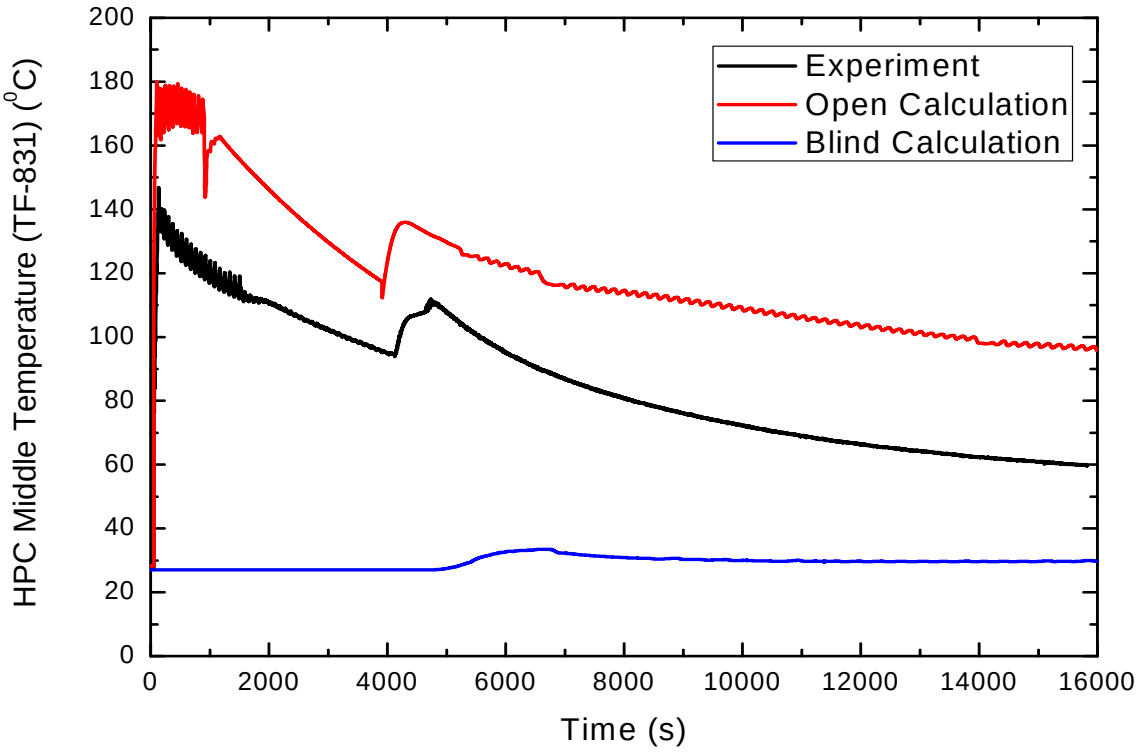

FIG. 4-38. HPC temperature at 3.17 m axial location.

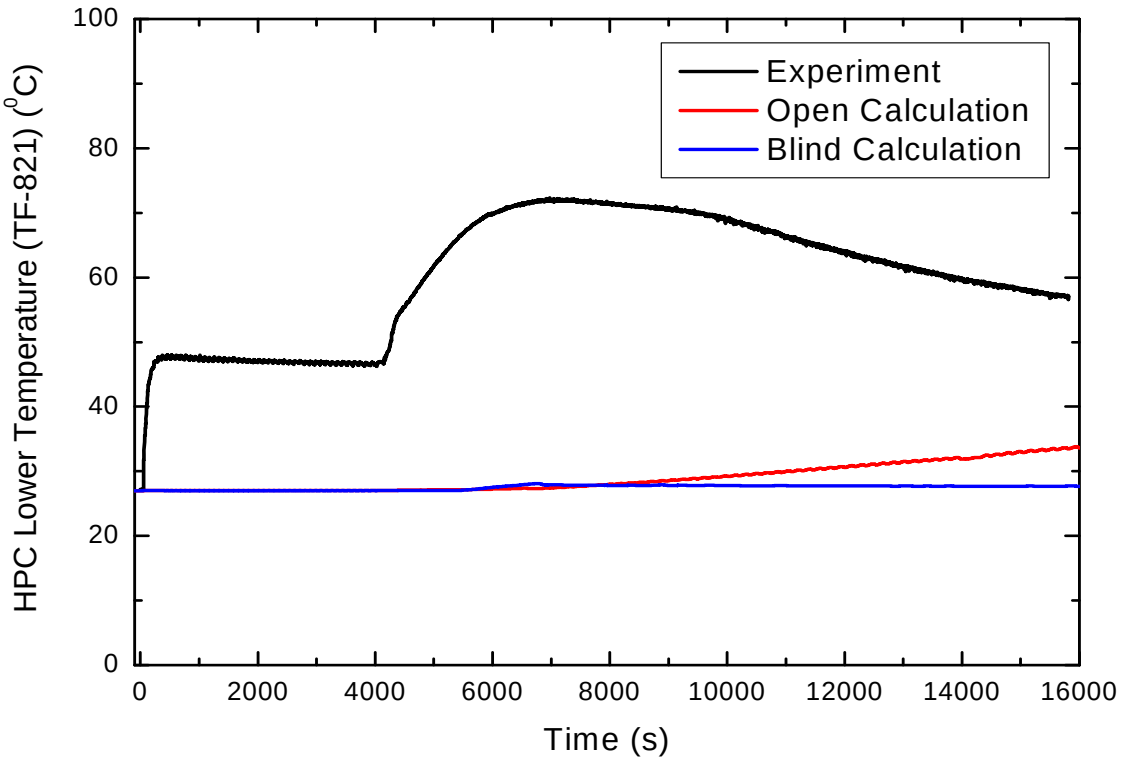

FIG. 4-39. HPC temperature at 1.57 m axial location.

4.2.3.4. CPV thermal-hydraulic behaviour

Cooling pool vessel (CPV) is maintained at ambient pressure and temperature. Time dependent volume is used to maintain the CPV pressure and temperature as ambient. Figures 4-40 to 4-43 show the variation in CPV temperatures during the SP2 test. Figure 4-40 shows the CPV fluid temperature at an axial location of 4.67 m. It is observed that the rate of rise in fluid temperature is more for experiment followed by blind and open calculations respectively. In blind calculations the CPV top level temperature reaches close to boiling temperature due to more heat transfer from HPC to RPV. Figures 4-41, 4-42 and 4-43 show the CPV fluid temperature at 4.16 m, 3.17 m and 1.57 m axial locations respectively.

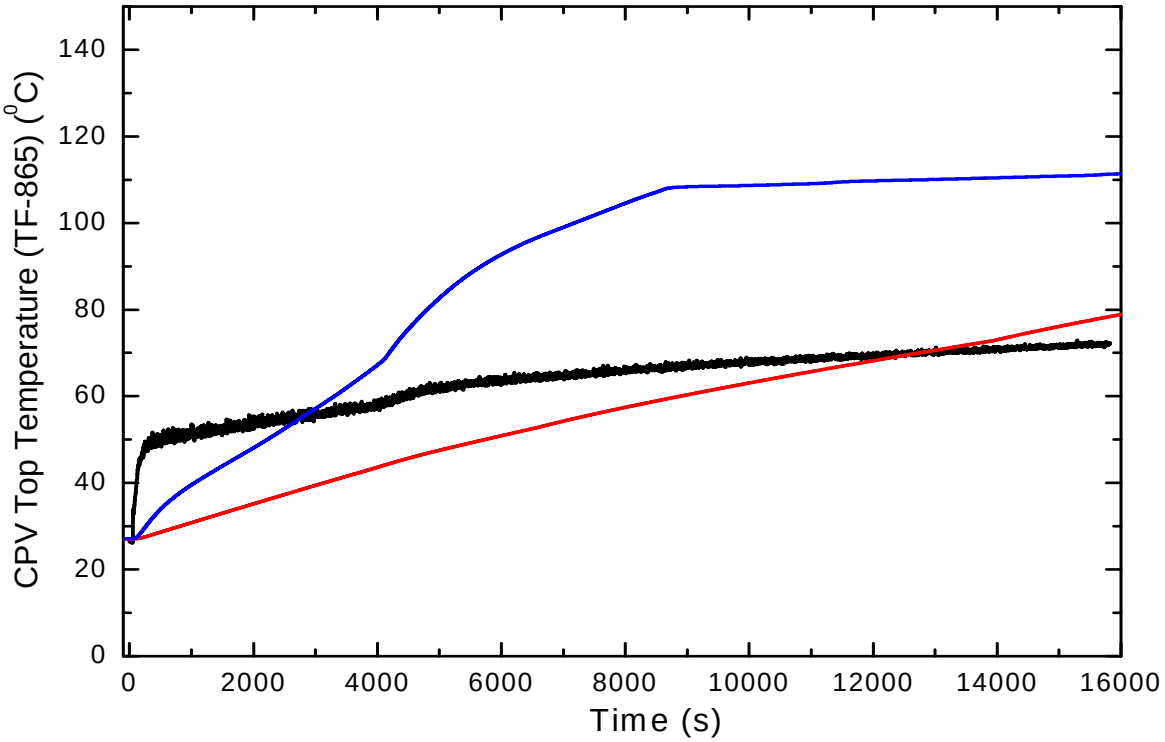

FIG. 4-40. CPV temperature at 4.67 m axial location.

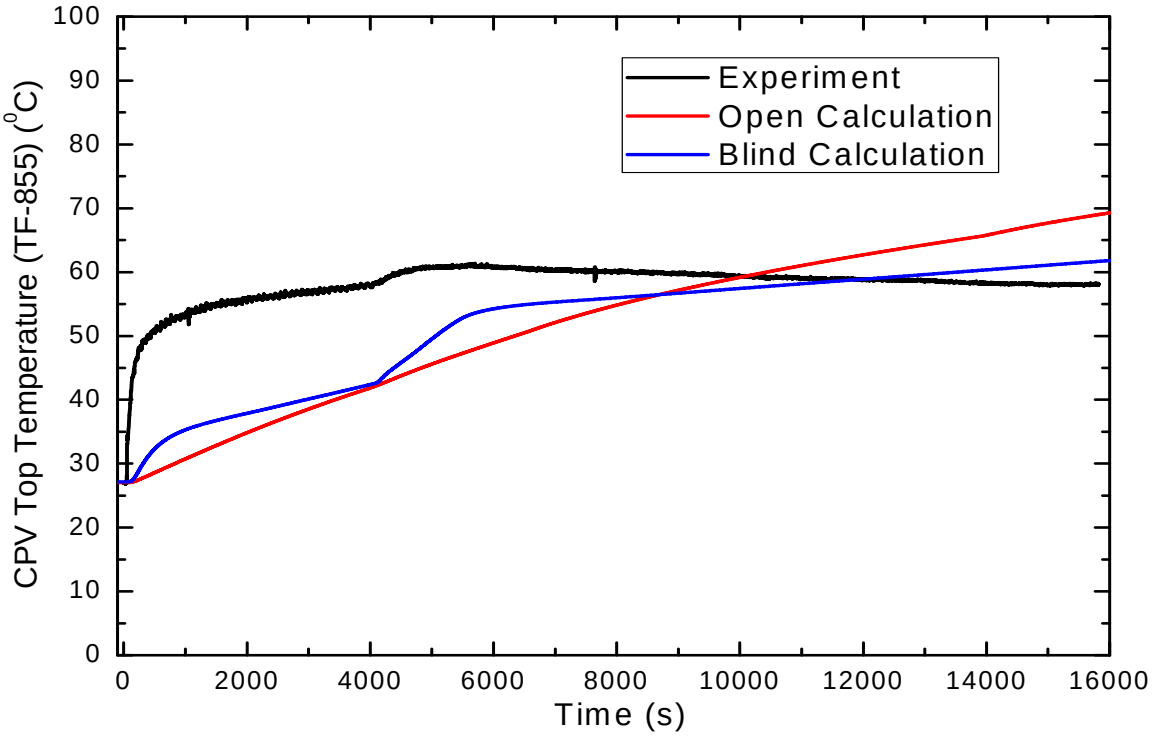

FIG. 4-41. CPV temperature at 4.16 m axial location.

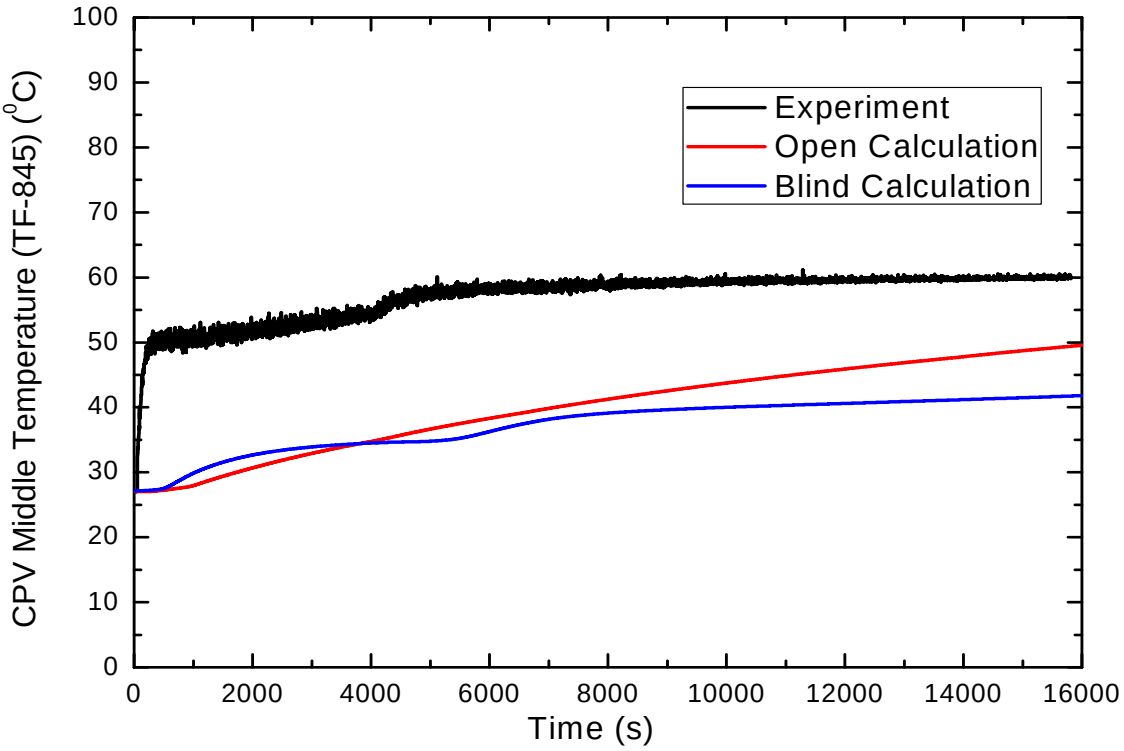

FIG. 4-42. CPV temperature at 3.17 m axial location.

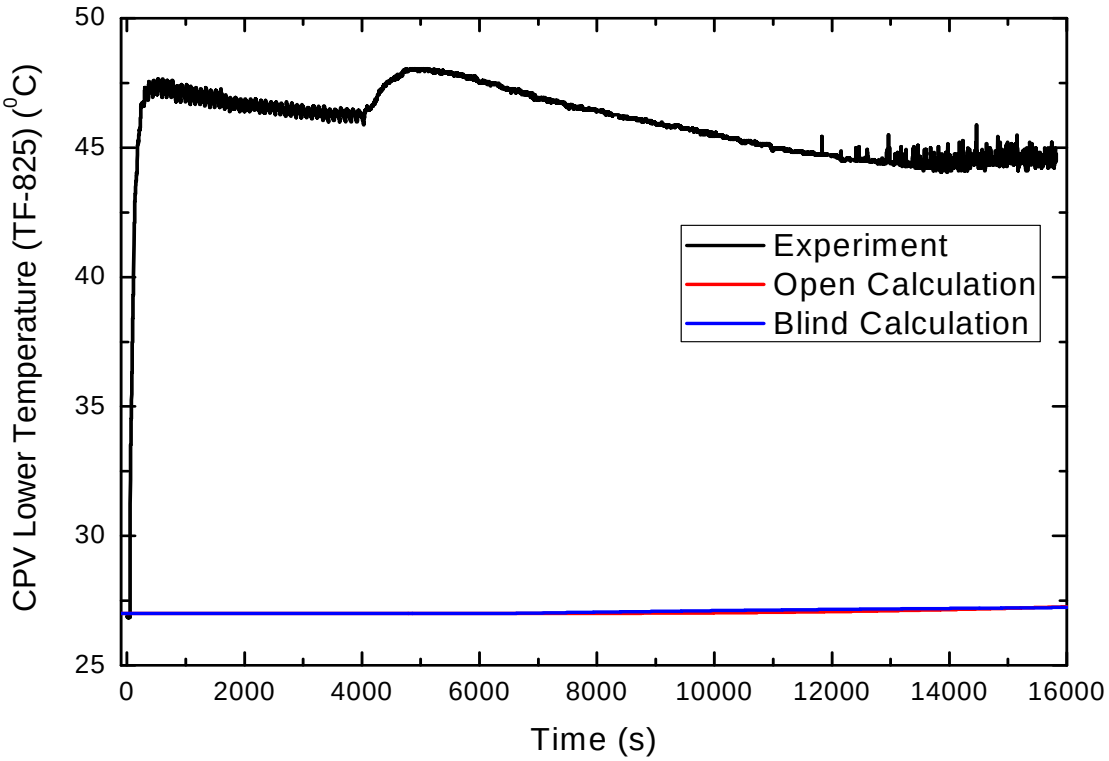

FIG. 4-43. CPV temperature at 1.57 m axial location.

4.2.4. Analysis results for power manoeuvring (SP3)

The steady state calculation was carried out assuming initial conditions of pressurizer level of 0.38 m, RPV pressure of 8.719 MPa(a) and core heater power of 40 kW. The heat loss to ambient was set to be of the order of 5 kW. The secondary side inlet mass flow rate was calculated by energy balance to obtain average steam temperature of 255.5°C (average of TF-611 to 615, TF-621 to 625 and TF-631 to 634 provided as initial steady state conditions). PZR heaters were considered to operate under automatic mode (switching on only if RPV pressure falls below 8.719 MPa(a). The steady state obtained is compared with experiment as per Table 4-3.

TABLE 4-3. STEADY STATE PARAMETERS FOR POWER MANOEUVRING (SP3 TEST)

Parameter	Experimental data	Blind calculation	Open calculation
RPV pressure (MPa(a))	8.719	8.719	8.719
Power (kW)	40	40	40
Heater inlet temperature (°C)	250.0	258.0	249.0
Heater outlet temperature (°C)	262.0	270.0	259.0
Primary mass flow rate (kg/s)	0.50	0.63	0.8
Steam outlet temperature (°C)	255.0	261.0	255.0

4.2.4.1. RPV thermal-hydraulic behaviour

Figures 4-44 to 4-51 show the variation of important RPV parameters for SP3 transient. The initial steady state flow rate (0.63 kg/s for blind calculations and 0.8 kg/s for open calculations) is observed to increase with increase in power as seen in Figure 4-44. Figure 4-45 shows the RPV pressure variation during the test. For calculations, RPV pressure increases above the nominal value of 8.719 MPa(a), due to mismatch between the heat removed in the SG and heat supplied to the core heaters while pressure does not increase for experiment. Figure 4-46 shows the pressurizer temperature variation during the transient which also follows the RPV pressure trends for both the calculations. Less flow of feed water during the very initial phase of transient (given as boundary condition for feed flow), leads to rise in the primary pressure and temperature of RPV. Figure 4-47 shows the pressurizer level variation, which remains more or less constant during the test. The RPV level is maintained by injecting the cold water from the lower plenum to ensure complete submergence of core heaters and pressurizer heaters to maintain safety of the heaters. The sequences of injection of water lead to lowering the lower plenum temperatures and hence the heater inlet and outlet temperatures, which can be seen in Figures 4-48 and 4-49. Figures 4-50 and 4-51 show the measured and predicted pressure drops across the heated section and downcomer section respectively. The predicted pressure drops are found to be in good agreement with experimental values.

4.2.4.2. SG thermal-hydraulic behaviour

Figures 4-52 to 4-54 show the variation of various SG parameters during the transient. The steam temperature at SG outlet depends directly on the feed water flow rate. Initial temperature of steam at SG coil outlet is matched with that of experiment by adjusting the feed water flow rate. The feed water flow rate is calculated by energy balance. Figure 4-52 shows the feed water temperature and Figure 4-53 shows the feed water mass flow rate, which is used as an input. Figure 4-54 shows the steam temperature at coil outlet, which is found to be in good agreement with experiment. The steam temperature falls nearly at 2800 s due to injection of cold water in RPV. The feed water boils within short length (0.4 m for saturation) of the SG coils and remaining length is used for superheating.

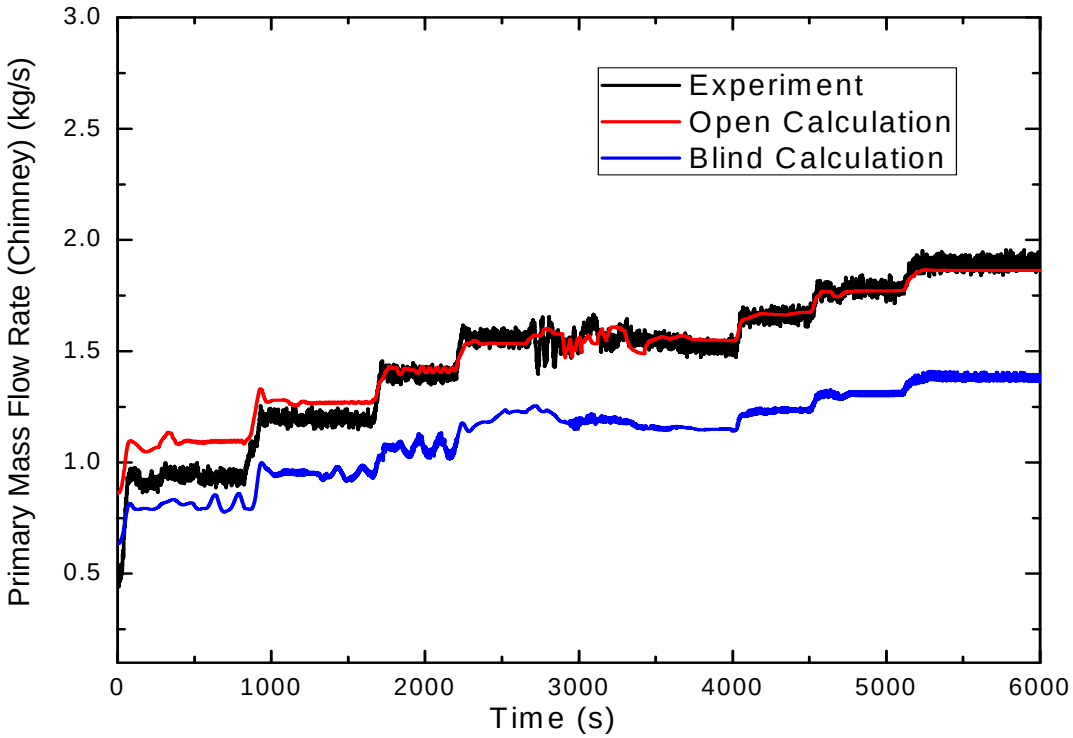

FIG. 4-44. Primary mass flow.

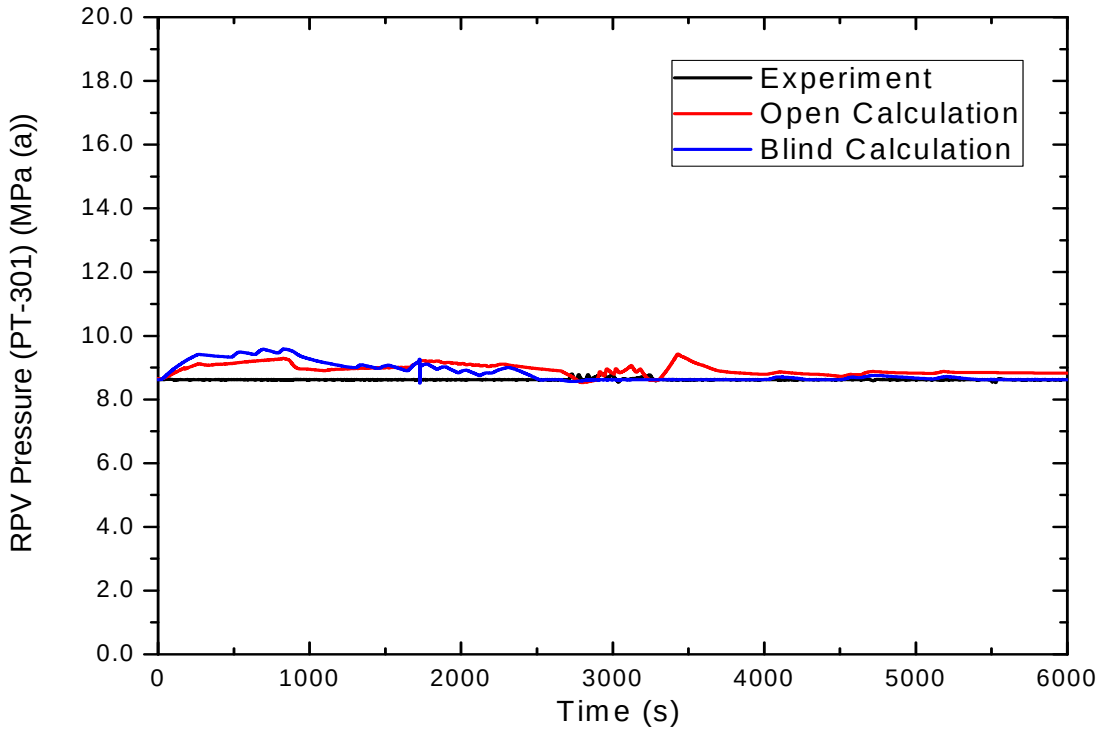

FIG. 4-45. RPV pressure.

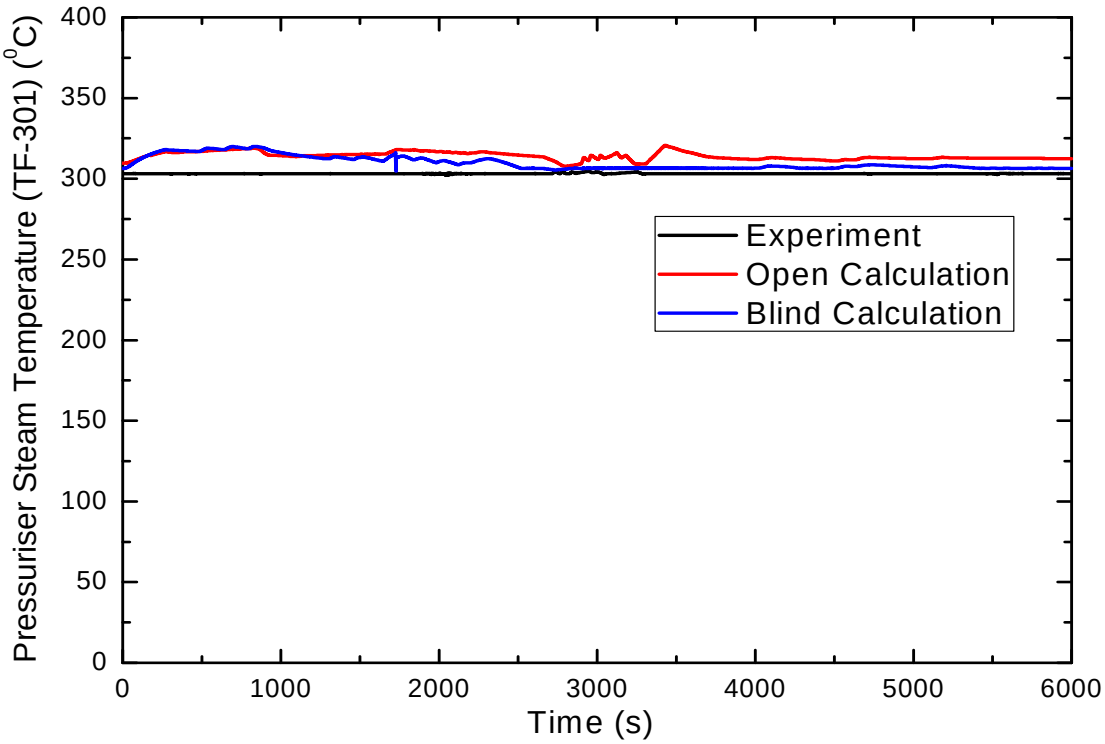

FIG. 4-46. Pressurizer steam temperature.

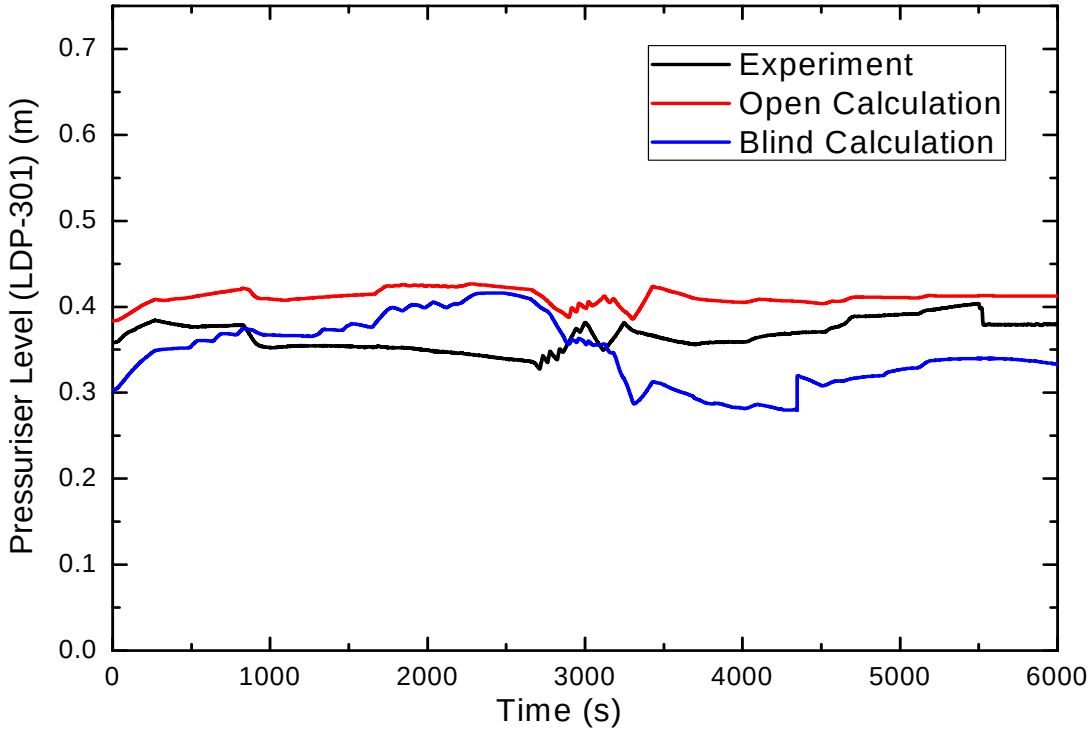

FIG. 4-47. Pressuriser level.

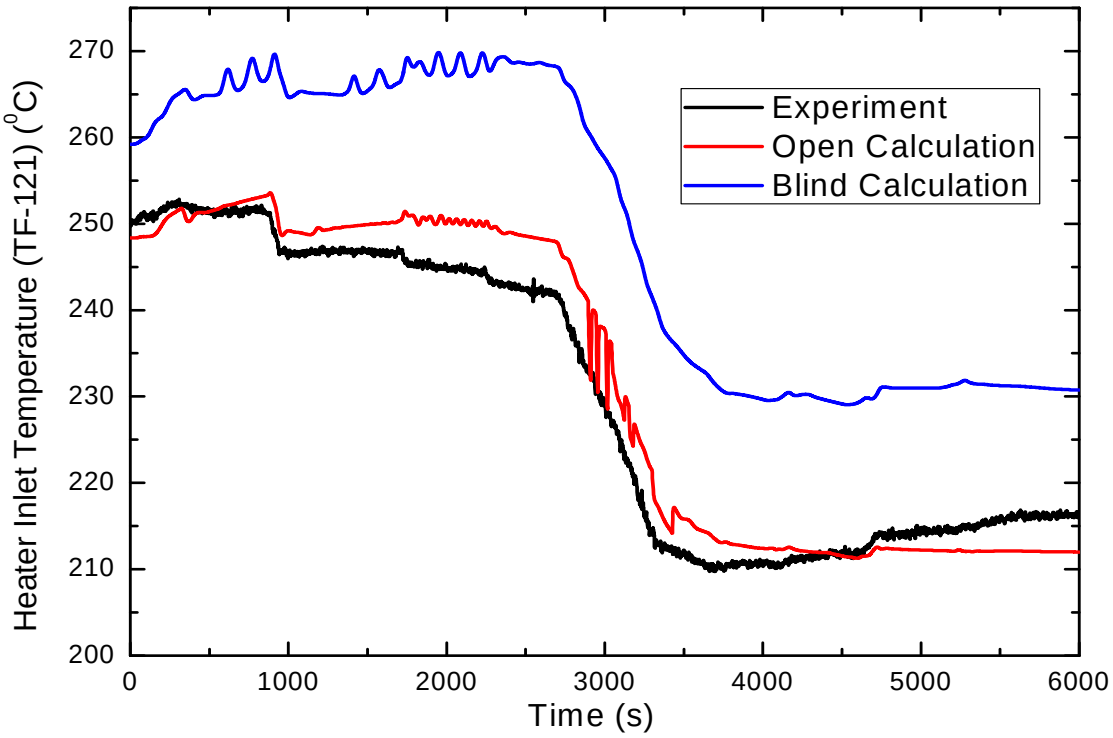

FIG. 4-48. Heater (core) inlet temperature.

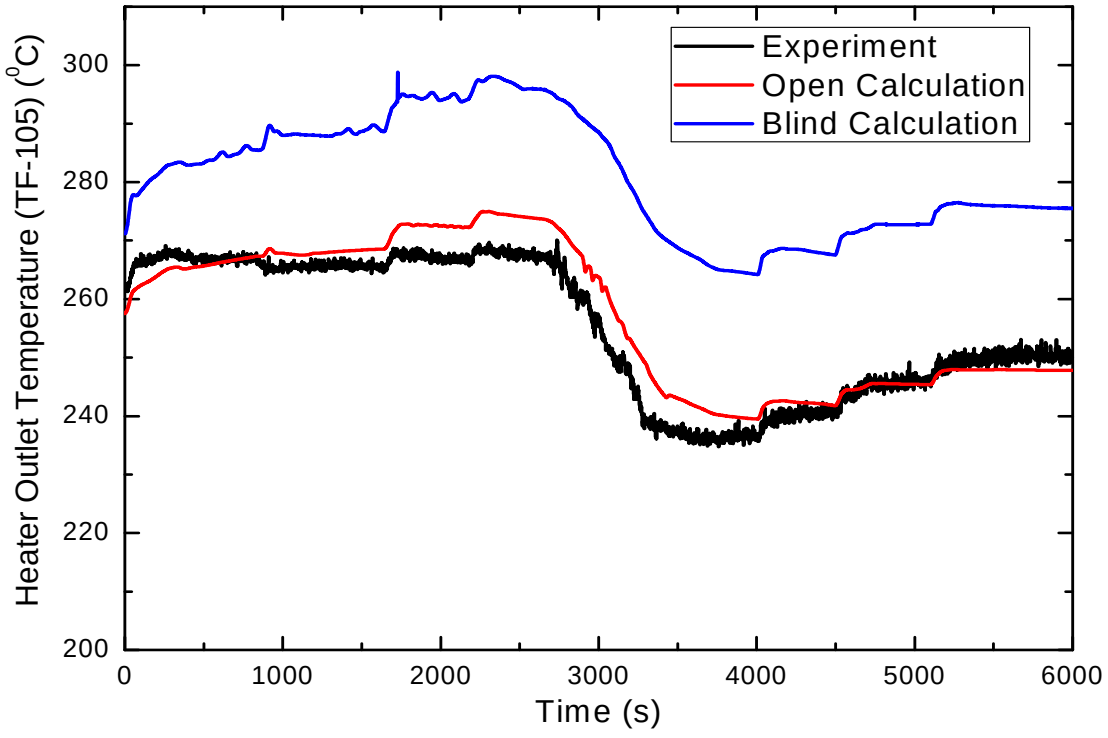

FIG. 4-49. Heater (core) outlet temperature.

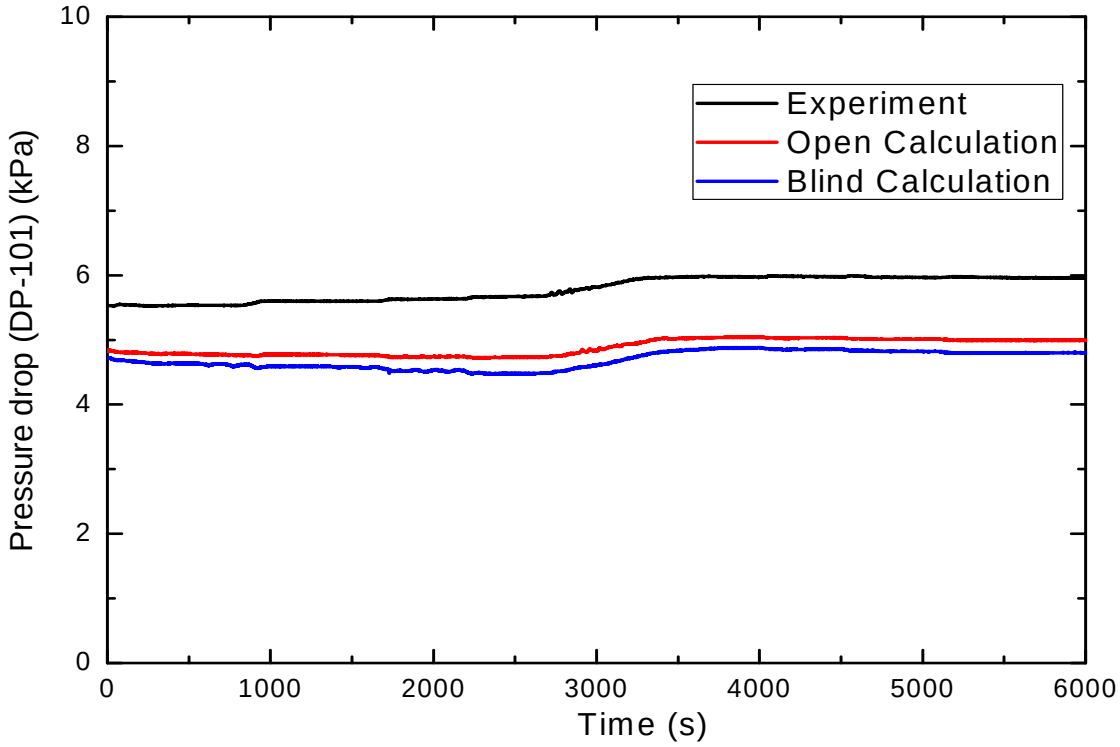

FIG. 4-50. Core pressure drop (DP-101).

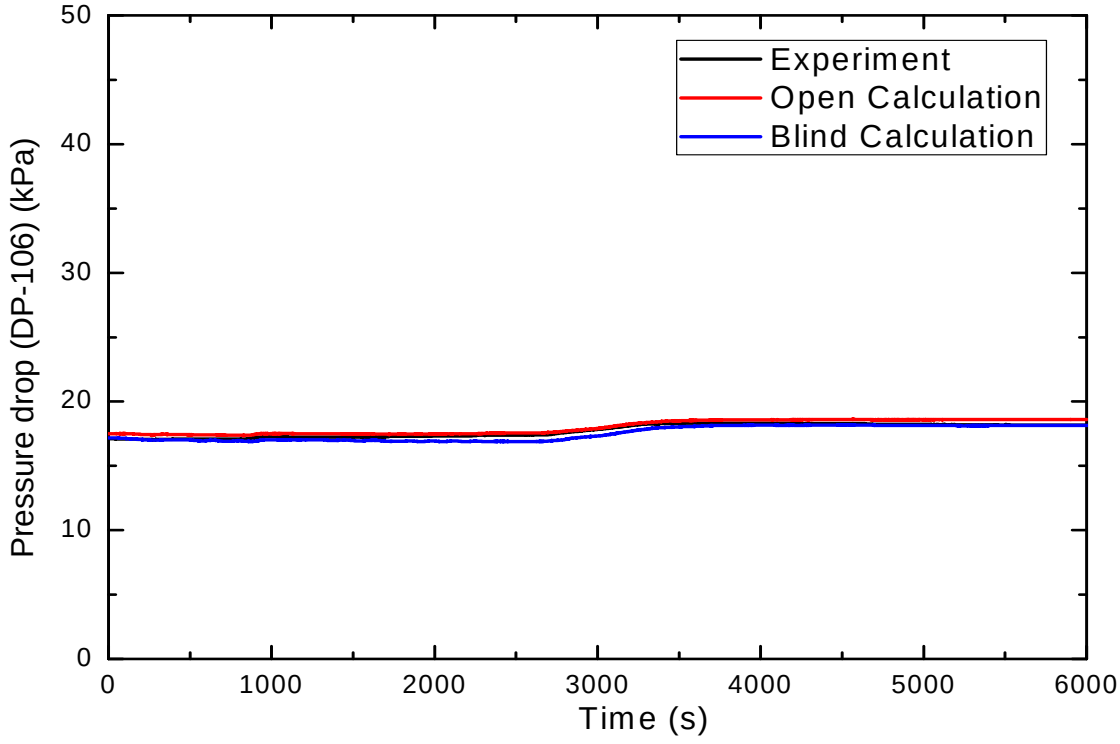

FIG. 4-51. Downcomer pressure drop (DP-106).

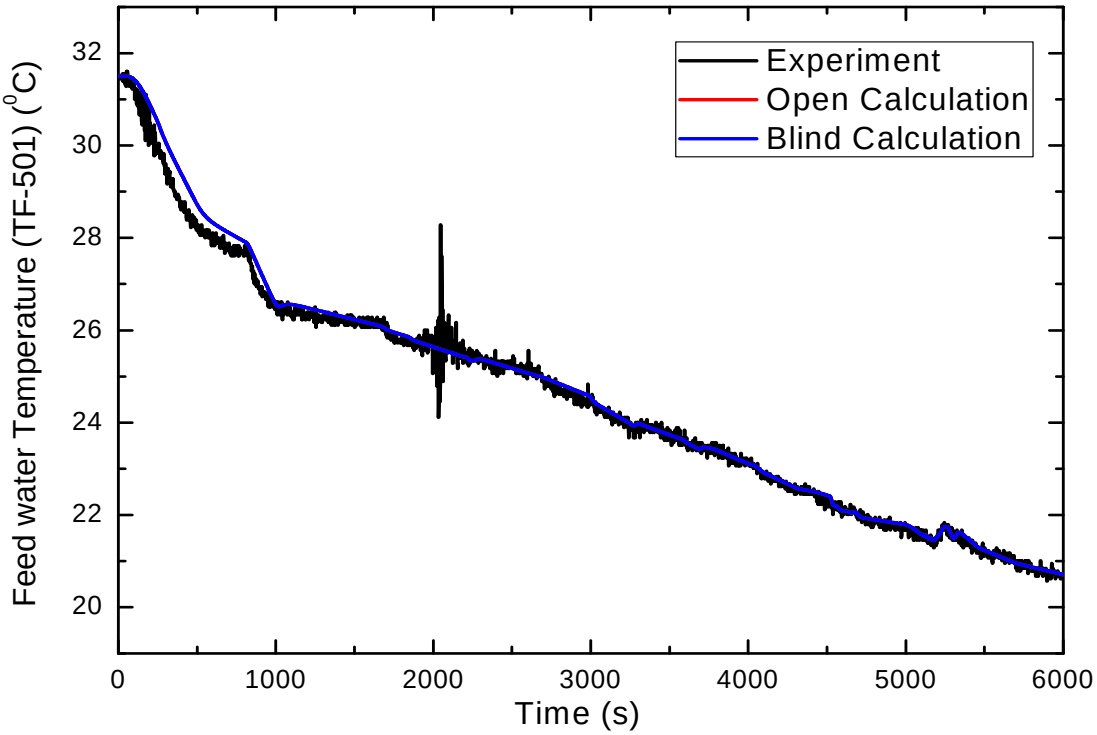

FIG. 4-52. Feed water temperature.

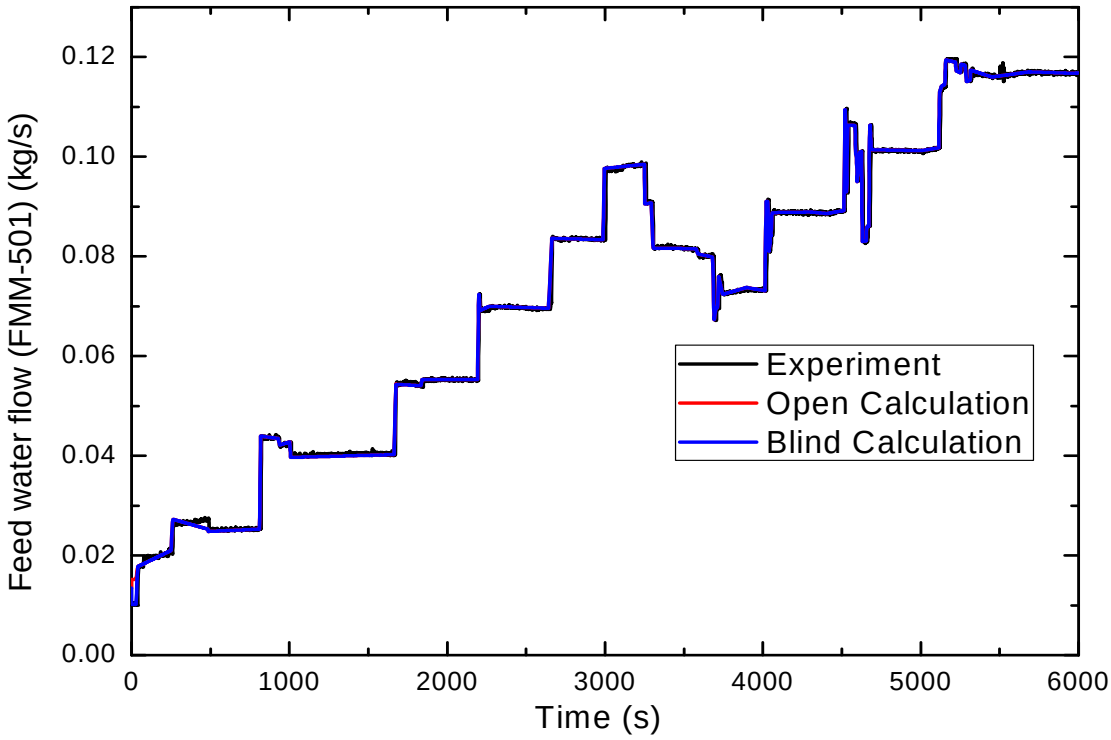

FIG. 4-53. Feed water flow rate.

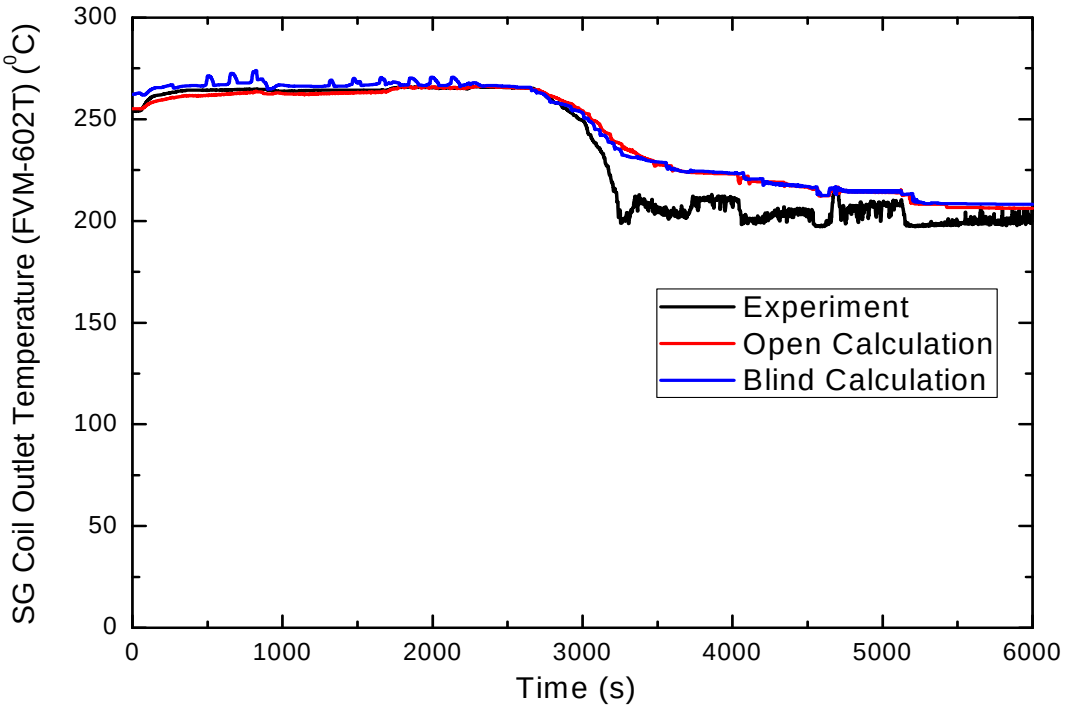

FIG. 4-54. Steam temperature at coil outlet.

4.3. CIAE - CHINA

4.3.1. Computer code

RELAP5/MOD3.3 is used for the present blind and open calculations. It is a one-dimension, two-fluid, six-equation code, and contains non-condensable components in the steam phase. In the code there is no specific model for heat transfer in helical coil SG, but the available model is for a pipe with longitudinal flow, which underestimates the heat transfer of SG. In the present calculation it is simply modeled by a "pipe" with heat structure of increased heat transfer area. The non-condensables is treated as a mixture of the same velocity and temperature as steam for the energy and momentum equation, and the condensation heat transfer with non-condensables is based on Collbum-Hougen diffusion model. The one-dimension code can not model the distribution and variation of the concentration of non-condensables with time in a volume. In SP-2 it is simulated with a constant reduced area throughout the transient. The flow in ADS lines is calculated by choked model with discharge coefficient of 1.0.

4.3.2. System idealization

4.3.2.1. System idealisation for blind calculation

Same nodalization of RELAP5 for both the blind and open calculations is used, as shown in Figure 4-55**.**

Hydraulics modeling

The core is modeled with 6 "volume" nodes, and the SG with 8 "volume" nodes. The HPC and CPV are modeled with two paths respectively, so that the natural circulation can be simulated. Because the condensation heat transfer is sensitive to the variation of liquid level, a fine nodalization is used in HPC and CPV, and they are modeled with 44 and 36 "volume" nodes, respectively.

A calculation of OSU-MASLWR-002 by RELAP5 has shown that with a fixed local flow resistance factor the primary mass flow rate can't be calculated reasonably for wider range of flow rate or power.

Therefore, in the present calculation some local resistance factors are reduced appropriately at higher power.

Heat structures modelling

The heat transfer for the core heater, the SG, the RPV chimney hot leg to cold leg, the HPC to CPV and the PZR heaters are simulated with heat structures. In addition, for simulation of heat loss, the insulations in RPV, HPC and CPV are modeled, and the convection heat transfer coefficient to ambient is set as 10 W/m^2-K. The SG heat transfer in helical coil tubes is modeled by a "pipe" with an increased heat transfer area by a factor of 2.5. For the heat transfer of HPC to CPV the condensation plate area is reduced by 32% to consider the degradation of condensation efficiency due to the accumulating effect of non-condensables in the near-wall region. For PZR the heater power is set "on" (12 kW) before the initiation of ADS, and "off" after that.

Control logic

The actions for ADS valves, the MFP and core power are simulated by trips as the test procedure.

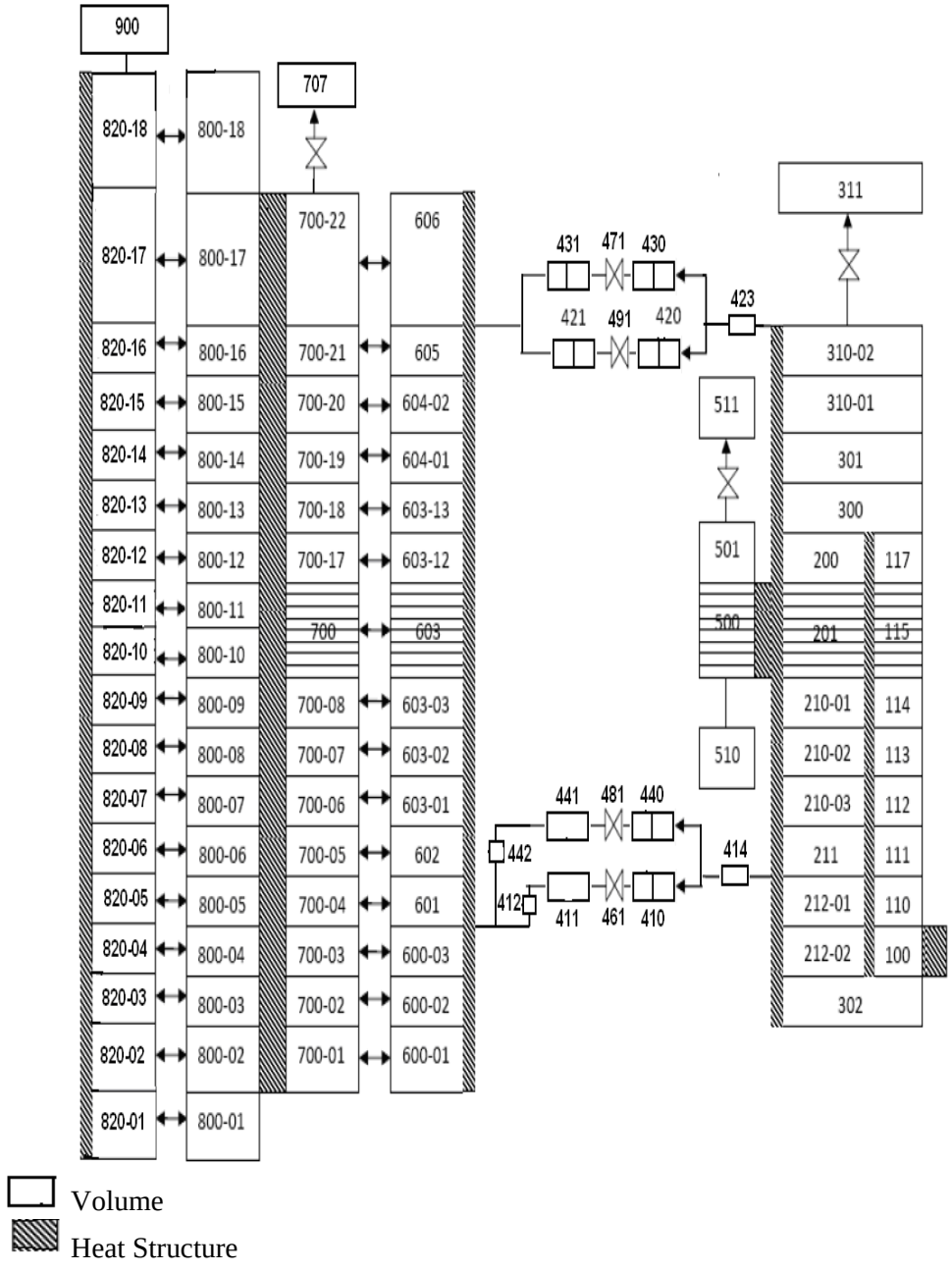

FIG. 4-55. Nodalization diagram for RELAP5 calculation.

4.3.2.2. Modelling change for open calculation

Minor modifications are made from the blind calculation to open calculation, as follows:

- For modeling the SG heat transfer, the increased heat transfer area of SG in heat structure is changed by a factor from 2.5 in blind calculation to 3.0 in open calculation.
- For SP-2, in open calculation the PZR heater power is switched “off” before activation of decay power mode, rather than “on” in blind calculation.

4.3.3. Analysis results for loss of feed-water transient

The timings for major events are listed in Table 4-4.

TABLE 4-4. SP-2 TIME SEQUENCE OF EVENTS

Event	Experiment (s)	Blind cal. (s)	Open cal. (s)
Stop MFP Close HPC vent valve SV-800	0	0	0
PZR pressure (PT-301) reaches 9.064 MPa(a) (1300 psig) Enter decay power mode	30	9.6	28.4
PZR pressure (PT-301) reaches 9.409 MPa(a) (1350 psig) De-energize PZR heaters Open ADS vent valve (PCS-106A)	NA 48	NA 9.6 27.6	NA 0 46.4
First opening time for PCS-106A Last opening time for PCS-106A	4024	4065	3976
Start long-term cooling when pressure difference between primary system and HPC (PT-301 minus PT-801) becomes less than 5 psi (0.034 MPa) Open and remain open of PCS-106A and PCS-106B Open and remain open of PCS-108A and PCS-108B	4043	4304	4181

4.3.3.1. RPV thermal-hydraulic behavior

The results are shown in Figures 4-56 to 4-68 by comparing the experiment, as denoted by “Exp”, with the blind calculation and open calculation, as by “B.C.” and “O.C.”, respectively.

The experimental values of decay heat are used as input of code (Fig. 4-56). The steady-state is established at the conditions consistent with the experiment, i.e., the core pressure PT-301 = 8.72 MPa(a), High pressure containment (HPC) pressure PT-801 = 0.126 MPa(a), core power = 297 kW and the Feedwater flow rate FMM-501 = 0.107 kg/s. The transient is started by setting FMM-501 to zero at 0 s, resulting in a rapid increase in the RPV pressure. The decay power mode activates at PT-301 = 9.062 MPa(a). Afterwards the pressure increases further. The maximum pressure reaches 9.18 MPa(a) by calculation, versus 9.2 MPa(a) in experiment. The evolutions of the pressures of RPV and HPC are shown in Figure 4-57. The vent valve PCS-106A opens at 18 s after the activation of decay heat mode. It leads to sharp decrease in PT-301. When the primary water becomes saturated, the pressure decreases slowly due to evaporation, and it exhibits oscillation behaviour as a result of the action of PCS-106A. The last open of PCS-106A is at 4065 s in blind calculation and 3976 s in open calculation, versus 4024 s in experiment. Shortly the long term cooling starts by opening the PCS-106B, 108A and 108B. In this stage the PT-301 decreases steadily and slowly.

Figure 4-58 shows the variation of primary mass flow rate. It is seen that as the result of alternate open and close of PCS-106A the primary flow rate oscillates severely, producing an effect on the core heat transfer (Fig. 4-56). In the period of long-term cooling, the core power is low, and thus the flow rate is relatively low and stable.

Figure 4-59 shows the variations of core inlet and outlet water temperature, and Figure 4-60 shows the variation of RPV water level. After loss of feed-water, at first the core outlet temperature increases

slightly, and the core inlet temperature increases towards the outlet temperature due to the loss of SG heat transfer. Afterwards, the inlet and outlet temperatures decrease at decay heat mode. After activation of long term cooling a distinct drop in the core inlet temperature is observed, but only a minor drop is calculated. It is a result of returning water from HPC, and would be related to the flow instability, as will be discussed later. The action of ADS leads to continuous decrease in the primary liquid level. About 80 s after the initiation of long term cooling the level in RPV reaches a minimum value of 3.13 m in experiment, versus 3.02 m by calculation. Then the liquid level recovers and reaches 3.37 m in experiment, versus 3.20 m in blind and open calculations. It indicates that the core is covered by water throughout the transient. Since at decay heat mode the core power is low, the heater temperatures are close to the saturation temperature and no heat-up occurs (Fig. 4-61).

4.3.3.2. SG thermal-hydraulic behavior

Figure 4-62 shows the calculated SG heat transfer. After loss of feed-water the SG removes the heat by evaporation of the remaining liquid in the coil. When the liquid is evaporated completely in about 30 s, the SG function of heat transfer loses. In this period the core inlet temperature TF-121 increases towards the outlet temperature TF-132 (Fig. 4-59). This behavior is reproduced essentially by the calculation, though it is not so sensitive due to rough nodes.

4.3.3.3. HPC thermal-hydraulic behavior

The variation of HPC pressure PT-801 is shown in Figure 4-57. After initiation of ADS the PT-801 increases. Under the procedure for the action of vent valve PCS-106A, the PT-801 oscillates between the open set-point of 1.824 MPa(a) and close set-point of 1.479 MPa(a). In this period the RPV level decreases (Fig. 4-60), accompanying increase in the HPC level LDP-801 (Fig. 4-63). Just after the initiation of long term cooling at 4043 s, the RPV pressure is slightly higher than the HPC. Hence, both the steam in the vent lines and the water in the sump return lines flow from RPV to HPC, and thus in a short period the PT-301 decreases and PT-801 increases (Fig. 4-64), and LDP-801 increases further. In experiment a sudden fluctuation of PT-801 occurs at 4,123s. Then, LDP-801 turns to decrease and LDP-106 turns to increase, suggesting that a natural circulation is developed in which the steam flows from RPV to HPC and the water flows from HPC to RPV. The instantaneous fluctuation of the PT-801 would be a result of some instability. It could promote the mass exchange between the RPV and HPC, and lead to the distinct decrease in the core inlet temperature. The instability is not predicted by the code properly and only a minor drop of TF-121 is calculated. In the later period the RPV pressure is essentially in balance with the HPC (Fig. 4-57), and thus the liquid level varies very small.

Figures 4-65 and 4-66 show the temperature distributions at different elevations of HPC for experiment and calculations, respectively. TF-811 and TF-821 are always located under the water level, representing the water temperature. They are below the saturation temperature and exhibit stratification feature. The TF- 841, 851 and 861 are always above the liquid level, representing the temperatures of the mixture of air with discharged steam, which are close to the saturation temperature. Before 4000 s they exhibit oscillation due to the pressure oscillation, and after then decrease steadily as the pressure decreases. TF-831 experiences uncovered to covered then uncovered condition again by water, and thus varies strongly.

Figure 4-67 shows the calculated heat removed from HPC to CPV, the core power and the heat losses for RPV, HPC and CPV. As seen, in the later stage the heat losses are negligible, and the HPC-CPV heat transfer is higher than the core power, suggesting its domination for the pressure decrease of HPC and RPV in the later period.

4.3.3.4. CPV thermal-hydraulic behavior

The CPV is fully filled with water. During transient the water temperatures increase gradually and exhibit stratification feature, as shown in Figure 4-68. At the end of transient the temperature increase at the top is about 27°C, while it is about 5°C at the button.

In general, the major phenomena in the transient are reproduced by the blind calculation, and reasonable agreements for main parameters are obtained with the experiment. The timing of initiation

of decay power mode is predicted at 9.6 s in blind calculation, versus 30 s in experiment. Before actuation of decay power mode the PZR pressure is higher than the normal value (8.72 MPa(a)). Therefore, in open calculation, the heater is set “off”, rather than “on” in blind calculation, so that the timing is predicted at 28.4 s, which is close to the experiment (30 s). With this modification the calculation results for other parameters in open calculation are not different obviously from blind calculation.

For HPC and CPV, the temperature stratification behavior is reproduced by the calculations qualitatively. It is understandable that the thermal-hydraulic behavior of natural circulation in HPC and CPV would be three dimensional and unstable in nature. It could not be predicted by one-dimensional code accurately for the temperature distribution in HPC and CPV, and could have effect on the core inlet temperature.

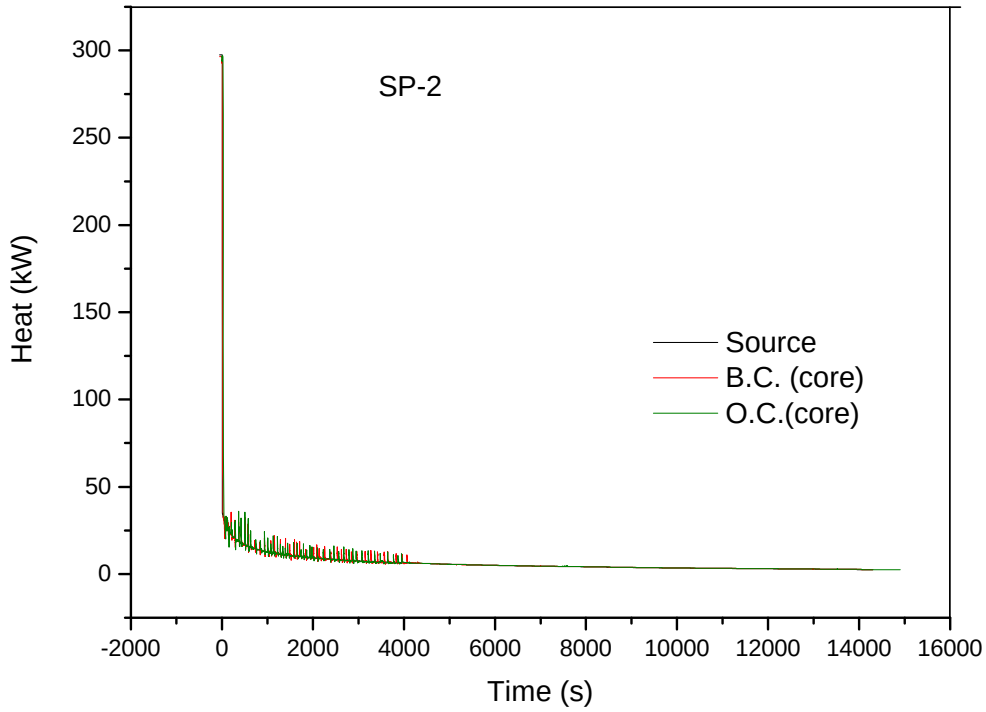

FIG. 4-56. Core power and heat transfer in the core.

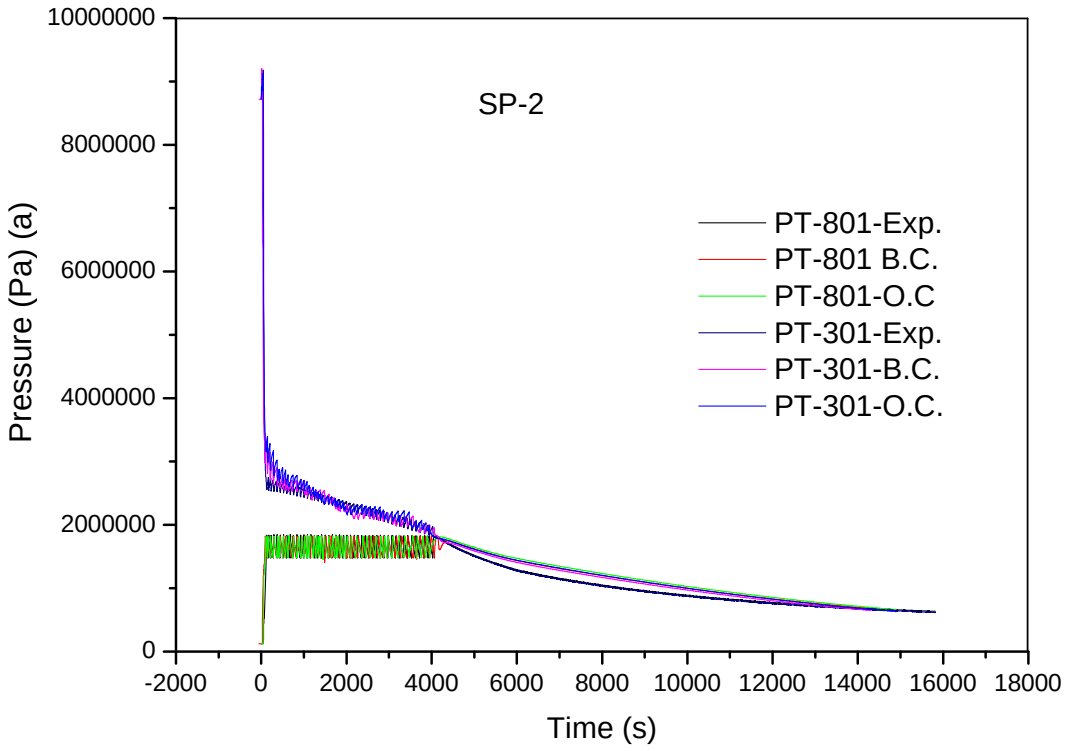

FIG. 4-57. RPV and HPC pressures.

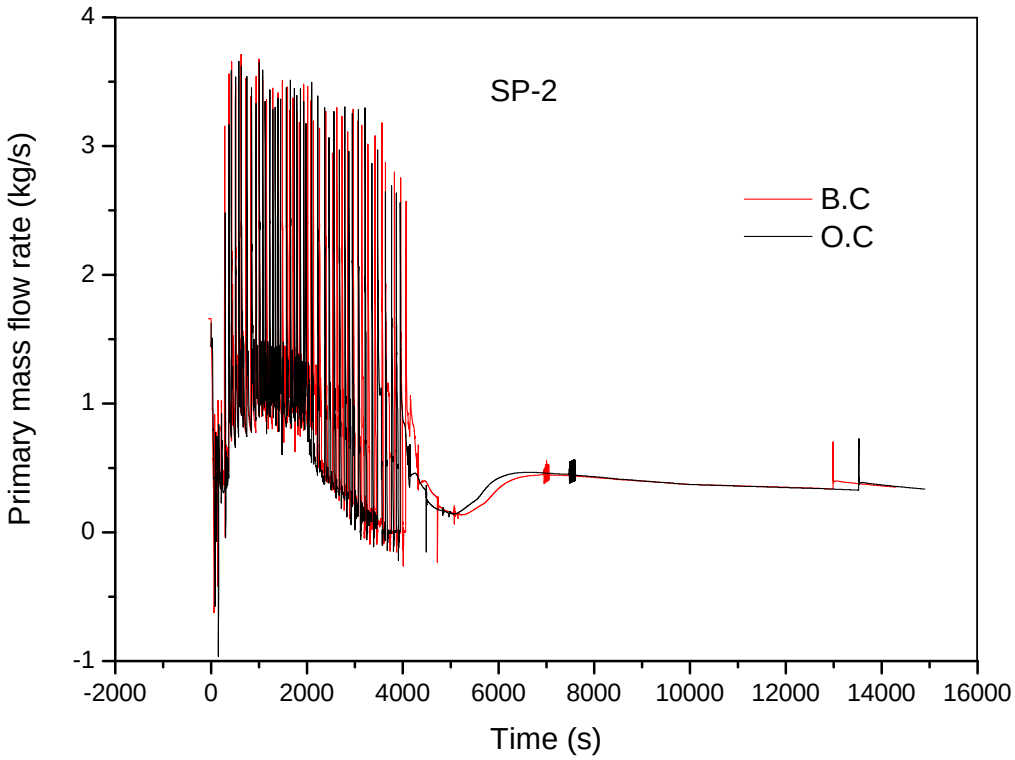

FIG. 4-58. Primary mass flow rate.

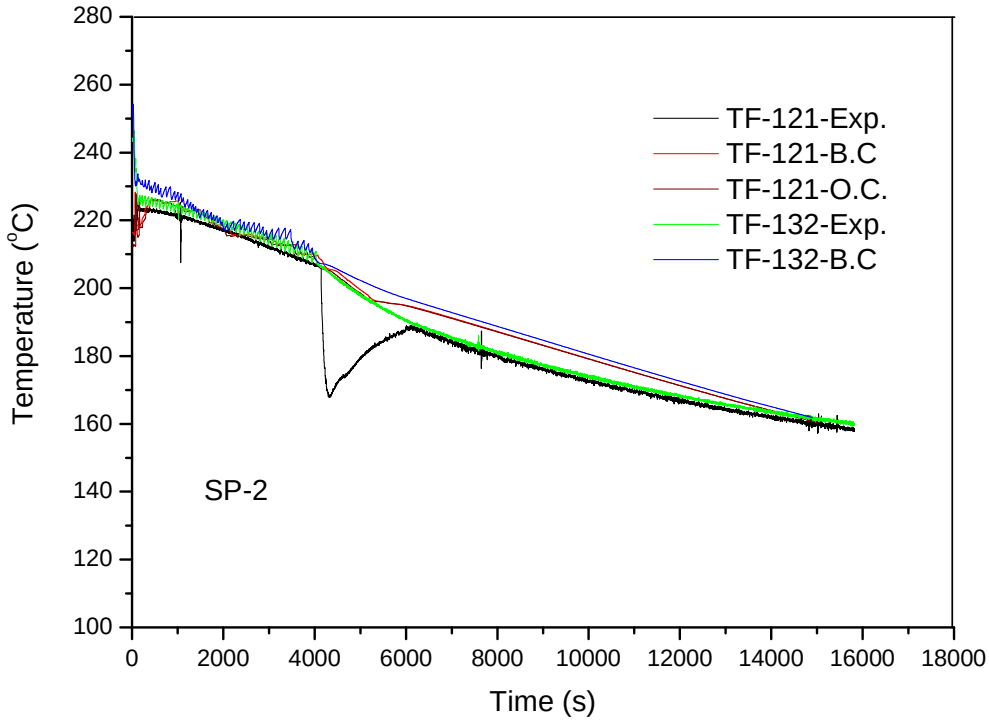

FIG. 4-59. Core inlet temperature TF-121 and outlet temperature TF-132 (no O.C.).

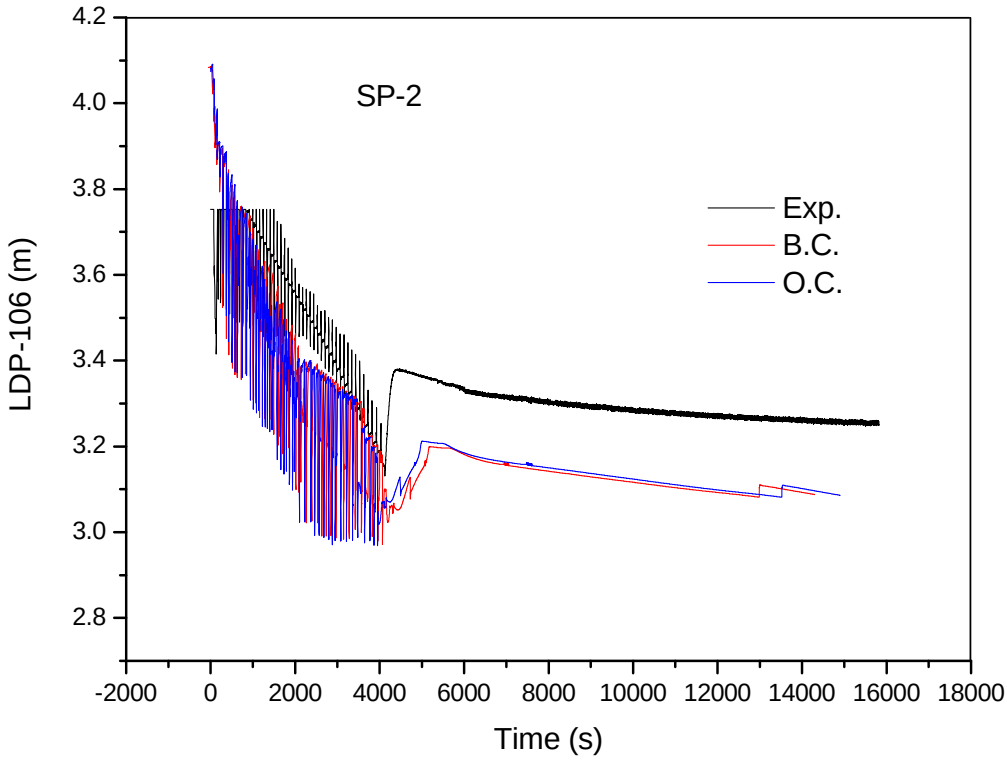

FIG. 4-60. Core liquid level LDP-106.

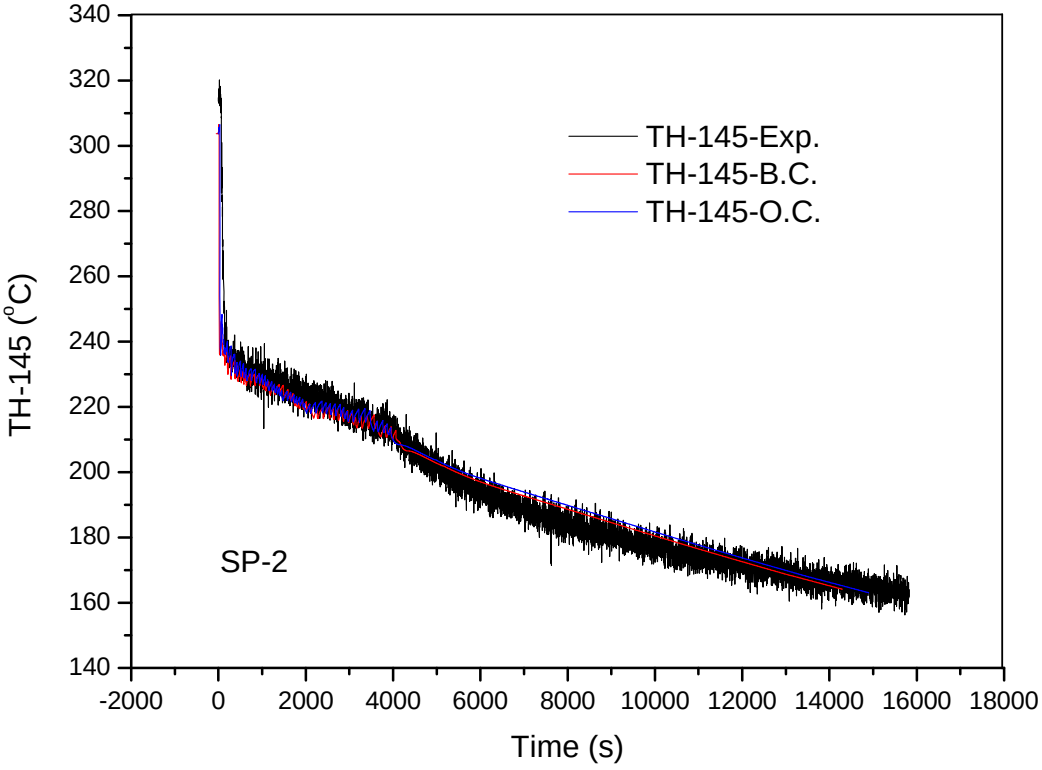

FIG. 4-61. Core rod temperature TH-145.

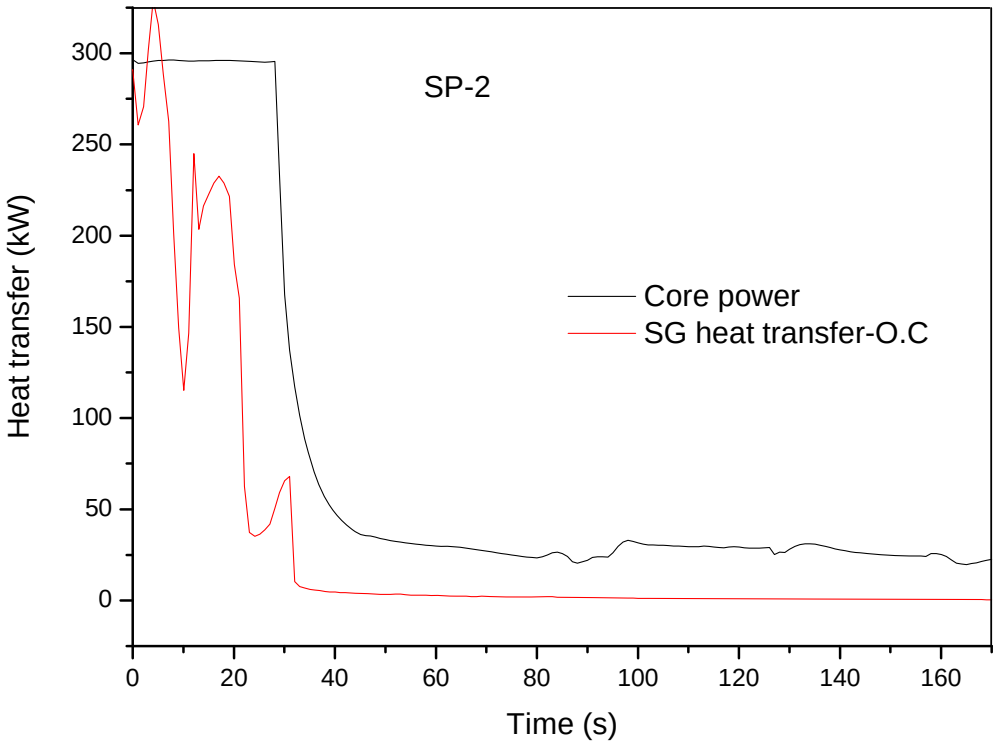

FIG. 4-62. Core power and the heat transfer in the core and SG.

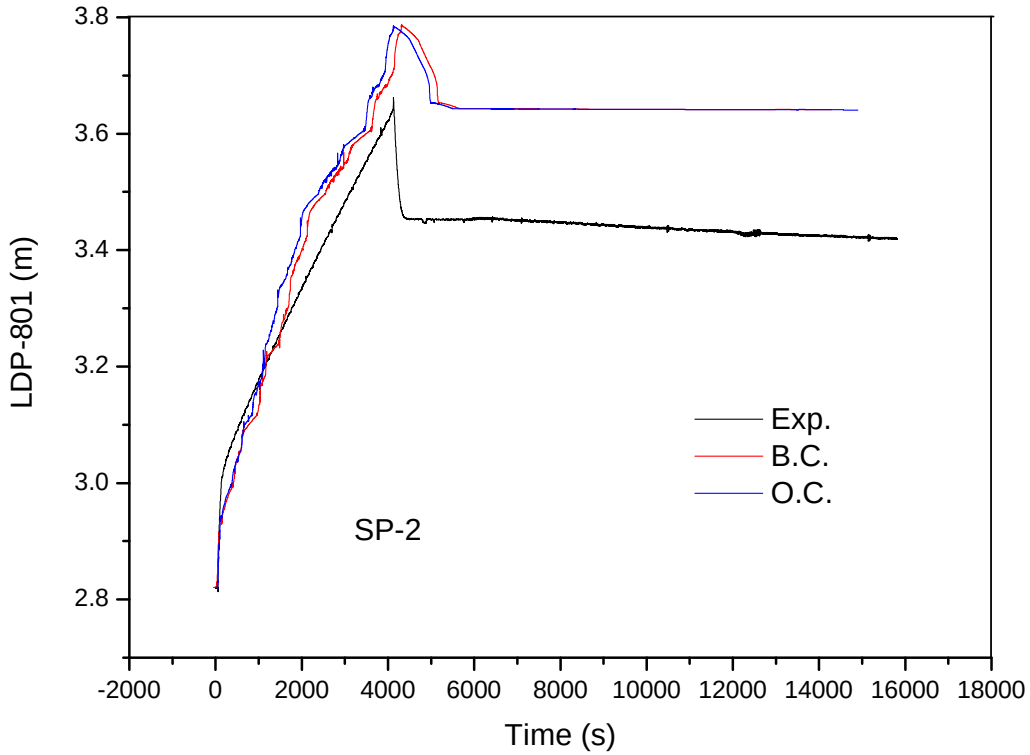

FIG. 4-63. Variation of the water level in the HPC.

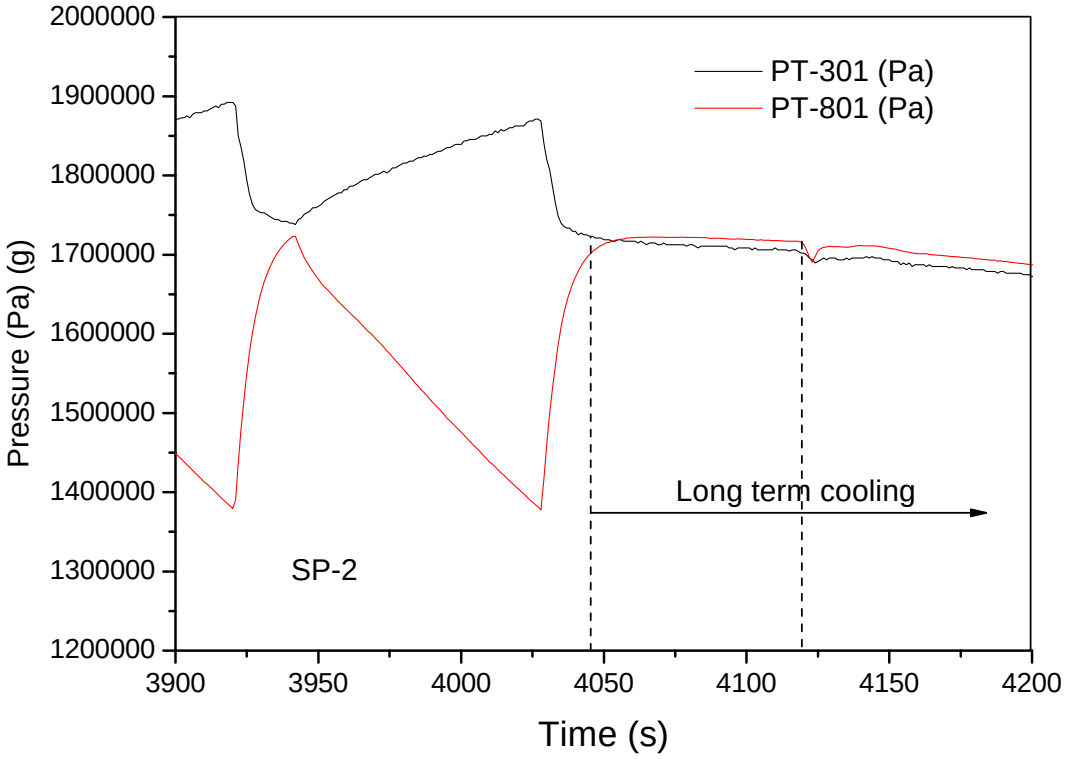

FIG. 4-64. Variations of PT-301 and PT-801 after the initiation of long term cooling.

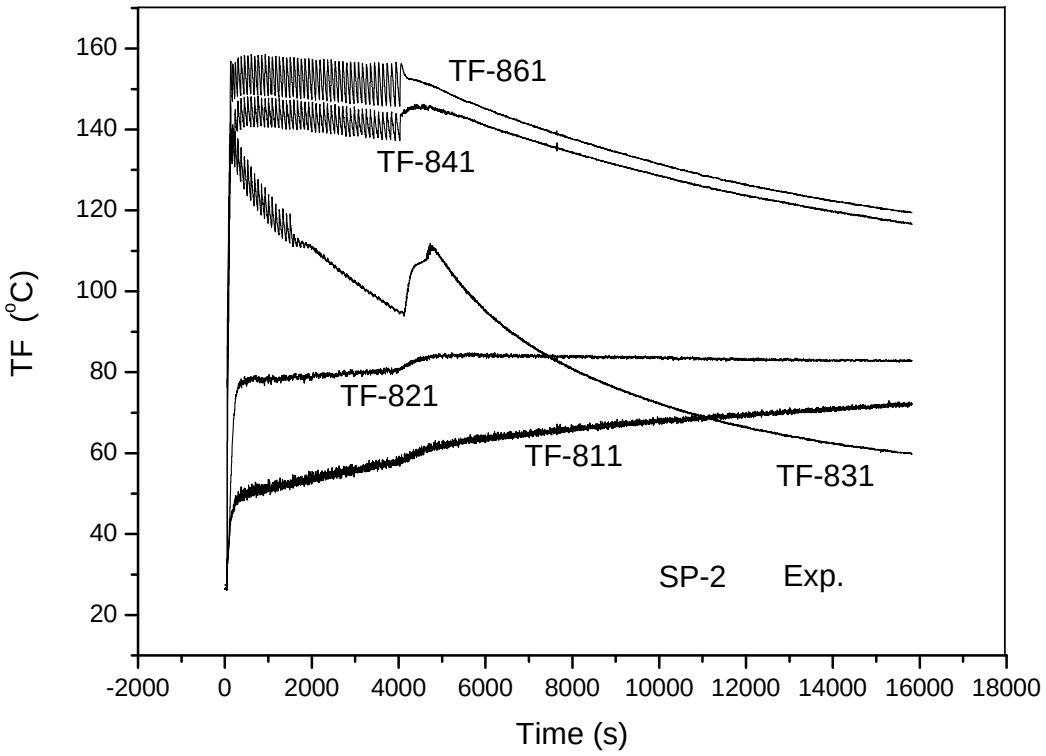

FIG. 4-65. Temperature distribution of the HPC measured in experiment.

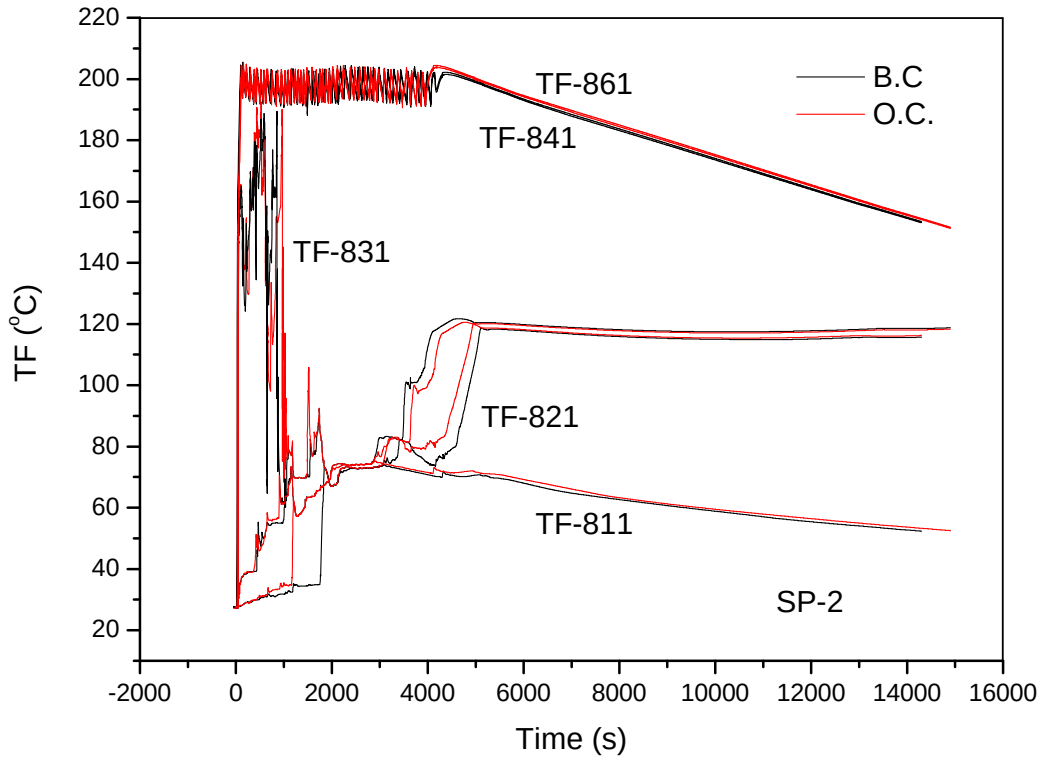

FIG. 4-66. Temperature distribution of the HPC by calculations.

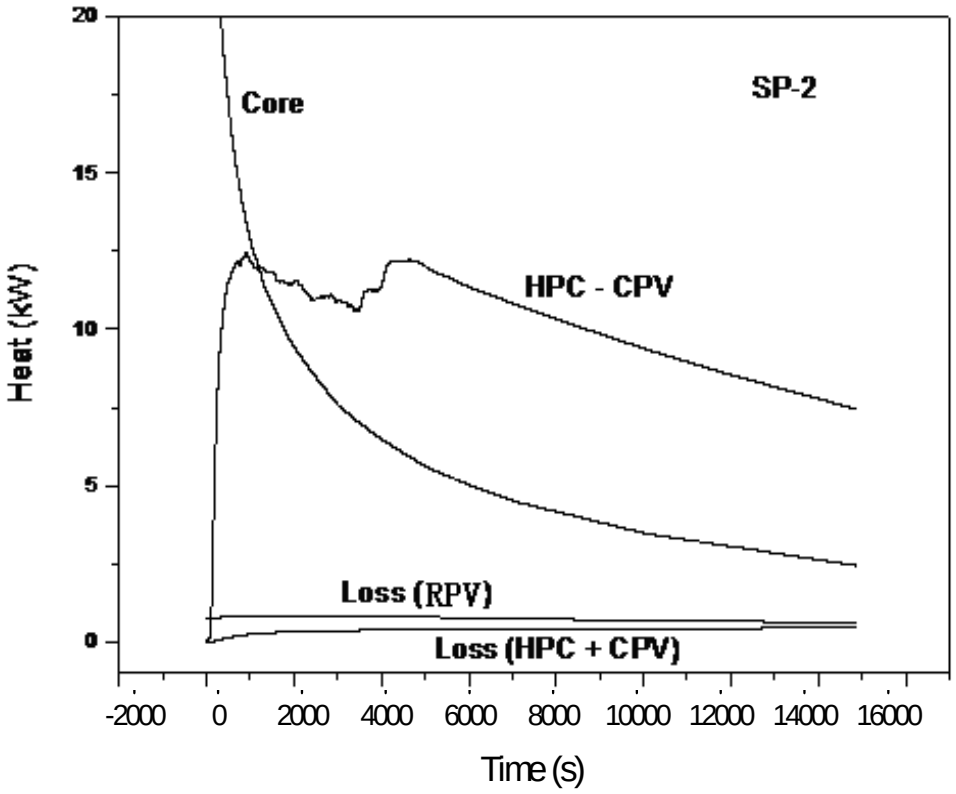

FIG. 4-67. Core power, the HPC to CPV heat and the heat losses.

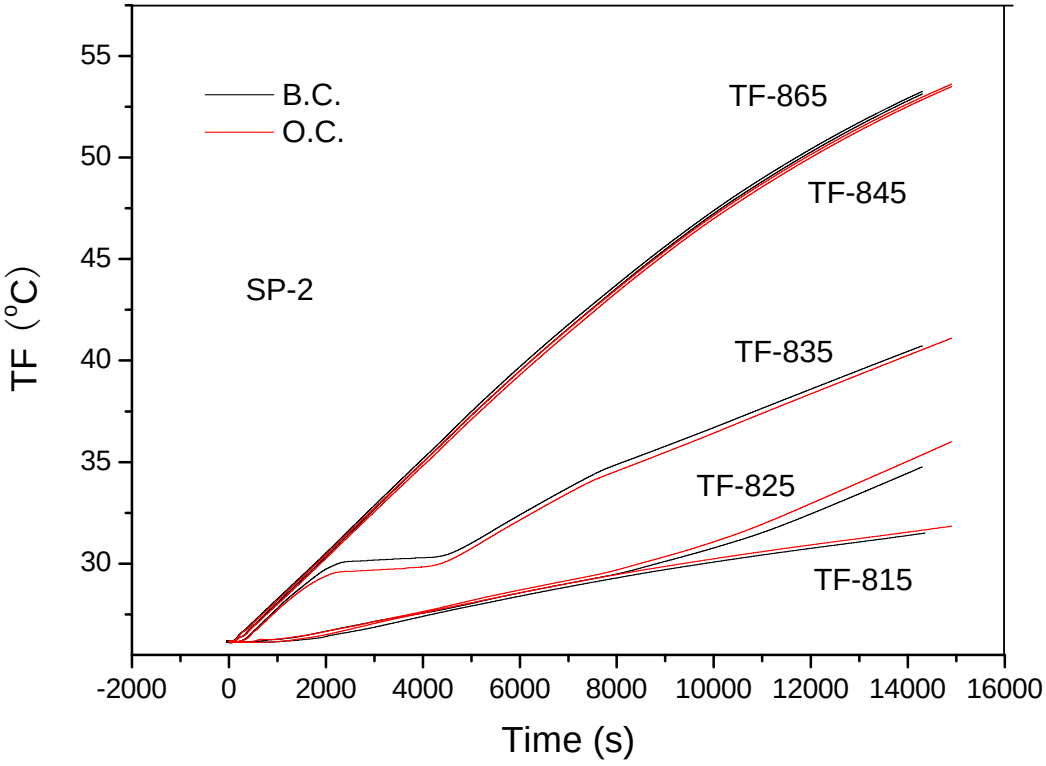

FIG. 4-68. Temperature distribution of the HPC in calculations.

4.3.4. Analysis results for power maneuvering

4.3.4.1. RPV thermal-hydraulic behavior

The experimental data of the core power and feed-water flow rate are used as the code inputs, as shown in Figures 4-69 and 4-70, respectively.

The PZR pressure is shown in Figure 4-71, and the core inlet and outlet temperature are shown in Figure 4-72. With different power level the primary pressure PT-301 remains around the nominal value (8.72 MPa(a)). For t < 2600 s the RPV water temperature is higher, hence, to keep the pressure in normal range the PZR heater power of 12 kW is switched on and off alternately with relatively high frequency, resulting in some minor disturbance in the calculations of pressure, flow rate and temperature. In the later stage the RPV water temperatures are lower, thus the heater power in PZR is always kept on, and thus the disturbance is not observed in experiment and calculations.

For t < 2600 s, the water temperatures are higher. After that it decreases by about 30°C, and remains at lower level in later stage. This trend is dominated by the SG heat transfer, as will be explained in next paragraph. In blind calculation the core water temperatures are slightly over-predicted with the maximum of about 10°C. In open calculation the heat transfer area of SG is increased by 20%, so the maximum deviation decreases to about 5°C. In both blind and open calculations the temperature differences between the inlet and outlet of the core are very close to the experiment, suggesting that the primary mass flow rate is well predicted. This can also be confirmed by the calculation of primary mass flow rate, as shown in Figure 4-73.

Figure 4-74 shows the liquid temperature and heater temperature at the upper portion of the core. For t < 1000 s with power of 80 kW or less the heater surface temperature is below the saturation temperature. For power higher than 100 kW, it exceeds the saturation temperature, indicating the rod in subcooled boiling regime. In the period of 2650 – 3700 s, as the water temperature decreases the heater surface temperature drops below the saturation point. For t > 4000 s, as a result of further increase of power the heater temperature increases slightly above the saturation temperature. The agreements of water temperature with experiment are mostly within 5°C for blind calculation and 3°C for open calculation.

The variation of RPV liquid level is shown in Figure 4-75. It is related to the primary mass and the water temperature. In later stage, though the water temperature is decreased by about 30°C, the level is remained at nearly constant. This is the result of injecting water of about 9.2 kg.

It is also seen in Figure 4-74 that for the condition of TH-146 below the saturation temperature the temperature difference, TH-146 – TF-106, is calculated properly, suggesting the suitability of the correlation on convection heat transfer coefficient for single phase flow. While for TH-146 above saturation temperature the wall superheat is calculated smaller than the experiment, suggesting an over-prediction of heat transfer coefficient for subcooled boiling.

4.3.3.2. SG thermal-hydraulic behavior

The RPV water temperature is dominated by SG thermal-Hydraulic behavior strongly. Figure 4-76 shows the steam temperature at the exit of coil. In lower power region (t < 2500 s) the temperatures are around 260°C, afterwards, they drop sharply and remain in the range of 194 - 220°C. It is controlled by the heat balance, and thus determined by the power removal and the feed-water parameters. This trend partially dominates the RPV water temperature (Fig. 4-72). In the region of lower power (t < 2500 s) with feedwater flow rate less than 0.055 kg/s, the steam flow rate and temperature calculated are strongly oscillatory. It disappears in later period with higher power and feed-water flow rate. In the period of 2650 to 3700 s the heat removed by SG is higher than the core power, as seen in Figure 4-77. This partially explains the decrease in the water temperature in RPV.

In general, for SP-3 the calculation result is essentially dominated by the modeling of SG heat transfer. The heat transfer coefficient in the helical coils is much higher than that in pipe with longitudinal flow. By proper modeling the SG heat transfer the calculation results are in good agreement with the experiment for the major parameters.

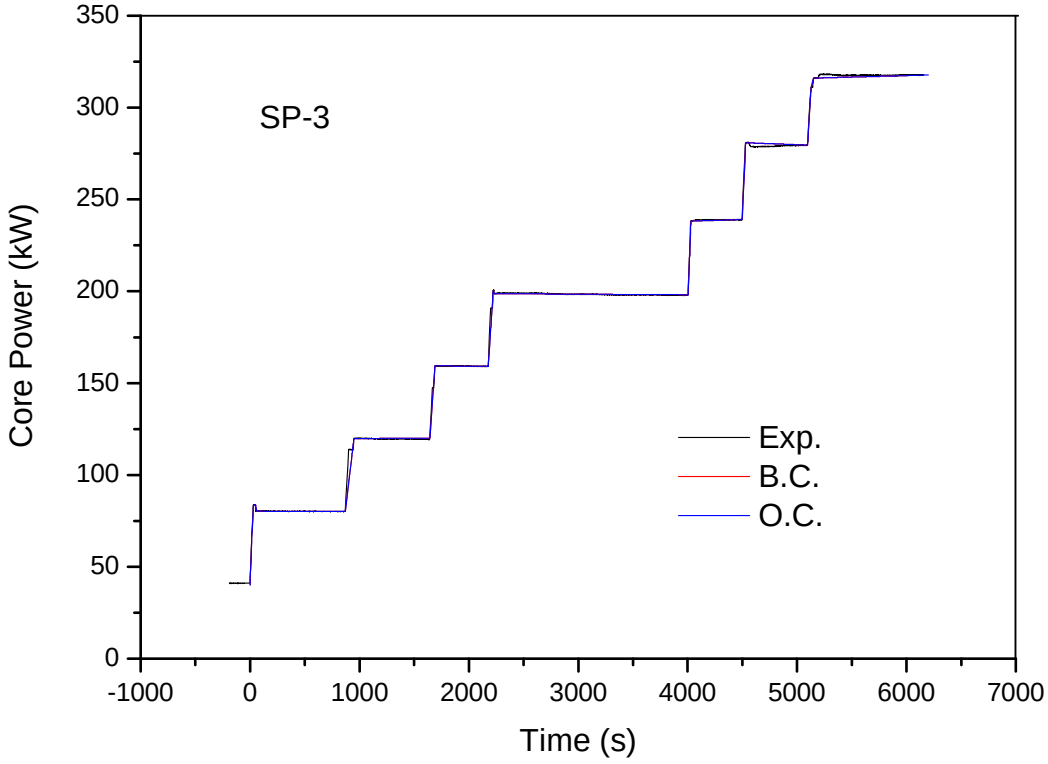

FIG. 4-69. Input of core power.

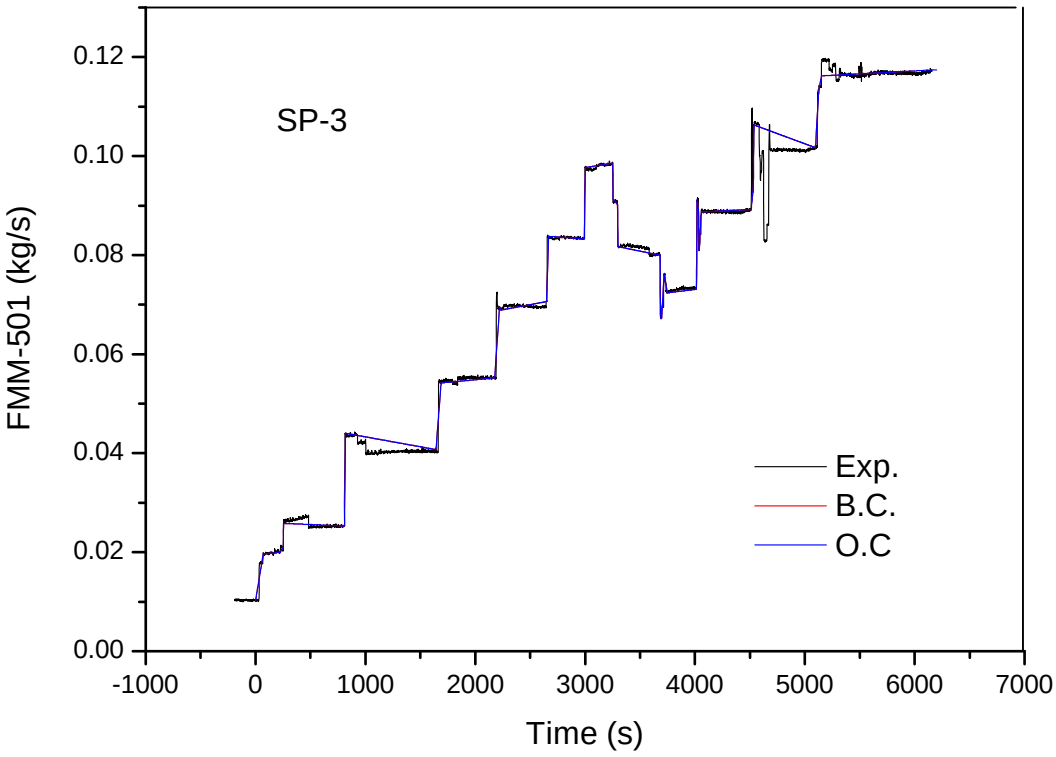

FIG. 4-70. Input of Feed-water flow rate.

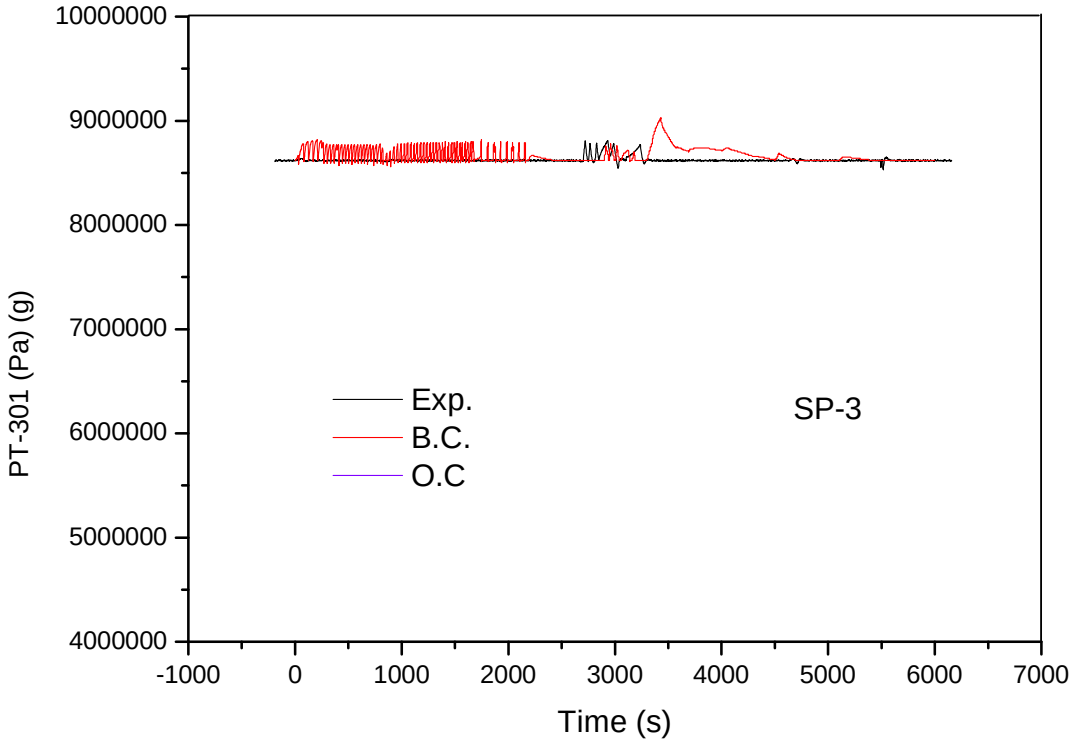

FIG. 4-71. PZR Pressure PT-301.

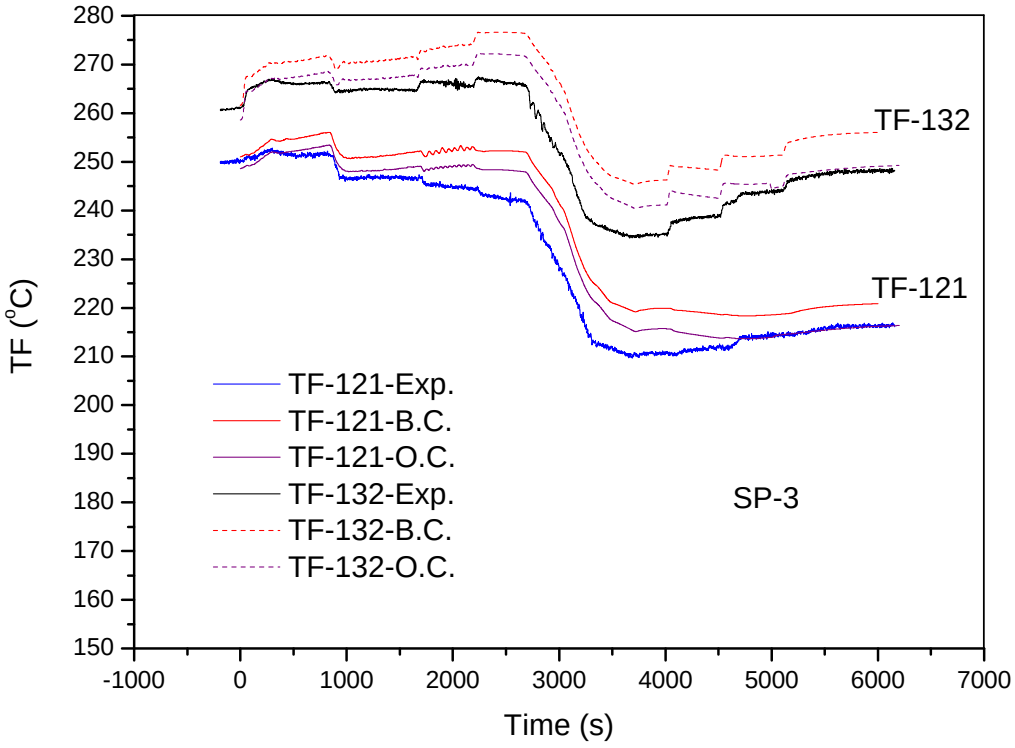

FIG. 4-72. Core inlet temperature TF-121 and outlet temperature TF-132.

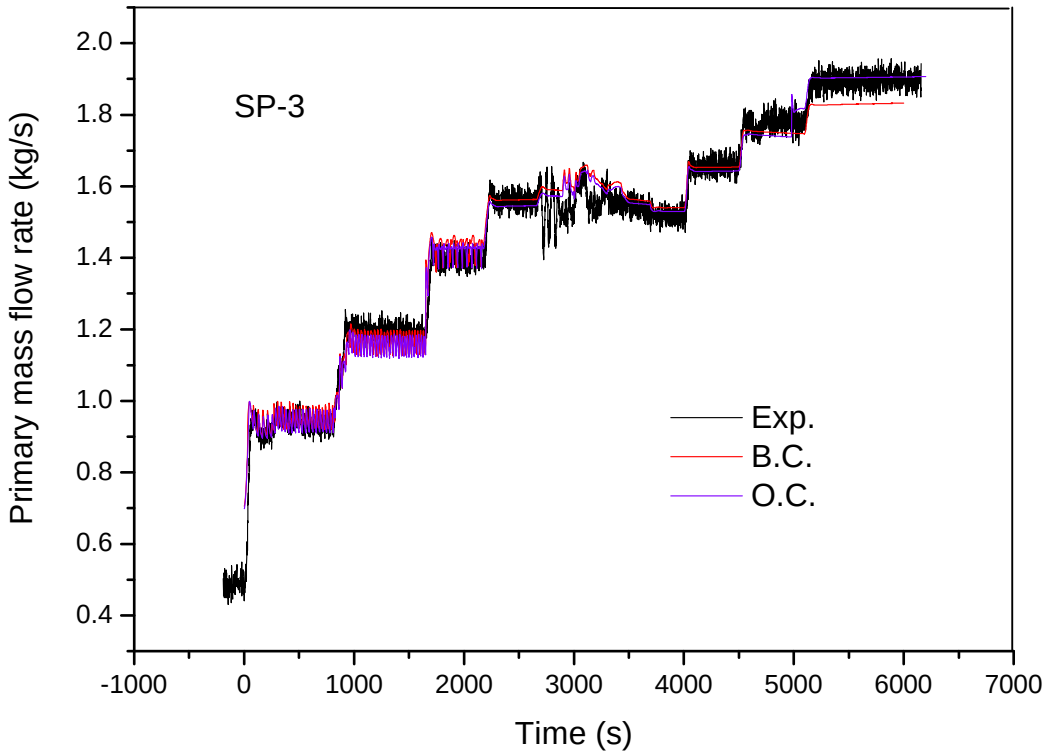

FIG. 4-73. Primary mass flow rate (FDP-131).

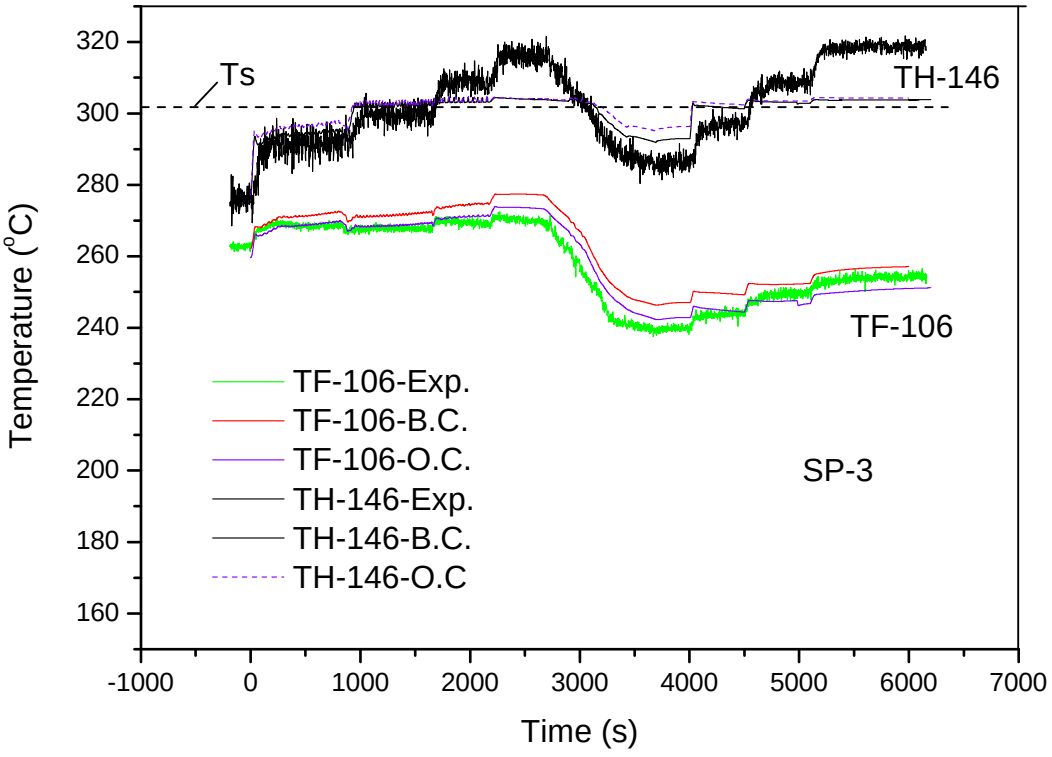

FIG. 4-74. Core water and heater temperatures.

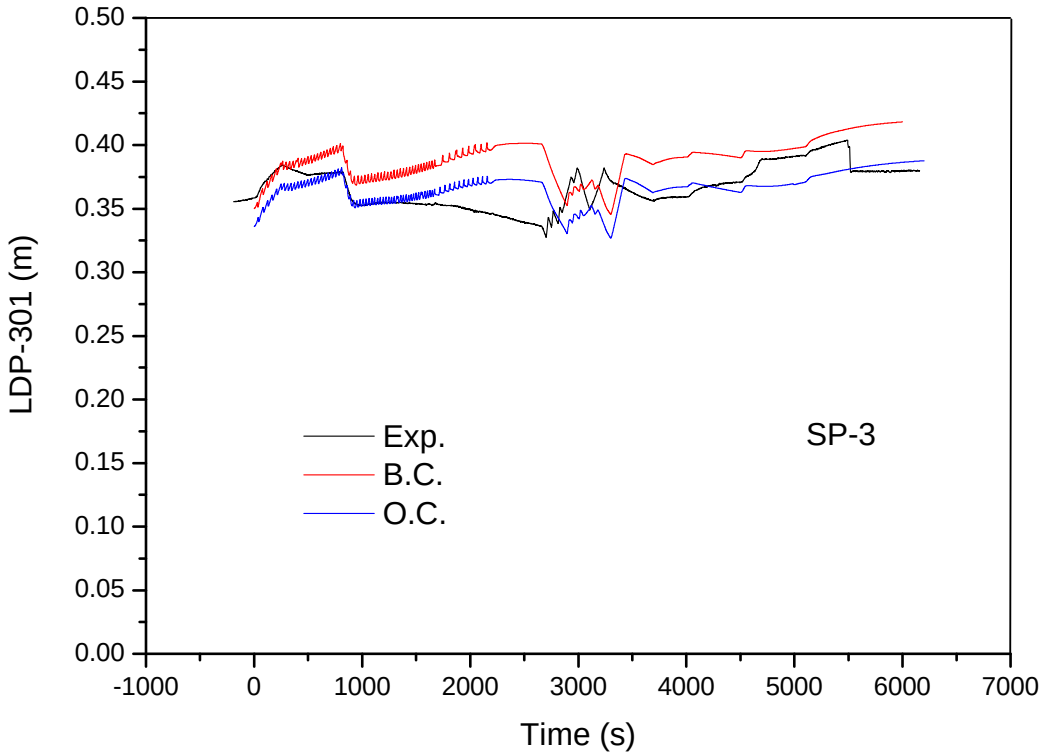

FIG. 4-75. PZR water level LDP-301.

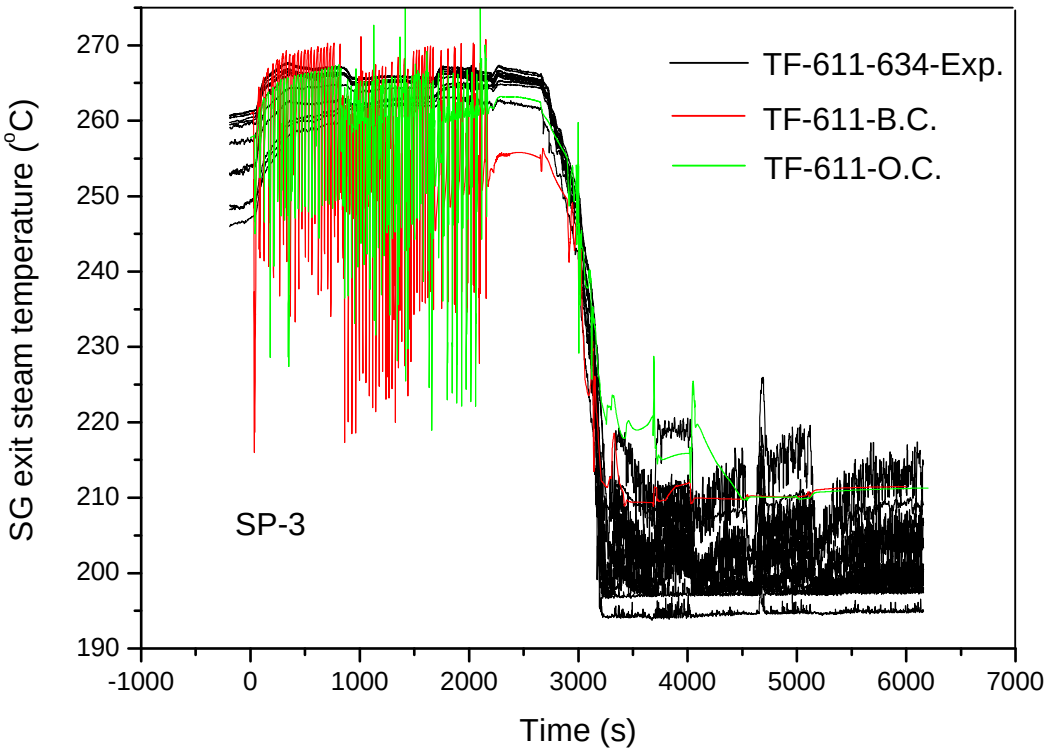

FIG. 4-76. Steam temperature just downstream of the coil.

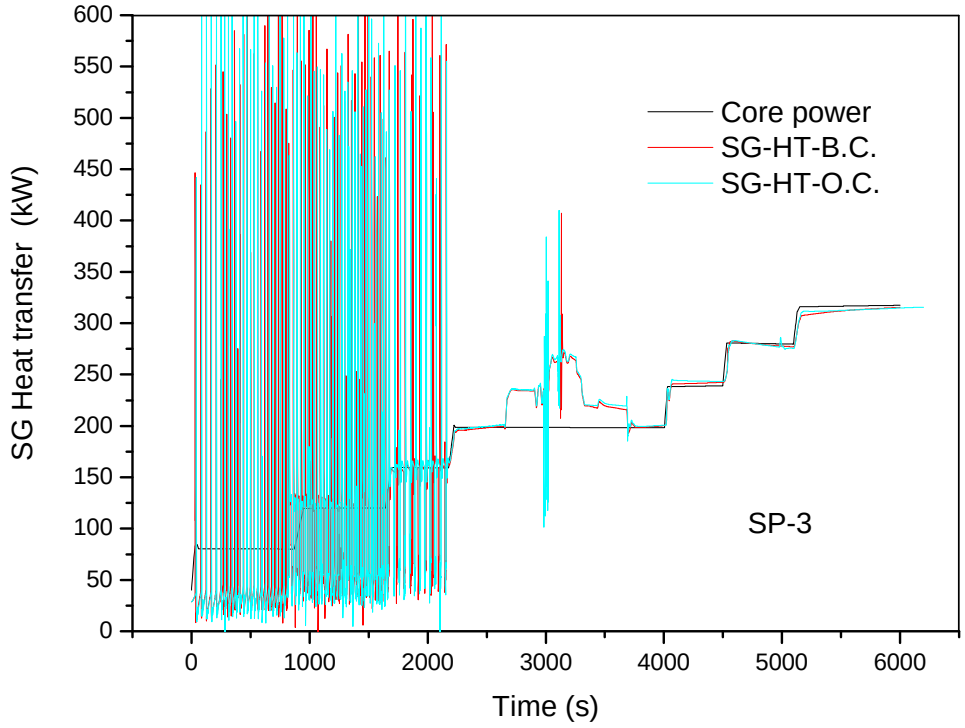

FIG. 4-77. Core power and SG heat transfer.

4.4. ENEA – ITALY

4.4.1. Computer codes

RELAP5 code [5, 6, 7] is a thermal-hydraulic (TH) code for nuclear system analysis and constitutes the object of continuous assessment in various international institutions. Wide qualification projects and sensitivity and uncertainty analyses of physical models have been performed all over the world [8]. A wide literature exists about the code description, capability and application. The light water reactor (LWR) transient analysis code, RELAP5, was developed at Idaho National Engineering Laboratory (INEL) for the U.S. Nuclear Regulatory Commission (NRC). The RELAP5 code has been developed for best estimate simulation of LWR coolant system transients during normal and off normal conditions. The code models the coupled behavior of the reactor coolant system and the core (point kinetic) for simulating accidents in LWR: such as loss of coolant accident (LOCA), anticipated transients without scram (ATWS) and operational transients, such as loss of feed-water (LOFW), loss of offsite power (LOOP) and turbine trip. A generic modeling approach is used. It permits simulating a variety of thermal-hydraulic systems such as turbines, condensers and secondary feed-water (FW) systems. The component models include also pumps, valves, pipes, heat releasing or absorbing structures, reactor point kinetics, electric heaters, jet pumps, etc. In addition, special process models are included for effects such as form loss, flow at an abrupt area change, branching, choked flow (Ramson/Trapp or Henry Fauske models), boron tracking, and non-condensable gas transport. This code is highly generic and can be used for simulation of a wide variety of hydraulic and thermal transients also in non-nuclear systems involving mixtures of steam, water, non-condensable and solute.

Based on one-dimensional, transient, non-homogeneous and non-equilibrium hydrodynamic model for the steam and liquid phases, RELAP5/Mod3 code uses a set of six partial derivative balance equations and can treat a non-condensable component in the steam phase. It is assumed to move with the same

velocity and have the same temperature as the vapor phase. Therefore, all properties of the gas phase are mixture properties of the steam/non-condensable mixture [5].

A semi-implicit numeric scheme is used to solve the equations inside control volumes connected by junctions. The fluid scalar properties (pressure, energy, density and void fraction) are the average fluid condition in the volume and are viewed located at the control volume center. The fluid vector properties, i.e. velocities, are located at the junctions and are associated with mass and energy flows between control volumes that are connected in series, using junctions to represents flow paths. The direction associated to the control volume is positive from the inlet to the outlet.

Heat flow paths are also modeled in a one-dimensional direction, using a staggered mesh to calculate temperatures and heat flux vectors. Heat structures and hydrodynamic control volumes are connected through heat flux. These structures are used to simulate pipe walls, heater elements, nuclear fuel pins and heat exchanger surfaces. There are many factors which influences the convective heat transfer coefficient correlation to use (e.g. presence of non-condensable; temperature of the wall; status of the fluid; geometry, etc.). An important factor that affects the magnitude of heat transfer coefficients, besides obvious parameters such as velocity, is the flow field or hydraulic geometry surrounding the surface. The flow field next to the wall influences the velocity profile and turbulence. The user can use pre-defined convection boundary types for available configurations (i.e. tube, parallel plates, vertical bundle with and without cross flow, horizontal bundle, etc.). No coding has been implanted for helical-pipes in vertical structures or bundle with staggered tubes, cross-flow in horizontal structures [9].

4.4.2. System idealization

4.4.2.1. System idealization for blind calculation

RELAP5 nodalization of OSU-MASLWR is simple and can be divided into five systems (Fig. 4-78): primary system (PS), secondary system (SS), High Pressure Containment (HPC), Cooling Pool Vessel (CPV), and six lines connecting the primary system with the HPC (i.e. 2 ADS vent, 2 ADS and 2 SUMP lines).

The primary system is modeled with five RELAP5 components:

- 2 BRANCH components represent the bottom region, connecting the downcomer (DC) part and the core zone and the region below the top plate of the primary system, which separates the PRZ zone, the ascending hot leg and steam generator (SG) entrance zone.
- 2 PIPE components, having 33 sub-volumes each, model the hot side (core zone, riser and hot leg) and the cold side (primary side steam generator, cold leg and downcomer).
- The PIPE component on the top represents the PRZ region

The secondary system is modeled with:

- 2 TIME DEPENDENT VOLUME and 1 TIME DEPENDENT JUNCTION components for setting the boundary conditions according with the test specifications (i.e. pressure at the outlet and coolant temperature and mass flow rate at the inlet);
- 2 PIPES components having 42 sub-volumes and representing the steam generator helical-coil tubes and the plugged tube.

The CPV and the HPC are modeled with two parallel stacks of PIPE and BRANCH components, representing the inner and the outer volumes. The CPV has cross-junctions connecting each sub-volume of the PIPE components. On the contrary, the HPC has cross connections, set-up according with the expected fluid paths in the system [10]. Both systems are connected on the top with a TIME DEPENDENT VOLUME representing the environment (i.e. atmospheric pressure) through a motor valve, which is operated on a high pressure signal, in the case of HPC and always open in the case of CPV.

The main features of the RELAP5 model are reported hereafter:

- The elevations of the different parts of the facility are maintained in the nodalization.

- A sliced approach is applied at all systems (i.e. primary, secondary, HPC, CPV and interfacing systems).
- The node to node ratio is kept uniform with a maximum ratio of 1.2 between adjacent sub-volumes.
- The helical-coil tubes of the steam generator are represented with a single equivalent tube using the "average" inclination angle of the real geometry, thus horizontal flow regime is applied.
- The heat transfer correlations applied for the helical-coil tubes inner side is "corrected" with a proper fouling factor.
- The cross connections of the HPC are set-up according with the expected fluid paths in the system.
- The energy loss coefficients in the junctions are evaluated or estimated on the basis of the system geometry [11, 12].
- The roughness is set 5.0 x 10^{-5} m with the exception of the core region and the SG tubes.
- The chocked flow is calculated using Henry Fauske model.
- The material proprieties are taken by the IAEA ICSP documentation [4], when available.

More information about the hydraulic and thermal structures data of the nodalization or the control actuated are reported in Refs. [13] and [15].

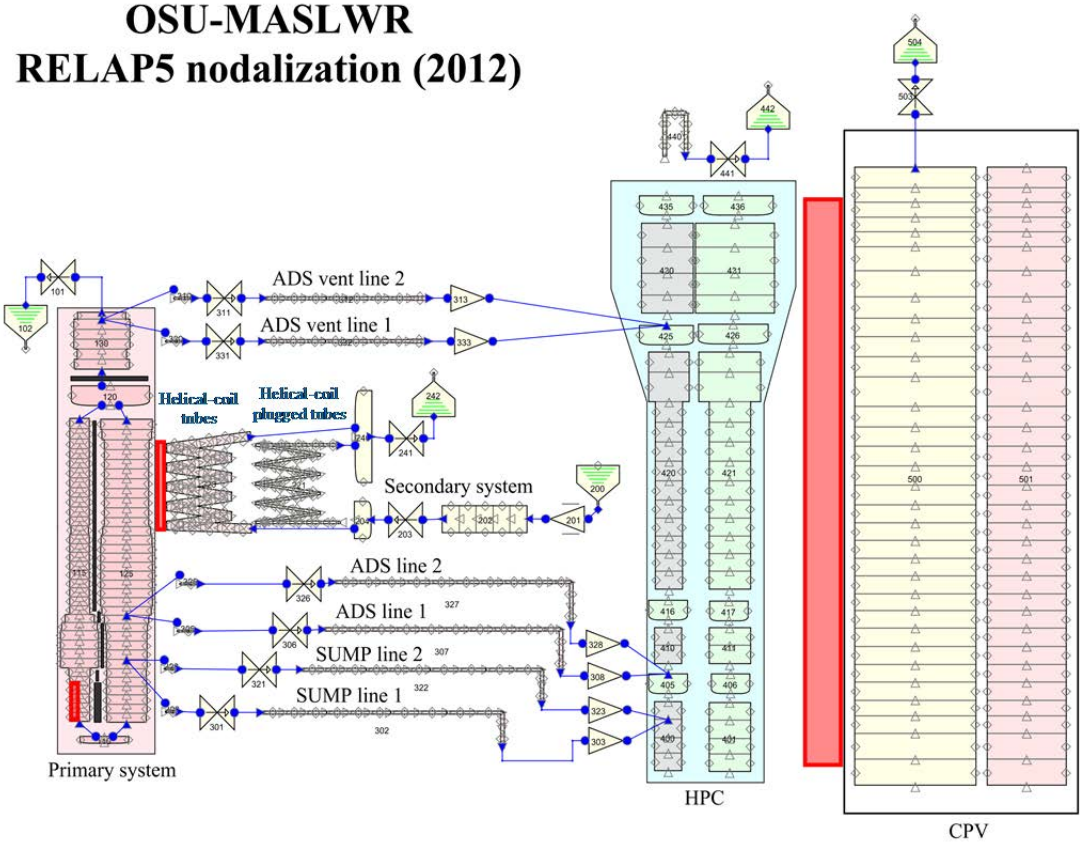

FIG. 4-78. ENEA nodalization, overall sketch.

4.4.2.2. Modeling change for open calculation

The open calculations of the tests SP2 and SP3 are carried out with few modifications in the input deck:

- The pressure drops of the primary system have been set-up according with the results of test SP3. The main contribution on the experimental measure data is the gravity head term. The experimental data of pressure drop in the system were available when the open calculation phase was completed.
- The heat exchange through the SG tubes secondary side has been modified in the range of powers, where a large overestimation was detected; see the conclusions in Ref. [14].

- The heat structure of the core power was corrected (typo error) with respect to the blind calculation of test SP2. Thus, 100% of the electrical power is available in the core instead of about 95% (this modification was already available in the blind calculation of test SP3).
- Henry Fauske critical flow model was changed with Ramson Trapp model. The gas phase discharge coefficient was reduced to 0.7, to avoid the over-prediction of the discharged mass [16].
- Modifications have been implemented in the control variable of the RPV level, which does not include the PRZ.
- The model of the CPV has been reviewed in order to improve the comparisons between the thermocouple measures and the code predictions. In particular, the hydraulic volumes, where the heat exchange is modeled, is drastically reduced in term of volume.

4.4.3. Analysis results for loss of feedwater transient

The test SP2 is a LOFW with ADS operation and long term cooling. The results of two code simulations are presented: the blind calculation, performed on the basis of selected initial and boundary conditions and the open calculation. The initial conditions of the experiment and at the end of the steady state calculations are compared in Table 4-5.

Steady state and initial conditions are achieved accordingly with the specifications for the blind calculation. Few minor deviations are observed among the code results and the experimental data. The main differences of the open calculations are connected with the modifications implemented in the input deck and reported in bullet 1 and 3 of section 4.4.2.2. The modification of the pressure drop in primary system, set-up on the basis of the SP3 open calculation (see next section), implied a larger mass flow rate in primary system, thus an overall reduction of the temperature difference across the core. The correction of the electrical core heat structure explains the larger overall energy in primary system achieved at the end of the steady state calculation.

The HPC and CPV are initialized with liquid water at 0.101 MPa(a) and 25°C. The upper volumes, above the liquid level free surface, are initialized with nitrogen. The HPC has a valve on the vessel top, which is activated on high pressure signal (> 2 MPa(a)) in HPC. The CPV system is opened during the overall transient.

The comparison of the resulting sequences of main events is reported in Table 4-6. Sample experimental and calculated parameter trends are reported below. The full set of comparisons is in Ref. [15].

Four phases and related phenomena are identified in the transient, as hereafter discussed. The following relevant TH phenomena are common to all phases of the transient. They are [17]: pressure drop at discontinuities; wall to fluid friction; heat transfer in covered core; heat transfer in passive structures and heat losses; global multidimensional coolant temperatures and flow distributions; and single phase natural circulation in primary system. Specific phenomena occurring/expected in each phase are reported hereafter.

Phase 1 – *increase of energy in primary system (0 - 51 s)*: from loss of FW up to the ADS vent valve 1 opening. Interesting phenomena for this phase are:
- condensation in stratified conditions (PRZ);
- heat transfer in SG primary and secondary sides;
- parallel channel instability in SG tubes.

Phase 2 – *primary system depressurization (54 - 131 s)*: from the ADS vent valve 1 opening up to the high pressure signal in HPC. Interesting phenomena for this phase are:
- critical flow at ADS vent valve 1;
- two phase natural circulation in primary system;
- pool thermal hydraulics in HPC and CPV;
- heat transfer across the HPC-CPV wall;
- thermal mixing and stratification in HPC and CPV;
- condensation in stratified conditions in the HPC wall and on the liquid free surface;
- non-condensable effect.

Phase 3 – *ADS vent valve 1 cycling (131 – 4024 s)*: from the first high pressure signal in HPC up to the low pressure difference between primary system and HPC. Interesting phenomena for this phase are:

- critical flow in valve (vapor phase);
- two phase natural circulation in connected primary system – HPC;
- pool thermal hydraulics in HPC and CPV;
- heat transfer across the HPC-CPV wall;
- thermal mixing and stratification in primary system, HPC and CPV;
- condensation in stratified conditions on the HPC wall and on the liquid free surface;
- boiler condenser mode in connected primary and HPC systems;
- non-condensable effect.

Phase 4 – *long term cooling (4024 – 15821 s)*: from the low pressure difference between primary system and HPC up to the end of transient. Interesting phenomena for this phase are:

- flow in valves (ADS and SUMP);
- two phase natural circulation in connected primary system – HPC;
- heat transfer across the HPC-CPV wall;
- thermal mixing and stratification in PS, HPC and CPV;
- boiler condenser mode in connected primary and HPC systems;
- non-condensable effect.

The test starts (phase 1) with the primary system in single phase natural circulation. The mass flow is driven from the balance between driving and resistant forces. Driving forces are the result of fluid density differences occurring between ascending (core side, inner zone) and descending sides (SG side, annular zone) of the main vessel. Resistant forces are due to irreversible friction pressure drops along the entire loop. The correct prediction of this phase is mainly connected with the calculation of the pressure drop in the system, thus the setup of the energy loss coefficients, the calculation of the heat exchange across the core and the SG (mainly for achieving the steady state conditions), the heat losses in primary system and the condensation in PRZ. The heat transfer in covered core is correctly calculated by the code. On the contrary, model deficiencies (convective heat transfer in the inner SG tubes) and user effect are critical issues for the heat transfer across the SG and for the pressure drop evaluations.

At time 0 s, the feedwater pump is switched off. From this time on, the loss of heat sink causes the unbalance of energy in the primary system, and the primary pressure (Fig. 4-79) starts to rise. The rate of pressure increase is driven by the difference between the core power (plus the heaters) and the heat losses, assuming that the total primary system mass inventory is correct (no experimental data is available). Once the first high pressure signal is met, the electrical core power is switched to decay heat mode. The coolant temperature difference across the core decreases rapidly (Fig. 4-80), nevertheless primary pressure continues to increase until the second high pressure signal (9.409 MPa(a)) in primary system is met (Fig. 4-79). This is the set point of the ADS vent valve 1 opening and of PRZ heaters off (beginning of phase 2).

The mass flow of steam discharged through the ADS vent valve 1 is calculated by the chocked flow model at the valve. The model Henry Fauske with default coefficients, used for the blind simulation, is expected to overestimate the single steam phase critical flow [8]. On the contrary, Ramson Trap model with the reduced gas phase discharge coefficient to 0.7, used for the open calculation, should adequately simulate the single gas phase critical flow [16]. Indeed, the opening of the valve at the top of the PRZ causes a large discharge of energy and a small discharge of mass from the primary system to the HPC, as demonstrated by the pressures (Fig. 4-79) and the levels trends (Fig. 4-81). This is evidenced by the experimental trend of the level in HPC, which increases smoothly. On the contrary, during the first discharge the code predicts liquid phase transported through the break (two phase critical flow) in both simulations, i.e. blind and open. No substantial difference is in both simulations, notwithstanding a sensible reduction of the maximum mass flow rate at valve opening in the open calculation.

The discharge of mass from the primary system towards the containment causes the increase of temperature of the water and of the metallic structures in HPC (Figs 4-83 and 4-84). The steam is condensed on the cold structures and on the liquid surface of the HPC. The energy is rapidly transferred through the heat exchanger plate to the CPV. This process is qualitatively predicted by the code simulations. In particular, the temperature increase in the higher part of the containment is observed also in the blind and open simulations (Fig. 4-83). Nevertheless, the wall temperatures, HPC and CPV sides, are rather underestimated. This might be explained with an incorrect set-up of the thermal capacity and conductivity of the plate material in the code simulations. Larger is the difference among the code calculations and the experimental results of the fluid temperatures in CPV (Fig. 4-85). In this case, this can be also connected with the position of the thermocouples in the facility, which measure a local temperature close to the plate structure (whereas the code provides a value averaged on a volume). This has been improved by means of the nodalization modification of the CPV, mentioned in section 4.4.2.2. Moreover, it should be noted that Figures 4-83 and 4-84 highlight the onset of coolant temperature stratification in HPC during this phase. The correct prediction of the coolant thermal mixing and stratification phenomena cannot be accurately predicted by RELAP5 code. However, they can be roughly calculated by means of “fictitious” 2D modeling of the tank, based on parallel stacks of pipes. The nodalization (or user) effect is crucial. Indeed, depending upon the nodalization scheme the mixing can be very limited or largely overestimated.

Once the high pressure signal in HPC is met (1.82 MPa(a)), the ADS vent valve 1 is closed (beginning of phase 3) to avoid the over pressurization of the system. This implies that the primary pressure increases again, whereas the HPC pressure decreases because the heat exchanged through the plate with the CPV (besides the heat losses). When the HPC pressure drops below 1.48 MPa(a), the ADS vent valve 1 is opened again. The cycling of the valve across the two set points (1.82 MPa(a) closure and 1.48 MPa(a) opening) lasts until the difference between the primary side and the HPC pressures is 0.034 MPa. This event is calculated after 4011 and 3882 s from the starting of the transient in the open and blind calculations respectively. Thus, it is slightly anticipated.

During this phase, at about 2000 s, the natural circulation in the primary system is almost at rest (Fig. 4-82). The figure highlights with spikes when the ADS vent valve is opened.

The low pressure difference signal between the primary system and the HPC represents the beginning of phase 4 with the full opening of 2 Sump and 2 ADS vent valves (cooldown procedure). The primary and the HPC systems are connected. The flow circulation between the systems is effective to remove the electrical core power through the HPC-CPV wall. No CHF conditions are observed during overall transient. The experiment is stopped at 15,821 s, with the primary system pressure equal to 0.51 MPa(a) and the coolant temperature at core outlet equal to 160°C. The blind (open) simulation predict a primary pressure equal to 0.33 MPa(a) (0.36 MPa(a)) and a coolant temperature of 145°C (150°C) after the same span of time.

In summary, the blind (and open) simulation demonstrates RELAP5 has the capability to reasonably predict the main phenomena and processes of the test. The trends of the primary system and HPC pressures are well predicted. Analogous considerations are applicable to the coolant temperatures in the primary system. Improvements might be possible if the knowledge of the experimental facility features/characteristics is improved too (e.g. materials). However, some phenomena occurring in the test are challenging for the models and correlations of the code (e.g. coupling primary system containment, the condensation in presence of non-condensable in the HPC). Some other phenomena, such as the mixing and thermal stratification in HPC, notwithstanding simulated, are beyond RELAP5 capabilities and only bounding analyses are possible.

TABLE 4-5. STEADY-STATE COMPARISON (SP-2)

Parameter	Tag No	Unit	Exp	Blind Calc	Open Calc
PRZ pressure	PT-301	MPa(a)	8.72	8.64	8.71
PRZ level	LDP-301	m	0.36	0.33	0.35
Power to core heater rods	KW-101/102	kW	--	297.3	299.7
FW temperature	TF-501	ºC	21.4	20	21.4
Steam temperature	FVM-602-T	ºC	205.4	202	203.6
Steam pressure	FVM-602-P	MPa(a)	1.41	1.45	145
Ambient air temperature	--	ºC	--	24	20
HPC pressure	PT-801	MPa(a)	0.127	0.135	0.135
HPC water temperature	TF-811	ºC	26.7	23.1	24.8
HPC water level	LDP-801	m	2.82	2.88	2.86
CPV water temperature	TF-815	ºC	--	23	24.8
PS flow at core outlet	FDP-131	kg/s	--	1.48	1.80
PS coolant temperature at core inlet	TF- 121/122/ 123/124	ºC	215.0	210	213
PS coolant temperature at core outlet	TF-106	ºC	251.5	250	248.5
Feedwater flow	FMM-501	kg/s	--	0.126	0.126
Steam flow	FVM-602-M	kg/s	--	0.126	0.126
PS coolant subcooling at core outlet	--	ºC	--	50	51.5
Total heat loss through PS	--	kW	--	--	4.7
Heat transfer through SG	--	kW	--	278	295
Max. surface temp. of core heater rods	--	ºC	--	303	302
Location from the SG secondary inlet to reach - saturation - superheat	--	m	--	Heated length (0-6.15) 1.7 5.2	Heated length (0-6.15) 1.55 4.85

TABLE 4-6. RESULTING SEQUENCE OF MAIN EVENTS (SP-2)

Phase	Event	Time (S)		
		Exp.	Blind Calc.	Open Calc.
Phase I (0-51s)	Start of simulation – steady state	0	0	0
	Stop MFP. Close HPC vent valve SV-800	0	0	0
	PT-301 (P_{PRZ}) = 9.064 MPa(a)(1300 psig). Enter decay power mode	30	37.4	34.2
	PT-301 (P_{PRZ}) = 9.409 MPa(a) (1350 psig) PZR heaters off. Open ADS vent valve (PCS-106A)	48	54	54
Phase II (54-131s)	1^{ST} closure of ADS vent valve (PCS-106A)	131	168	155
Phase III (131-4024 s)	Record opening and closing times for PCS-106A	Ref. [15]		
	Record opening and closing times for SV-800	--	--	
Phase IV (4024-15821 s)	Long-term cooling: PT-301 (P_{PRZ}) - PT-801 (P_{HPC}) < 0.034 MPa (5 psi) PCS-106A/B, PCS-108A/B opened	4024	3882	4011
	End of test if (or): - PZR pressure ≤ 0.135 MPa(a) (5 psig) - Primary coolant temperature (TF-132) ≤ 35 ºC - 5 hours have elapsed	15821	15821	15821

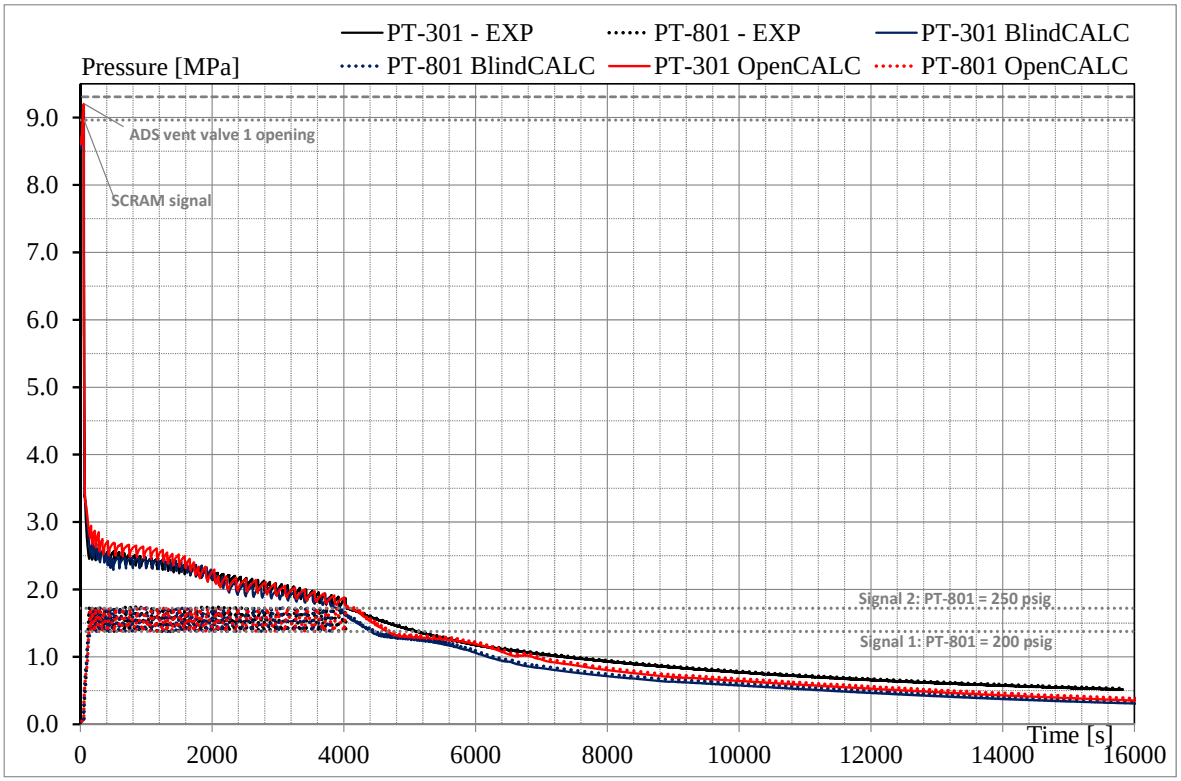

FIG. 4-79. Primary and HPC pressures (absolute, SP-2).

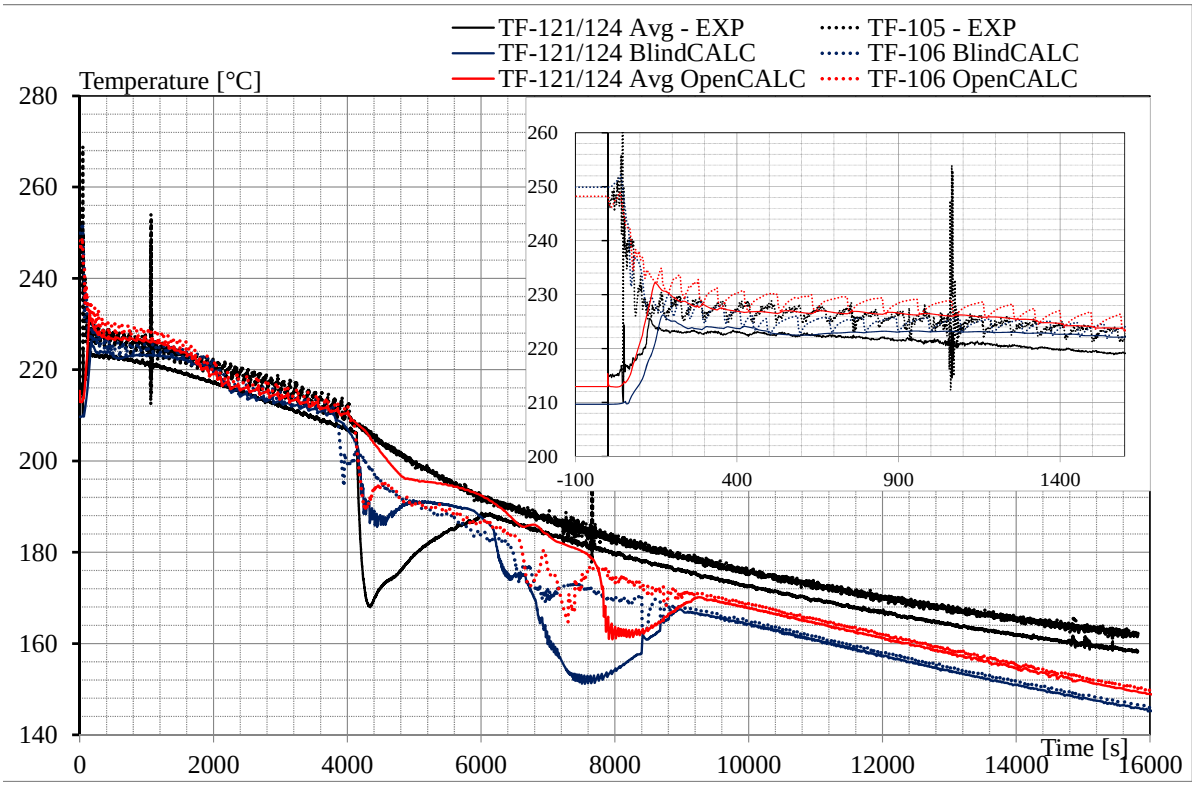

FIG. 4-80. Primary coolant temperatures at core outlet and at SG outlet (dotted line, SP-2).

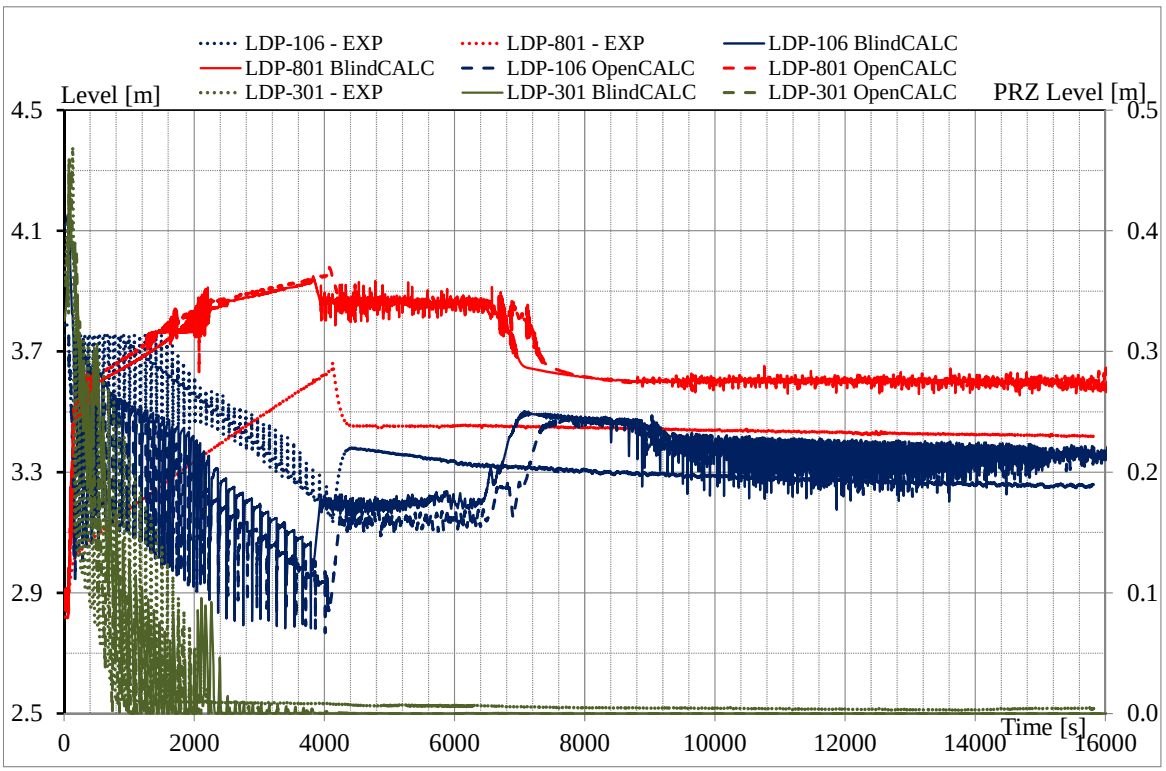

FIG. 4-81. Primary system, HPC and PRZ levels (SP-2).

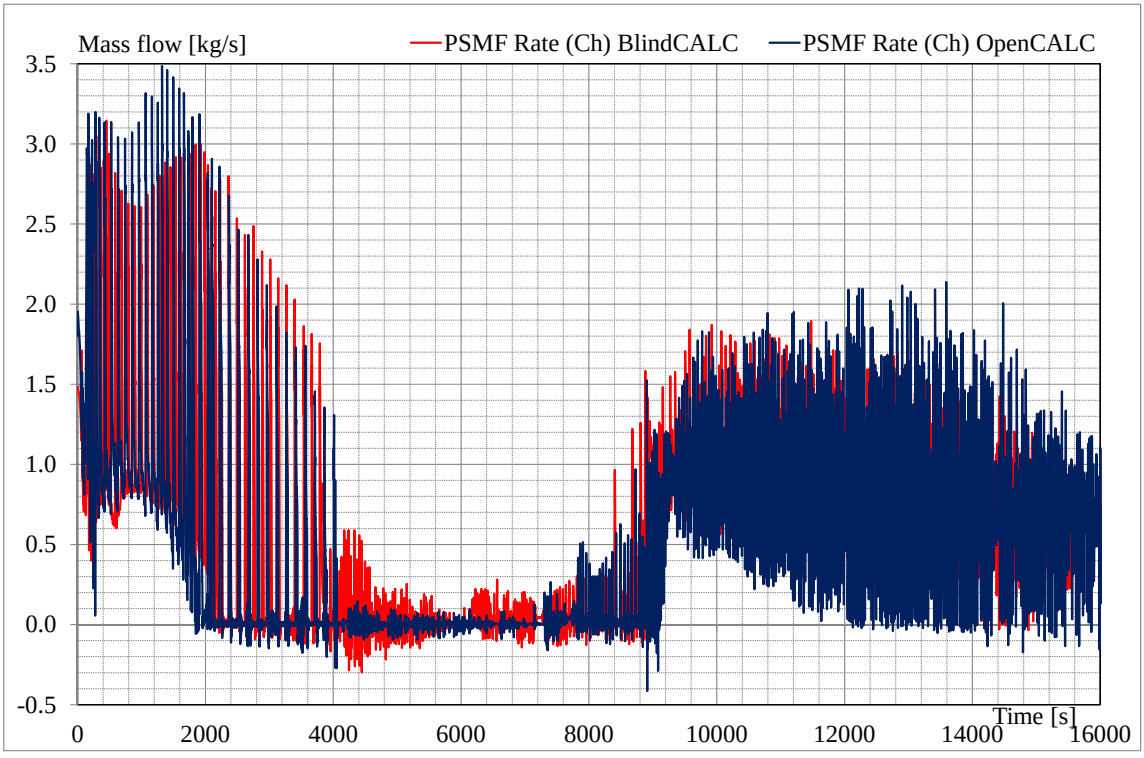

FIG. 4-82. Primary coolant mass flow rate at hot leg riser (SP-2).

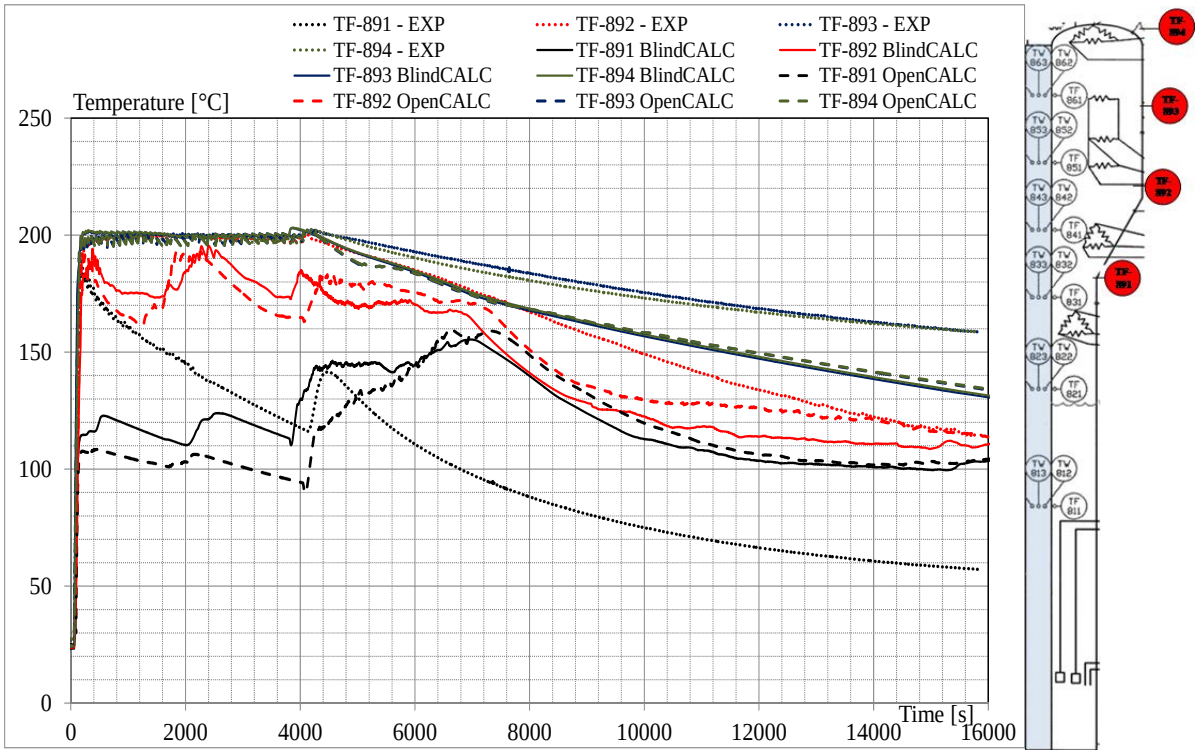

FIG. 4-83. Coolant temperatures in HPC (SP-2).

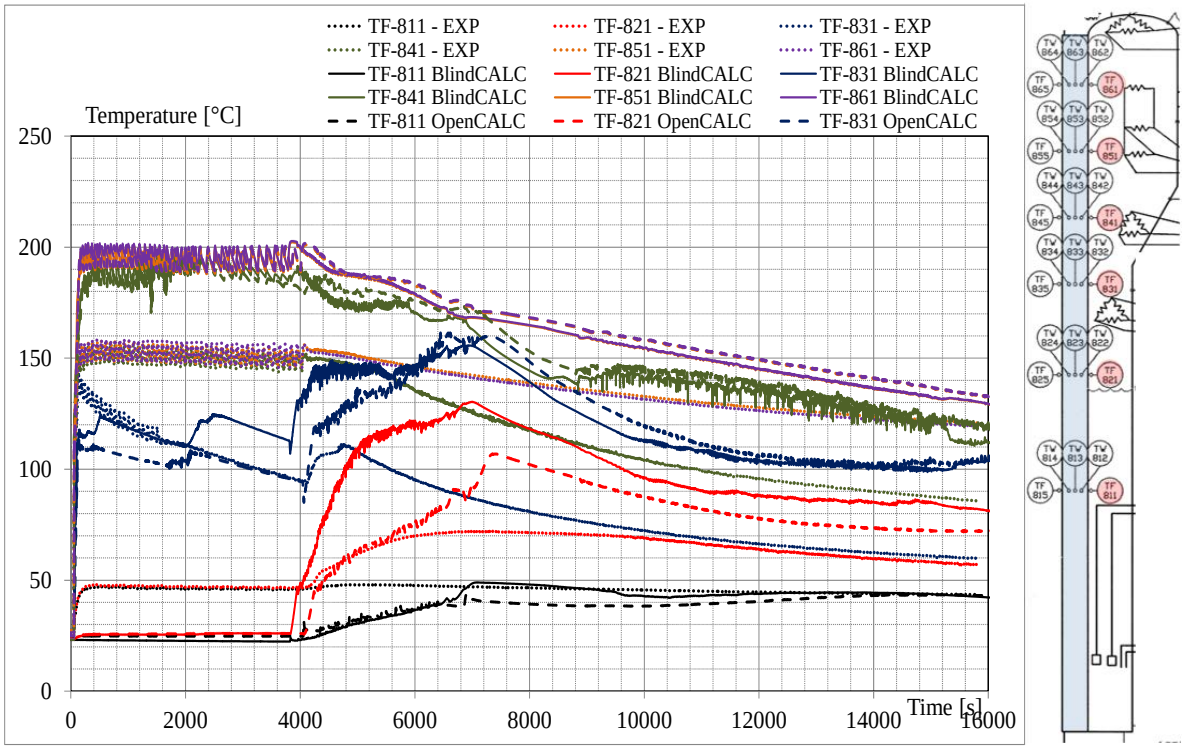

FIG. 4-84. Coolant temperatures in HPC close to HPC- CPV heat exchange plate (SP-2).

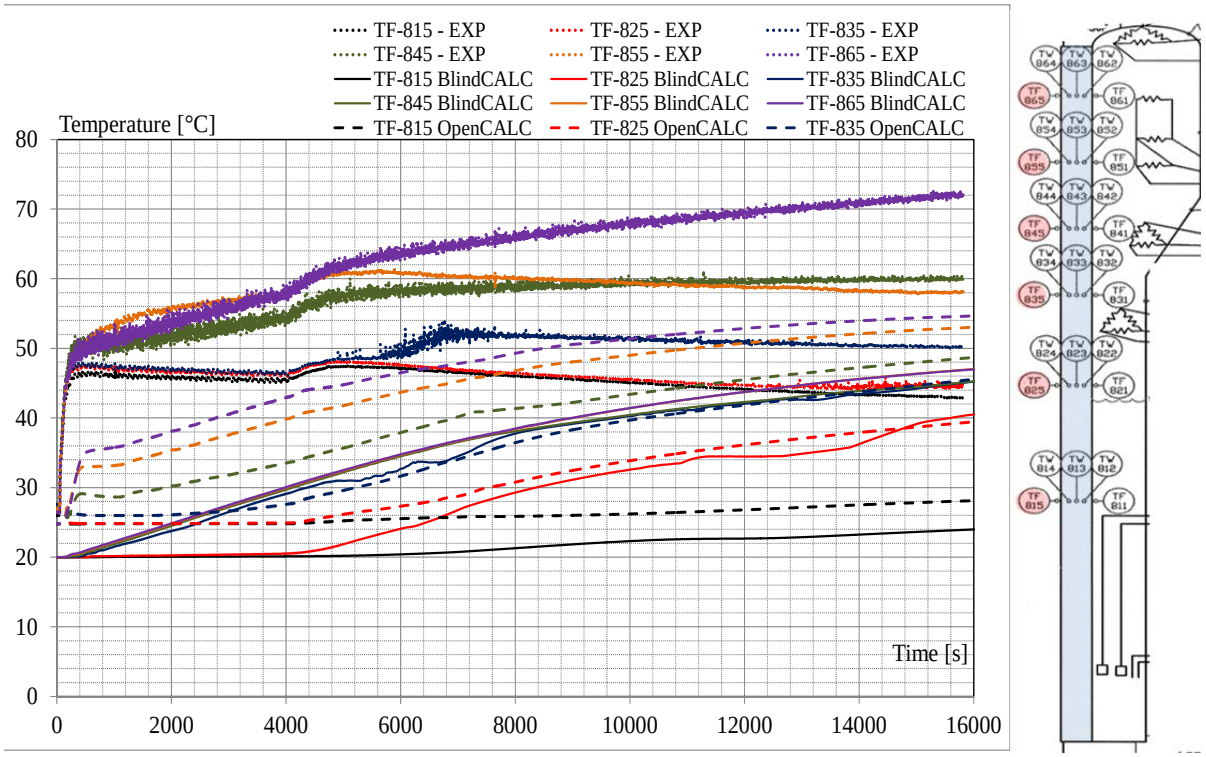

FIG. 4-85. Coolant temperatures in CPV close to HPC- CPV heat exchange plate (SP-2).

4.4.4. Analysis results for power maneuvering

The nodalizations used for the blind and open calculations do not differ from those applied for the simulations of test SP2, discussed in section 4.4.3.

The experiment is a natural circulation test at different core power levels (from 40 to 320 kW). Only the primary and the secondary systems are involved in the analysis. Single phase natural circulation is expected in primary system during overall transient. The initial conditions of test and of code simulations are reported in Table 4-7. They are achieved accordingly with the specifications [4], after a null transient of 3000 s.

Few minor deviations are observed. The simulations evidence a coolant temperature at core inlet rising with a rate of about 0.004°C/s. This is considered acceptable and, also, observed in the experimental data. Indeed, the thermal balance calculated with the available data implies that a stable condition is achievable only if the heat losses in primary system are larger than 11 kW (about double than in the RELAP5 model). According with the experimental data, the power removed by the SG is less than 29 kW, which is calculated assuming that the superheated steam at the outlet of all tubes is 262°C. Assuming (conservatively) that the pressurizer heaters are switched off (power equal to 0 kW), and considering that the core power is 40 kW, the balance of power in the system is achieved with 11 kW of heat losses.

The main difference between the experimental and the code results is the temperature of the vapor at SG tubes outlet. The calculated temperatures are about 262°C, which are close to the most frequently measured temperatures at the outlet of the SG tubes. On the contrary, the experimental measure of steam temperature in steam line, recorded by the transducer FVM-602-T, is not reliable at the beginning of the transient. Indeed, it is affected by the thermal inertia of the cold metallic structures, which are not pre-heated [18].

Finally, some considerations shall be done with respect to the mass flow rate at the beginning of the transient. The measured mass flow rate is 0.50 kg/s, see Table 4-7. The blind calculation overestimates the mass flow rate, whereas it is well matched in the open simulation. This difference is explained with the modification of the input deck mentioned in the first bullet of section 4.4.2.2, using Reynolds depended energy loss coefficients. Nevertheless, it is observed that the temperature difference between

core inlet and outlet is ~ 12°C, 12°C and 15.5°C in the experiment, blind and open calculations, respectively. The code results might be both correct and are inconsistent with the experimental values of coolant temperatures across the core and of mass flow rate.

The code simulations are set up imposing the core power, the FW flow and temperature versus time (according with the specifications [4]). The PRZ heaters are operated to control the primary pressure stable. Sample experimental and calculated parameter trends are reported below. The full set of comparisons is in Ref. [15]. The relevant thermal-hydraulic phenomena and processes of the test are:

- pressure drop at discontinuities;
- wall to fluid friction;
- condensation in stratified conditions (in PRZ);
- global multidimensional coolant temperatures and flow distributions;
- heat transfer in covered core;
- heat transfer in SG primary and secondary sides;
- heat transfer in passive structures and heat losses;
- parallel channel instability in SG tubes;
- single phase natural circulation in primary system.

The test starts with the system in single phase natural circulation. The mass flow (Fig. 4-86) is driven from the balance between driving and resistant forces (as described in section 4.4.3 for the phase 1). The correct prediction of this phase is mainly connected with the calculation of the pressure drop in the system (estimated on the basis of the geometry for the blind calculation and set-up accordingly with the experimental result of mass flow rate in the open calculation), and the calculation of the heat exchange across the core and the SG. No “quasi” steady state conditions are achieved after about 1000 s up to about 3000 s (power range 120 – 200 kW) in the blind simulation. This is highlighted by the coolant temperature trends in primary system (Fig. 4-88).

The calculated heat exchange highlights that the convective heat transfer inside the SG tubes is under-predicted, from 1000 to 3000 s. Pseudo stationary conditions are roughly achieved for the others power levels. The larger increase of coolant temperature observed in the blind simulation after 3000 s is explained with the lower mass flow rate, as demonstrated by the open calculation results. The open calculation shows a reasonable prediction of the parameter trends in the time interval 1000 – 3000 s, which has been achieved increasing the convective heat transfer in the steam generator tube side (Fig. 4-91). This is also evident by the steam temperature trends in Figure 4-90. The open calculation shows an improved prediction of the coolant temperature at the SG tube outlet, which is largely under-estimated in the blind calculation.

The duration of each plateau in the experiment would be longer to ensure the parameter trends are stabilized, with particular regards to the SG steam temperatures at tubes outlet and in the steam line (Fig. 4-90). The experimental FW flow (Fig. 4-89) is inconsistent (larger) with the overall power to be removed between 2700 and 3700 s (Fig. 4-91). As consequences, during this time the primary pressure (Fig. 4-86) is kept constant by PRZ heaters in the test and in the simulations. During this time interval, water is injected in the experiment from the bottom of the RPV [18]. The injection is implemented in the open calculation, but not in the blind simulation because the information was not available. No CHF conditions are met in the simulations as well as in the experimental results during the overall transient.

In summary, the blind and open simulations demonstrate RELAP5 has the capability to reasonably predict the main phenomena and processes of the test. It is observed that the availability of a specific correlation for helical-coil tubes would be useful to improve the prediction of the convective heat transfer the steam generator.

TABLE 4-7. STEADY-STATE COMPARISON (SP-3)

Parameter	Tag No	Unit	Exp.	Blind Calc.	Open Calc.
PRZ pressure	PT-301	MPa(a)	8.72	8.70	8.71
PRZ level	LDP-301	m	0.36	0.347	0.35
Power to core heater rods	KW-101/102	kW	40	40	40
FW temperature	TF-501	ºC	31.5	31.5	31.5
Steam temperature	FVM-602-T	ºC	205.4*	262.0	262.3
Steam pressure	FVM-602-P	MPa(a)	1.35	1.45	1.35
Ambient air temperature	--	ºC	--	24.0	20.0
PS flow at core outlet	FDP-131	kg/s	0.50	0.677	0.49
PS coolant temperature at core inlet	TF-121/122/ 123/124	ºC	250-251	253.0	251.5
PS coolant temperature at core outlet	TF-106	ºC	262-263	264.8	267.4
FW flow	FMM-501	kg/s	0.0102	0.0102	0.0102
Steam flow	FVM-602-M	kg/s	--	0.0102	0.0102
PS coolant subcooling at core outlet	--	ºC	--	36.5	33.7
Total heat loss through PS	--	kW	--	6.7	6.1
Heat transfer through SG	--	kW	--	29.0	29.0
Max. surface temp. of core heater rods	--	ºC	--	264.9	268.0
Location from the SG secondary inlet to reach - saturation - superheat	--	m	--	Heated length (0-6.15) 0.38 0.96	Heated length (0-6.15) 0.20 0.80
* *from 242 to 260°C at SG tubes outlet.*					

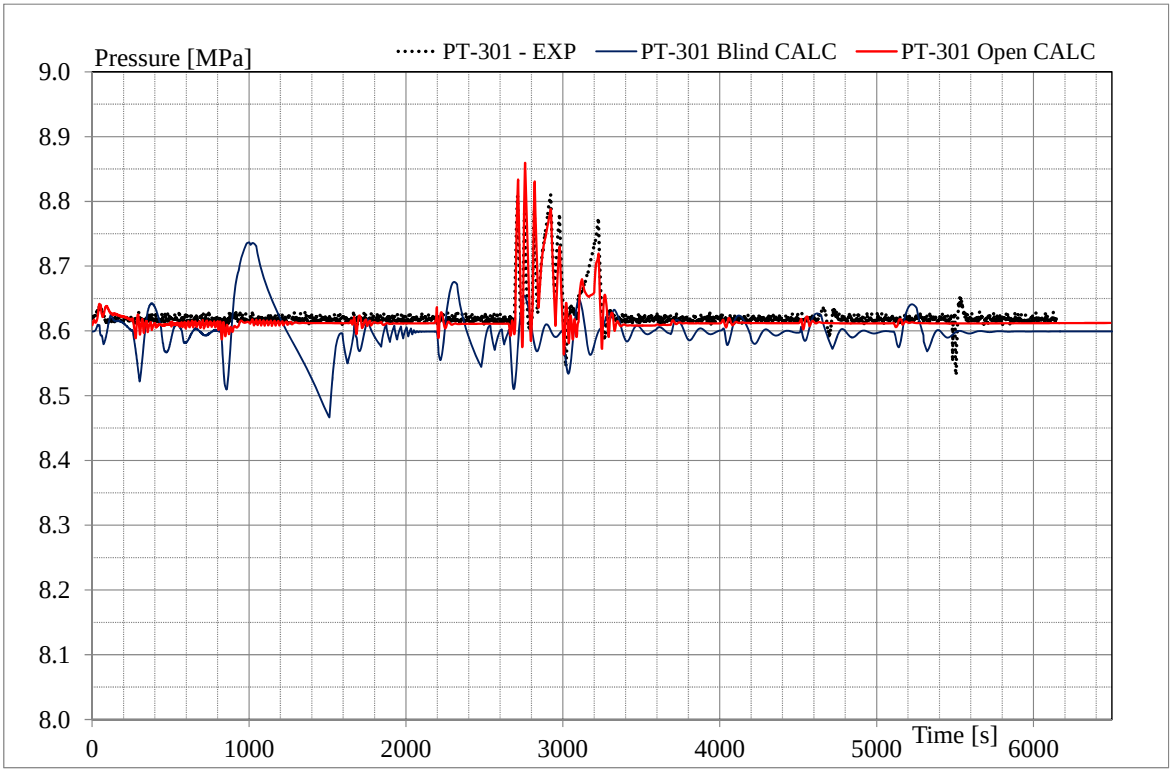

FIG. 4-86. Primary pressure (absolute, SP-3).

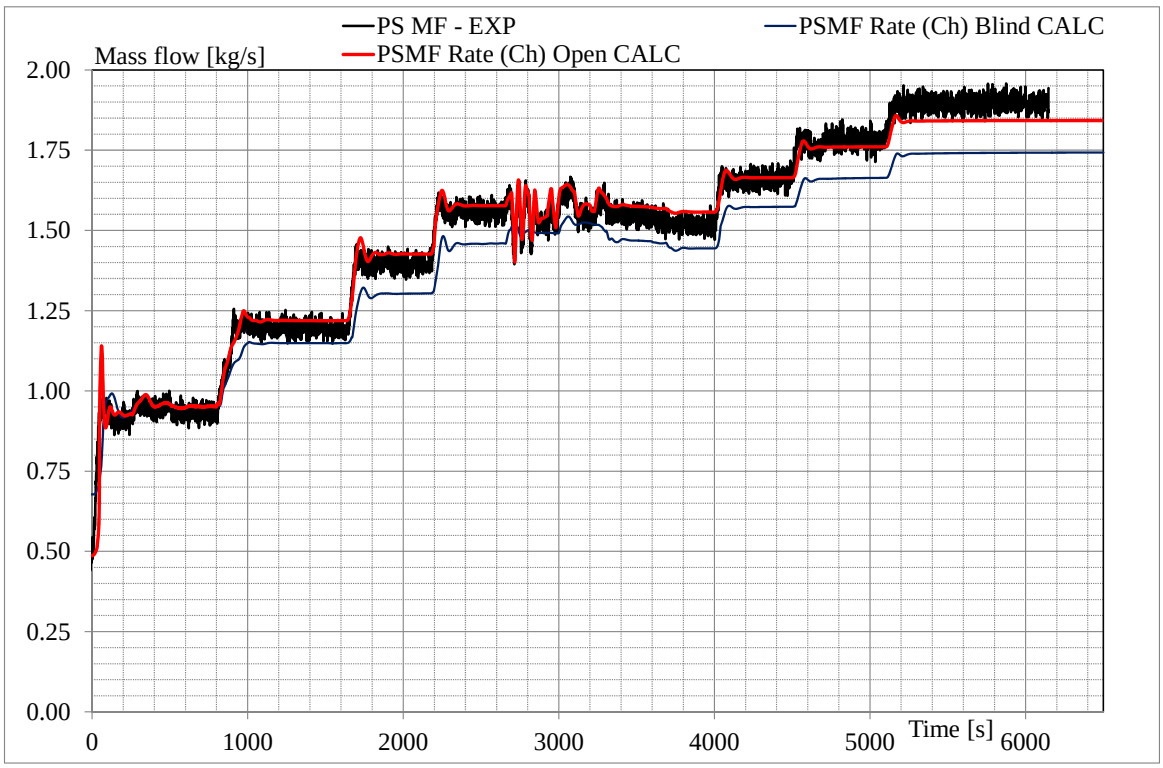

FIG. 4-87. Primary coolant mass flow rate at hot leg riser (SP-3).

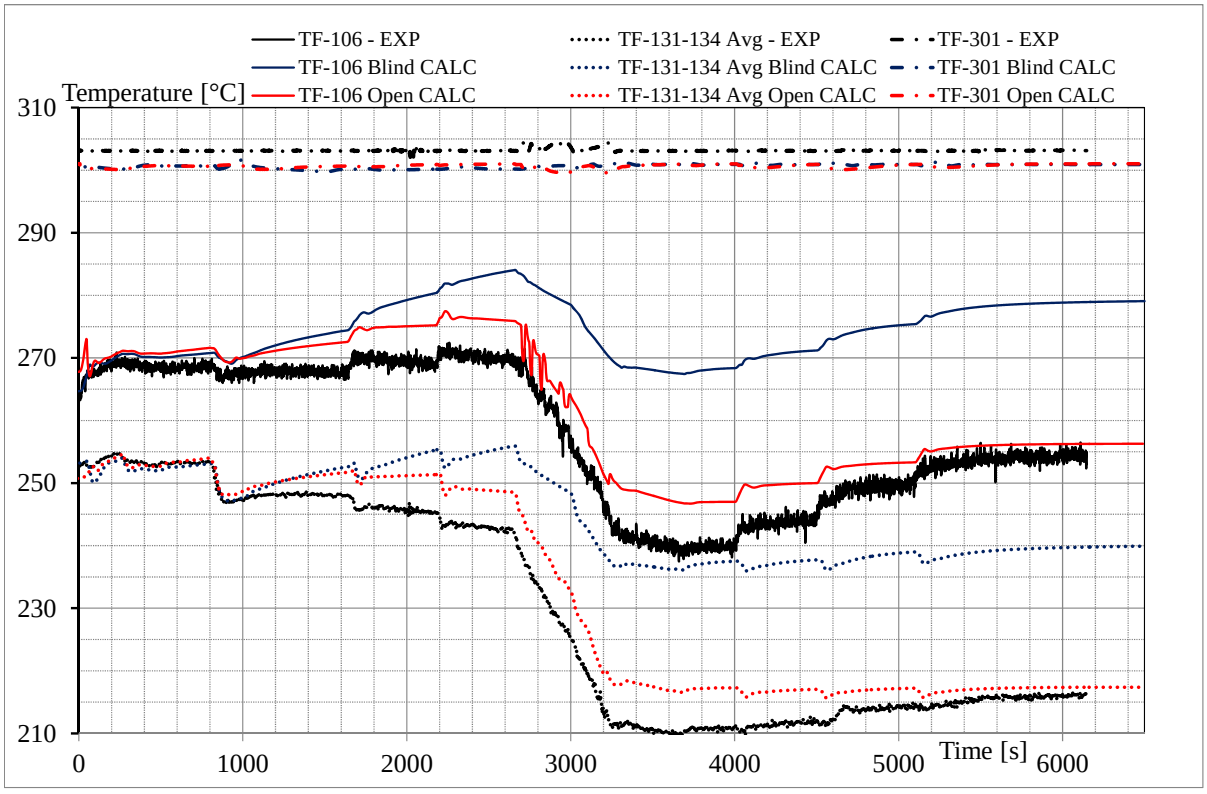

FIG. 4-88. Primary coolant temperatures at core outlet, at SG outlet (dotted line) and PRZ (SP-3).

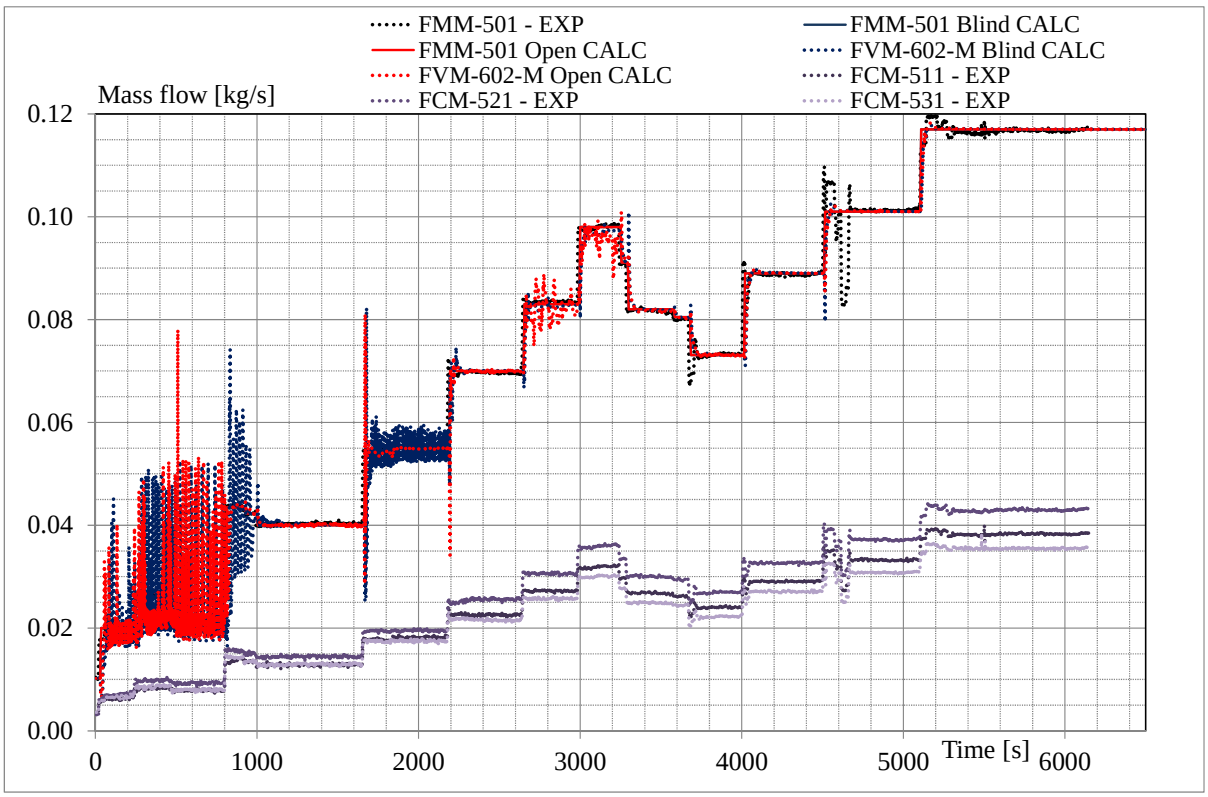

FIG. 4-89. FW (FMM-501) and steam (FVM-502) line mass flow rate (FCM-511, FCM-521, FCM-531 FW experimental mass flow rate in each SG tube group, SP-3).

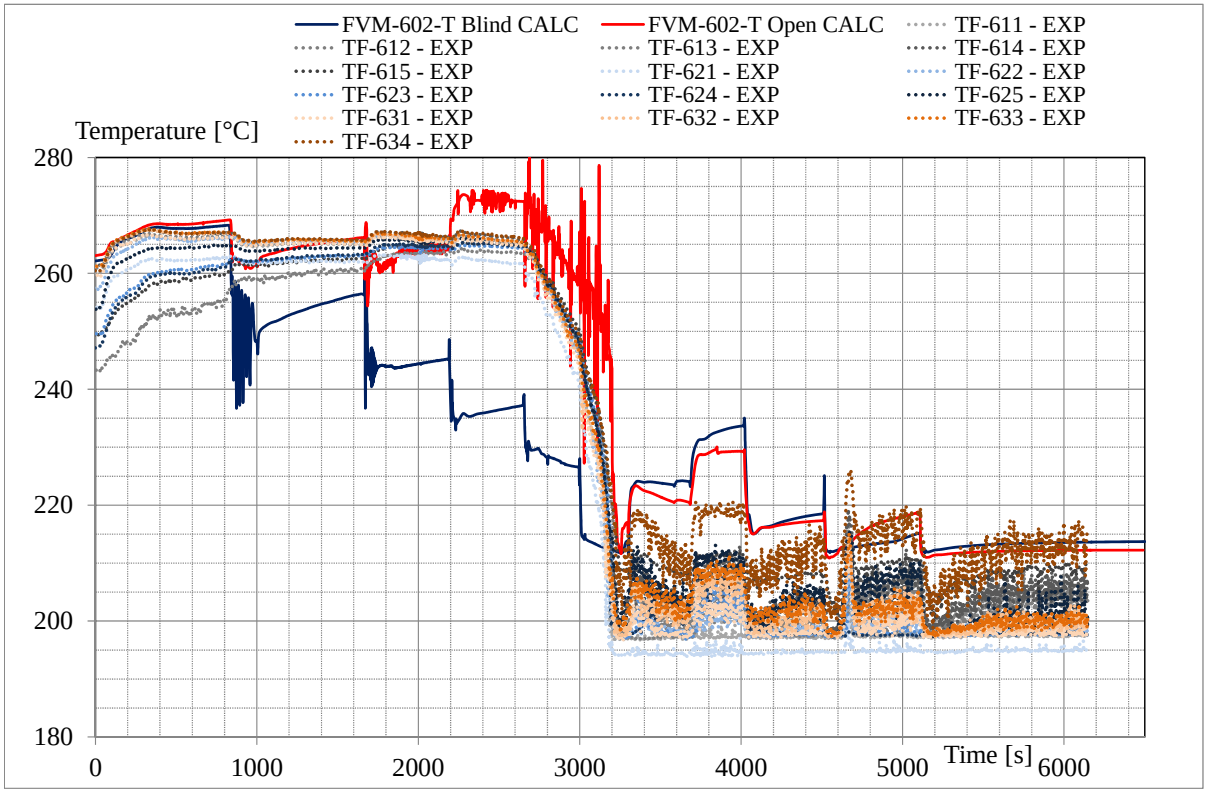

FIG. 4-90. SG secondary temperatures (SP-3).

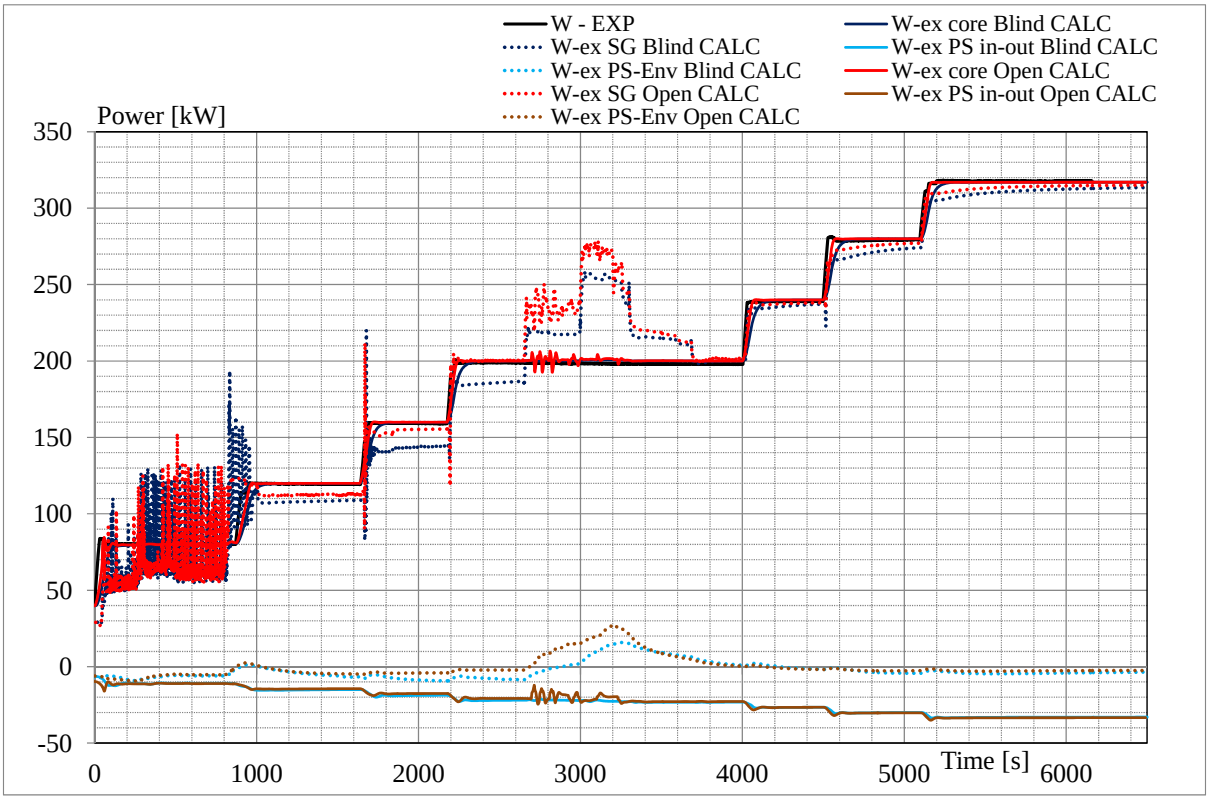

FIG. 4-91. Power transferred to fluid in the core, power exchanged in SG, across the chimney and heat losses (SP-3).

4.5. GIDROPRESS — RUSSIAN FEDERATION

4.5.1. Computer codes

Russian thermal hydraulic code KORSAR/GP was used for blind and open calculations of MASLWR thermal-hydraulic behaviour during the SP-2 and SP-3 experiments. KORSAR/GP is a best estimate code and it is intended for analyses of LWR processes in steady-state, transient and accident conditions. Modelling of thermal hydraulic processes in KORSAR/GP is carried out on the basis of completely non-equilibrium two-fluid model (three conservation equations for water and steam phases) in one-dimensional approach.

Possibility to model of the specific physical phenomena is provided. They are the behaviour of non-condensable gases, choked flow, “flooding” of water and water steam counter flows, heat exchange crisis with boiling in coolant and steam-generating channels, reflooding, two-phase flow stratification in vertical channels, radiation heat exchange, etc.

Basic principles of numerical scheme model:

– Balance method of differential conservation equation writing.
– Chess grid.
– Donor principle of writing convective members of equation (upwind difference scheme).
– Semi-implicit numerical scheme.
– Linearization of implicit members of equation (non-iterative scheme).

4.5.2. System idealization

4.5.2.1. System idealization for blind calculation

The main modeling assumptions used for Blind Calculation as follows:

– All core heaters are lumped together.
– All SG coil tubes are lumped together.
– Three helical SG coils are modeled as single pipe volume with the flow and heat transfer areas kept the same.
– Two parallel channels, connected with each other, were used for HPC modelling.
– Each pair of ADS lines is modeled as single equivalent channel.
– Choked flow model is implied at all valves on vent lines.
– PRZ heaters, HPC heaters, feed water lines are not modeled.
– A surface roughness of 1.0×10^{-6} m was used for all MASLWR components.
– The KORSAR nodalization diagram of the MASLWR test facility is shown in Figure 4-92. It contains the main components and features of the test facility, see Table 4-8.
– All the geometric data have been collected or calculated from information found in [4, 11, 19].

TABLE 4-8. ELEMENTS OF THE KORSAR NODALIZATION SCHEME

KORSAR Component	KORSAR Component Type	MASLWR Region
Ch100, Ch1, Ch2, Ch3, Ch30	Channel	Primary system
Ch10, Ch20, Ch40	Channel	Secondary system
Ch200, Ch300	Channel	High pressure containment
Ch400, CH500 *	Channel	Cooling pool
Ch106, Ch107, Ch108	Channel	ADS lines
VAL106, VAL107, VAL108	Valve	ADS valves
HCS1	Heat structure	Core heater rods
HCS4, HCS3, HCS22, HCS25	Heat structure	RPV wall RPV Features
HCS10	Heat structure	SG tubes
HCS20, HCS23, HCS24	Heat structure	Steam drum
HCS40	Heat structure	Steam line wall
HCS200, HCS201	Heat structure	HPC wall
HCS106	Heat structure	Vent line (PCS106) wall
HCS300	Heat structure	Heat transfer plate
HCS30 *	Heat structure	Pressurizer heaters
bvol_t1, bvol_t2, bvol_t3	Boundary cell	-
bljun_1	Impenetrable connection	-
* for open calculation only		

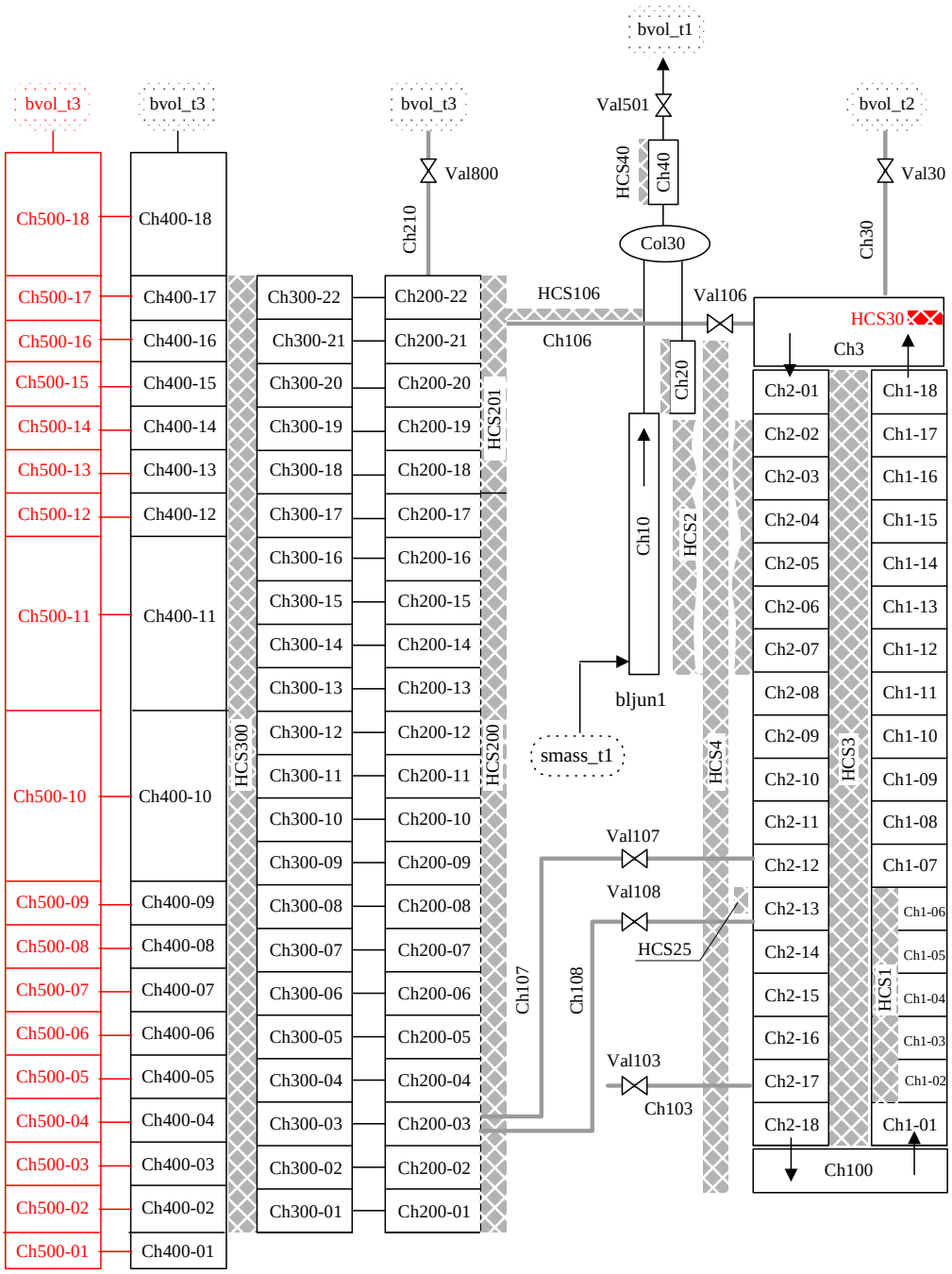

FIG. 4-92. KORSAR nodalization diagram of the MASLWR test facility – open calculaton.

4.5.2.2. Modelling change for open calculation

After the analysis of the SP-2 and SP-3 experimental data the following changes were made for nodalization scheme used for open calculation:

- The steam line pressure (PT602) is used as the secondary side boundary condition for transient.
- The geometrical characteristics of two vertical channels located inside the HPC which model the thermal heat boundary layer (Ch300) near the heat transfer plate and other HPC volume (Ch200) are changed. Ch300 cross section area is significantly less than Ch200 one in open calculation. For blind calculation the cross section areas of both channels were equal each other.
- One channel model was used for cooling pool vessel in blind calculation. Two channels located inside the cooling pool vessel model the thermal heat boundary layer near the heat transfer plate (Ch400) and other CPV volume (Ch500) in open calculation. The elements of the channels Ch400

and Ch500 are connected by the junctions. Ch400 cross section area is significantly less than Ch500 one.

– Heat transfer plate is modeled as two dimensional heat structures.
– The pressurizer heaters and additional heat losses are modeled for SP-3 open calculation.

Modeling changes for open calculation are shown in red in Figure 4-92 and Table 4-8.

4.5.3. Analysis results for loss of feed-water transient

4.5.3.1. RPV thermal-hydraulic behavior

SP-2 time sequence of events is summarized in Table 4-9. After the MFP trip and HPC vent valve SV-800 closing the pressurizer pressure increases up to 9.064 MPa(a) at 17 s (Fig. 4-93) and core power becomes equal to decay power.

After the PCS-106A opening (53 s) the primary pressure is fast decreasing and becomes equal to the saturation pressure at ~85 s. During the blowdown and long-term cooling stages the primary pressure is slowly decreasing due to the core power decreasing and vapor release through PCS-106A and PCS-106B. Natural circulation (single phase) at the beginning of transient and natural circulation (two phase) at the blowdown stage takes place (Figs 4-95 and 4-96). As primary pressure is going down, the primary mass flow rate is decreasing too. The ejection of vapor from RPV to HPC leads to RPV water level decrease to upper edge of the chimney and later on to SG inlet. Average value of void fraction at core outlet is about 0.1 during blowdown stage (Figs 4-97 and 4-98). Chocked flow phenomenon takes place in the vent line A.

At the moment of opening the valve the mass flow rate through PCS-106A is about 0.68 kg/s, then it is decreasing, and at the moment of the first PCS-106A closing it is less than 0.07 kg/s. At second opening the peak value of flow rate doesn't exceed 0.08 kg/s and every next value becomes lower than the previous one. After 4105 s the vent valves are kept open, and the flow rate slowly decreases due to primary cool down.

Start of long-term cooling is obtained as 4143 s. At this time cumulative discharge through PCS-106A from primary circuit into HPC is about 50 kg. The void fraction in upper part of RPV is equal to 1.

TABLE 4-9. SP-2 TIME SEQUENCE OF EVENTS

Event	Time (s)		
	Experiment	Blind	Open
Start of simulation – steady state	-	from -1000.0 to 0.0	
Stop MFP Close HPC vent valve SV-800	0.0	0.0	0.0
PZR pressure (PT-301) reaches 9.064 MPa(a) (1300 psig) Enter decay power mode	18.0	17.0	35.0
De-energize PZR heaters Open ADS vent valve (PCS-106A)	48.0	53.0	47.0
Record opening and closing times for PCS-106A	See Table 4-10		
Record opening and closing times for SV-800	No opening		
Start long-term cooling when pressure difference between primary system and HPC (PT-301 minus PT-801) becomes less than 5 psi (0.034 MPa) Open and remain open of PCS-106A and PCS-106B Open and remain open of PCS-108A and PCS-108B	4024.0	4143.0	4250.0
End of test when one of the following conditions is reached: - PZR pressure (PT-301) ≤ 0.61 MPa(a) (75 psig)	15820.0	14000.0	14800.0

TABLE 4-10. SP-2 PCS-106A OPERATION

# of Events	Experiment		KORSAR BLIND		KORSAR OPEN	
	Open (s)	Close (s)	Open (s)	Close (s)	Open (s)	Close (s)
1	48.00	131.00	54.00	147. 00	47.00	85.00
2	165.00	175.00	178.00	188.00	100.00	118.00
3	222.00	231.00	228.00	237.00	137.00	154.00
…	…	…	…	…	…	…
46	3917.00	3938.00	…	…	3982.00	4018.00
47	4024.00	null	…	…	4112.00	null
…			…	…		
53			4003.00	4034.00		
54			4105.00	null		

4.5.3.2. SG thermal-hydraulic behavior

Steam generator tube wall heat transfer and reactor power are equal at the start of the transient. At the time 0.0 s according to SP-2 procedure the feedwater flow to SG was terminated. At the same time the vapor flow from SG was terminated, too. After the feedwater loss the heat transfer to secondary side is decreased to about zero. During the transient the heat transfer in SG is directed to primary coolant, therefore the secondary side temperature and pressure follow to the primary coolant parameters (see Figs 4-99 and 4-100).

4.5.3.3. HPC thermal-hydraulic behavior

A rapid increase of the HPC pressure takes place, but it does not exceed the limit for SRV-800 opening (Fig 4-100). During ADS actuation pressure drops behavior are in accordance with water level drop and pressure decreasing (Figs 4-101 and 4-102). The volume of the HPC is filled with steam condensing in the containment wall transferring energy to the CPV (Figs 4-103 and 4-104).

Thermal stratification in the HPC and in the CPV is observed (Figs 4-105 and 4-106). The water and heat transfer plate (HTP) temperatures in the low part of HPC depend on the depth of penetration of steam jet in water volume.

From the analysis of the SP-2 experimental data it results, that the thermal heat boundary layer is located inside the HPC near the heat transfer plate. This layer is formed in result of the contact of the steam jet from PCS-106A and HPC wall. After the contact the steam flows down along the wall and reaches the HPC bottom. The boundary layer temperature is significantly higher than steam and water temperatures inside the other HPC volume. The boundary layer is not modeled for the blind calculation. This phenomenon is taken into consideration for the open calculation.

When the pressure differences between the RPV and HPC are less than 0.034 MPa, PCS 106 A and B and PCS 108 A and B stay permanently open. During the interval from 4143 to 4400 s the mass flow through PCS-108A (PCS-108B) has the direction from RPV to HPC, because of the steam mass flow through PCS-106A/B line after one opening isn't enough for the HPC pressure stabilisation. The reason of this phenomenon is the incorrect large value of the loss coefficient for PCS-106A/B line. For open calculation the value of loss coefficient for PCS-106A/B line is reduced, so water flow is directed to the RPV after PCS 108 A and B opening (Fig. 4-107).

4.5.3.4. CPV thermal-hydraulic behaviour

The HPC wall is cooled down via the heat plate (between CPV and HPC). There is the thermal heat boundary layer located inside the CPV near the heat transfer plate. The boundary layer temperature is significantly higher than steam and water temperatures inside the other CPV volume. This phenomenon is also taken into consideration for the open calculation (Fig. 4-108).

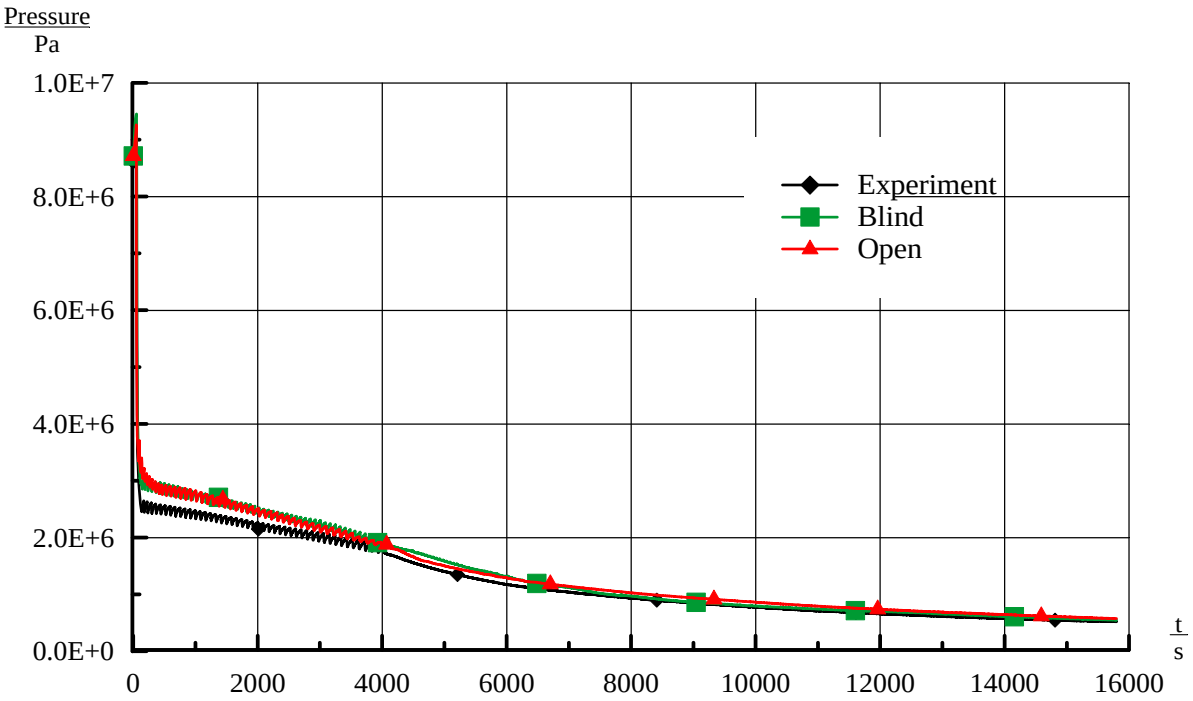

FIG. 4-93. Pressurizer pressure (PT-301).

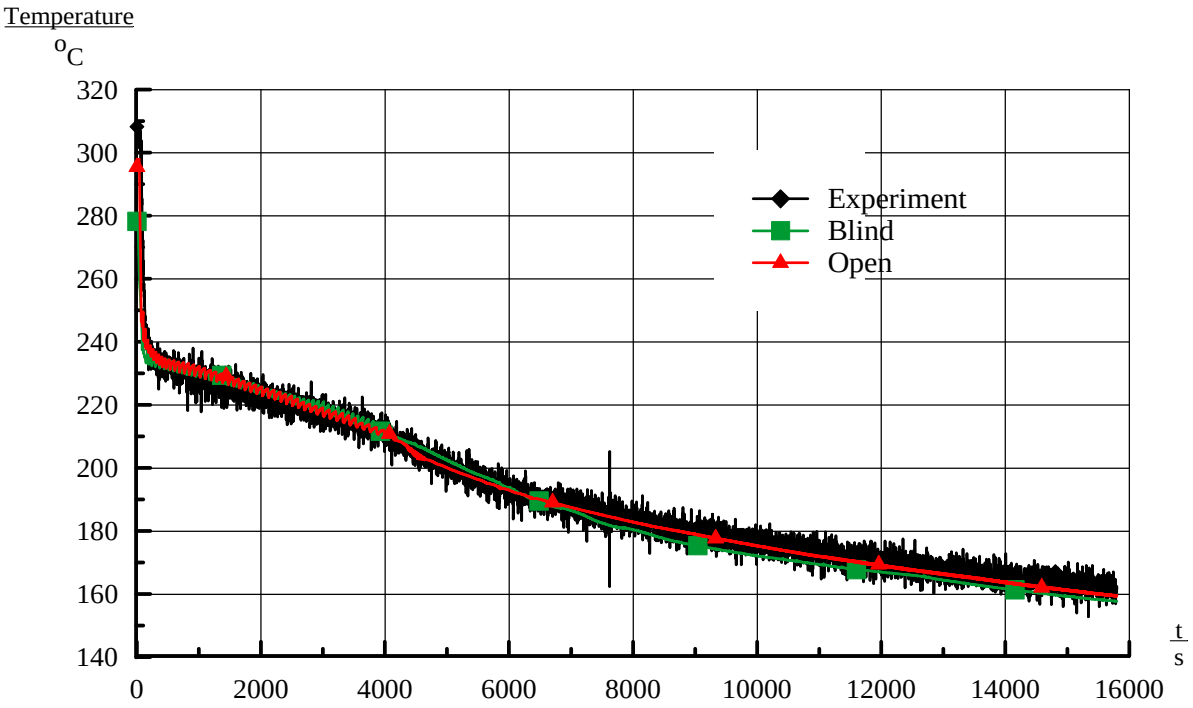

FIG. 4-94. Core heater rod temperature (TH-142).

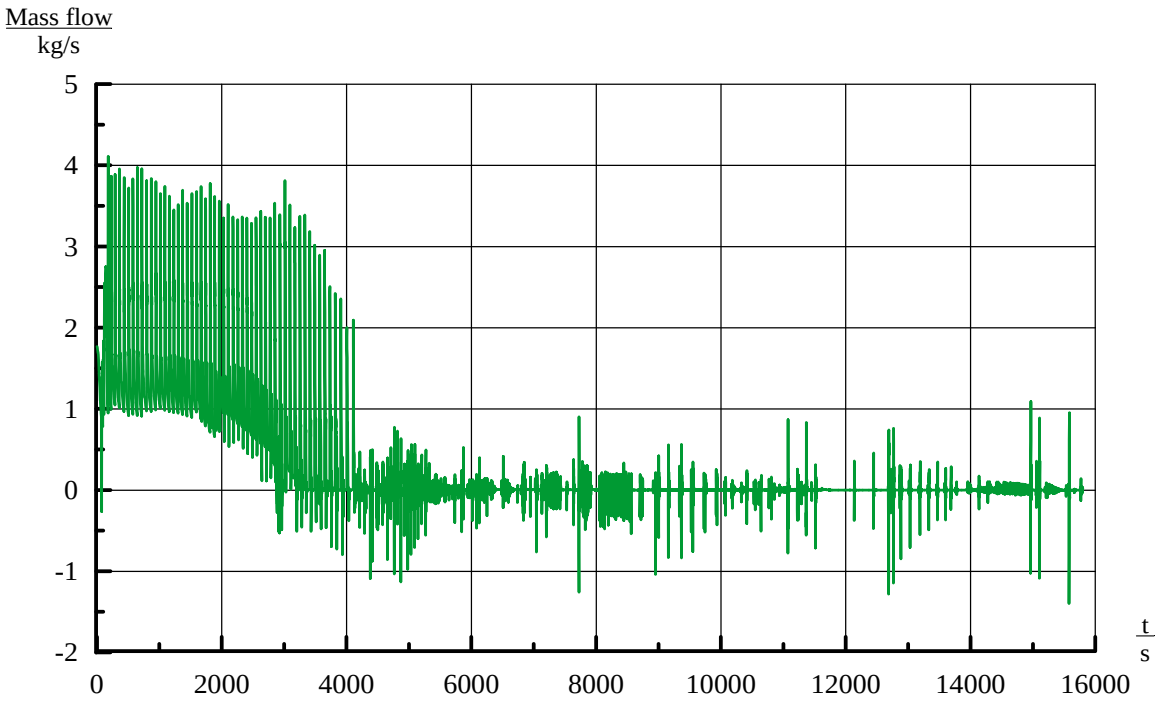

FIG. 4-95. Primary mass flow rate (chimney) – blind.

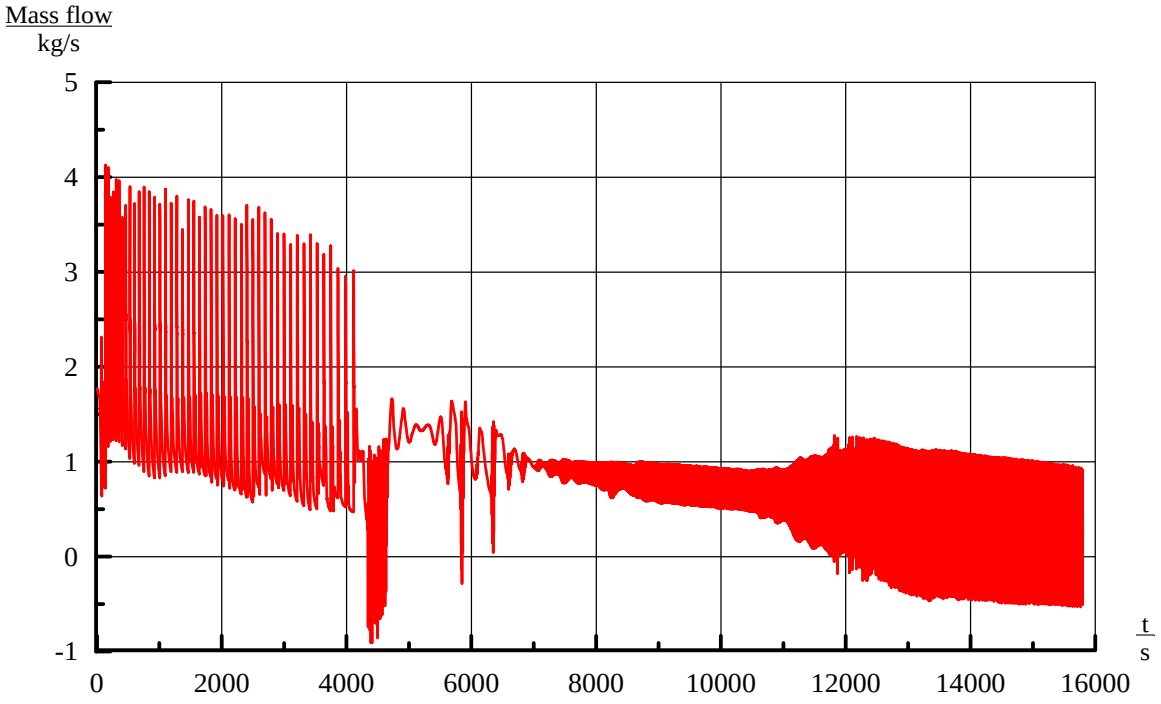

FIG. 4-96. Primary mass flow rate (chimney) – open.

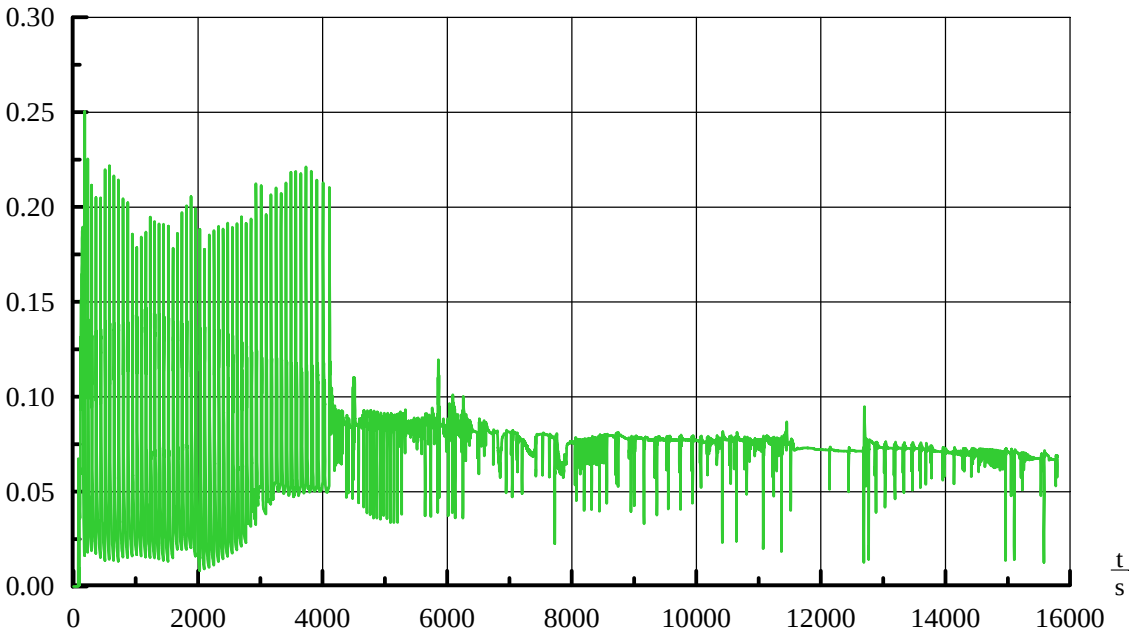

FIG. 4-97. Void fraction (core outlet) – blind.

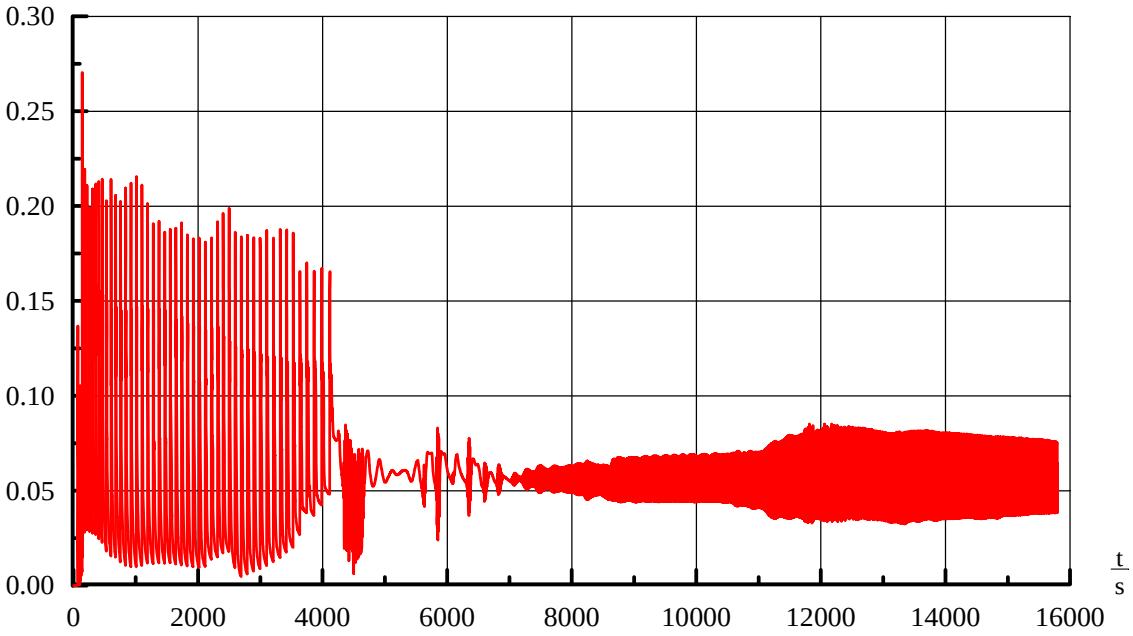

FIG. 4-98. Void fraction (core outlet) – open.

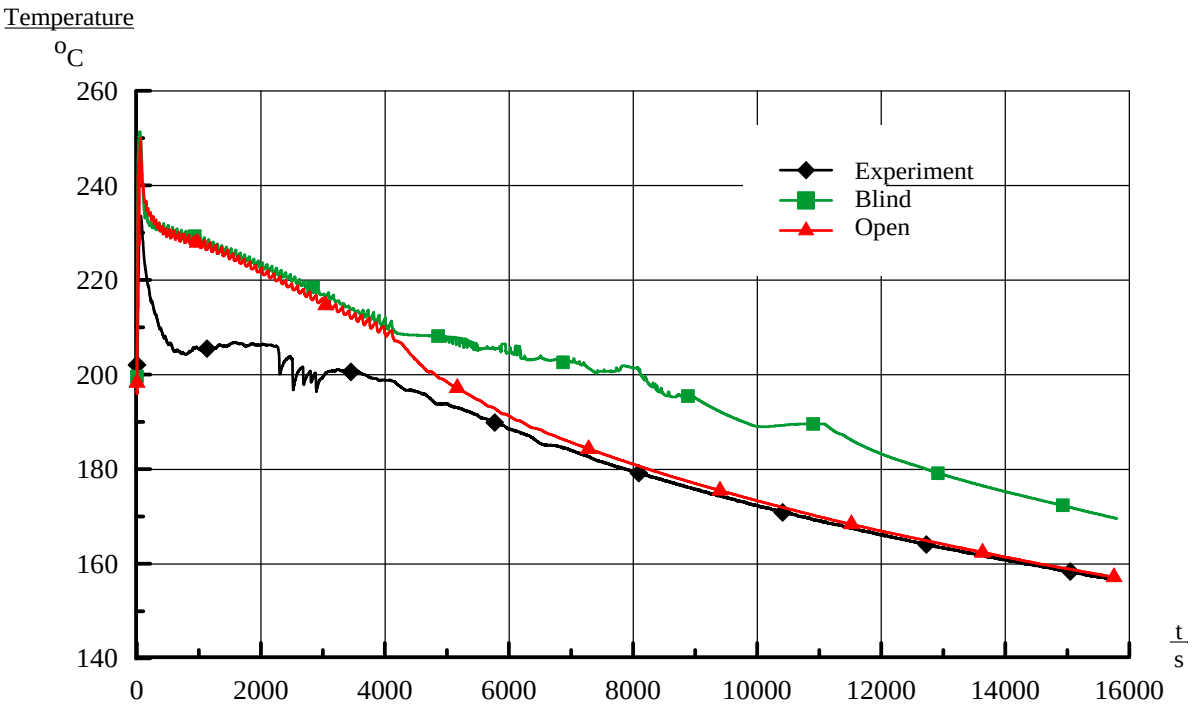

FIG. 4-99. Temperature at SG coil exit (TF-611/621/.../634 Average).

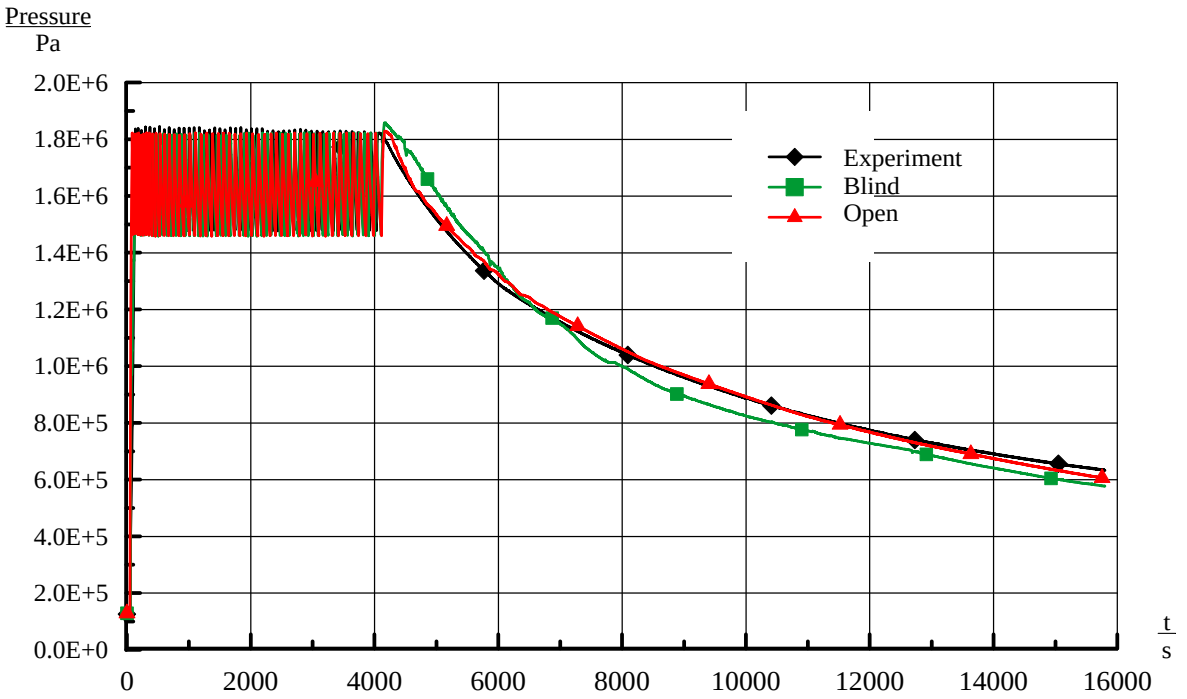

FIG. 4-100. HPC pressure (PT-801).

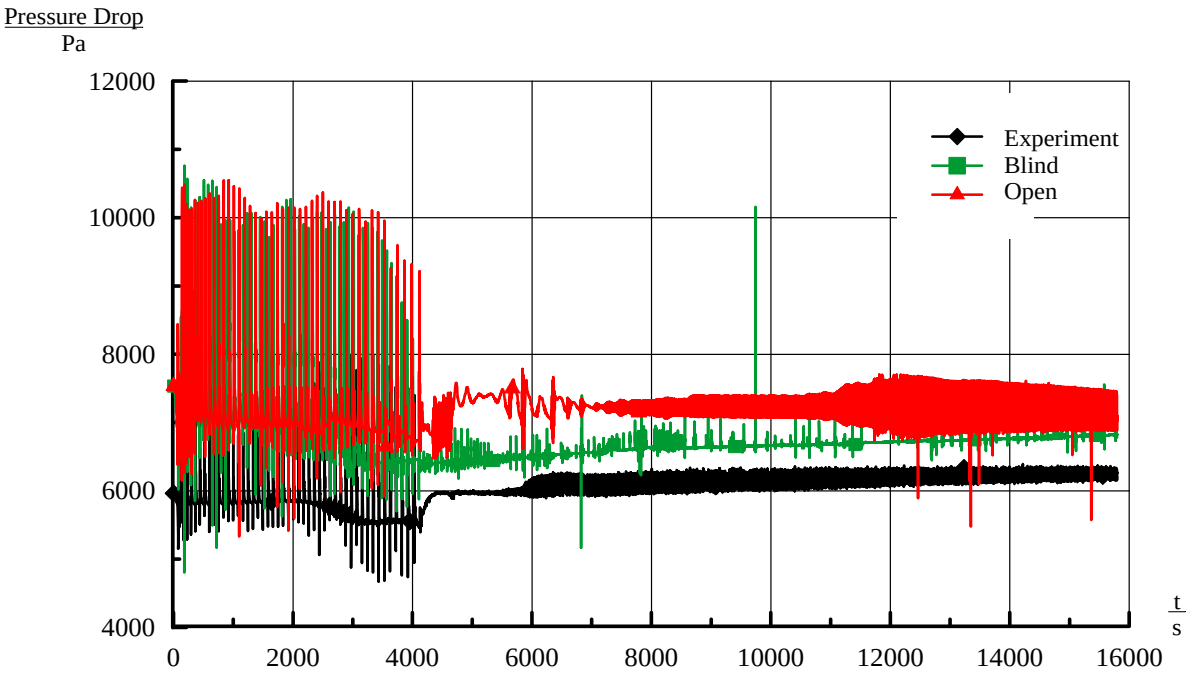

FIG. 4-101. Core pressure drop (DP-101).

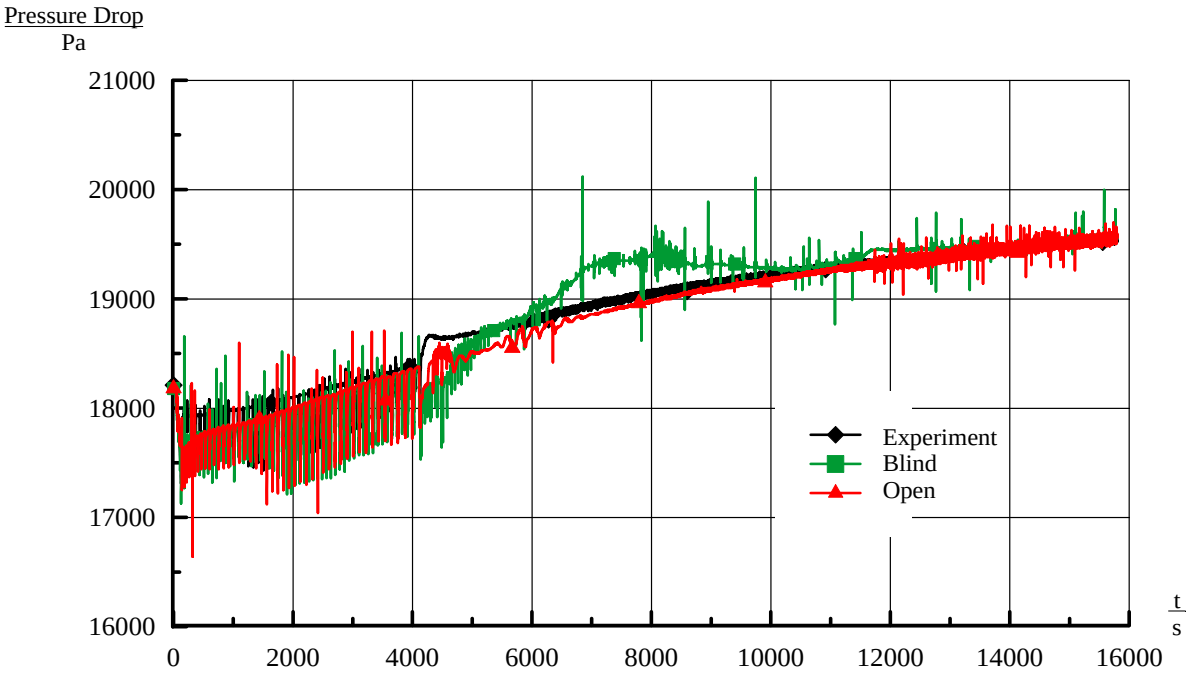

FIG. 4-102. Pressure drop in the annulus below SG (DP-106).

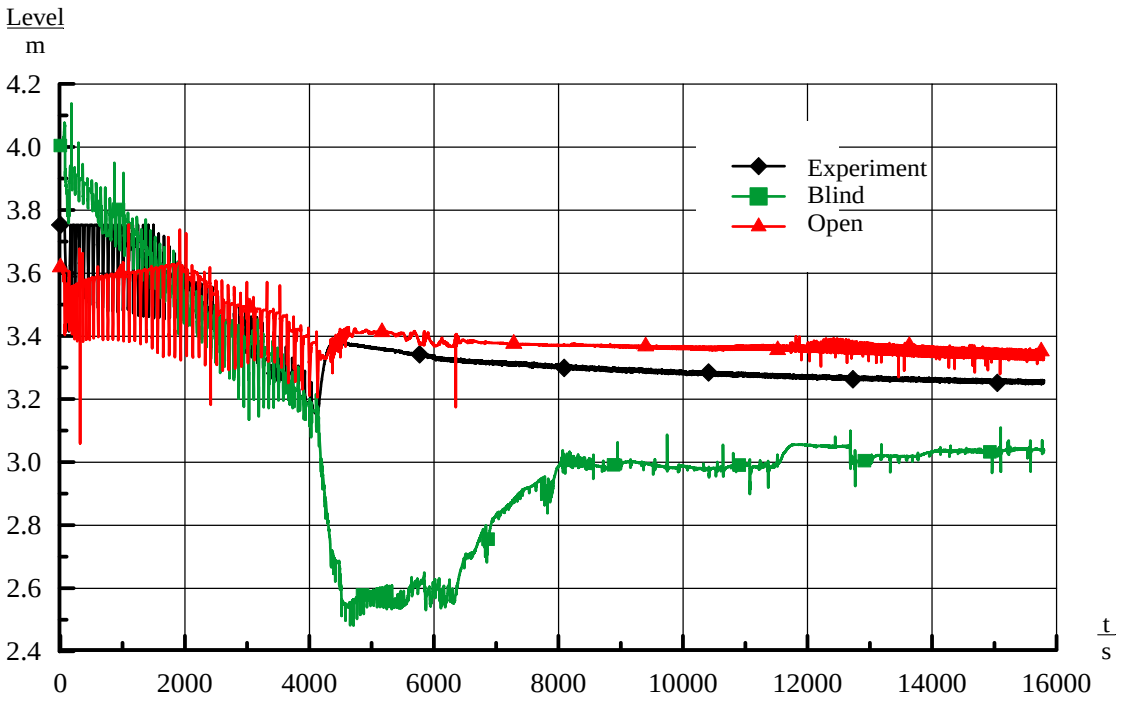

FIG. 4-103. RPV water level (LDP-106).

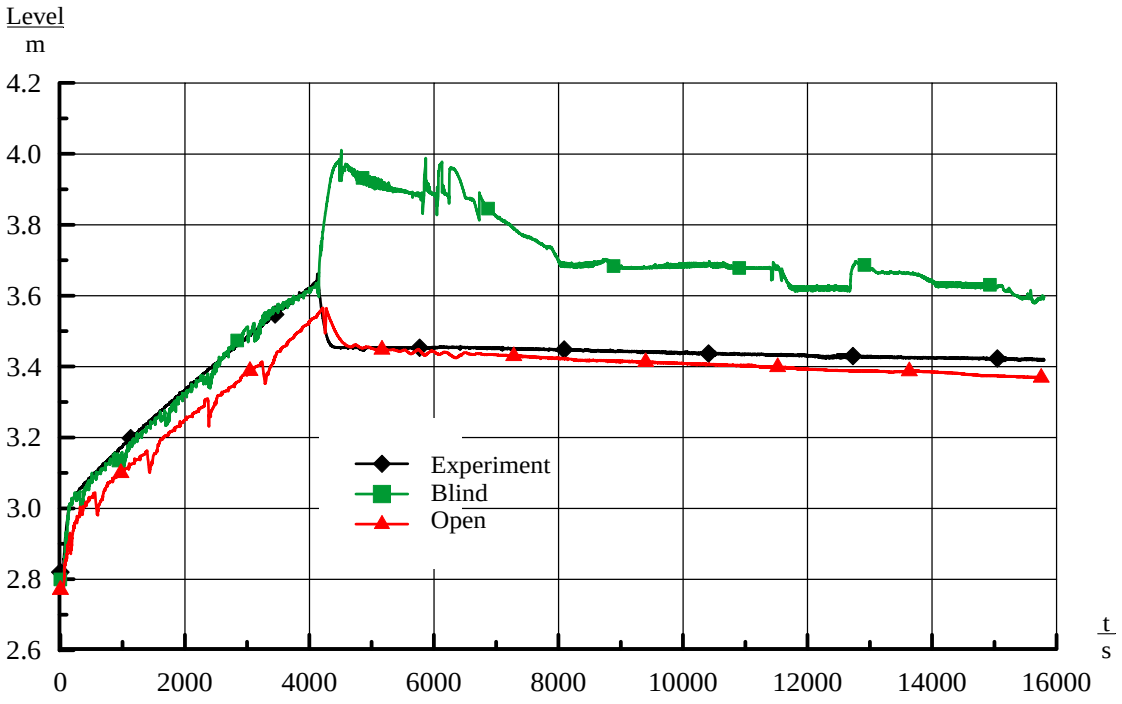

FIG. 4-104. HPC water level (LDP-801).

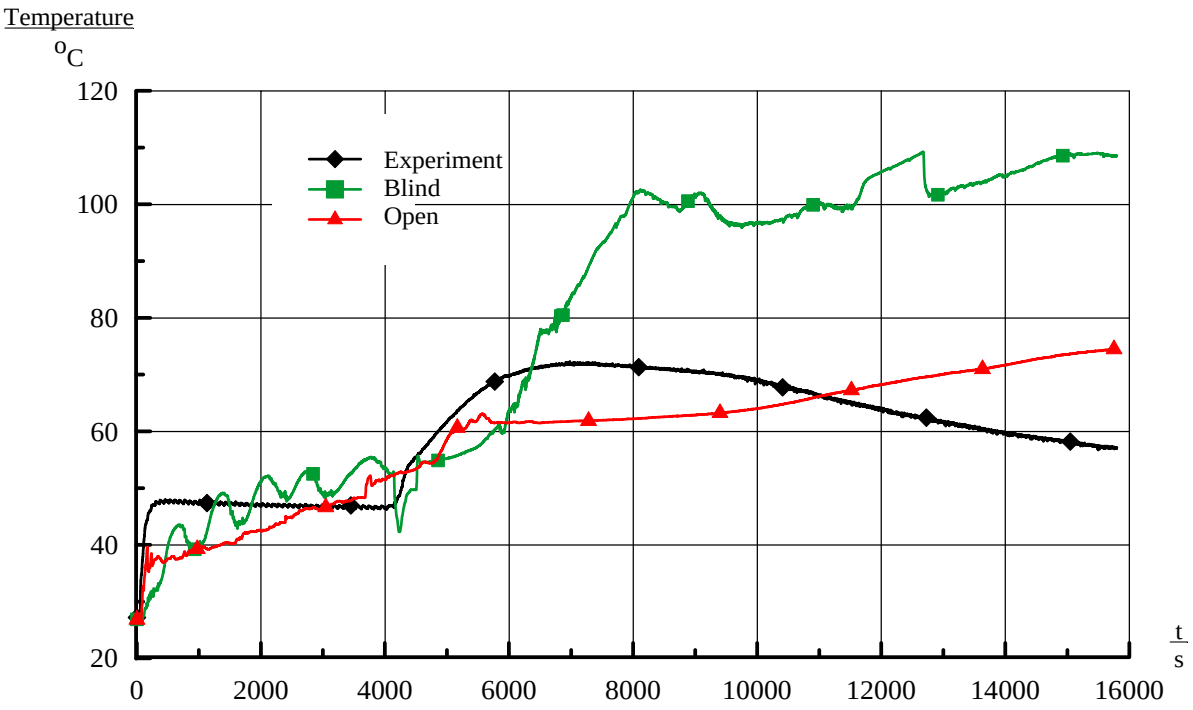

FIG. 4-105. HPC water temperature at 157 cm (TF-821).

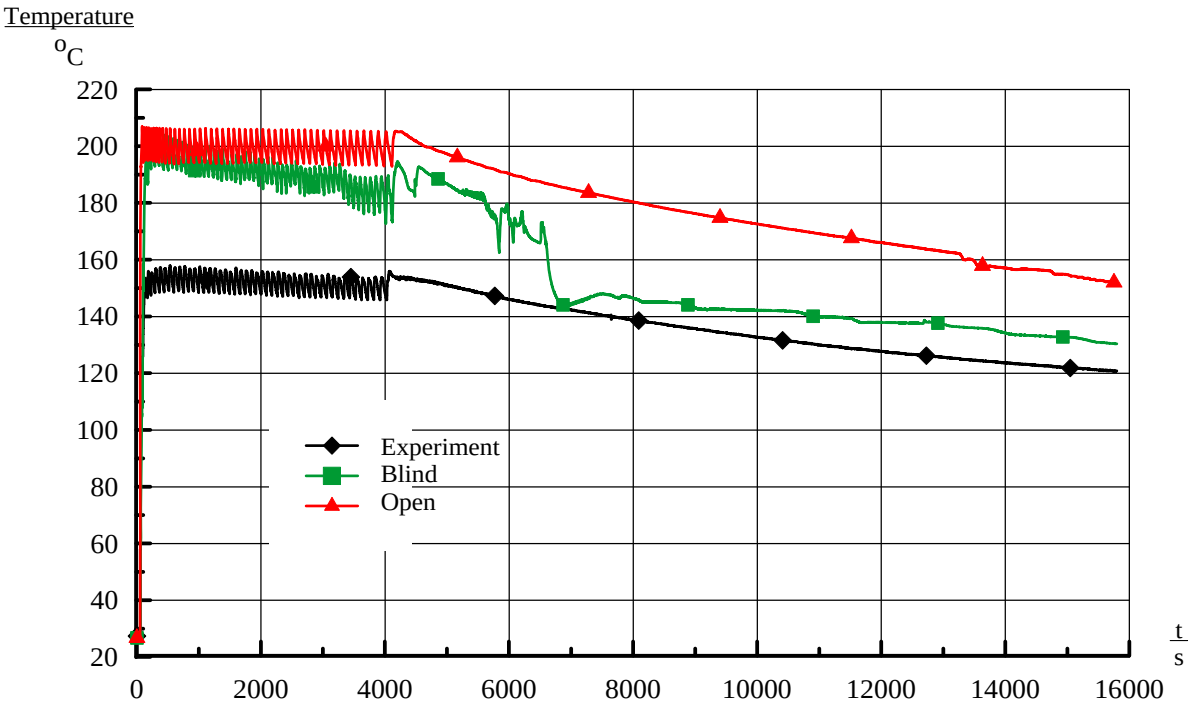

FIG. 4-106. HPC water temperature at 416.9 cm (TF-851).

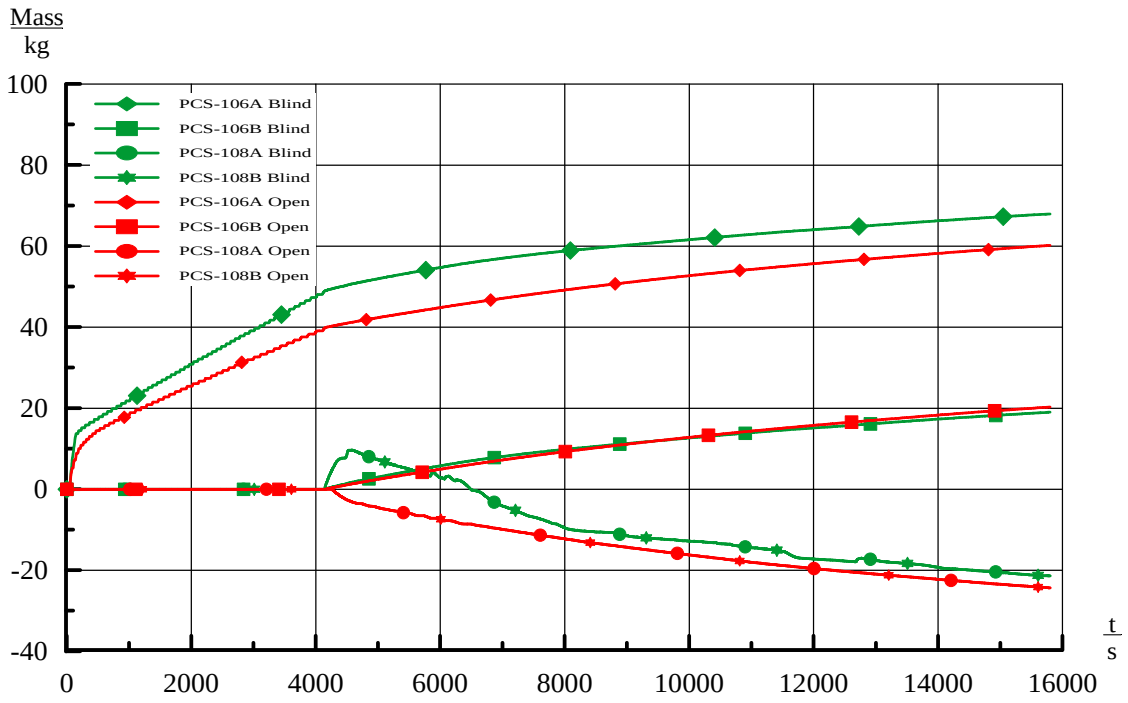

FIG. 4-107. Cumulative discharge.

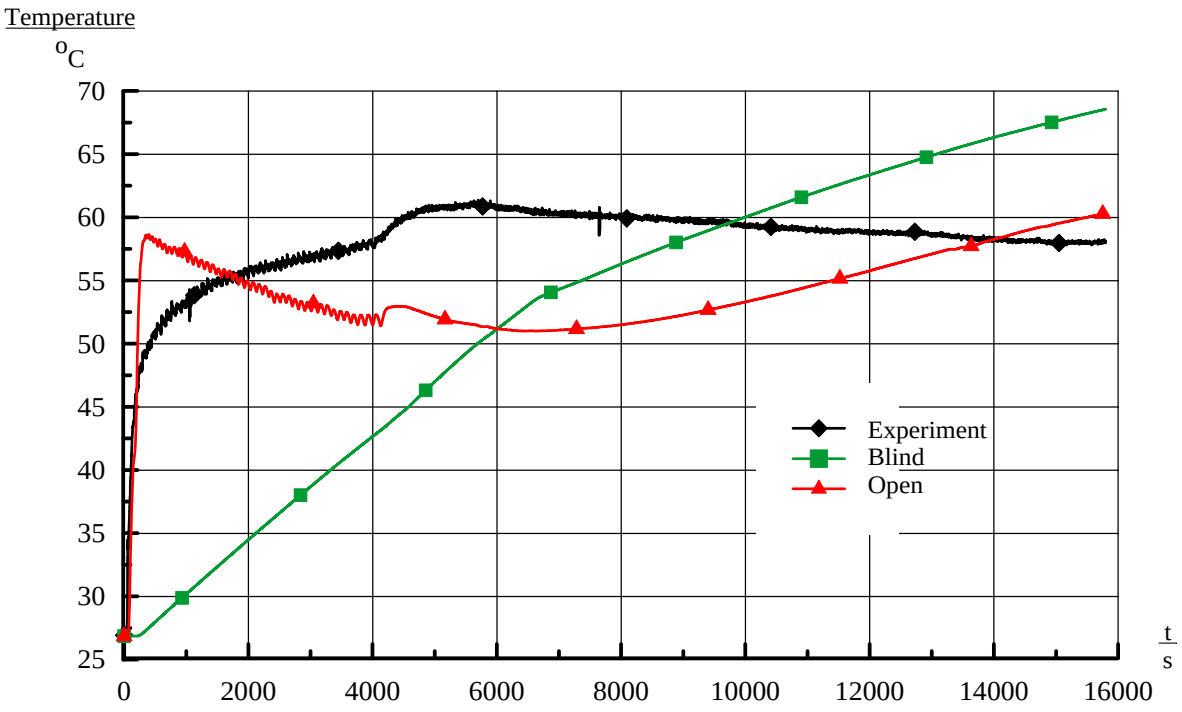

FIG. 4-108. CPV water temperature at 416.9 cm (TF-855).

4.5.4. Analysis results for power maneuvering

4.5.4.1. RPV thermal-hydraulic behavior

The behavior of primary and secondary parameters is defined by the boundary conditions: the core power and feed water flowrate.

The increasing of the core power results in the increase of:

– the core mass flowrate, the core exit temperature;
– the core temperature difference;
– the heat transfer from primary to secondary side.

Steam generator tube wall heat transfer and core power are equal at the start of the SP-3. The step by step increasing of core power is followed by the core mass flow increasing (Fig. 4-109).

At about 2700 s the large rise of feed water flow rate occurs. Heat transfer to secondary side becomes larger than core power, and the farther behaviors of primary and secondary parameters depend from this rise (Figs 4-110, 4-111 and 4-112).

TABLE 4-11. SP-3 TIME SEQUENCE OF EVENTS

Event	Experiment (s)	KORSAR (s)
Start of simulation – steady state	0.0	0.0
	According to [20]	
Initiate core power increase to 80 kW	0	0
Initiate core power increase to 120 kW	870	870
Initiate core power increase to 160 kW	1642	1642
Initiate core power increase to 200 kW	2177	2177
Initiate core power increase to 240 kW	4004	4004
Initiate core power increase to 280 kW	4498	4498
Initiate core power increase to 320 kW	5096	5096

4.5.4.2. SG thermal-hydraulic behavior

At about 2700 s steam temperature at SG coil exit is decreased (Figs 4-115 and 4-116) because the heat transfer to secondary circuit becomes larger than core power (secondary mass flow rate increases while the core power is constant).

Steam generator tube wall heat transfer and core power are equal at the start of the SP-3. The step by step increasing of core power is compensated by the feed water flow and steam flow increasing (Figs 4-117 and 4-118).

4.5.5. Summary

The developed model of MASLWR experimental facility on the basis of KORSAR code allows the prediction of SP-2 and SP-3 natural circulation experiments. Results of blind calculation of SP-2 and SP-3 experiments well coincide with experimental data.

At the open calculation some correction of model discrepancies from the blind calculation are made. In particular, the boundary condition at steam line output is corrected, the loss coefficient for PCS-106A/B line is corrected also. The assumption on formation of boundary layers nearby HTP inside HPC (because of steam jet penetration into water volume) and CPV is made. Modeling changes for the consideration of these phenomena are made. Open calculation with corrected model reduced the differences between code and experimental data for SP-2 (RPV and HPC water levels, HPC, HTP and CPV temperatures, etc.).

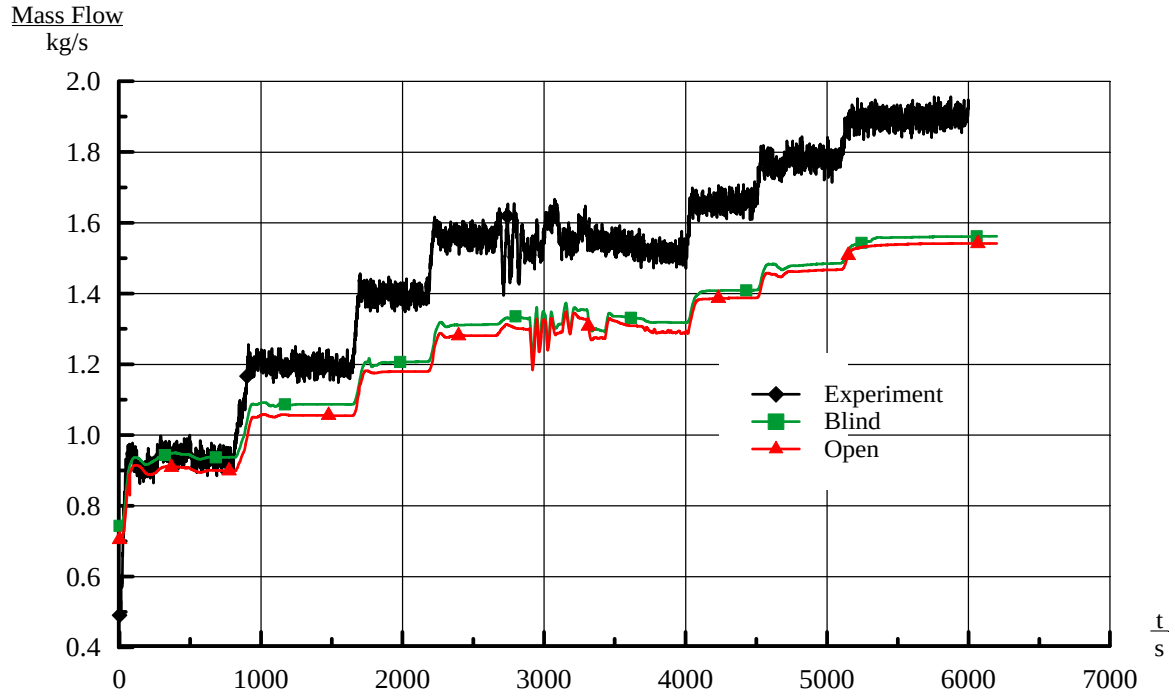

FIG. 4-109. Primary mass flow rate (chimney).

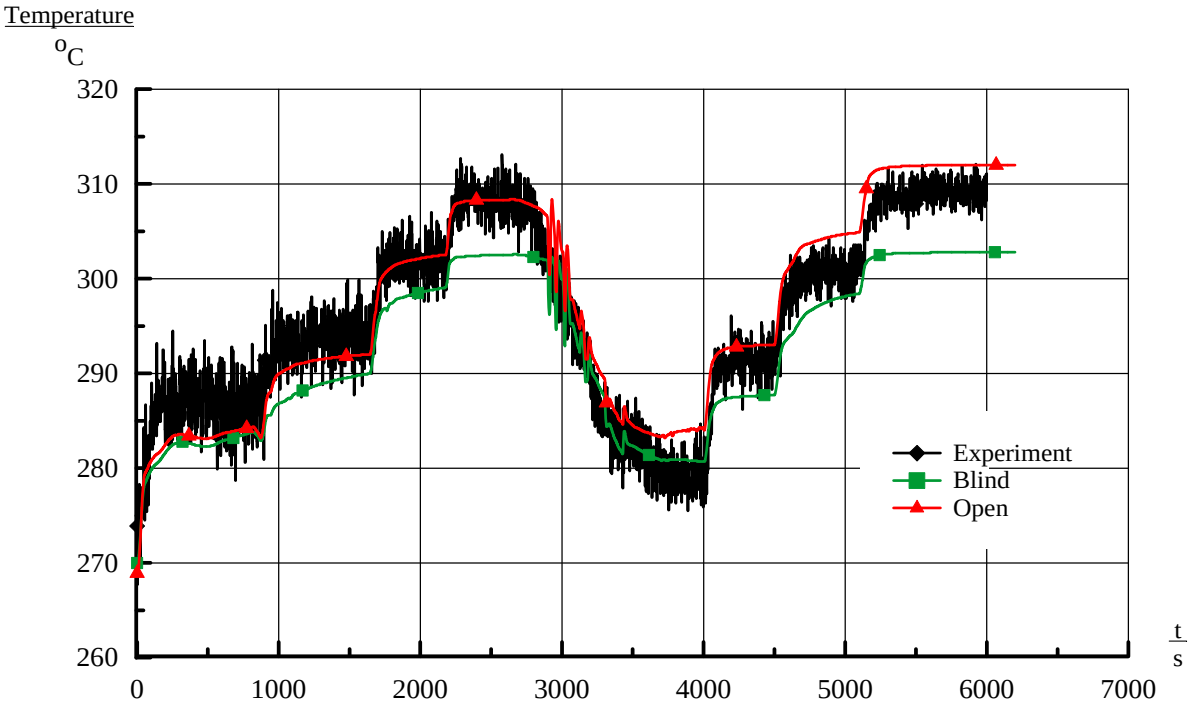

FIG. 4-110. Core heater rod temperature (TH-142).

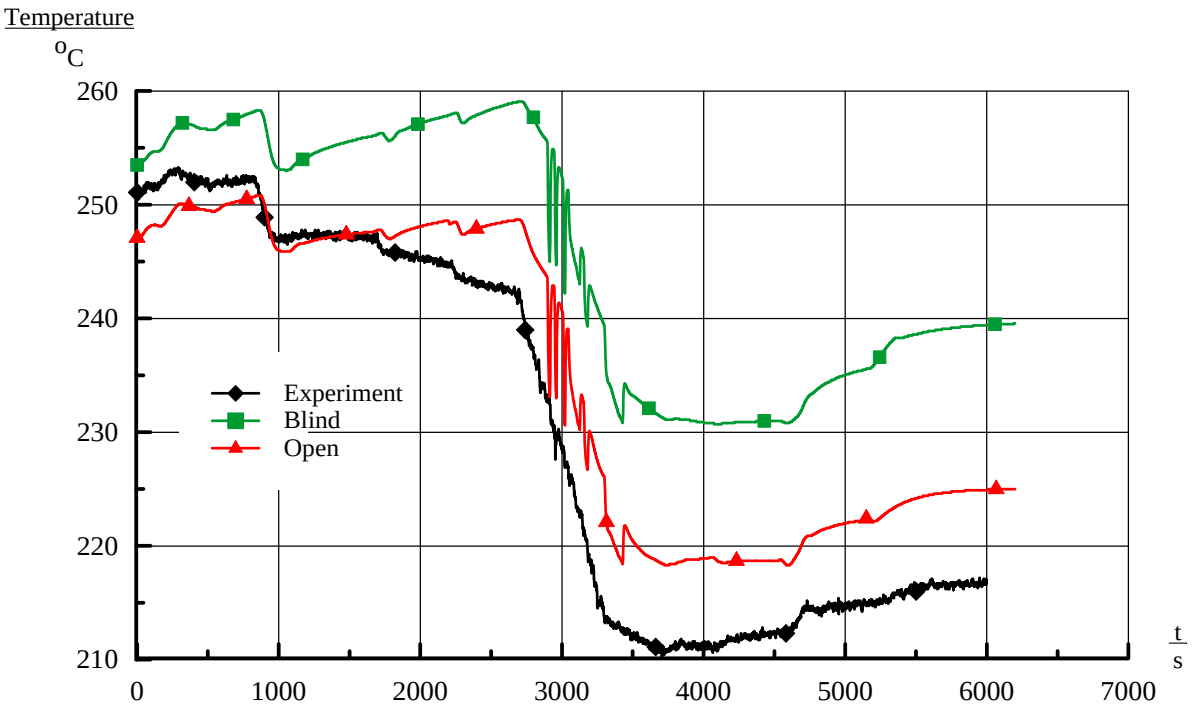

FIG. 4-111. Core inlet temperature (TF-121/122/123/124 Average).

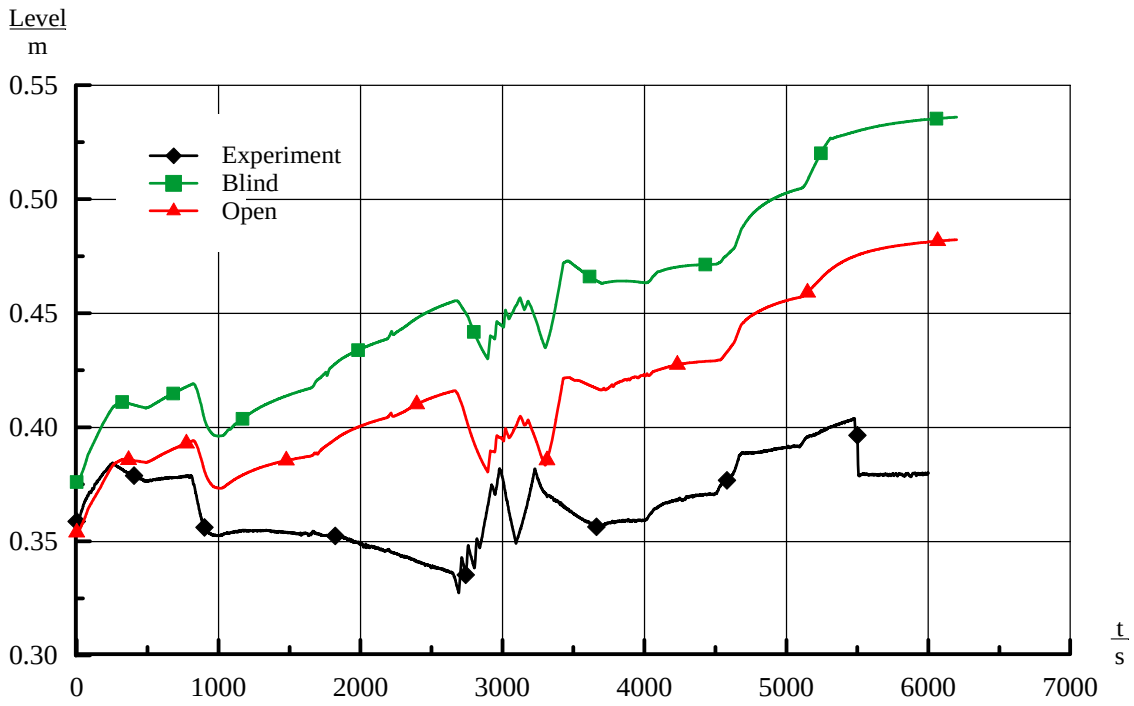

FIG. 4-112. Pressurizer level (LDP-301).

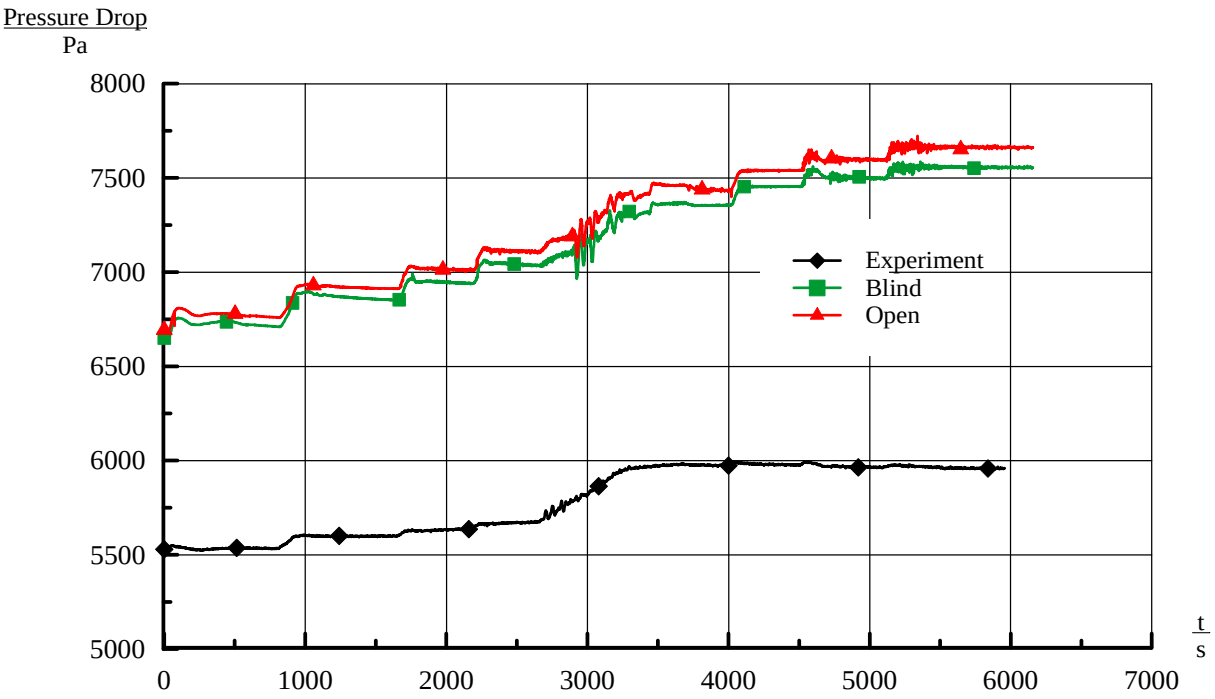

FIG. 4-113. Core pressure drop (DP-101).

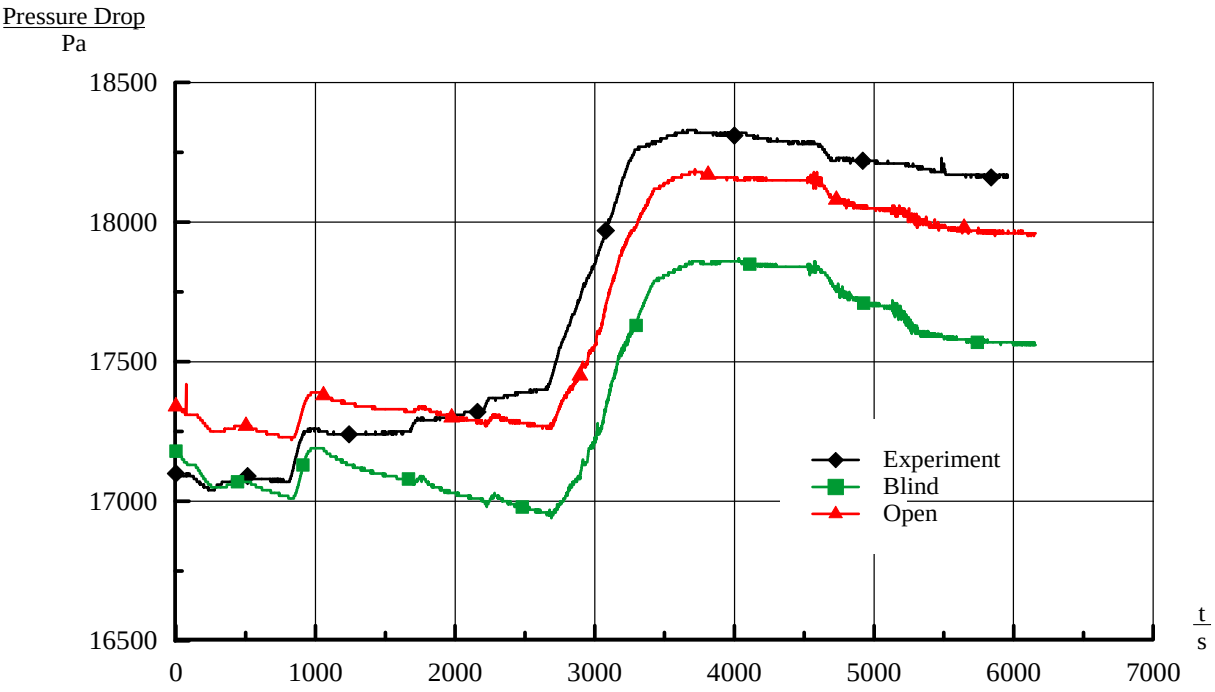

FIG. 4-114. Pressure Drop in the annulus below SG (DP-106).

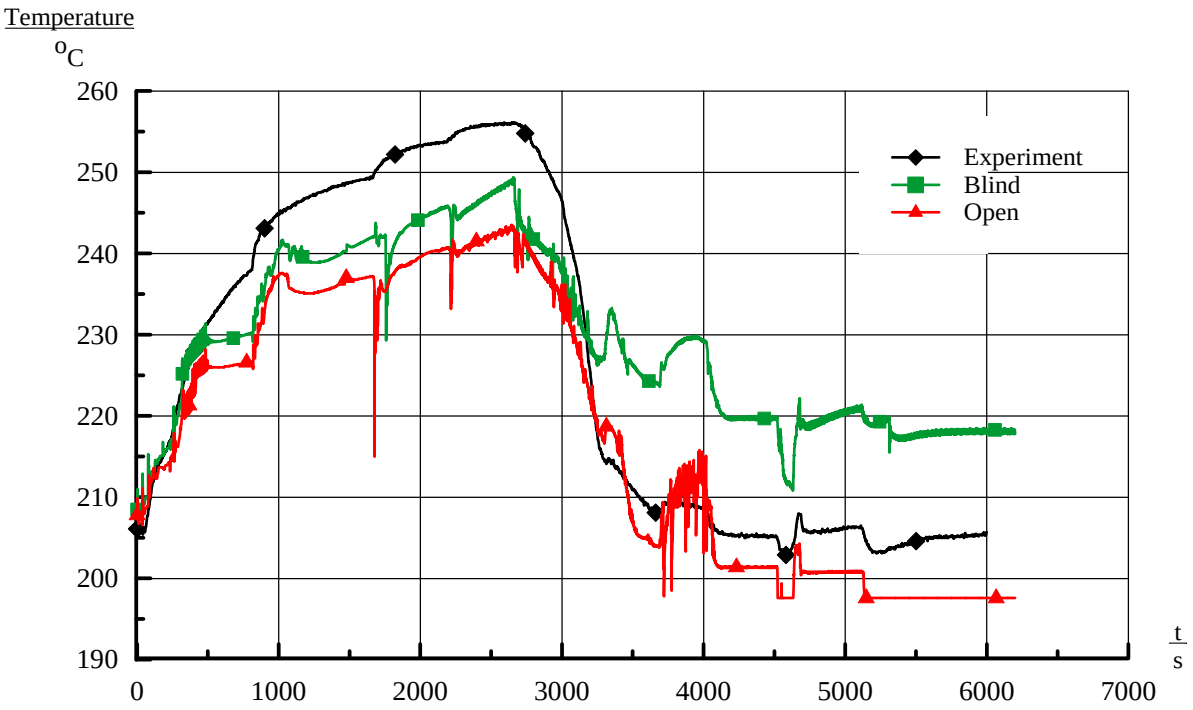

FIG. 4-115. Main steam temperature (FVM-602-T).

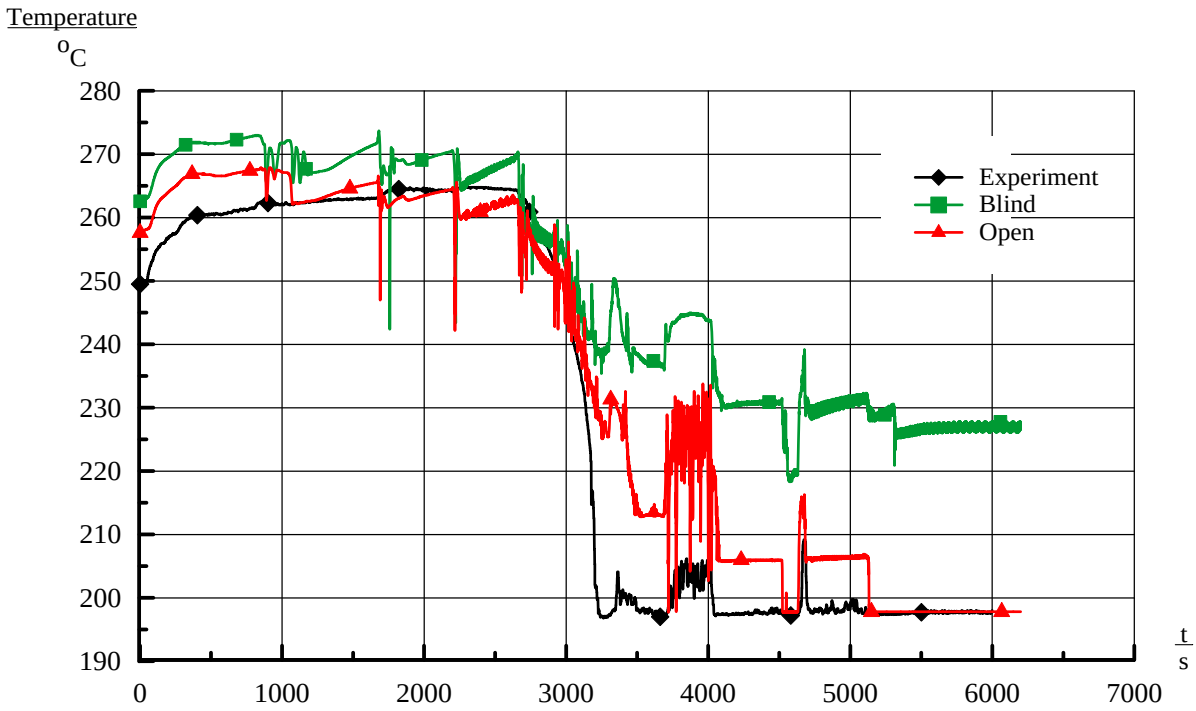

FIG. 4-116. Steam temperature at SG coil outlet (TF-611/612/…/634 Average).

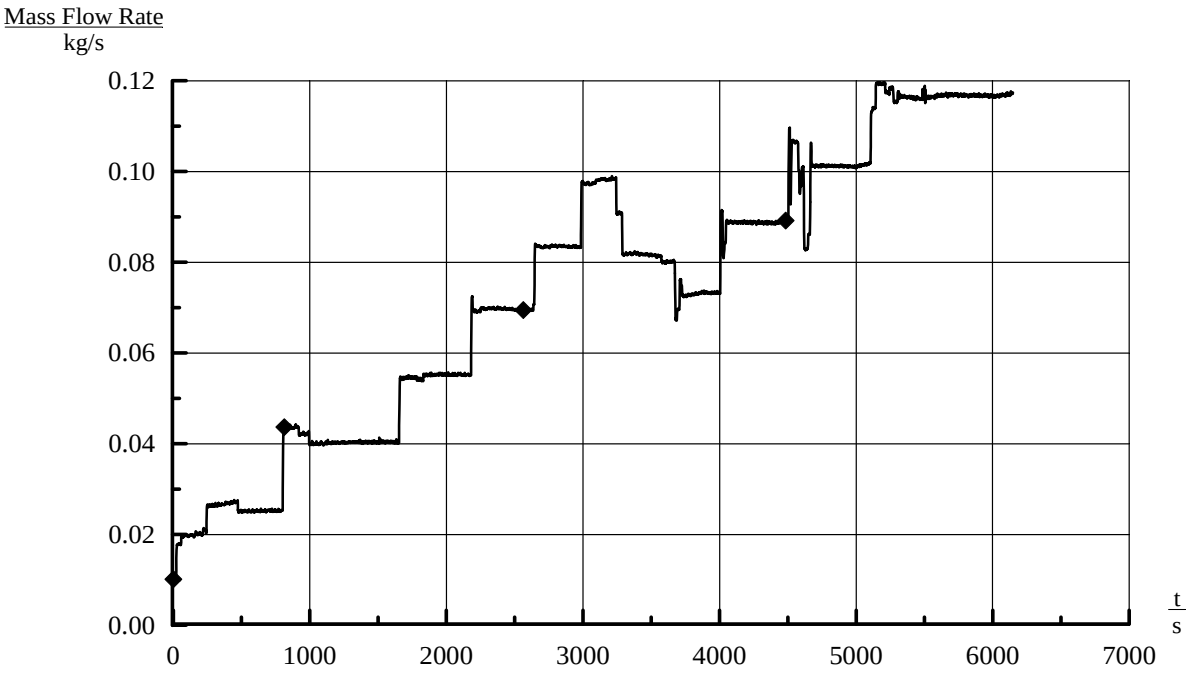

FIG. 4-117. Feed water mass flow rate (SUM FMM-511/521/531).

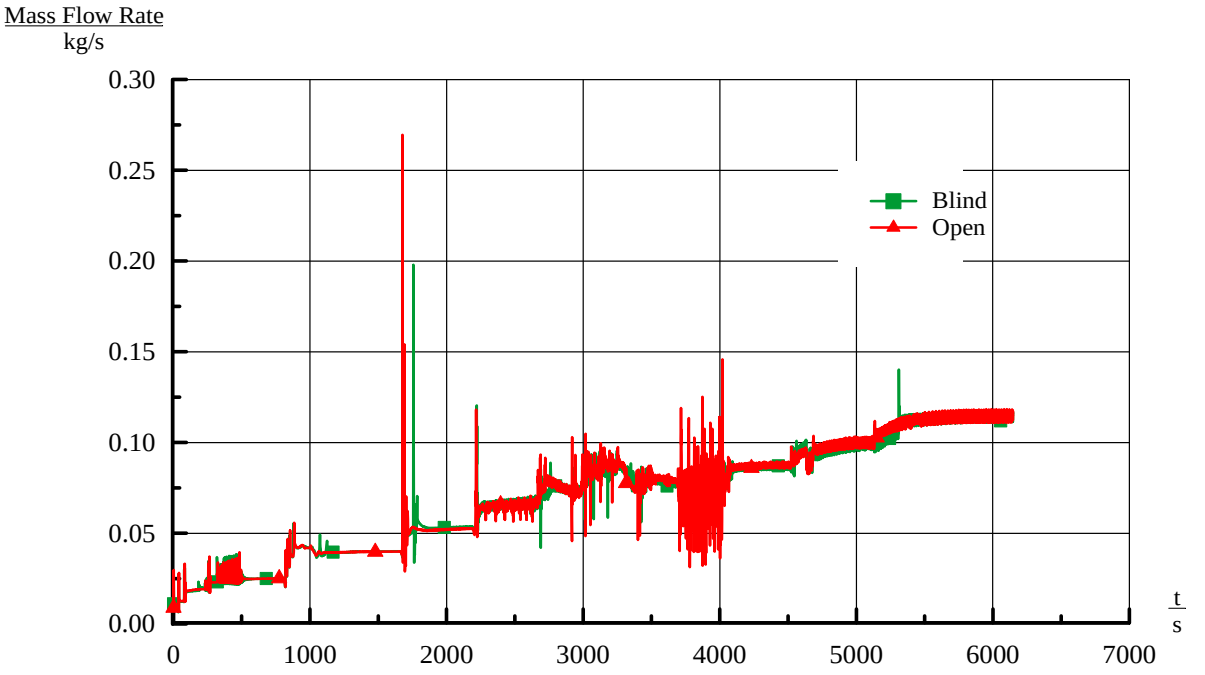

FIG. 4-118. Steam mass flow rate (FVM-602-M).

4.6. IBRAE — RUSSIAN FEDERATION

4.6.1. Computer codes

SOCRAT (System Of Codes for Realistic AssessmenT of severe accidents) is a computer code intended for a coupled modeling of a wide range of thermal-hydraulic, physicochemical, thermo-mechanical and aerosol effects at all stages of accident progression, from initiating event up to corium release following the reactor vessel failure and consequent ex-vessel processes in containment. For instance, SOCRAT allows simulation of the following processes taking place in severe accidents at LWR NPP: core heat up and melting, melt progression, hydrogen generation and release, radioactive fission products generation, release, transport and deposition on surfaces, degradation and failure of the reactor vessel, corium-concrete interaction, and corium retention in the core catcher. The code models take into account the specific geometry of VVER reactors.

SOCRAT includes several modules coupled together. Some of these modules are computer codes developed by different scientific institutes of Russian Federation. The main modules are as follows:

- RATEG (thermal hydraulic processes);
- SVECHA (degradation of the core and in-vessel structures);
- HEFEST (thermal and chemical processes inside corium after its relocation in lower plenum, corium-vessel interaction leading to vessel melt through and melted material release in reactor cavity);
- KUPOL-M (thermal hydraulic processes in containment);
- PROFIT (processes of the fission product transport in the primary circuit).

In calculations of MASLWR SP-2 and SP-3 only RATEG module was used. RATEG module is intended for simulation of thermal hydraulic behavior of the primary and secondary circuits. It contains models for different elements such as channels, chambers, pumps, valves, etc., and models for control and instrumentation systems allowing development of the full scale nodalization schemes for complex thermal hydraulic systems.

Modeling of the coolant flow in RATEG is realized with a two-fluid two-phase hydraulic heterogeneous approach. The coolant is assumed to be in a liquid and/or gaseous phases. Each phase is characterized by its own volume, velocity and temperature and may include several components. For example liquid phase may contain water and dissolved boric acid or non-condensable gases, gaseous phase contains steam and non-condensable gases. Interactions of phases (heat and mass transfer, friction) and heat transfer to solid structures depend on geometry and flow regime. RATEG module allows simulation of different flow regimes under normal operation and accident conditions.

The basic thermal hydraulic variables are pressure, void fraction, phasic enthalpies, and non-condensable qualities (nitrogen, hydrogen, oxygen) defined in the center of control volume, and phasic velocities defined at the boundaries between successive control volumes. The basic equations are approximated using a linear semi-implicit finite-difference scheme allowing violation of the Courant limit. Spatial approximation of mass continuity and energy conservation equations is based on control volumes method with donor formulation for flux terms. The momentum conservation equations are approximated in a non-divergent form using upstream formulation for convective derivatives.

Heat transfer in solid structures (fuel rods, control rods, SG tubes, barrel, shrouds etc.) can be modeled either in one-dimensional or two-dimensional approaches. Two-dimensional heat conduction equation is approximated using linear implicit splitting scheme. All heat structures in RATEG module have cylindrical or conic geometry.

4.6.2. System idealization

Nodalization diagram for OSU MASLWR Test Facility that was used in SOCRAT calculations of SP-2 and SP-3 is shown in Figures 4-119 to 4-122. Strategy of nodalization was based on a minimal number of cells allowing correct physical modeling and matching the configuration of test facility, using Table 2.3 of OSU-MASLWR-07002 [21].

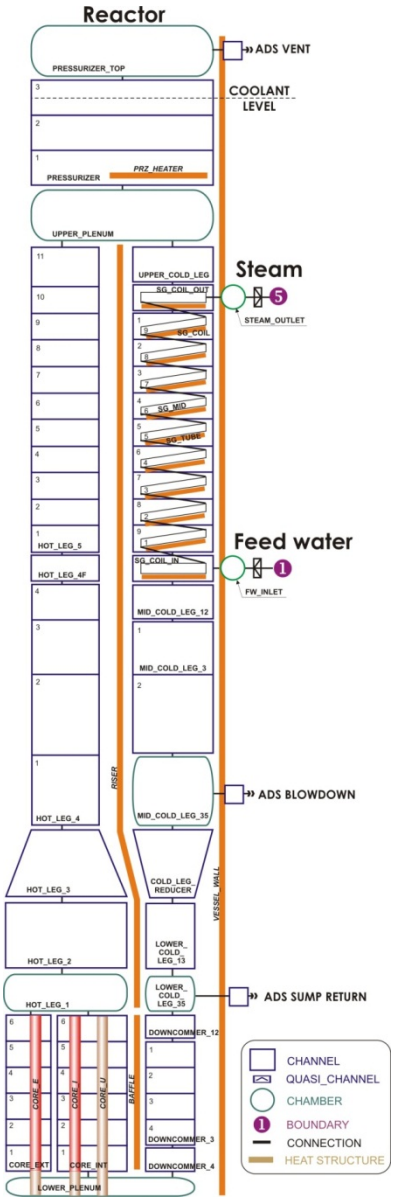

FIG. 4-119. Reactor nodalization scheme.

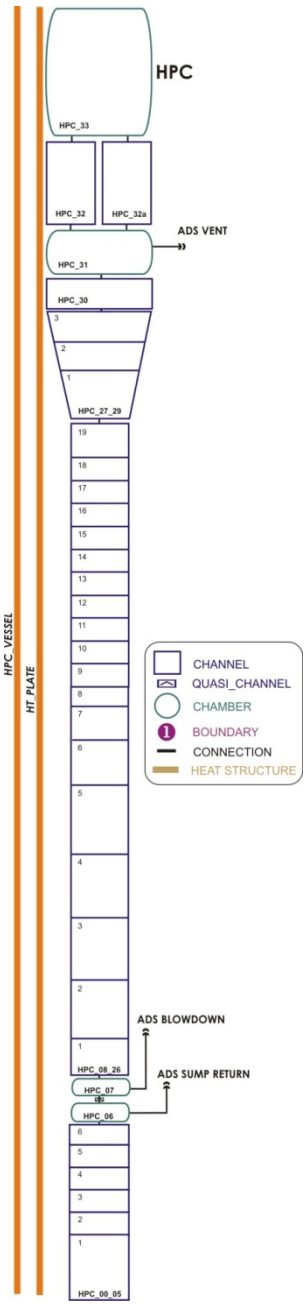

FIG. 4-120. HPC nodalization scheme (blind calculations).

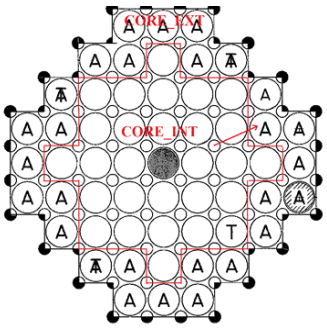

FIG. 4-121. Nodalization scheme of core.

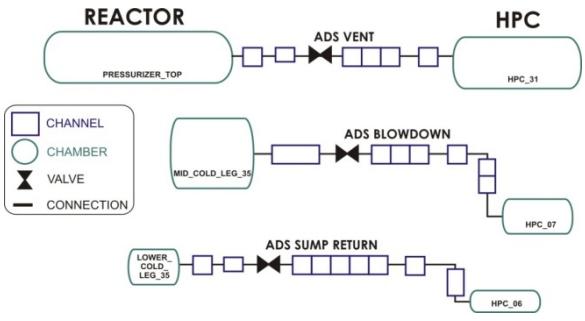

FIG. 4-122. Nodalization scheme of ADS connections.

Core channels were represented by 2 effective channels, surrounding 29 rods in core center and 28 other rods at core periphery. Correspondingly, all core rods were also divided into 2 effective heat structures. Pressurizer heaters were modeled by a stainless steel structure with internal heat source. Steam generator helical coil tubes were lumped in 1 effective straight tube. Zhukauskas cross flow heat transfer correlation was implied at SG tube bundle (primary side) [22]. Blowdown lines, two vent lines and two sump recirculation lines were represented as separate components. A choked flow model was implied at all valves on vent lines.

Heat structures of HPC heaters and steam line walls were ignored in a model. Feed water system was represented by feedwater collector only. Two-dimensional heat transfer (radial and axial directions) was modeled in following solid structures: fuel rods, vessel internals, ADS lines, HPC wall and heat transfer plate, CPV wall. Vessel bottom was modeled with solid cylinder plate.

Form loss coefficients were set at abrupt area changes, diaphragm locations, flow turns and blockings: namely, core inlet and outlet, downcomer inlet and outlet, pressurizer inlet, 4 sections in the cold leg, vent lines. The values for direct and inverse flows were set identical. The values were specified by tuning the calculated mass flow rates to experimental data from tests 001, 002, 003a and 003b [1].

The ambient temperature in SP2 and SP3 was set constant and equal to 25°C. The other modeling assumptions include the following simplifications:

- No consideration for heat losses from sump return and blowdown lines;
- Form loss coefficient at coolant flow 90° turn equal to 0.5;
- CPV always considered at adiabatic conditions.

Insulation on RPV was modeled explicitly in accordance with ICSP specification [21]. Insulation material of HPC, CPV and ADS lines was not modeled.

Time step size was selected to be the maximum allowed value (0.04 s) throughout the steady-state and transient. However its automatic decrease and increase back to maximum value is possible depending on intrinsic logic of the code (for example, during condensation processes or abrupt changes of parameters time step is reduced).

4.6.2.1. System idealization for blind calculation

The nodalization schemes for blind and open calculations are almost identical (Figs 4-119 to 4-123) except for HPC which in blind calculations was modelled with one channel, and in open calculation with a stack of two cross-coupled channels. Besides, for blind calculations heat transfer coefficient (HTC) from isolation surface to air was set 20 W/m^2-K, effective HTC from HPC steel to air was set 5 W/m^2-K, effective HTC from ADS steel lines to air was set 10 W/m^2-K.

4.6.2.2. Modelling change for open calculation

In open calculations HPC nodalization was subdivided into two stacks of cells with cross-junctions (Fig. 4-123). Also, heat losses to ambient air from RPV, HPC and ADS were adjusted: HTC from isolation surface was reduced to 15 W/m^2-K, effective HTC from HPC steel to 2 W/m^2-K, effective HTC from ADS steel lines to 1 W/m^2-K.

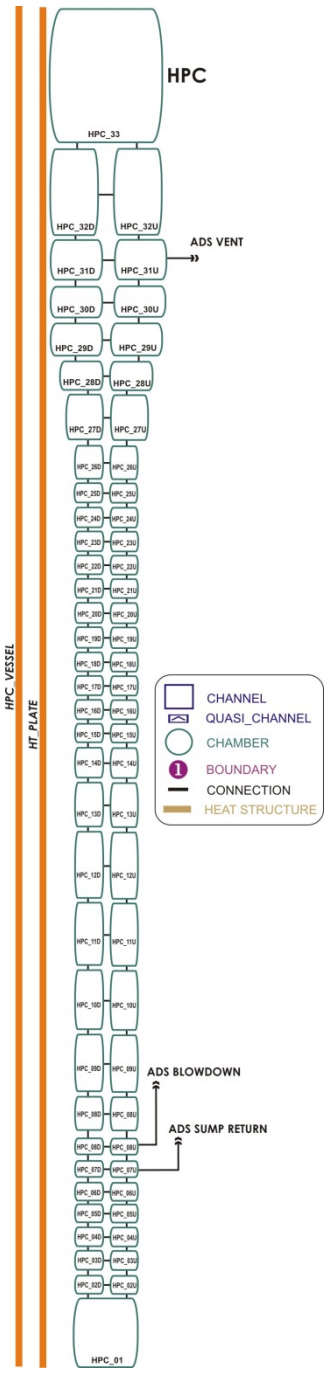

FIG. 4-123. HPC nodalization scheme for SOCRAT (open calculations).

4.6.3. Analysis results for loss of feed-water transient

The comparison of calculation results and test data for SP-2 steady-state is presented in Table 4-12. A good compliance for all parameters can be noted, except for secondary superheat. It is overestimated by about 25 degrees. But it should be noticed that the measured value corresponded to point far downstream from SG exit, and the calculated value is given for exit plane of SG tubes. However, in terms of power that deviation is small compared to the heat transferred from primary to the secondary side.

TABLE 4-12. STEADY-STATE COMPARISON FOR TEST SP-2

Parameter	Unit	Experimental Value	SOCRAT results	
			Blind	Open
Pressurizer pressure	MPa(a)	8.720	8.718	8.73
Pressurizer level	cm	36.07	34.55	35.2
Power to core heater rods	kW	149.39/147.94	149.39/147.94	149.39/147.94
Feedwater temperature	ºC	21.39	21.35	21.35
Steam temperature	ºC	205.38	231.16*	231.54*
Steam pressure	MPa(a)	1.411	1.411	1.421
Ambient air temperature	ºC		25	25
HPC pressure	MPa(a)	0.127	0.132	0.132
HPC water temperature	ºC		26.70	26.70
HPC water level	cm	282.04	282.22	279
Primary flow at core outlet	kg/s		1.68	1.68
Primary coolant temperature at core inlet	ºC	215.34/214.82 214.42/215.11	215.55	217.0
Primary coolant temperature at core outlet	ºC	251.52	252.44	251.8
Feedwater flow	kg/s		0.1102	0.11
Steam flow	kg/s		0.1055	0.11
Primary coolant subcooling at core outlet	ºC		48.27	47
Total heat loss through primary system	kW		2.0	2.4
Heat transfer through SG	kW		296.5	295.7
Maximum surface temperature of core heater rods	ºC		302.6	304
Location from the SG secondary inlet to reach - saturation - superheat	m		 1.5 5.0	 1.5 5.0

* exit plane of SG tubes

Below some SP-2 transient results are discussed and compared to test data.

4.6.3.1. RPV thermal-hydraulic behavior

Break flow is modeled in SOCRAT at first opening of vent valve PCS-106A. The timing of PCS-106A operation in numerical modeling is very similar to test data.

The flow rate through PCS-106A depends on void fraction of coolant (steam and water until 100 s and steam thereafter in blind calculations), RPV pressure (slightly decreasing from 100 to 4050 s in blind calculations) and state of the valve (open or closed) (Fig. 4-124). Because of PCS-106A valve cyclic actuation, coolant discharge flow is oscillating. On average peak values of flow rate are lowering with time in conformance with decrease of pressure drop between RPV and HPC. First peak of flow rate is much higher than the next peaks because at first opening coolant passing through PCS-106A contains water. Flow rate is further smoothing to average rate of 8 g/s (Fig. 4-125). After 4050 s oscillations disappear as vent valves are kept open, and the flow rate slowly decrease due to primary cool down.

After vent line opening a stable flow of vapor from RPV to HPC through PCS-106A, PCS-106B valves and backward flow of water from HPC to RPV through PCS-108A, PCS-108B is establishing, assuring the natural calculation coupling between RPV and HPC (Fig. 4-125). Opening of SV-800 never happens due to pressure decrease. These phenomena are correctly reproduced in calculations.

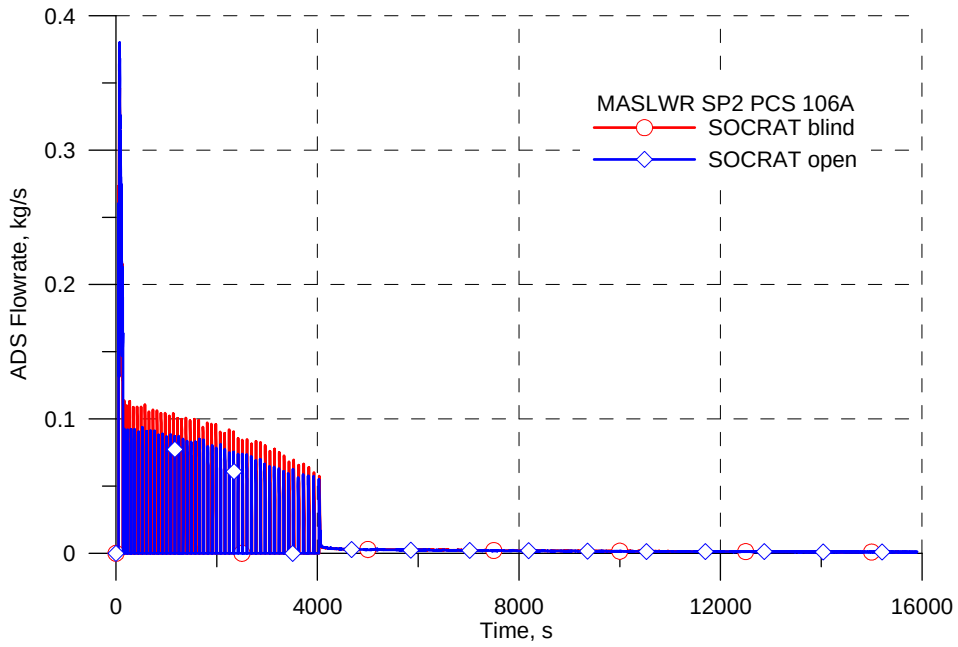

FIG. 4-124. Calculated flow rate through PCS-106A (calculation results).

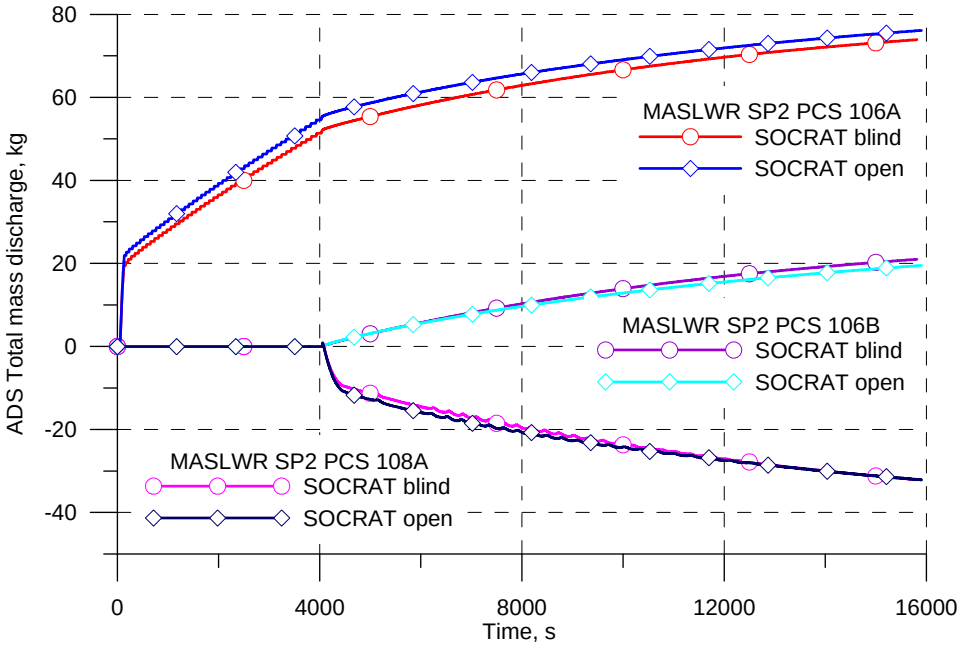

FIG. 4-125. Accumulated mass discharge through vent and sump return lines (calculation results).

Calculated collapsed level of RPV coolant is decreasing from 0 to 4050 s (Fig. 4-126) because of vapor discharge to HPC, followed by primary pressure decrease and coolant evaporation. RPV water level comes down to upper edge of the chimney and later on, down to SG inlet. Calculated void fraction at core outlet is about 5 % (depending on correlations used it can reach 10 %). The oscillating behavior of the level is explained by PCS-106A cycling. At 4050 s opening of PCS-108A and PCS-108B valves let the water flow from HPC to RPV. Consequently, a water level build up is observed in RPV. Since the hot primary water is mixed with colder water coming from HPC, the average primary water temperature is decreasing, its density is increasing and primary level slowly goes down.

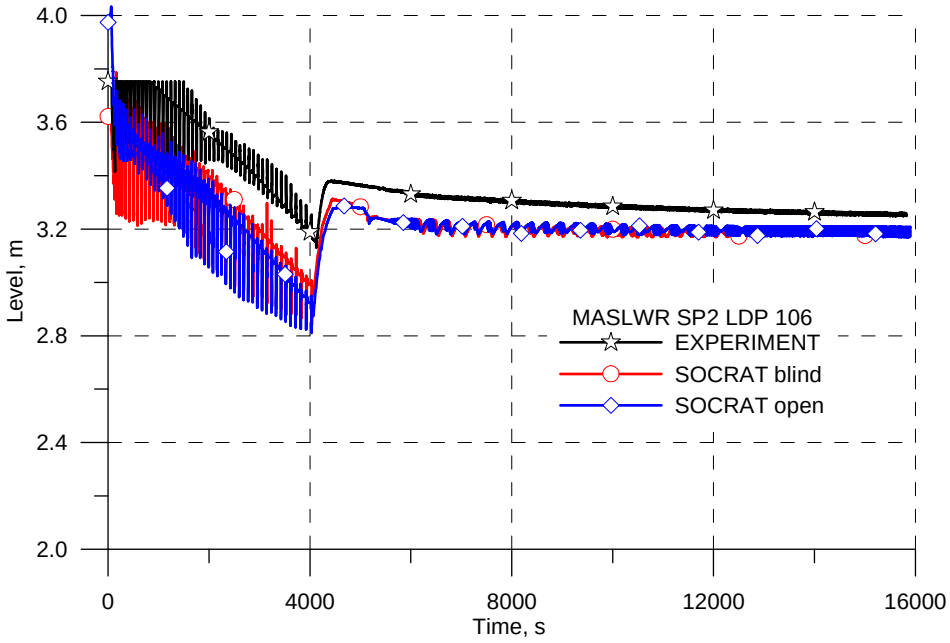

FIG. 4-126. Change of collapsed level of water in RPV.

Pressure change in primary circuit is shown at Figure 4-127. The test data are fairly well reproduced by SOCRAT. Primary pressure dramatically sinks immediately after the first opening of PCS-106A valve and then stabilizes at a saturation value corresponding to coolant temperature. Up to 4050 s primary pressure is governed by HPC pressure which, in turn, depends on condensation rate and heat transfer to CPV. On average pressure is slightly decreasing because the mass of vapor generated between two successive PCS-106A openings is less than the mass of vapor released to HPC every PCS-106A cycle. Vapor generation is determined by the following processes:

– heat transfer in the core (core power);
– heat transfer to RPV wall;
– heat transfer through the plate;
– water mixing in a large pool of water.

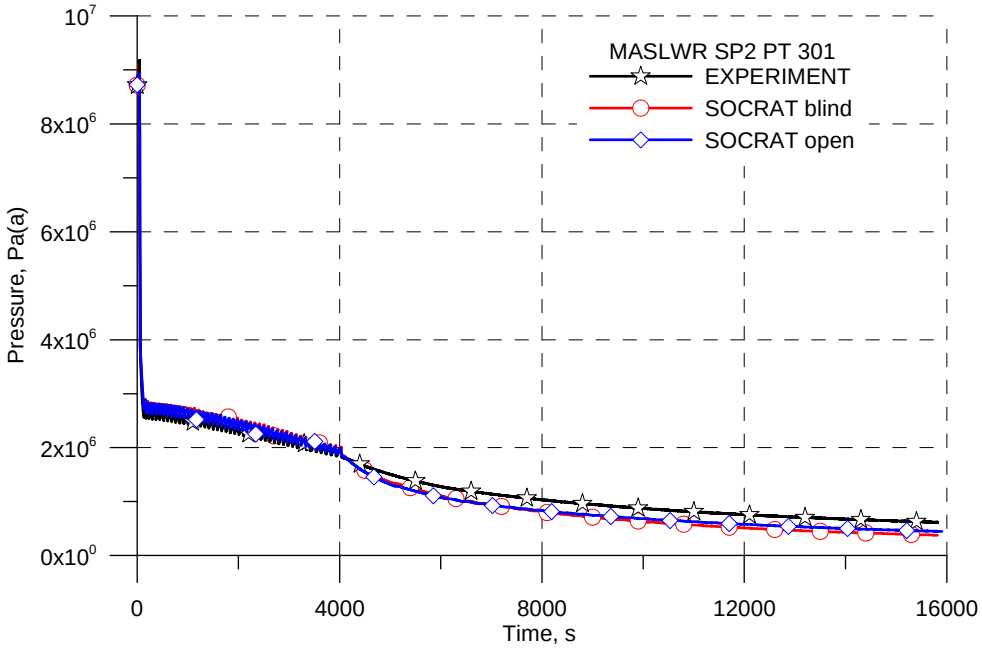

FIG. 4-127. Primary pressure.

As primary pressure goes down, the flow rate through the chimney is also decreasing (Fig. 4-128). The flow rate peaks are caused by pressure drop in RPV with every PCS-106A opening, which provokes a coolant boiling in its full volume and vapor rise to the upper plenum.

According to blind calculation results, primary circulation flow rate comes to zero at around 2500 s when primary water level drops down to the chimney upper edge, and natural circulation breaks up (Fig. 4-128). From that time the flow along chimney is provided only by PCS-106A openings.

After opening of all valves (at vent and recirculation lines) the cold water comes from HPC to the lower part of RPV downcomer. In SOCRAT calculations cold water from HPC is instantly mixed with hot water in RPV downcomer. It is due to one-dimensional nodalization of downcomer in calculation. One should note that in experiment a cold plug is moving to core inlet by one side of the downcomer and provokes temperature drop at core inlet (Fig. 4-129). As we don't have enough experience of modeling a non-uniform mixing of a cold jet in annular pool of hot water with 1D hydraulic elements, we didn't try this in blind calculation by SOCRAT.

In blind calculation the cold mixture of water was cooling down the upper part of the core because of the overestimated heat transfer across the chimney wall. That explains why from 4050 to 5000 s a temperature drop at core outlet is observed in blind calculation (Fig. 4-130). In open calculation the heat exchange across chimney wall was corrected: temperature drop at core outlet became much smoother, and water at core inlet is now colder than in blind calculation. During this stage circulation through the chimney almost disappears, because the core power is spent to coolant heat up. When water in HPC bottom becomes hotter, the primary subcooling at core inlet decreases, and vapor reappears at core outlet.

In contrast to blind results with SOCRAT, test data demonstrate that HPC water is quite fast heating up from top to bottom. The reason for this can be explained by vent line configuration which makes hot vapor jet discharge right in HPC water surface, thus provoking its intense mixing. Because of this HPC water coming to RPV is hotter than in blind calculations, and restart of vapor circulation through the chimney comes earlier. Due to one-dimensional limitation of RATEG models, effect of a fast heat up of HPC bottom regions could not be reproduced quantitatively neither in blind nor in open calculations, but the code reproduced the effect qualitatively. From 4050 s the primary coolant temperatures in SOCRAT calculations are lower than in experiment (Figs 4-129 and 4-130), though up to 4050 s they are correlating quite well. Correspondingly the core rod temperature is also 10-20 degrees underestimated in SOCRAT calculations after recirculation valves opening (Fig. 4-131).

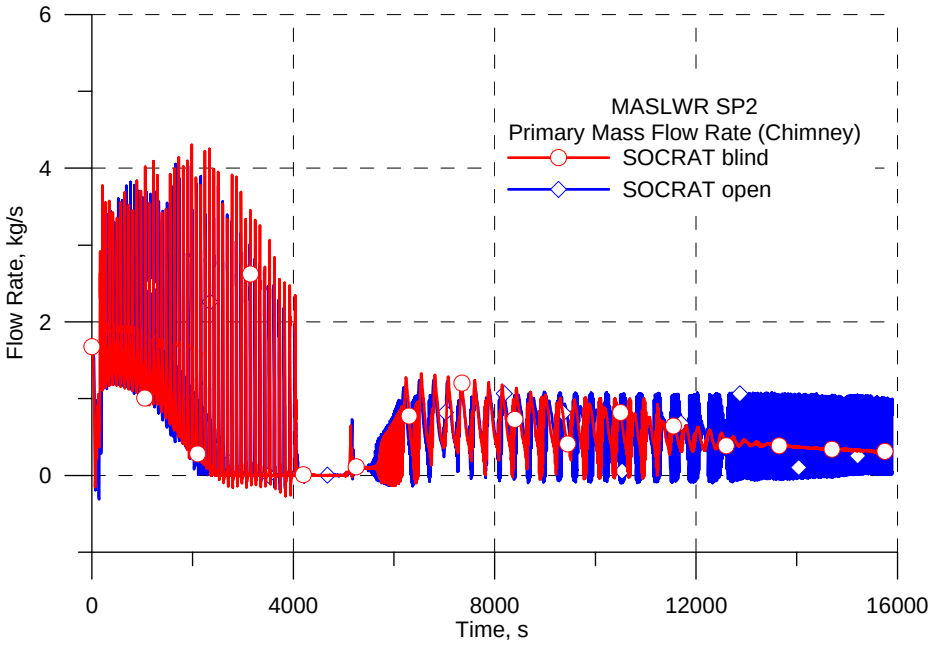

FIG. 4-128. Primary flow rate in chimney (calculation results).

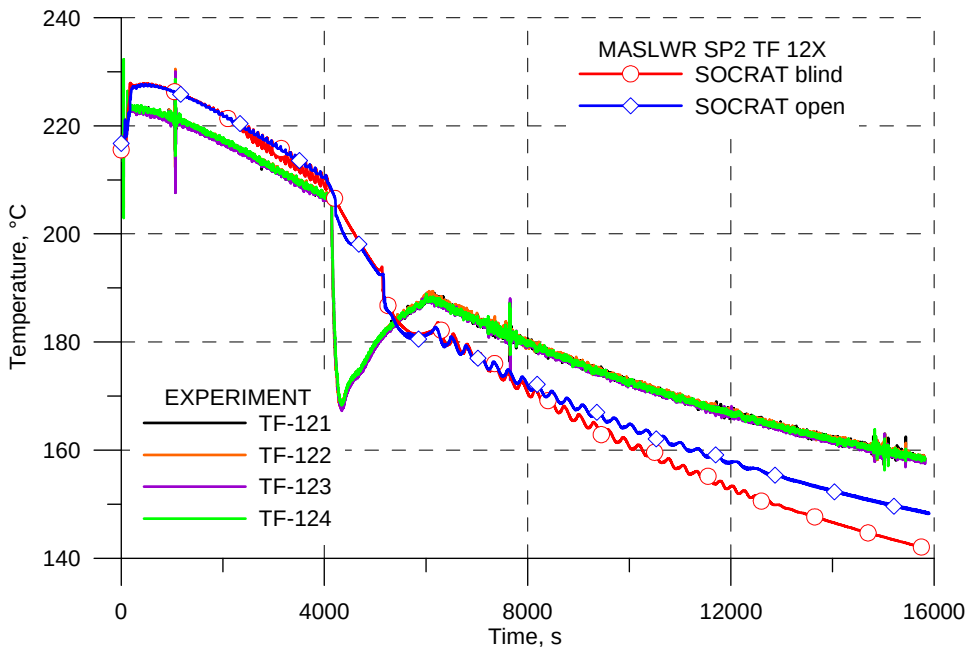

FIG. 4-129. Coolant temperature at core inlet.

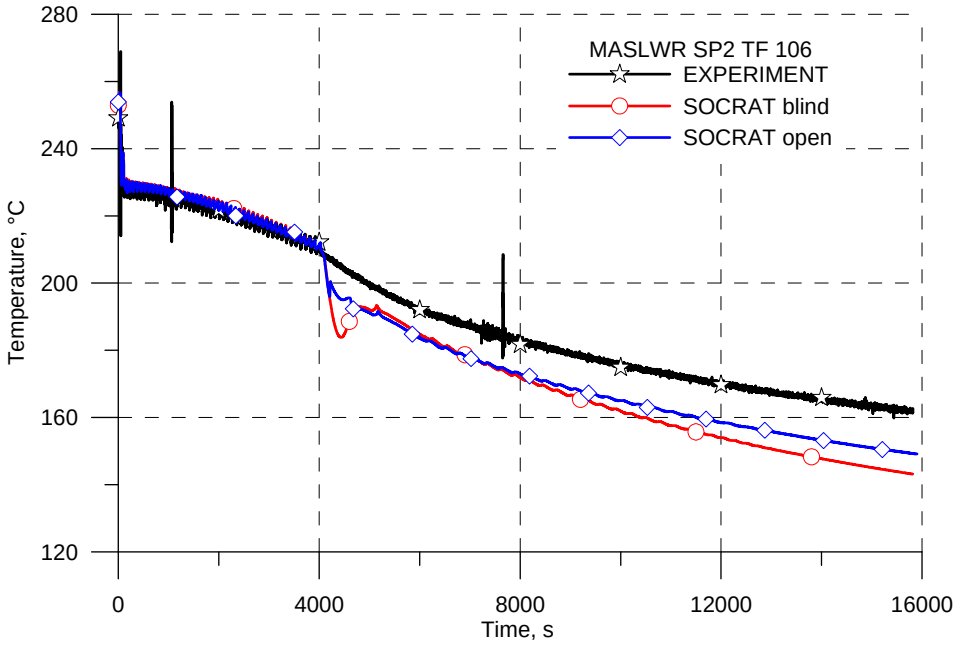

FIG. 4-130. Coolant temperature at core outlet.

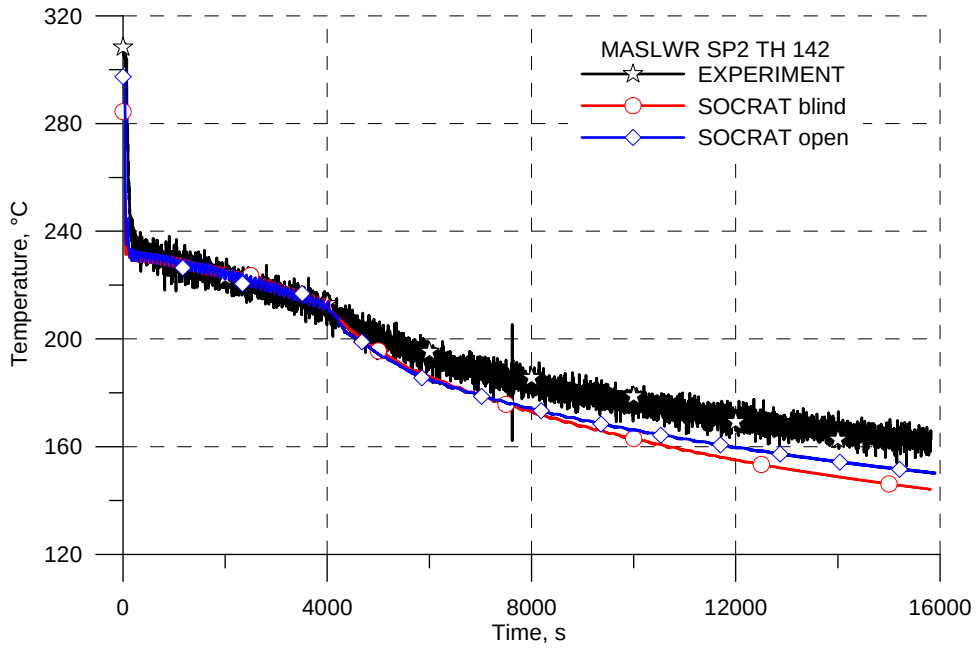

FIG. 4-131. Core rod temperature.

Results of calculation of pressure drops along RPV with SOCRAT are in good agreement with experimental results (Figs 4-132 to 4-134). Measurements for DP102 and DP105 seem to be corrupted (probably they reached their range limits), so they are not presented here. In all regions both blind and open calculations correctly predicted the trend of pressure drop change. The difference between measured and calculated values is constant throughout the transient and may be due to calibration feature at time zero. With the same initial pressure drop the difference would not exceed 5-10% in all range of parameters.

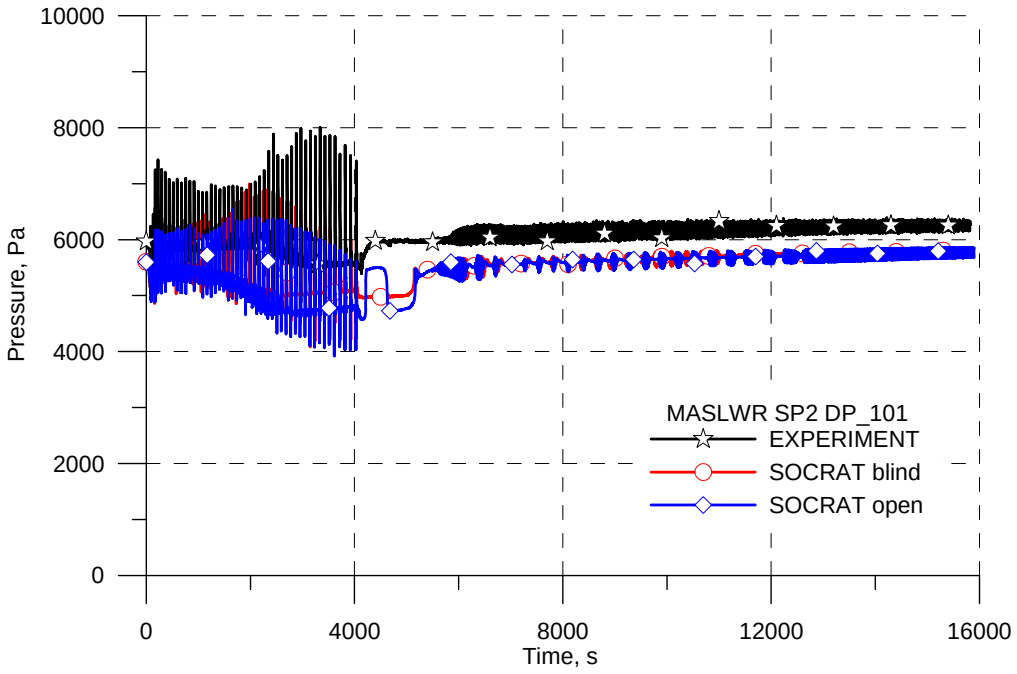

FIG. 4-132. Pressure drop at the core in SP-2.

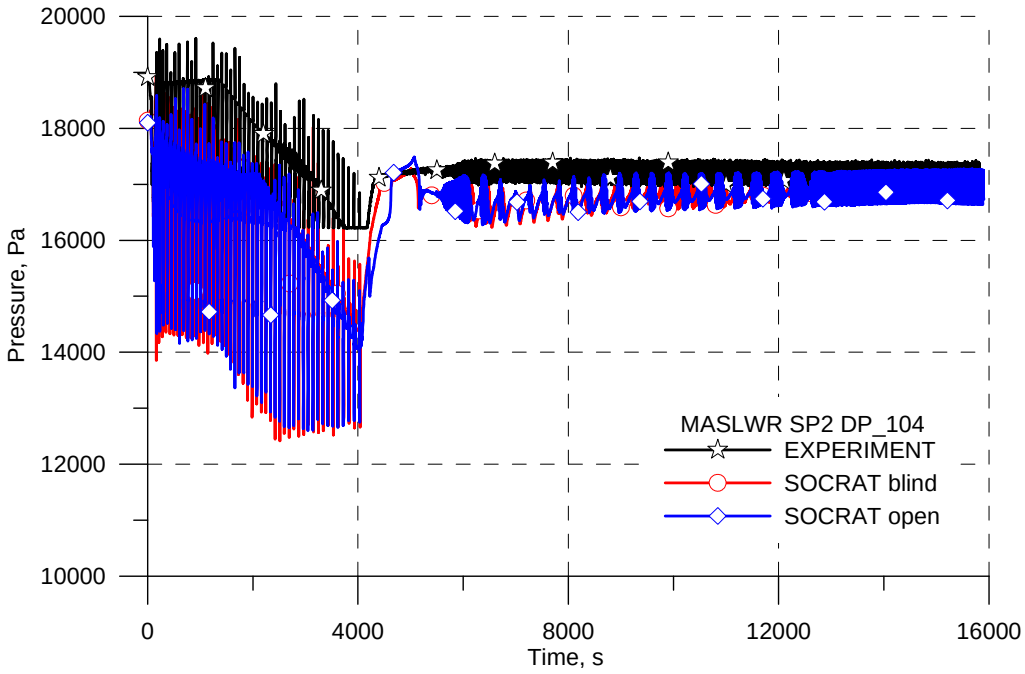

FIG. 4-133. Pressure drop at hot leg in SP-2.

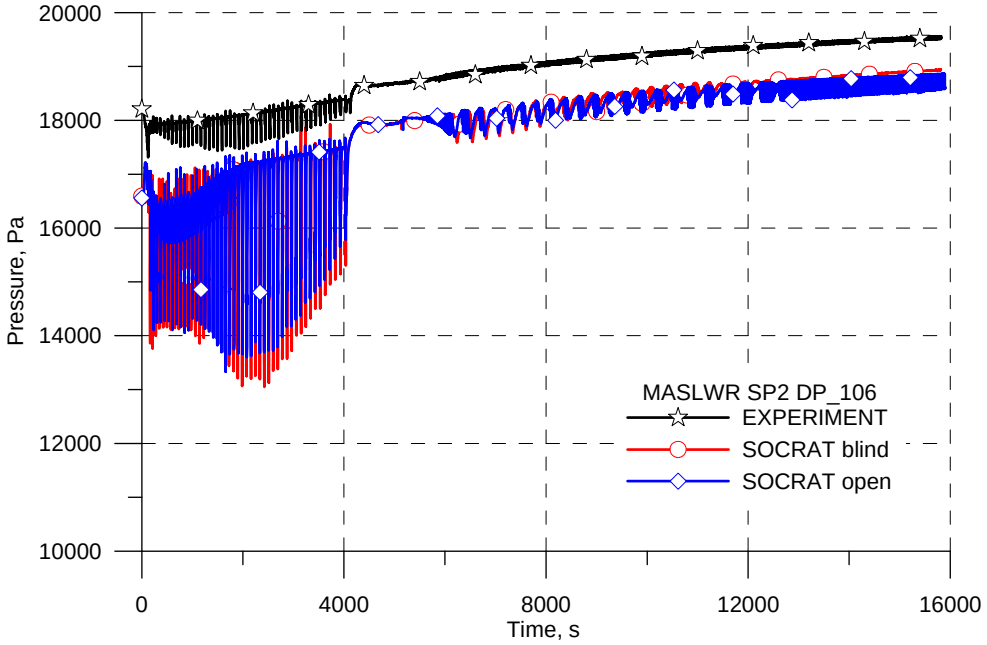

FIG. 4-134. Pressure drop at cold leg and downcomer in SP2.

4.6.3.2. SG thermal-hydraulic behavior

In conformance to SP-2 procedure the feedwater flow through SG was stopped as initiating event. At the same time the vapor flow from SG was stopped too, in blind calculations. After feedwater loss the power transferred to secondary side dropped to almost zero. Throughout the transient the heat transfer in SG remained at a very low level and was directed to primary coolant, because the secondary side temperature is following the primary cool down. In open calculation the vapor release from SG tubes was not blocked, and the results reproduced well the test data (Fig. 4-135).

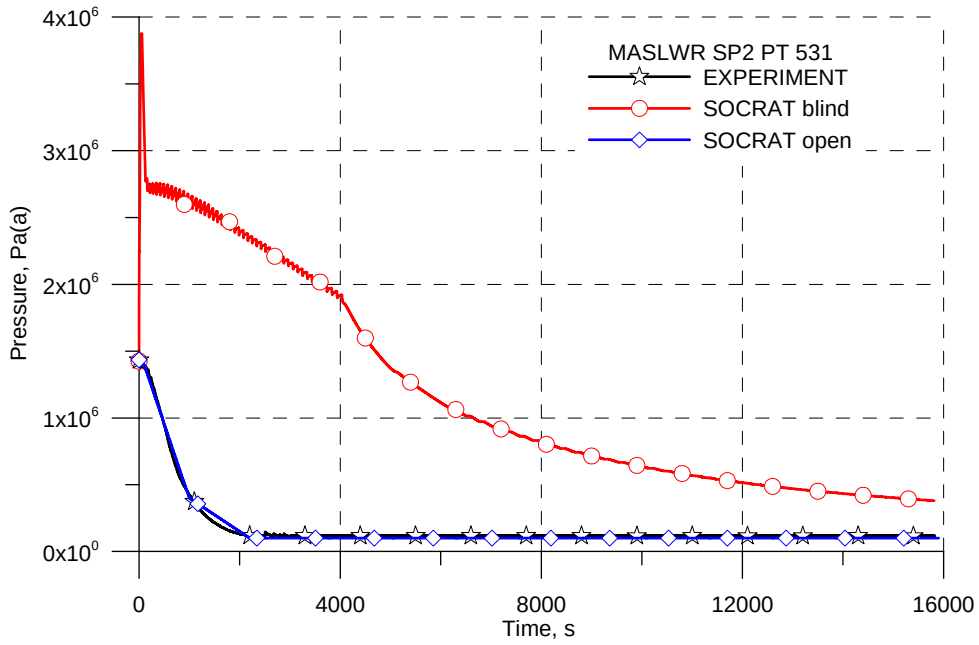

FIG. 4-135. Feedwater pressure for SG inner coil.

4.6.3.3. HPC thermal-hydraulic behavior

Average HPC pressure remains stable till 4050 s while it is experiencing large oscillations following PCS-106A valve blowdown (Fig. 4-136). Condensation of vapor coming from RPV to HPC free volume is efficient enough for pressure remaining stable. After opening of a second vent line there is a small peak in pressure but it is not exceeding the limit for SRV-800 opening. In calculations the rate of pressure decrease after 4000 s is higher than in experiment. That is probably due to the absence of a film-tracking model for HPC wall in SOCRAT.

Condensation process is also confirmed by HPC level rise as long as PCS-106A is releasing primary vapor to HPC (0 to 4050 s in Fig. 4-137). At time of sump return valves opening the level drops down because of water flow from HPC to RPV. Next it is slowly going down in accordance with pressure decrease and water density increase.

At vent valve opening, vapor coming from RPV in free volume of HPC leads to temperature rise in its upper region (TF-831 to 861). At this moment temperatures in the HPC upper region (free volume) are governed by vapor condensation on walls and they are close to saturation values (Figs 4-139 and 4-141). Then, as water level in HPC rises due to condensation process, the control volume with thermocouple TF-831 becomes filled with relatively cold water and temperature inside the control volume goes down (Fig. 4-138). At 4050 s the water level in HPC drops down by about 0.4 m, the cold water in control volume with TF-831 is replaced by hotter water falling down from control volume upside, and TF-831 is reheated. Afterwards heat transfer to CPV causes water cooling in this control volume. Further cooling of the system determines the almost equal rate of HPC temperature decrease at different elevations. The described processes are adequately reproduced by SOCRAT results.

Heat transfer in HPC bottom region is qualitatively reproduced by SOCRAT open calculation, though water temperature remains underestimated till recirculation line opening. In blind calculation a fast heat up of a bottom part of HPC could not be reached because of one-dimensional HPC nodalization (Fig. 4-140).

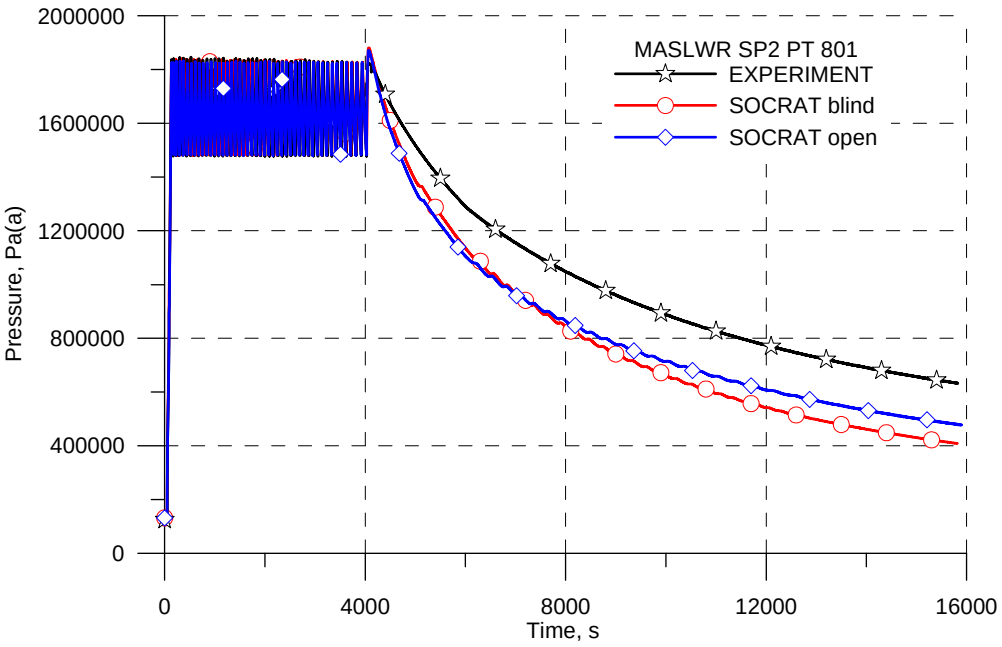

FIG. 4-136. Pressure in HPC.

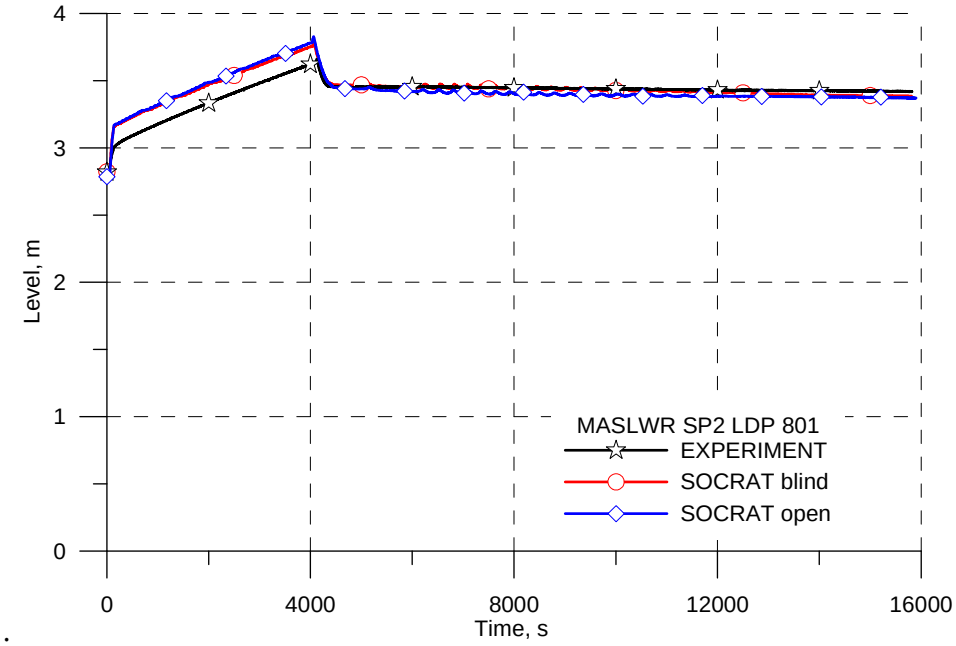

FIG. 4-137. Collapsed water level in HPC.

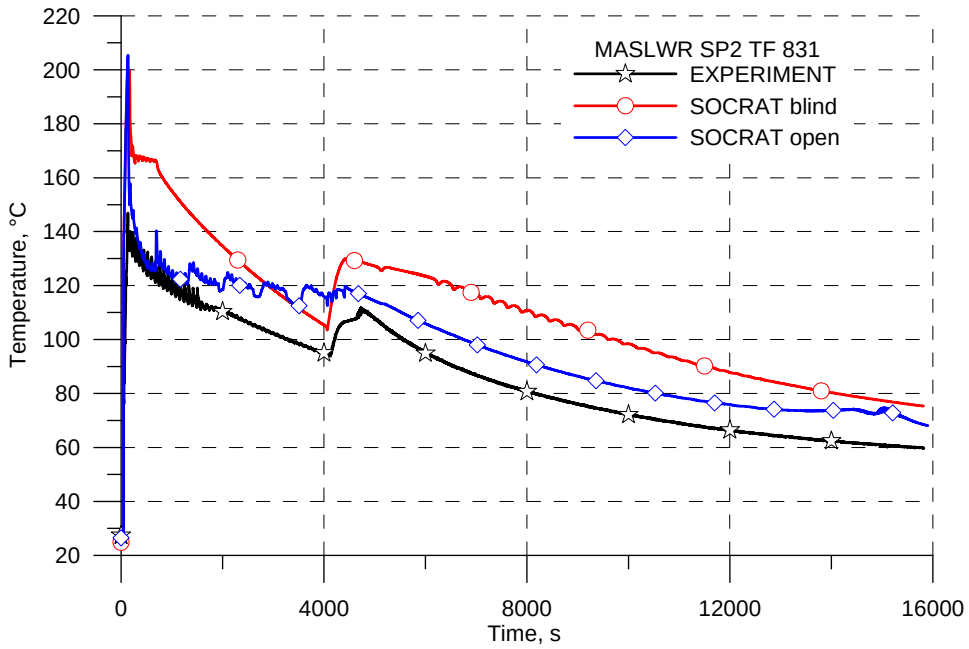

FIG. 4-138. HPC water temperature at level 3.

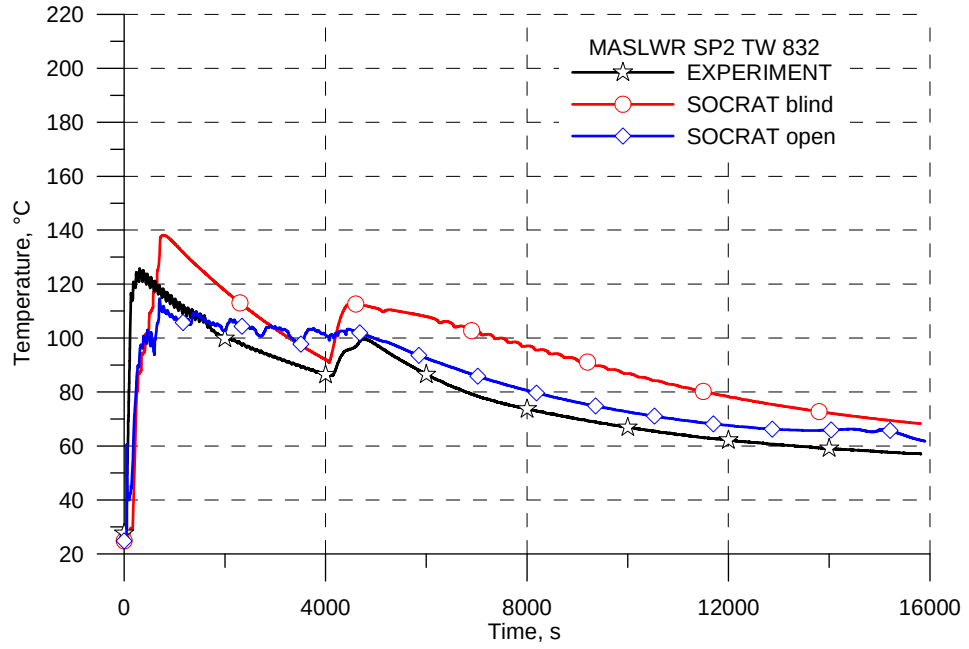

FIG. 4-139. Heat transfer plate internal temperature at level 3.

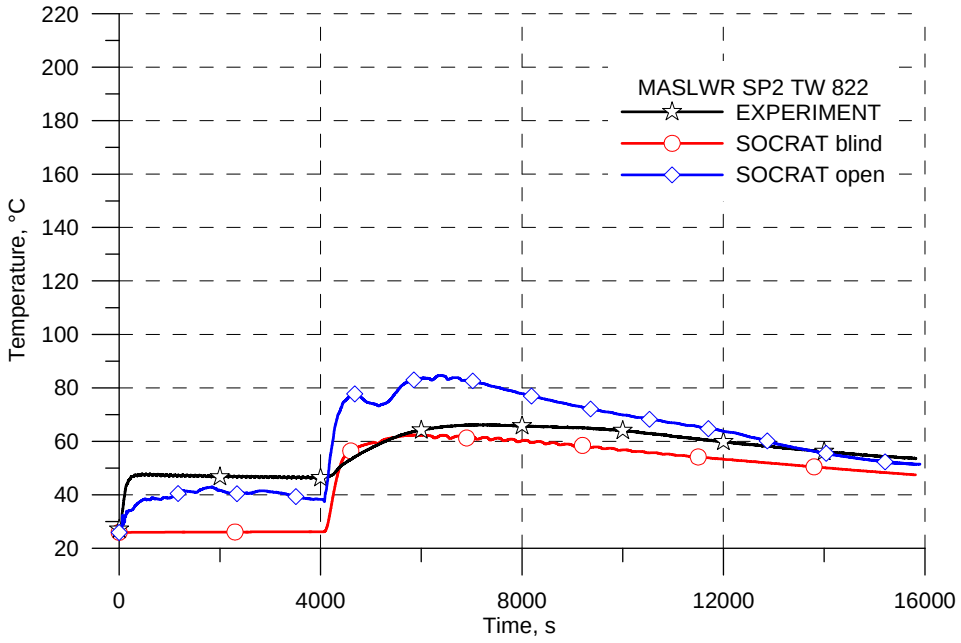

FIG. 4-140. Heat transfer plate internal temperature at level 2.

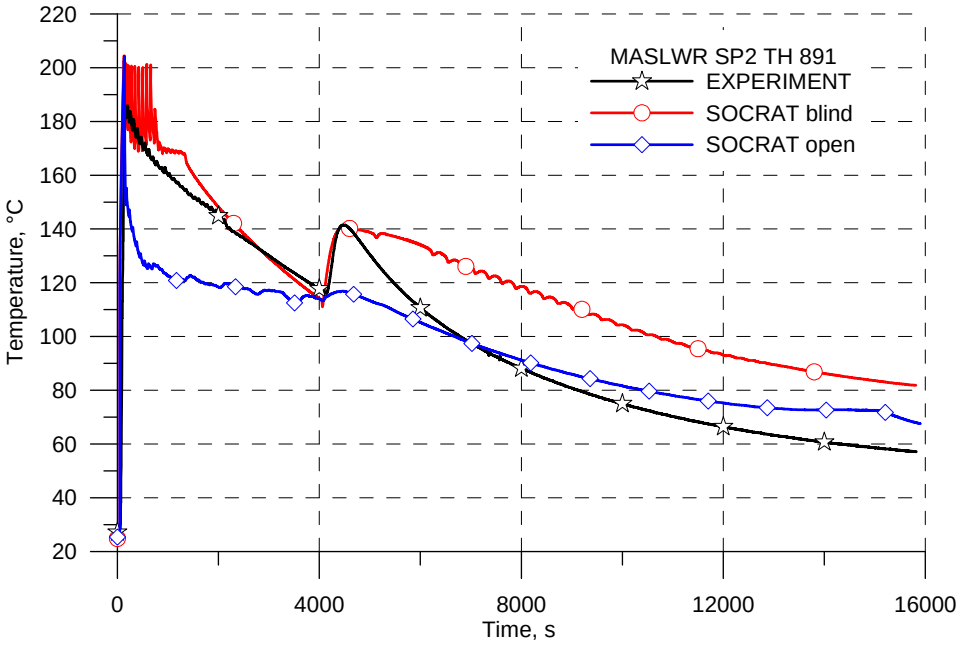

FIG. 4-141. HPC internal wall temperature.

4.6.3.4. CPV thermal-hydraulic behaviour

Thermal stratification in large pools of liquid is not reproduced correctly enough in SOCRAT calculation because RATEG module uses one-dimensional thermo-hydraulics and the nodalization loop for natural circulation in HPC could not simulate fairly the mixing of water. As one can see from test data (Figs 4-142 and 4-143), water in bottom (TF-825) and upper (TF-845) regions of CPV pool is heated by HPC water in some few minutes after vent valve opening. In calculations by SOCRAT water temperature rises very slowly in upper region and remains constant for about 4000 s in CPV bottom. It is explained by slow water heat-up in HPC and by the fact that in SOCRAT a CPV pool was

presented by only one channel. Test data reflect temperature at near-plate region while in SOCRAT temperature is given in a whole volume of the hydraulic cell (so it is an averaged value).

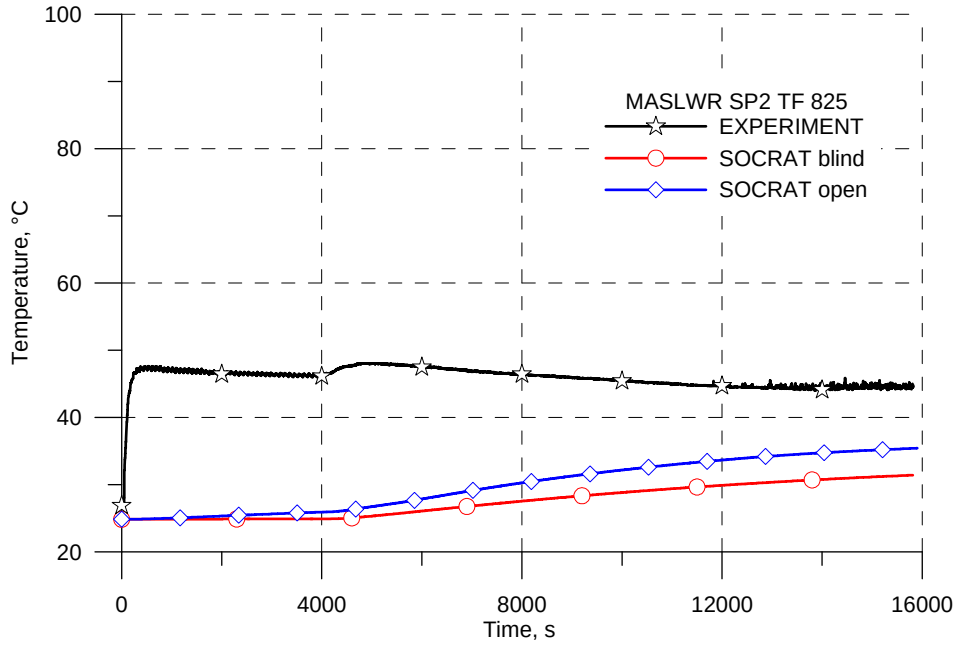

FIG. 4-142. Temperature of water in CPV bottom.

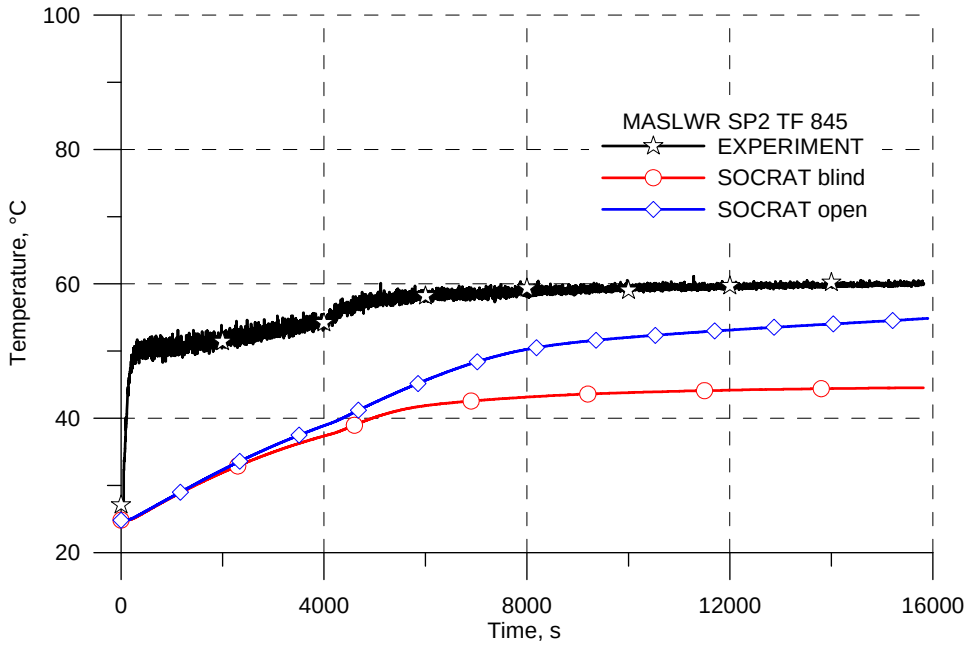

FIG. 4-143. Temperature of water in CPV upper region.

4.6.4. Analysis results for power maneuvering

Comparison of calculation results with test data in SP-3 steady-state is presented in Table 4-13. As for SP-2, again a good compliance for all parameters was achieved in SP-3. The deviation of the secondary superheat value is because SOCRAT value corresponds to SG tubes exit, and the test value was measured far downstream from SG. It will be shown in paragraph 4.6.4.2 that at SG exit the calculated and measured steam temperatures are in good agreement.

Besides, the modeling results show that a true steady state was not achieved in experiment, a primary temperature deviation of 0.004 K/s remained.

4.6.4.1. RPV thermal-hydraulic behavior

In blind calculation core power was step-wise increasing in conformance with transient scenario and the corresponding secondary mass flow rate was increasing in conformance with boundary conditions (Fig. 4-144). To get a better reproduction of test data in open calculation a secondary flow rate at transient stage was increased by 0.0035 kg/s (Fig. 4-144). That value is considered to be of the order of measurement system error of flowmeter. This change has had almost no effect on primary flow rate and core rod temperature (Figs 4-145 and 4-150), but a corresponding increase of the primary-to-secondary heat transfer by about 4 kW lead to a better modeling of some other parameters (Figs 4-146 to 4-149).

Primary flow rate shown in Figure 4-145 is governed by temperature difference between coolant in RPV bottom and upper part, and hence, power balance in core–SG system.

As can be seen from Figures 4-146 and 4-147, temperature difference at core edges increases with core power rise. Coolant temperature at core exit is increasing with time while water in downcomer gets colder. However coolant heat up is not large enough for reaching saturation.

Between 2700 and 3700 s heat transfer to the secondary side becomes larger than core power, because in test scenario core power is kept constant and secondary mass flow rate is increased. Primary water is cooled down and becomes colder than RPV walls. From 3700 s on, core power is again increased and that leads to coolant heat-up and coolant temperature at core outlet starts rising. All these variations in coolant temperature are reasonably correlating with blind calculation results and are quite well reproduced in open calculations.

As coolant is subcooled throughout the test progression, all collapsed level changes are determined by water density versus temperature variations, and by vapor density versus pressure variations. In open calculations increase of primary-to-secondary heat flux allowed primary water cooling, thus getting much better agreement of collapsed level calculation to level measurement (Fig. 4-148).

Primary pressure is regulated by pressurizer heaters. On average pressure in RPV is kept constant throughout the transient (Fig. 4-149). Again blind calculation results are in a reasonable agreement with test data, and are significantly improved in open calculations.

Temperature margin between walls of core rods and coolant depends on core power and in calculations makes ~25 degrees at 200 kW and ~40 degrees at 320 kW. In last case a generation of bubbles on core rod walls becomes possible. This is because wall temperature exceeds saturation temperature by 3 – 4 degrees. However bubbles are not transported from rods to the core of flow channels.

As in case of SP-2, results of calculation of pressure drops along RPV got with SOCRAT for SP-3 are in good agreement with experimental results (Figs 4-151 to 4-153). Explanation for differences between calculated and measured values is given in paragraph 4.6.3.1.

TABLE 4-13. STEADY-STATE COMPARISON FOR TEST SP-3

Parameter	Unit	Experimental Value	SOCRAT Calculations*	
			Blind	Open
Pressurizer pressure	MPa(a)	8.719	8.718	8.729
Pressurizer level	cm	35.74	34.40	35.49
Power to core heater rods	kW	21.19/21.00	21.19/21.00	21.19/21.00
Feedwater temperature	ºC	31.49	31.50	31.5
Steam temperature	ºC	205.44	259.70*	257.9*
Steam pressure	MPa(a)	1.446	1.444	1.444
Ambient air temperature	ºC		25	25
Primary flow at core outlet	kg/s		0.78	0.80
Primary coolant temperature at core inlet	ºC	250.11/250.69 250.21/------	251.30	249.4
Primary coolant temperature at core outlet	ºC	262.76	261.67	259.9
Feedwater flow	kg/s		0.012	0.0135
Steam flow	kg/s		0.012	0.0135
Primary coolant subcooling at core outlet	ºC		39.6	40
Total heat loss through primary system	kW		4.7**	3.2**
Heat transfer through SG	kW		33.7	37.7
Maximum surface temperature of core heater rods	ºC		273.4	274.3
Location from the SG secondary inlet to reach - saturation - superheat	m		 0.2 0.7	 0.2 0.7

* exit plane of SG tubes
**coolant to vessel

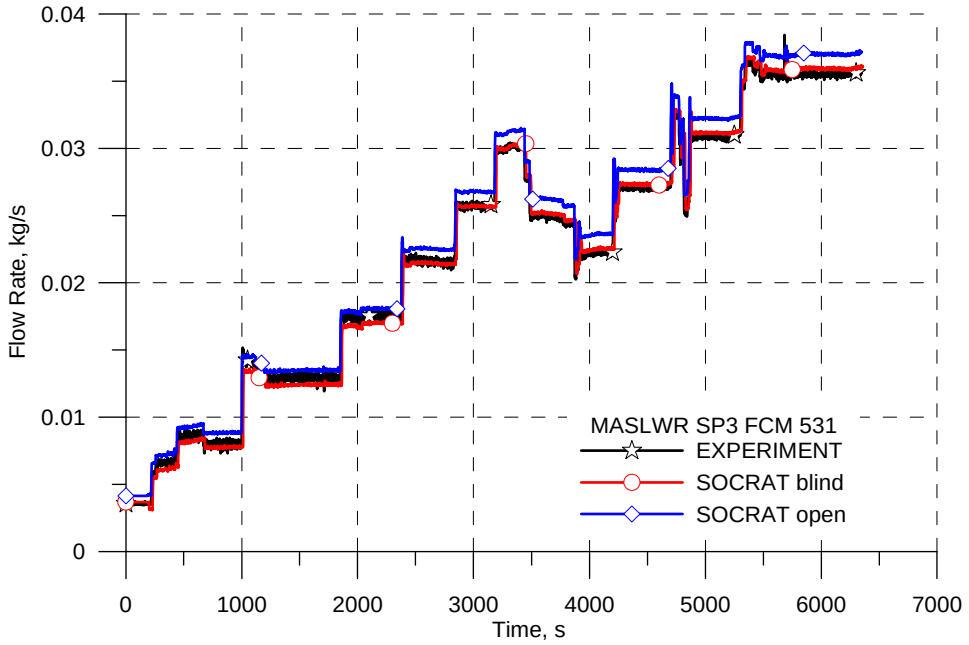

FIG. 4-144. Change of the secondary flow rate.

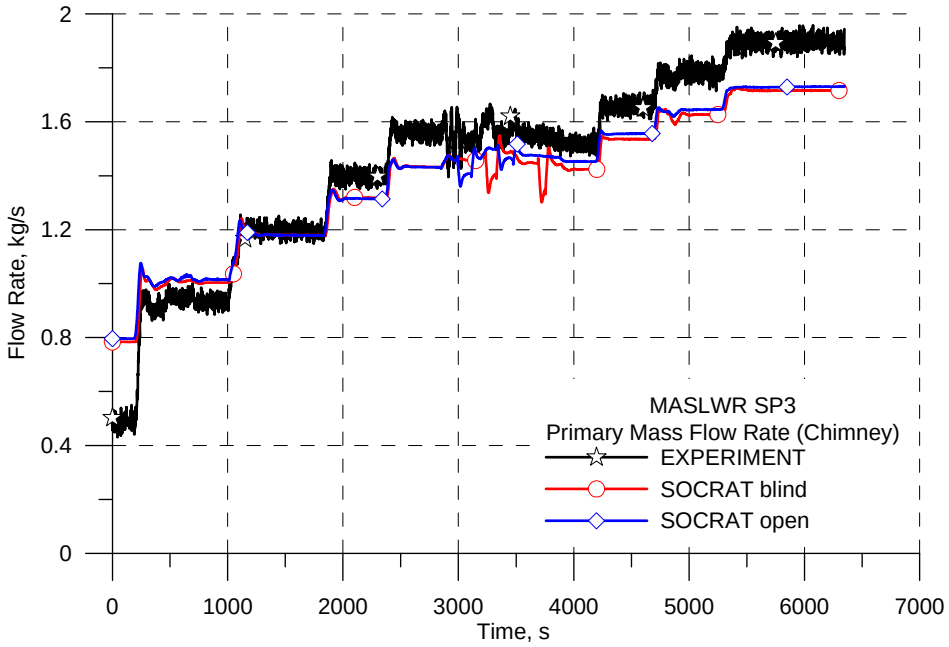

FIG. 4-145. Primary flow during the transient.

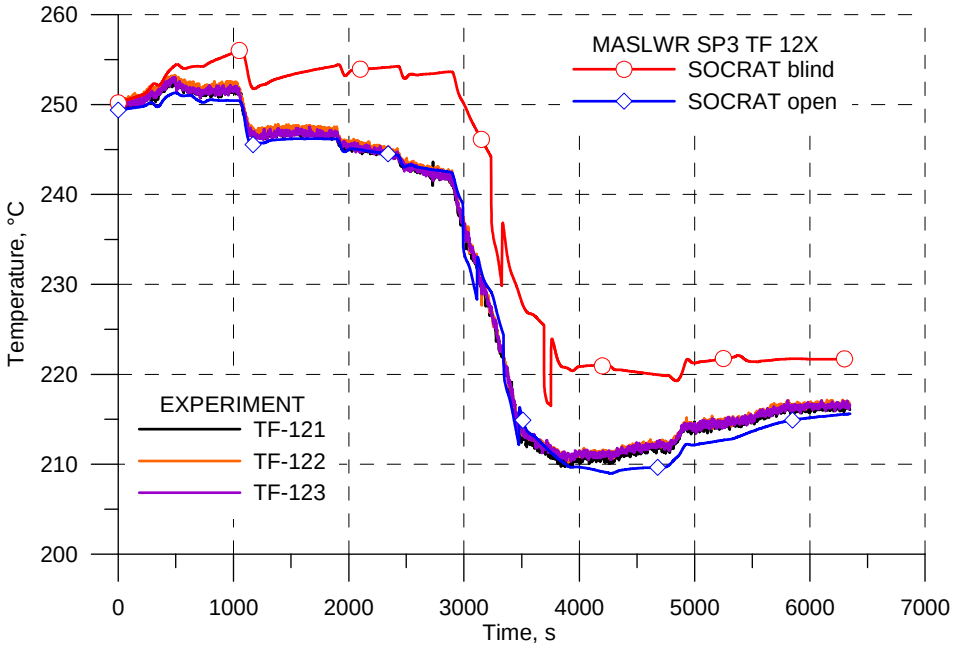

FIG. 4-146. Core inlet temperature during the transient.

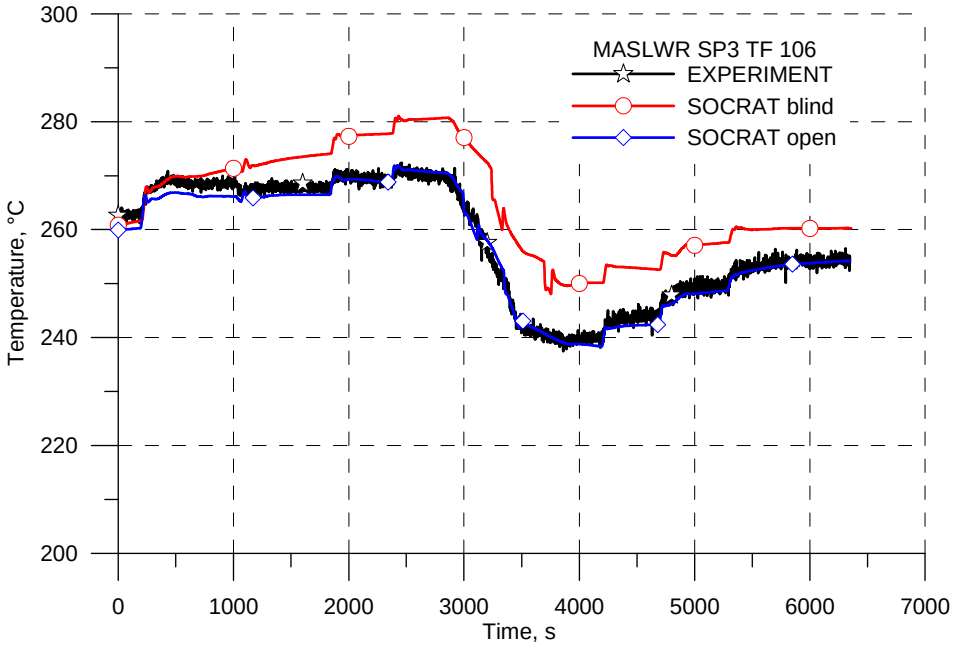

FIG. 4-147. Core outlet temperature during the transient.

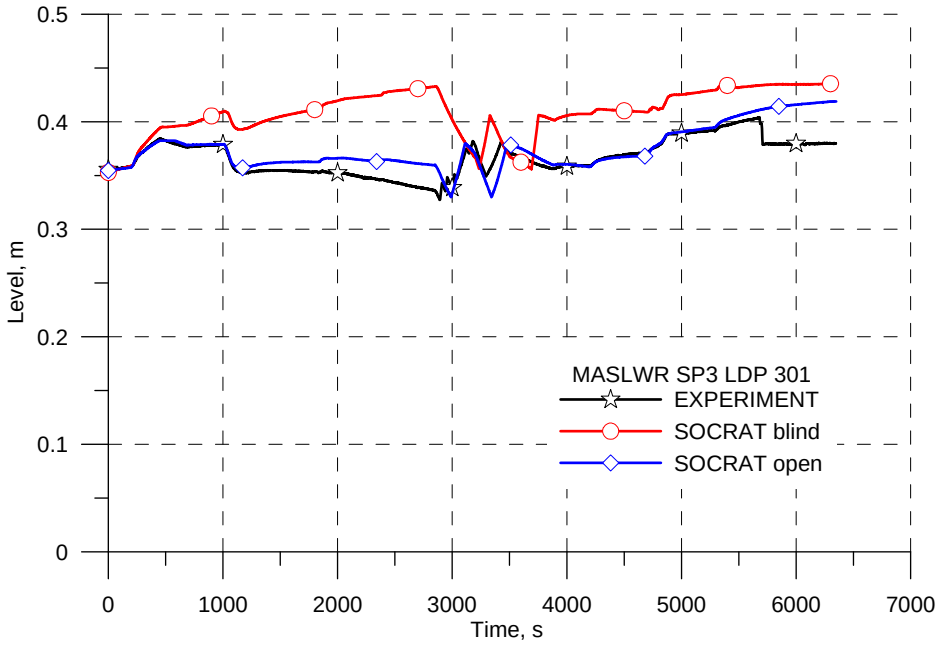

FIG. 4-148. Water level in RPV.

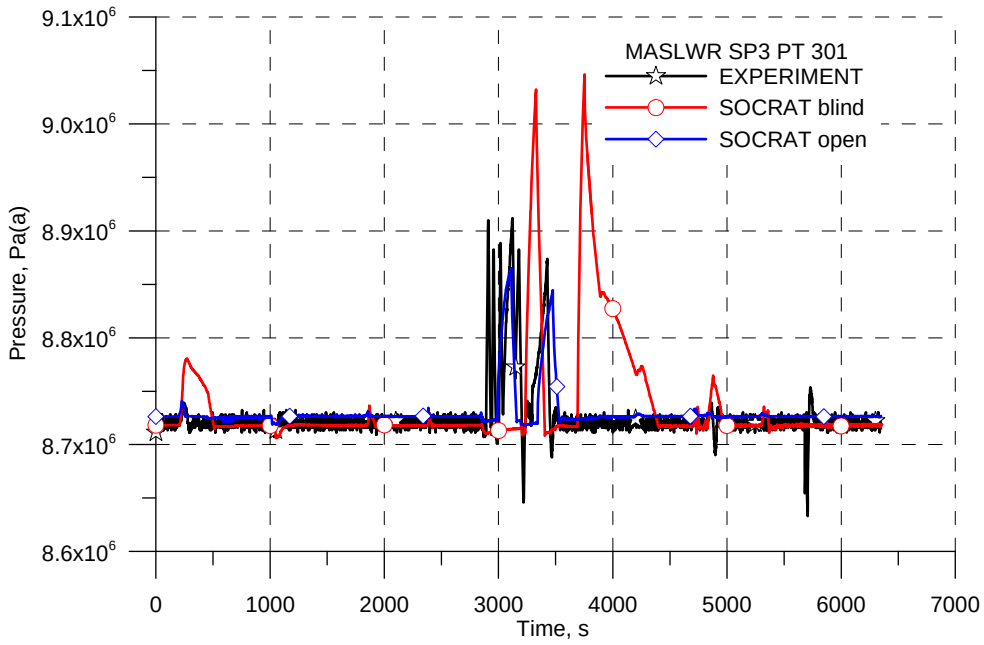

FIG. 4-149. Primary pressure during the transient.

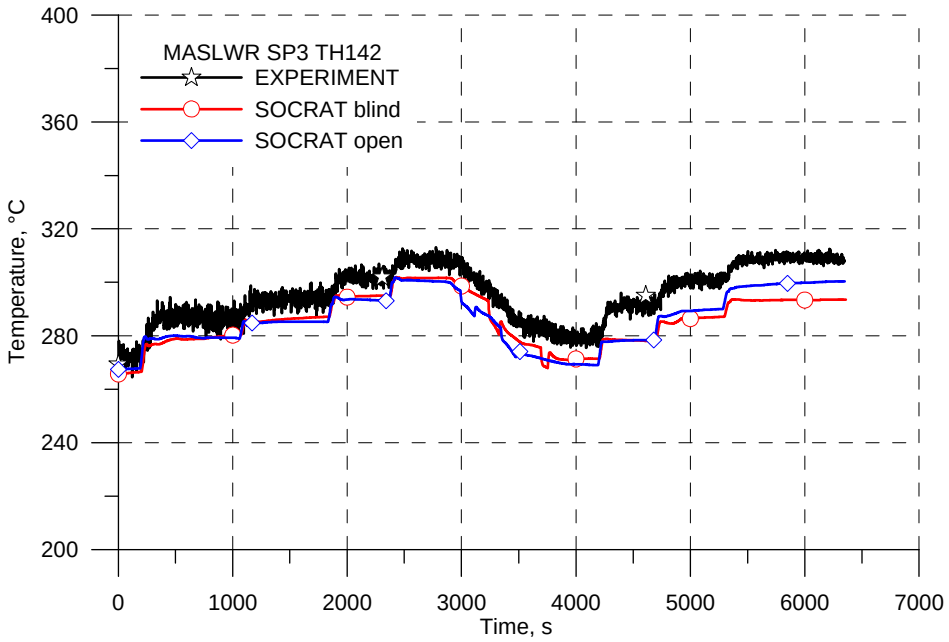

FIG. 4-150. Wall temperature of core rods.

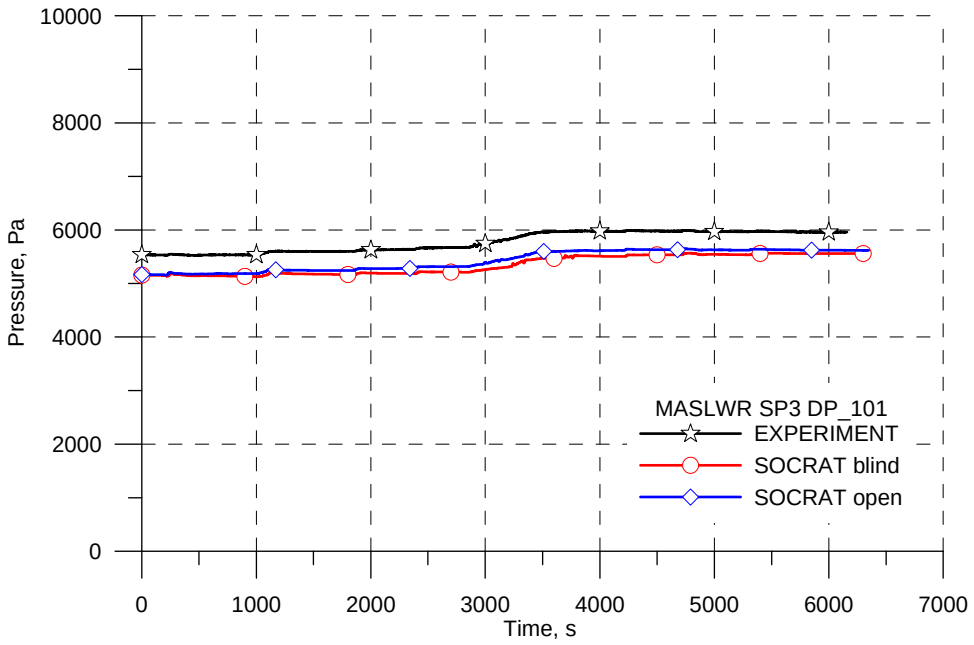

FIG. 4-151. Pressure drop at the core in SP-3.

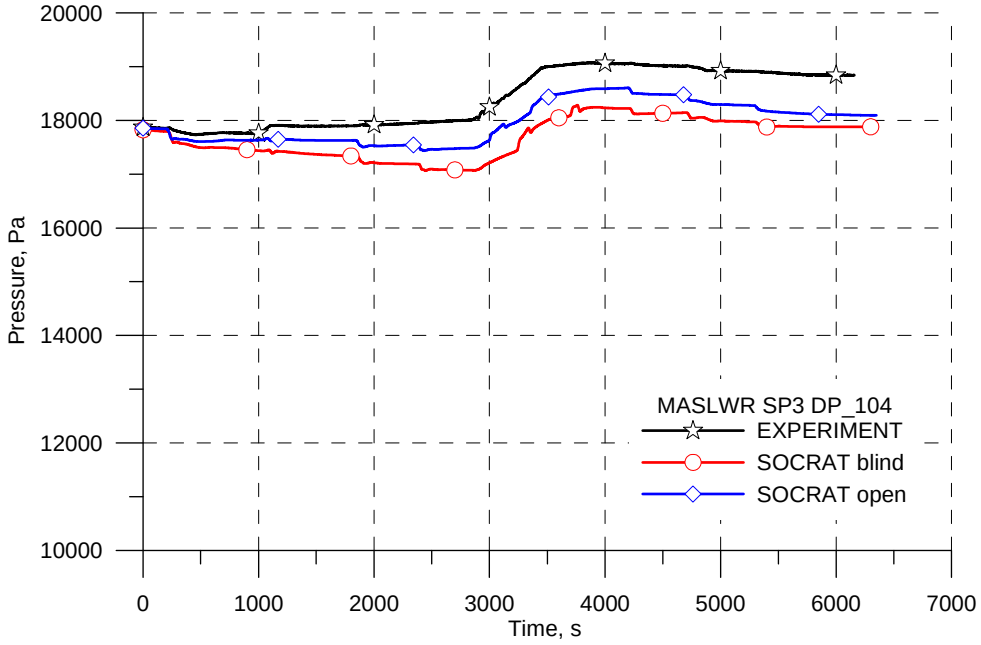

FIG. 4-152. Pressure drop at hot leg in SP-3

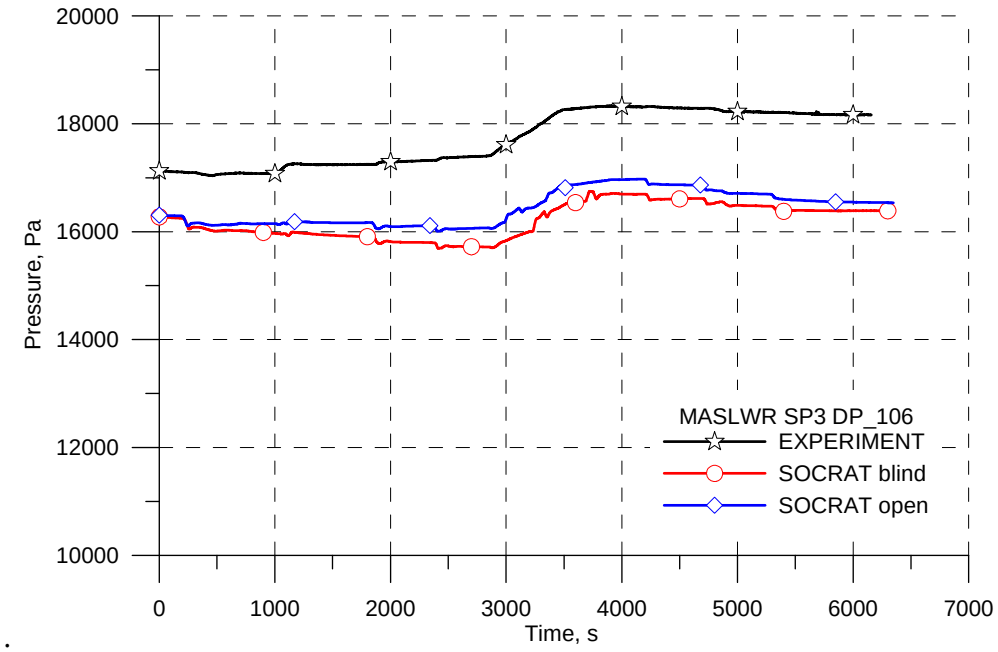

FIG. 4-153. Pressure drop at cold leg and downcomer in SP-3.

4.6.4.2. SG thermal-hydraulic behavior

Increasing secondary flow rate in open calculations allowed a better agreement of secondary steam temperature (Fig. 4-154) and pressure (Fig. 4-155) with test data.

As shown in Figure 4-154, vapor superheat at SG tubes outlet remains almost constant after 4000 s. By this time RPV metal structures are cooled down, since from 2500 to 4000 s heat transfer to the secondary side prevailed over core power generation. From 4000 s on, some part of core power was reheating the RPV and chimney walls and heat transferred to the secondary side was not enough to increase secondary superheat. For steam superheat of 10 degrees about 0.5 % of nominal core power is needed, and 10°C overestimation of steam temperature after 3500 s has almost no influence on general results.

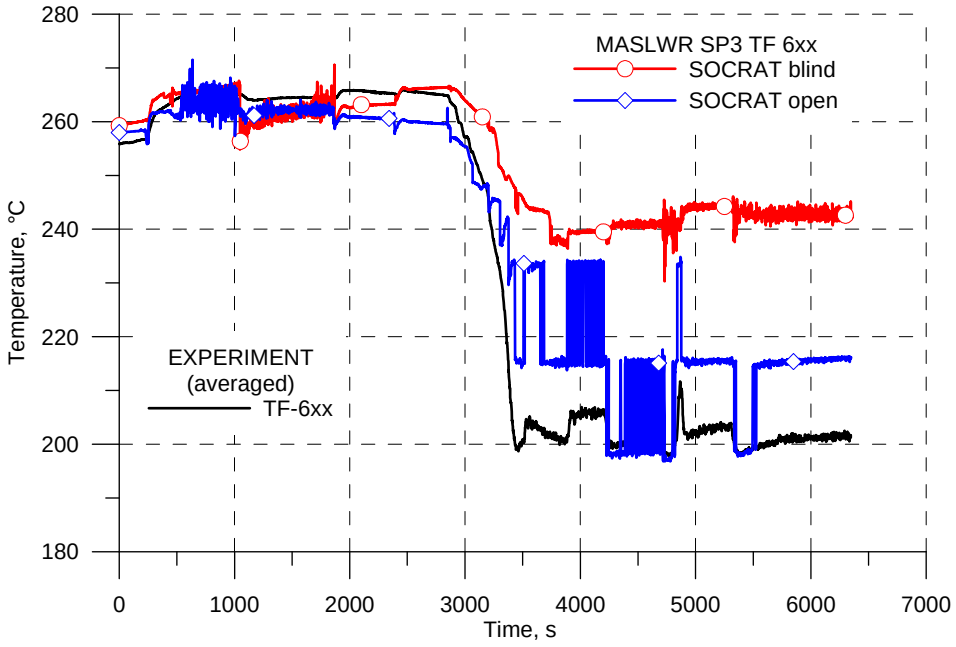

FIG. 4-154. Secondary steam temperature.

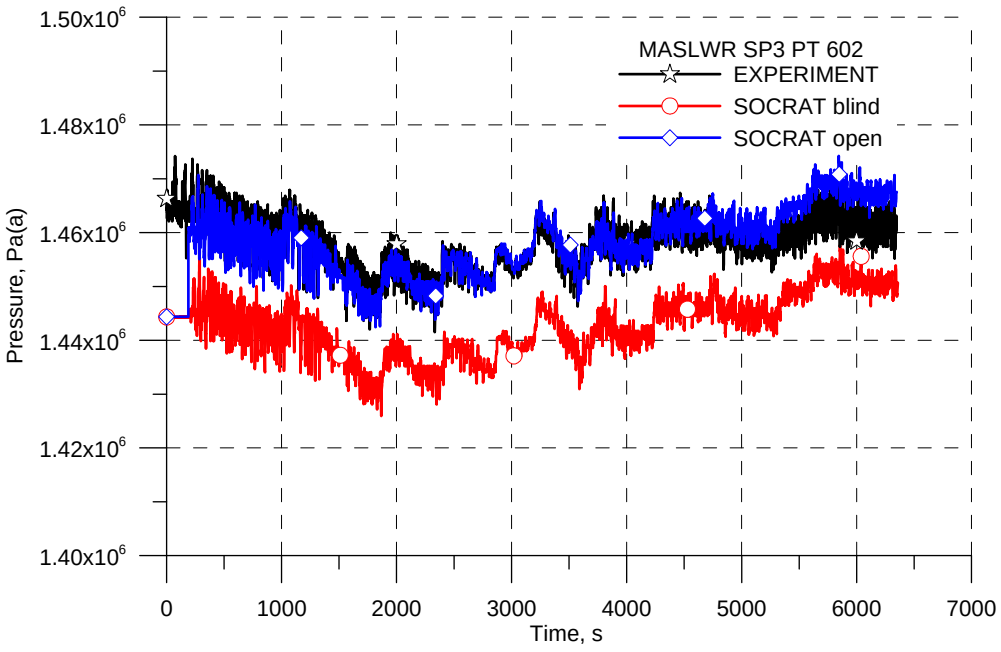

FIG. 4-155. Secondary pressure.

4.7. KAERI — REPUBLIC OF KOREA

4.7.1. Computer Codes

TASS/SMR-S code has been used. TASS/SMR-S is a thermal-hydraulic system analysis code that is developed by KAERI, focused on an integral PWR [23]. The main purpose of the code is to simulate all relevant phenomena, processes and conditions of reactor system that may occur during transients. And several conservative transient models are adopted in the code to describe thermal-hydraulic behaviours of plants.

Analysis with TASS/SMR-S code is based on system modelling consist of node and path. Node is a control volume that has mass and energy, and each node is connected through path. Nodes can consist of water, steam and non-condensable gas, and its thermal-hydraulic behaviours are calculated with 3-equation Homogeneous Equilibrium Model (HEM) with drift flux model. The drift-flux model makes up for the weak point in the 3-equation HEM model. The drift-flux model can consider relative speed of steam in the two-phase flow condition.

Besides the conservation equation, TASS/SMR-S code has several component models that are capable of integral PWR system analysis, especially the SMART plant. The core model is capable of heat transfer calculation in the core. The Reactor Coolant Pump (RCP) model is used for primary coolant flow rate calculation, as well as RCP coast down. The steam generator model is capable of heat transfer calculation on once-through helically coiled steam generator, and passive heat removal system model is capable of describing the passive residual heat removal system of SMART.

4.7.2. System idealization

4.7.2.1. System idealization for blind calculation

For general, core is modeled by 6 nodes with same height. Core power fraction is evenly distributed to 6 core nodes. Steam generator is nodalized with 10 nodes with same height. Code embedded steam generator model is applied on steam generator modelling. Heat transfer through inactive region is ignored. Every structure of primary system such as vessel and barrel, and HPC are considered as heat structure. However, structures for secondary system and CPV system are not considered as heat structure except heat transfer plate between HPC and CPV. Ambient heat loss is given as boundary condition for each analysis and proportionally distributed by node height to vessel-adjoining nodes.

Geometric input of TASS/SMR-S code is based on node and path. Node is a control volume that shares common thermal-hydraulic properties and path is a connection for mass and energy exchange. The system analysis should be started from proper nodalization. Figure 4-156 shows nodalization of the MASLWR facility for TASS/SMR-S code analysis. Diagrams with black number mean nodes and lines with red number mean paths at the nodalization. Nodalization includes all the vessels including RPV, HPC and CPV as well as ADS lines. Nodes for RPV are assigned to node 1 to 48. Core region is divided by 6 nodes and SG region is divided by 10 nodes, respectively. The nodes for hot leg region and downcomer region are nodalized with 13 nodes each. The hot leg and downcomer nodes are connected to lower and upper plenum, then make a closed coolant loop for PRV. Pressurizer is modelled with one node to adopt the code-embedded pressurizer model.

The HPC and CPV are nodalized by 12 nodes each. The node height for HPC and CPV is modeled to achieve a consistency in elevation between center of the nodes and the thermocouples. Also every neighbouring node in HPC and CPV is connected with path to simulate the natural circulation of HPC and CPV.

For the secondary system, steam generator is nodalized by 10 nodes. And 14 steam generator tubes are merged into 1 tube with same heat transfer area. A huge node is connected with steam generator tube outlet as steam boundary.

Also ADS lines are fully modeled as each path. The ADS area is assumed as ADS pipe cross-sectional area, not the minimum flow are of ADS valves.

For SP-2 analysis, the feedwater flow rate and the core power are given as boundary condition that follows test procedure. The ADS valve operation logics are fully embedded on analysis. The feedwater isolation valve is closed at the beginning of transient with no stroking time, and the ADS valves are operated with no stroking time. Ambient heat loss for steady-state calculation is assumed as 41.71 kW, which is about 14% of initial core power. Ambient heat loss for transient calculation is assumed as 11.86 kW that is induced from SP-3 calculation. Heat losses for ADS line, HPC and CPV are ignored.

For SP-3 analysis, the core power is given by boundary condition that follows experimental data, not as test procedure. Also feedwater flow follows experimental data, not as secondary system control logic. The charging flow logic is added to the RPV lower plenum directly. The ambient heat loss for steady-state is assumed as 11.86 kW.

4.7.2.2. System idealization for open calculation

The heat structure model at the HPC is added to improve the pressure behaviour in the HPC. The system nodalization for open calculation is the same as blind calculation. However some modelling are modified to improve calculation results. The heat structures for heater rods are added to calculate heater surface temperature. The heat balances to estimate ambient heat loss is re-calculated.

For SP-2 analysis, the ambient heat loss for steady-state calculation is assumed by 44.50 kW, which is about 15% of initial core power. The Ambient heat loss for transient calculation is given by 15% of the current decay power. Heat losses for ADS line, HPC and CPV are ignored.

For SP-3 analysis, the ambient heat loss for steady-state and transient is assumed by 12.25 kW, which is about 4% of maximum core power.

4.7.3. Analysis results for loss of feed-water transient

For steady state calculation, thermal-hydraulic values such as core power and feedwater flow rate should be given as boundary condition. But some of values remained unknown. So, these unknown variables are estimated from heat balance calculation. Figure 4-157 shows the calculation procedure. From the core power and core region enthalpy change, primary coolant flow rate could be calculated. Then, SG heat transfer from primary to secondary could be calculated from primary coolant flow rate and SG region enthalpy change. At last, feedwater flow rate could be decided from SG heat transfer and secondary enthalpy change. With the calculated condition, steady state calculation is performed. The calculated steady state conditions are compared with experimental values in Table 4-14.

SP-2 test is a loss of feedwater transient with decay power. Therefore feedwater flow rate and core power are given as boundary conditions. Figure 4-158 represents core power for experiment, blind calculation and open calculation. Feedwater supply is ceased at 0.0 s, and core power is decreased at 38.0 s. The ADS vent valve is opened at 51.0 s, manually. Ambient heat loss for transient is also given as boundary condition. The ambient heat loss is given by 15% of the current decay power.

4.7.3.1. RPV Thermal-Hydraulic Behaviour

Figure 4-159 shows primary mass flow rate at chimney. The mass flow rate decrease continuously from the beginning of transient to first opening of ADS vent valve. The natural circulation of RPV is sustained by heat generation of core and heat removal by SG. However, the heat removal is lost at the beginning of transient. Therefore the single phase natural circulation of RPV is decreased until first opening of ADS vent valve.

The opening of ADS vent line causes RPV depressurization as a result of steam discharge. Figure 4-160 shows the PZR pressure behaviour. The depressurization causes saturation temperature decrease, and then the RPV coolant starts boiling. Figure 4-161 represents the void fraction of core outlet. The boiling of coolant is the main reason of flow instability at early phase of transient. And there is a significant difference between blind and open calculation result. It comes from difference of pressure behaviour. The depressurization of open calculation is more significant than blind calculation. Therefore, the coolant of open calculation reaches at saturation point earlier than blind calculation.

After first oscillation for 60.0 to 300.0 s, the mass flow rate increases up to around 2.5 kg/s and decreases until ADS sump operation. Figure 4-162 shows the ADS vent line discharge flow rate. During this period, the coolant of RPV is discharged into HPC and void fraction of RPV is increased by ADS vent line operation. Therefore the mass flow rate is decreased by increase of path void fraction. Also core power reduction is a reason of mass flow rate decrease.

At 2939.0 s, pressure difference between PT-301 and PT-801 is smaller than 0.034 MPa. So, the sump line valve opened at that time and it causes second flow instability. Figures 4-163 and 4-164 show the HPC pressure behavior and the sump line flow rate. Also the core inlet temperature is decreased by surge flow from HPC to RPV. Figure 4-165 represent the averaged core inlet temperature. But, the temperature drop due to surge flow is not significant in calculation. The reason for this difference is the flow instability that is induced by sump line opening. Due to the flow instability, the HPC coolant is not surged into RPV fully. Therefore the core inlet coolant temperature is not dropped as experiment.

For the ADS behavior, PZR water levels of calculation both blind and open are much higher than experimental result as shown as Figure 4-166. And the water levels of calculations reach at ADS vent line elevation for some period. Therefore two-phase coolant is discharged through the vent line. The solidation of PZR is a characteristic of system analysis code based on HEM model. At the HEM model, the void fraction of RPV nodes is over-estimated. And PZR in-surge flow is over-estimated by void fraction over-estimation. That is the reason for most of difference between experiment and calculation.

For heat transfer in the core, Figure 4-167 shows the heater surface temperature for experiment and open calculation. The heater surface temperature of calculation is much lower than experiment, but very similar with coolant temperature of calculation. From the result, the difference of heater surface temperature comes from under-prediction of coolant temperature.

Figure 4-168 shows the heat transfer across chimney. The heat transfer across chimney is decided by coolant temperature difference between hot leg and cold leg. And the coolant temperature difference comes from heat balance between heat generation of core and heat removal of SG. Therefore the heat transfer across chimney is reduced from beginning of transient until sump valve operation.

4.7.3.2. SG thermal-hydraulic behaviour

SP-2 transient is a scenario for a loss of feedwater. Therefore heat transfer across SG is eliminated as Figure 4-169. However the sump valve operation makes the primary coolant temperature decrease, and SG stored energy is transferred reversely into primary coolant. Figures 4-170 and 4-171 show

secondary steam temperature and pressure. Secondary steam temperature and pressure are not changed as much as other thermal hydraulic behavior of RPV due to loss of feedwater.

4.7.3.3. HPC thermal-hydraulic behaviour

Figure 4-163 shows HPC pressure behaviour. The ADS vent line operates properly and maintain HPC pressure between control criteria. Also sump valve is opened by control logic and makes natural circulation path between the HPC and the RPV with ADS vent line. Figure 4-164 shows the sump line flow rate.

Figure 4-172 shows the HPC temperature of top and bottom. The thermal stratification is observed at both results from experiment and calculation. Until the sump valve operation, hot water comes from upside of HPC and top temperature is much higher than bottom temperature. Therefore natural circulation inside HPC is very restricted. It makes such a thermal stratification. But the operation of sump valve makes natural circulation inside HPC. And it makes the temperature difference between top and bottom of HPC coolant small. But the temperature difference of open calculation is less than experimental result after sump valve operation. It means natural circulation over-prediction of TASS/SMR-S code.

4.7.3.4. CPV thermal-hydraulic behavior

Figure 4-173 shows the coolant temperature behavior of CPV. The coolant temperatures increased continuously by the heat transfer through plate. And thermal stratification is observed as HPC. The sudden increase of HPC coolant temperature on experiment is a consequence of large amount of heat transfer at early phase of transient. But the heat transfer model could not predict it.

TABLE 4-14. STEADY-STATE COMPARISON FOR TEST SP-2

Parameter	MASLWR	Unit	Experimental Value	Calculation Value
Pressurizer pressure	PT-301	MPa(a)	8.719	8.721
Pressurizer level	LDP-301	m	0.3606	0.3610
Power to core heater rods	KW-101/102	kW	297.40	297.37
Feedwater temperature	TF-501	ºC	21.23	21.37
Steam temperature	FVM-602-T	ºC	205.33	204.78
Steam pressure	FVM-602-P	MPa(a)	1.431	1.429
Ambient air temperature		ºC		N/A
HPC pressure	PT-801	MPa(a)	0.1268	0.1455
HPC water temperature	TF-811	ºC	26.26	27.02
HPC water level	LDP-801	m	2.820	2.820
CPV water temperature	TF-815	ºC	25.95	27.02
Primary flow at core outlet	FDP-131	kg/s	*Not Given	1.691
Primary coolant temperature at core inlet	TF-121/122/ 123/124	ºC	215.08	215.23
Primary coolant temperature at core outlet	TF-106	ºC	249.14	251.94
Feedwater flow	FMM-501	kg/s	1.0736e-4	2.3436e-8
Steam flow	FVM-602-M	kg/s	2.2953e-5	0.09286
Primary coolant subcooling at core outlet		ºC		48.78
Total heat loss through primary system		kW		44.494
Heat transfer through SG		kW		252.874
Maximum surface temperature of core heater rods		ºC		299.81
Location from the SG secondary inlet to reach - saturation - superheat		m		 ~1.58 ~5.99

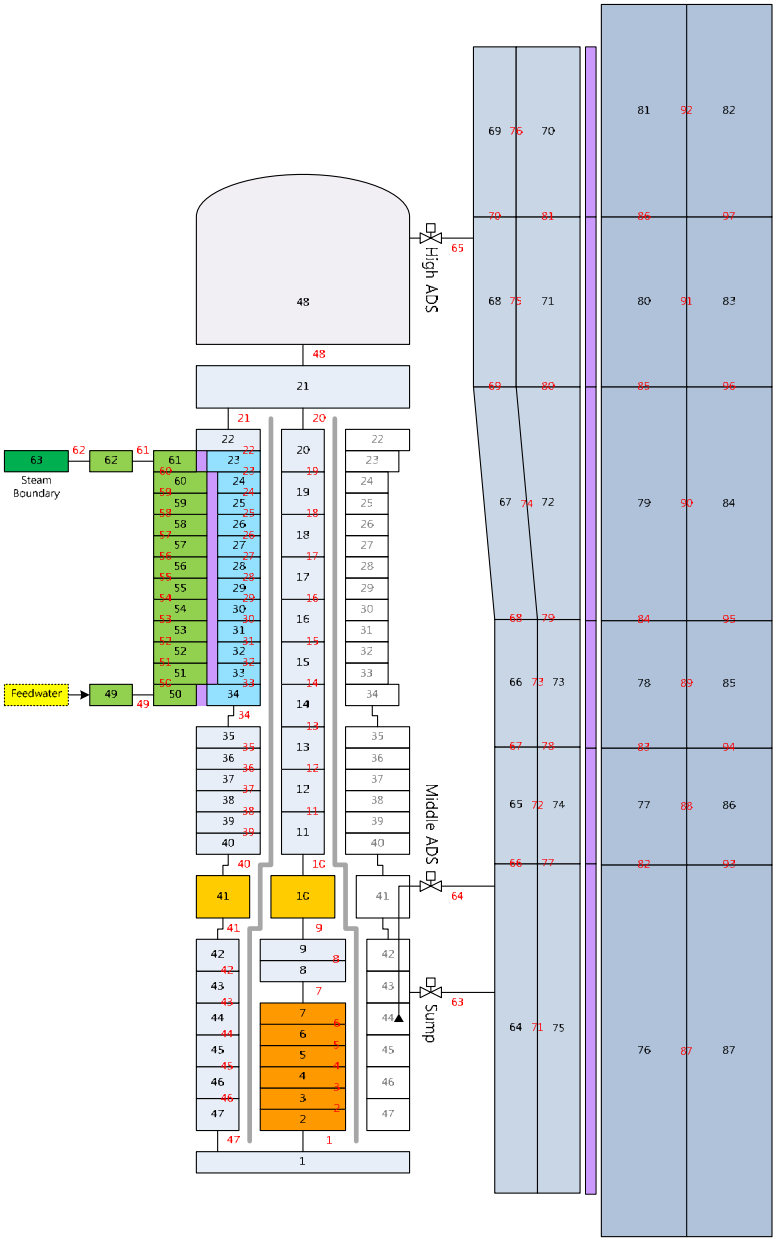

FIG. 4-156. TASS/SMR-S nodalization for MASLWR facility.

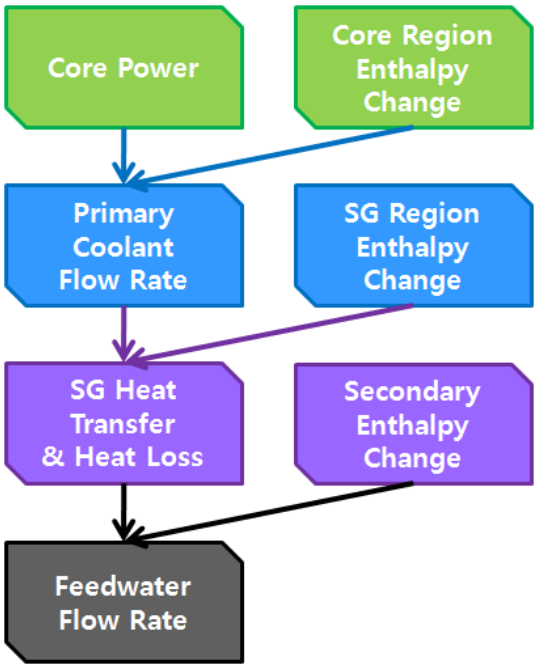

FIG. 4-157. Heat balance calculation procedure.

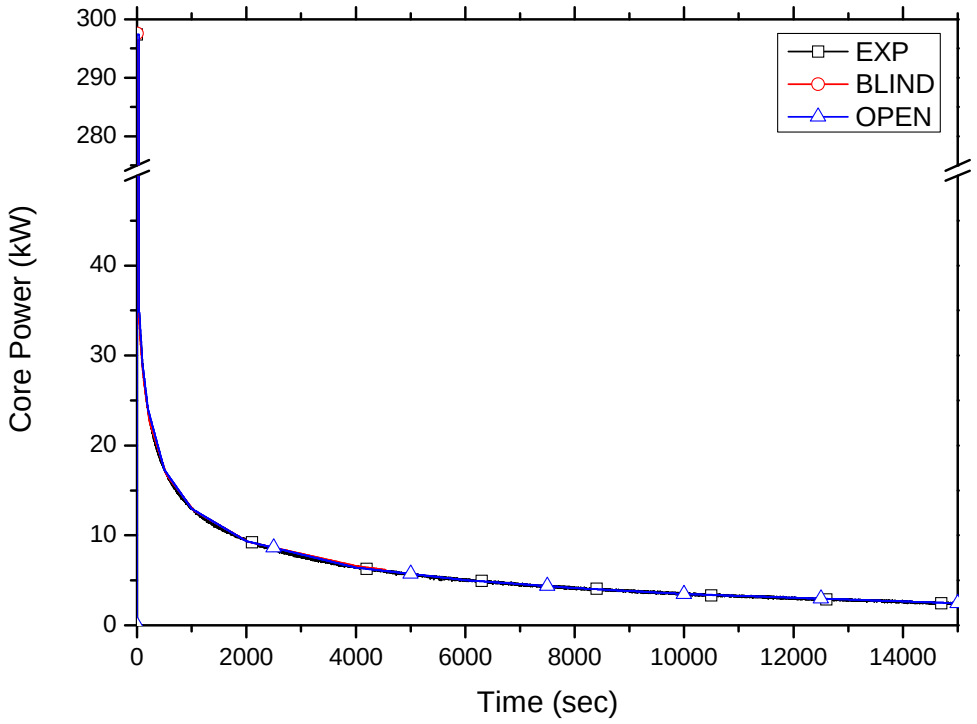

FIG. 4-158. Core power for SP-2.

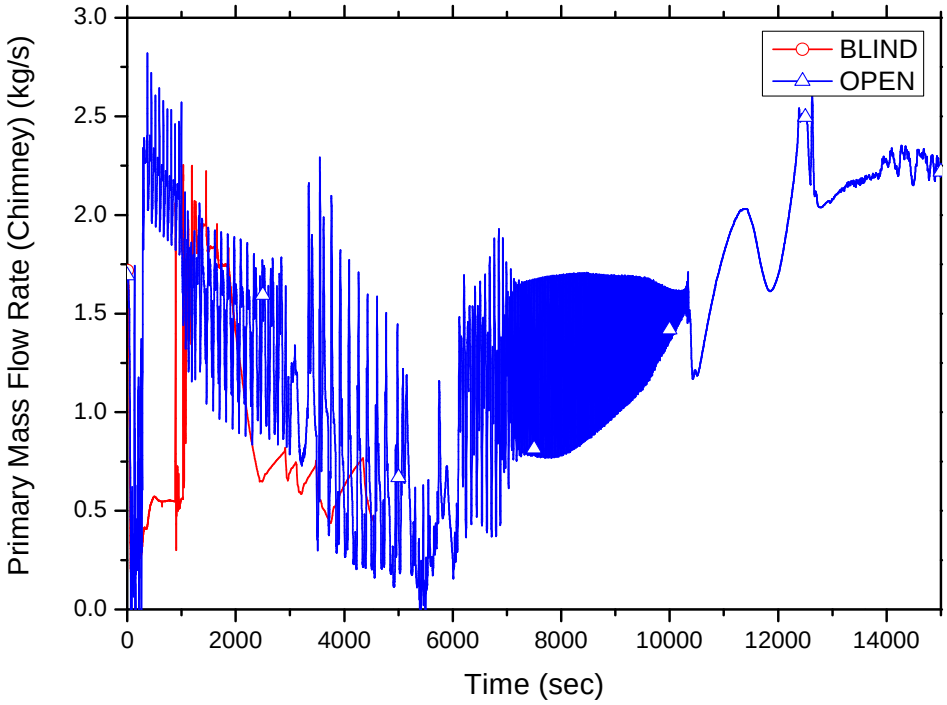

FIG. 4-159. Primary flow rate (chimney).

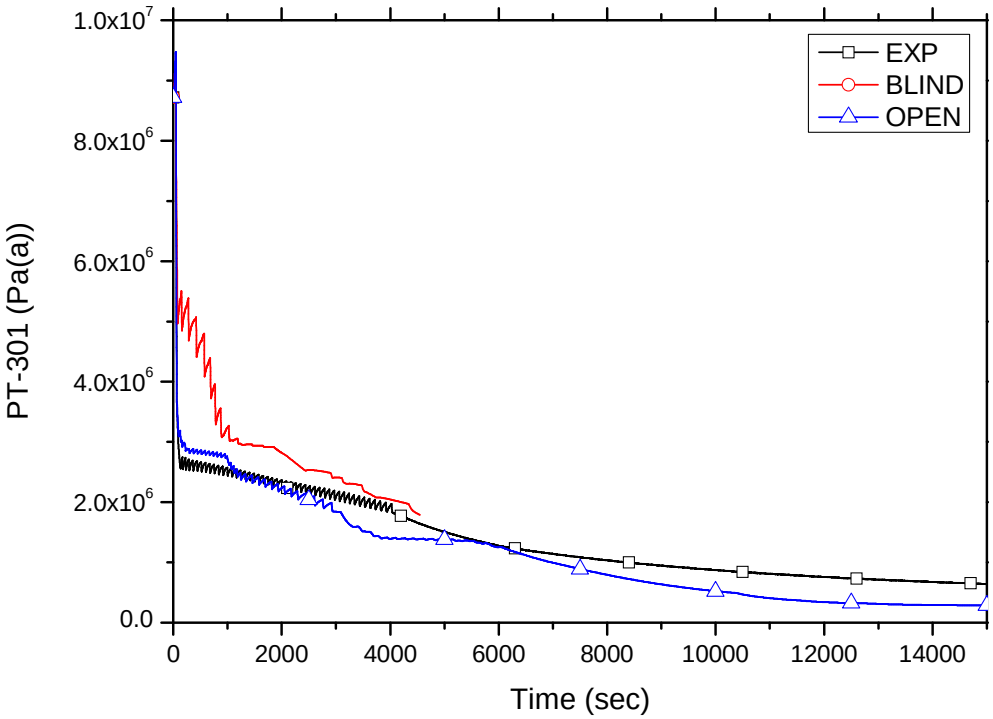

FIG. 4-160. PZR pressure.

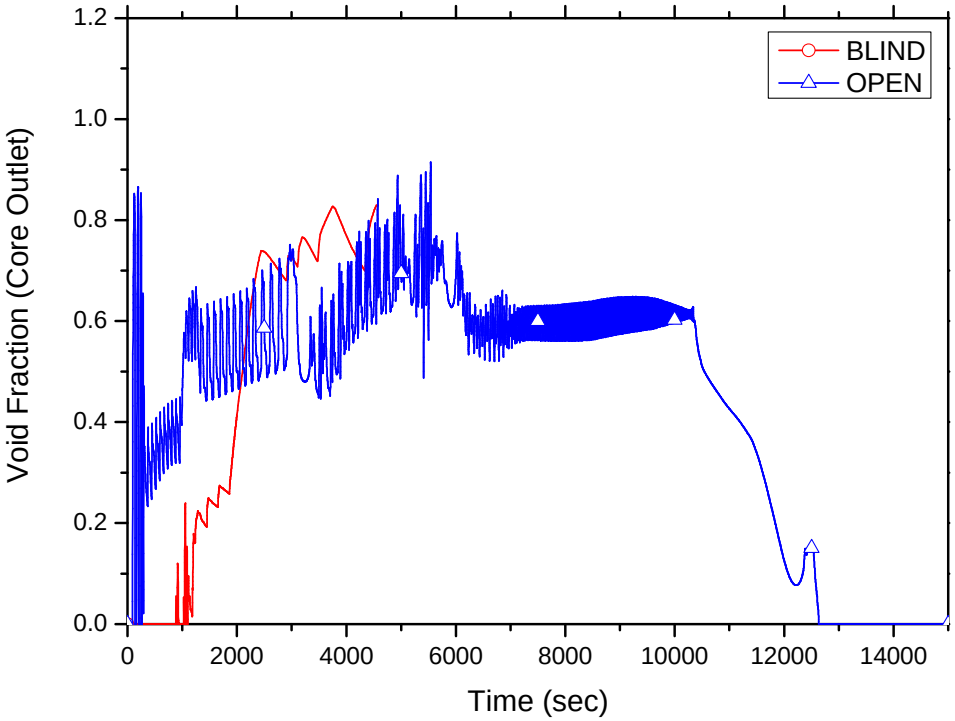

FIG. 4-161. Core outlet void fraction.

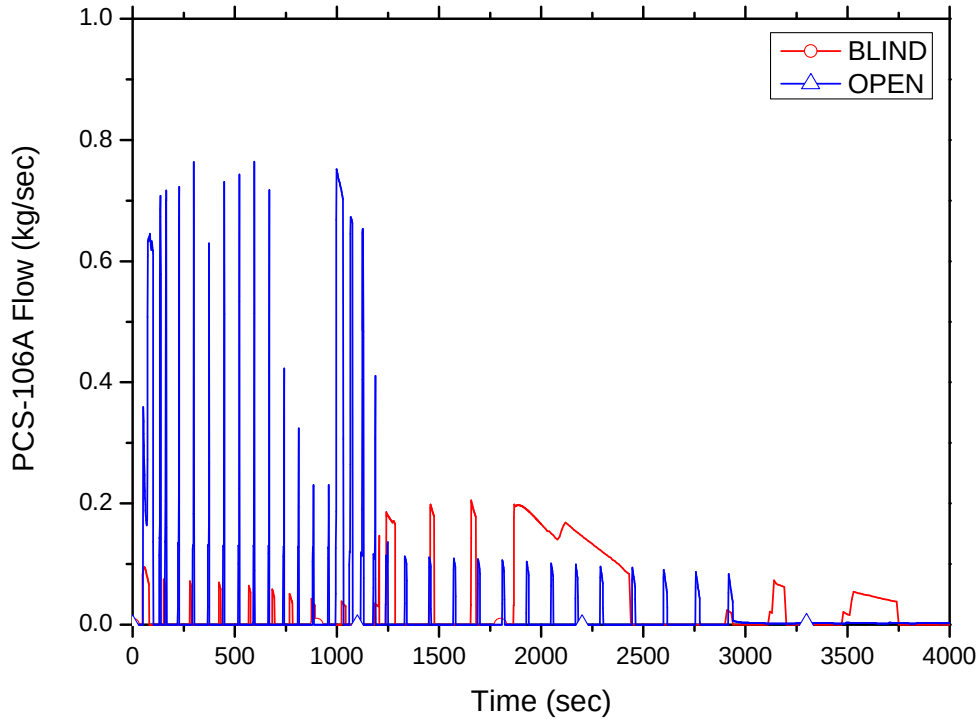

FIG. 4-162. ADS vent line flow rate.

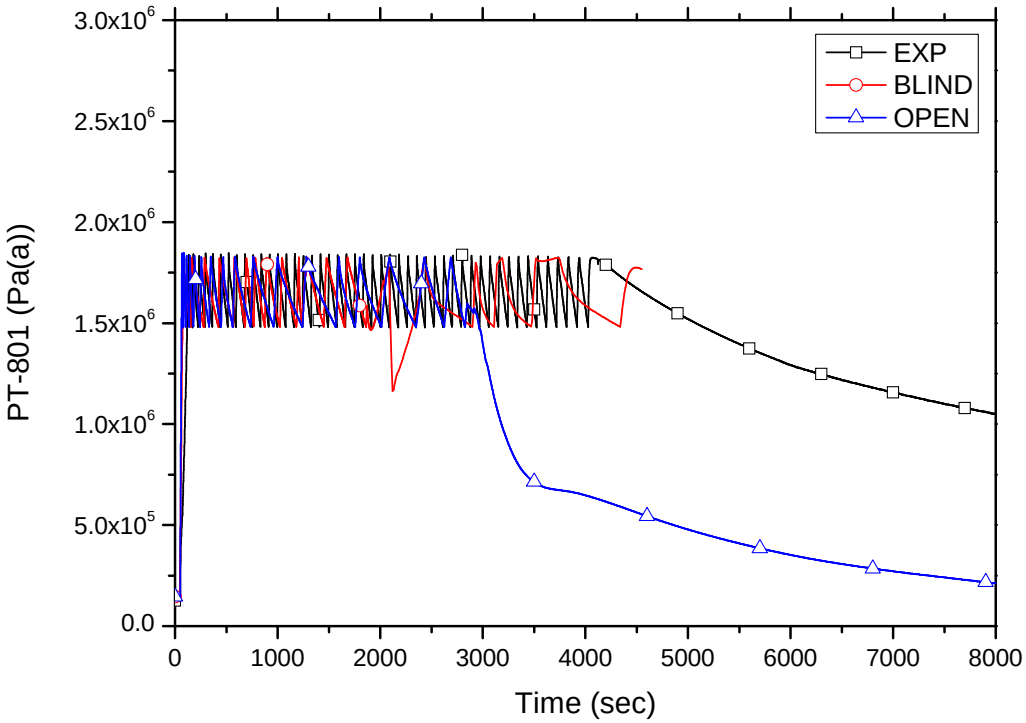

FIG. 4-163. HPC pressure.

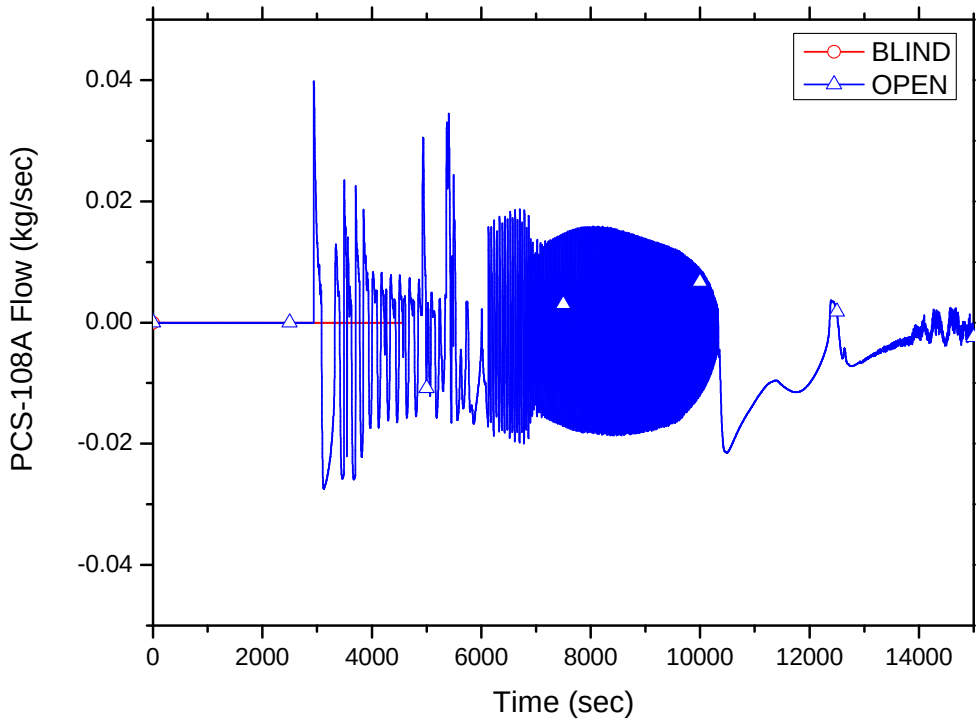

FIG. 4-164. ADS sump line flow rate.

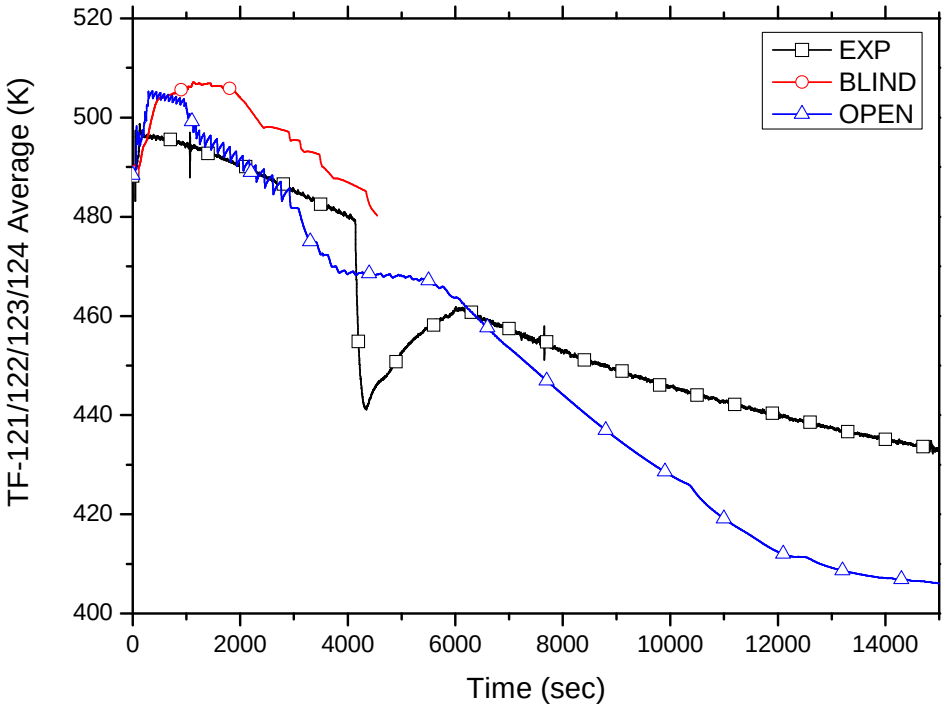

FIG. 4-165. Core inlet temp.

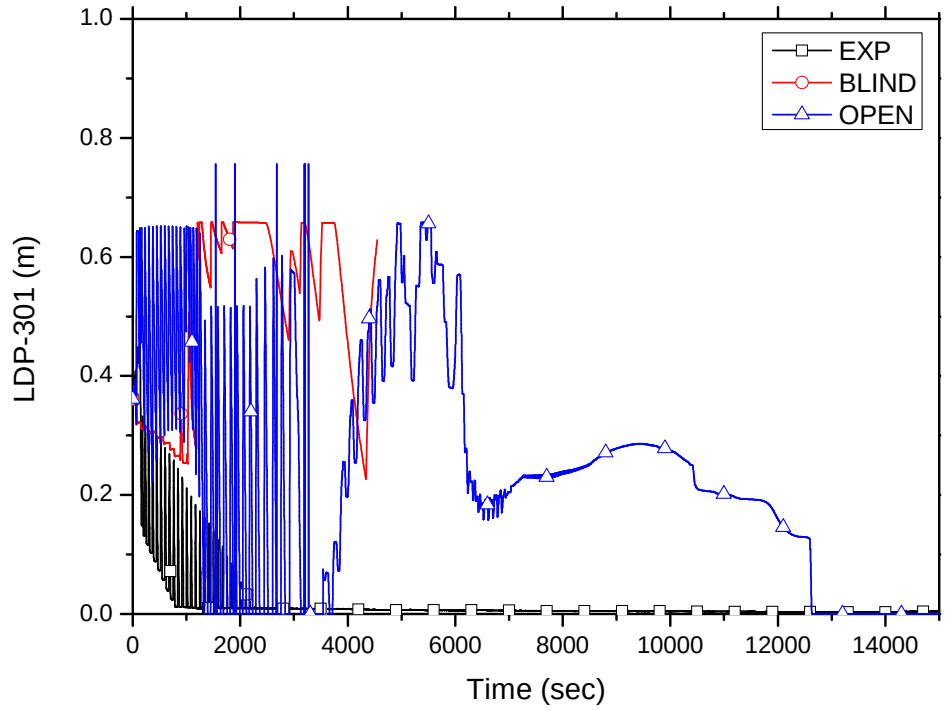

FIG. 4-166. PZR water level.

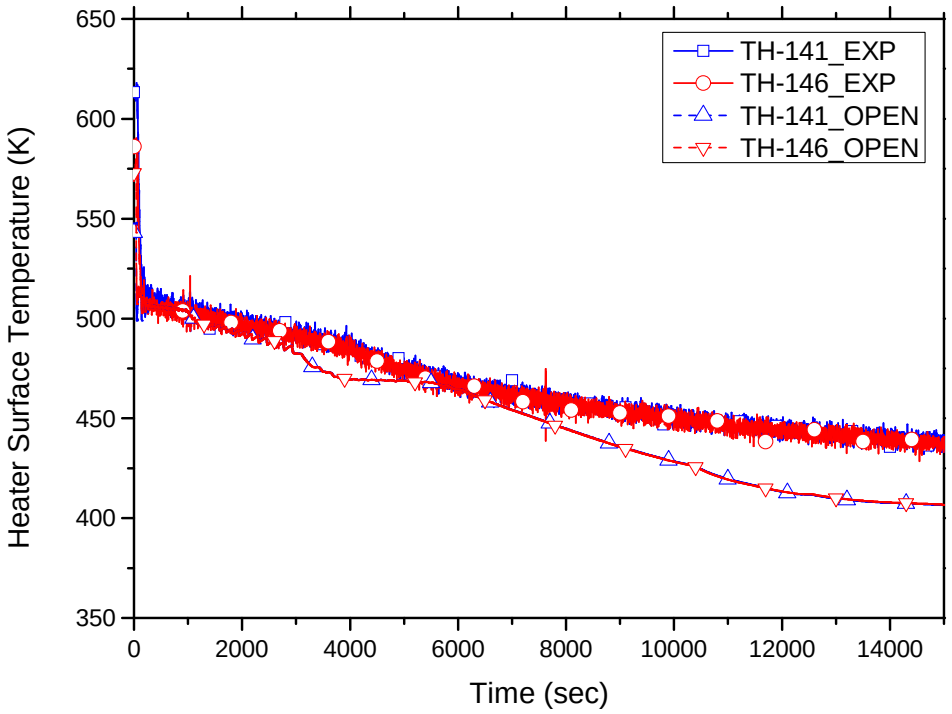

FIG. 4-167. Heater surface temp.

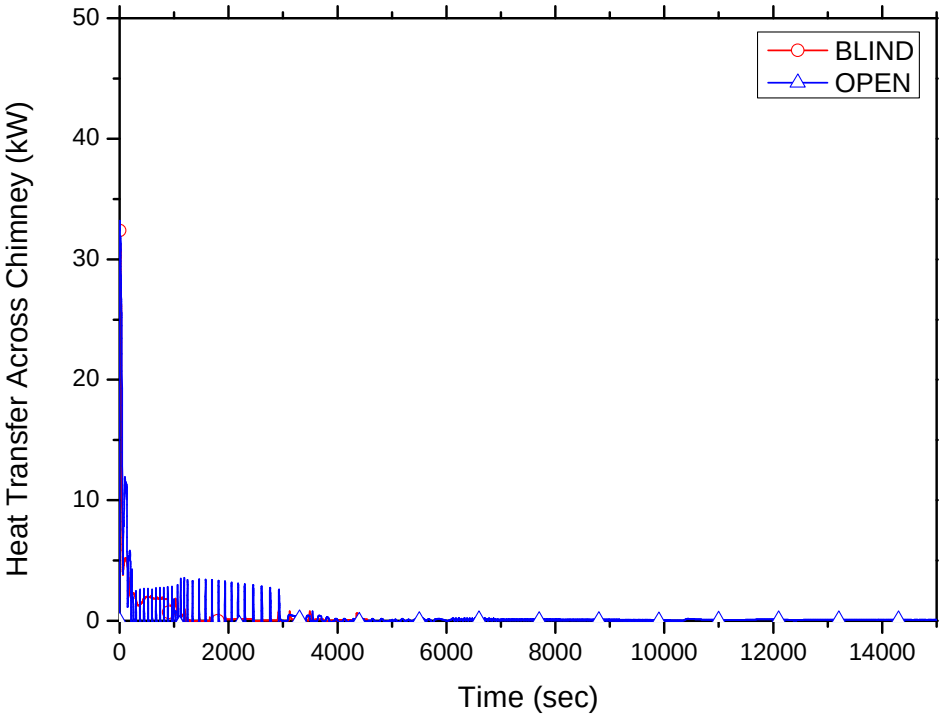

FIG. 4-168. Heat transfer across chimney.

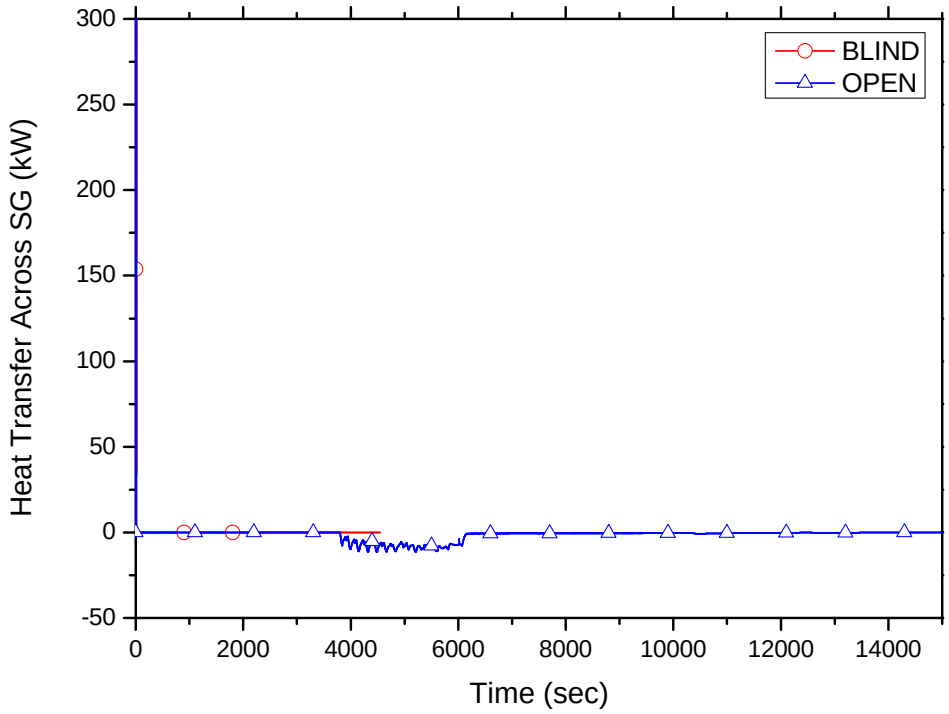

FIG. 4-169. Heat transfer across SG.

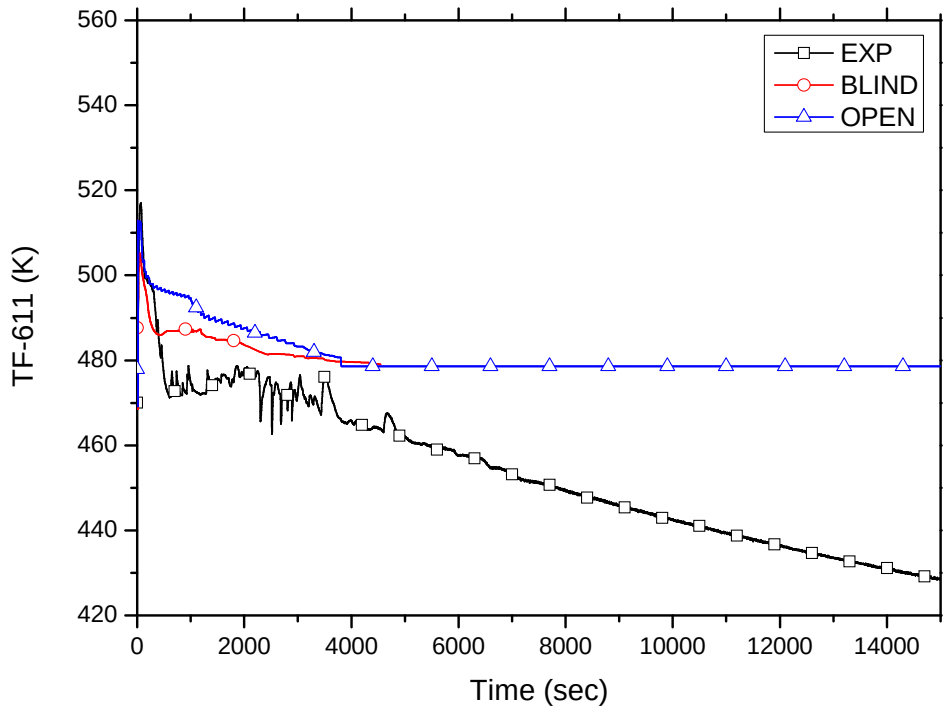

FIG. 4-170. Secondary SG outlet temperature.

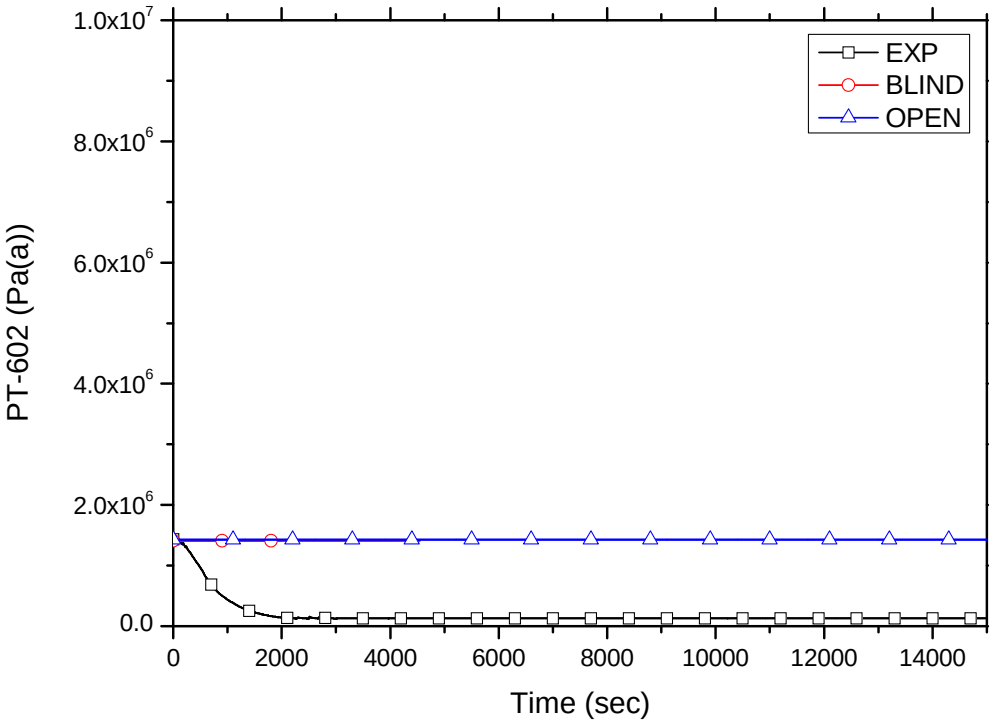

FIG. 4-171. Secondary steam line pressure.

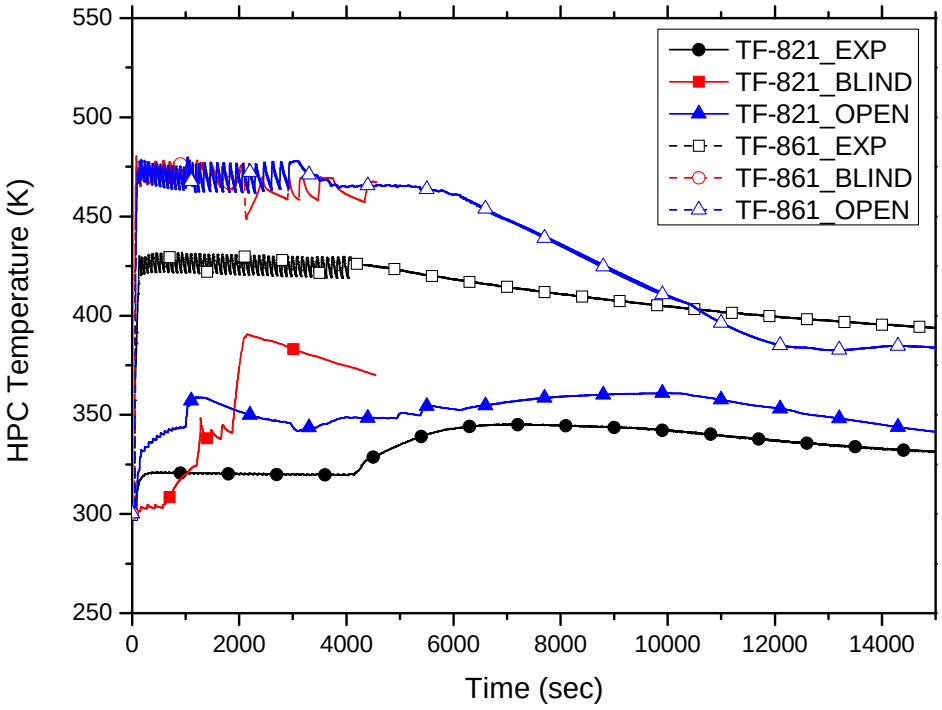

FIG. 4-172. HPC temperature.

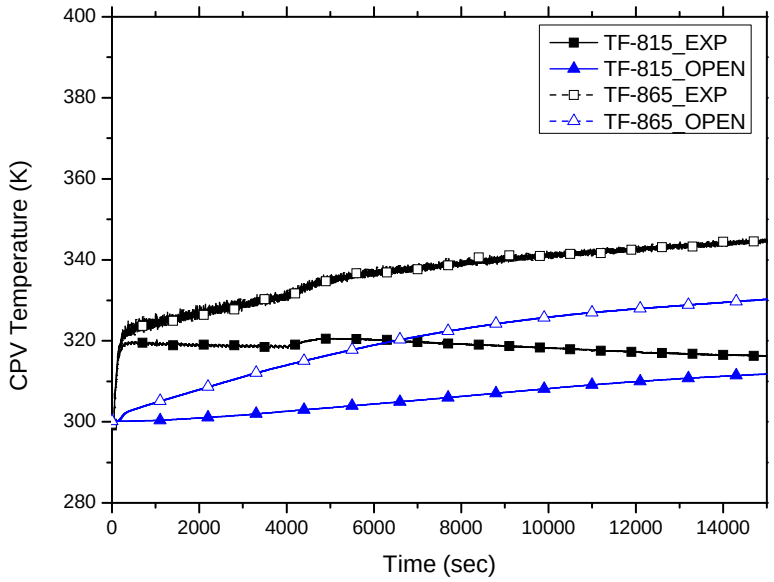

FIG. 4-173. CPV temperature.

4.7.4. Analysis results for power maneuvering

The steady state calculation is carried out using initial conditions with pressurizer water level of 0.36 m, pressurizer pressure of 8.72 MPa(a) and core heater power of 41.1 kW. The heat loss to ambient is assumed 12.24 kW from experimental results. This value is calculated by power difference between the core heater power and the steam generator power.

The initial steady state is simulated as a 5000 s transient calculation, taking the initial boundary conditions. Initial inlet and outlet temperature in the core is calculated to be 250.82°C and 262.76°C, respectively. The secondary side mass flow rate is kept as 0.01016 kg/sec which is 1.5% smaller than experimental value in order to balance between the generated power in the core and the transferred power in the steam generator. The superheat at the steam generator outlet is predicted 64.4°C, which is 5°C higher than the experiment and the average clad surface temperature is under-predicted slightly. TASS/SMR-S code predicted well the initial conditions as shown in Table 4-15.

4.7.4.1. RPV thermal-hydraulic behavior

Figures 4-174 and 4-175 show the core heater power and feedwater flow rate as boundary conditions. The core heater power is stepped up by about 40 kW from 40 to 320 kW. The feedwater temperature is assumed a constant value of the initial temperature for the blind calculation but it is used the same value with the experiment for the open calculation.

The transient initiated by an increase of the core power heaters step by step. A natural circulation flow is developed as shown in Figure 4-176 due to a density difference between a heat generation in the core and a heat removal through the steam generator. The flow rate increases with the core heater power. The TASS/SMR code over-predicts the primary natural circulation flow at the beginning of the 40 kW but the code under-predicts it at the end of 320 kW. The mass flow increases to 1.9 kg/s from 0.5 kg/s for the power of 320 kW from 40 kW in the experiment however the mass flow rate increases to 1.48 kg/s from 0.67 kg/s in the calculation. The TASS/SMR code does not predict well the increase rate with power change.

Figure 4-177 shows pressurizer water level. The charging flow to maintain pressurizer water level causes in-surge flow into the pressurizer that induces rapid pressure change. The pressurizer pressure behavior is shown in Figure 4-178, which is depending on the surge flow. The pressurizer pressure is over-predicted about 5 % of nominal pressure at the end of transient, which seems to result from the calculated surge flow.

Figure 4-179 shows the fluid temperature at the core inlet and outlet sides. Generally, the fluid temperature at the inlet and outlet is predicted well by the TASS/SMR-code although the temperature difference between the inlet and outlet sides is over-predicted owing to under-prediction of the primary mass flow by the code.

The TASS/SMR code predicts the differential pressure properly at the cold side of the reactor vessel as shown in Figure 4-180. The difference of initial value of the experiment and the calculation results from the difference between the measured DP height and the calculated DP height for DP-105. The calculated differential pressure for those DP will follow the experimental value well during whole transient if a constant value at DP-105 is added to the calculated value in order to compensate the elevation difference between the experimental height and the calculated height.

4.7.4.2. SG thermal-hydraulic behavior

It is assumed that the steam pressure is constant for a whole transient because a magnitude of the pressure change is less than 0.7% of initial pressure for the transient.

Heat transfers of primary system are shown in Figure 4-181. The heat transfer at the steam generator should be equal to the core power minus ambient heat loss when the system maintains a steady state condition. If this value is not equal, some parameters will be changed. The feedwater flow is supplied more than the required flow to remove the power generated in the core during 2800 - 3800 s as shown in Figure 4-182. As a result of much feedwater supply, primary coolant temperature decreases and the steam temperature becomes a saturation state from the superheated steam as shown in Figure 4-183. The superheated condition is collapsed at around 3400 s due to much feedwater flow. The TASS/SMR code predicts to appear this phenomenon at 3200 s. For the experiment, the heat balance between the core power and steam generator power plus heat loss recovers as the feedwater flow maintains the core power level at around 4200 s. Also, the pressurizer pressure has a constant value. For the calculation, the removed power at the steam generator plus the heat loss is less than the generated power in the core. Accordingly, the pressurizer pressure is over-predicted.

TABLE 4-15. STEADY-STATE COMPARISON FOR TEST SP-3

Parameter	MASLWR	Unit	Experimental Value	Calculation Value	
				Blind	Open
Pressurizer pressure	PT-301	MPa(a)	8.72	8.72	8.72
Pressurizer level	LDP-301	m	0.36	0.36	0.36
Power to core heater rods	KW-101/102	kW	41.05	40.00	41.1
Feedwater temperature	TF-501	ºC	31.49	31.47	31.59
Steam temperature	FVM-602-T	ºC	255.94	260.65	261.43
Steam pressure	FVM-602-P	MPa(a)	1.46	1.45	1.46
Ambient air temperature		ºC		N/A	N/A
Primary flow at core outlet	FDP-131	kg/s	0.50	0.66	0.67
Primary coolant temperature at core inlet	TF-121/122/123/124	ºC	250.34 (Average)	251.16	250.82
Primary coolant temperature at core outlet	TF-106	ºC	262.72	262.81	262.76
Feedwater flow	FMM-501	kg/s	0.01031	0.00999	0.01016
Steam flow	FVM-602-M	kg/s	0.01031	0.00999	0.01016
Primary coolant subcooling at core outlet		ºC		38.25	38.29
Total heat loss through primary system		kW		11.87	12.25
Heat transfer through SG		kW		28.13	28.65
Maximum surface temperature of core heater rods		ºC		288.72 (326.3)	276.57
Location from the SG secondary inlet to reach - saturation - superheat		m		 ~0.32 ~1.58	 ~0.32 ~1.58

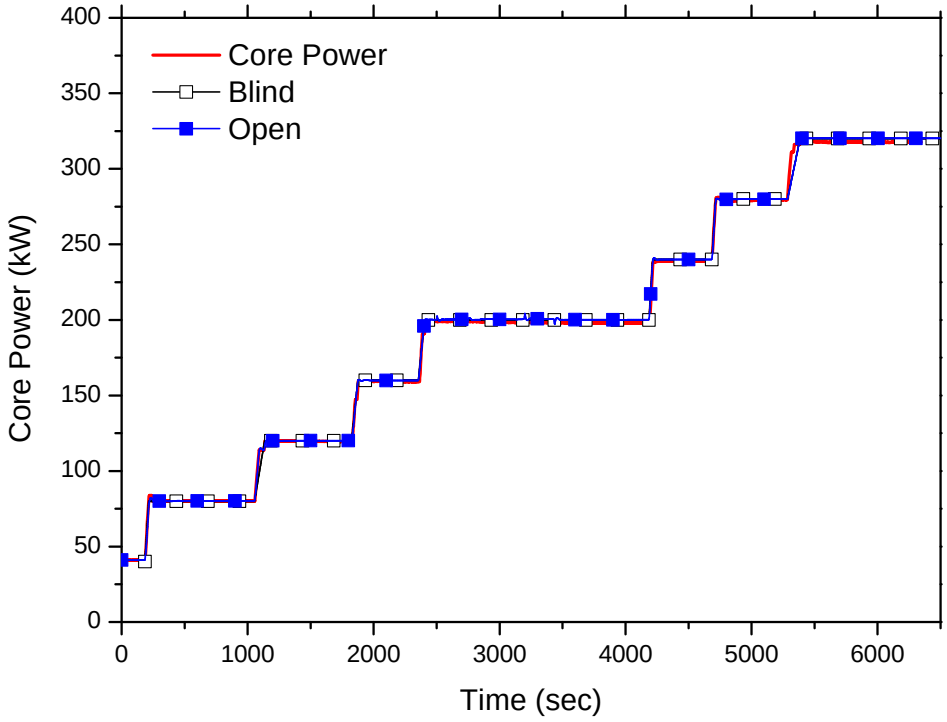

FIG. 4-174. Heater rod power for SP-3.

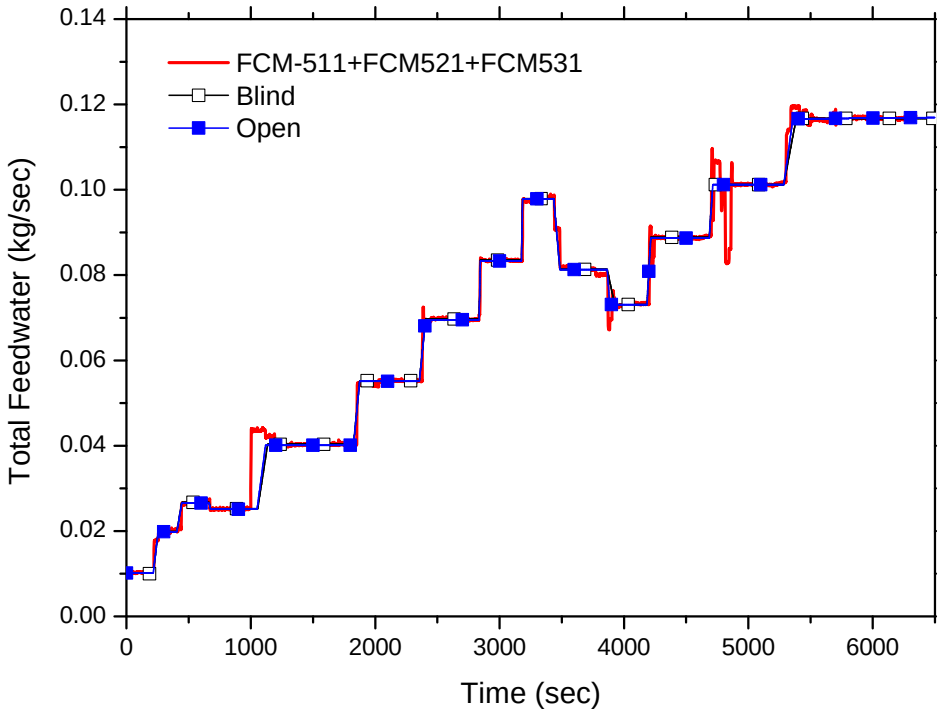

FIG. 4-175. Feedwater flow rate for SP-3.

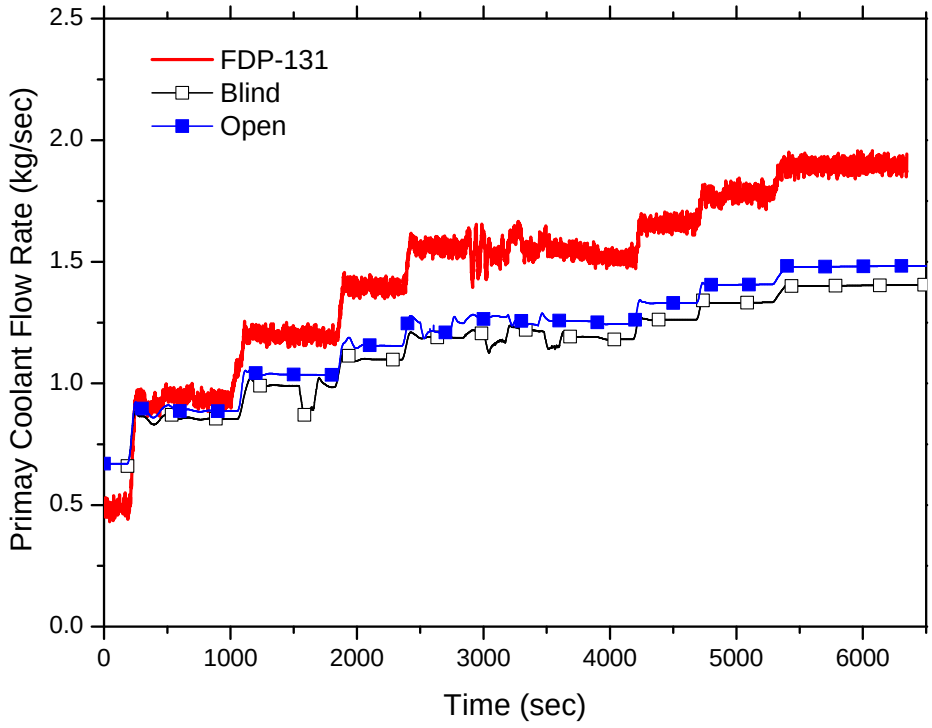

FIG. 4-176. Primary mass flow rate for SP-3.

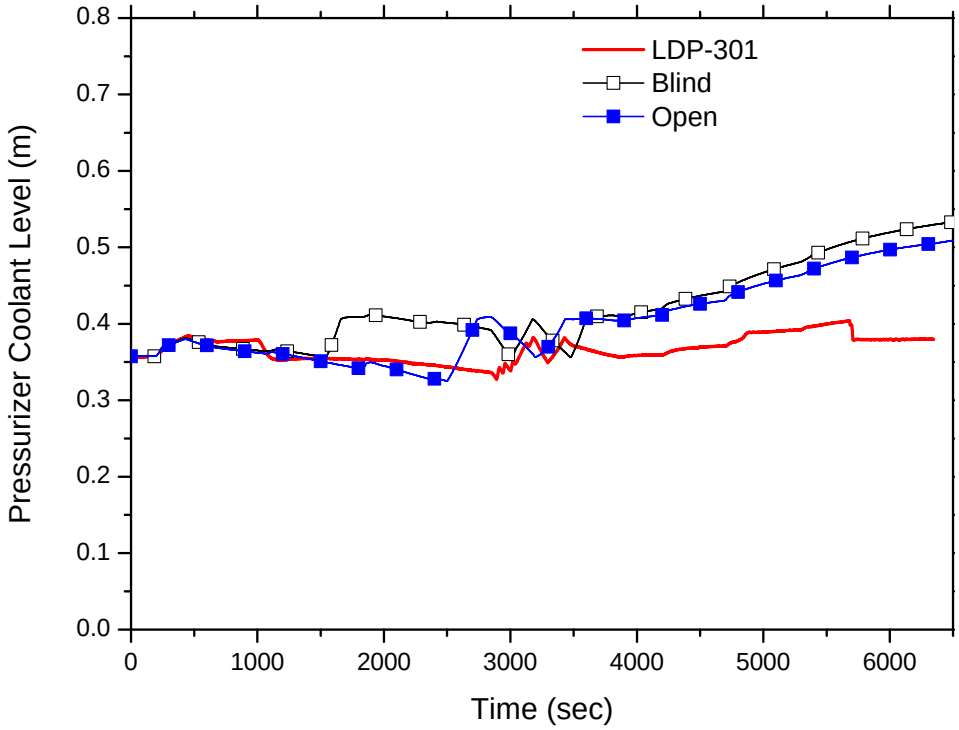

FIG. 4-177. Pressurizer water level for SP-3.

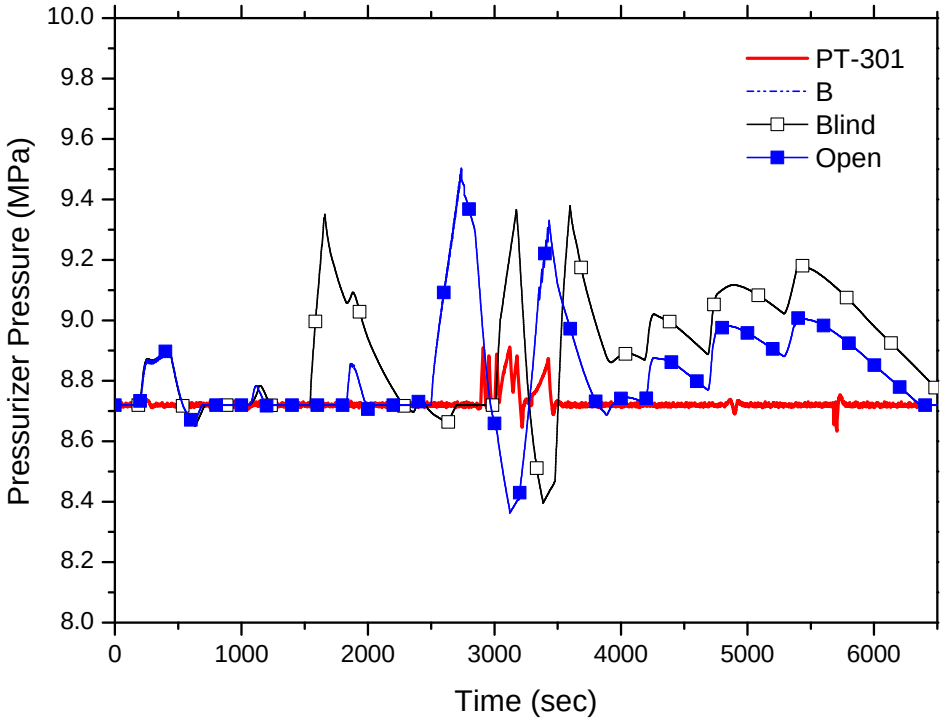

FIG. 4-178. Pressurizer pressure for SP-3.

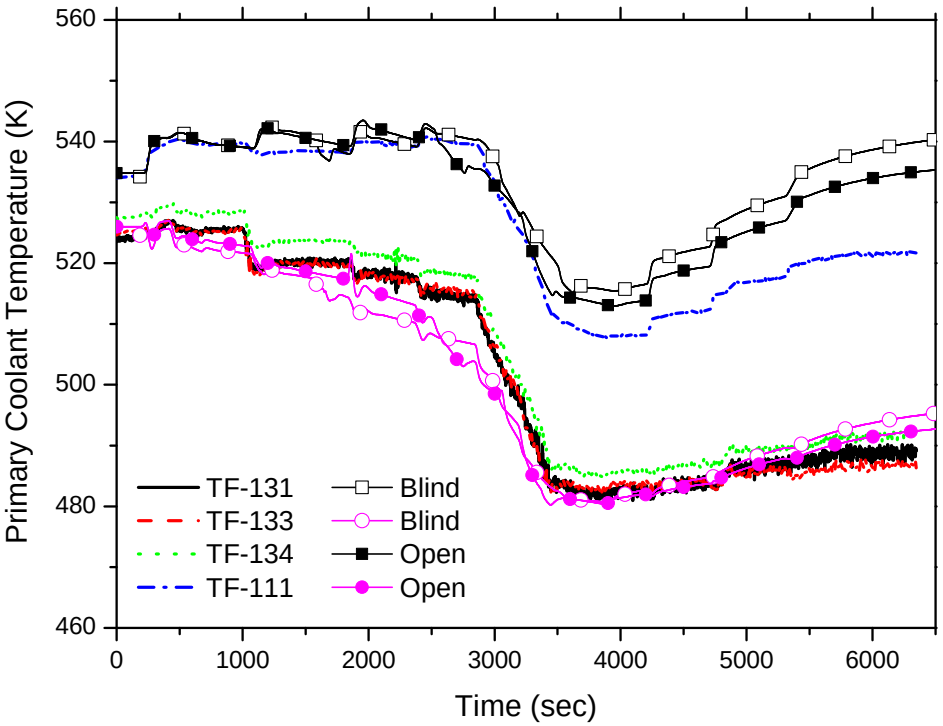

FIG. 4-179. Core inlet and outlet temperature for SP-3.

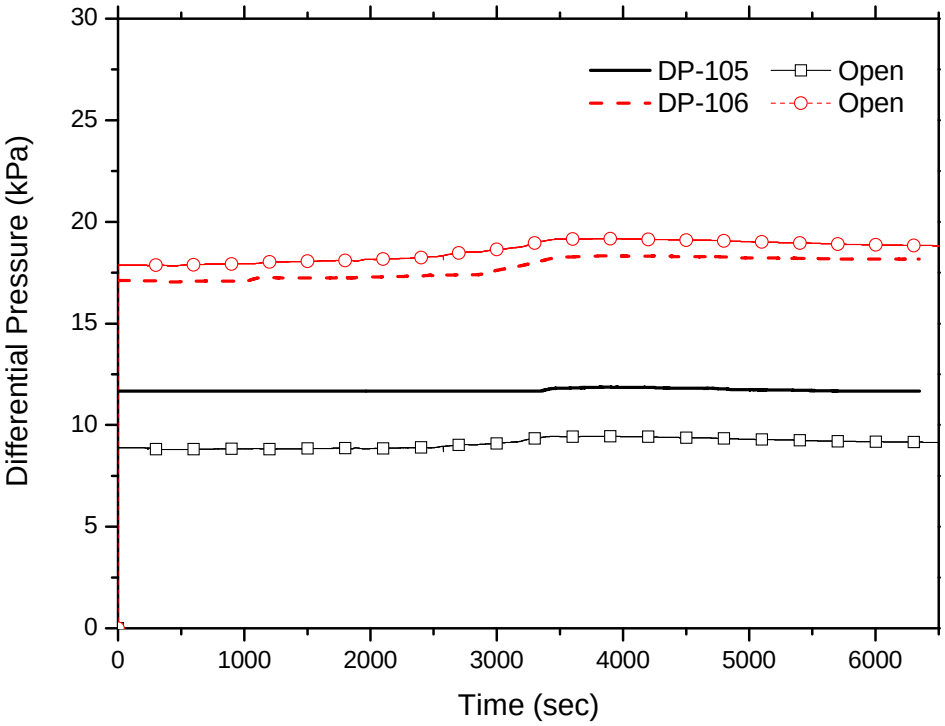

FIG. 4-180. Cold side differential pressure for SP-3.

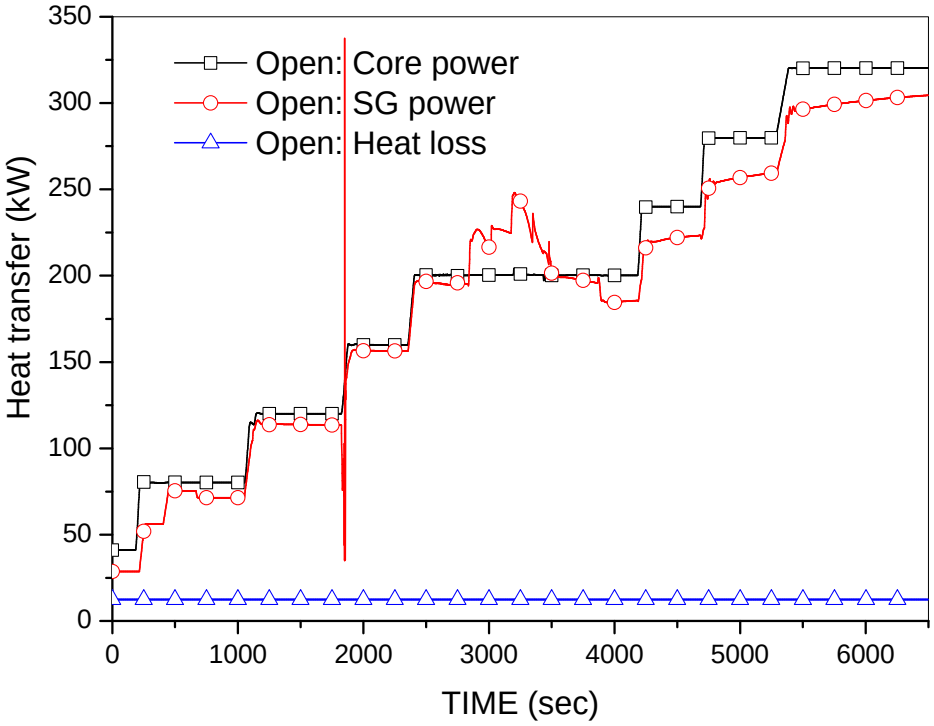

FIG. 4-181. Primary power for SP-3.

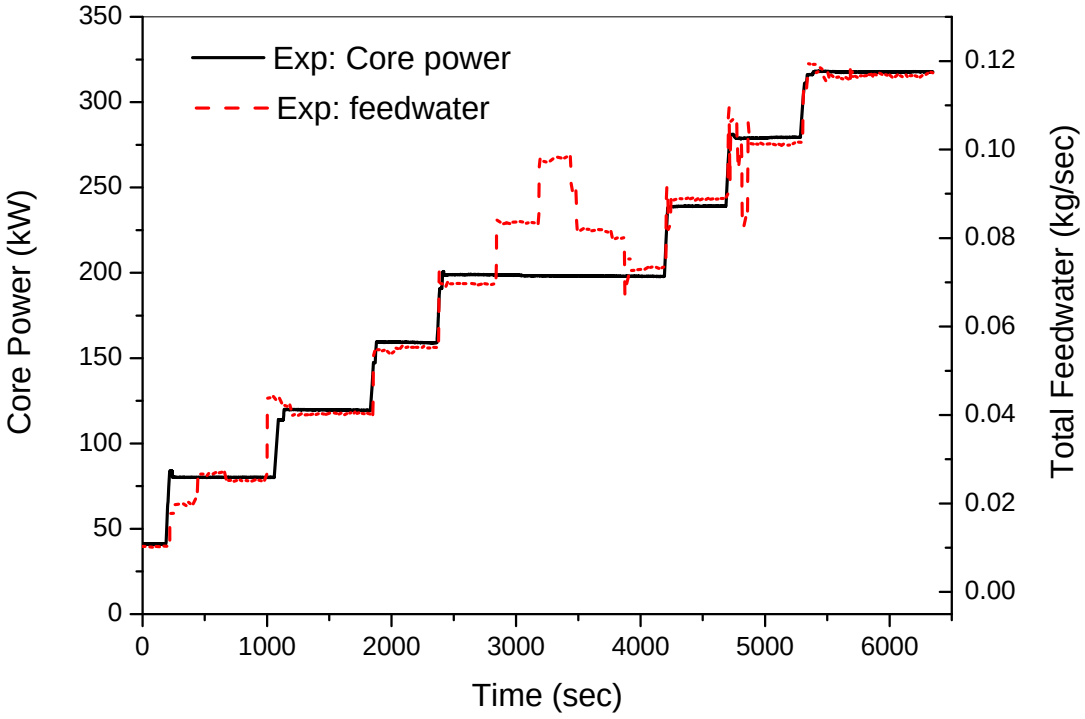

FIG. 4-182. Core power and feedwater flow for SP-3.

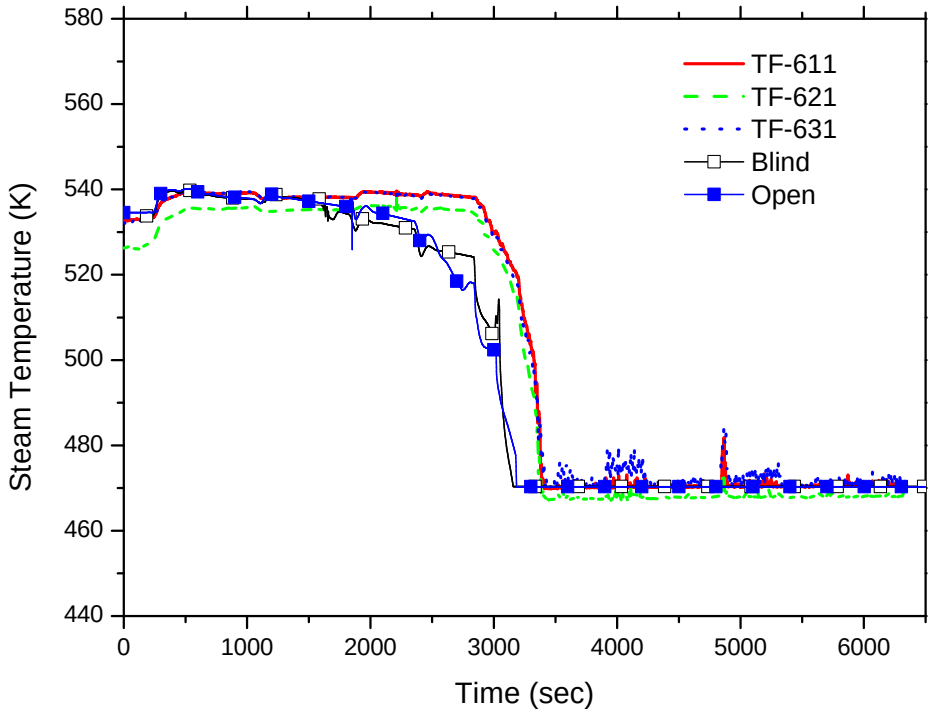

FIG. 4-183. Steam temperature for SP-3.

4.8. KINS — REPUBLIC OF KOREA

4.8.1. Computer codes

In blind and open calculations of the SP-2 and the SP-3 transients of IAEA ICSP for MASLWR test facility, MARS code (KS-002 version) [24] with helical coil geometry specific wall-to-fluid heat transfer model was used. MARS stands for Multi-dimensional Analysis of Reactor Safety and the code is a thermal-hydraulic system code that has been developed based on RELAP5 Mod3.2 and COBRA-TF codes. The MARS code adopts two fluid models and it solves total eight equations for pressure, vapor volume fraction, phase specific internal energies, phase specific velocities, non-condensable quality and boron density.

Most of convective heat transfer packages included in the MARS code are the same as those of RELAP5 code but unlike the RELAP5 code, the MARS code is equipped with special helical coil geometry specific heat transfer models. To make this specific heat transfer models operable in calculations, special option numbers for convective boundary condition should be chosen in developing input deck. For instance, convection boundary condition (#114) was chosen for inside wall-to-fluid heat transfer of the helical tube, which activates modified Chen heat transfer model based on Mori-Nakayama's single phase heat transfer model for helical tube geometry [25]. For outside wall-to-fluid heat transfer of the helical tube, Zukauskas' single phase heat transfer model for horizontal tube bundle [26] was turned on by selecting convection boundary condition (#135).

In the simulation of loss of feed water transient (i.e. SP-2), high pressure and high temperature steam of RPV was vented to HPC and as a result choked flow evolved through vent line of automatic depressurization system of MASLWR facility [21]. To simulate choked flow phenomenon, Henry-Fauske choked flow model which is a default model of the MARS code was used in the present simulation. As for non-condensable gas which is present in upper region of HPC and CPV, the same approach of that in the RELAP5 code is applied in the MARS code.

Besides the MARS code, the USNRC SNAP tool was utilized in developing input decks for blind and open calculations of IAEA ICSP. The version used was 2.0.7(August 15, 2011).

4.8.2. System idealization

4.8.2.1. System idealization for blind calculation

Major modelling assumptions used for blind calculation of the SP-2 transient are as below;

- Non-condensable gas (i.e. saturated air at 300.15°K) fills the upper part of HPC and CPV, respectively.
- Water temperatures of both HPC and CPV are 300.15°K.
- No heat loss (No heat structures) through RPV, HPC and CPV is assumed.
- CPV is modelled as isolated from atmosphere.
- Valves in vent lines and in sump return lines of automatic depressurization system of MASLWR facility are assumed as trip valve.
- HPC and CPV are modelled as full two pipes, respectively.

Nodalization diagram used in the blind calculation of the SP-2 transient is given by Figure 4-184.

Also, major modelling assumptions specific to the SP-3 blind transient analysis to the exclusion of the SP-2 related assumptions are as below;

- Heat loss from RPV to surrounding atmosphere was assumed (Heat structures of RPV except pressurizer were included in the model).
- Pressurizer heater with on-off control logic was modelled.
- RPV injection flow was not assumed.

Nodalization diagram used in the blind calculation of the SP-3 transient is given by Figure 4-185.

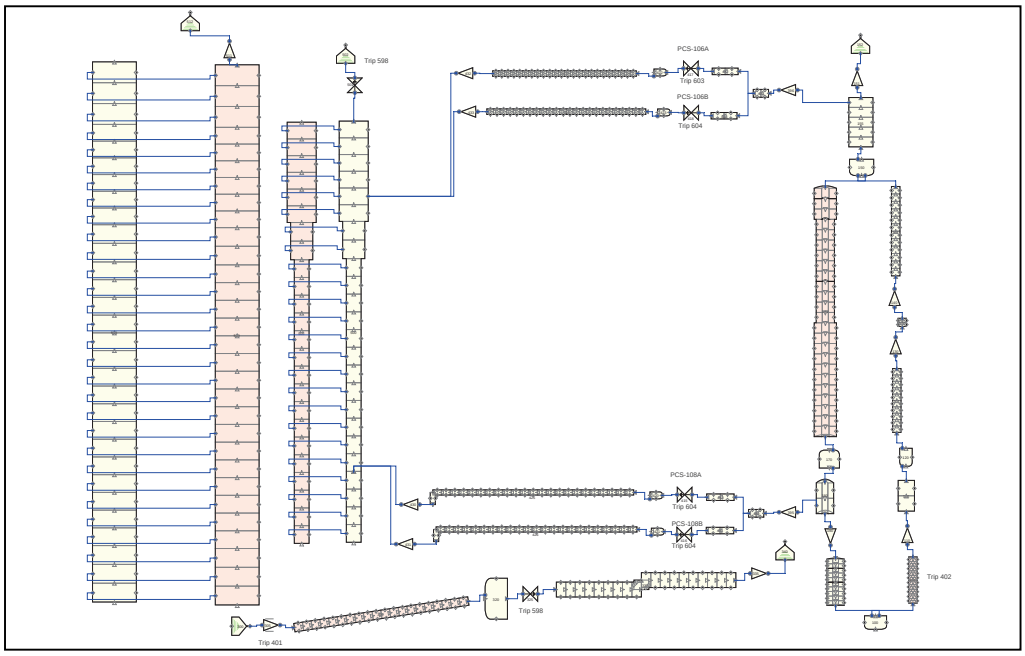

FIG. 4-184. Nodalization for SP-2 analysis in blind calculation.

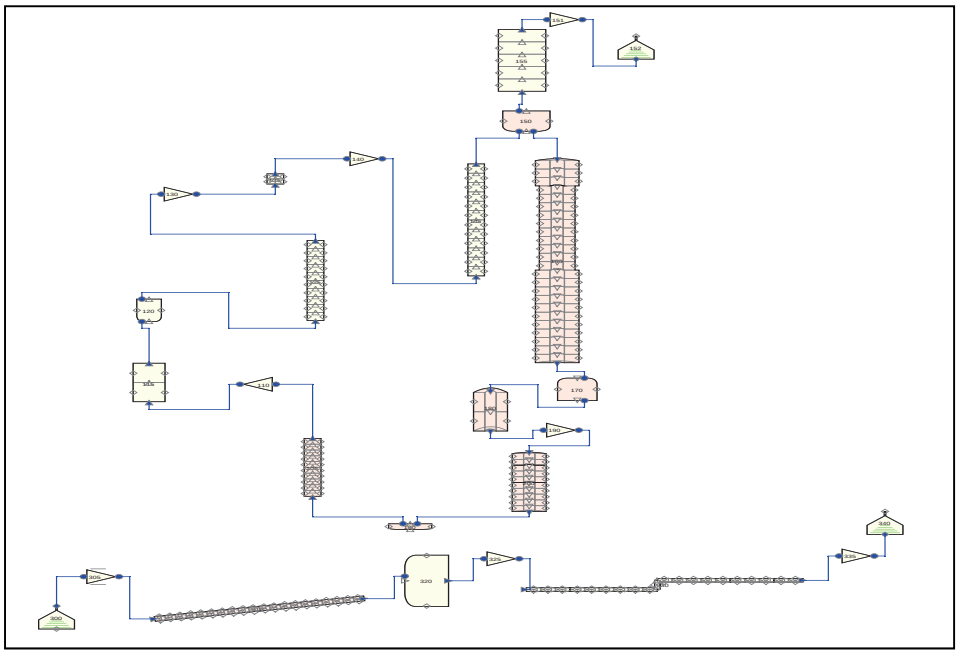

FIG. 4-185. Nodalization for SP-3 analysis in blind calculation

4.8.2.2. Modelling change for open calculation

Modelling changes made for the open calculation of the SP-2 transient are as below;

– CPV is modelled as open to atmosphere during whole transient. (CPV was isolated from atmosphere in the blind calculation).
– HPC and CPV are modelled as partial two pipes to improve agreement between experimental data and the code simulation results (HPC and CPV were modelled as full two pipes in the blind calculation).

Nodalization diagram used in the open calculation of the SP-2 transient is given by Figure 4-186. Note that multiple junction components for connecting two pipes volume of HPC and CPV are omitted in the open calculation model in comparison with the blind calculation model.

Additional modelling changes made for the SP-3 transient analysis in the open calculation are as below;

- Pressurizer heater with proportional-integral control logic was modelled in the open calculation (On-off control logic for the pressurizer heater was employed in the blind calculation).
- Flow injection to RPV during the SP-3 transient was included in the open calculation (RPV injection flow was not included in the blind calculation).
- Junction head loss coefficients of some components in the primary system (i.e. within RPV) was changed from values of the SP-2 transient analysis to revised ones in the open calculation of the SP-3 transient analysis to fit initial primary mass flow rate given by experimental data (Junction head loss coefficients of the primary system remained unchanged for both of the SP-2 and the SP-3 in the blind calculation.).

Nodalization diagram used in the open calculation of the SP-3 transient is given by Figure 4-187.

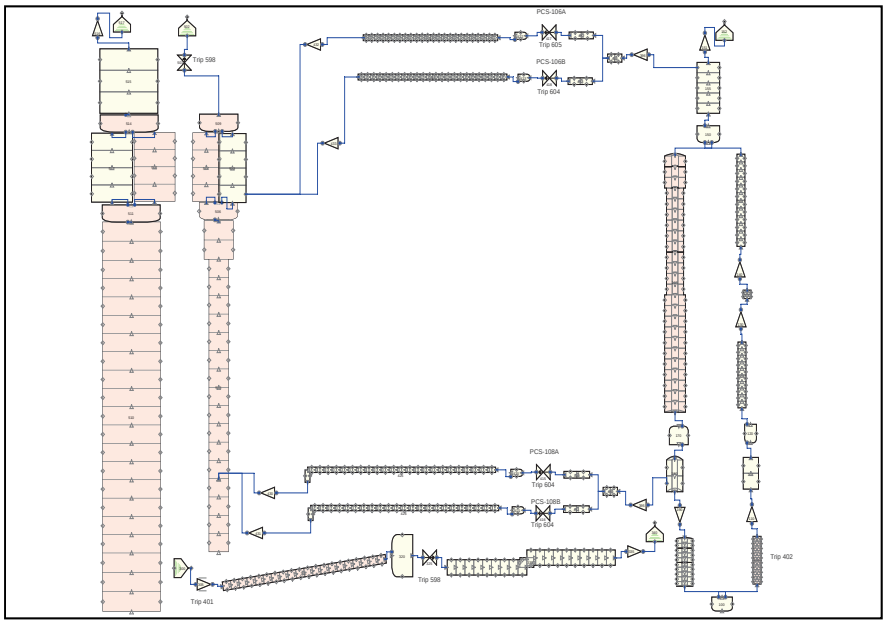

FIG. 4-186. Nodalization for SP-2 analysis in open calculation.

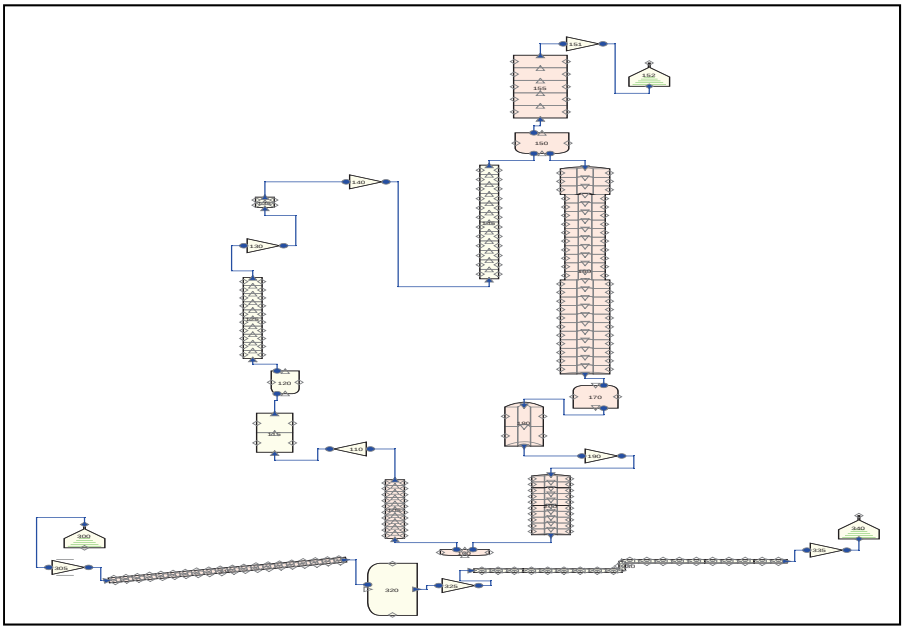

FIG. 4-187. Nodalization for SP-3 analysis in open calculation.

4.8.3. Analysis results for loss of feed-water transient

Major time sequence of events for the SP-2 transient is given in Table 4-16.

TABLE 4-16. SP-2 TRANSIENT MAJOR TIME SEQUENCE OF EVENTS

Event	Time (s)		
	Open Calculation	Blind Calculation	Experiment
Stop MFP Close HPC vent valve SV-800	0	0	0
PZR pressure (PT-301) reaches 9.064 MPa(a) (1300 psig) Enter decay power mode	31.5	29.6	N/A
PZR pressure (PT-301) reaches 9.409 MPa(a) (1350 psig) De-energize PZR heaters Open ADS vent valve (PCS-106A)	49.5	47.6	48
First opening time for PCS-106A	49.5	47.6	48
Record opening and closing times for SV-800	Not open	Not open	Not open
Start long-term cooling when pressure difference between primary system and HPC (PT-301 minus PT-801) becomes less than 5 psi (0.034 MPa) Open and remain open of PCS-106A and PCS-106B Open and remain open of PCS-108A and PCS-108B	4161	807	4024(PCS-106A) 4111(PCS-106B) 4116(PCS-108A) 4117(PCS-108B)
End of test when one of the following conditions is reached: - PZR pressure ≤ 0.135 MPa(a) (5 psig) - Primary coolant temperature (TF-132) ≤ 35 ºC (95ºF) - 24 hours have elapsed	N/A	N/A	N/A

4.8.3.1. Steady state

Table 4-17 shows steady state calculation results for the SP-2 and comparison with experimental data. As shown in Table 4-17, almost all variables calculated agree well with the experimental data. Note that there exist only minor differences between the blind and the open calculations.

4.8.3.2. Transient phenomena

Using the steady state run results as initial conditions, the SP-2 transient is simulated. Transient results calculated are shown in Figures 4-188 to 4-204. In the figures, experimental data are compared with blind and open calculation results except Figures 4-202 and 4-204.

Pressure behaviors of pressurizer (PT-301) and HPC (PT-801) are shown Figure 4-188. In the blind calculation, pressure equilibrium time between pressurizer and HPC was calculated to be short compared to experiment data and this was identified as large condensation effect in the HPC. Therefore, fouling factor to heat transfer correlation for heat transfer plate was slightly changed from original value of 1.0 to 0.8 in the open calculation to reduce large condensation in the HPC. Considering that heat loss around the heat transfer plate could arise and that real fouling could exist at the heat transfer plate, this slight change of fouling factor to heat transfer correlation seems to be reasonable. Furthermore, HPC and CPV modeling was changed in the open calculation compared to the blind calculation. That is, fully two pipes volumes were used for modeling of HPC and CPV in the blind calculation. Otherwise, partially two pipes volumes were used for vapor regions of HPC and CPV in the open calculation. In spite of this improvement in the pressure equilibrium time, calculated pressure of pressurizer in the open calculation shows some discrepancy compared to experimental data. Especially, calculated pressurizer pressure is estimated higher than experimental data at the end of initial blowdown stage of pressurizer pressure. This phenomenon seems to be due to reduced condensation in HPC by adjusting the fouling factor of the heat transfer plate to 0.8 and it can be eliminated by restoring the fouling factor to 1.0 with inclusion of additional heat structures such as RPV etc. of the MASLWR test facility in the simulation model to give more heat to the primary side fluid. However, overall predictability is improved greatly in the open calculation compared to the blind calculation.

TABLE 4-17. STEADY-STATE COMPARISON OF SP-2 EXPERIMENT WITH SIMULATIONS

Parameter	MASLWR	Unit	Experiment	Steady-State (Blind Cal.)	Steady-State (Open Cal.)
Pressurizer pressure	PT-301	MPa(a)	8.718	8.720(BC)	8.718(BC)
Pressurizer level	LDP-301	m	0.3606	0.3998	0.3434
Power to core heater rods	KW-101/102	kW	297.4	299(BC)	299(BC)
Power of PZR heater		kW		N/A (no PZR heater modelling)	N/A (no PZR heater modelling)
Feedwater temperature	TF-501	ºC	21.2	21.39(BC)	21.39(BC)
Steam temperature	FVM-602-T	ºC	205.4	205.09	203.85
Steam temperature	Avg. of TF-611 to TF-634	ºC	203.1	210.09	207.21
Steam pressure	FVM-602-P	MPa(a)	1.411	1.411(BC)	1.411(BC)
Ambient air temperature		ºC	25	N/A(no heat loss modelling)	N/A(no heat loss modelling)
HPC pressure	PT-801	MPa(a)	0.127	0.127665	0.127653
HPC water temperature	TF-811	ºC	26.7	27.7	27.0
HPC water level	LDP-801	m	2.820	2.810	2.813
Primary flow at core outlet	FDP-131	kg/s	1.82	1.846	1.734
Primary coolant temperature at core inlet	TF- 121/122/ 123/124	ºC	215.1	215.71	214.97
Primary coolant temperature at core outlet	TF-106	ºC	251.5	250.50	251.96
Feedwater flow	FMM-501	kg/s	0.106	0.1094	0.1099
Steam flow	FVM-602-M	kg/s	N/A	0.1094	0.1099
Primary coolant subcooling at core outlet		ºC		50.8	49.3
Total heat loss through primary system		kW		N/A (no heat loss modelling)	N/A (no heat loss modelling)
Heat transfer through SG		kW		299	299
Maximum surface temperature of core heater rods		ºC		290.00	293.39
Location from the SG secondary inlet to reach - saturation - superheat		m		1.815m (saturation) 5.445m (superheat)	1.815m (saturation) 5.7475m (superheat)
CPV water level	LDP-901	m	6.35	6.41	6.41
CPV water temperature	TF-815	ºC	25.95	27.12	27.0

Figure 4-189 shows comparison of pressurizer temperature (TF-301) among experiment, blind and open calculations. Overall agreement between experimental data and the open calculation result is much improved compared to the blind calculation. However, a steam exit temperature such as average of TF-611 to 634 shows some discrepancy between experimental data and simulation results (Fig. 4-190). Blind calculation result agrees well with the experimental data in early phase of the SP-2 experiment. Otherwise, open calculation result agrees well with the experimental date in late phase. Mid chimney temperature (TF-132) comparison also shows good agreement between the experiment and the open calculation result (Fig. 4-191). Figures 4-192 and 4-193 show averaged core inlet (Avg. TF-121~124) and outlet (TF-105) temperatures. Excellent agreement is achieved for the open calculation. Especially, core inlet temperature drop due to opening of PCS-108A/B valves is well predicted. Various pressures drops (DP-101~106) predictions of the open calculation show reasonable trends compared with experimental data and absolute values of pressure drops calculated are also well agreed with the experimental data. Contrary to the open calculation results, the blind calculation results for pressure drops do not show good agreement. Especially, overall trends of pressure differences show some deviation compared to experimental data. (Fig. 4-194)

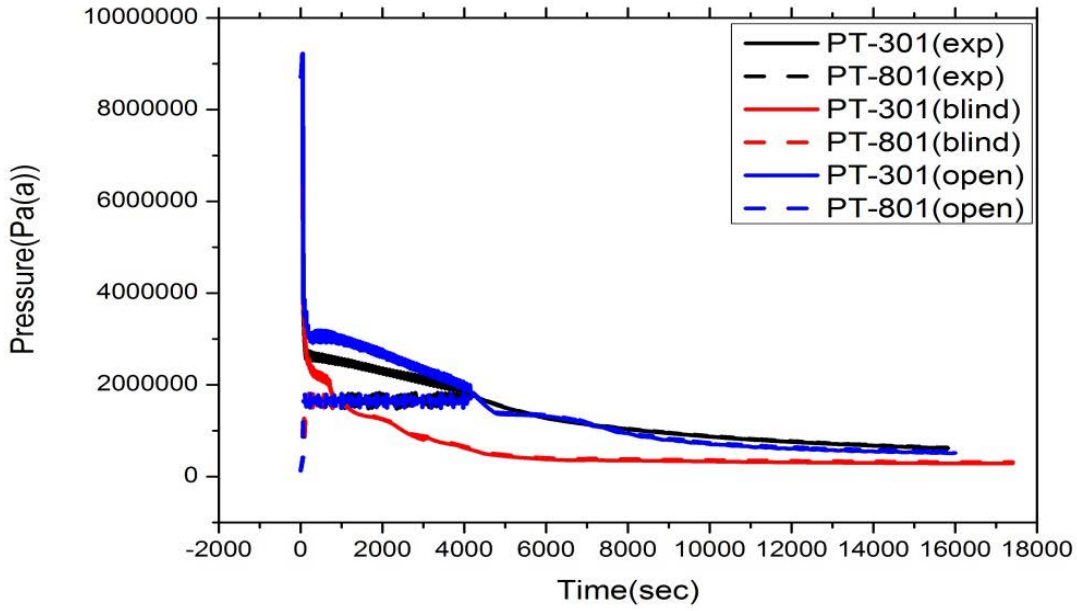

FIG. 4-188. Comparison of PZR and HPC pressures (SP2).

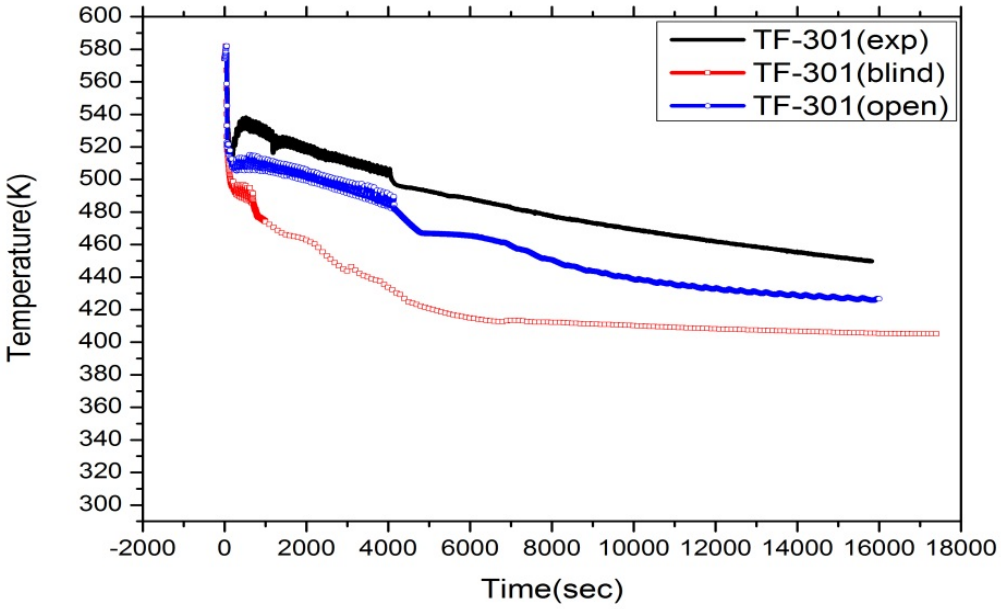

FIG. 4-189. Comparison of PZR temperature (SP2).

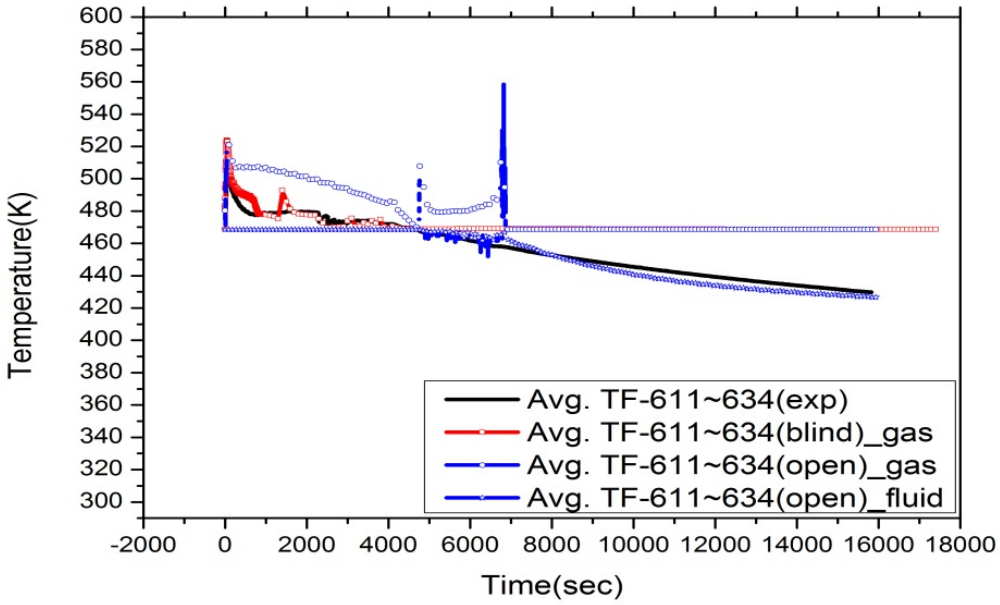

FIG. 4-190. Comparison of SG exit temperature (SP-2).

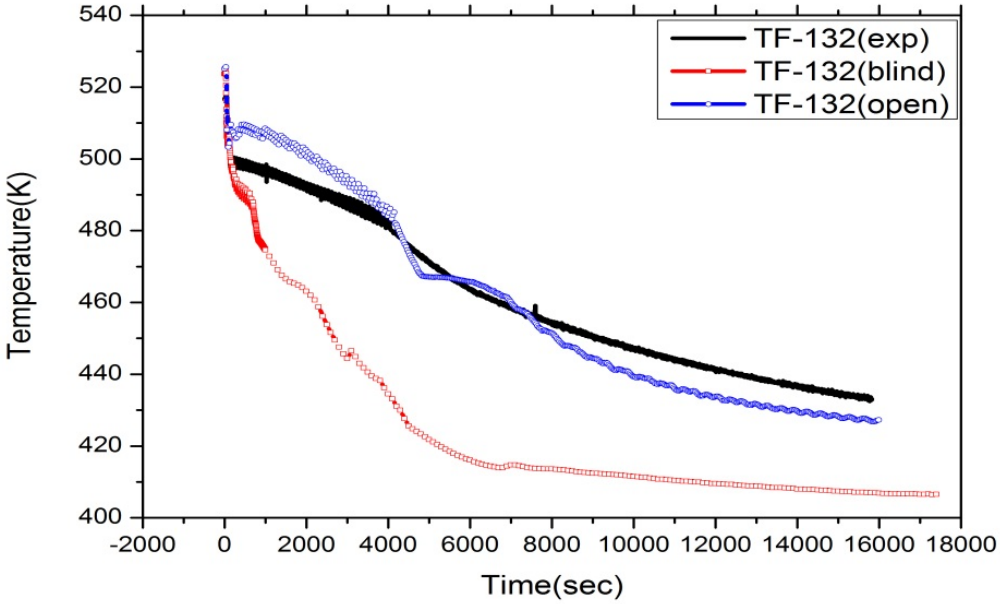

FIG. 4-191. Comparison of mid chimney temperature (SP-2).

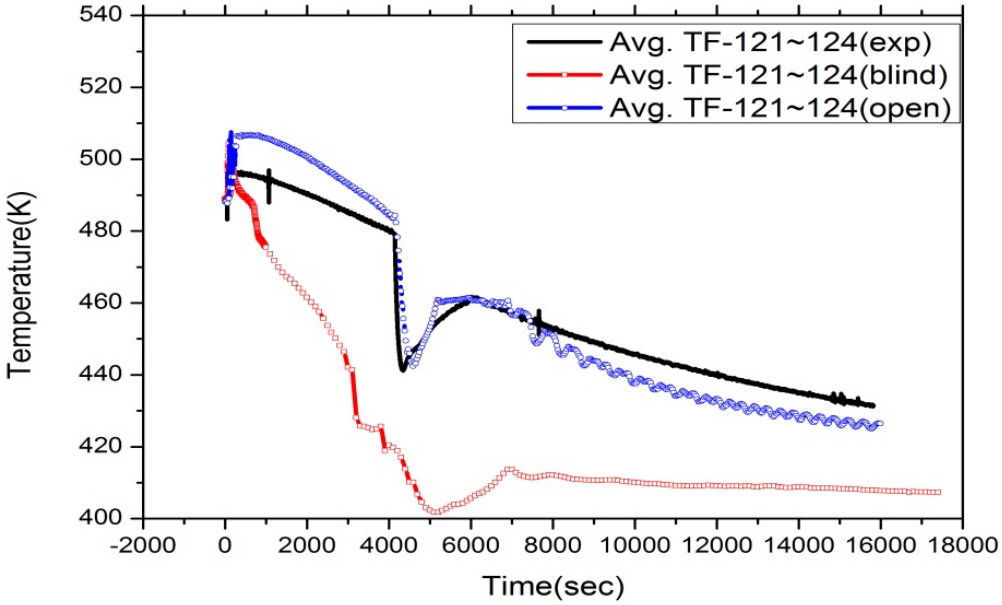

FIG. 4-192. Comparison of core inlet temperature (SP-2).

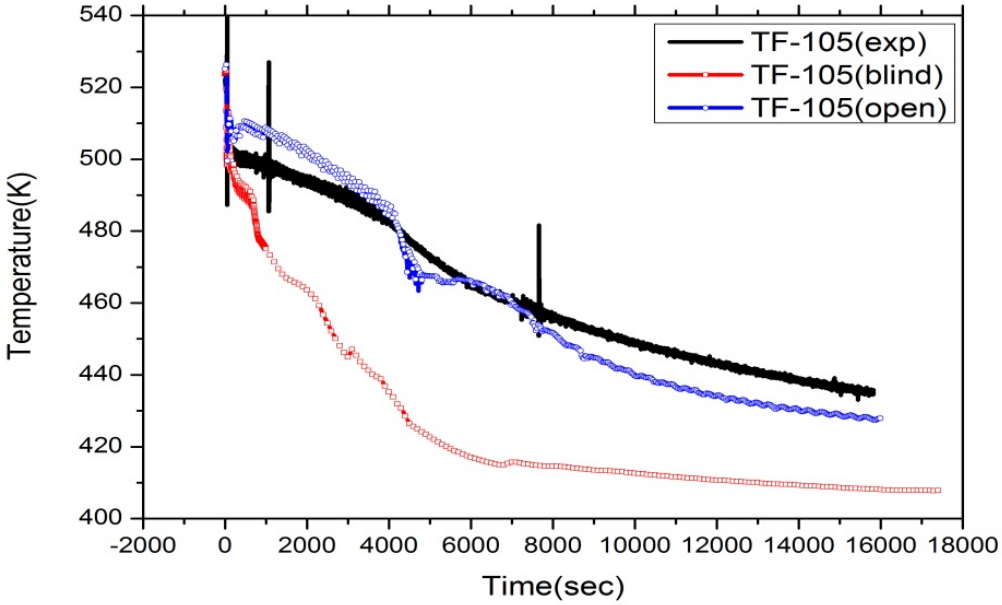

FIG. 4-193. Comparison of core outlet temperature (SP-2).

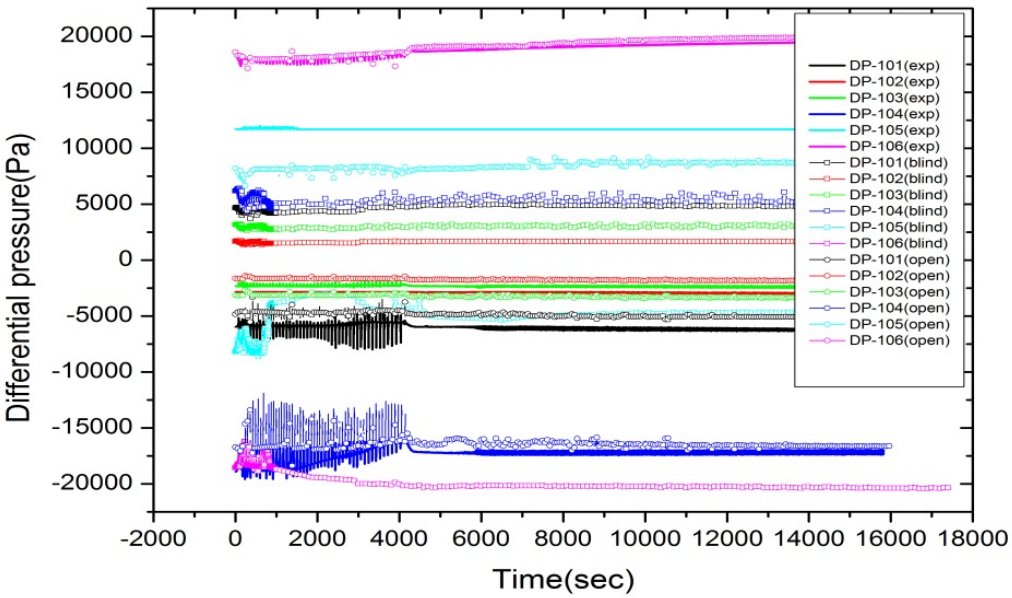

FIG. 4-194. Comparison of differential pressures (SP-2).

In Figure 4-195, various levels trends for RPV (LDP-106), HPC (LDP-801), CPV (LDP-901) and pressurizer (LDP-301) are shown. Agreement between the experiment and the open calculation is excellent. Core heater rod temperature (Avg. TH-141~146) and HPC water temperature (TF-831 & 861) also show good agreement (Figs 4-196 and 4-197). Especially, increase of temperature of TF-831 in HPC just after the opening of all valves of the automatic depressurization system is well predicted in the open calculation. However, for water temperatures in HPC near heat transfer plate (TF-811~TF-861), some discrepancies are identified (Fig. 4-198). Simulated behaviors of TF-831 and 841 are different from experimental data. Also magnitude of temperatures for TF-841, 851 and 861 are estimated lower than experimental data. Compared to the open calculation, blind calculation results do not give reasonable agreement with experimental data for levels, core heater rod temperature and water temperature in HPC.

Figures 4-199 to 4-201 show wall temperatures within the heat transfer plate (TW-812 & 862, TW-814 & 864) and fluid temperatures in CPV. Global trends of temperatures show reasonable agreement between the experimental and the open calculation results. That is, temperature increasing trend with respect to increasing temperature sensor height is well produced in the open calculation. However, quantitative aspect of agreement is not so good. Especially, abrupt temperature increase observed during early period of the SP-2 experiment is not well produced in the simulation. Magnitude of temperature is not well predicted, either. The main reason of these discrepancies seems to the fact that three-dimensional effect such as circulation of flows within HPC and CPV is not well produced by the simulation. Since in the present study, HPC and CPV are modeled one-dimensional pipe component, intrinsic modeling deficiency in the present simulation could be inevitable. For these variables, blind calculation results also show poor agreement.

Figure 4-202 shows core power comparison between the experiment and the open calculation. Fluctuation shown in calculated core power is due to the fact that the calculated core power is estimated by convective heat flux output of the MARS code at core multiplied by heat transfer area.

Figure 4-203 shows some simulated variables in the open and the blind calculations, which are not given in the experimental data. Cumulative masses through PCS-106A/B and PCS-108A/B show reasonable trends. Considering cumulative mass sign, one can find fluid within RPV exits to HPC through PCS-106A/B valves and enter to RPV through PCS-108A/B valves. Results from the blind calculation shows much faster increase of cumulative flow compared to the open calculation. The primary mass flowrate (FDP-131) is also given in Figure 4-204. The behavior of the primary mass

flowrate shows some difference for the open and the blind calculations. Blind calculation result shows much oscillation and persisting behavior in the primary mass flow rate compared to that of the open calculation.

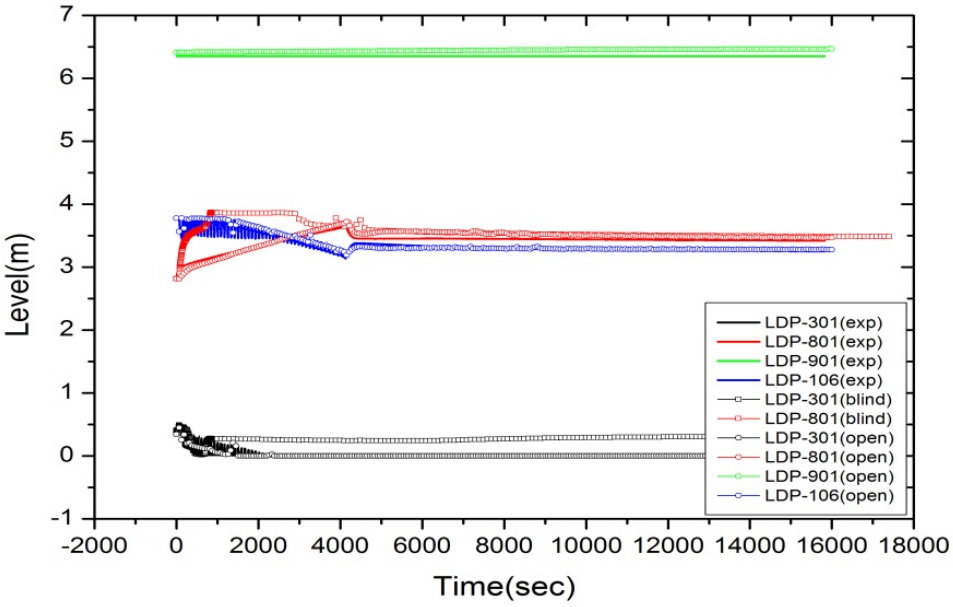

FIG. 4-195. Comparison of various levels (SP-2).

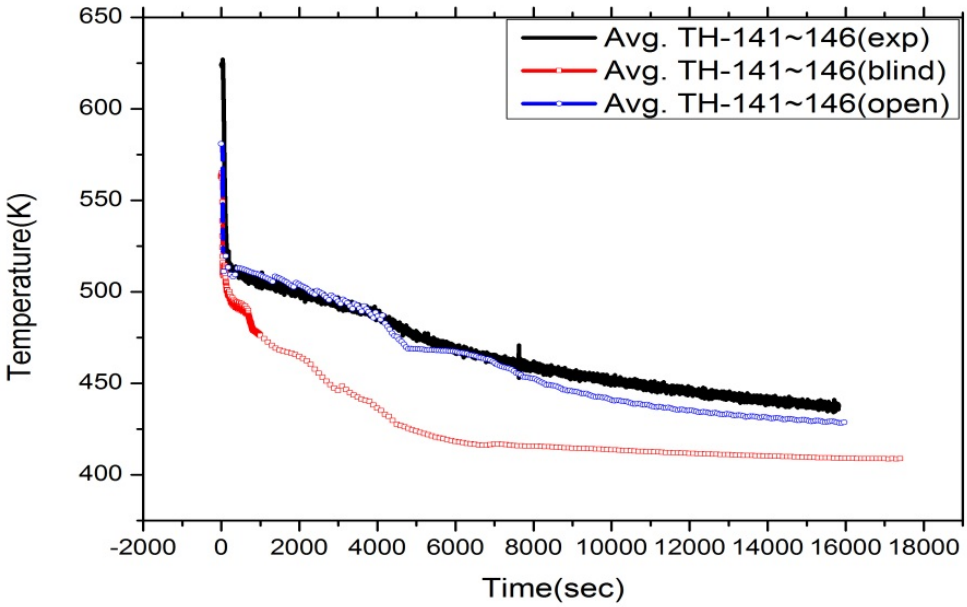

FIG. 4-196. Comparison of core heater rod temperature (SP-2).

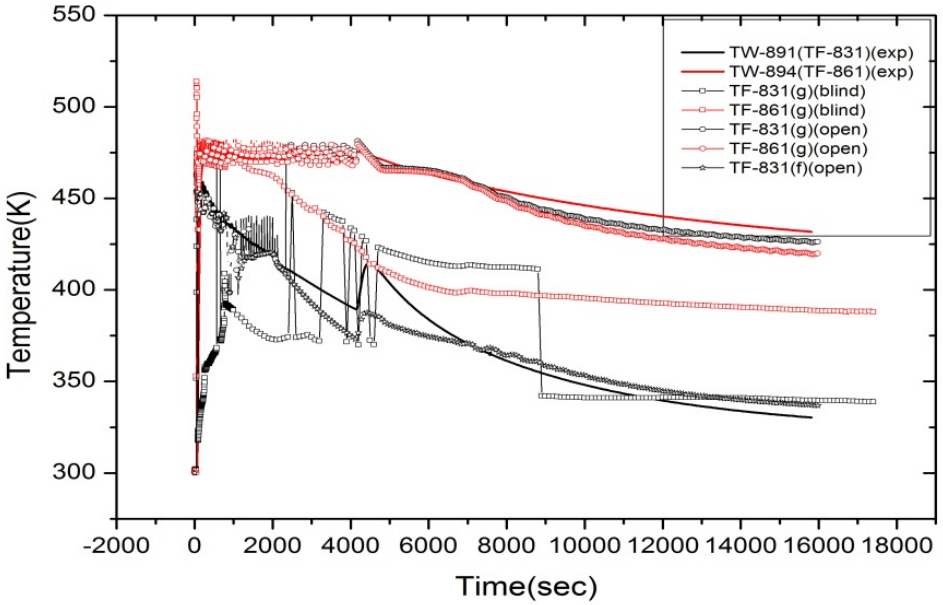

FIG. 4-197. Comparison of fluid temperature in HPC (SP-2).

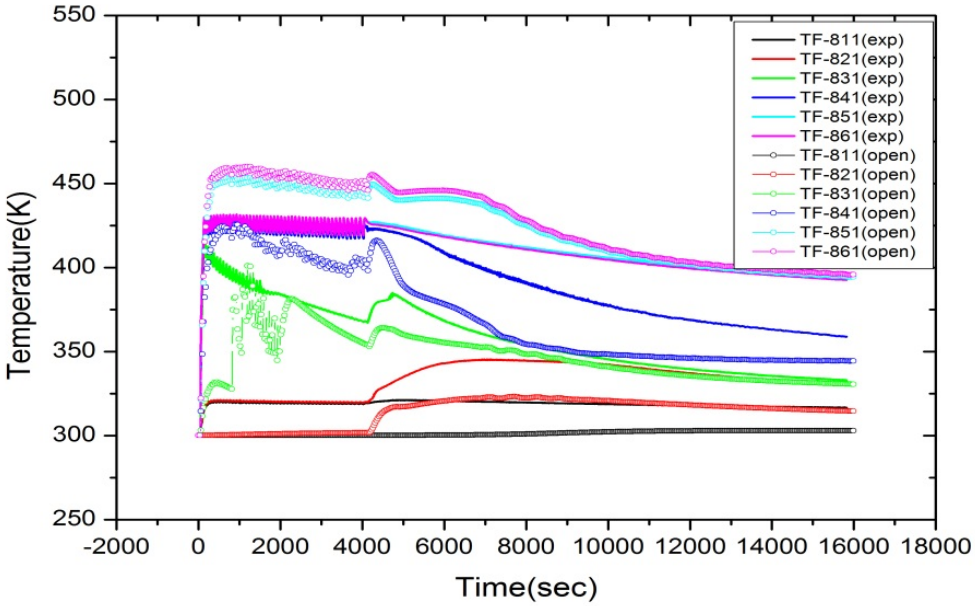

FIG. 4-198. Comparison of fluid temperature in HPC near heat transfer plate (SP-2).

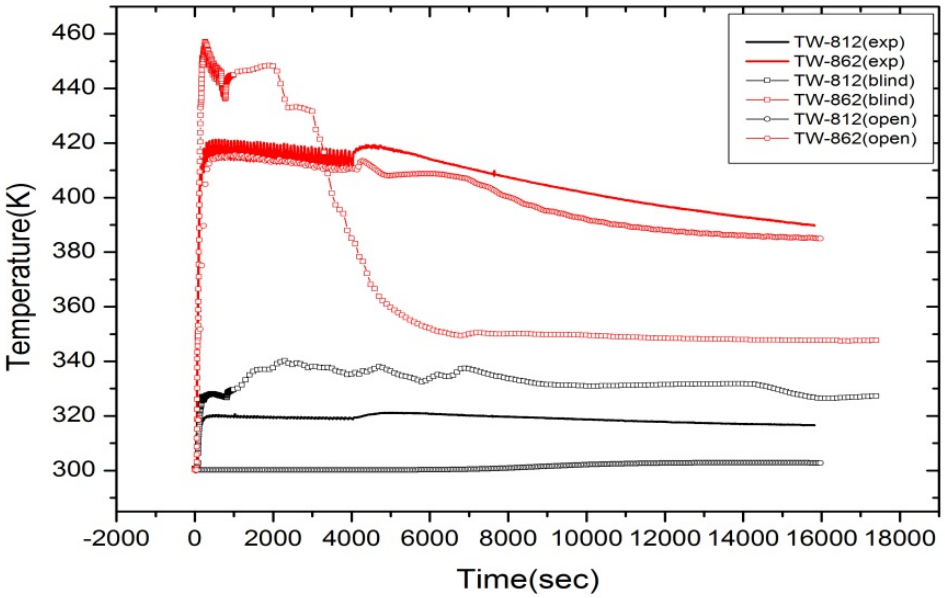

FIG. 4-199. Comparison of wall temperature in heat transfer plate near HPC (SP-2).

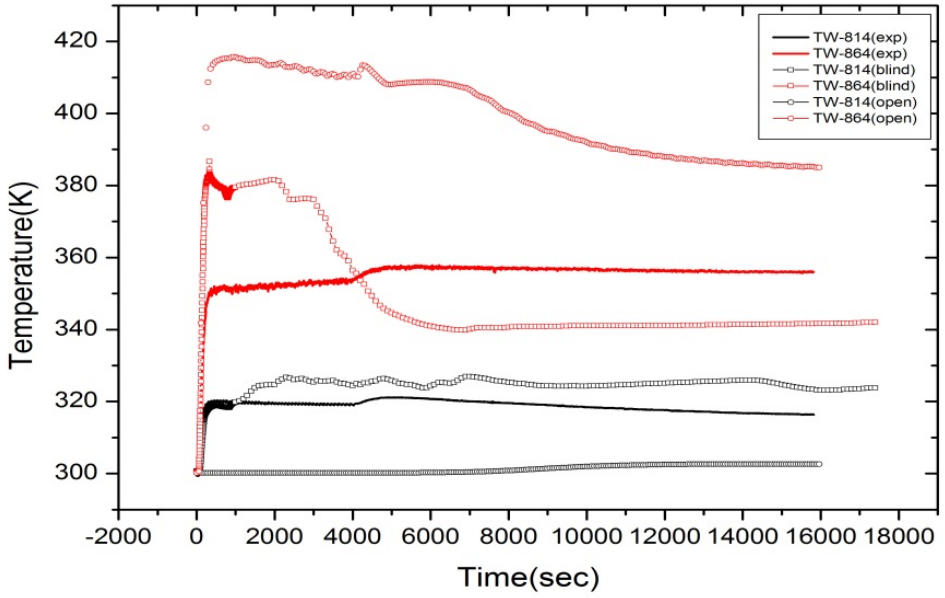

FIG. 4-200. Comparison of wall temperature in heat transfer plate near CPV (SP-2).

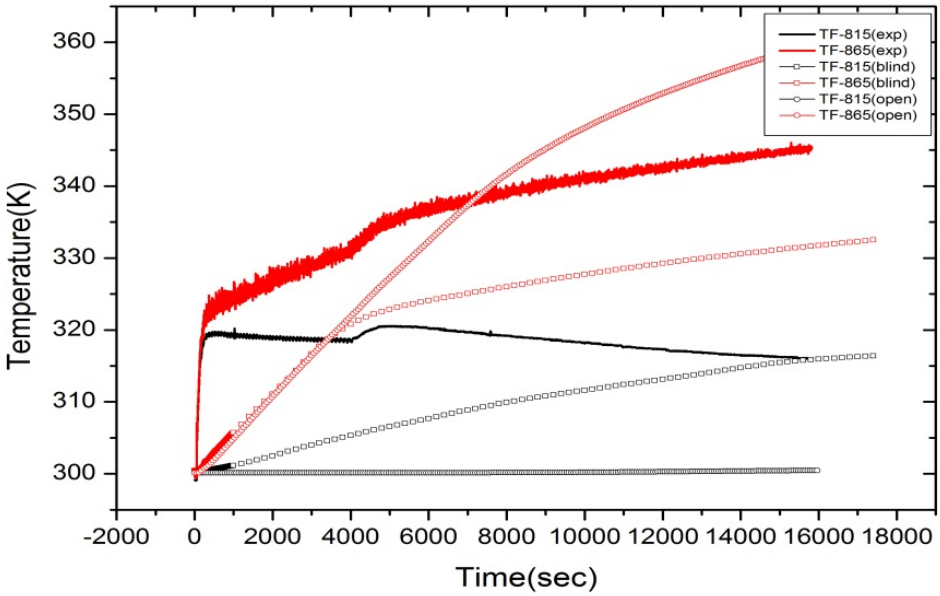

FIG. 4-201. Comparison of CPV fluid temperature (SP-2).

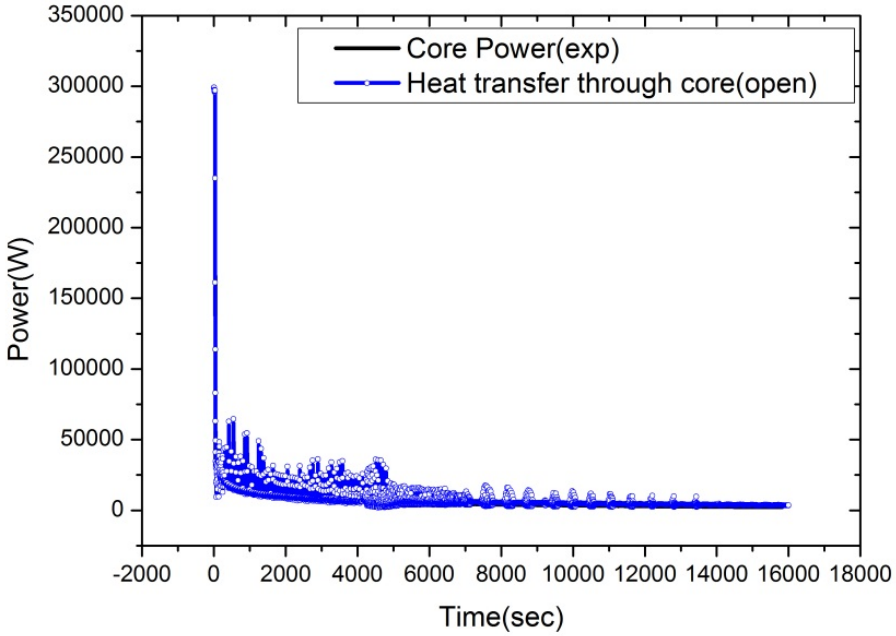

FIG. 4-202. Comparison of core power (SP-2).

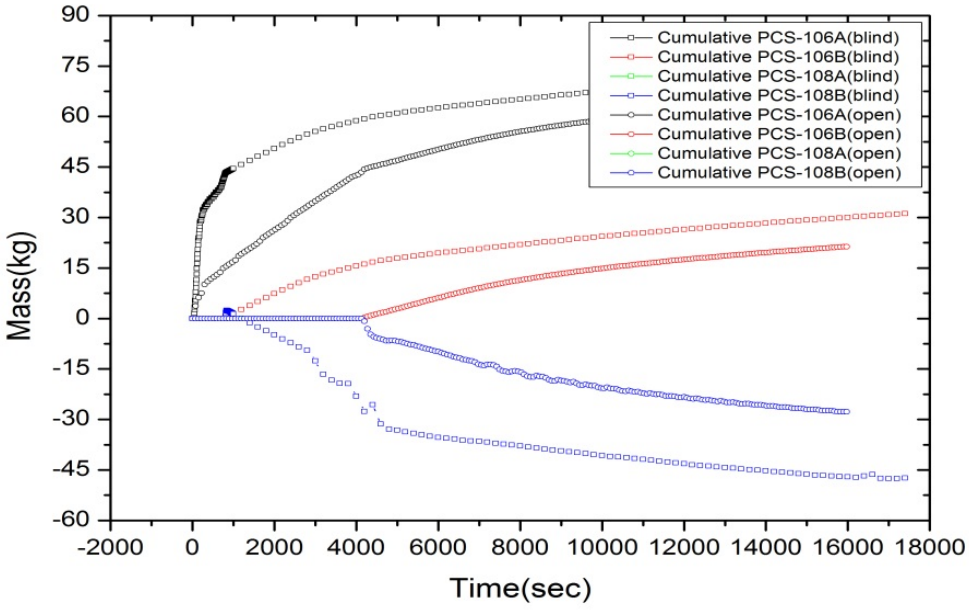

FIG. 4-203. Comparison of cumulative masses through ADS system (SP-2).

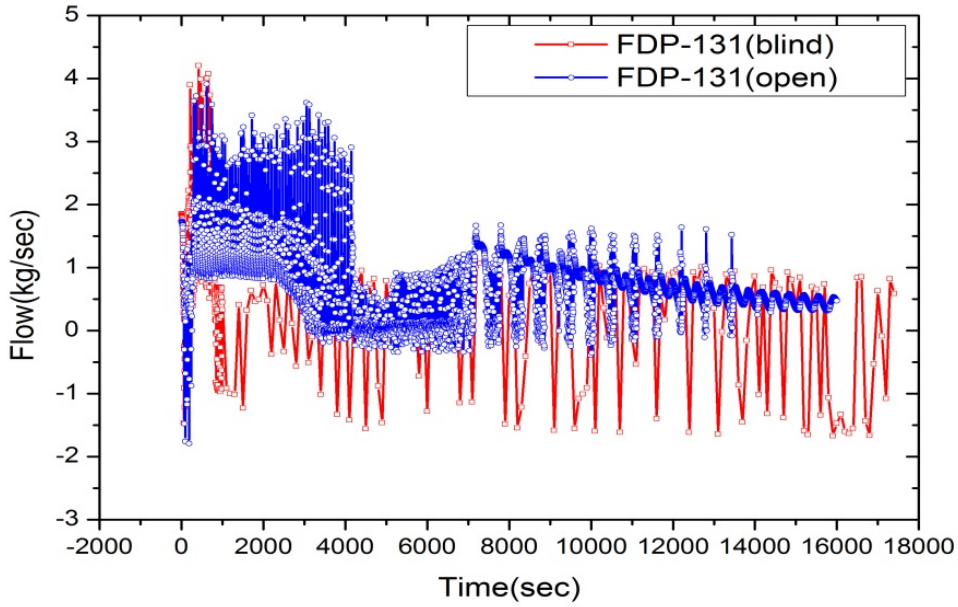

FIG. 4-204. Comparison of primary mass flowrate at core outlet (SP-2).

4.8.4. Analysis results for power manoeuvring

Major time sequence of events for the SP-3 transient is given in Table 4-18. Boundary conditions used in the SP-3 transient analysis are summarized in Figures 4-205 to 4-209.

TABLE 4-18. SP-3 TRANSIENT MAJOR TIME SEQUENCE OF EVENTS

Event	Time (s)
Start of simulation – steady state (start of data collection)	0
Initiate core power increase to 80 kW	27
Initiate core power increase to 120 kW	908
Initiate core power increase to 160 kW	1690
Initiate core power increase to 200 kW	2221
Initiate core power increase to 240 kW	4030
Initiate core power increase to 280 kW	4527
Initiate core power increase to 320 kW	5136

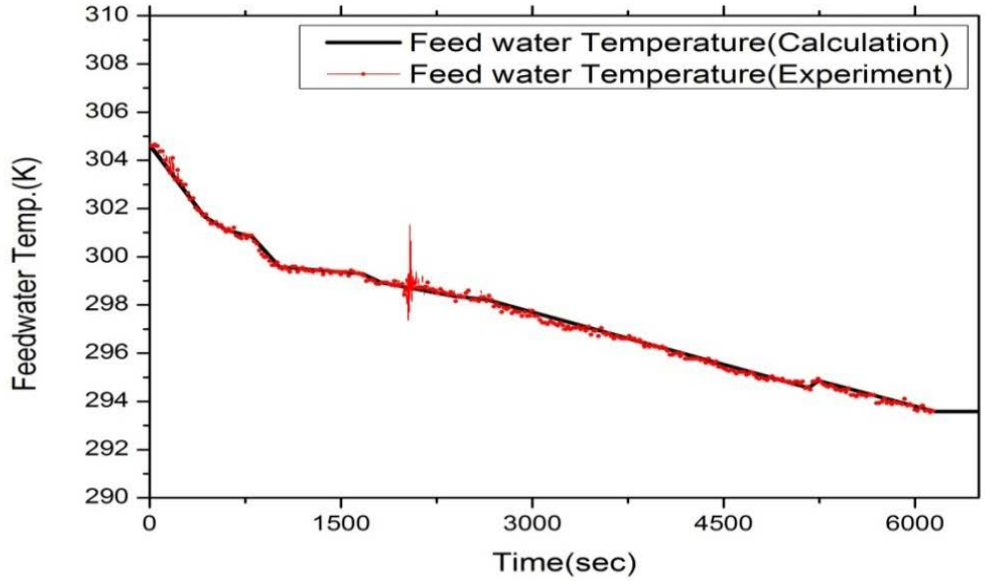

FIG. 4-205. Feed water temperature for the SP-3 transient analysis.

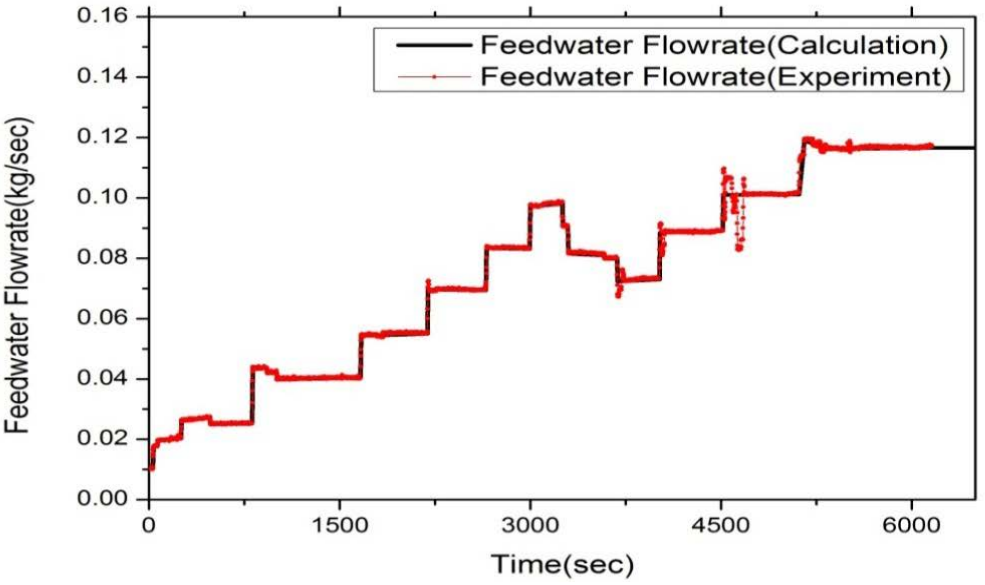

FIG. 4-206. Feedwater inlet flowrate for the SP-3 transient analysis.

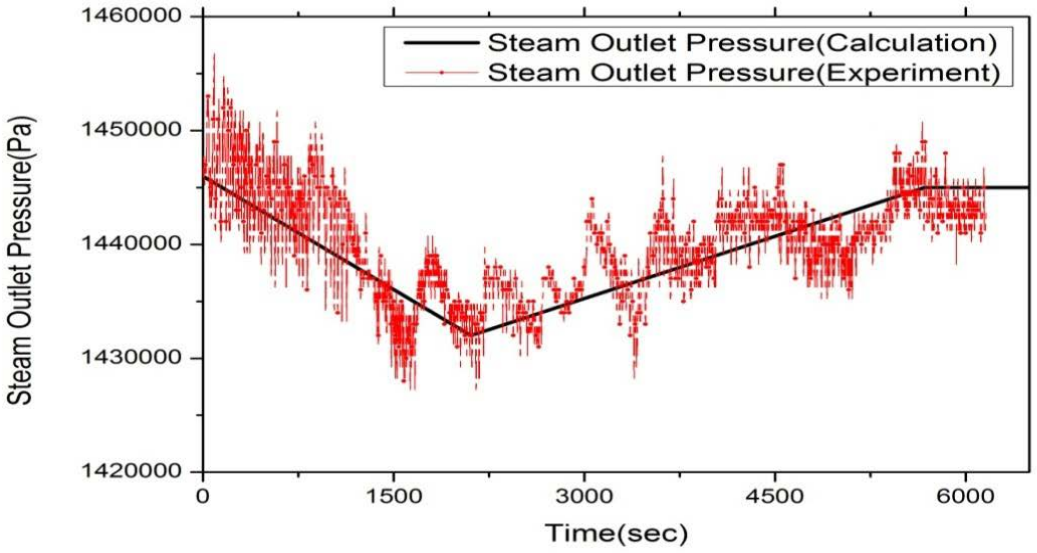

FIG. 4-207. Steam outlet pressure for the SP-3 transient analysis.

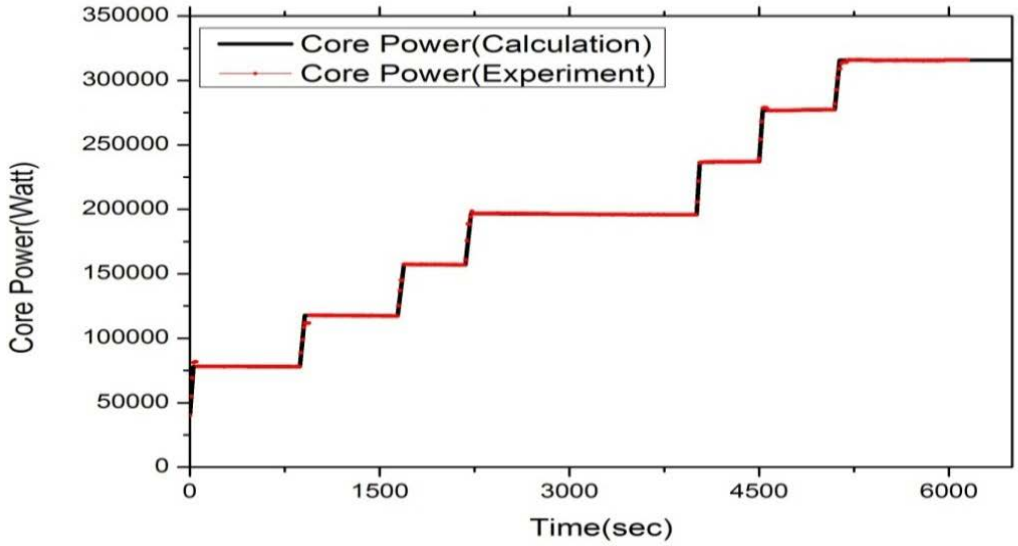

FIG. 4-208. Core power levels for the SP-3 transient analysis.

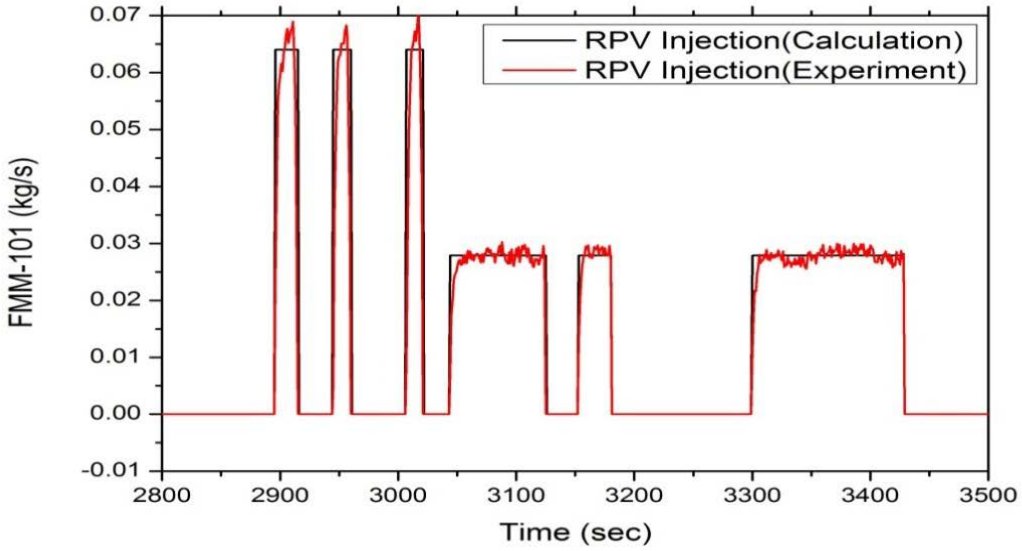

FIG. 4-209. RPV injection flow for the SP-3 transient analysis in the open calculation.

4.8.4.1. Steady state

Table 4-19 shows steady state calculation results for the SP-3 and comparison with experimental data given in the blind and the open calculations. As shown the table, almost all variables calculated agree well with experimental data

TABLE 4-19. STEADY-STATE COMPARISON OF SP-3 EXPERIMENT WITH SIMULATIONS

Parameter	MASLWR	Unit	Experiment	Steady-State (Blind Cal.)	Steady-State (Open Cal.)
Pressurizer pressure	PT-301	MPa(a)	8.718	8.719325(BC)	8.719325(BC)
Pressurizer level	LDP-301	m	0.3574	0.3826	0.3541
Power to core heater rods	KW-101/102	kW	42.1	40(BC)	40(BC)
Feedwater temperature	TF-501	ºC	31.5	31.49(BC)	31.49(BC)
Steam temperature	FVM-602-T	ºC	205.4	205.35	255.3
Steam temperature	Avg. of TF-611 to TF-634	ºC	256.4	259.32	262.91
Steam pressure	FVM-602-P	MPa(a)	1.446	1.446(BC)	1.446(BC)
Ambient air temperature		ºC	20-24	22(BC)	22(BC)
Primary flow at core outlet	FDP-131	kg/s	0.68	0.87531	0.68997
Primary coolant temperature at core inlet	TF- 121/122/ 123/124	ºC	250.3	250.42	251.69
Primary coolant temperature at core outlet	TF-106	ºC	262.8	259.82	263.54
Feedwater flow	FMM-501	kg/s	0.010	0.01018	0.01011
Steam flow	FVM-602-M	kg/s	0.010	0.01018	0.01011
Primary coolant subcooling at core outlet		ºC		41.437	37.718
Total heat loss through primary system		kW		11.4	12.34
Heat transfer through SG		kW		28.60	27.66
Maximum surface temperature of core heater rods		ºC		269.3	276.8
Location from the SG secondary inlet to reach - saturation - superheat		m		 0(saturation) 0.9075(superheat)	 0(saturation) 0.605(superheat)

4.8.4.2. Transient phenomena

Almost all variables calculated are well agreed with the experimental data of the SP-3 transient. Since differences between the blind and open calculation results are small, Figures 4-210 to 4-220 only show comparisons of the open calculation results with the experimental data of the SP-3 transient.

In Figure 4-210, steam temperature (FVM-602-T) shows some discrepancy between experiment and simulation. However, this is due to the fact that the secondary system's outlet boundary condition is designated by steam temperature and static quality of 1.0 in the transient analysis. Therefore, steam temperature was simply calculated as saturated temperature at the designated pressure in the present calculation. Otherwise, steam temperature at steam generator exit (Avg. TF-611~634) as shown in Figure 4-211 shows good agreement between the calculation and the experiment.

Figure 4-212 shows pressure differences for DP-101 through DP-106. As shown in the figure, overall trends of pressure differences calculated are well compatible with experimental data. In spite of good prediction in pressure difference, agreement between the calculation and the experiment in the primary mass flowrate (FDP-131) is poor. Especially, discrepancy becomes larger as mass flowrate increases (Fig. 4-213). One of the reasons of this discrepancy is due to the fact that junction loss coefficients within RPV were further optimized from those of the SP-2 transient for best fit of the primary mass flowrate at the initial core power level 40 kW of the SP-3 and this optimization was done in the

direction of increasing original junction loss coefficient values. However, exact reason of this discrepancy is not clear.

Figure 4-214 also shows core heater rod temperature comparison (Avg. TH-141~146). Overall trend of the core heater rod temperature shows good agreement but magnitude of calculated values shows smaller than that of experiment because of coarse meshing of core heater rod in the simulation model. Core power as seen in Figure 4-215 shows good agreement except some fluctuation in 200 kW region. This fluctuation is due to the fact that calculated core power is obtained by convective heat flux output of the MARS code multiplied by heat transfer area. In Figure 4-216, core inlet/outlet temperatures (Avg. TF-121~123/TF-105~106) are shown. All calculated temperatures are agreed with experimental data reasonably. Figures 4-217 and 4-218 show comparison of pressurizer pressure (PT-301) and temperature (TF-301) and they show that pressurizer control implemented in the present simulation is reasonable. Good agreement in feedwater pressure (Avg. PT-511~531) is shown in Figure 4-219.

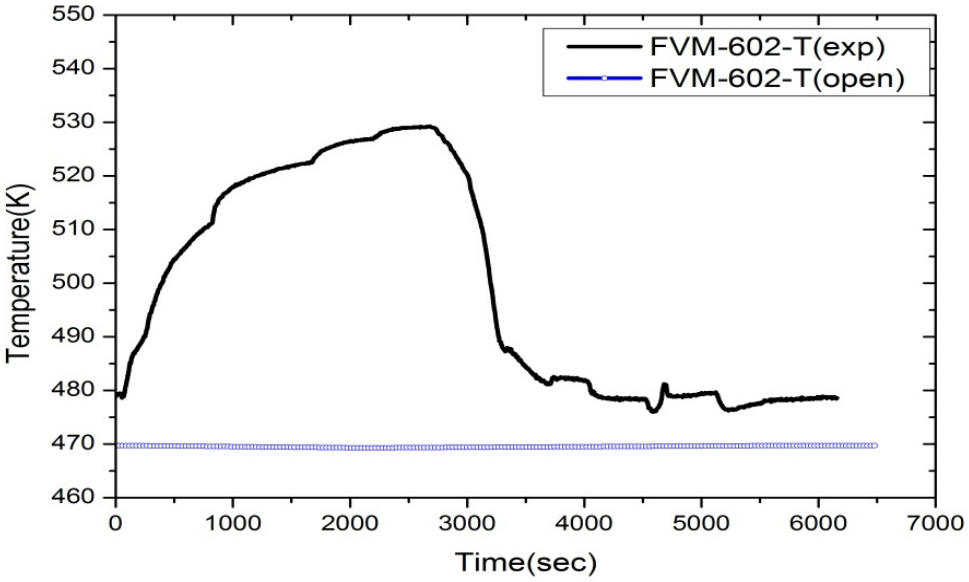

FIG. 4-210. Comparison of steam temperature (SP-3).

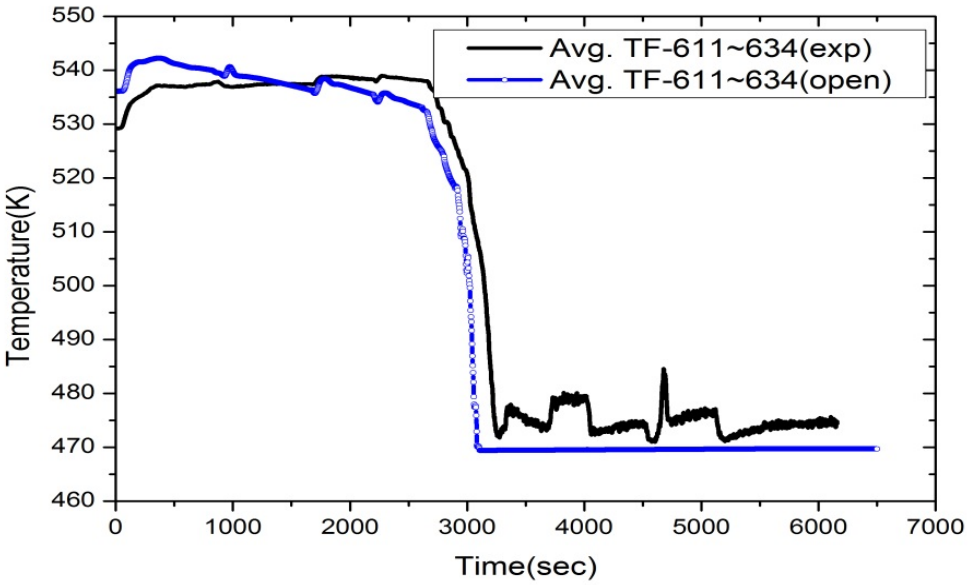

FIG. 4-211. Comparison of steam temperature at SG exit (SP-3).

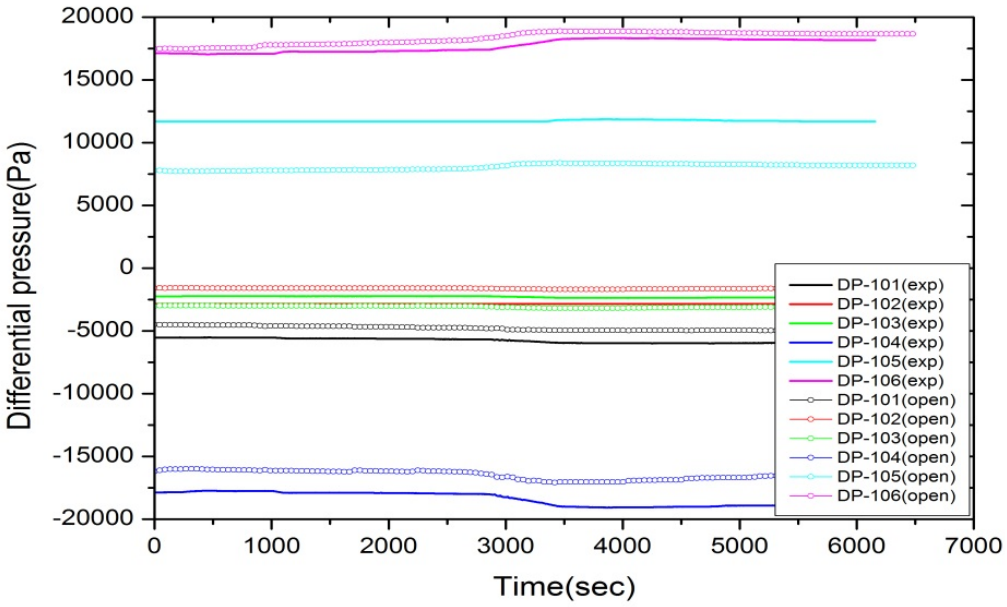

FIG. 4-212. Comparison of differential pressure (SP-3).

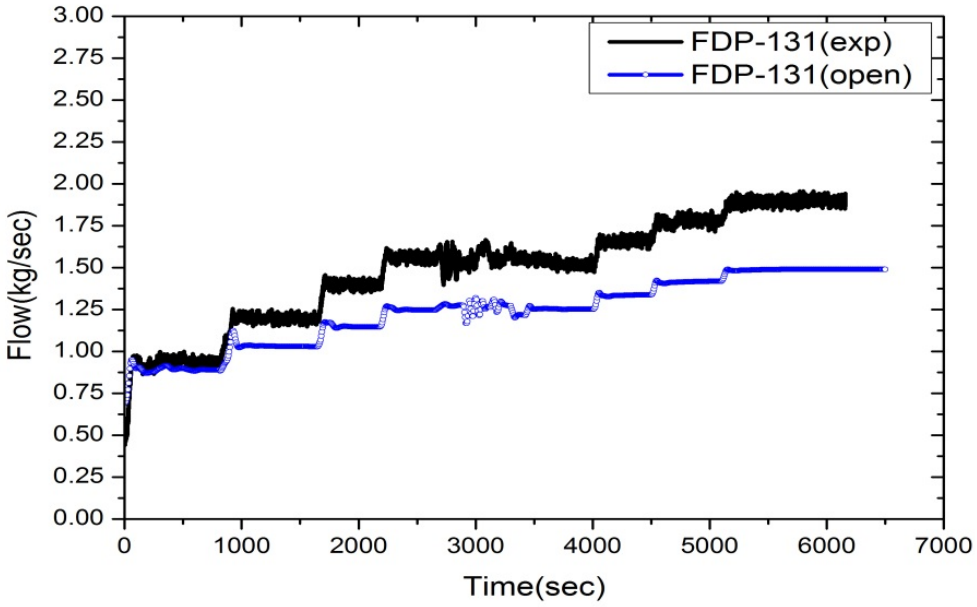

FIG. 4-213. Comparison of primary mass flowrate (SP-3).

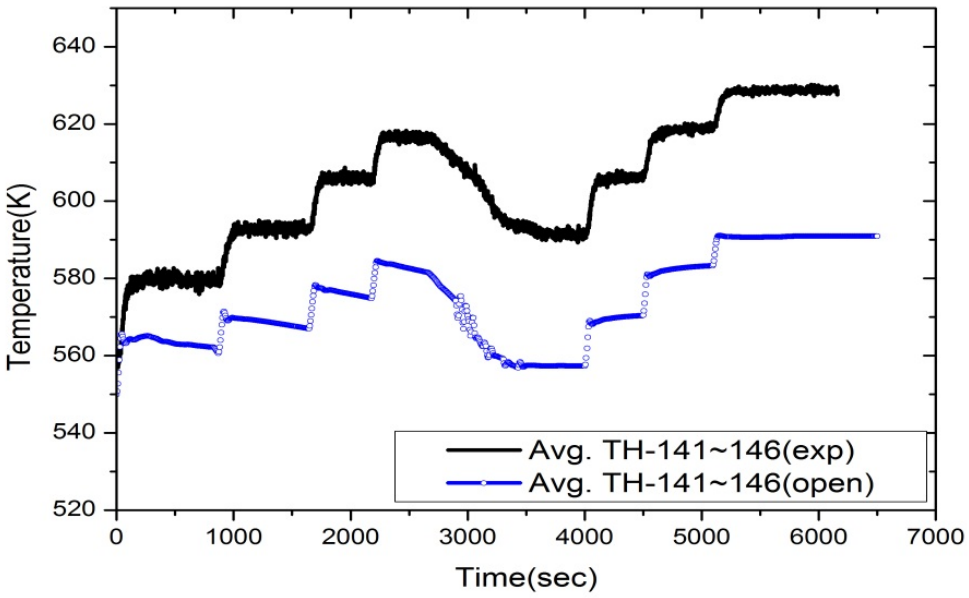

FIG. 4-214. Comparison of core heater rod temperature (SP-3).

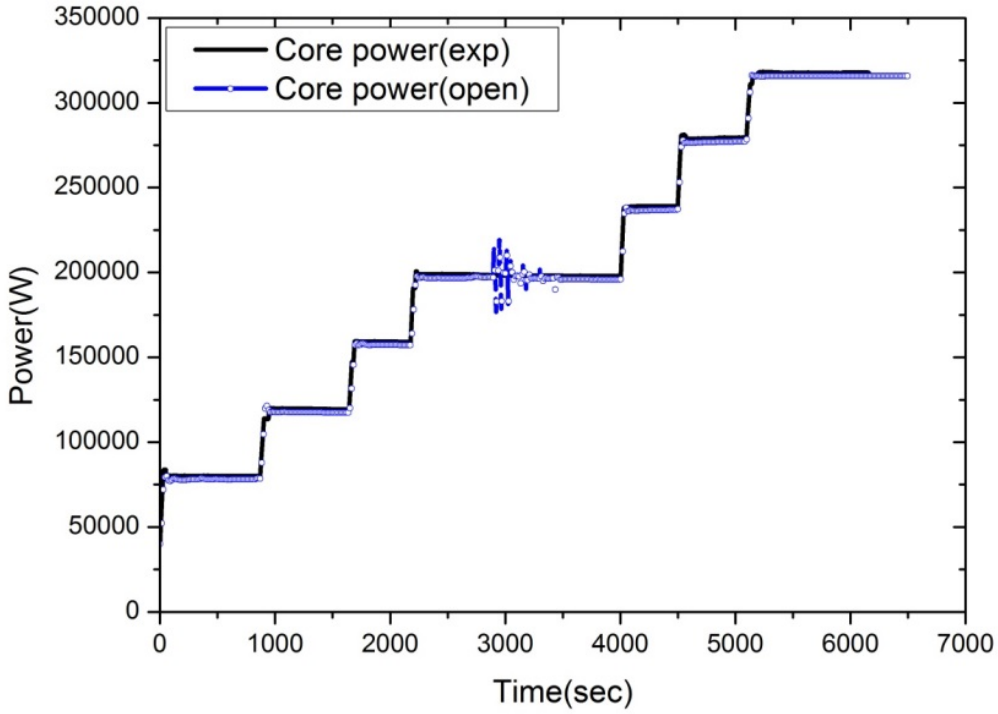

FIG. 4-215. Comparison of core power (SP-3).

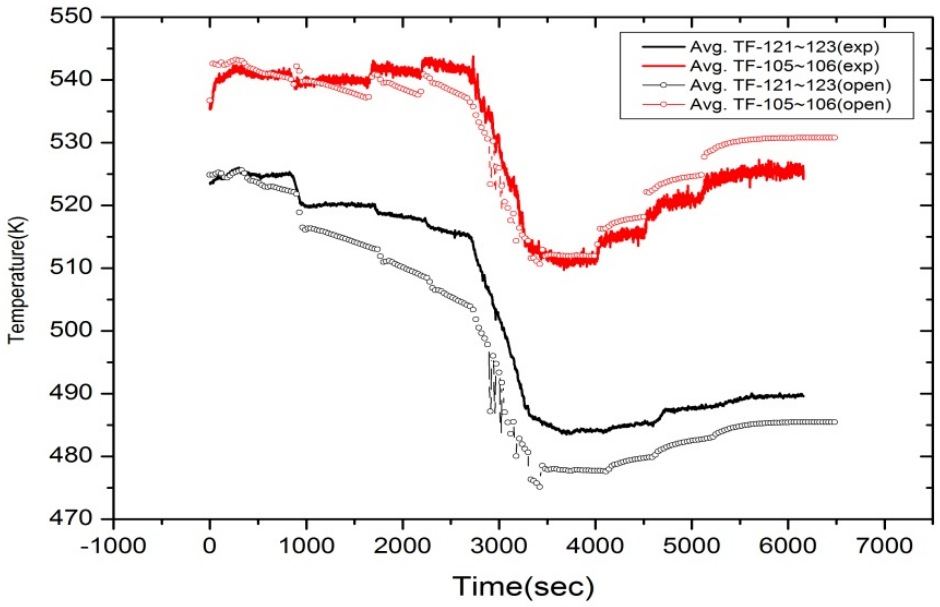

FIG. 4-216. Comparison of core inlet/outlet temperatures (SP-3).

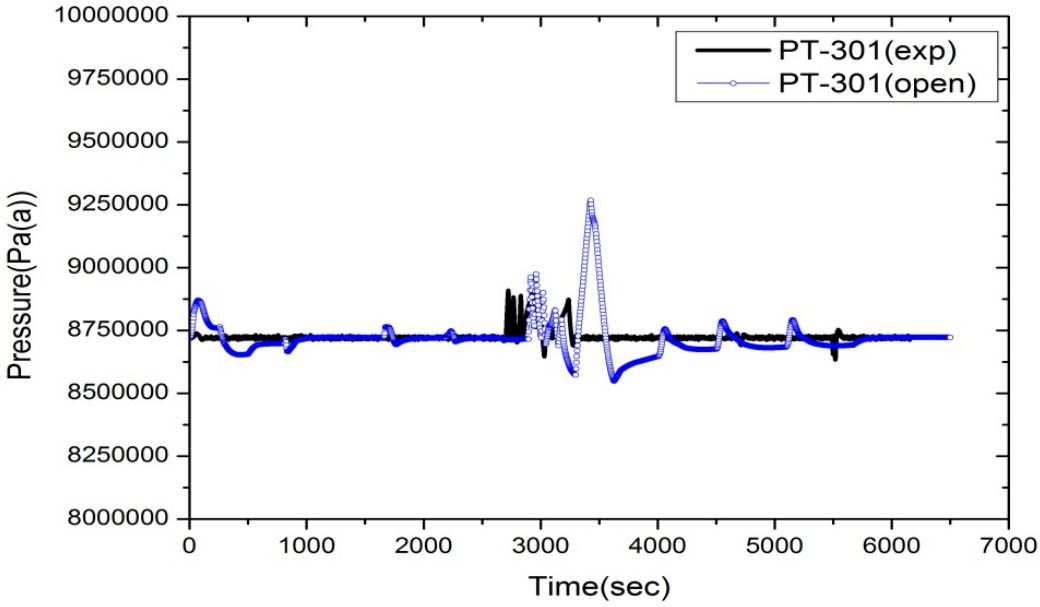

FIG. 4-217. Comparison of PZR pressure (SP-3).

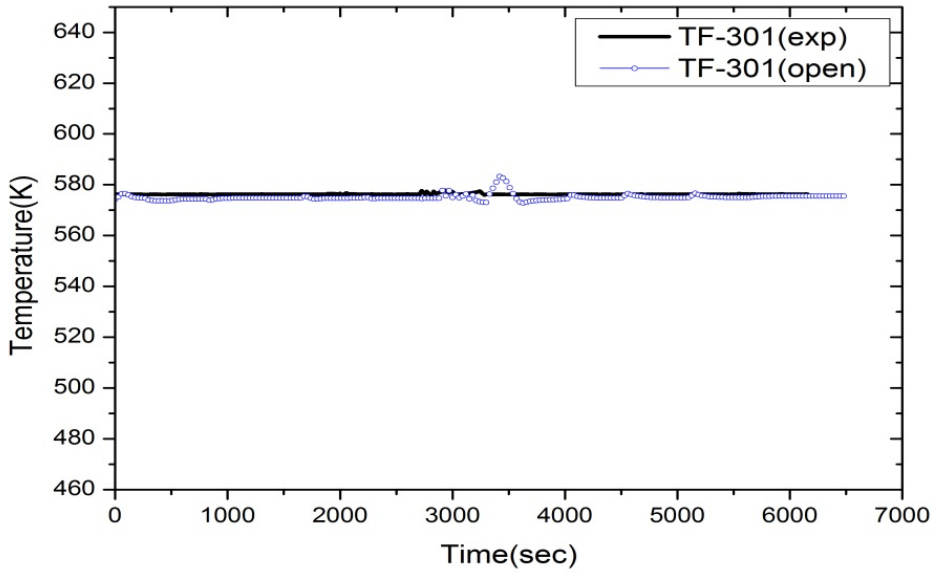

FIG. 4-218. Comparison of PZR temperature (SP-3).

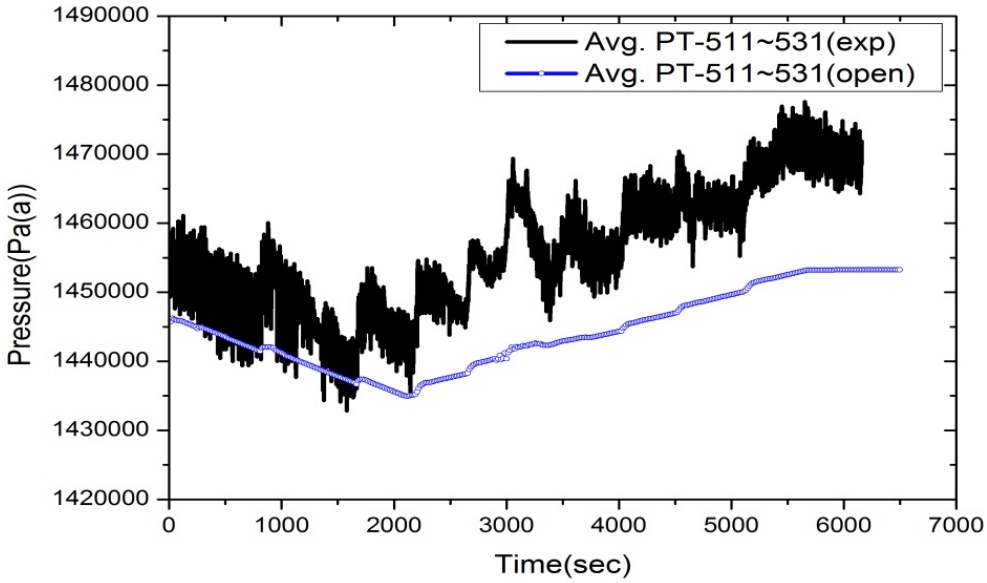

FIG. 4-219. Comparison of feedwater pressure(SP-3).

4.9. NPCIL - INDIA

4.9.1. Computer code

RELAP-5/MOD 3.2 computer code is used for calculations of blind and open predictions for both tests i.e. Loss of Feed water Transient with Subsequent ADS Operation and Long Term Cooling (SP-2) and primary loop flow in normal Operating Conditions at Different Power Levels (SP-3) performed on MASLWR test facility.

The RELAP-5/MOD 3.2 hydrodynamic model is a one-dimensional, transient, two-fluid model for flow of a two-phase steam-water mixture that can contain non-condensable components in the steam phase and/or a soluble component in the water phase. The numerical solution scheme used is either by

a semi implicit scheme or nearly implicit numerical scheme to optimize calculation time step. The difference equations are based on the concept of a control volume (or mesh cell) in which mass and energy are conserved. This results in defining mass and energy volume-average properties and requires knowledge of velocities at the volume boundaries. The velocities at boundaries are obtained through the use of momentum control volumes (cells) centered on the mass and energy cell boundaries. Therefore, the scalar properties (pressure, energy, and void fraction) of the flow are defined at cell centers, and vector quantities (velocities) are defined on cell boundaries. A physical system consisting of flow paths, volumes, areas, etc., is simulated by constructing a network of control volumes connected by junctions. The RELAP-5 hydrodynamic model contains several options such as thermal tracking model, level tracking model, water packing model, stratification model, wall friction model along with thermal equilibrium and non-equilibrium models. RELAP-5 also has several options for hydrodynamic junction such as CCFL model, choking model, homogeneous and non-homogeneous models etc. These options can be used independently or in combination. The RELAP-5 thermal-hydraulic model solves eight field equations for eight primary dependent variables.

Heat structures represent the solid structures bounding hydrodynamic volumes (i.e. pipe walls) or structures internal to the volumes (fuel pin/heater). The one dimensional heat conduction equation is used to compute temperature distributions within heat structures. Hydrodynamic volumes and heat structure conditions are coupled through heat structure boundary conditions. The constitutive relations include models for defining flow regimes and flow-regime-related models for inter-phase drag and shear, wall friction, wall heat transfer, and inter-phase heat and mass transfer. Heat transfer regimes are defined and used for wall heat transfer.

RELAP-5/MOD3.2 includes many generic components (e.g. pump, valve, accumulator, separator etc.) used for simulation of any thermal hydraulic system. RELAP-5 includes material property libraries and associated physical models for commonly used materials in nuclear applications.

4.9.2. System idealization

4.9.2.1. System idealization for blind calculation

The RELAP-5/MOD-3.2 idealization of the MASLWR test facility for tests SP-2 and SP-3 consisting of RPV, secondary system (SG-Coil), HPC, CPV and associated heat structure are shown in Figure 4-220. The RPV consists of lower plenum connecting to core and cold leg, conical region, chimney in hot leg, down comer in cold leg and upper plenum connecting to hot and cold leg and pressurizer region. The RPV is modelled from component No.100 to 128 as shown in Figure 4-220. The reactor core heater is modelled as one equivalent heat structure simulating the 56 electric heaters. Pressurizer is modelled as a single pipe component and represented as component No. 111 in idealization diagram. The three pressuriser heater elements are modelled with one equivalent heat structure.

The HPC vessel consisting of three sections: a lower cylindrical section, an upper cylindrical section, and an eccentric cone section that joins the two. The HPC is modelled from component No. 601 to 660. The CPV is long cylinder and is modelled from component No. 801 to 808. Secondary side SG coil is modelled from component No. 280 to 340. The secondary side steam generator outlet is modelled using time dependent volume (TDV) to provide boundary conditions of SG pressure. To simulate the time varying feed water (FW) flow rates and temperature as boundary condition, a time dependent junction (TDJ) and TDV at inlet side of SG coil is modelled.

The secondary side steam generator (SG) consists of three parallel banks of helical coil, located within the pressure vessel in the annular space between the hot leg riser and the inside surface of the reactor pressure vessel (RPV). The outer and middle coils consist of five tubes each while the inner coil consists of four tubes. In the modelling, all tubes of three parallel coils are lumped together and model as a single representative tube.

To simulate the heat transfer from HPC to CPV through heat transfer plate, a heat structure is modelled and shown in Figure 4-220. Heat structures are also modelled to simulate core heater rods, heat transfer to SG coils, heat transfer from hot leg to cold leg and heat loss from RPV to atmosphere. The ADS blow-down lines connect the RPV cold leg to HPC are appropriately modelled and shown in Figure 4-220.

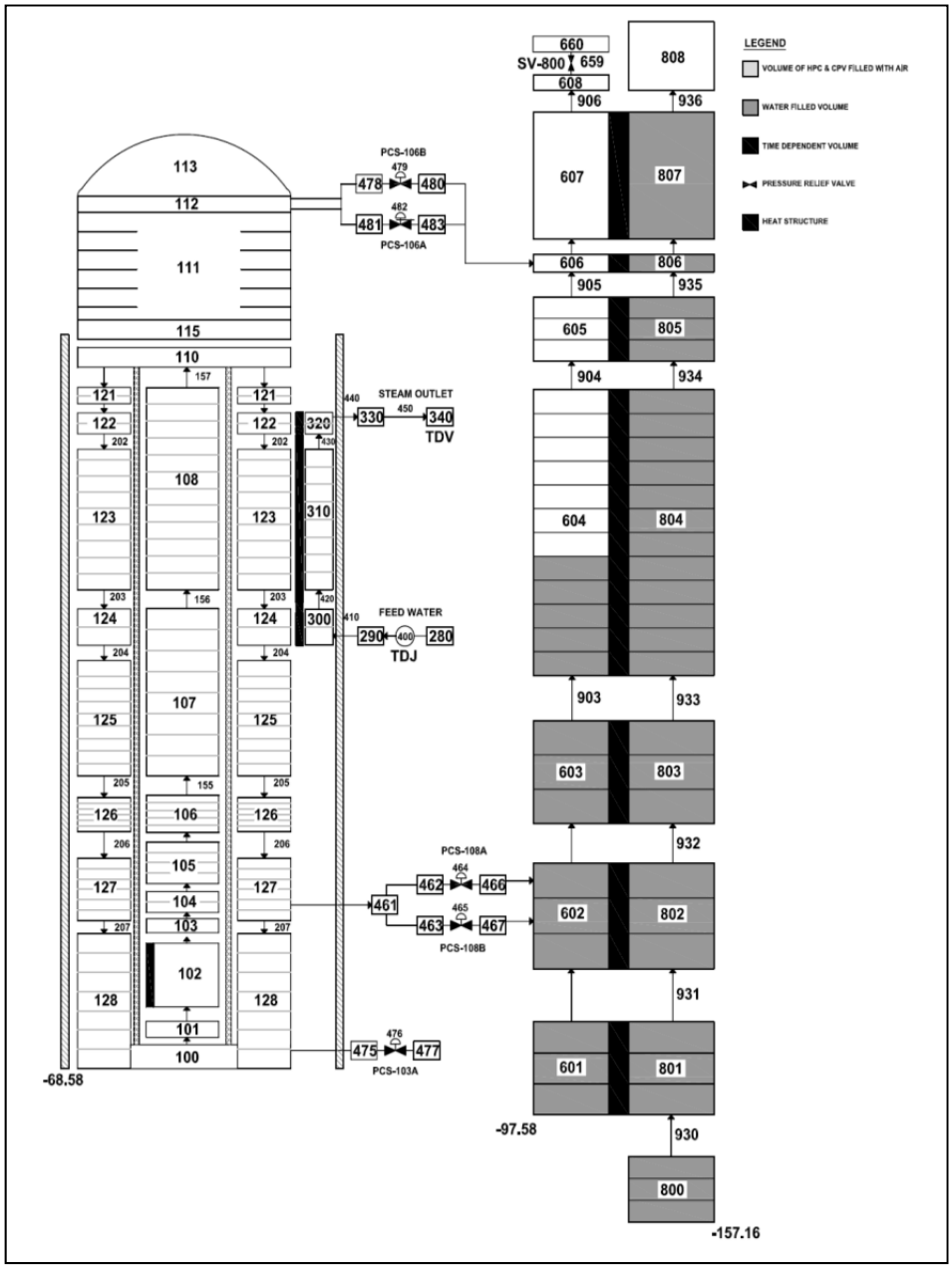

FIG. 4-220. Idealization diagram for simulation of MASLWR test facility.

Logics for operation of pressurizer heater ON/OFF, actuation of various ADS and blow-down valves, steam generator feed flow are modelled appropriately as per the test procedures. In idealization scheme used for simulations, due consideration is given for instrumentation to capture accurate transient behaviours as per the actual test facility.

4.9.2.2. Modelling change for open calculation

Modelling and system idealization of entire test facility of MASLWR for both tests for open calculation are generally same as used in Blind calculation. After the comparison of blind calculation with experimental results, based on deviations among them, following changes have been made for open calculation:

– Heat structure for modelling of heat loss from hot leg to cold leg has been modified to include the heat loss from core and conical region to down comer of cold leg.

- End-loss coefficients have been appropriately allocated in the RPV to match primary flow obtained in experimental results for Test SP-2.
- Thermal capacity of pressuriser heater has been modelled appropriately.
- Material properties of heat transfer plate between HPC and CPV has been incorporated as found in open literature for heat transfer plate material SA240 TP304 SS for lower temperature range.
- For the connection of RPV to HPC, exact location of ADS sump return valve-108A & 108B has been re-idealized.
- Heat loss from RPV to atmosphere is modelled based on atmospheric temperature for SP-2 whereas in case of SP-3 heat loss is modelled based on heat transfer coefficient to accommodate heat loss of 5.0 kW.
- Latest provided boundary conditions as provided have been used for Test SP-3 for core heater power, secondary side feed water flow rate and temperature.

4.9.3. Analysis results for loss of feed-water transient

In the blind/open simulation of this test, steady state run is performed for a period of 50,000 s. Subsequently, main SG feed pump tripped to initiate the transient as per the experiment to simulate loss of feed water transient. Following termination of feed flow, de-energisation of pressurizer heaters and conversion of heater power to decay power mode has been simulated on RPV pressure high (as per the test procedure). Initial steady state conditions achieved in open calculation for test SP-2 are given in Table 4-20 which also includes the initial conditions observed during the experiment as well as in blind calculation.

TABLE 4-20. STEADY-STATE COMPARISON FOR TEST SP-2

Parameter	MASLWR	Unit	Experiment	Steady-State Prediction	
				Blind Calculation	Open Calculation
Pressurizer pressure	PT-301	MPa(a)	8.718	8.718	8.718
Pressurizer level	LDP-301	m	0.3606	0.3584	0.3584
Power to core heater rods	KW-101/102	kW	297.4	298	298
Feed water temperature	TF-501	ºC	21.2	21	21
Steam temperature	FVM-602-T	ºC	205.4	204.01	205.26
Steam pressure	FVM-602-P	MPa(a)	1.411	1.427	1.427
Ambient air temperature		ºC	25	25	25
HPC pressure	PT-801	MPa(a)	0.127	0.128	0.128
HPC water temperature	TF-811	ºC	26.7	27.0	27.0
HPC water level	LDP-801	m	2.82	2.827	2.827
Primary flow at core outlet	FDP-131	kg/s	1.82	1.79	1.79
Primary coolant temperature at core inlet	TF-121/122/ 123/124	ºC	215.1	222.57	222.05
Primary coolant temperature at core outlet	TF-106	ºC	251.5	257.85	258.62

4.9.3.1. RPV thermal-hydraulic behavior

In this test, transient starts with tripping of main feed pump at 0.0 s. Following termination of feed water supply to SG, heat removal from SG ceases and heat generated in core remains stored in RPV which results in rise of RPV pressure (Fig. 4-221). Due to accumulation of core heat in RPV, level swell is also observed in pressurizer (Fig. 4-226). Primary water down flow temperature after steam generator and core inlet temperature starts rising just after tripping of main feed pump due to loss of heat sink (Fig. 4-222). In about 28 s, RPV pressure increases to around 1300 psig (9.1 MPa(g)) at which, heater power reduces to decay power mode. Thereafter, RPV pressure and temperature rises at

a slower rate due to reduction in heater power to decay power level in the absence of heat sink (Fig. 4-222).

As per logic, ADS vent valve PCS-106A opened at 48 s and steam flows from RPV to HPC. Following opening of ADS valve PCS-106A, water level in RPV (Fig. 4-225) starts decreasing whereas water level in pressurizer (Fig. 4-226) increases till the closing of valve PCS-106A due to flashing of RPV water. This rise and fall in the level of the RPV is related with the opening of PCS-106A, but total inventory in RPV decreases with each opening of the valve PCS-106 A. It is observed that during experiment PCS-106A opened 47 times prior to opening of all valves (PCS-106B, 108A and 108B) and same number of PCS-106A operation are observed in the blind and open predictions.

At around 4148 s (4024 s in experiment and 4780 s in blind prediction), all ADS valves (PCS-106B, PCS-108A and PCS-108B) including PCS-106A get opened on sensing pressure difference between RPV and HPC below 5 psi. On opening of all ADS valves, the water level in HPC sharply reduces whereas water level in RPV increases to equalize the static head. On opening of valve PCS-108A & B, relatively cold water of HPC gets transferred to RPV which results further reduction in RPV temperature (Figs 4-222 and 4-223).

Figure 4-224 shows the core heater rod temperature (TH-145). It is found that predicted results in blind and open calculation are in good agreement with the experimental results.

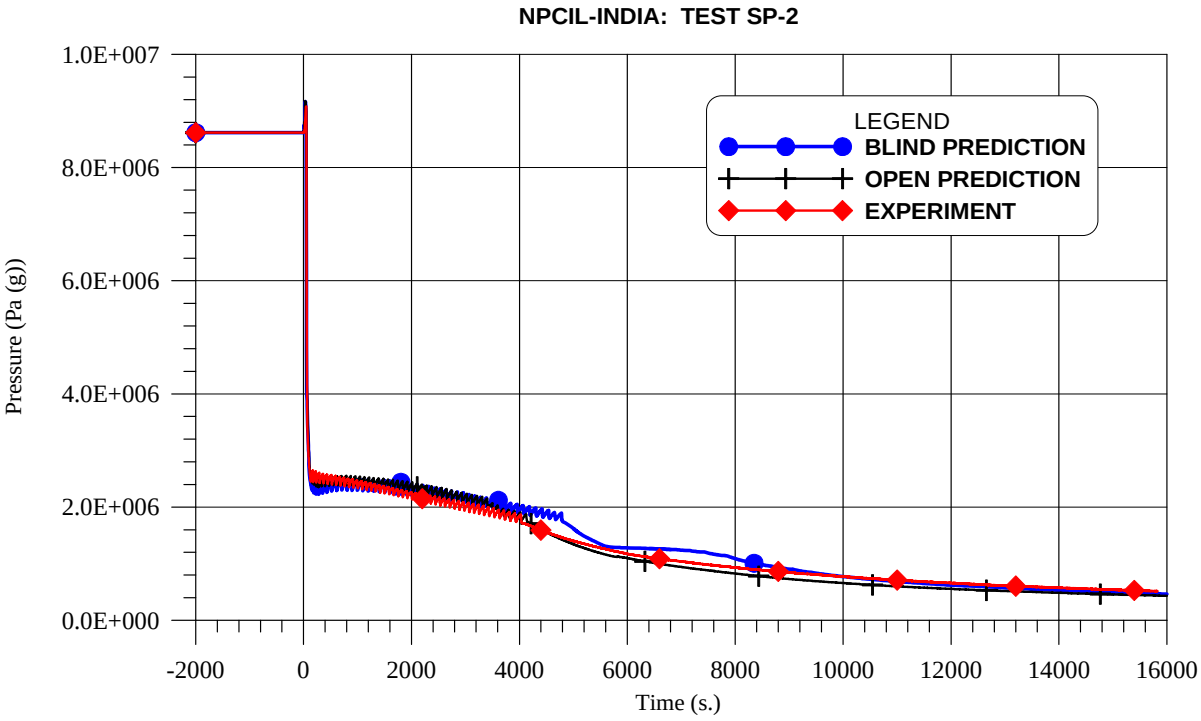

FIG. 4-221. RPV pressure PT-301(Pa)/steam pressure in pressuriser.

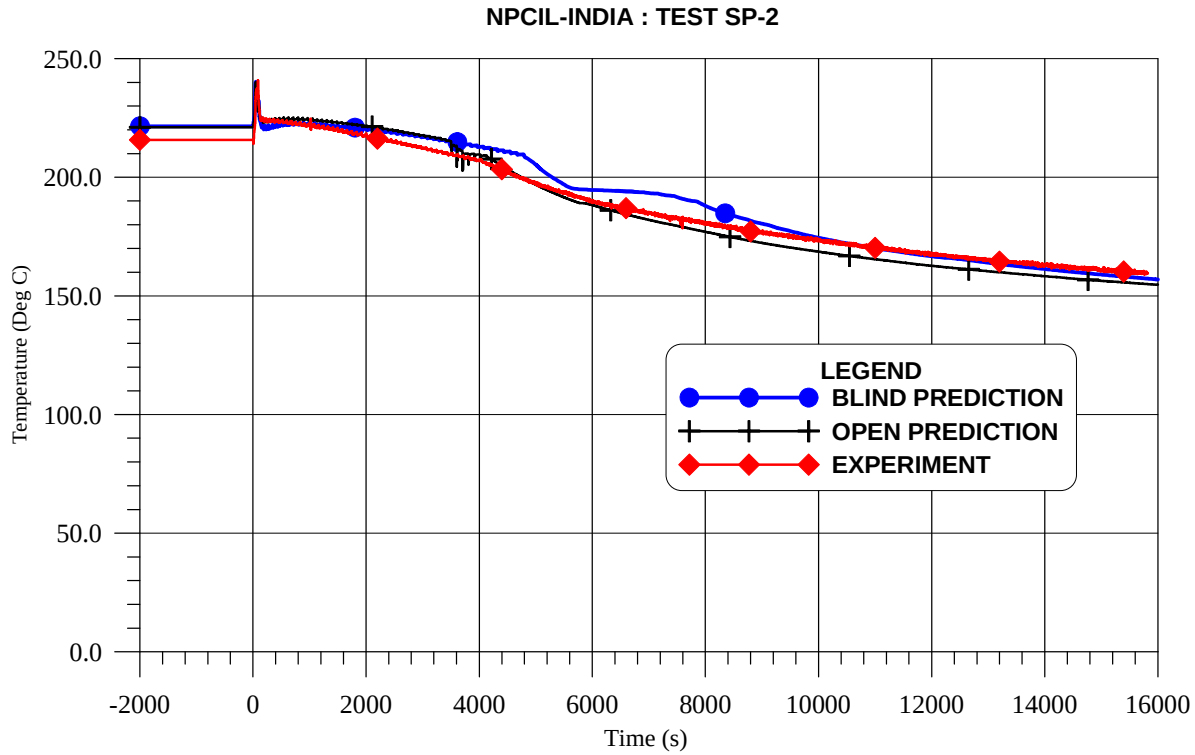

FIG. 4-222. Primary water down flow temperature after steam generator (TF-131).

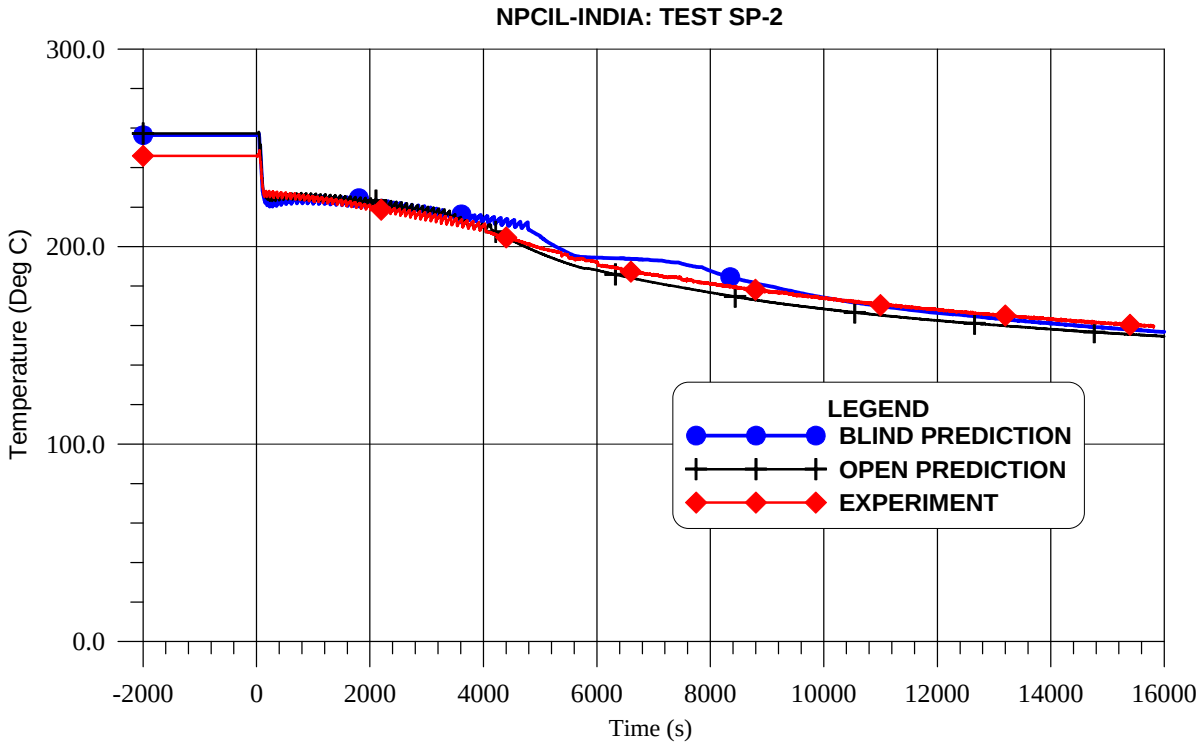

FIG. 4-223. Primary water temperature at top of chimney (TF-111).

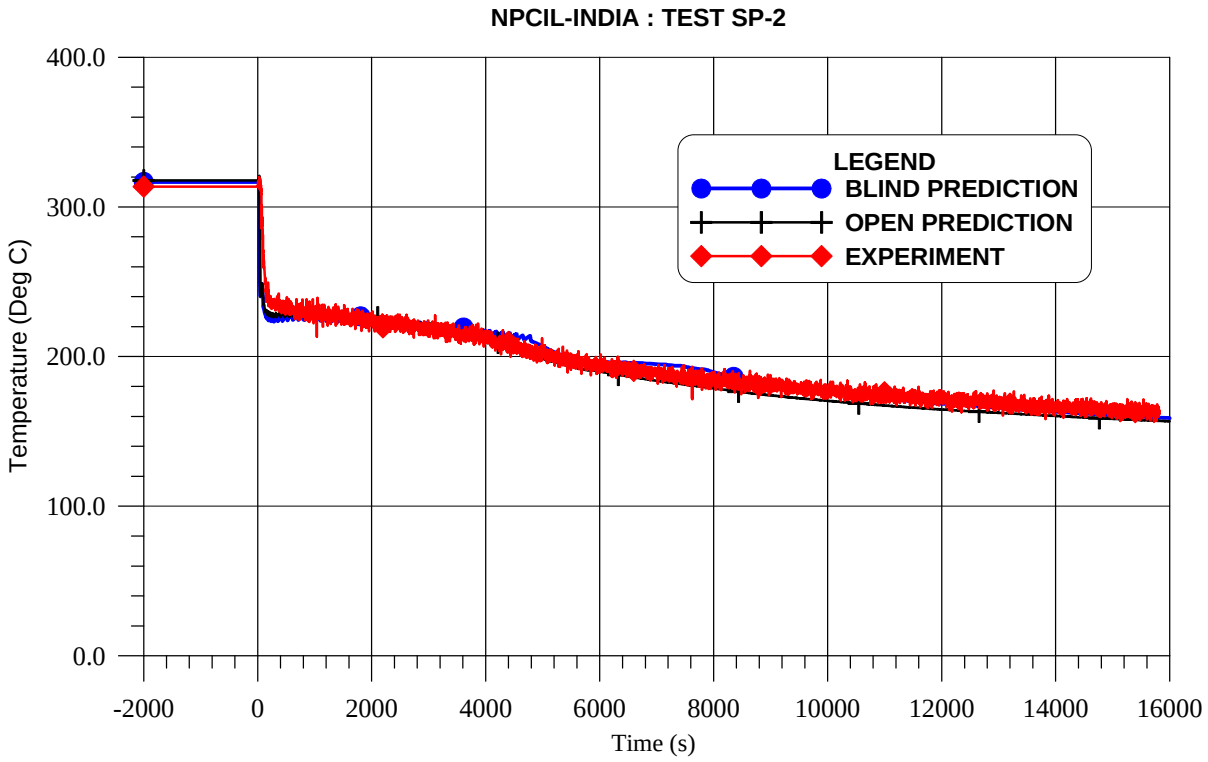

FIG. 4-224. Core heater rod temperature (TH-145).

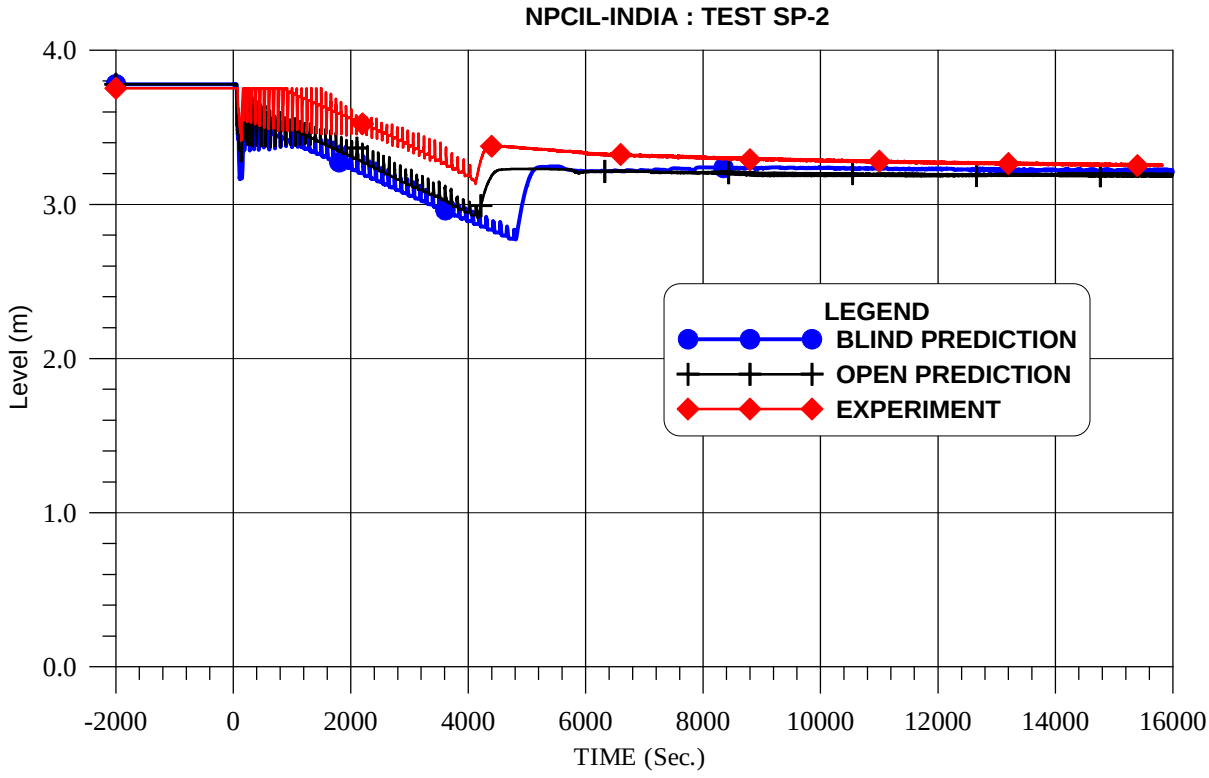

FIG. 4-225. Primary water level (LDP-106).

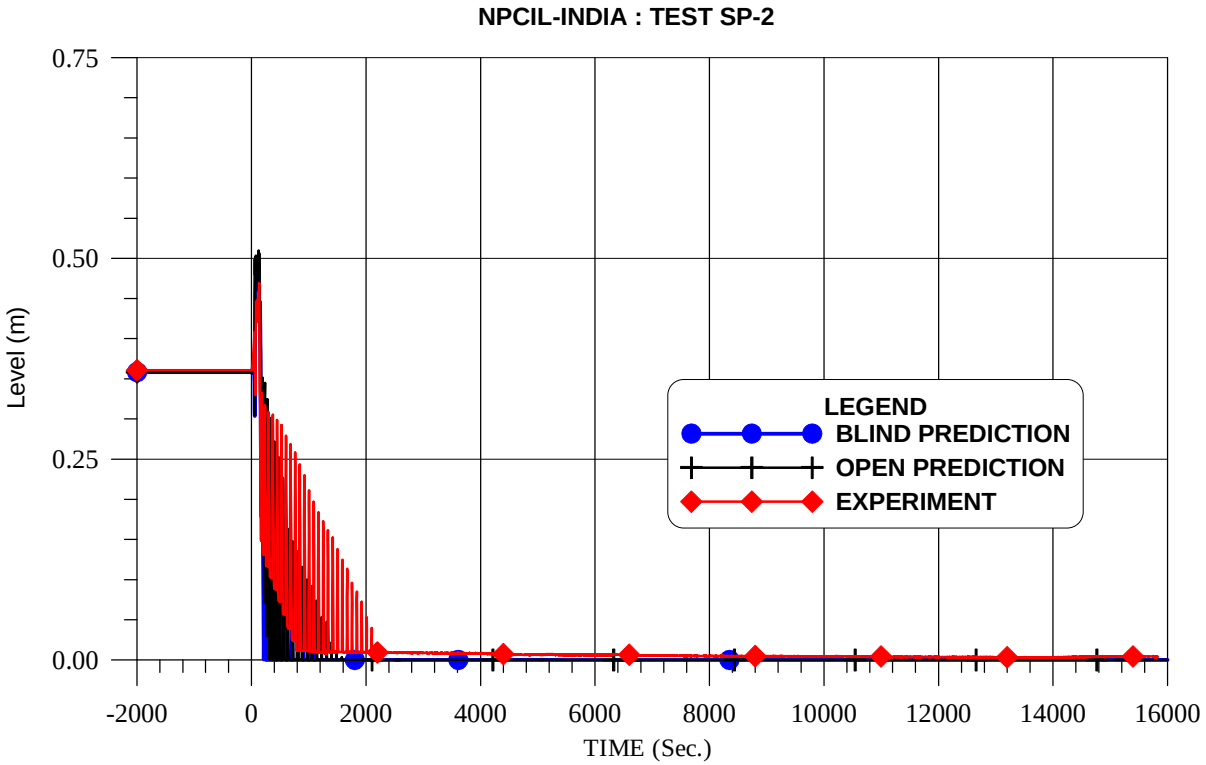

FIG. 4-226. Primary Water Level in Pressuriser (LDP-301).

4.9.3.2. SG thermal-hydraulic behaviour

Steady state has been achieved and steady state values of SG feed pressure, temperature and flow rate are 1.33 MPa(g), 21.44ºC and 0.111 kg/s respectively. Whereas, steady state values of steam outlet pressure, temperature and flow rate are achieved as 1.32 MPa(g), 205.26ºC and 0.111 kg/s respectively. As per the test procedure of SP-2, feed water pump stops and feed flow to SG coil reduces to zero in the beginning of transient. SG pressure is kept constant in blind calculation whereas in open calculation SG pressure in transient is taken same as in experiment as boundary condition.

4.9.3.3. HPC thermal-hydraulic behaviour

Following opening of ADS valve PCS-106A, steam flow occurs from RPV to HPC which results in sharp rise of pressure (Fig. 4-227), water level and temperature in the HPC. Following closing of ADS valve PCS-106A at around 141 s, HPC pressure starts reducing due to combined effect of heat transfer from HPC to CPV through heat transfer plate and condensation of discharge steam in HPC. Once, HPC pressure reduced to 200 psig (1.478MPa (a)) at around 153 s in which ADS valve again open as per given logic (Fig. 4-227). On opening of ADS valve, RPV pressure starts further reducing and HPC pressure starts increasing from 200 psig to 250 psig. At around 167 s blowdown valve gets closed on sensing HPC pressure more than 250 psig. It is observed that duration of ADS valve opening is significantly reduced at this time from around 93 s to around 14 s. This is because large amount of energy transferred through PCS-106A is utilized for heating HPC structure and heat transfer plate in first opening of ADS valve. Thereafter, in subsequent opening of valve, large part of energy is utilized to increase HPC pressure. Similar phenomenon is observed in blind and open predictions. Water level in HPC is (Fig. 4-228) continuously increases and reaches to maximum water level of 3.7 m at 4158 s. During the transient, ADS valve (PCS-106A) got opened for 47 times before achieving the condition for opening of other valves (PCS-106B, PCS-108A and PCS-108B) on pressure difference between RPV and HPC less than 5 psig. Sharp spikes in HPC pressure are observed during the transient due to frequent opening and closing of ADS valve PCS-106A.

As steam discharge to HPC, water temperature in upper portion of HPC increases sharply to around 180°C (Fig. 4-230) in open calculations whereas in blind calculations and in experiment it increases to around 200°C and 160°C respectively. It is observed that in experiment part of heat is getting

transferred to HPC lower portion through conduction by heat transfer plate, resulting rise in water temperature in HPC lower portion also. Whereas in blind/open prediction, water temperature at the lower part of HPC does not increase during the operation of ADS valve-106A and remain at around initial temperature (Fig. 4-229). Subsequent opening of valve 108A and 108B, water gets transferred from HPC to RPV which results in lowering of water level in HPC (Fig. 4-228). Transfer of hot water from upper portion to lower portion of HPC causes rise in water temperature at the lower part of the of HPC also which has been well predicted in blind and open calculation (Fig. 4-229).

4.9.3.4. CPV thermal-hydraulic behaviour

As the pressure and temperature in the HPC increases, heat transfer takes place from HPC to CPV through the heat transfer plate which leads to increase in the water temperature of the CPV (Fig. 4-232). During the initial opening of ADS valve, predicted water temperature in the lower portion of CPV is maintained at around initial temperature (Fig. 4-231). After opening of all ADS valves, water temperature in the lower portion of CPV is also increases slowly. Water temperature in CPV is maintained at relatively lower temperature which indicates that CPV is capable of removing the decay heat of the core and long term cooling is maintained. Water level in CPV remains almost at the initial steady state level due to water temperature in the CPV is not increasing significantly. It is seen that water temperature is increased by 40°C in the upper part of the CPV, while temperature is increased by 20°C in the lower part of CPV.

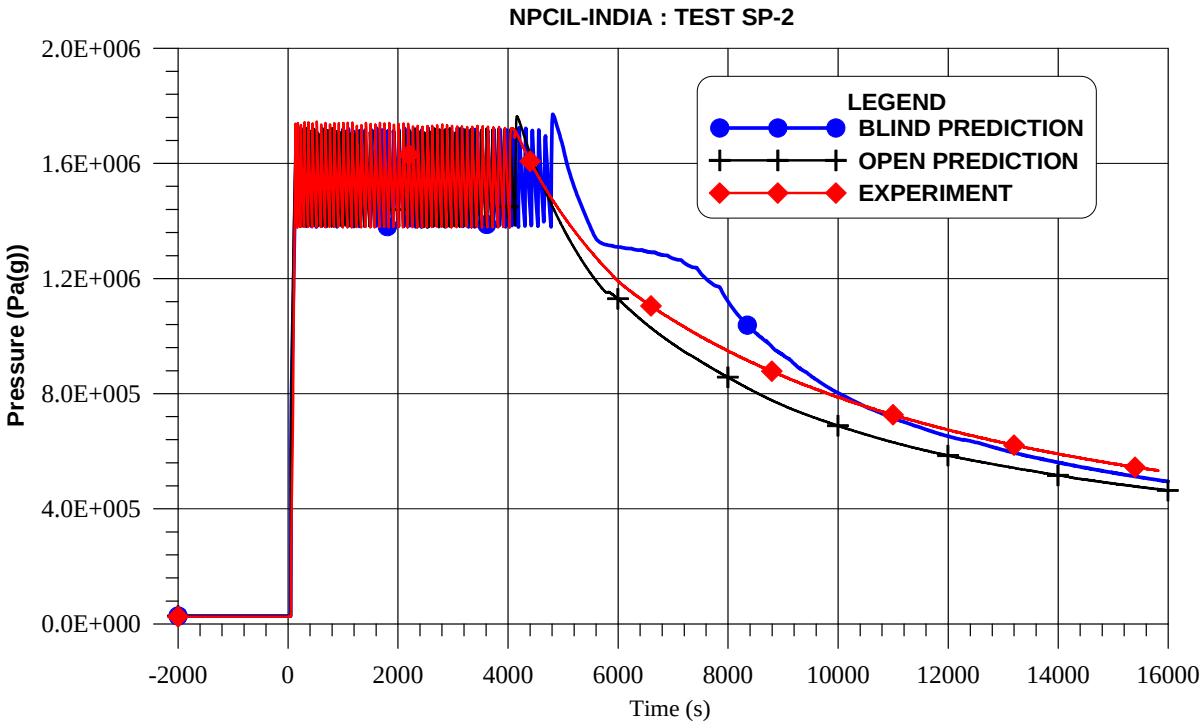

FIG. 4-227. High pressure containment pressure (PT-801).

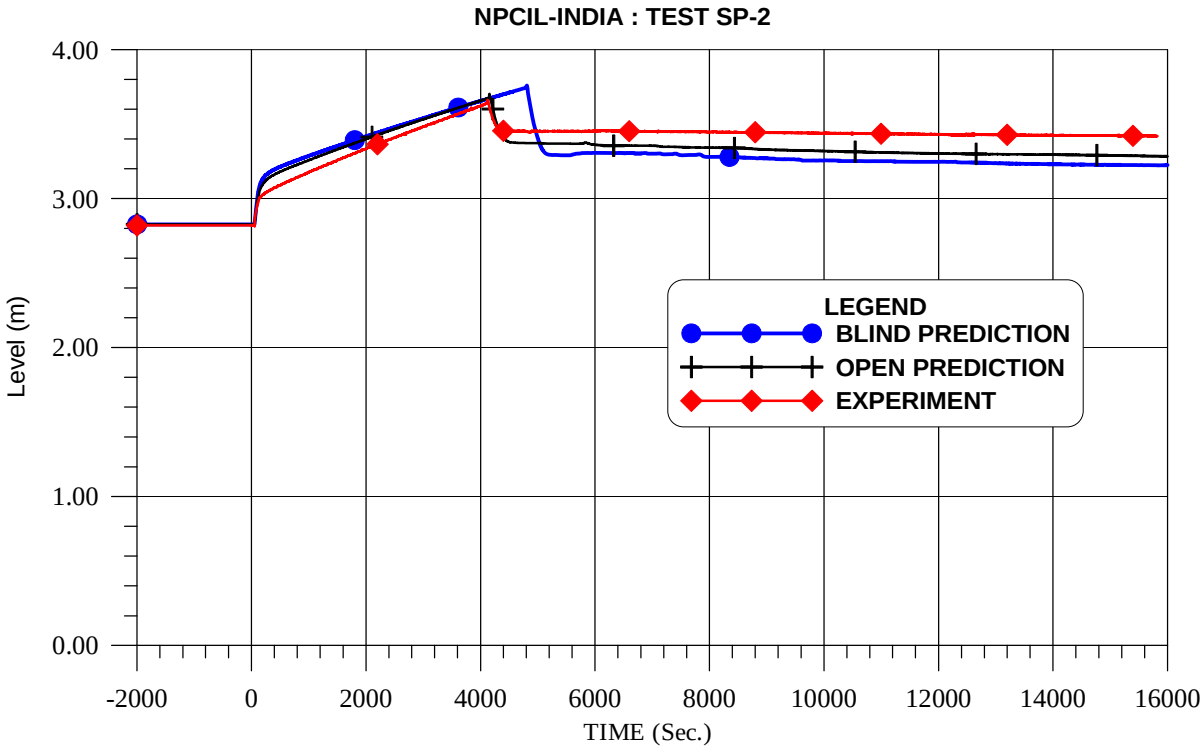

FIG. 4-228. Containment water level (LDP-801).

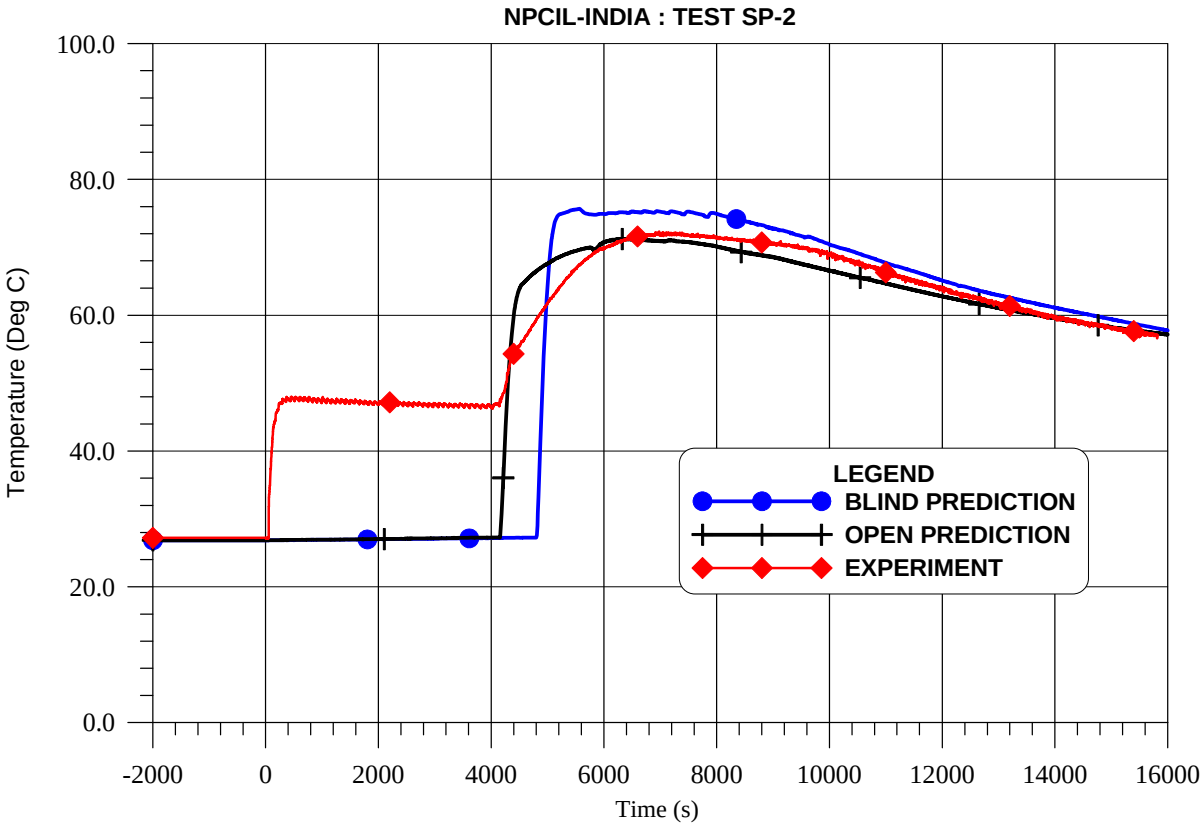

FIG. 4-229. Water temperature located inside the high pressure containment (TF-821).

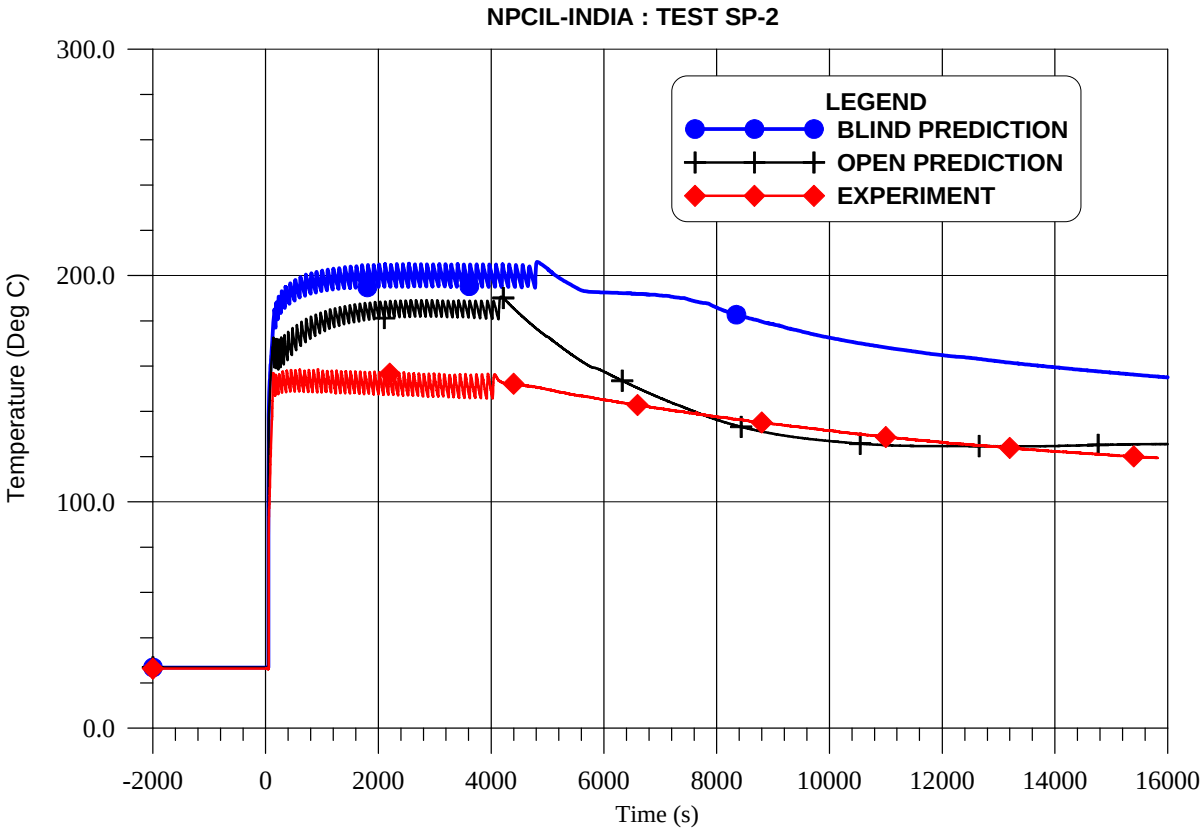

FIG. 4-230. Water temperature located inside the high pressure containment (TF-861).

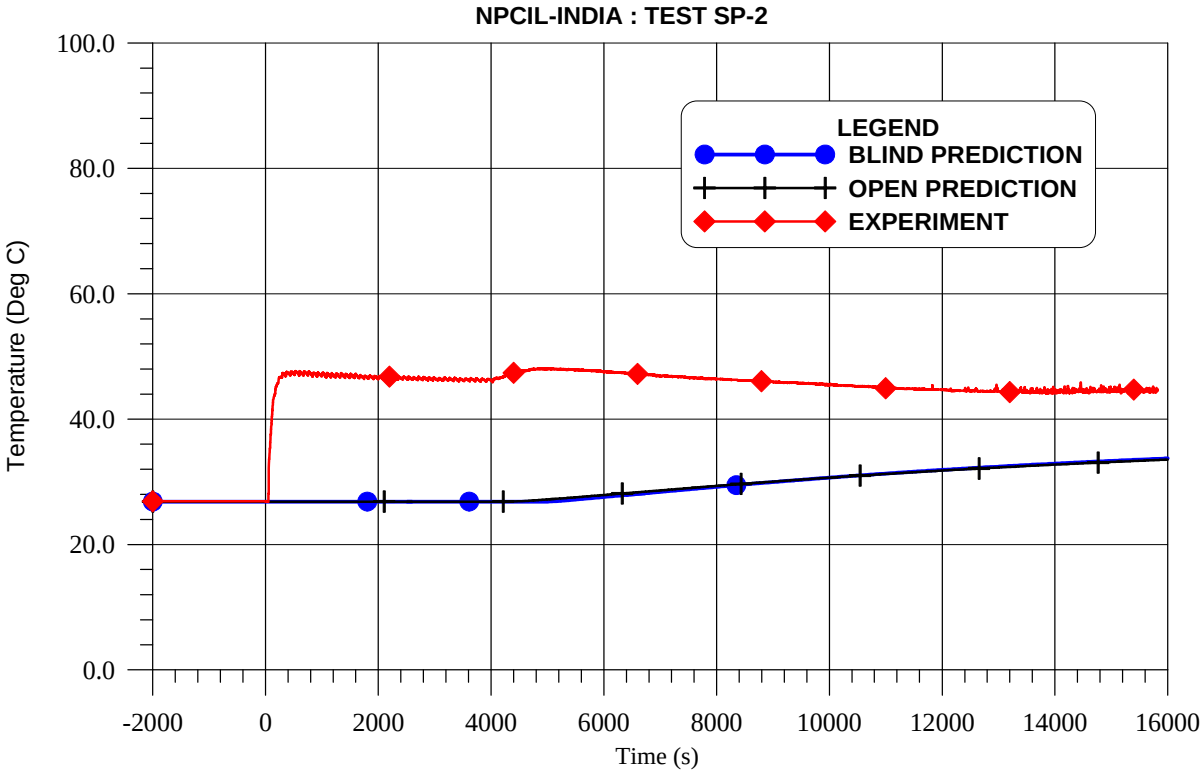

FIG. 4-231. Water temperature located inside the CPV near heat transfer plate (TF-825).

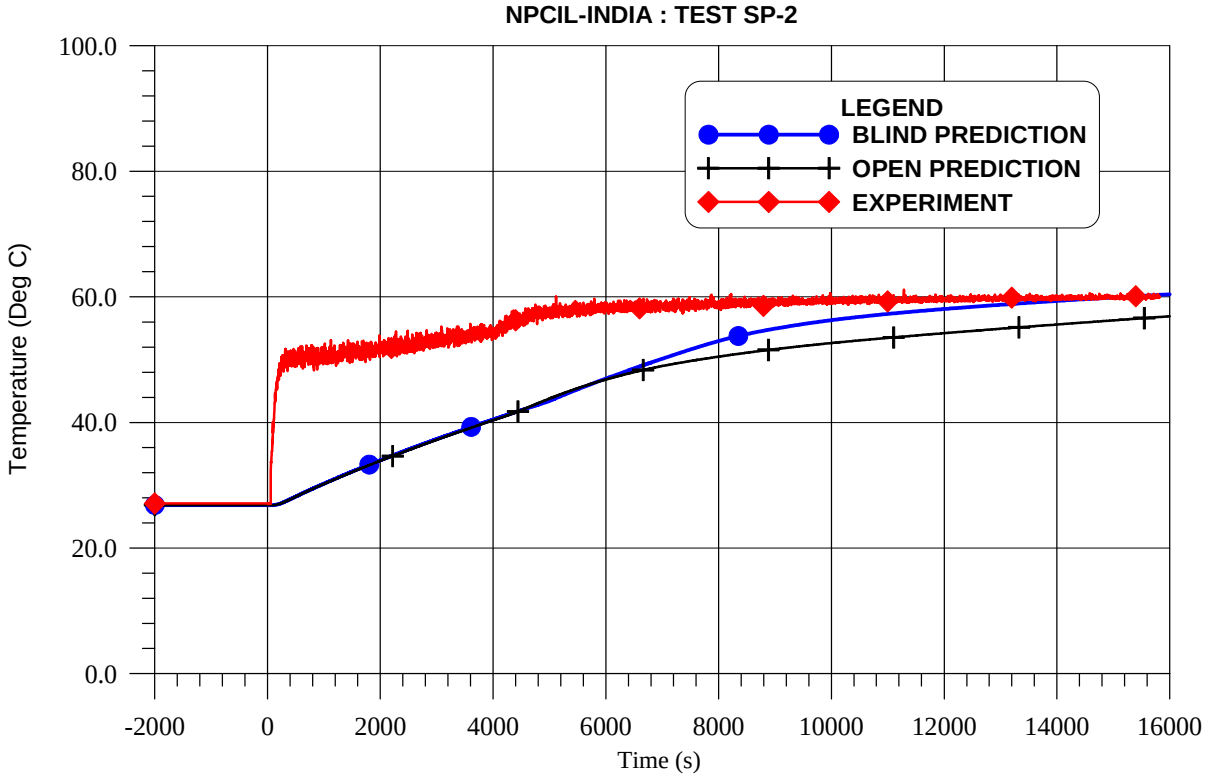

FIG. 4-232. Water temperature located inside the CPV near heat transfer plate (TF-845).

4.9.4. Analysis results for power manoeuvring

The purpose of this test is to investigate fluid flow rate through the primary loop in normal operating conditions at different power levels. This experiment is conducted at power level of 40 kW and after achieving the steady state, power has been increased stepwise (with step size of 40 kW) to 320 kW in various steps in period of around two hours. It has been observed from steady state experimental data that power in the core heaters is 40 kW whereas the actual power transferred to the primary fluid is only around 30 kW (based on energy balance). To overcome this mismatch, 35 kW power is considered in core heaters which is used as boundary condition in this analysis along with 5 kW heat losses from RPV to atmosphere for achieving the steady state as discussed in the 3rd meeting held at Republic of Korea. To achieve specified initial conditions, steady state run of 100,000 s is performed. The achieved initial conditions for open calculations are presented in Table 4-21 along-with the experimentally observed initial conditions and conditions predicted in the blind calculations.

4.9.4.1. RPV thermal-hydraulic behaviour

In the analysis, core heater power, SG coil feed water flow rate and temperature are taken as boundary condition. It is observed that pressure (Fig. 4-233) and temperature of pressurizer remain nearly same in the entire transient similar to experimental results. Similarly, the water level in RPV (Fig. 4-239) remains nearly at the steady state value throughout the transient. Water level in pressurizer shows slight changes due to change in temperature in RPV.

As seen from Figures 4-234 to 4-235, core inlet temperature and cold leg temperature remain same till 3000 s irrespective of increase in core power. At the same time, core outlet temperature increases with core power (Fig. 4-236). It is seen that heater temperature increases with increase in core power (Fig. 4-237). In the subsequent period from 3000 to 4000 s, core power remained constant but SG feed has increased as observed in experiment, resulting in reduction of temperatures at all locations in RPV. Subsequent to 3500 s, temperatures at all locations start rising slowly.

TABLE 4-21. STEADY-STATE COMPARISON FOR TEST SP-3

Parameter	MASLWR	Unit	Experiment	Steady-State Value	
				Blind Cal.	Open Cal.
Pressurizer pressure	PT-301	MPa(a)	8.718	8.716	8.716
Pressurizer level	LDP-301	m	0.3574	0.3585	0.3586
Power to core heater rods	KW-101/102	kW	42.1	40	35
Feed water temperature	TF-501	ºC	31.50	31.65	31.61
Steam temperature	FVM-602-T	ºC	256.4	263.9	261.43
Steam pressure	FVM-602-P	MPa(a)	1.446	1.465	1.465
Ambient air temperature		ºC		25	25
Primary flow at core outlet	FDP-131	kg/s	0.48	0.85	0.81
Primary coolant temperature at core inlet	TF- 121/122/ 123/124	ºC	250.3	255.1	253.29
Primary coolant temperature at core outlet	TF-106	ºC	262.8	264.6	261.86
Feed water flow	FMM-501	kg/s	0.01	0.013	0.0108
Steam flow	FVM-602-M	kg/s	-	0.013	0.0108
Total heat loss through primary system		kW		5.10	5.06
Heat transfer through SG		kW		36.53	31.65
Maximum surface temperature of core heater rods		ºC		278.8	274.86

It is seen that major part of differential pressures are due to elevation difference because velocities are small under natural circulation. Since elevation difference remains same, differential pressures are also almost same throughout the transient. Small deviations are due to change in velocity and change in temperature. To match sign of differential pressure with experimental values, differential pressures are calculated by subtracting upstream pressure from downstream pressure (Fig. 4-238). Large deviations are observed in experimental data as compared to code predictions (Fig. 4-238).

For prediction of primary loop flow, end loss coefficients have been fixed in the entire loop for test SP-2 results in well matching of RPV flow with experimental data at higher power levels. However, for lower power levels, code predicts higher RPV flow (Fig. 4-240). It may be due to the higher friction factors at lower Reynolds number in natural circulation mode. It is seen that core heater temperatures are well in agreement with experimental results. Primary water level is well predicted by the code (Fig. 4-239).

Analysis is terminated after a transient period of 6350 s in which core power is increased from 35 kW to 320 kW in various steps. It is observed that overall transient of key identified thermal hydraulic parameters such as RPV pressure, temperature at various location of RPV are well predicted by the code and mainly governed by rate of rise of core heater power and SG feed water flow rate.

4.9.4.2. SG thermal-hydraulic behaviour

Feed water pressure (PT-511) to the Steam generator remains at around 1.465 MPa(a). Feed water mass flow rate (FMM-501) to the Steam generator is used as boundary condition. It increases from 0.0108 kg/s to 0.1174 kg/s as the power is increased from 35 kW to 320 kW. Feed water temperature (TF-501) which is used as boundary condition falls from steady state value of 32 to ~ 20°C as the power rise from 35 kW to 320 kW. Main steam pressure remains constant at around 1.464 MPa(a) throughout the simulation, however average main steam temperature falls from 261.4°C to 206.3°C (Fig. 4-241) during the entire transient.

It is observed that during 2800 to 3200 s, power to the core heater remains constant at 200 kW whereas feed water supply to the steam generator is increased during above period results in lowering of steam temperature in the outlet of the steam generator (Fig. 4-241).

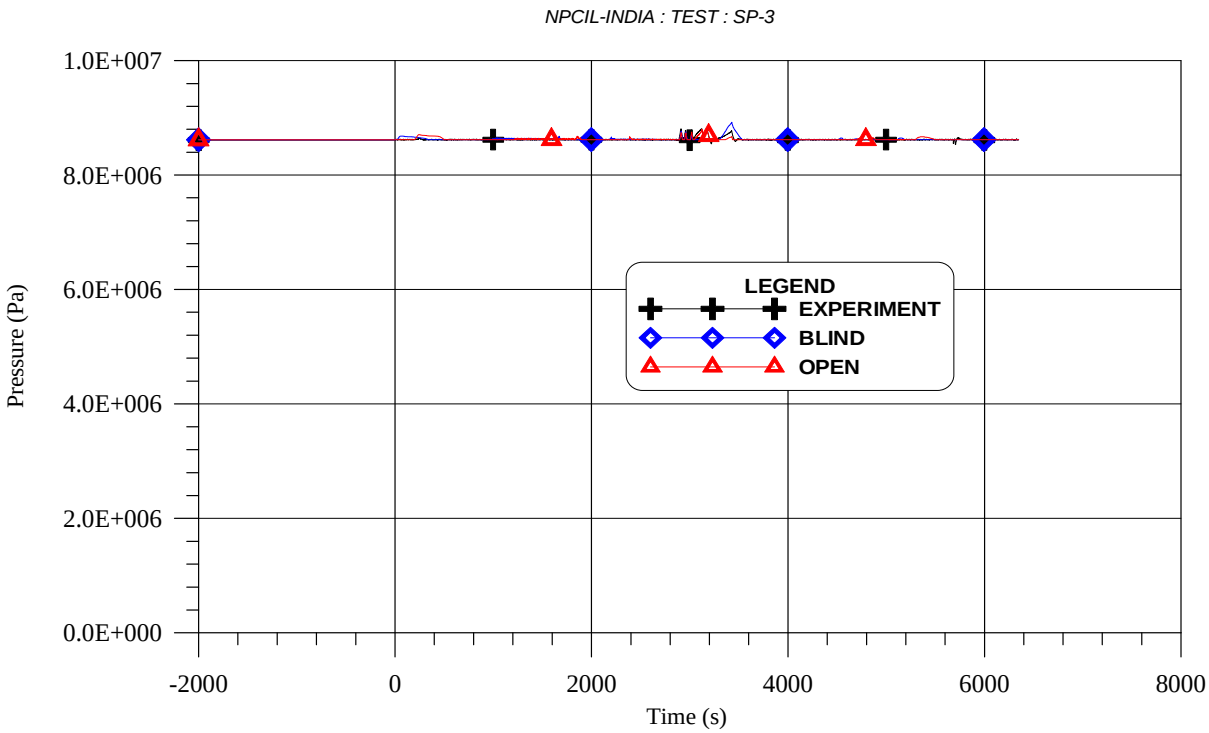

FIG. 4-233. Steam pressure in pressurizer (PT-301).

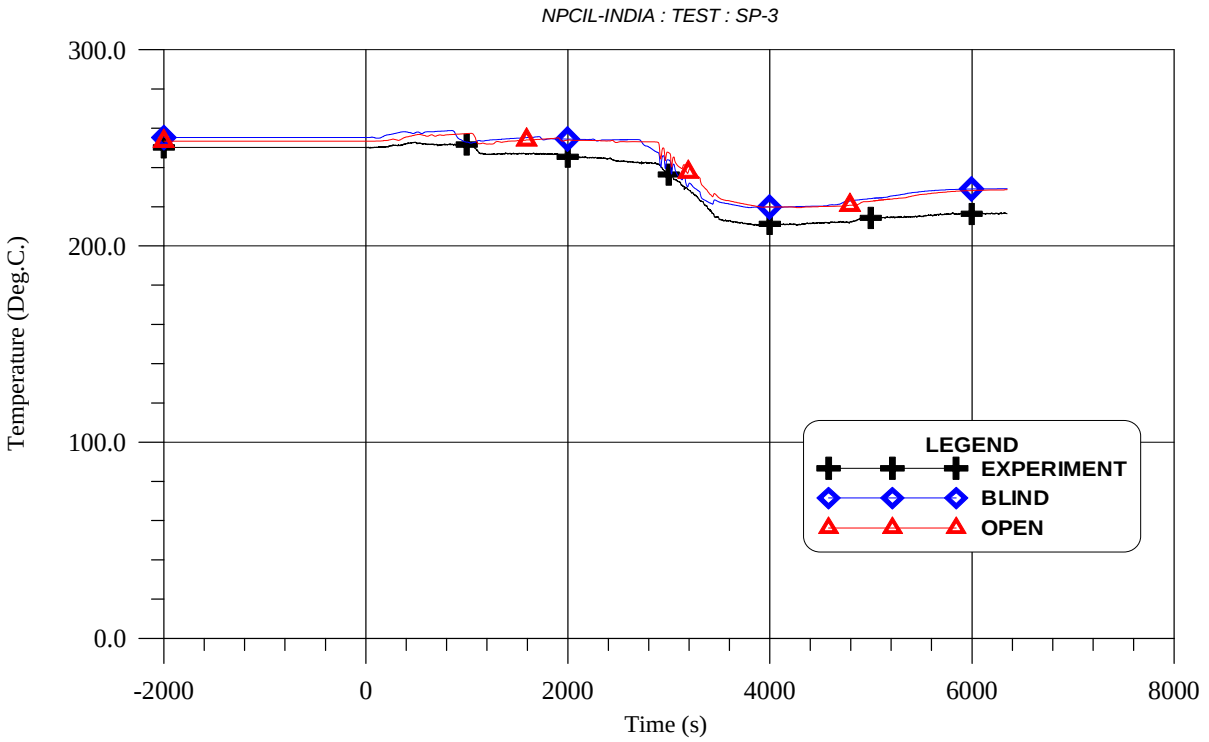

FIG. 4-234. Core inlet temperature (TF-121).

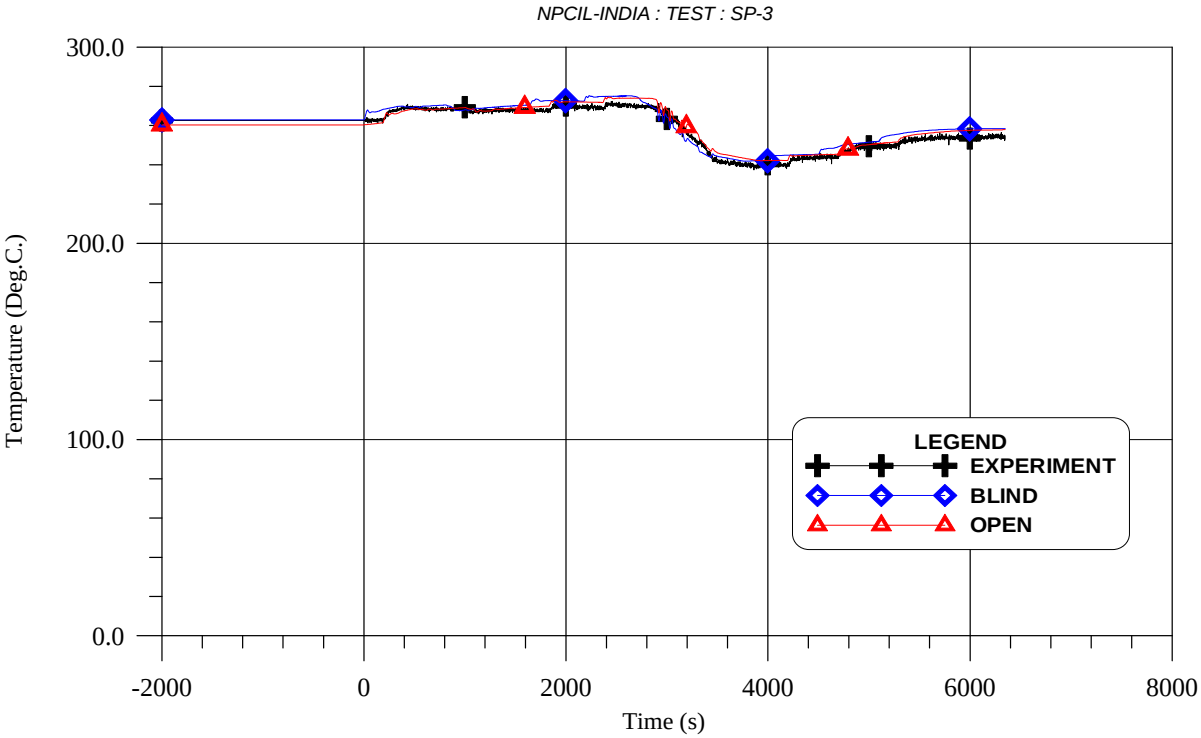

FIG. 4-235. Water temperature at centre of core (TF-106).

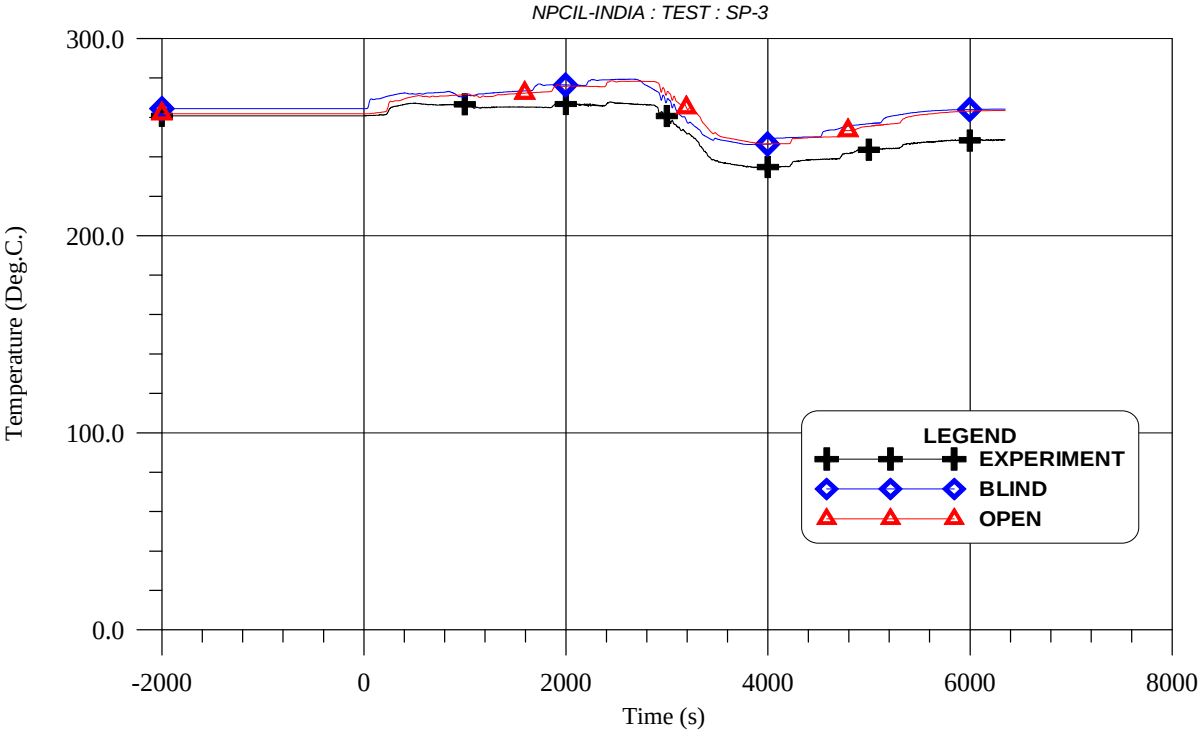

FIG. 4-236. Primary water temperature at top of chimney (TF-111).

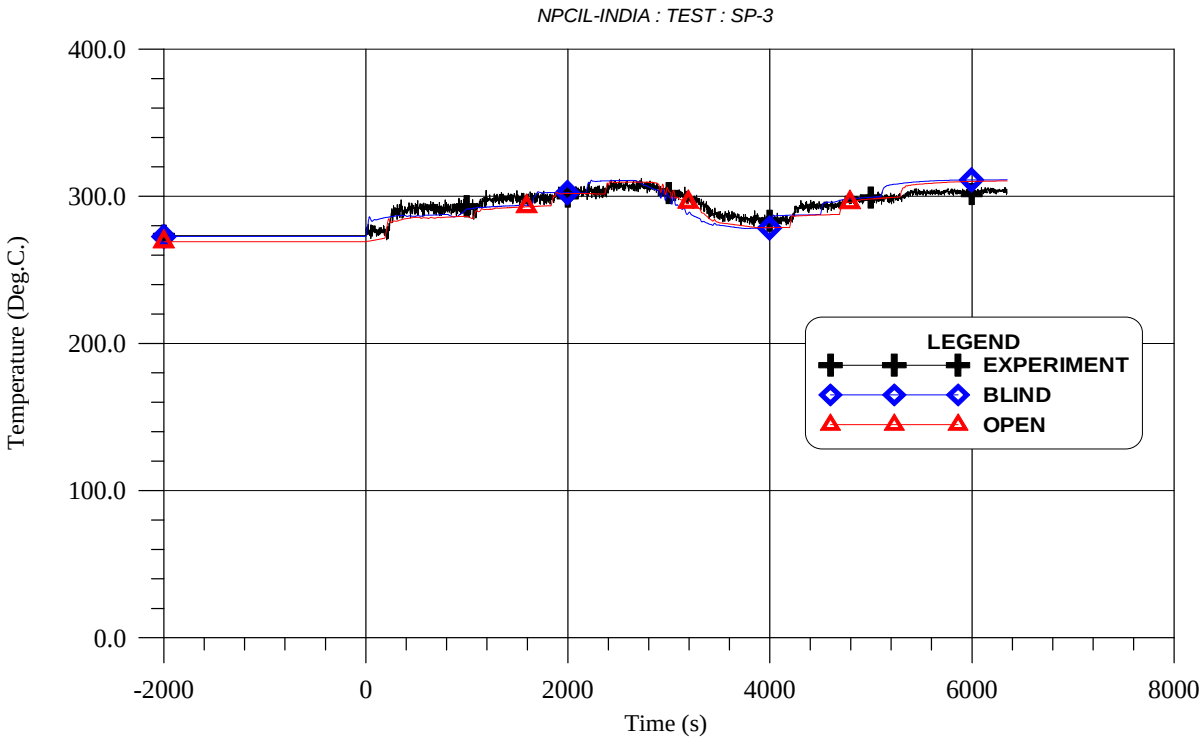

FIG. 4-237. Core heater rod temperature (TH-143).

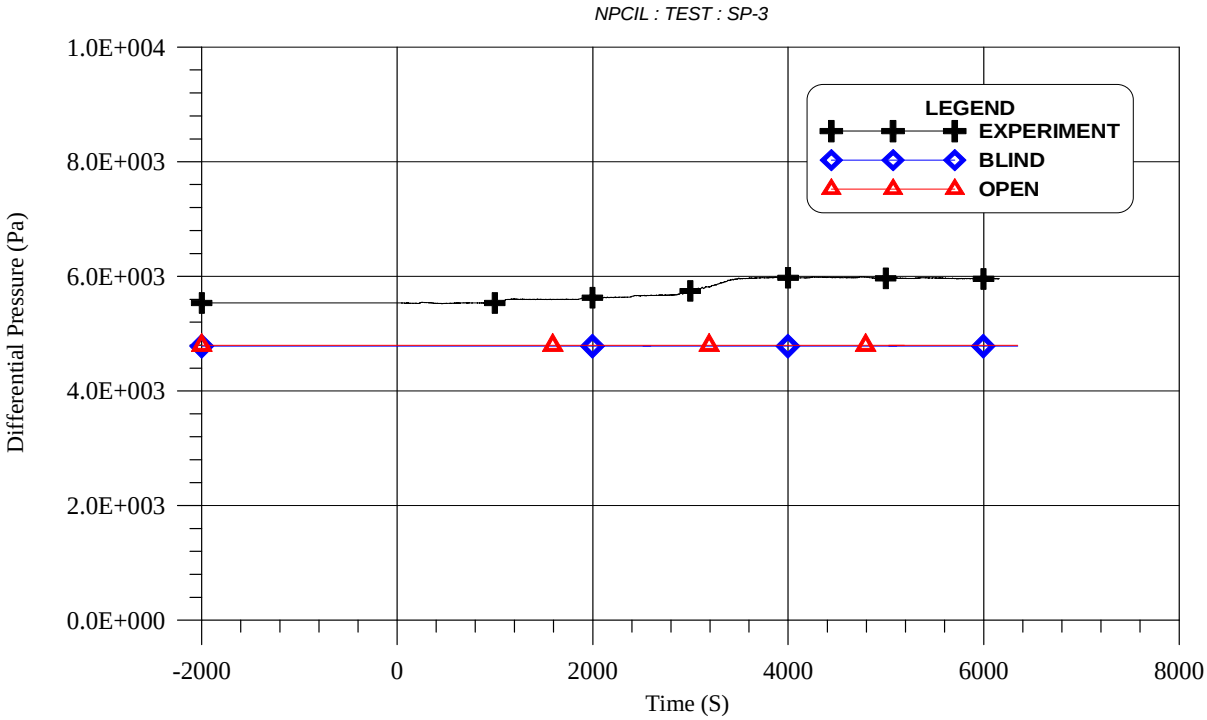

FIG. 4-238. Pressure loss in the core (DP-101).

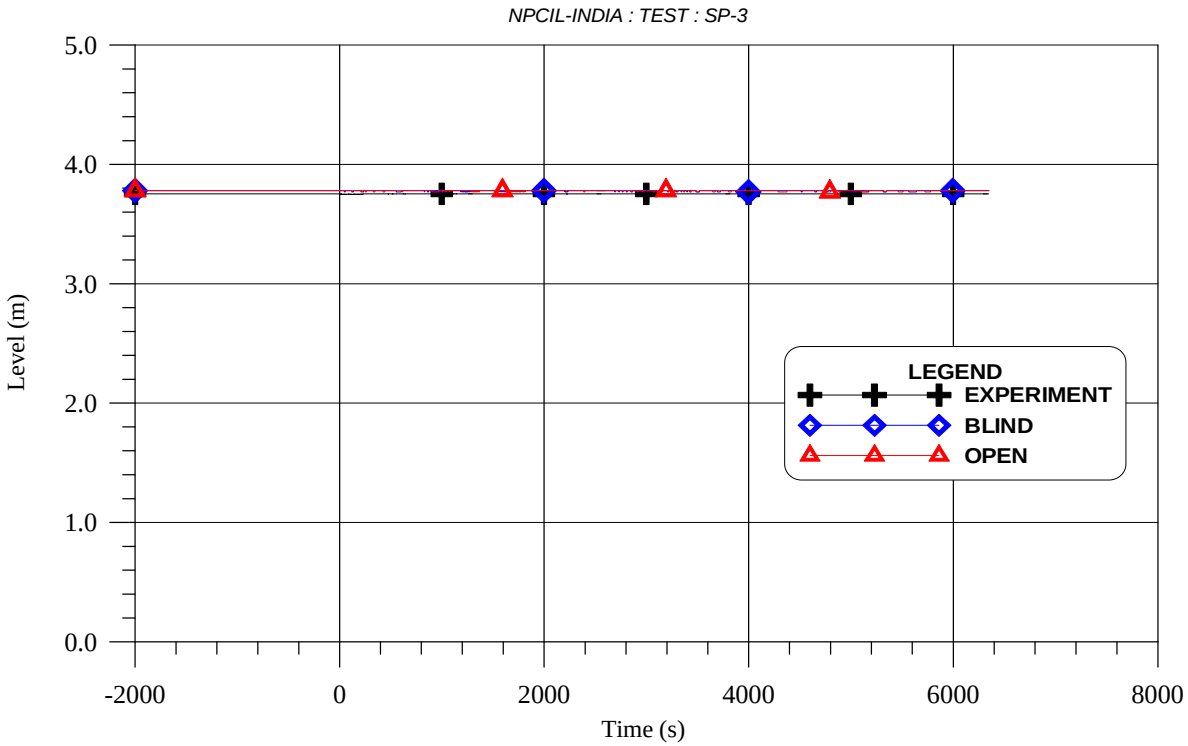

FIG. 4-239. Primary water level (LDP-106).

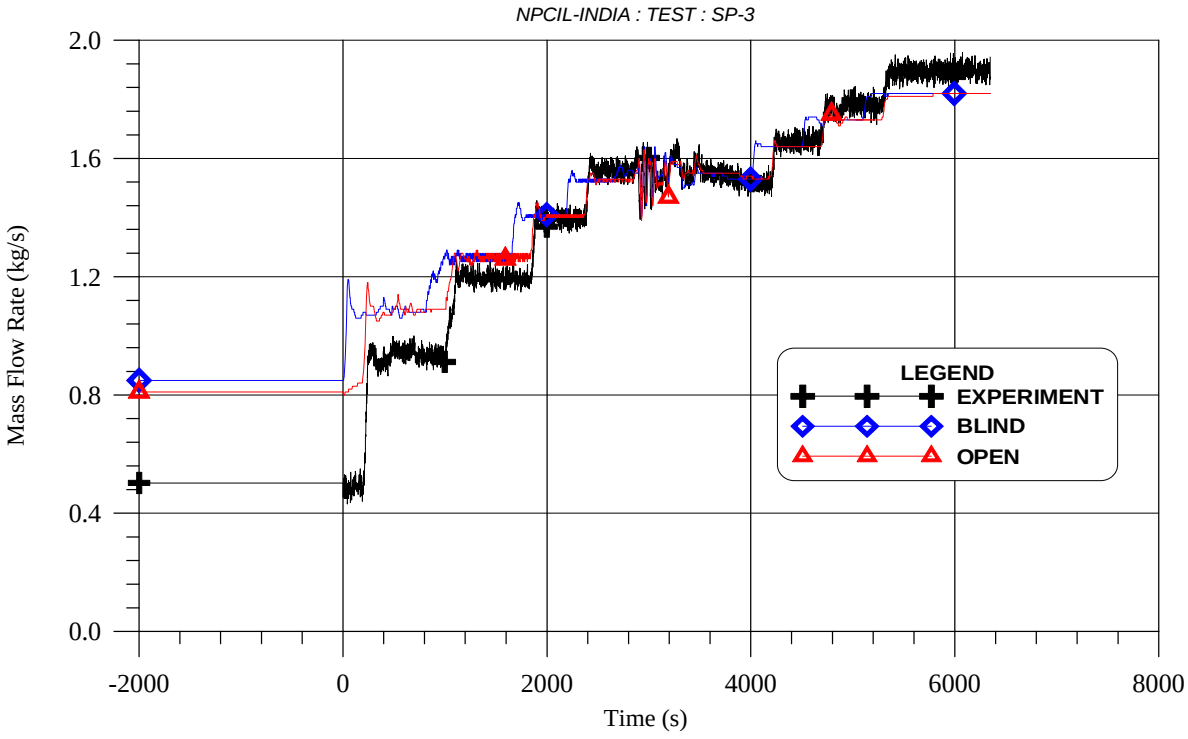

FIG. 4-240. Primary mass flow rate in chimney.

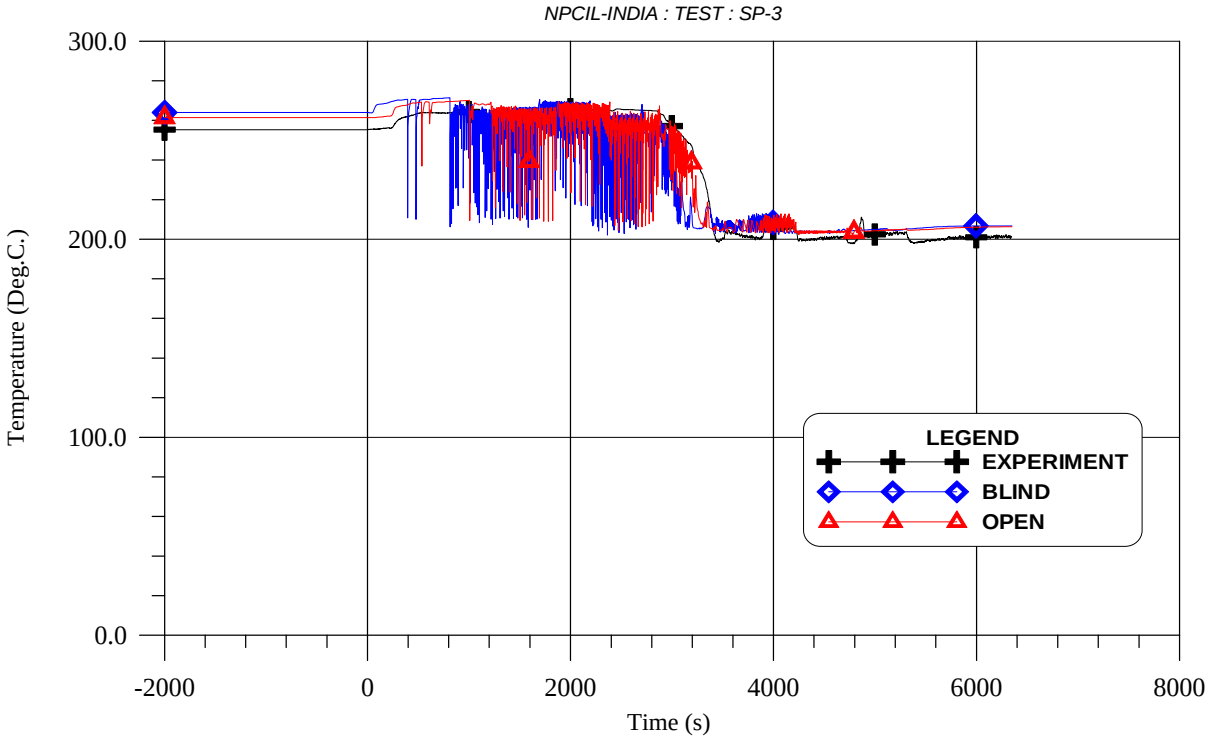

FIG. 4-241. Average Main steam temperature.

4.10. NRC – USA

4.10.1. Computer codes

In order to analyze the thermal hydraulic behaviour of LWR reactors, the USNRC has maintained four codes, the RAMONA, the RELAP5, the TRAC-B and the TRAC-P. In the last years the NRC is developing an advanced best estimate thermal hydraulic system code, by merging, among other things, the capability of the previous codes into a single code. This new code is called TRAC/RELAP Advanced Computational Engine or TRACE, and is a component-oriented code designed to perform best estimate analyses for LWR. In particular this code is developed to simulate operational transient, LOCA, other transient typical of the LWR and to model the thermal hydraulic phenomena taking place in the experimental facilities used to study the steady state and transient behaviour of reactor systems. TRACE is a finite volume, two fluid, code with 3D capability which gives user the possibility to model heat structures and control systems that interact with the component models. It can be run coupled with the 3D reactor kinetics code PARCS as well. TRACE can be used together with a user-friendly front end, Symbolic Nuclear Analysis Package (SNAP), able to support the user in the development and visualization of the model, to show a direct visualization of selected calculated data using the animation model capability, and accepts existing RELAP5 and TRAC-P input. The computational complexity of a generic TRACE model is only limited by the availability of the computer memory. The code is based on two fluid, two-phase field equations. This set of equations consists of the conservation laws of mass, momentum and energy for liquid and gas fields. The resulting equation set is coupled to additional equations for non-condensable gas, dissolved boron, control systems and reactor power. Relations for wall drag, interfacial drag, wall heat transfer, interfacial heat transfer, equation of state and static flow regime maps are used for the closure of the field equations. The interaction between the steam-liquid phases and the heat flow from solid structures is also considered. These interactions are in general dependent on flow topology and for this purpose a special flow regime dependent constitutive-equation package has been incorporated into the code. TRACE uses a pre-CHF flow regime, a stratified flow regime and a post-CHF flow regime. In order to study the thermal history of the structures the heat conduction equation is applied to different geometry. A 2D(r and z) treatment of conduction heat transfer is taken into account as well. A finite volume numerical method is used to solve the partial differential equations governing the two-phase

flow and heat transfer. By default, a multi-step time-differencing procedure that allows the material Courant-limit condition to be exceeded is used to solve the fluid-dynamics equations. Figure 4-242 shows the TRACE/SNAP environment architecture.

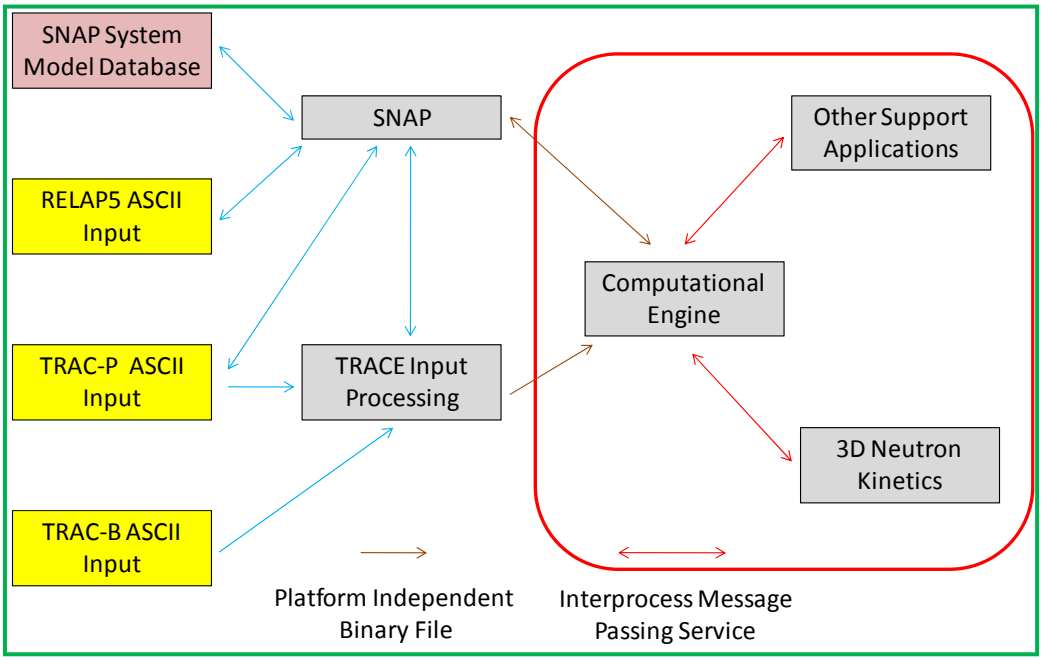

FIG. 4-242. TRACE/SNAP environment architecture.

TRACE version 5.0 Patch 3 was used in analyzing the standard problems. The graphical user interface tool used is SNAP version 2.2.1. Field equations, choked flow models are standard TRACE models and the helical coils were modeled with standard PIPE components. These models are explained in the TRACE user's manual in detail.

Specific model assumptions for SP-2;

- SV-800 was assumed to be open during steady state operation until the transient begins when the valve was closed. This is based on the noncondensible air pressure given in the boundary condition spreadsheet.
- The ambient temperature was given as heat loss boundary condition based on the ambient temperature data released in December 2011. Heat loss coefficient is assumed to be constant as 8 W/m^2-K to achieve total heat loss of 8.7 kW for reactor vessel.
- The valve rate for PCS-106A, B and PCS-108A, B is assumed to be 0.2 sec^{-1} based on the PCS-106A open/close timing results released by OSU.
- Decay power magnitude follows the spreadsheet value (the experiment curve).

Specific model assumptions for SP-3;

- Level control is achieved by a PI level controller through FILL 3 and 4 boundary components during steady state initialization. During power ramping, the level control is manual. Makeup flow boundary condition is provided by OSU to be used in the model boundary condition.
- The core heater power and feedwater flow/temperature released are given as boundary condition for the simulation.
- The ambient temperature was given as heat loss boundary condition based on the ambient temperature data released in December 2011. Heat loss coefficient is assumed to be constant as 8 W/m^2-K as in ICSP2.
- Steady state operation was run for 6000 section to ensure the exit steam temperature is steady and close to the boundary condition released in the spreadsheet. All major parameters in primary system are steady.

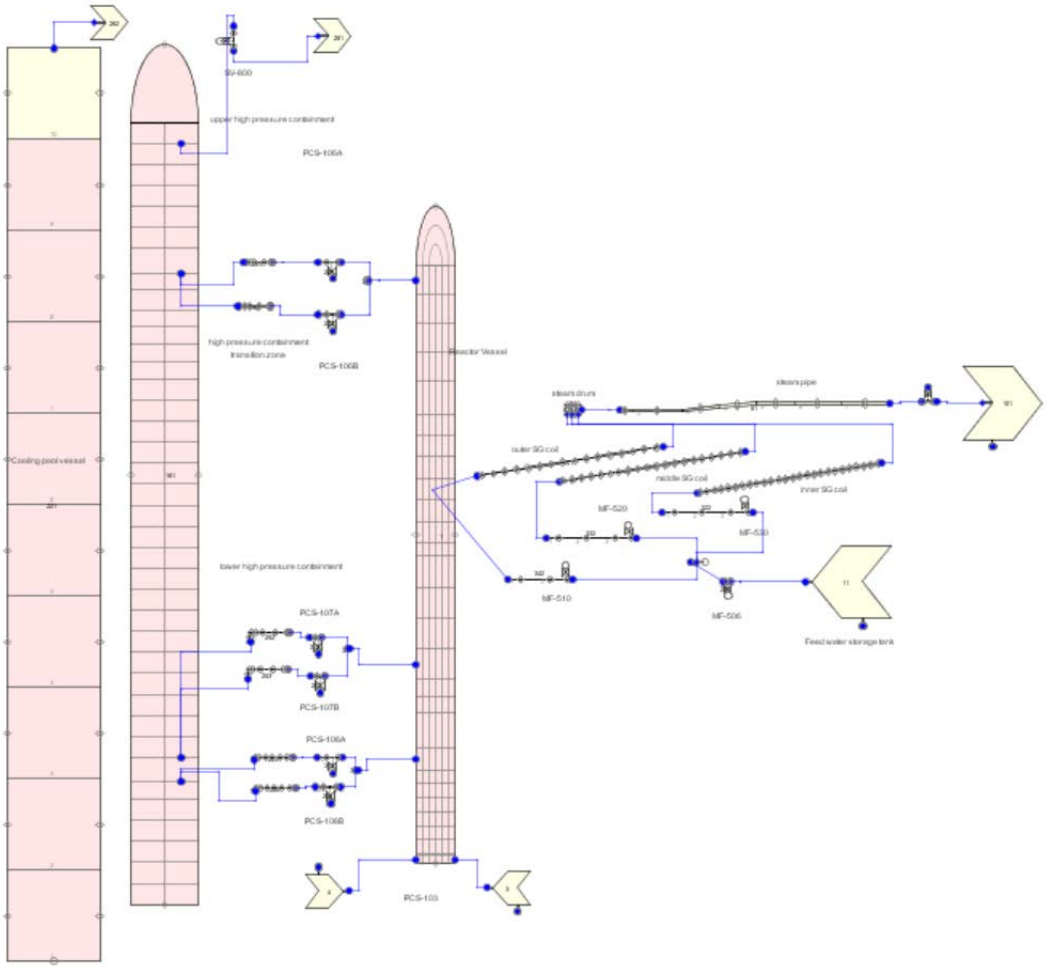

FIG. 4-243. TRACE MASLWR nodalization for blind/open calculation.

4.10.2. System idealization

4.10.2.1. System idealization for blind/open calculation

Figure 4-243 shows TRACE MASLWR nodalization for blind/open calculation.

4.10.2.2. Modelling change for open calculation

Model for open calculation is the same as blind prediction except the core channel baffle flow area and helical tube steam generator heat transfer coefficients;

- The core flow area was changed to reflect the core baffle area. The core plate was laid against the core baffle area. Based on the picture in the specification document, the zig-zag shape baffle area should be accounted for area deduction. After deduction, the core flow area is close to the area listed in the Table 2.3 of MASLWR specification document.
- The initial core average steady state temperatures were much higher than data in blind prediction. Assuming correct geometry, the only way to reduce the core average temperature is to increase heat transfer between the primary and secondary side. 20% of the heat transfer coefficients on the inner and outer surfaces of helical tubes were increased to improve the heat transfer.
- Changed the number of nodes in mid coil (PIPE 51) of steam generator from 40 to 20. Modified the heat structure coupling to the hydraulic nodes in order to damp out the oscillation during steady state calculation. The outer shell side hydraulic conditions of the heat structure reflect the vessel radial ring 3 conditions instead of alternating between ring 2 and 3.

The initial temperature for cooling pool vessel, high pressure containment and reactor vessel were adjusted to be closer to the experimental data.

4.10.3. Analysis results for loss of feed-water transient

Table 4-22 shows the steady state conditions for SP-2 from experiment, blind and open predictions. In the following figures and tables, pressure unit Pa, MPa represent SI unit absolute pressures and Pa(g), MPa(g) represent SI unit gauge pressures.

Table 4-23 shows the time sequence of events from experiment, blind and open calculations.

TABLE 4-22. STEADY-STATE COMPARISON FOR TEST SP-2

Parameter	MASLWR	Unit	Experimental Value	Steady-State Value (Blind Prediction)	Steady-State Value (Open Calculation)
Pressurizer pressure	PT-301	MPa(a)	8.720	8.7195	8.7195
Pressurizer level	LDP-301	m	0.3607	0.3610	0.3632
Power to core heater rods	KW-101/102	kW	149.46/147.87	299/2	299/2
Feedwater temperature	TF-501	ºC	21.40	21.35	21.35
Steam temperature	FVM-602-T	ºC	205.38	204.50	198.18
Steam temperature	Avg. of TF-611 to TF-634	ºC	203.1	215.5	199.61
Steam pressure	FVM-602-P	MPa(a)	1.411	1.481	1.480
Ambient air temperature		ºC	25.0	25.0	25.0
HPC pressure	PT-801	MPa(a)	0.12685	0.12684	0.12684
HPC water temperature	TF-811	ºC	26.72	20.45	26.46
HPC water level	LDP-801	m	2.82	2.85	2.85
Primary flow at core outlet	FDP-131	kg/s	N/A	1.6111	1.5590
Primary coolant temperature at core inlet	TF-121/122/123/124	ºC	215.34/214.82 214.42/215.11	230.98/230.98 229.61/229.61	222.02/222.02 221.01/221.01
Primary coolant temperature at core outlet	TF-106	ºC	251.52	267.60	260.53
Feedwater flow	FMM-501	kg/s	0.106	0.11135	0.11134
Steam flow	FVM-602-M	kg/s	N/A	0.110117	0.11126
Primary coolant subcooling at core outlet	N/A	ºC	N/A	33.5	38.91
Total heat loss through primary system	N/A	kW	N/A	8.753	8.144
Heat transfer through SG	N/A	kW	N/A	299.0	299.79
Maximum surface temperature of core heater rods	N/A	ºC	N/A	303.24	302.73
Location from the SG secondary inlet to reach - saturation - superheat	N/A	m	N/A	(mid-coil) from SG inlet 1.7835 m to saturation 3.3056 m to superheat	(mid-coil) from SG inlet 1.847 m to saturation 5.842 m to superheat
CPV water level	LDP-901	m	6.35	6.35	6.35
CPV water temperature	TF-815	ºC	25.95	20.0	26.37

TABLE 4-23. ICSP-2 TIME SEQUENCE OF EVENTS

Event	Time (s) MASLWR	Time (s) Blind Calculation	Time (s) Open Calculation
Start of simulation – steady state (start of data collection)	0.	0.	0.
Stop MFP Close HPC vent valve SV-800	0.	0.	0.
PZR pressure (PT-301) reaches 9.064 MPa(abs) (1300 psig) Enter decay power mode	43.0	37.1	39.28
PZR pressure (PT-301) reaches 9.409 MPa(a) (1350 psig) De-energize PZR heaters Open ADS vent valve (PCS-106A)	N/A 48.0 48.0	N/A 55.1 55.1	N/A 57.28 57.28
Record opening and closing times for PCS-106A	See released initial condition spreadsheet	See released initial condition spreadsheet	See released initial condition spreadsheet
Record opening and closing times for SV-800	Stays closed	Stays closed	Stays closed
Start long-term cooling when pressure difference between primary system and HPC (PT-301 minus PT-801) becomes less than 5 psi (0.034 MPa) - Open and remain open of PCS-106A/B - Open and remain open of PCS-108A/B	4051.9 for pressure equalization 4024.0 s for PCS 106A 4114-7 s for PCS 106B, 108A/B	4717.5 for pressure equalization 4695.5 for PCS 106A 4801.5 for PCS 106B, 108A/B	3983.9 for pressure equalization 3949.6 for PCS 106A 4051.7 for PCS 106B, 108A/B
End of test when one of the following conditions is reached: - PZR pressure ≤ 0.135 MPa(a) (5 psig) - Primary coolant temperature (TF-132) ≤ 35 ºC (95 ºF) - 24 hours have elapsed	15660 sec (4hr 21 min)	15000 sec (4.16 hr) simulation ends and the PZR pressure reaches 36 psig and primary coolant temperature TF-132 reaches 137.8 C	15000 sec (4.16 hr) simulation ends and the PZR pressure reaches 35.8 psig and primary coolant temperature TF-132 reaches 137.9 C

4.10.3.1. RPV thermal-hydraulic behaviours

At 0 s problem time, feedwater flow was turned off. The steam flow decreased accordingly and helical coils liquid inventory boiled off within a couple of hundred seconds. Figure 4-258 showed the steam and feedwater flow conditions of this transient.

In Figure 4-244, RPV and HPC pressures were shown. According to Table 4-23 experimental data, when pressure reached the set point at 43 s, RPV entered decay heat mode. After ADS vent valve (PCS-106A) opened at 48 s, the HPC pressure rose. At 4052 s, pressures of RPV and HPC equalized. Before equalization, RPV pressure decreased in a zigzag manner due to the open/close behavior of PCS-106A. After equalization, HPC pressure was slightly higher than RPV pressure and the reverse flows through PCS-108A, B took place. In blind prediction, the RPV entered decay heat mode at 38 s and PCS-106A opened at 56.0 s. The timing for pressure equalization was around 4715.5 s. Open prediction gave close initial timings – 39 s to enter decay heat mode and 57 s for PCS-106A opening. And the pressure equalization was improved to 3984 s. The increased heat transfer in open calculation sped up the pressure equalization. Both calculations showed same physical trends in pressure behaviors.

According to TRACE predictions in Figure 4-245, the heat transfer to the secondary side decreased significantly after feedwater was shut off. The helical coil liquid boil-off reduced the heat transfer. PZR heater power soon became zero due to the drop of RPV level below heater position (0.202m). In the calculations decay heat power from experiment was used as boundary condition. Open calculation results were similar to the blind prediction.

From experimental data in Figure 4-246, the reactor vessel level LDP-106 dropped below the baffle plate after 900 s and dropped below top of the riser at around 2100 s. Blind prediction gives faster and

stronger level drop (700 s below the baffle plate and 1600 s below top of the riser). During the transient, the RPV level remained above the top of core. According to blind predictions in Figure 4-247, the core flow became zero averagely when the level dropped below top of riser at around 2000 s. The core flow oscillated the entire period until the RPV and HPC pressures equalized around 4700 s. After the equalization, the two sector core flows demonstrated a circular pattern within core. Open prediction produces better timing result compared to the blind prediction.

The differential pressures across SG coil (DP-105) and cores (DP-101) were shown in Figure 4-248. Experimental pressure drops were higher than both predictions in general. The DP-101 data stopped oscillation at the pressure equalization point when the ADS vent valves closed, which affected the natural circulation and associated pressure drop. TRACE results were close to the data. DP-105 experimental data shows unreasonably flat response in significant portion of the period. It should be explored more to verify the accuracy. TRACE open calculation showed improved timing of the equalization point.

Core outlet (TF-105) and inlet temperatures (TF121-4) were shown in Figure 4-249. Both temperatures in experimental data dropped after pressure equalization point when recirculation flow (from HPC into RPV) started. The calculations showed higher initial temperatures for core inlet and outlet but the overall trends were similar. The higher core inlet and outlet temperature obtained in blind prediction implied underestimated heat transfer coefficient. The temperatures were improved in the open calculation by increasing heat transfer coefficients in steam generator. In open calculation the inlet temperature drop at the pressure equalization point was also improved in timing and magnitude. In both blind prediction and open calculation, the riser and core showed small amount of void in the transient, shown in Figure 4-250.

In Figure 4-251, according to data, the HPC level (LDP 801) rose when the RPV (LDP 106) level dropped in the first part of the transient - before the pressure equalization point. After pressure equalization, HPC maintained a slightly higher level for the recirculation flow through PCS-108A and B. Experimental data showed faster rise and fall of HPC level but slower drop of RPV level compared to the calculations. The timing in blind prediction was about 700 s off the data but the trends were the same. In open calculation, the timing deviation was significantly improved. The CPV level (LDP 901) does not change significantly in the transient.

Based on TRACE predictions, Figure 4-252 showed the vent flows through PCS-106A and B. Before RPV and HPC pressure equalized, the main depressurization mechanism was through PCS-106A. The flow magnitude decreased gradually due to the equalization of pressure. The oscillatory behavior was due to the cycling of PCS-106A. PCS-106B opened according to the set point in operating procedure, which was very close to the equalization point. Figure 4-253 shows the recirculation flow took place after equalization point. The safety valve (SV-800) did not open throughout the transient. Figure 4-254 shows the accumulative flow through all the ADS valves. PCS-106A was the main valve to relieve RPV pressure before the equalization point. The main performance difference between the blind prediction and the open calculation is the shift of pressure equalization timing.

In Figure 4-255, the core heater rods surface temperatures dropped after the core entered decay heat mode. From the plot, the experimental data started with higher values. The TH144 data is abnormally high. The scattering of measured temperatures in experiment is larger. The temperature curves changed slope around the pressure equalization point. The change of slope occurred at the pressure equalization point, which was about 4700 s for blind prediction and about 4000 s for open prediction. Surface temperatures dropped more after the equalization point because colder flow entered the core.

Cold leg (TF131-4) and core inlet (TF121-4) temperature differences are shown in Figure 4-256. The difference between these two temperatures represents the bypass heat transfer from core and hot leg to cold leg and downcomer. Before the pressure equalization point, the temperature difference was close between cold leg and core inlet. After the equalization point, colder water entered RPV core, the cold leg temperature after SG helical coils (TF131-4) became much higher than the core inlet (TF-121-4). The natural circulation path was terminated and the core inlet was cooled by the recirculation flow from HPC. The temperature rise between blind prediction and the experiment are close but the timing is off due to the opening times of recirculation valves. In open calculation, the timing has improved but the temperature rise is lower.

According to the data provided for PCS-106A opening times, the initial opening is at 48 s and the last reopening time was 4024 s. From Table 4-23, in blind prediction, TRACE predicted initial opening time of 56 s and the last reopening at 4696 s. TRACE showed longer depressurization for the transient in blind prediction due to higher initial energy in the pressure vessel. The core fluid temperatures were shown in Figure 4-249. In the open calculation, the depressurization period is much closer to the experiment.

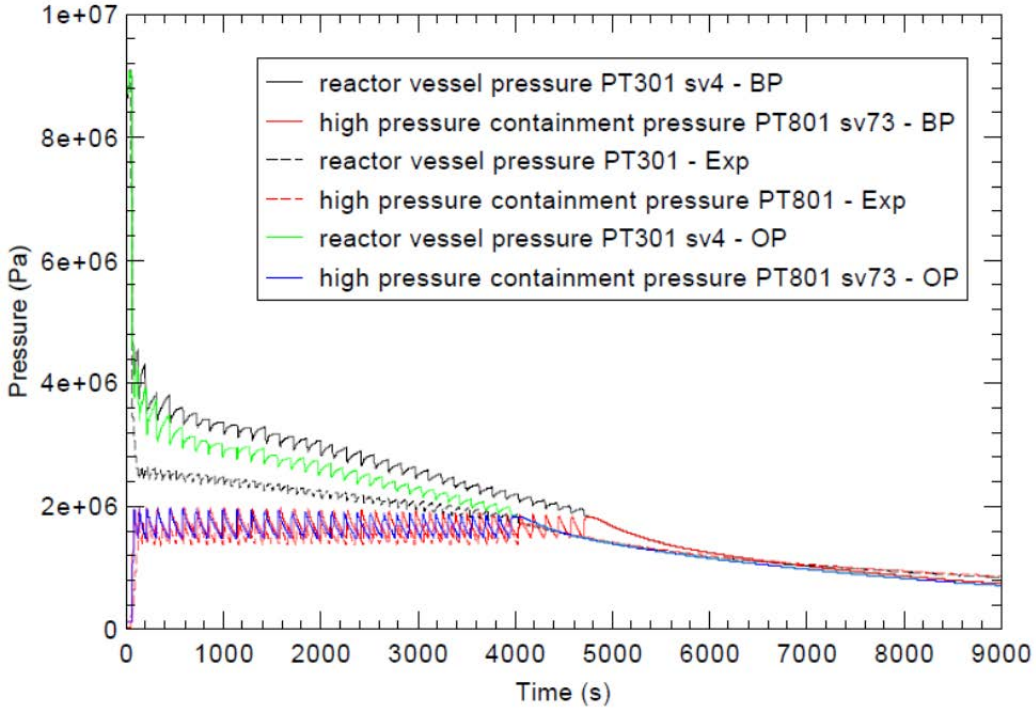

FIG. 4-244. Reactor vessel and high pressure containment pressure.

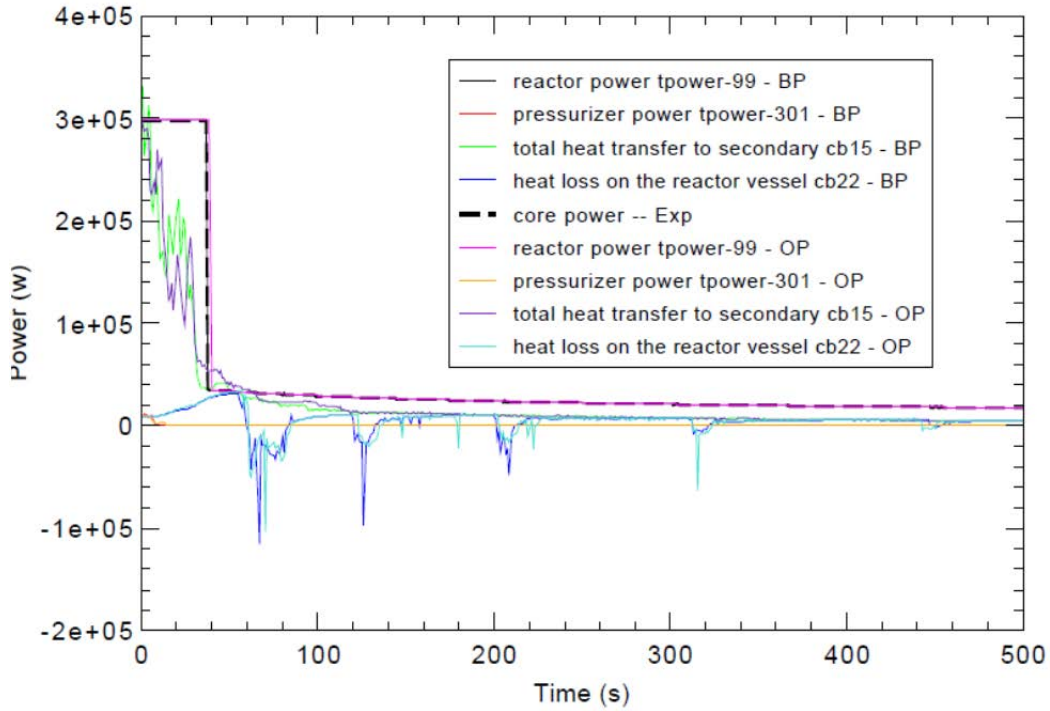

FIG. 4-245. Energy distribution.

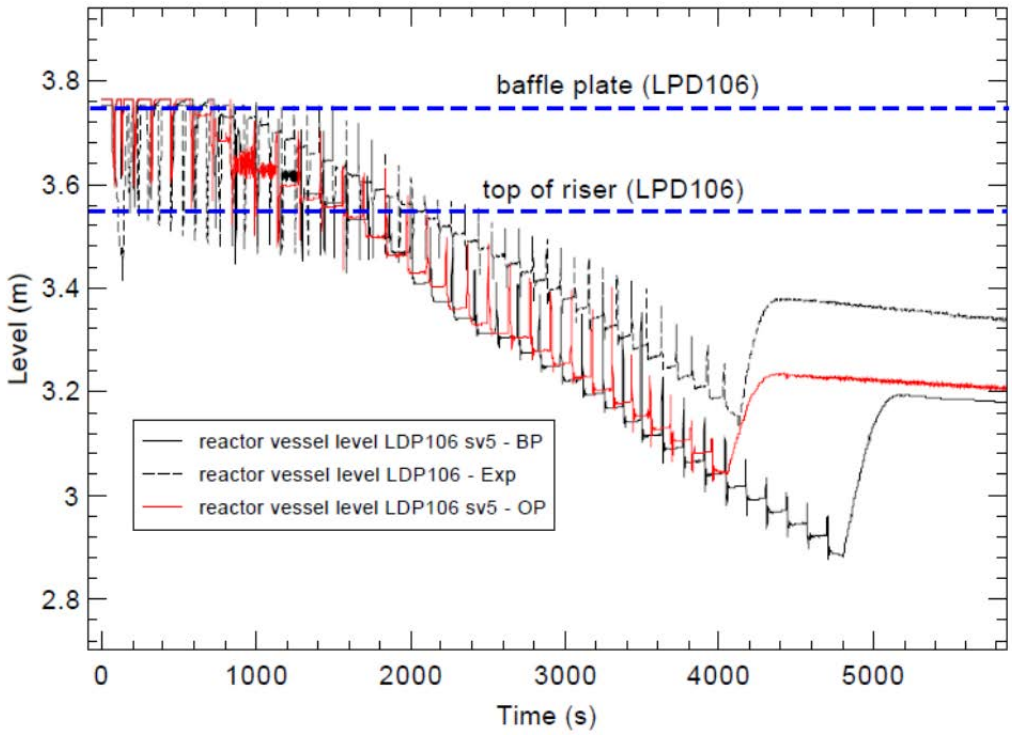

FIG. 4-246. Reactor vessel water level.

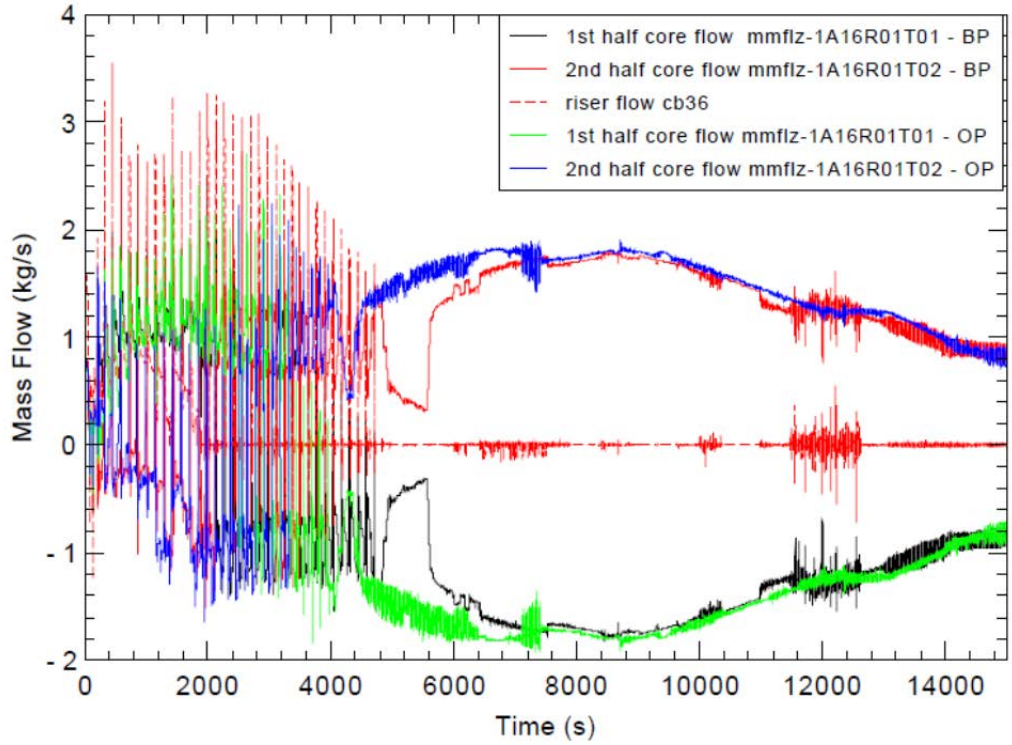

FIG. 4-247. Core flow.

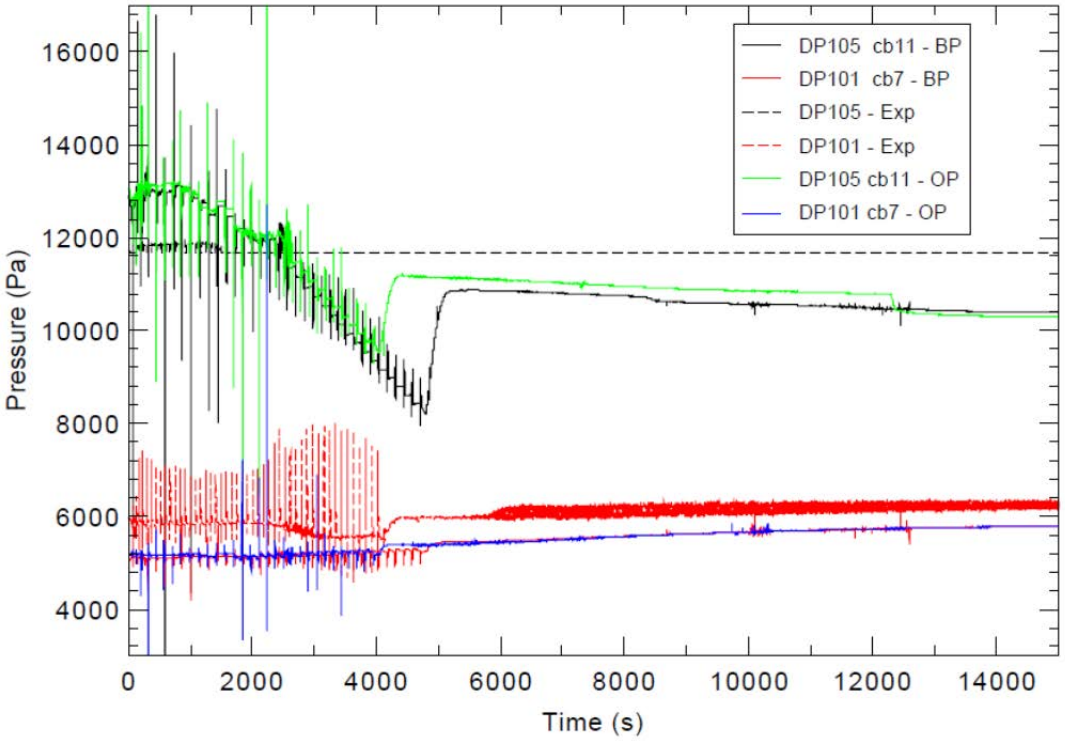

FIG. 4-248. Pressure drop across core and SG.

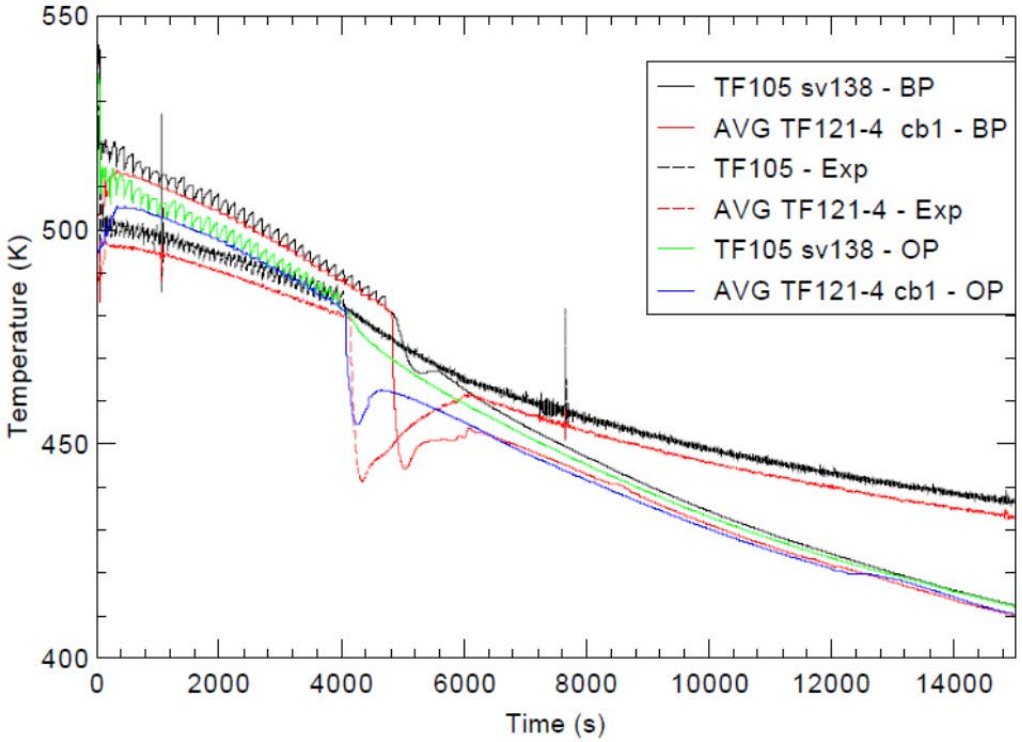

FIG. 4-249. Core inlet and outlet temperature.

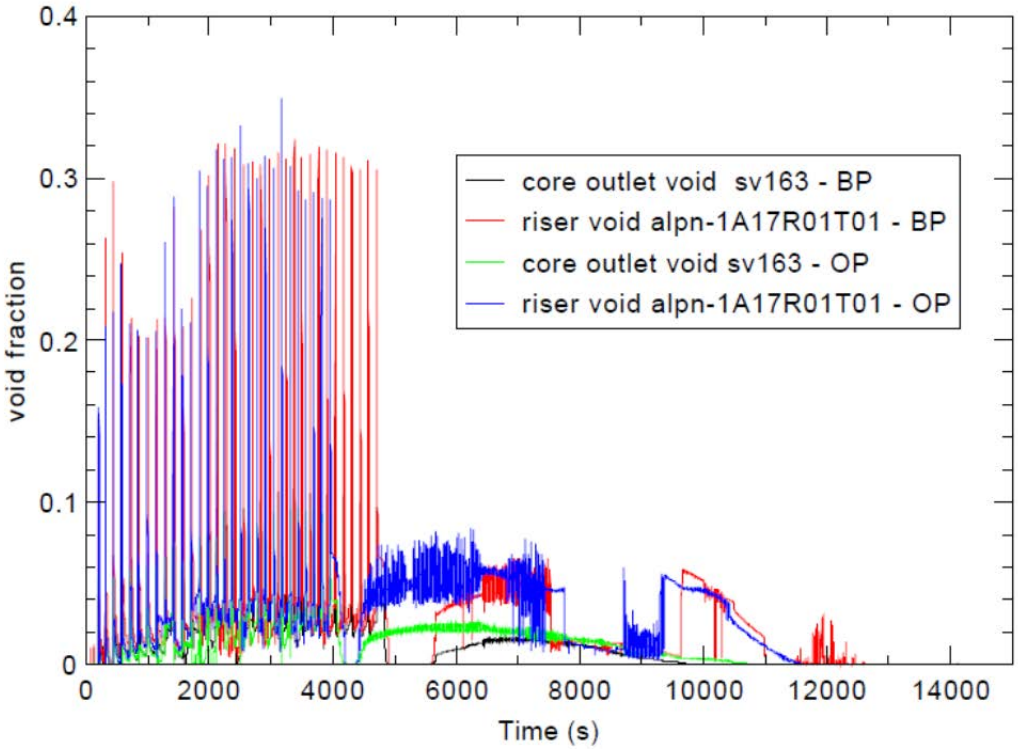

FIG. 4-250. Core outlet and riser void distribution.

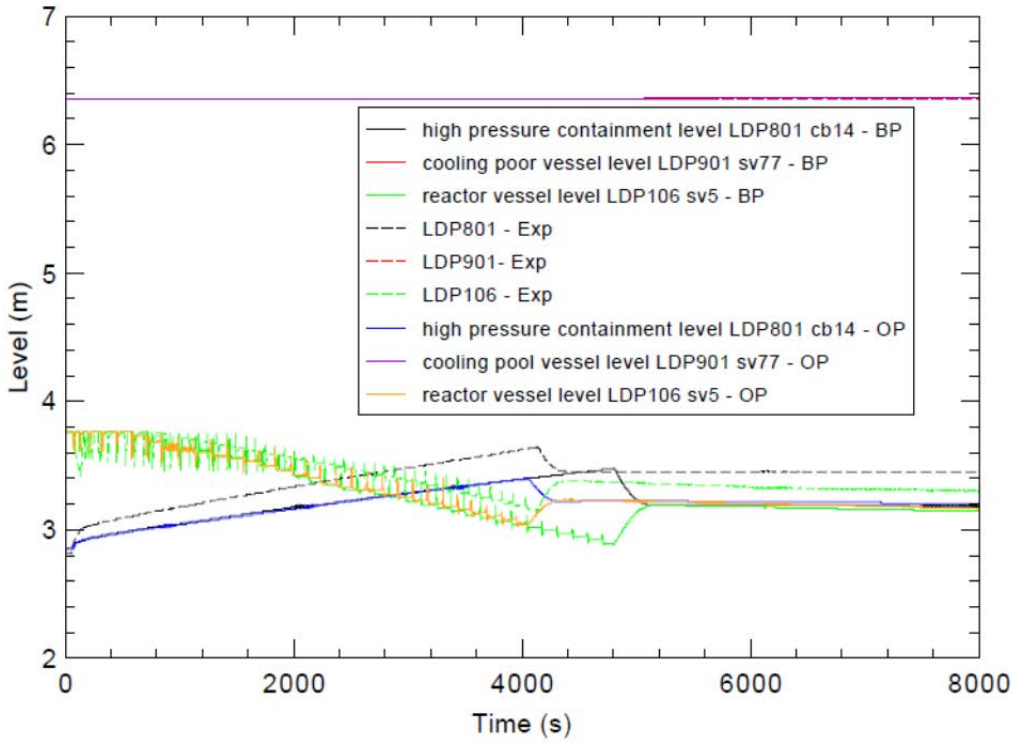

FIG. 4-251. RPV, HPC and CPV water level.

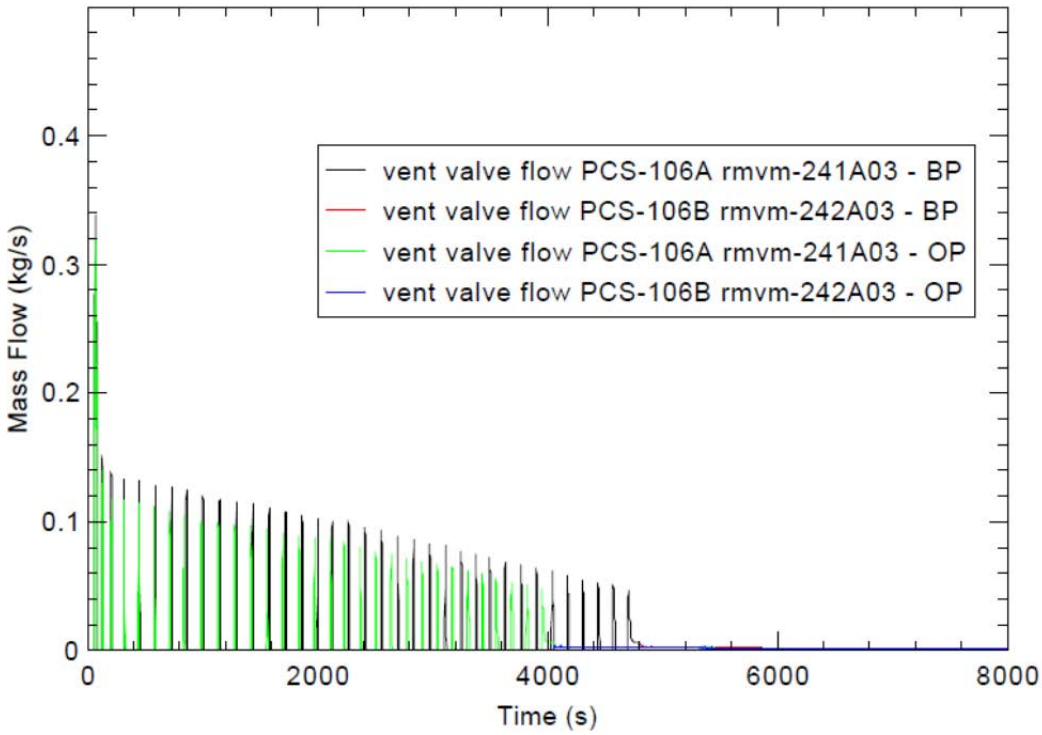

FIG. 4-252. ADS vent valve flow.

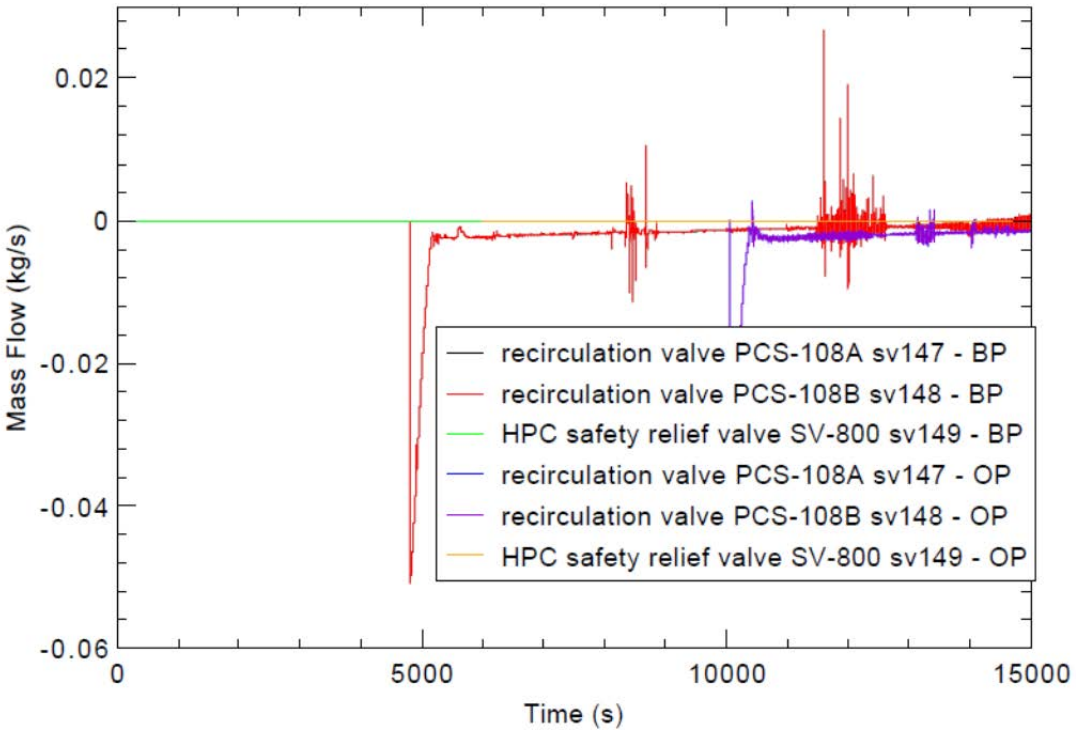

FIG. 4-253. ADS recirculation valves and HPC safety relief valve flow.

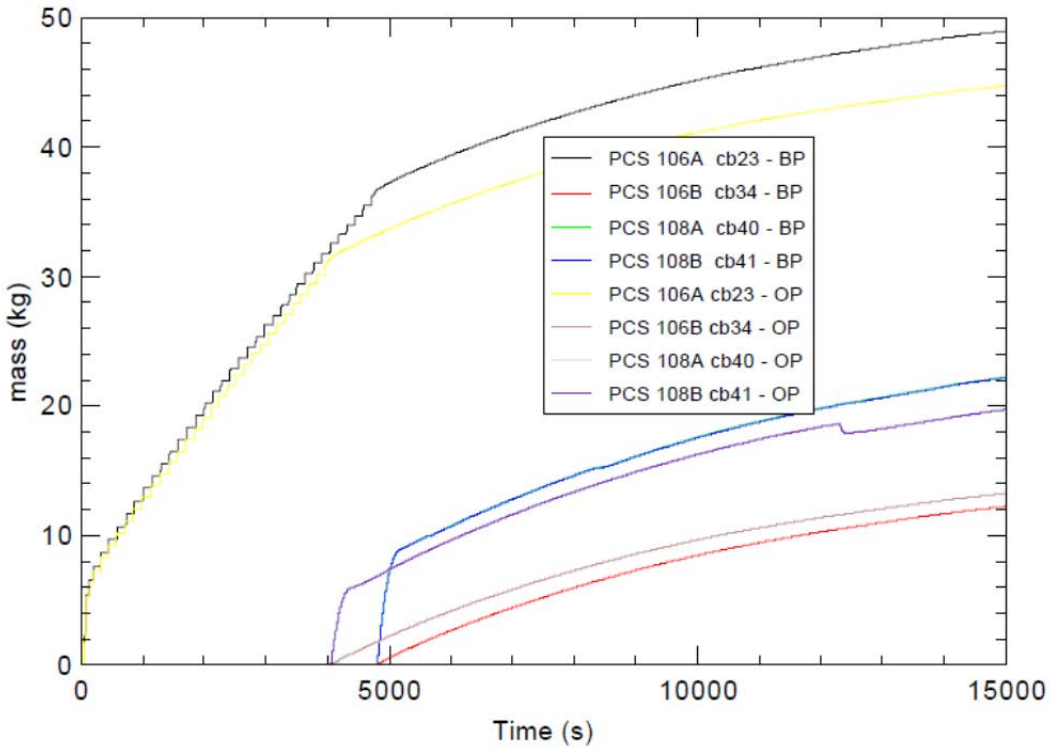

FIG. 4-254. ADS cumulative flow.

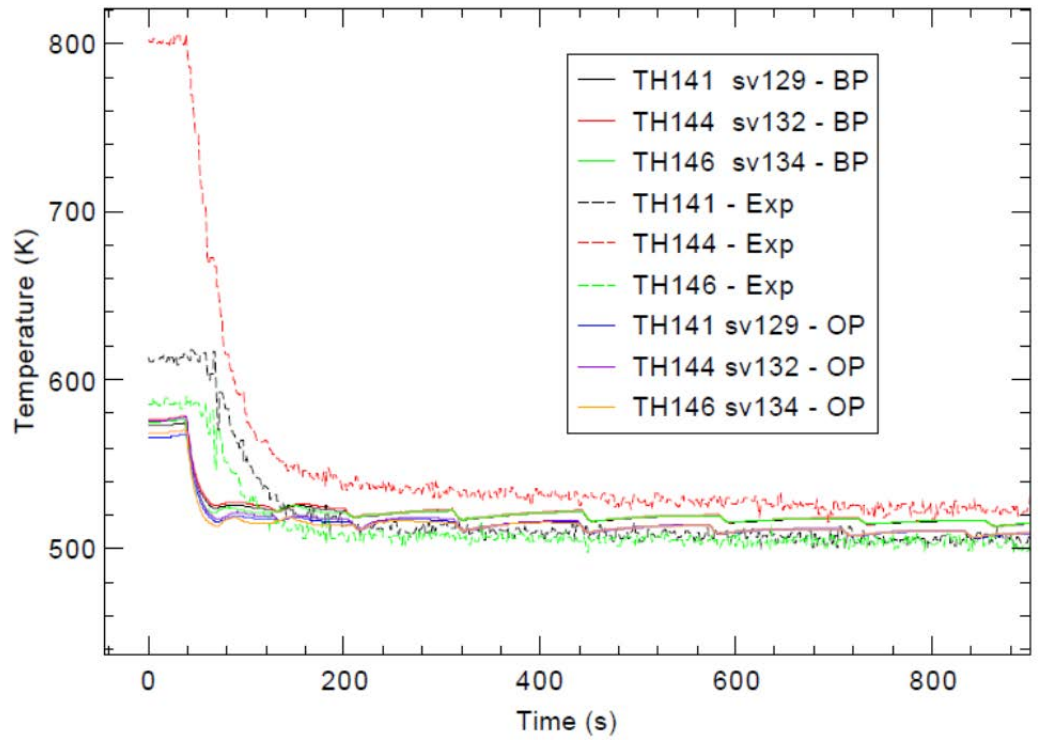

FIG. 4-255. Heater rods surface temperatures.

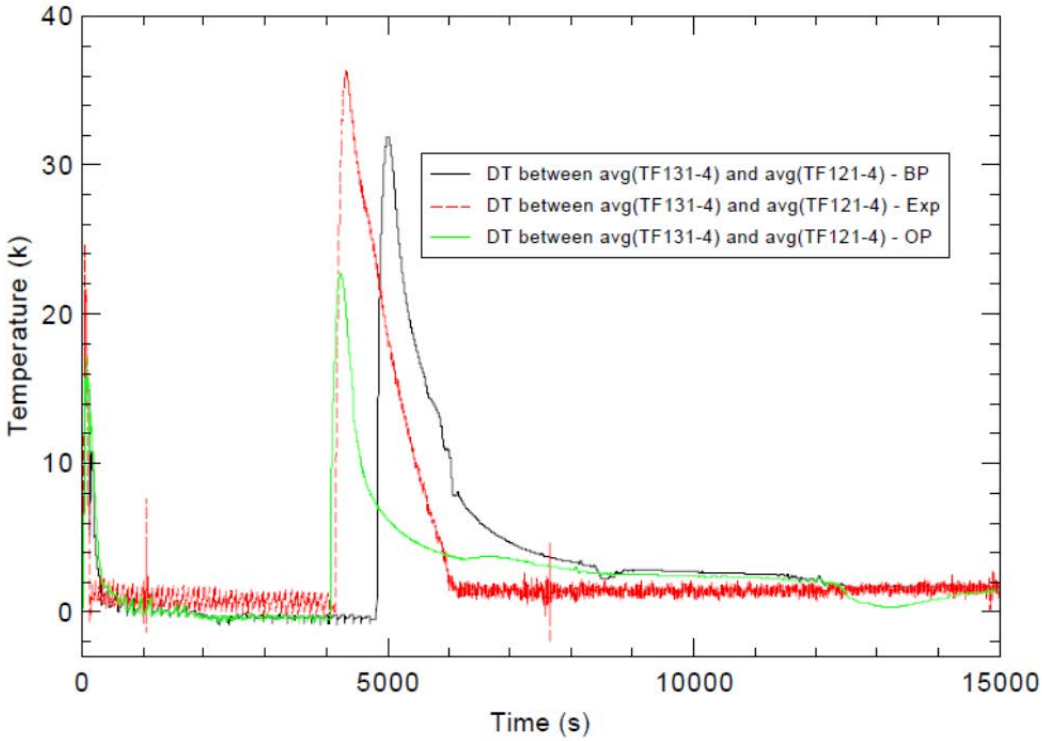

FIG. 4-256. Bypass heat transfer.

4.10.3.2. SG thermal-hydraulic behaviours

In Table 4-22, the released steady state steam pressure data (FVM-602P, 1.411MPa(a)) deviates from the procedure (1.480 MPa) greatly.

In Figure 4-258, both the blind prediction and open calculation showed the voiding of mid helical coil liquid inventory. Within 120 s, the coil liquid boiled off completely.

Exit steam temperatures are shown in Figure 4-259. The exit steam temperatures were dropping in the entire transient since the heat transfer from primary side was reduced, shown in Figure 4-245. In blind prediction, the SG exit steam temperatures, in particular TF-621, remained superheated until the equalization point. The experimental data showed similar trend. In blind prediction, the steam line temperature (FVM-602T) dropped to saturation temperature quickly and was much lower than the SG exit steam temperatures. In the experiment, the steam line temperature dropped significantly in early stage. A strong condensation could happen in the area near the sensor. The steam line temperature in both calculations stays high compared to the experiment is due to the fixed pressure boundary condition in the steam network. Feedwater temperature TF-501 remained constant in this transient and did not play much role since the flow was turned off.

Figure 4-260 shows the steam and feedwater pressures. The pressure in experiment dropped much faster than the calculations where fixed boundary condition set up in the steam network. It won't affect the results in primary side since no flow was available in the secondary side.

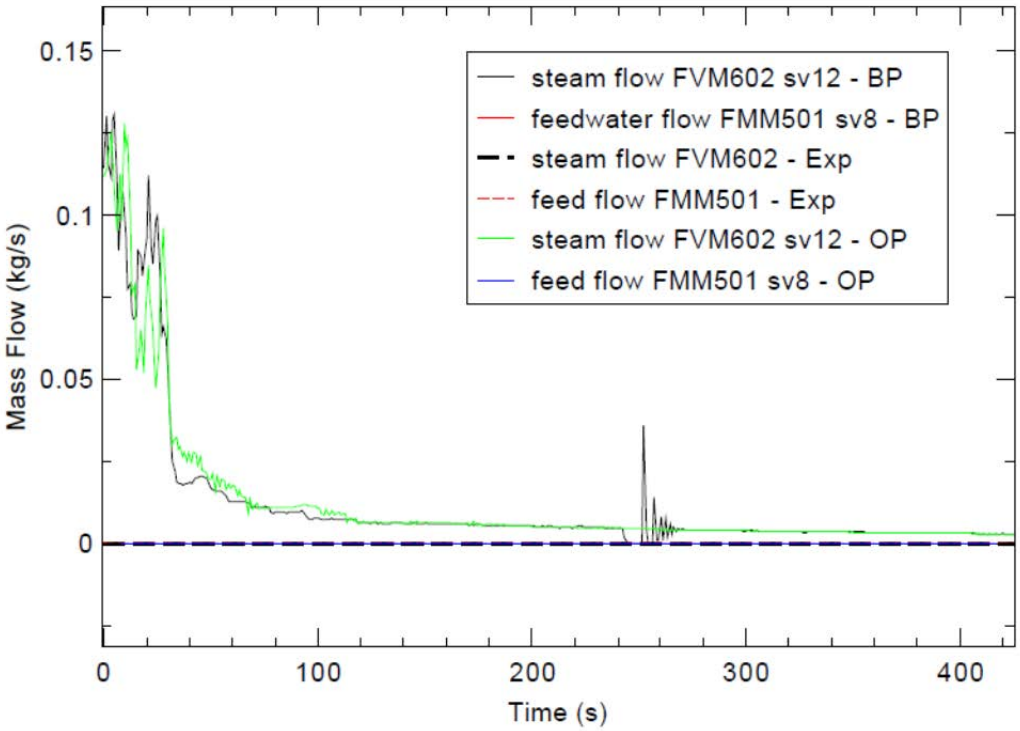

FIG. 4-257. Steam and feedwater flow.

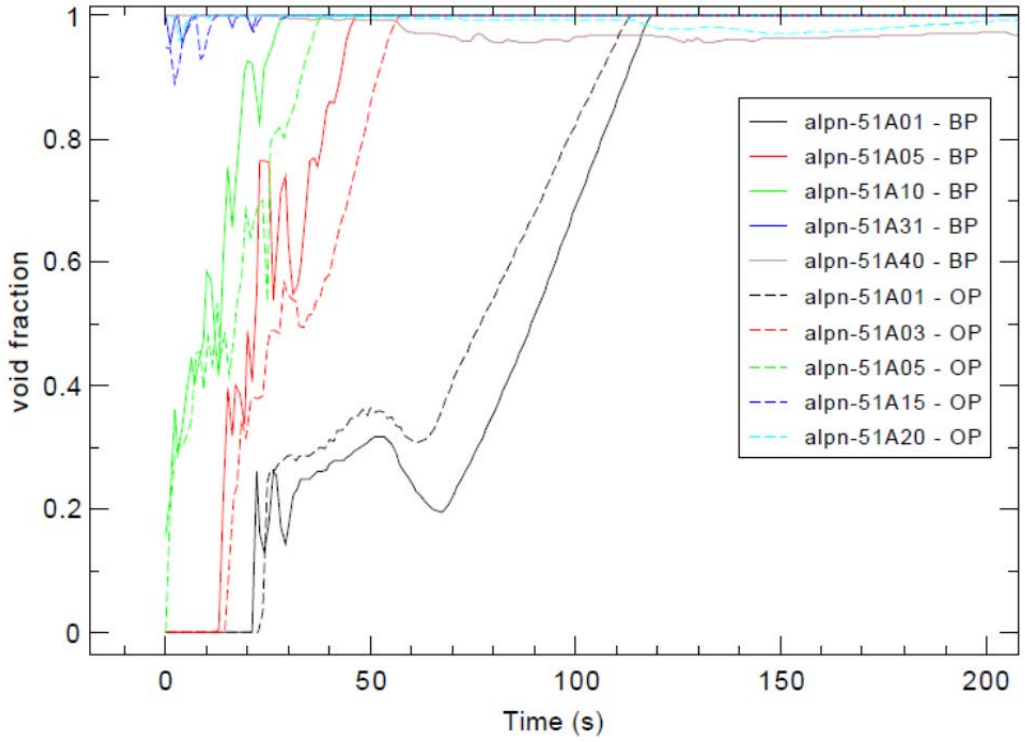

FIG. 4-258. Mid-coil void fraction.

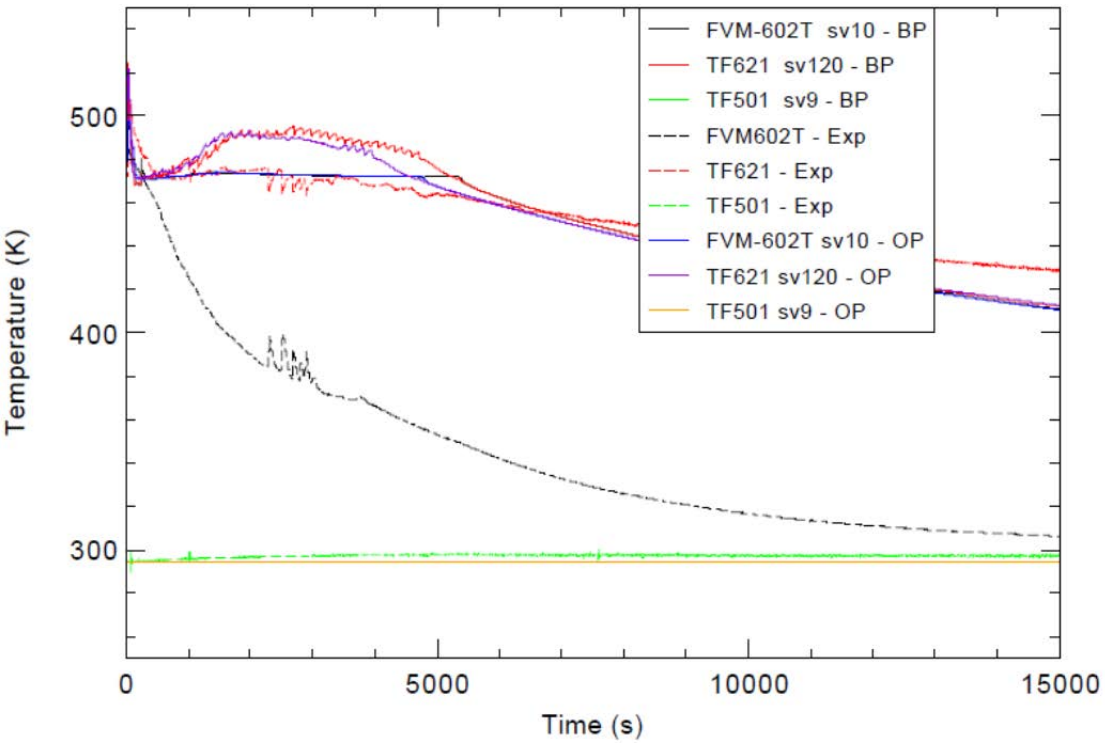

FIG. 4-259. Exit steam and feedwater temperature.

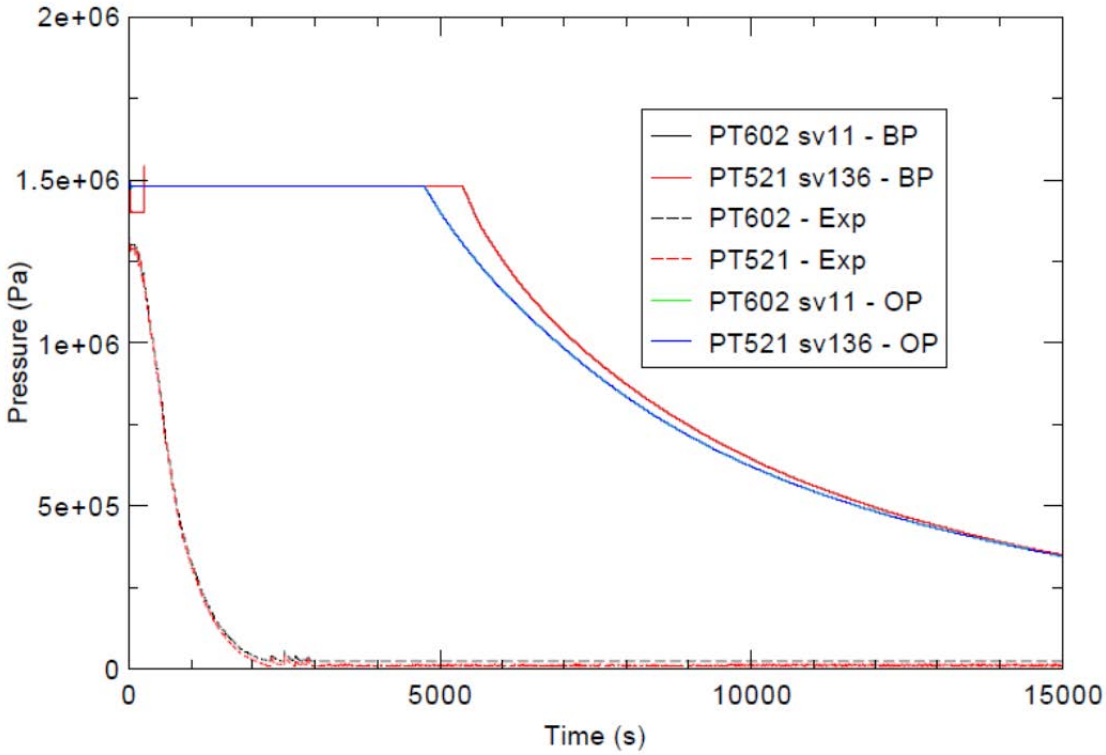

FIG. 4-260. Exit steam and feedwater pressure.

4.10.3.3. HPC thermal-hydraulic behaviours

Figure 4-261 shows the HPC bottom, top and air partial pressures. They started with a sudden increase due to the ADS vent flow. The control set points of PCS-106A caused the HPC pressure stays lower than the safety relieve valve limit. The pressure history exhibited cyclic behavior due to openings and closings of PCS-106A. After the equalization point, PCS-106A stopped cycling and stayed open, and HPC depressurized along with RPV. The air pressure occupied a small portion of the total pressure. Compared to open calculation, the blind prediction showed transfer of more energy from RPV into HPC and less condensation heat transfer because the HPC initial pressure increase was higher and pressure remains higher for a longer period.

In Figure 4-261, both calculations give maximum containment pressure of 1.9945 MPa(a) (i.e. 289.2 psia in HPC top), which was very close to the SV-800 set point of 1.9969 MPa(a) (289.7 psia). The experimental data shows a maximum of 1.7370 MPa(a) (252 psia). The max containment pressure depends on the valve rate of PCS-106A, B. In both predictions, 0.2 s^{-1} was assumed according to the close time provided in the boundary condition spreadsheet. However, the valve rate seems to be inadequate to control the HTC pressure between 1.3786MPa(a) and 1.7232MPa(a) (200 and 250 psia). This is possible due to higher initial energy inventory stored in the reactor pressure vessel and underestimated condensation heat transfer in the HPC.

Figure 4-262 shows the liquid temperature in HPC. The stratification phenomenon was clearly demonstrated. The temperatures of TF-831 to TF-861 were basically steam saturation temperatures and temperatures of TF-811 to TF-821 were liquid temperatures below the level interface. In the experiment and calculations, as time goes by, the steam temperatures reduced but the liquid temperatures increased due to heat up by the steam. However, experiment data shows lower temperatures with lower HPC pressure. It implies that the TRACE condensation heat transfer is weaker. It can also be seen from the temperature rise rate of the liquid temperatures. The liquid temperatures in experiment has faster rise compared to the blind prediction. Open calculation shows similar behaviors but with better timing on the pressure equalization point. Figure 4-263 shows the steam/air temperatures nears the ADS vent line. The steam temperatures drop at the pressure equalization point. In experiment, it occurs at around 4051 s and in blind prediction, it was 4717 s. In open calculation, the timing has improved to be closer to the experiment. The steam/air temperatures oscillated because the oscillatory ADS flow from RPV.

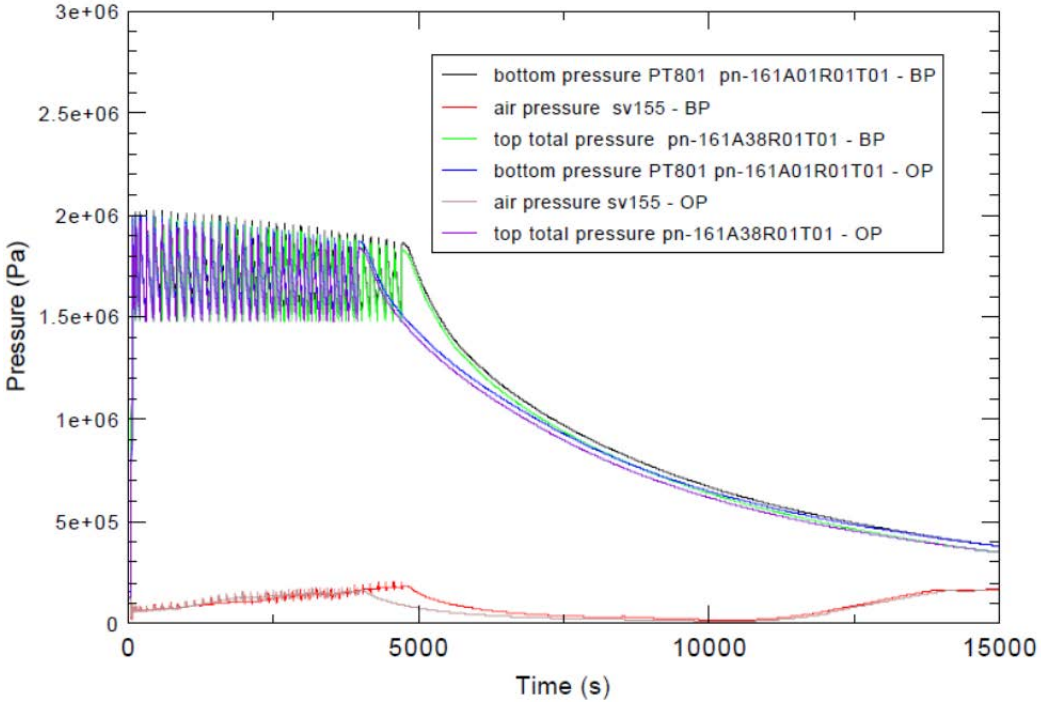

FIG. 4-261. HPC pressure.

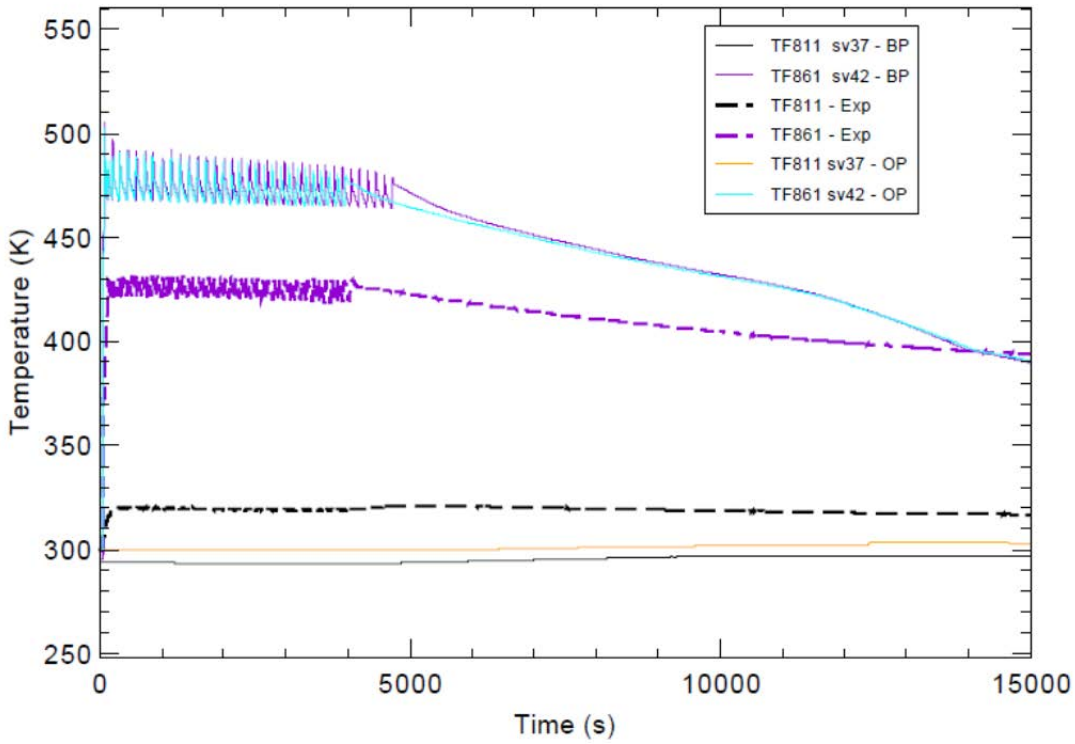

FIG. 4-262. HPC temperature.

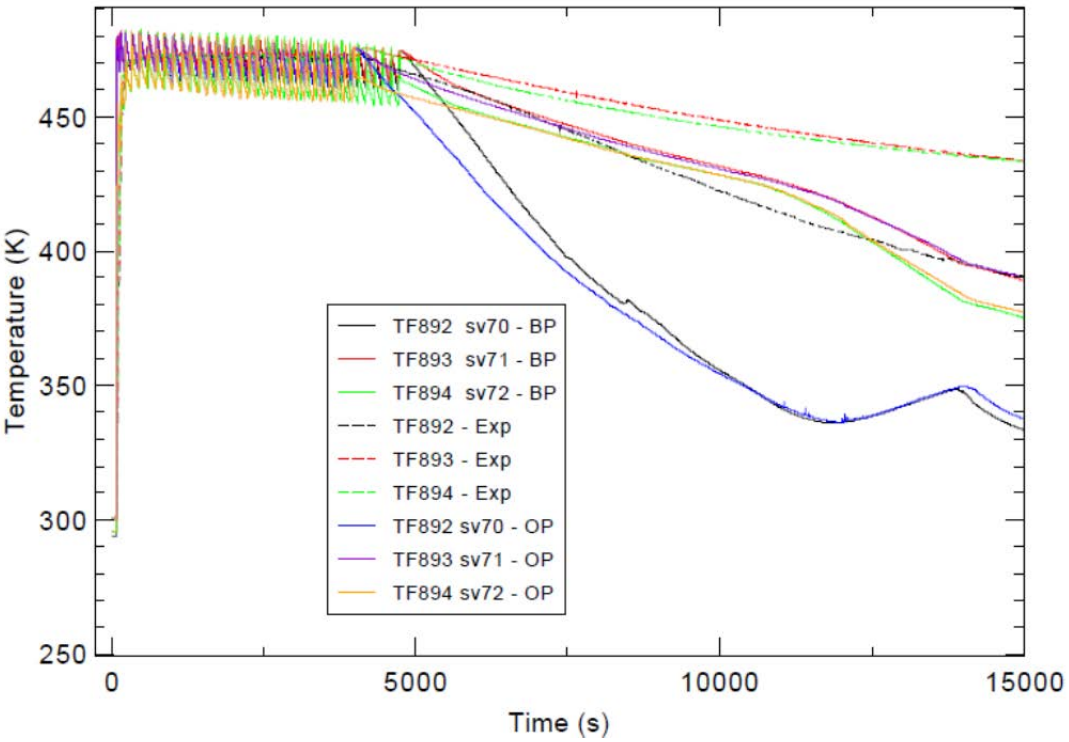

FIG. 4-263. HPC air/steam temperature.

4.10.3.4. CPV thermal-hydraulic behaviours

CPV fluid temperatures are shown in Figure 4-264. The fluid temperatures increased as the heat was transferred from RPV to HPC and then heat transfer slab. The experimental data shows fast rise of liquid temperatures compared to blind prediction. The rate of temperature rise was not realistic. In open prediction, the initial temperature was adjusted to match the experiment. However, the initial rise of water temperature in the experiment was not caught in the simulation. Final temperatures are close between the experiment and open calculation.

Figure 4-265 and 4-266 show the heat transfer plate temperatures on HPC side and CPV side. The blind prediction showed that the HPC side temperatures were about 50 degrees higher than CPV side, which was reasonable. The temperatures TW-842 to TW-846, TW-844 to TW-864 are located on the top part of the slab and they are closer to the temperature of the steam vented from RPV. Like the fluid temperatures in Figure 4-262, they decreased as transient progressed. But the temperatures on the lower part of the slab increased due to heat up of the HPC condensed liquid. The experimental data again showed that the temperature rise in the upper portion was lower compared to the blind prediction and open calculation as seen in Figure 4-262, which was consistent with the higher pressure rise in the calculations. The open calculation improved the timing of the temperature rise.

Figure 4-267 shows the mid layer heat transfer plate temperatures. TW813 has minimum temperature rise since it's located in the lower part of the slab. In Figure 4-268, the condensation heat transfer took place above the liquid interface. It confirmed that that the slab temperature above the interface was closer to the steam temperature, shown in Figure 4-262.

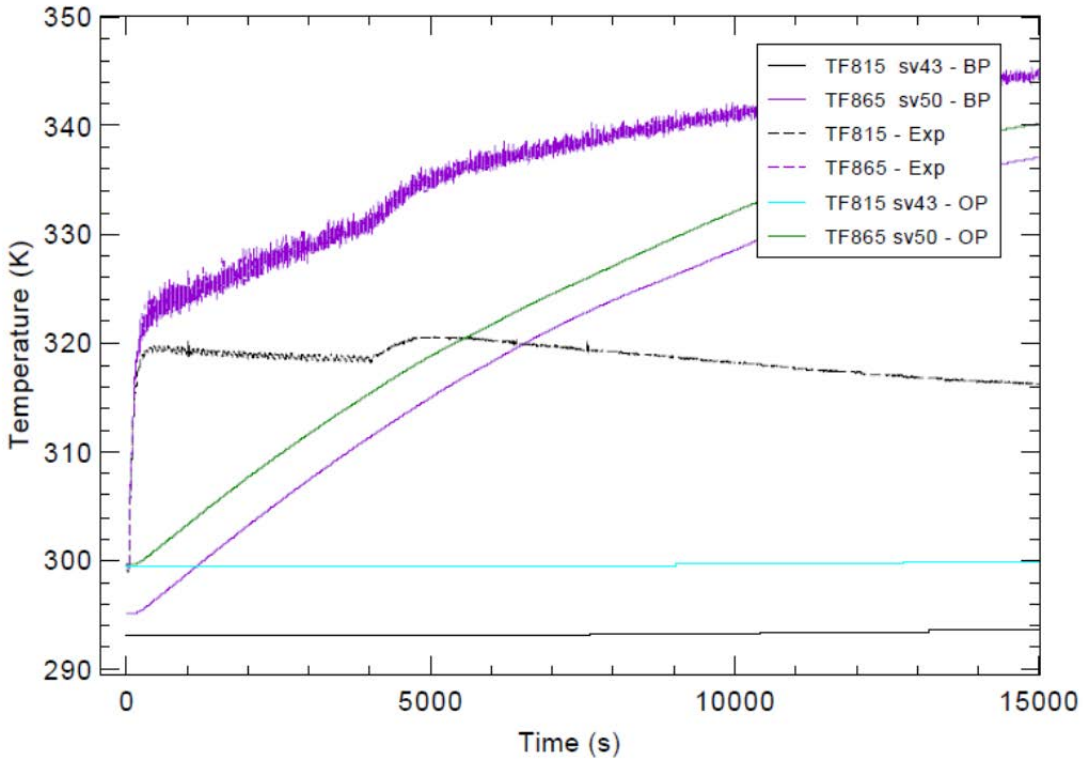

FIG. 4-264. CPV water temperature.

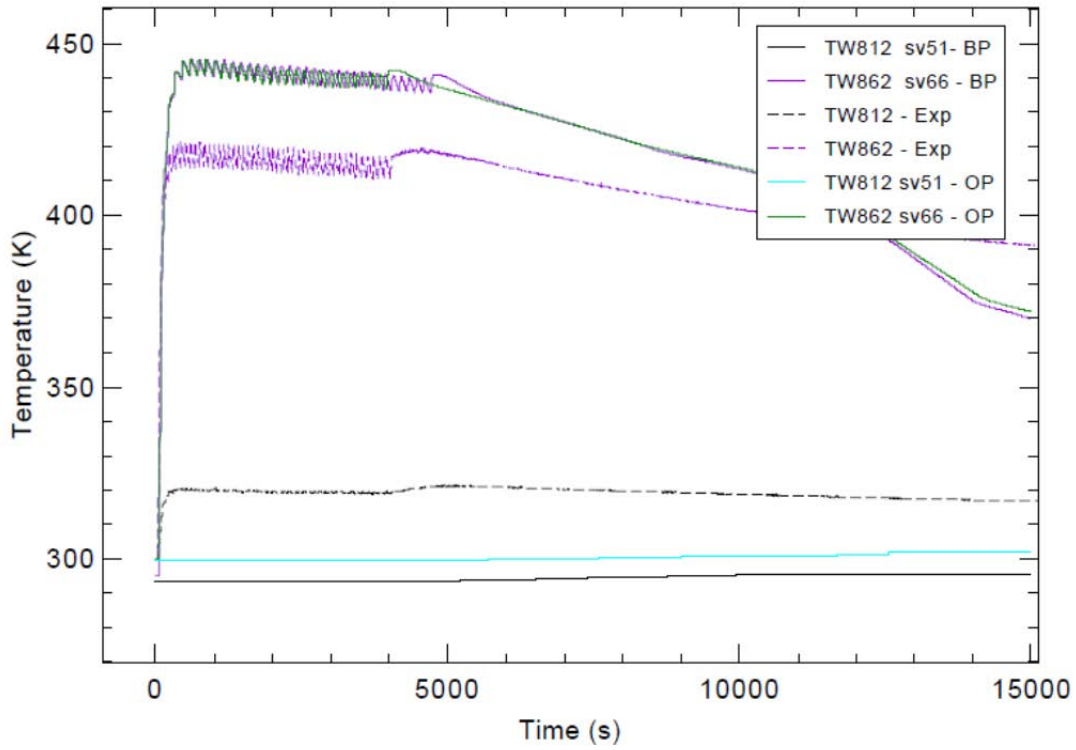

FIG. 4-265. Heat transfer slab HPC side temperature.

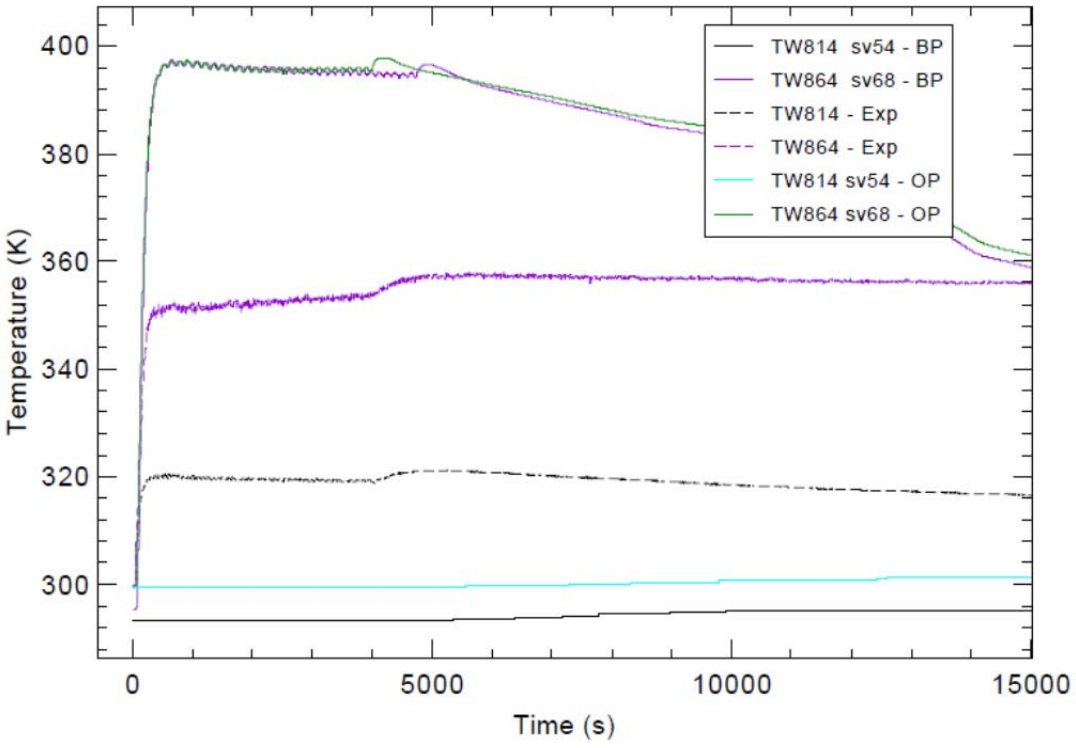

FIG. 4-266. Heat transfer slab CPV side temperature.

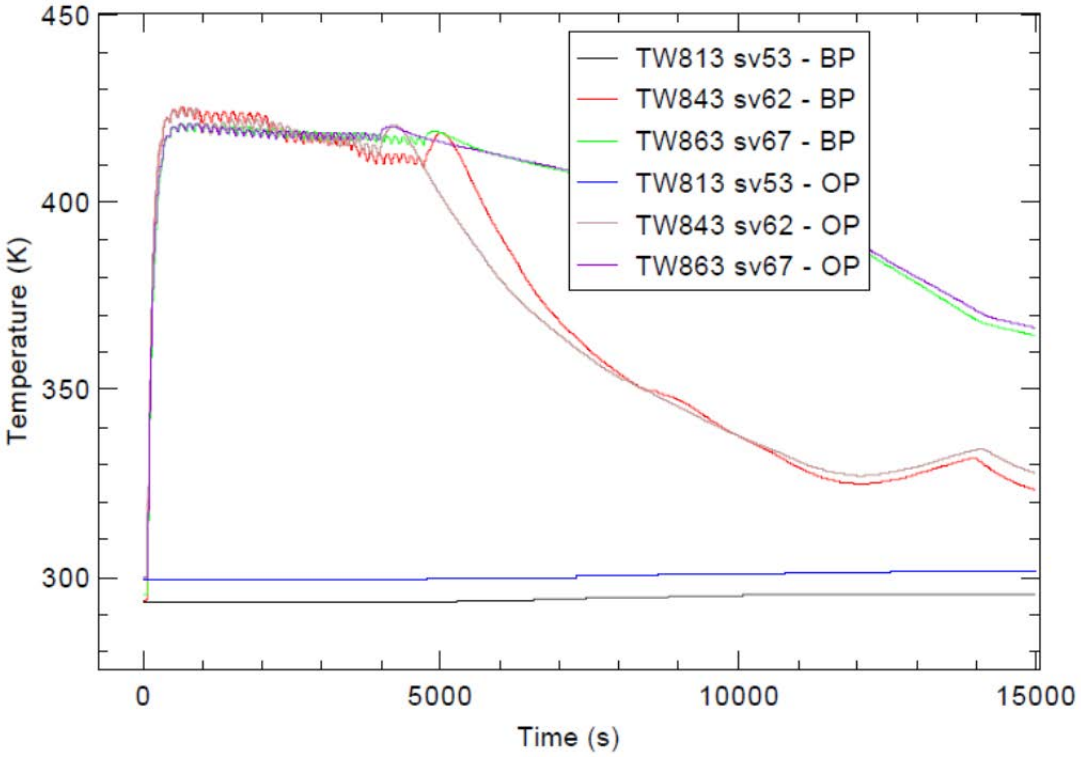

FIG. 4-267. Heat transfer plate temperature.

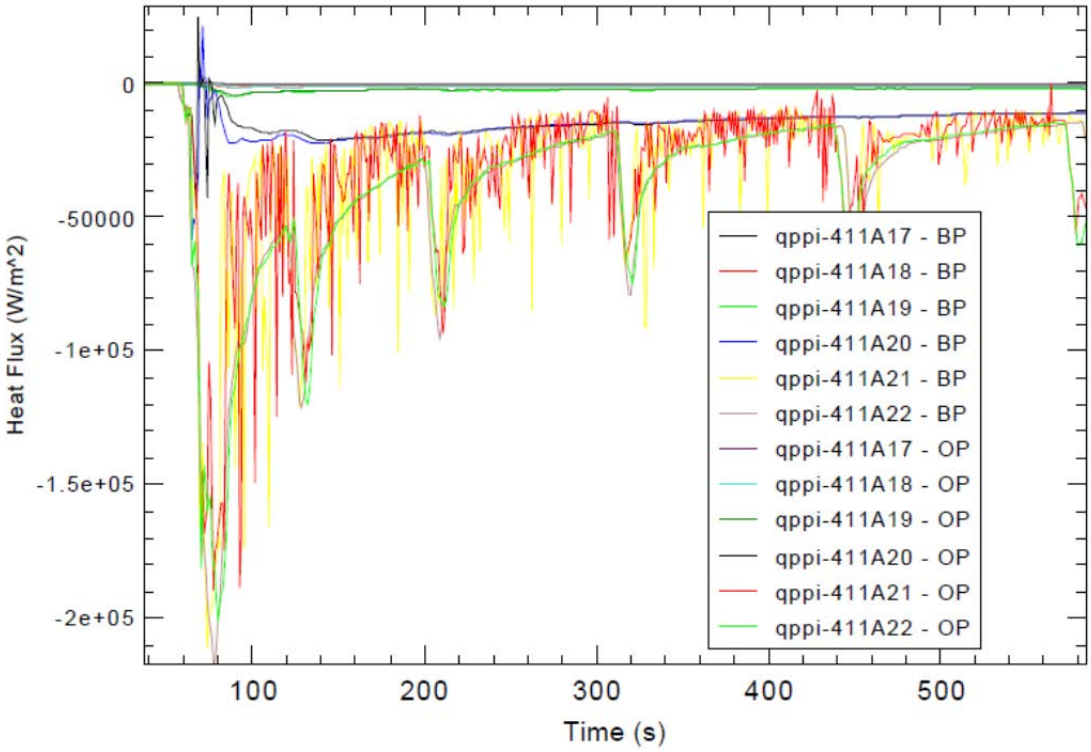

FIG. 4-268. Heat transfer near HPC level.

4.10.4. Analysis results for power manoeuvring

Table 4-24 shows the steady state conditions for SP-3 from experiment, blind and open predictions. In Table 4-24, experimental data shows that the steam exit temperatures (TF-611 to TF634 in initial condition spreadsheet) were between 250 and 260°C and yet the steam line temperature (FVM-602 T) was 205.44°C. The temperature drop was too huge to be considered as steady state. A possible reason is the steam condensation in steam pipe was strong at low power condition.

Table 4-25 shows the time sequence of events for SP-3 from experiment, blind and open calculations. In the figures and tables, pressure unit Pa, MPa represent SI unit absolute pressures and Pa(g), MPa(g) represent SI unit gauge pressures.

TABLE 4-24. STEADY-STATE COMPARISON FOR TEST SP-3

Parameter	MASLWR	Unit	Experimental Value	Steady-State Values (Blind Prediction)	Steady-State Values (Open Calculation)
Pressurizer pressure	PT-301	MPa	8.7193	8.7210	8.7195
Pressurizer level	LDP-301	m	0.3574	0.3590	0.3617
Power to core heater rods	KW-101/102	kw	21.12 / 21.00	42.10/2	42.10/2
Feedwater temperature	TF-501	ºC	31.5	31.5	31.5
Steam temperature	FVM-602-T	ºC	205.44	256.70	255.19
Steam temperature	Avg. of TF-611 to TF-634	ºC	256.4	259.0	259.2
Steam pressure	FVM-602-P	MPa(a)	1.446	1.447	1.447
Ambient air temperature	N/A	ºC	25.0	24.86	25.01
Primary flow at core outlet	FDP-131	kg/s	N/A	0.746	0.735
Primary coolant temperature at core inlet	TF-121/122/ 123/124	ºC	250.11 / 250.69 250.21 / ??	249.67/249.67 249.66/249.66	249.40/249.40 249.41/249.41
Primary coolant temperature at core outlet	TF-106	ºC	262.76	260.21	260.12
Feedwater flow	FMM-501	kg/s	0.01	0.01021	0.01021
Steam flow	FVM-602-M	kg/s	N/A	0.01150	0.01032
Primary coolant subcooling at core outlet	N/A	ºC	N/A	41.09	41.14
Total heat loss through primary system	N/A	kW	N/A	12.06	12.23
Heat transfer through SG	N/A	kW	N/A	30.07	28.03
Maximum surface temperature of core heater rods	N/A	ºC	N/A	270.07	269.97
Location from the SG secondary inlet to reach - saturation - superheat	N/A	m	N/A	(mid coil) from SG inlet 0.15375 m to saturation 0.615 m to superheat	(mid coil) from SG inlet 0.15375 m to saturation 0.615 m to superheat

TABLE 4-25. SP-3 TIME SEQUENCE OF EVENTS

Event	Time (s) MASLWR	Time (s) Blind Calculation	Time (s) Open Calculation
Start of simulation – steady state (start of data collection)	0.	0.	0.
Initiate core power increase to 80 kW	0	0	0
Initiate core power increase to 120 kW	809	809	809
Initiate core power increase to 160 kW	1642	1642	1642
Initiate core power increase to 200 kW	2176	2176	2176
Operator injected make-up water	2895-3429	2895-3429	2895-3429
Initiate core power increase to 240 kW	4004	4004	4004
Initiate core power increase to 280 kW	4498	4498	4498
Initiate core power increase to 320 kW	5094	5094	5094

4.10.4.1. RPV thermal-hydraulic behaviours

Figure 4-270 plots the core flow (FDP-131). In both blind and open calculation, TRACE results were higher than the experimental value in the low power range. As power went up, the prediction values were lower than the experimental one. OSU verified the experimental data considering the measurement uncertainties. TRACE results were consistent with the trend of most simulations. Figure 4-271 plots the DP measurement. TRACE predicted higher DP across steam generator (DP-105) but lower DP across core (DP-101). DP-105 data showed significant portion with flat response. It should be explored further to ensure the accuracy.

Figure 4-272 shows that the heat removal on the secondary side was much higher than the core power between 2800 and 3200 s. The overcooling of feedwater flow brought down the primary coolant temperature and secondary steam temperature. The pressurizer heater power was comparable to the heat loss from reactor vessel. The pressurizer heater was turned on and off to maintain the reactor pressure according to the set point. The blind prediction and open calculation did not show significant deviation in the power calculation.

In Figure 4-273, reactor level LDP-106 stayed constant since the water level was above the baffle plate throughout the transient. According to the experimental data, pressurizer level LDP-301 first increased in the beginning stage then decreased due to power/feedwater flow mismatch in power ascension before the over-cooling event. During the over-feeding period, levels dropped drastically as more energy was drawn to the secondary side. The operator tried to maintain the level above the PZR heater (around 0.202 m) so they injected make-up water from vessel bottom between 2896 to 3428 s. They successfully maintained the level above 3.25 m. After stopping the make-up water injection, the level continued to rise as the power increased. The reactor level increase due to make-up water in the experiment was more obvious than in both blind prediction and open calculation. And yet the trends are similar for the experiment and calculations.

In Figure 4-274, a substantial subcooling margin was maintained in the core outlet temperature and saturation temperature. The core outlet temperature increased first due to power ascension and then decreased during the feedwater over-cooling period, which was expected. The data showed that the overcooling event was more obvious in experiment than the blind prediction because the core outlet temperatures dropped lower. In open calculation, the outlet temperature matches better to data. The unexpected increase and drop of saturation temperature was due to an abnormal pressure drop. It was a code deficiency identified and will be explained below.

In Figure 4-275, at time between 3400 and 4600 s, the pressurizer pressure of both open calculation and blind prediction showed irregular behaviors. It's due to a TRACE 3D level tracking model deficiency – over flashing/condensation when level interface passes through nodal boundary. The impact to the transient response is relatively mild. A fix is in progress.

Heater rod surface temperatures are plotted in Figure 4-276. TH-143 and TH-144 are located in the inner core and the rest are in the peripheral locations. In blind and open calculation, the temperatures

in the inner locations appear to be lower than the outer locations. The reason is not clear, may be due to irregular flow distribution. In the experiment, TH-144 data appeared to be abnormally high.

In the transient, the fluid in the cold leg side was heated up through the core barrel due to the temperature difference between hot leg and cold leg. Cold leg (TF131-4) and core inlet (TF121-4) temperature differences were plotted in Figure 4-277. The temperature difference represented the bypass heat transfer from core to the cold leg. According to the data, in the lower power range, cold leg temperature TF131-4 was higher than core inlet temperatures TF121-4. As power went up, the flow increased and heat up effects were more obvious. Therefore the differences became smaller and eventually the core inlet temperatures were higher than the cold leg temperatures in the full power range. The blind prediction showed the same trend but with discrepancy in magnitude. During the over-feed period, the make-up water cooled the core inlet and caused the temperature difference to rise because the make-up water entered the vessel from core inlet area. Blind prediction and open calculation showed stronger effects than the experiment. The response of make-up water in temperature appeared not to be consistent with the level response shown in Figure 4-273.

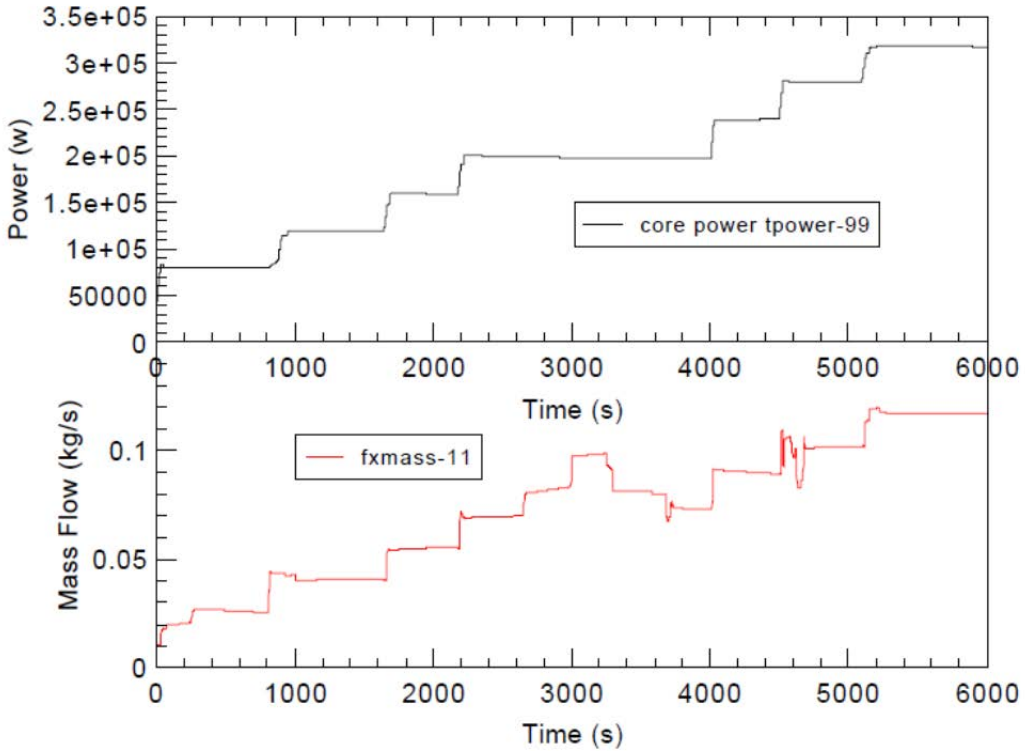

FIG. 4-269. Core power and feedwater flow boundary condition.

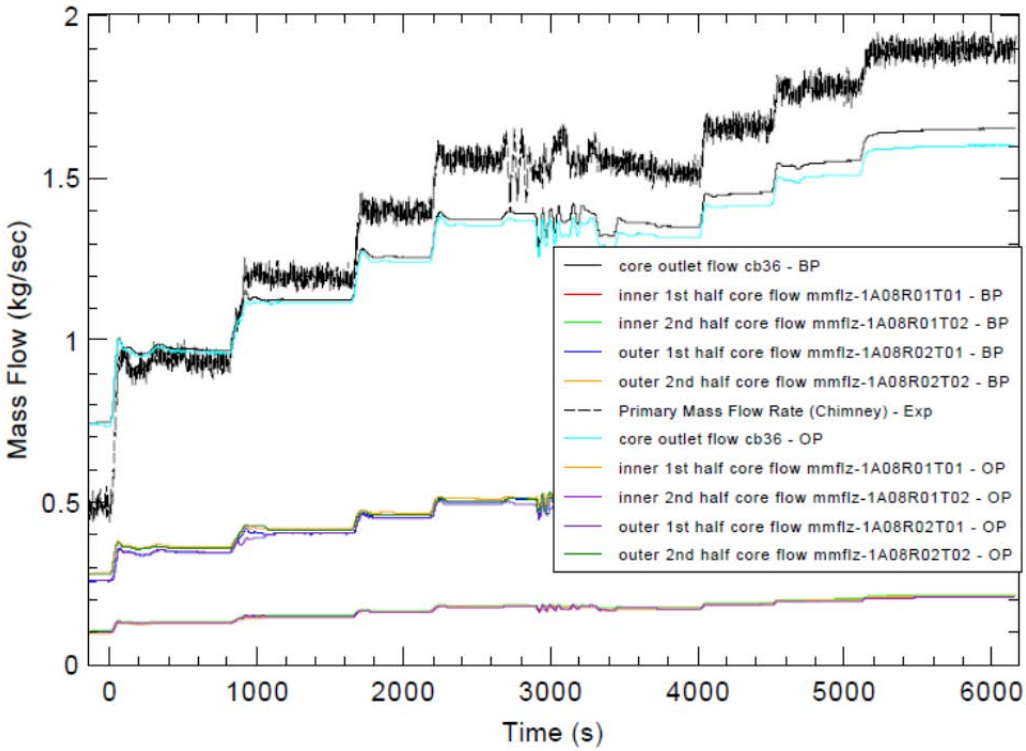

FIG. 4-270. Core outlet flow (FDP-131).

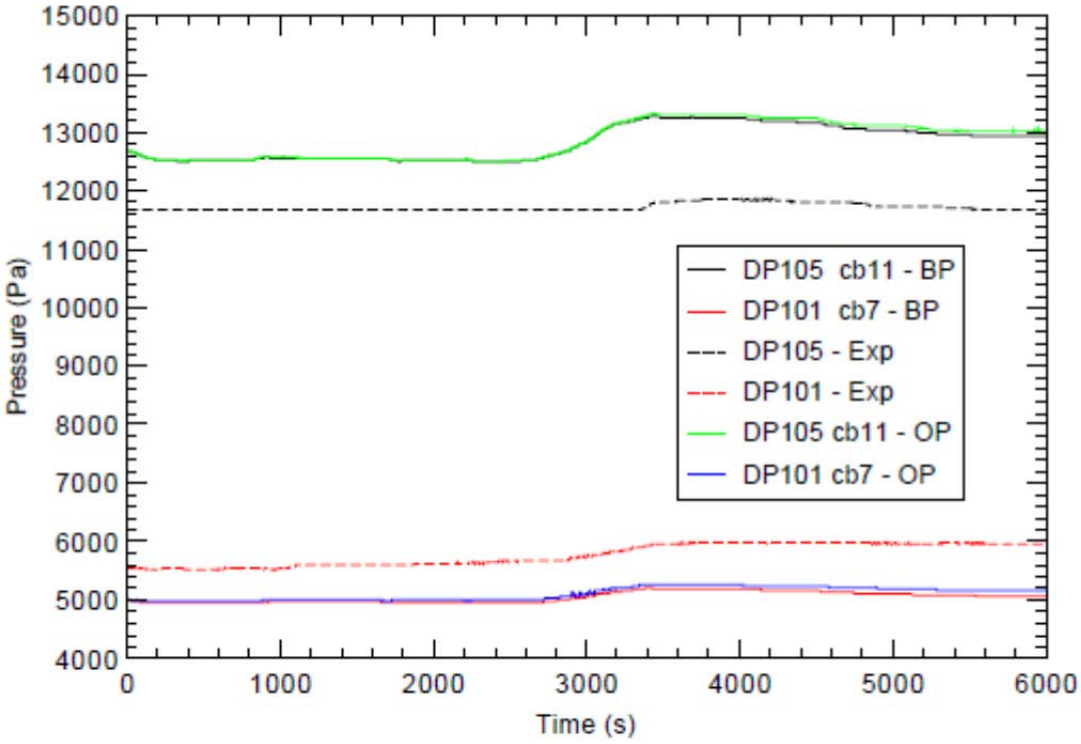

FIG. 4-271. Pressure drop across SG (DP-105) and core (DP-101).

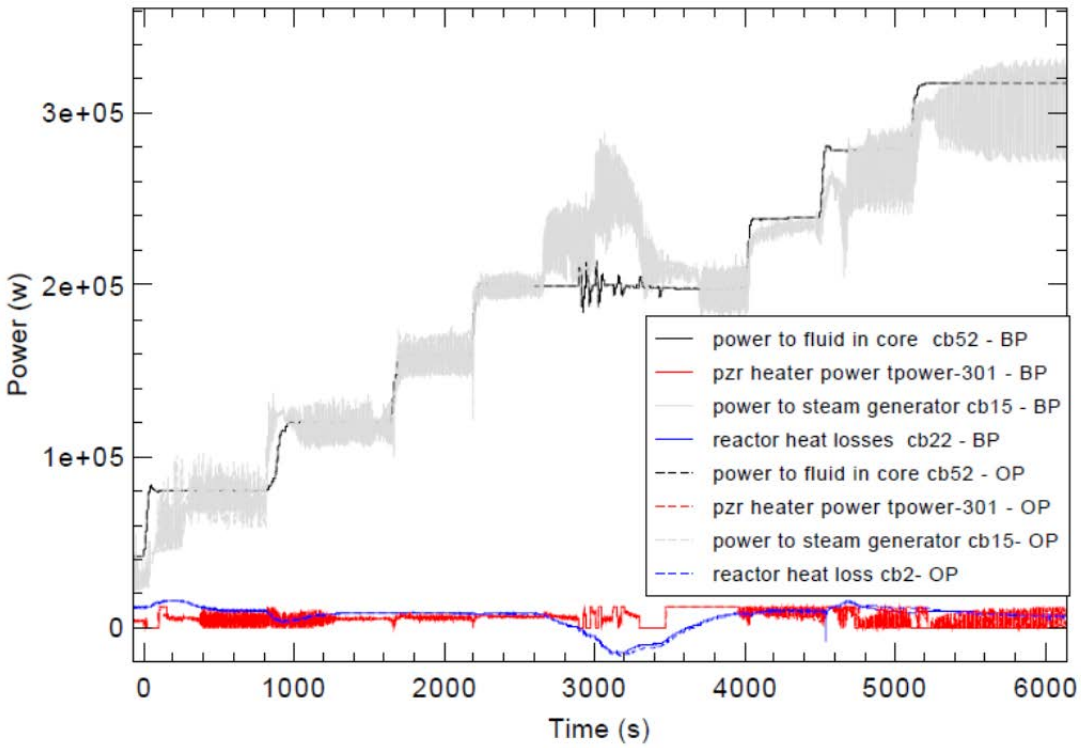

FIG. 4-272. Power to fluid in core.

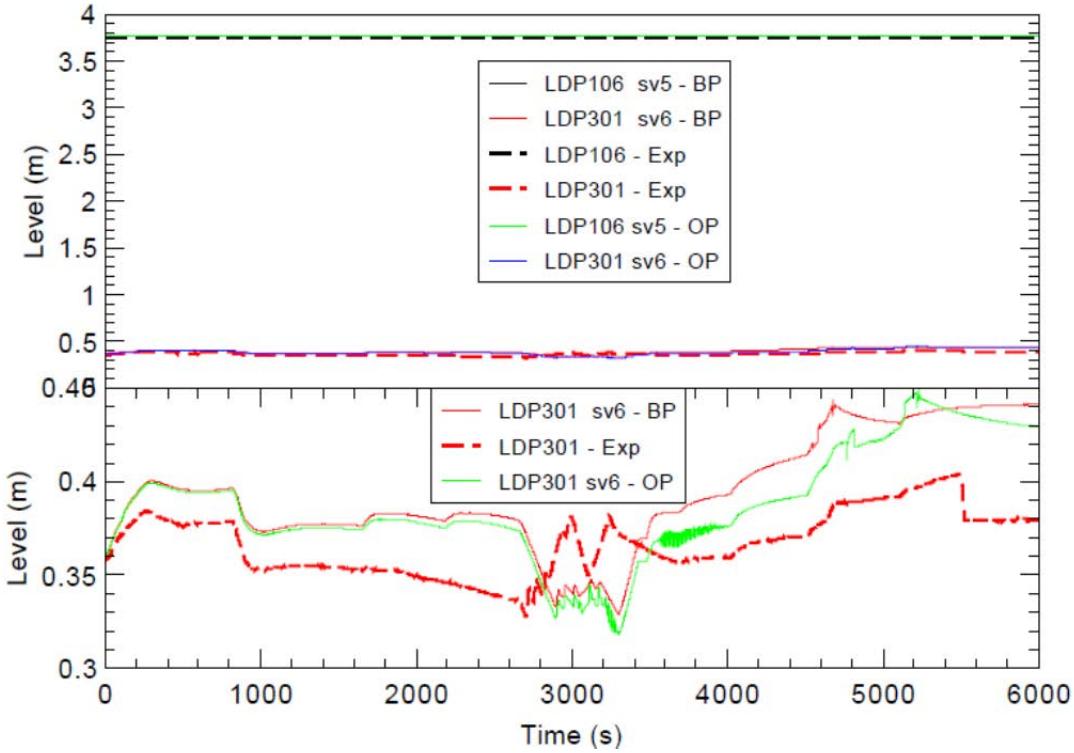

FIG. 4-273. Water level (LDP-106 and LDP-301).

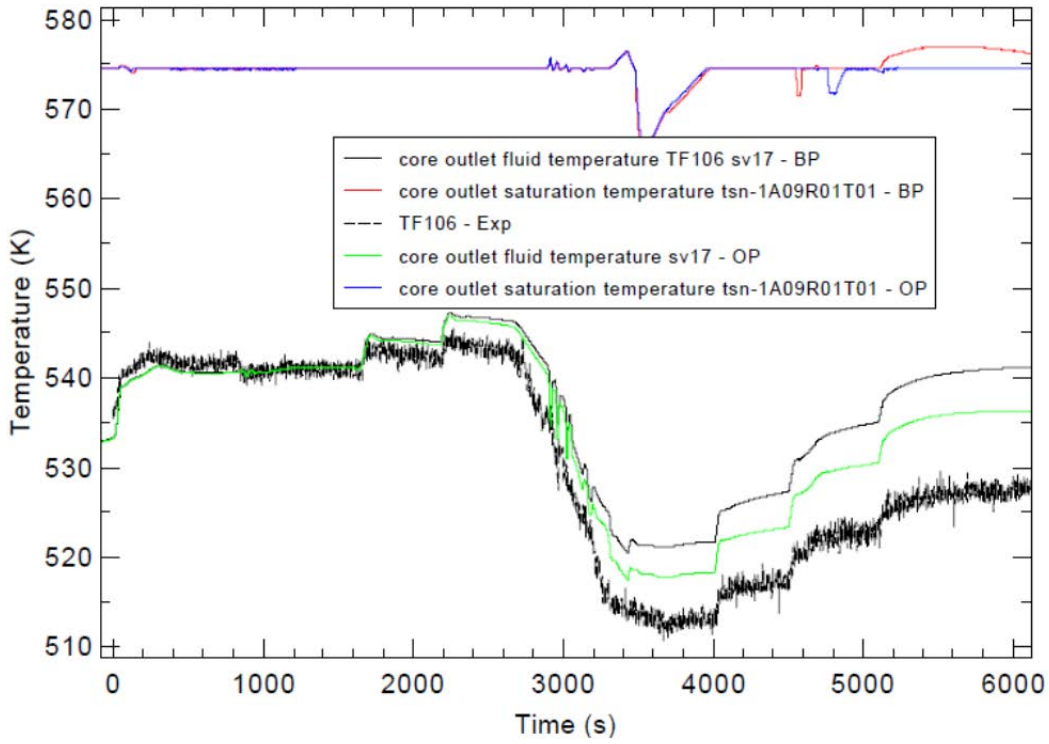

FIG. 4-274. Core outlet fluid temperature (TF-106).

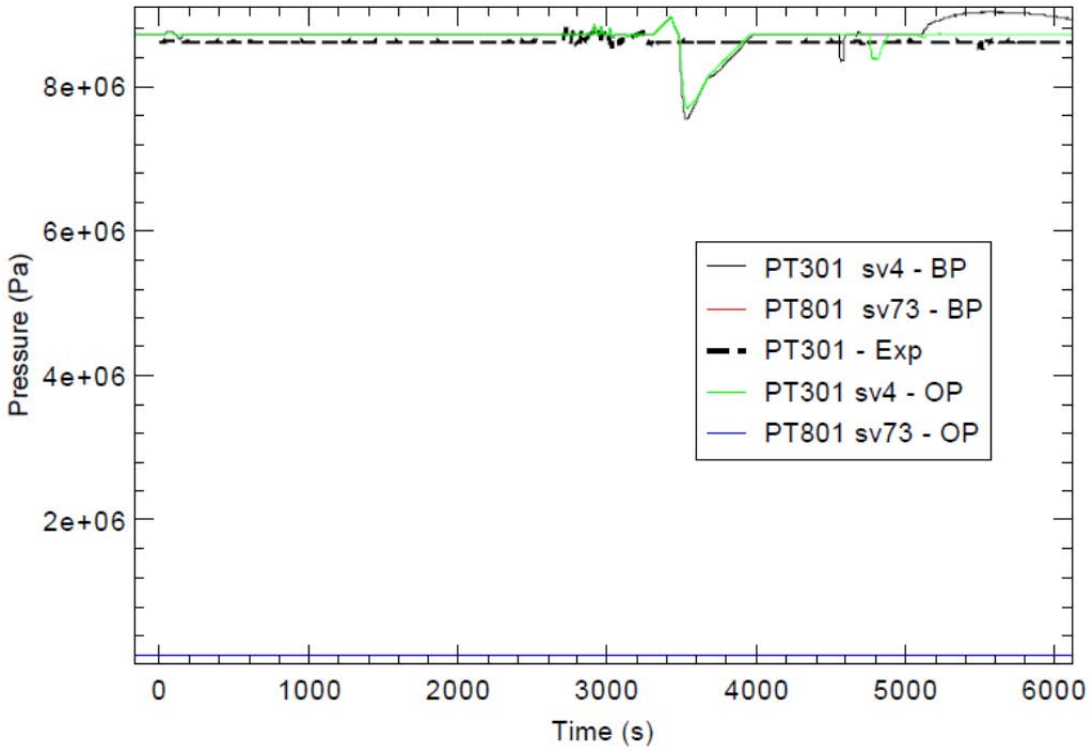

FIG. 4-275. Pressurizer pressure (PT-301).

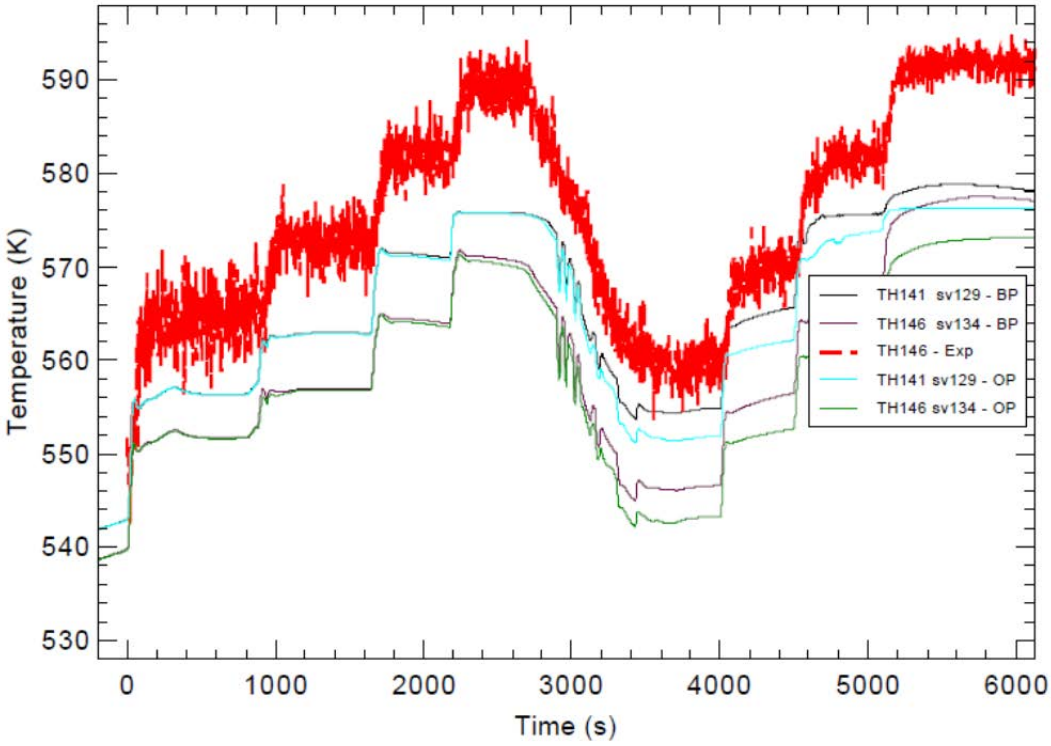

FIG. 4-276. Surface temperatures of core heater rods.

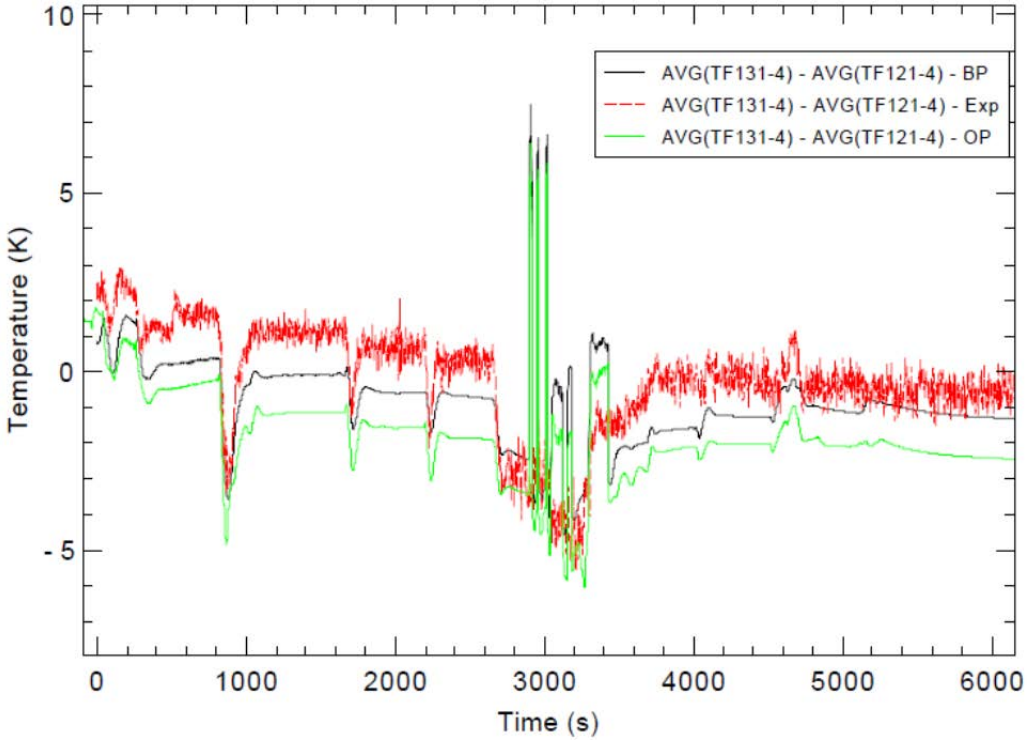

FIG. 4-277. Bypass heat transfer.

4.10.4.2. SG thermal-hydraulic behaviours

Figure 4-278 shows the steam and feedwater flow predictions. The feedwater flow was input as boundary condition. According to the data, between 2800 and 3200 s, the feedwater was higher than the steam flow averagely. This is the main event in this transient. The operator was trying to maintain the saturation condition in the procedure by lowering the exit steam temperature through feedwater flow. They increased the feedwater flow higher than the amount set by the power level for an extended period. It brought down the steam temperature from highly superheated condition to the saturation condition, which was consistent with the void distribution plot in Figure 4-279 and exit steam temperature plot in Figure 4-280. Open calculation results were close to the blind prediction.

Feedwater temperature (Fig. 4-281) from experimental data is approximated as boundary condition in blind prediction and open calculation. The decreasing trend in the entire period shows the cooling ability of feedwater became stronger as the power increased, which was opposite to the real plant operation where the feedwater gets better heating by extraction steam as power increases.

Steam line pressure and feedwater line inlet header pressures are plotted in Figure 4-282. The pressures increased slowly before the feedwater over-cooling period (2800 to 3200 s). Then both pressures increased significantly as feedwater flow was overly increased compared to the value set by the power during the over-cooling period. Then they both dropped as the exit steam became saturated after the over-cooling period. Both pressures increased again as operator continued to increase the feedwater flow. The pressure drop between feedwater inlet and steam pipe remained relatively constant. In both blind prediction and open calculation, the steam/feed network was maintained at a higher pressure boundary condition. While in the experiment, the boundary condition is flow condition.

The SG boiling length for the transient was not estimated. In steady state, the boiling length of saturation and superheat was a rough estimate according to the void distribution and heat transfer coefficient. The estimate could deviate from reality significantly.

In Figures 4-278 to 4-280, TRACE blind prediction calculation shows significant oscillation in SG coil flow and temperature. The oscillation has been improved in the open calculation by reducing the number of nodes in the mid coil of steam generator and the hydraulic condition coupling. To completely resolve the oscillation, the information of the restrictors before the helical coils is needed.

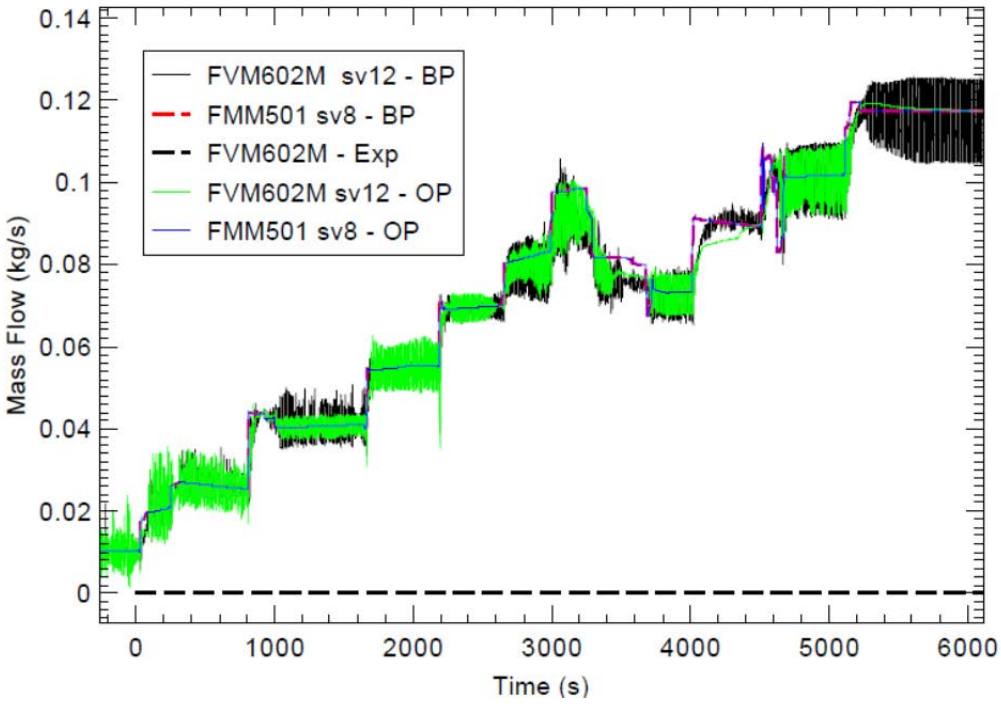

FIG. 4-278. Steam and feedwater flow.

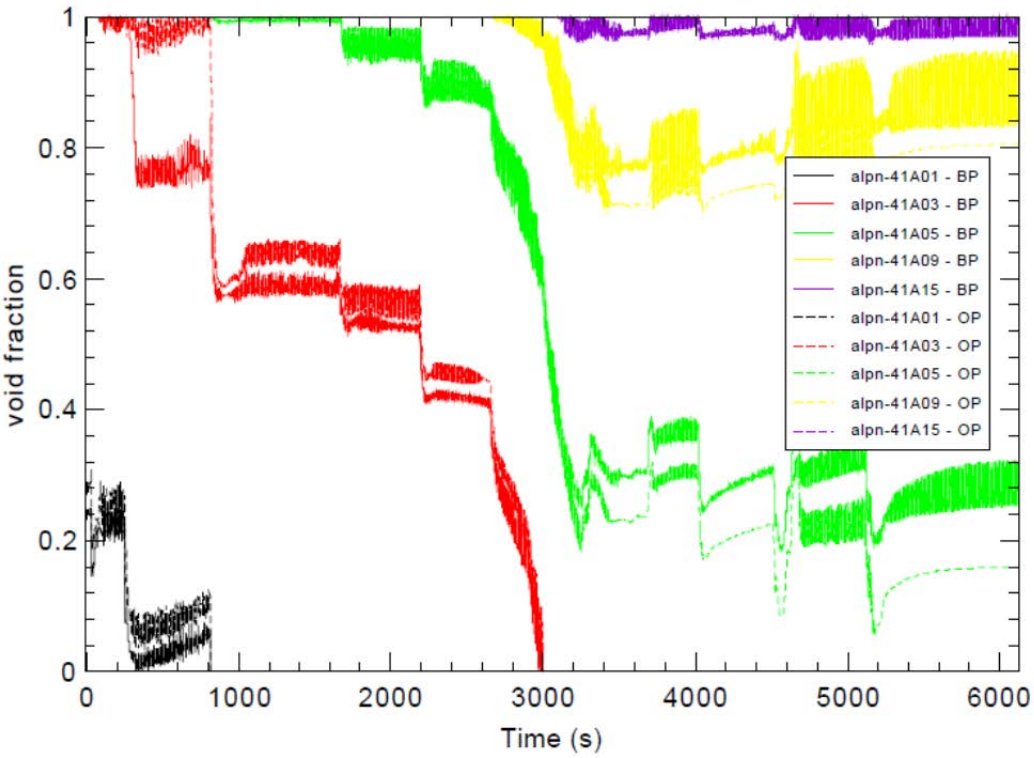

FIG. 4-279. Void fractions in SG outer coil.

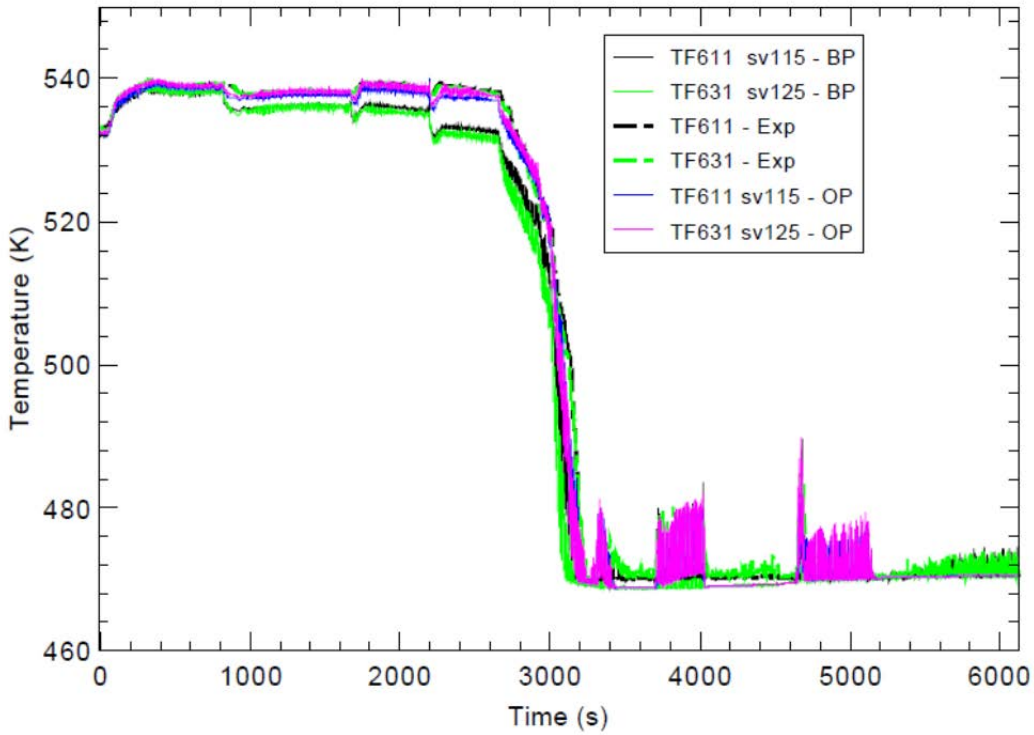

FIG. 4-280. Steam generator exit steam temperature.

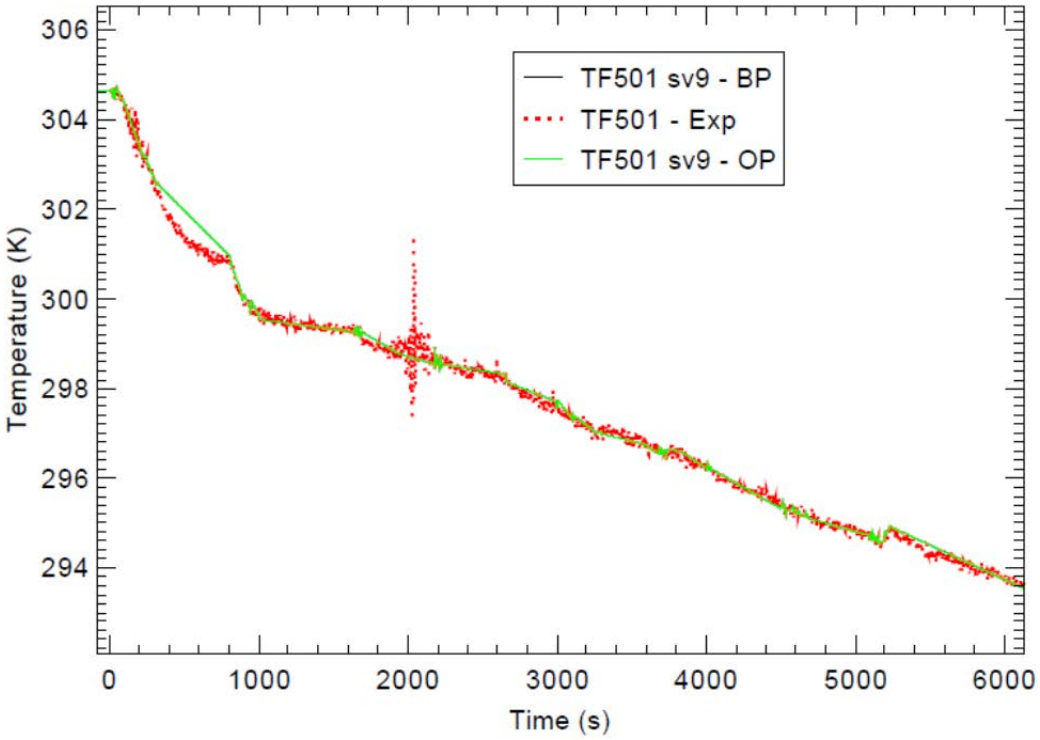

FIG. 4-281. Feedwater temperature.

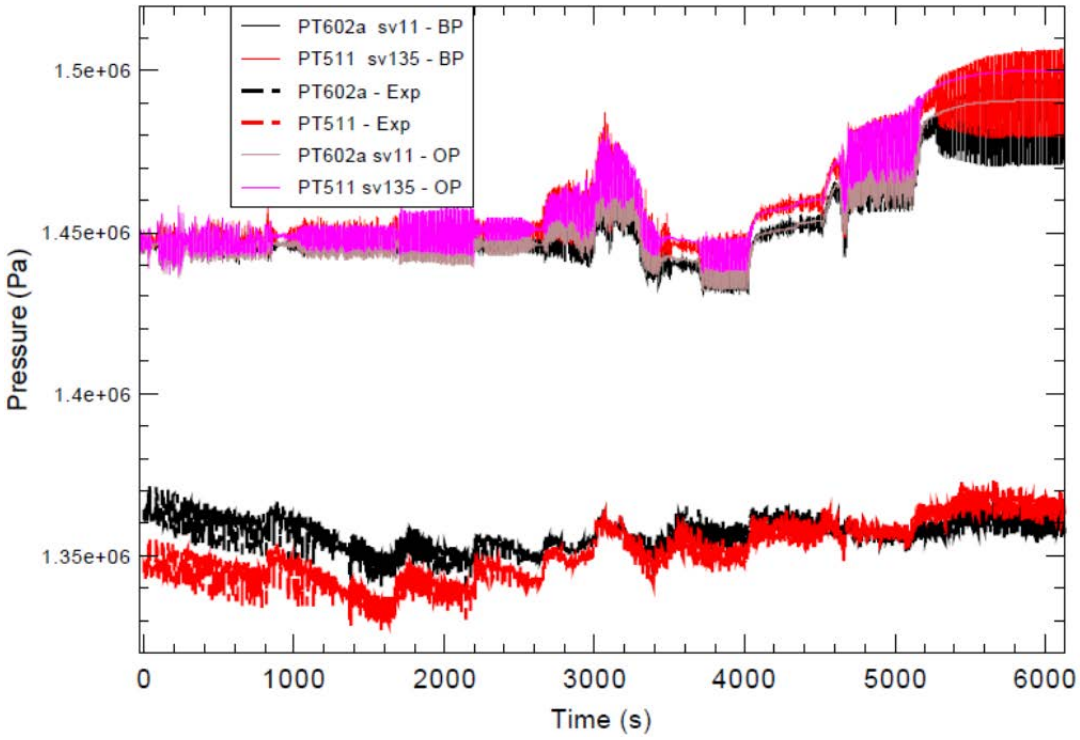

FIG. 4-282. Steam and feedwater pressure.

4.11. NUSCALE – USA

4.11.1. Computer codes

RELAP5/MOD3.3 has been used to simulate system thermal-hydraulics of the OSU MASLWR experimental test facility. RELAP5 has been developed for many years as a best estimate system thermal-hydraulics code for light water nuclear reactor applications. This code solves six field equations in the form of a one-dimensional, transient two-fluid model for two-phase steam-water mixtures which can contain noncondensible gas in the steam phase and solutes in the liquid phase. The dependent variables solved for with the field equations are, pressure, gas phase velocity, liquid phase velocity, gas phase internal energy, liquid phase internal energy, vapor void fraction, noncondensible quality, and boron density. The code solves for non-homogeneous non-equilibrium flow, however much simpler models can be invoked by user options. Volume and time averaged parameters are used in formulating the hydrodynamic equations of RELAP5, which are solved using semi-implicit finite differencing. RELAP5 does not contain a specific model for helical coil steam generators. It is a single pressure code, and therefore the non-condensable gas must be in equilibrium with the steam phase. Multiple choked flow models may be applied in RELAP5 however only the MOD3.3 default model is used in this study. The default model is a form of the Henry-Fauske choking flow model which uses empirical constants to account for non-equilibrium effects.

4.11.2. System idealization

This section will summarize the system nodalization changes that have been made between the blind and open calculations. In general, RELAP5 models can be expected to predict first-order one-dimensional phenomena for which the code was developed to predict. Specific RELAP5 components used in modelling the OSU MASLWR system include annulus for the downcomer region, and branches or pipes for all other volumes, except those which constitute boundary conditions. Time dependent volumes and time dependent junctions have been used to implement the proper boundary conditions in the model. All valves in the system are treated as zero-dimensional with loss coefficients specified to represent losses to the flow passing through them. Larger volumes in which relatively stagnant fluid may exist, such as the containment and cooling pool volumes, are represented by two pipes which are connected through cross junctions to allow for the effect of natural circulation to be accounted for. Heat transfer to and from heat structures to the surrounding volumes is only modelled in the radial direction, and no axial heat transfer is modelled in the system.

4.11.2.1. System idealization for blind calculation

The system nodalization used to obtain the results of the blind calculations for both SP-2 and SP-3 can be seen in Figure 4-283. The revisions made to this nodalization in order to obtain the open calculation results for SP-2 and SP-3 is listed in detail in the next section 4.11.2.2. The nodalization scheme does not include piping losses in the blowdown lines, vent lines, or sump recirculation lines.

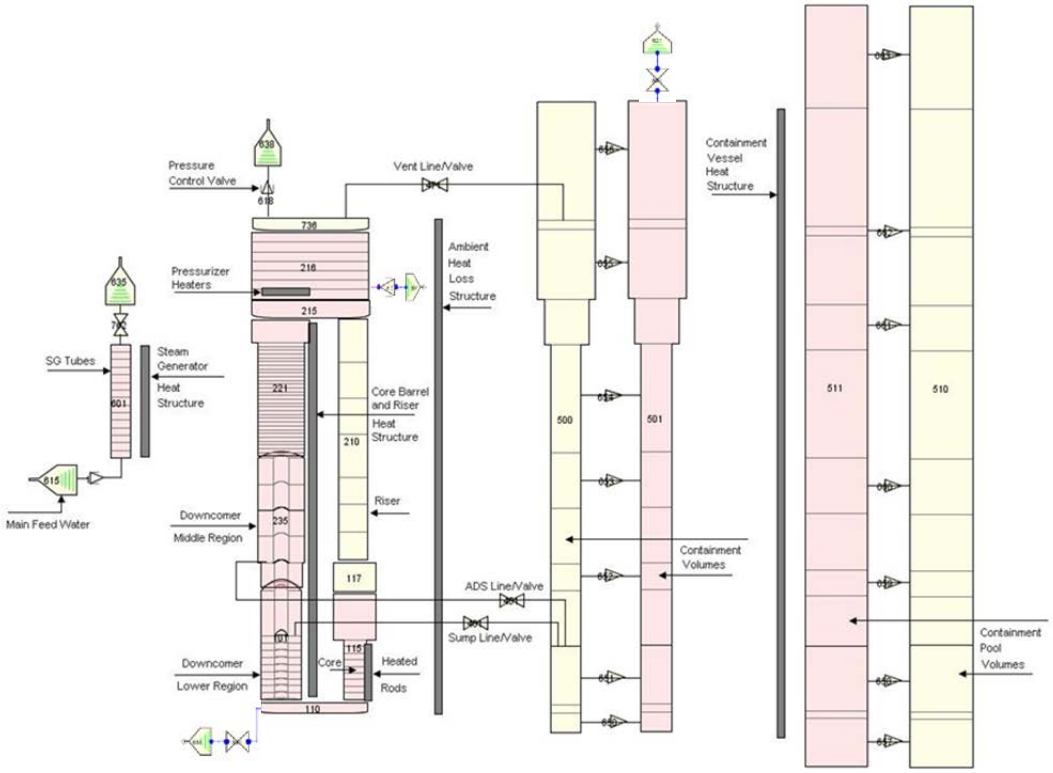

FIG. 4-283. Nodalization used for blind calculation.

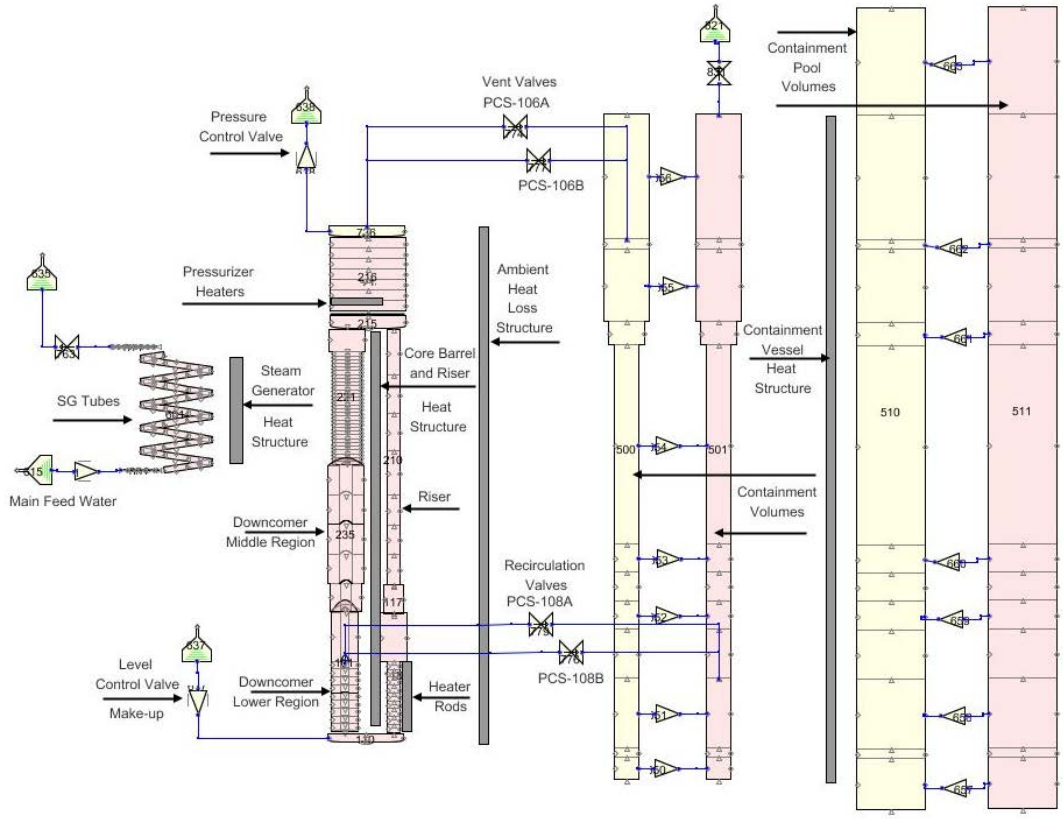

FIG. 4-284. Nodalization diagram for RELAP5 open calculations.

4.11.2.2. Modelling change for open calculation

The latest RELAP5 nodalization diagram used for the open calculations can be seen in Figure 4-284 and was generated using SNAP Version 2.1.3. The nodalization scheme has changed since the blind and double-blind calculation results. Changes made to the nodalization for the open calculations in comparison to the blind calculations include:

- The steam generator (SG) tubes are now modeled using an inclined single pipe with equivalent flow area and hydraulic diameter. The blind calculation nodalization scheme for the SG tubes used a vertical pipe.
- The number of nodes in the steam generator tubes has been doubled to 30 to match the number of nodes on the primary side.
- The main feed water and steam lines leading to and from the SG are now incorporated into the model.
- A check valve is placed at the exit of the steam line to model the back pressure control valve in the experiment and to prevent any back flow into the steam generator.
- The middle volumes of the containment and cooling pool have been lengthened to prevent solver issues related to non-condensable crossing volume boundaries.
- Errors found in the SG heat structure area have been corrected to reflect the experimental configuration.
- Both vent valves (PCS-106A, PCS-106B) and recirculation valves (PCS-108A, PCS-108B) are now modeled to reflect the experimental configuration.
- The main vent valve (PCS-106A) has been modeled as an actuated motor valve as opposed to a trip type.
- The flow area and heat structure area of the SG has been reduced to reflect the plugged outer SG tube in the facility.
- A level control system has been added to inject water if the water level falls below the pressurizer (PZR) heaters. This system is not used in this analysis.

4.11.3. Analysis results for loss of feed-water transient

The initial conditions were obtained by running identical RELAP5 models with steady state control logic. The main feed water mass flow rate was adjusted manual in an attempt to match conditions such as steam superheat to that of the experimental data. The initial conditions for all components were then imported into the transient model using SNAP, and the transient cases were then calculated. The loss of feed water transient SP-2 results are presented in the form of a table listing the time of major events (Table 4-26) and multiple figures showing thermal-hydraulic behavior for the different major components of the system in the following sections. The time sequence of events is referenced to time zero which indicates when the main feed water pumps stopped. As can be seen in Table 4-26, the time sequence of events for the open calculation results more closely represents the experiment than does the blind calculations. The most noticeable difference is the timing and number of times that the vent valve PCS-106A is opened and closed. While the open calculation predicts 9 more opening and closings, the timing of other major events is closely predicted by the open calculation results. The end of test conditions was never reached by either the experiment or calculations results and is represented by NA. The same is true for the opening of the safety-valve SV-800. More detailed analysis of the SP-2 open calculation results regarding the different components of the experimental facility (RPV, SG, HPC, CPV) is given in the following sections.

TABLE 4-26. SP-2 TIME SEQUENCE OF EVENTS

Event	Experiment Time (s)	NUSCALE (Blind) Time (s)	NUSCALE (Open) Time (s)
Stop MFP Close HPC vent valve SV-800	0	0	0
PZR pressure (PT-301) reaches 9.064 MPa(a) (1300 psig): - Enter decay power mode	~ 40	28	26
De-energize PZR heaters Open ADS vent valve (PCS-106A)	~ 48	46	44
Record opening and closing times for SV-800	NA	NA	NA
Start long-term cooling when pressure difference between primary system and HPC (PT-301 minus PT-801) becomes less than 5 psi (0.034 MPa): - Open and remain open of PCS-106A and PCS-106B - Open and remain open of PCS-108A and PCS-108B	~ 4024	552	3998
End of test when one of the following conditions is reached: - PZR pressure ≤ 0.135 MPa(a) (5 psig) - Primary coolant temperature (TF-132) ≤ 35 ºC (95 ºF) - 24 hours have elapsed	NA	NA	NA

4.11.3.1. RPV thermal-hydraulic behavior

In the following figures, the feed water flow is isolated (Stop MFP) at 0 s, which corresponds to time 0 in the time sequence of events, Table 4-26. At 0 s, the main feed pump is stopped and the pressure increases until the blowdown event is initiated by opening of the depressurization vent valve PCS-106A. Before PCS-106A is actuated, and 18 s after the pressurizer pressure reaches 9.064 MPa(a), the heater rods are entered into a decay mode operation.

As can be seen in Figure 4-285, there is a large initial pressure decrease during the first opening of the vent valve. The containment pressure increases to its upper limit of 1.825 MPa(a) during this same period, and the PCS-106A valve is closed until the pressure in the containment reduces due to steam condensation to its lower set point of 1.480 MPa(a). The pressure for the experiment and the blind and open calculations follow this protocol. The predicted primary pressure, however, is dramatically different between the blind and open calculations. This is primarily due to the correct modelling of the secondary side steam flow as well as corrections to errors in the heat transfer area and coefficient of the SG. The open calculation results show good agreement with the experiment, with the exception of the first few openings of the valve. Also, there is a slightly lower pressure predicted during the long term cooling. The initial pressure difference may be due to the models in-ability to properly predict liquid entrainment and two-phase choking at PCS-106A, as indicated by the pressurizer liquid levels, or slight differences in condensation rates in the containment. The experiment may very well have a higher initial condensation rate than predicted by RELAP5 which allows the RPV to lower its pressure slightly further before the HPC pressure increases to its set point. The difference in long term cooling pressure is most likely due to a slight difference in the predicted energy losses from the reactor pressure vessel. The code may predict slightly larger heat loss, however there is no experimental data available from this experiment to directly quantify this heat loss.

As can be seen in Figure 4-286, the liquid levels of the open calculation show much better prediction of the liquid levels when compared to the blind calculations. Initially, the pressurizer pressure increases mostly due to expansion of the liquid as well as possible swell due to phase change in the hottest parts of the RPV. As the valve is opened and the RPV depressurizes, naturally the pressurizer level decreases until it is emptied of liquid. During the same time, the RPV level shows similar trends to the pressurizer, until the recirculation valves are opened and water rapidly enters the RPV

increasing the level indication. As the steam is condensed the HPC level increases until the recirculation valves open at which point the levels start long term steady cooling. The water levels remain slightly apart during long term cooling possibly due to losses acquired across the lines between the RPV and HPC, which are not modeled. The CPV water heats up slightly which causes a very small increase in the water level due to fluid expansion.

Arguably, the most important parameter in this blowdown transient is the RPV fluid temperatures. These temperatures will determine the fluid properties which in turn determine the choking flow rate through the valve as well as the pressure response of the containment volume. The core outlet temperature predictions along with experimental data are seen in Figure 4-287. Again, it seems that the long term cooling and heat loss of the experiment may be over predicted by the open calculations. The large bumps in the blind calculation results around 8000 s are due to errors in the modelling of the secondary which allowed fluid to flow back into the steam generator adding energy to the system which was not physically possible in the experiment. Also, a level tracking model was applied to the containment volumes which provided for a more accurate prediction of water level and pressure in the containment, which is required during long term cooling in order to properly predict the direction of flow in the natural circulation loop between the RPV and HPC. As can be seen in Figure 4-288, the temperature rise across the core is very comparable to the open calculations. The large spike between 4000 and 6000 s is due to the flow of the much cooler HPC water into the downcomer region of the RPV. The thermocouple in the experiment measures a much cooler local liquid temperature, where as the code determines a volume averaged temperature which explains the difference in magnitude of the open calculations and experiment. Again, the blind calculations do not predict the trend of the data due to differences in the heat transfer to the secondary and the water level prediction in the containment.

The core natural circulation flow rate can be seen in Figure 4-289 which shows the open calculation and blind calculation results. There is no experimental data available for this parameter, however it can be seen that at the instant the blowdown begins, the natural circulation flowrate is interrupted and stops completely. Whether or not the flow is reversed cannot be determined from this particular analysis, however this should be investigated further. During the opening and closing period of the vent valve oscillatory behaviour is seen as expected due to thermal equilibrium conditions between the riser and downcomer. Also, the long term cooling shows oscillations which could be due to an imbalance of steam generation and condensation rates. It is expected that the flow rate found in the experiment is similar in magnitude and behaviour to that of the open calculation.

The flow rate through PCS-106A is seen in Figure 4-290. Again, no test data is available, but the trend of the calculation is expected to be similar to that of the experiment. As the pressure in the RPV decreases so does the flowrate associated with each opening of the vent valve. The flow rate decreases substantially when the HPC and RPV pressures equalize and PCS-106B, as well as PCS-108A and B open. A narrow range plot of the PCS-106A flow rate is shown in Figure 4-291. As can be seen the flow begins near 44 s in the simulation, near that of the experimental value of 48 s. Also, the final closing predicted in the open calculation is similar to that of the experiment, near 4000 s. One difference is the number of openings. The open calculations predict 9 more openings than that of the experiments. This difference is mostly accounted for early on in the transient, during the first few openings.

Temperature variation in the downcomer can be seen in Figure 4-272. Again, the temperature range and trends are predicted well by the open calculations, however there is some differences in magnitude most likely due code averaging, whereas the thermo-couple measurements are local. The differences in temperature are small and could also be corrected by more accurate prediction of the core temperature heat transfer characteristics of the SG and RPV.

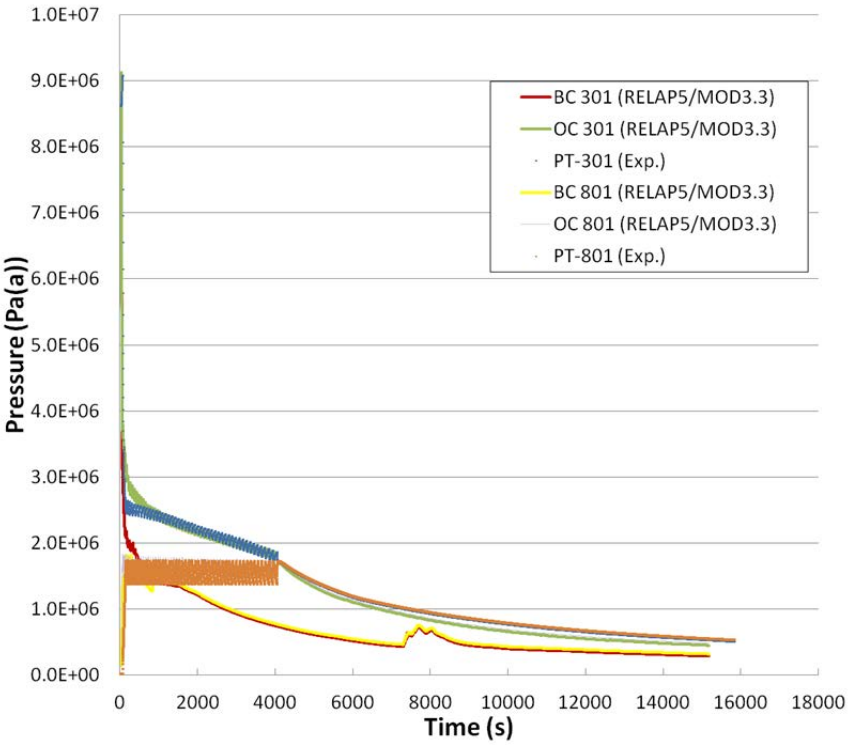

FIG. 4-285. Pressurizer pressure (PT-301) with HPC pressure (PT-801).

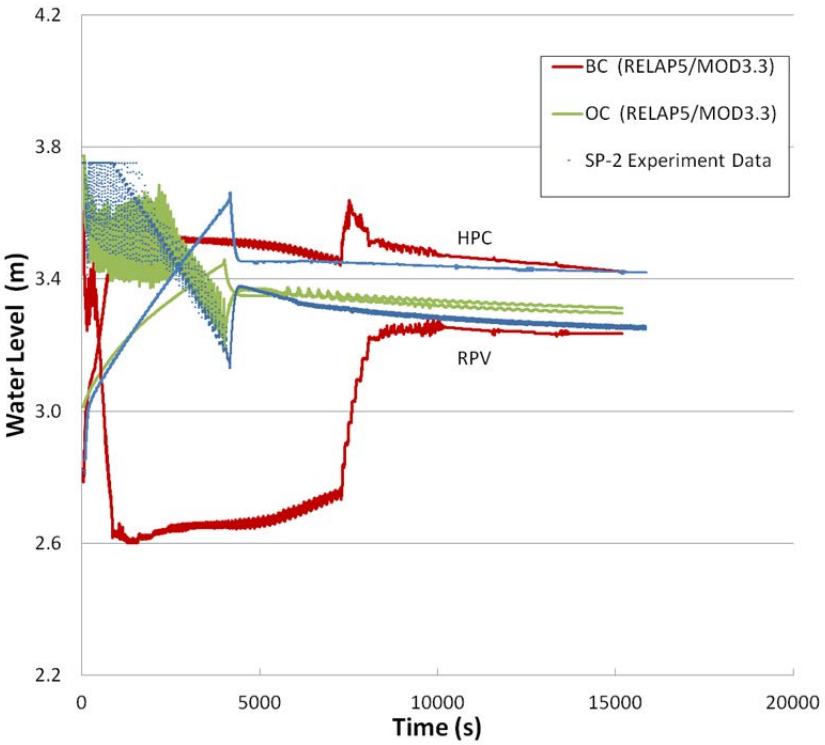

FIG. 4-286. RPV and HPC collapsed water levels.

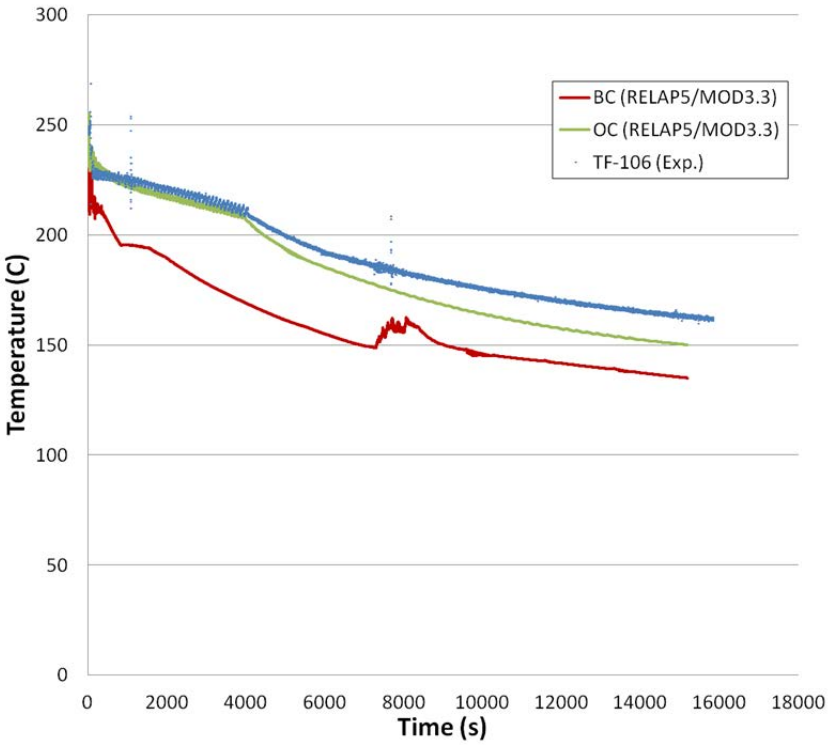

FIG. 4-287. Core outlet fluid temperature.

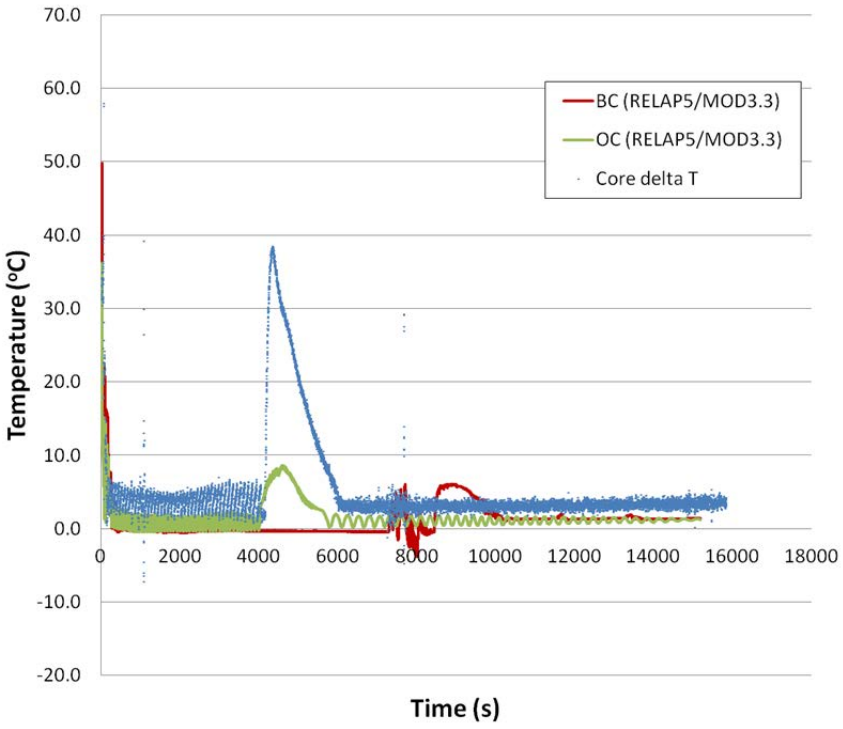

FIG. 4-288. Temperature rise across the core (TF-106 minus AVG(TF-121 to TF-124)).

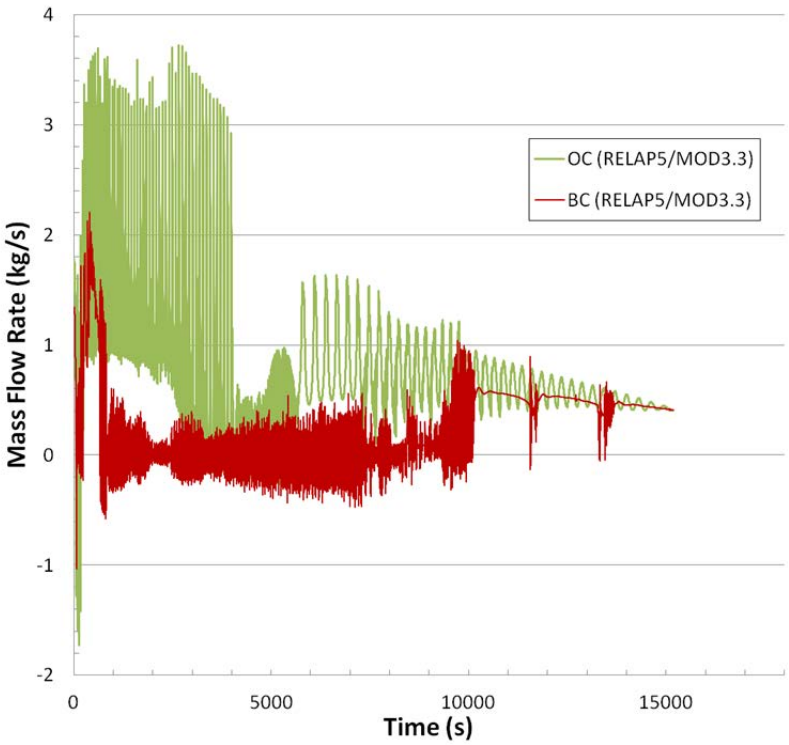

FIG. 4-289. Primary system flow rate.

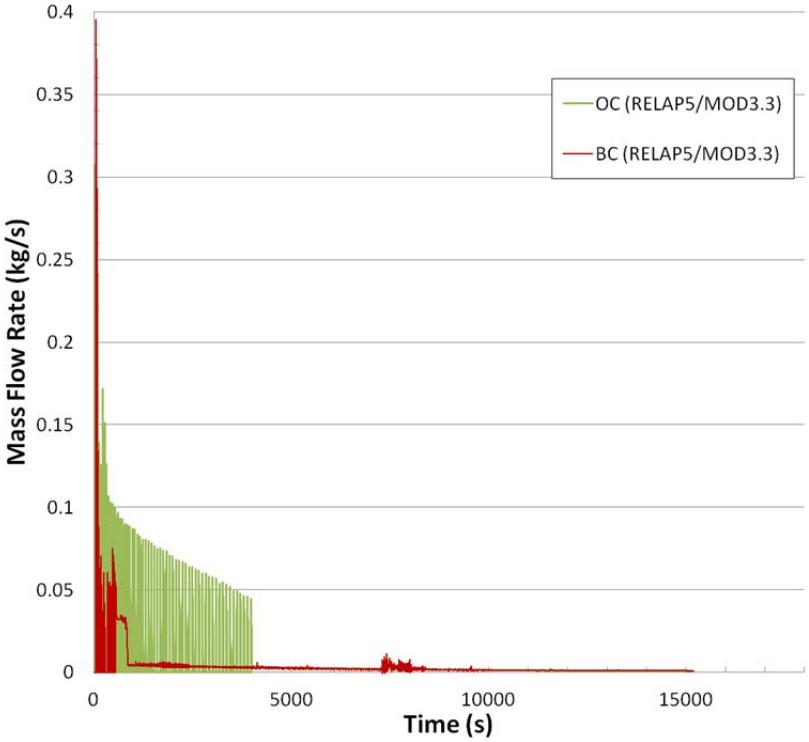

FIG. 4-290. ADS vent valve PCS-106A flow rate.

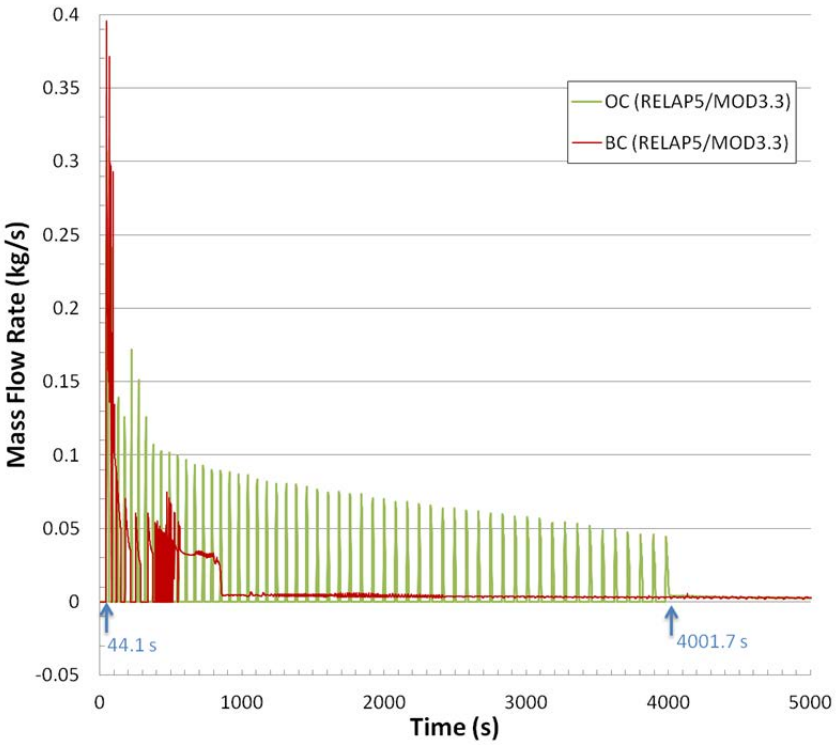

FIG. 4-291. ADS vent valve PCS-106A flow rate (short time scale).

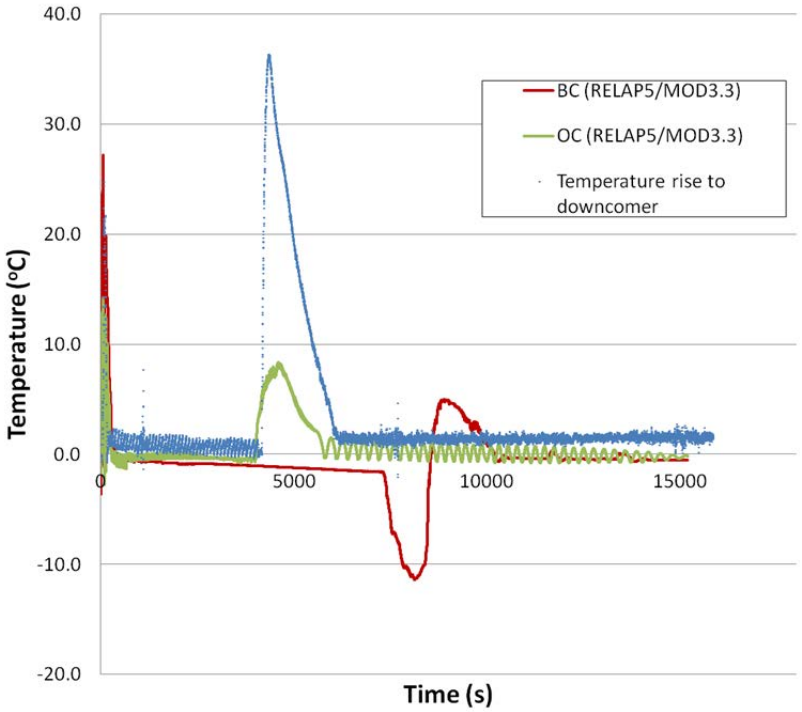

FIG. 4-292. Bypass heat transfer between riser and downcomer (AVG(TF-131 to 134) – AVG(TF-121 to 124)).

4.11.3.2. SG thermal-hydraulic behavior

The steam generator thermal-hydraulic behaviour is not well characterized by the experimental data. This is due to the fact that the steam pressure in the experiment is measured after a pressure regulating valve far downstream of the SG exit. These differences make it difficult to show the prediction capability of the model, and therefore the expected values for these parameters are plotted against the data available. These comparisons are not direct and therefore cannot be used to inform on the predictability or limitations of the model. The steam exit temperatures from the SG coils are shown in Figure 4-293. A lower steam exit temperature is seen in the experiment than that predicted. The difference in steam exit temperature predictions and experimental results may be due to a higher rate of boil off of the fluid remaining in the SG tubes under experiment conditions, or the heat transfer rate at the location of measurement. The pressure on the other hand is not suitable for comparison to the actual steam pressure in the SG tubes as shown by the open calculations results. Again, this is due to the location of the pressure measurement in the experiment which effectively removes it from other useful information. Figure 4-294 shows the open calculation expected pressures. This predicts that the steam pressure actual remains high during the boil off phase of the fluid remaining in the SG tubes, until eventually the pressure drop is determined by the heat loss of the fluid remaining in the SG tubes. According to the experimental setup, no flow out of the SG tubes would occur unless the pressure inside was higher than the set point (1.489 MPa(a)) of the pressure regulating valve at the exit of the SG, therefore forcing fluid to remain in the SG at all times. As seen in Figure 4-295, the feed flow is not well predicted in the blind calculation due to the before mentioned deficiencies in the model which allowed back flow into the SG tubes.

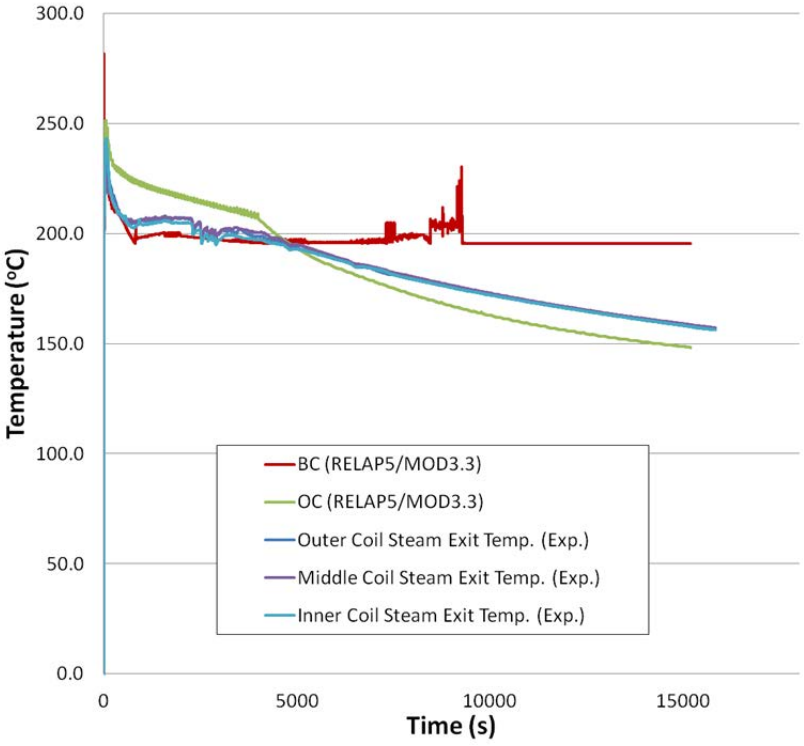

FIG. 4-293. Average steam exit temperature from SG coils.

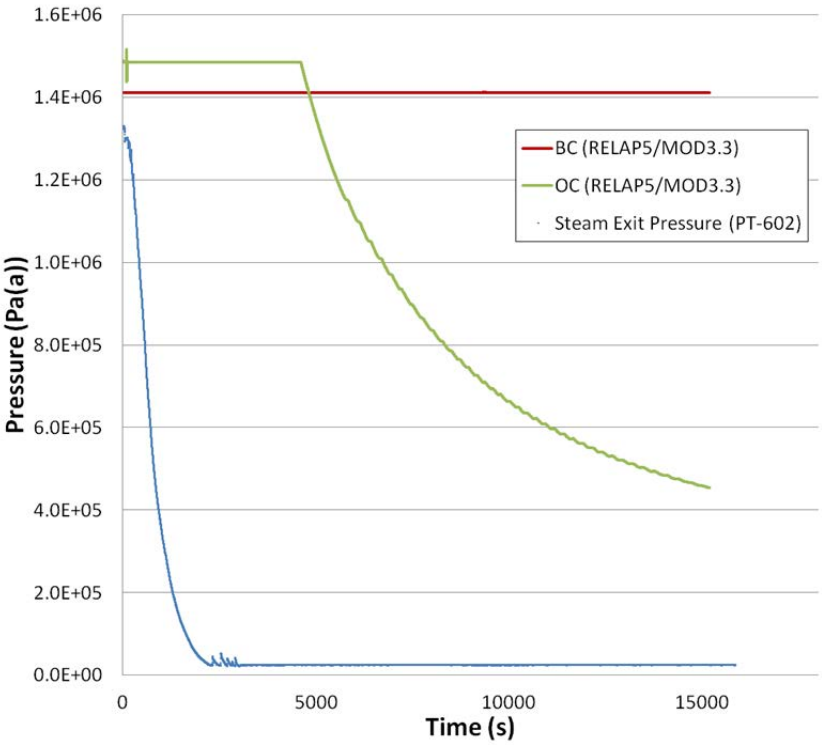

FIG. 4-294. Steam pressure (PT-602).

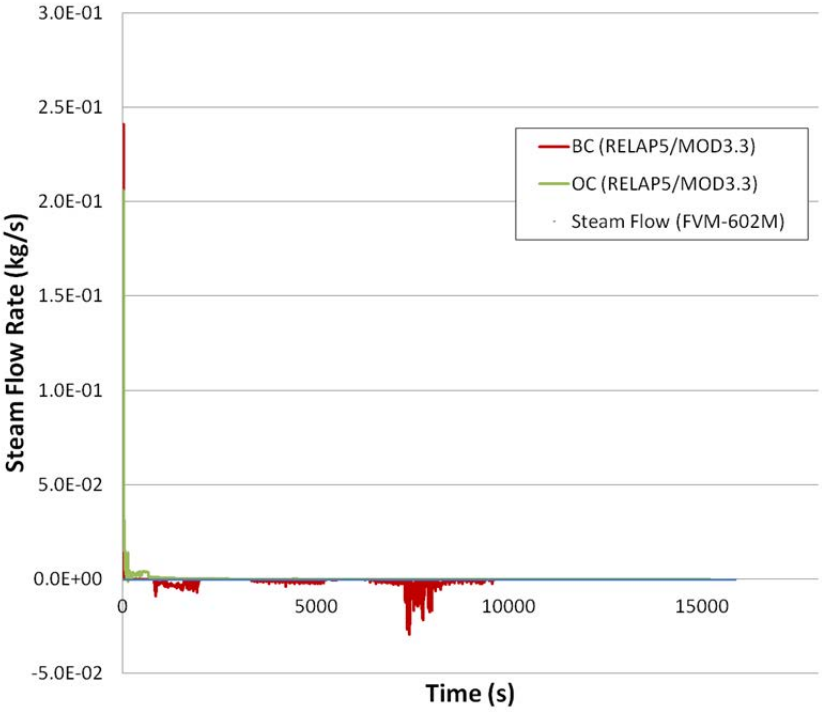

FIG. 4-295. Steam flow rate (FVM-602M).

4.11.3.3. HPC thermal-hydraulic behavior

Two figures are used to compare the experimental temperatures of the HPC fluid at different axial locations and those predicted by the open calculations. It is evident from Figure 4-296, that there is a large axial gradient in HPC temperature measurements. It is noticeable that the top few thermocouples TF-861, 851 and 841 are in the presence of steam from the blowdown process, while the lower two thermocouples are covered with the much cooler HPC water that was initially present at the beginning of the experiment. A concern might be that the thermocouples, especially in the steam volume are not measuring an average bulk fluid temperature and therefore cannot be well correlated with a one-dimensional volume averaged temperature as calculated by the RELAP5 code. In Figure 4-296, the upper thermocouples are measuring the steam to be approximately 150°C, which is approximately 50°C below saturation at the HPC pressure. It is likely, that these thermocouples are measuring the condensation film temperature on the wall of the heat transfer plate, and not the actual temperature of the steam present in the containment volume. The RELAP5 predictions of fluid temperatures at different axial locations along the containment are shown in Figure 4-297. These predictions show that RELAP5 predicts the bulk steam to be at or very near saturation temperature at the containment volume pressure. The condensate film thickness and temperature are not variables available for plotting in RELAP5. More thermocouple measurements would be required to accurately compare the experimental conditions involving fluid temperature in the containment to code predictions.

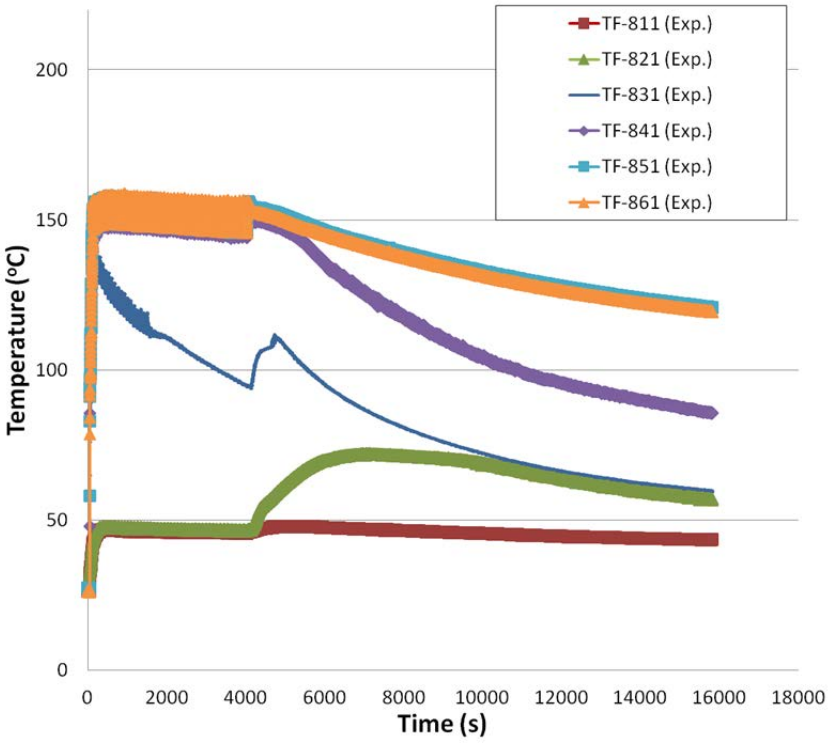

FIG. 4-296. HPC temperatures for SP-2 experiment.

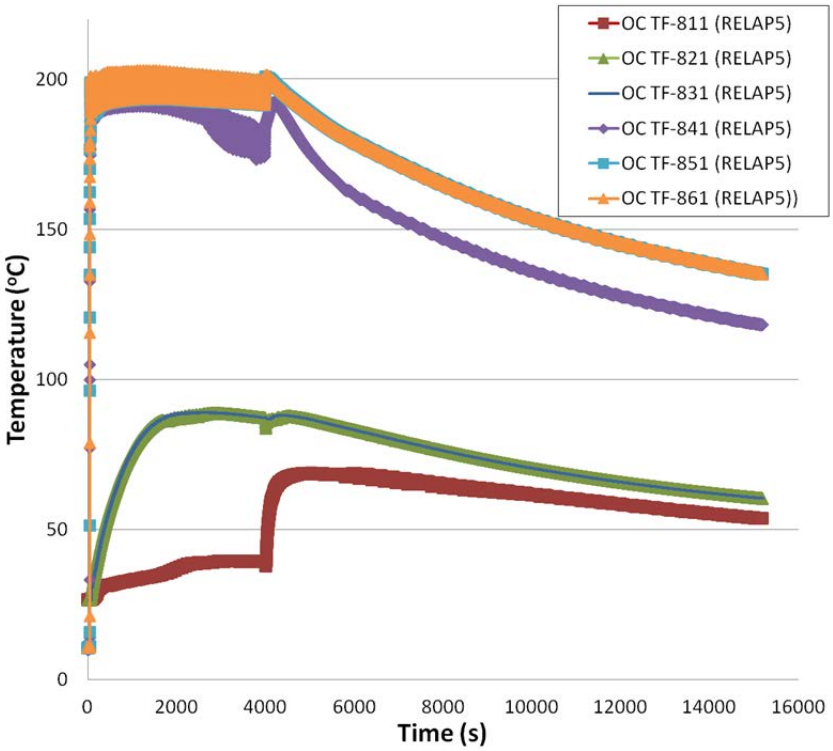

FIG. 4-297. HPC temperatures for RELAP5 Open Calculations.

4.11.3.4. CPV thermal-hydraulic behavior

Similarly, it is difficult and not advised to directly compare the thermocouple measurements of the fluid temperatures in the cooling pool to that of the code predictions. While overall trends may be similar, the temperatures measured and those calculated are not representative of each other. As can be seen in Figure 4-298, the cooling pool fluid axial temperatures measured increase with increasing height. The measurements do not show any obvious indications of thermal stratification. The code predictions however in Figure 4-299 indicate that the temperature increases with axial distance, however the 3 top thermocouples would read nearly identical fluid temperatures. This points to the possibility that thermal stratification may be present in the experiment, and that the thermal couple measurements are too close to the wall. It would be advised to increase the number of thermocouples in the fluid further from the wall allowing for a boundary layer quantification as well as an average fluid temperature.

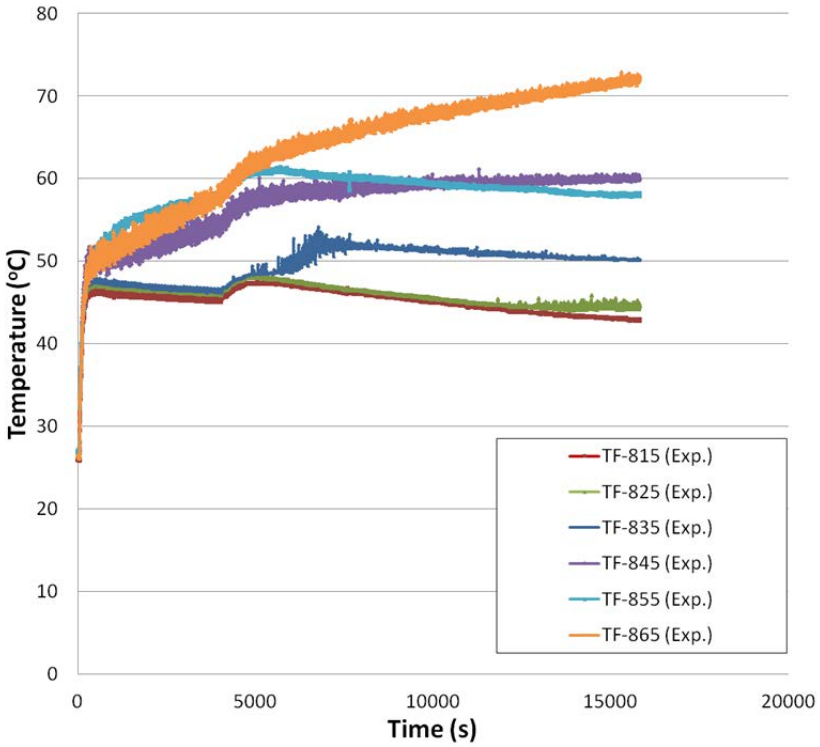

FIG. 4-298. CPV temperature for SP-2 experiment.

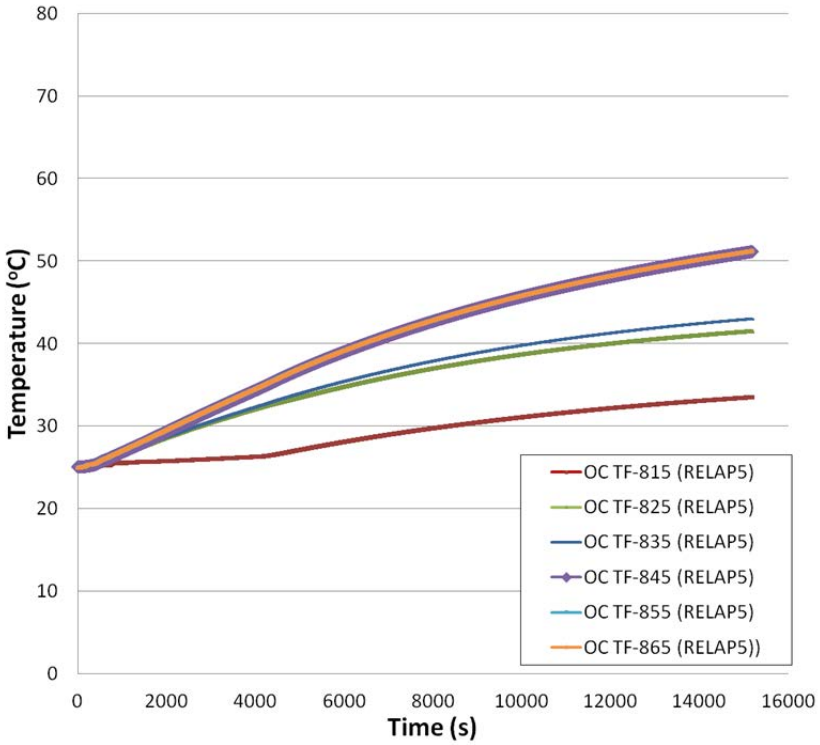

FIG. 4-299. CPV Temperature for RELAP5 open calculations.

4.11.4. Analysis results for power maneuvering

4.11.4.1. RPV thermal-hydraulic behavior

During this transient, core heater power is stepped up by approximately 40 kW from 40 to 320 kW according to provided data over approximately 6500 s. This is used as a boundary condition to the model input. The base main feed water flow rate is accordingly stepped from approximately 0.15 kg/s to 0.112 kg/s. The feedwater flow rate is given as a boundary condition and is consistent with the feedwater flow from the experiment as shown in Figure 4-300. Slight differences exist due to approximations made in tabular input versus time. The pressurizer pressure is seen in Figure 4-301. The blind calculation results had difficulty in controlling this parameter, whereas the open calculation is much improved. It seems as if the experiment was first being controlled by some RPV process measurement such as core exit temperature, and the steam superheat ignored. The steam superheat during the first half of the experiment was very large, and subsequently it was lowered. During this lowering it was necessary to inject make-up water to the RPV which is what caused the oscillations around 3000 s in the data seen here.

The pressurizer level is predicted well up until the completion of the water injected, after which the open calculation predicts a slightly lower value. It is unknown whether more water was injected which the authors were unaware of. This is one of the few possible explanations for the discrepancy in the PZR experimental water level and the open calculations. The RPV level indicates that the water level remained constant and above the baffle plate.

The heat transfer to and from the downcomer fluid is analyzed using the temperature difference between the fluid exiting the primary side of the SG and the lower plenum as seen in Figure 4-303. The open and blind calculation results are both able to capture the trend of the temperature difference well, however they both slightly underpredict the experimental values. This could be due to the models over prediction of the heat loss to the environment or over prediction of heat transfer to the SG secondary side. The core exit temperature predicted by the open calculation is nearly identical to that of the experiment at low powers, however at higher powers after the reduction in the steam superheat, the model predicts slightly higher core exit temperatures. Overall, the open calculation predictions are much improved over the blind calculations with only minor changes to the model, mostly related to the heat transfer to the secondary. As shown in Figure 4-305, the open calculation natural circulation flow rate in the primary compares well with the data. At the lower powers, the model has difficulty predicting the flow rate due to the fact that the model control system is tuned for full power operation, while some experimental parameters are adjusted manual. Also, the steady state condition predicted for the start of this transient may not have been observed in the experiment. This data is not available for comparison however. The changes in the steam superheat during the experiment are detailed in the next section.

4.11.4.2. SG thermal-hydraulic behavior

The adjustment of the steam superheat nearly half way through the experiment is dramatic and can be seen in Figure 4-306. Initially, the secondary was operated at near 60 degrees superheat, while the objective was to have near saturation conditions. This was adjusted by increasing the secondary flow, which increased the heat transfer to the primary, lowering the primary pressure and inherently the primary liquid level. This required cold make-up water to be injected to the lower plenum as described earlier. Again, the open calculations are able to predict this large swing in steam superheat well, while the blind calculations simply did not center around the same set points. The secondary steam mass flow rate is seen in Figure 4-307 and shows an increase in the steam flow as the power is increased. The data provided however seems to be in error possibly caused by a measurement hardware malfunction.

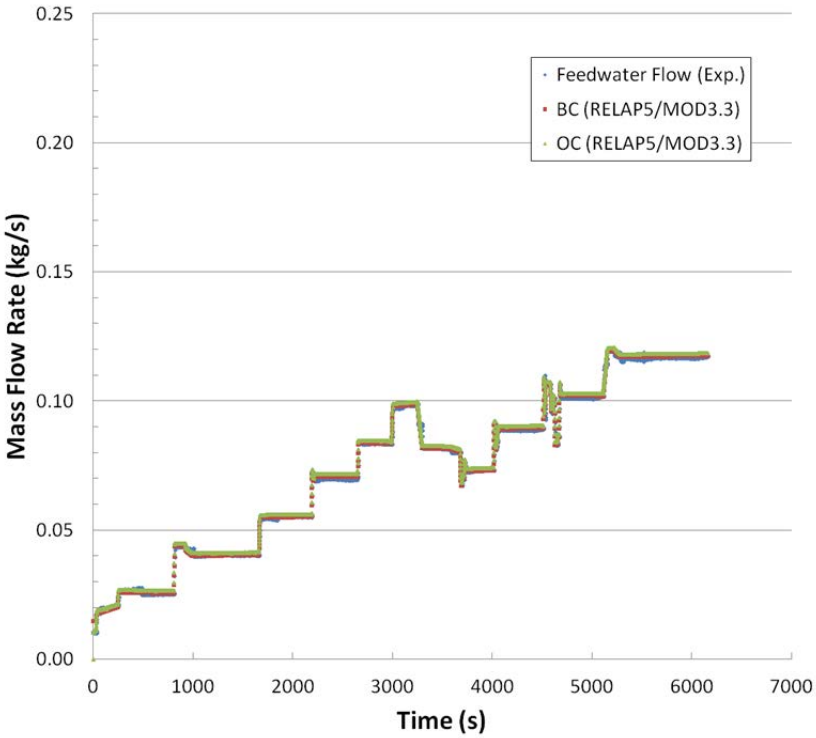

FIG. 4-300. Main feed water flow.

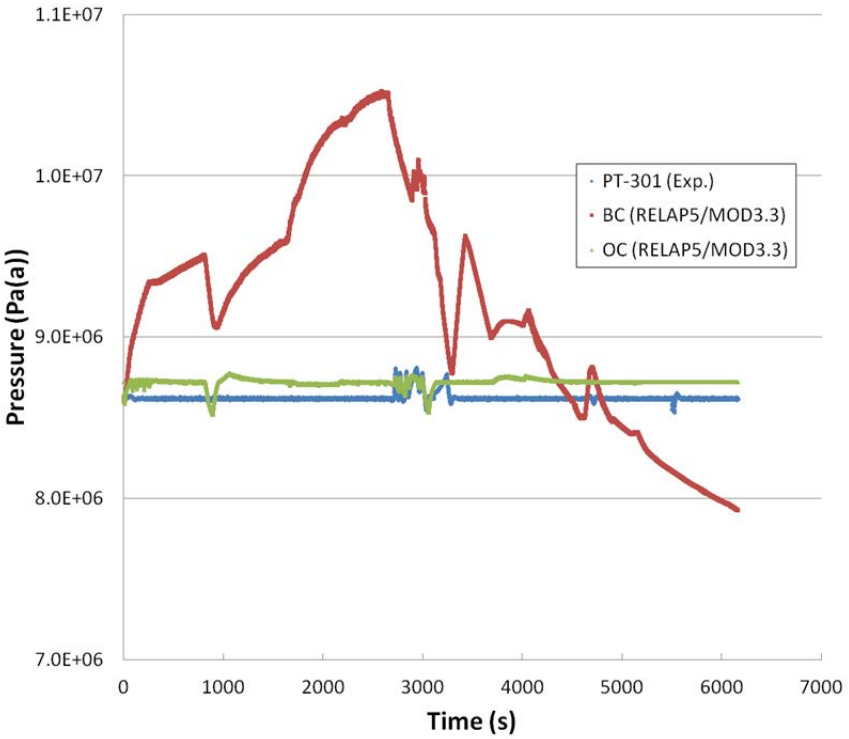

FIG. 4-301. Pressurizer pressure (PT-301).

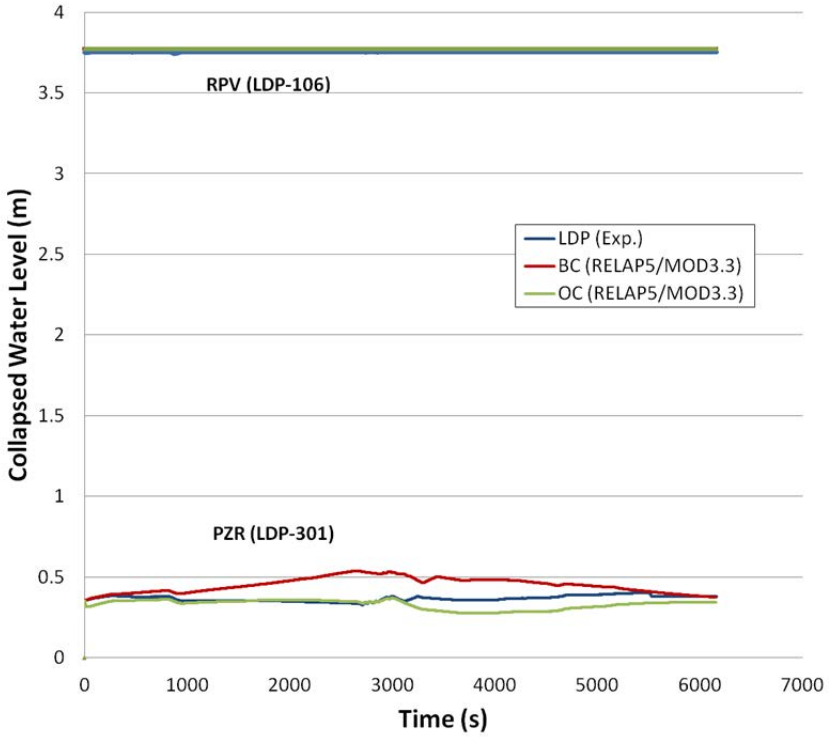

FIG. 4-302. Pressurizer and RPV collapsed water levels.

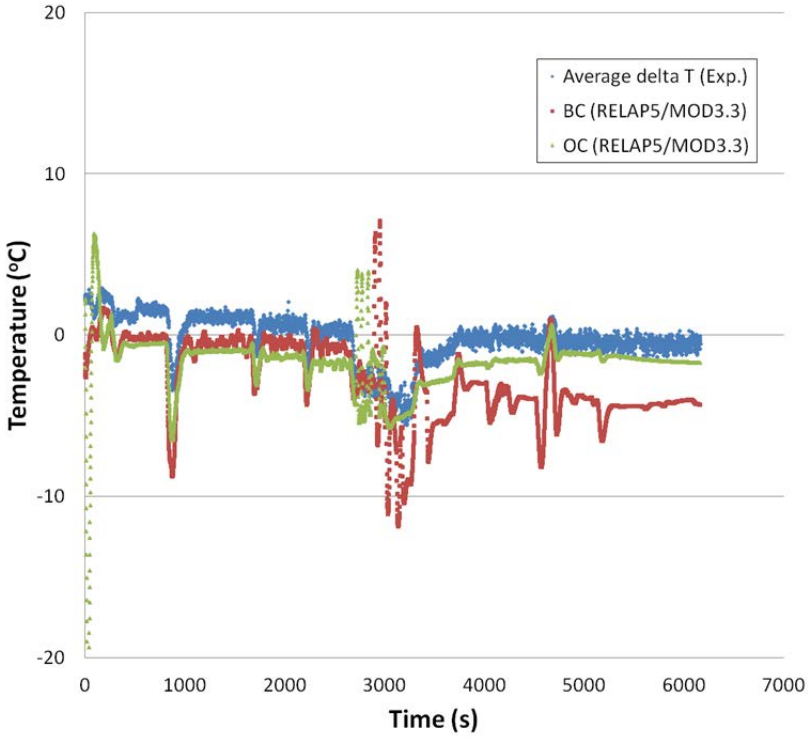

FIG. 4-303. Temperature difference between riser and downcomer.

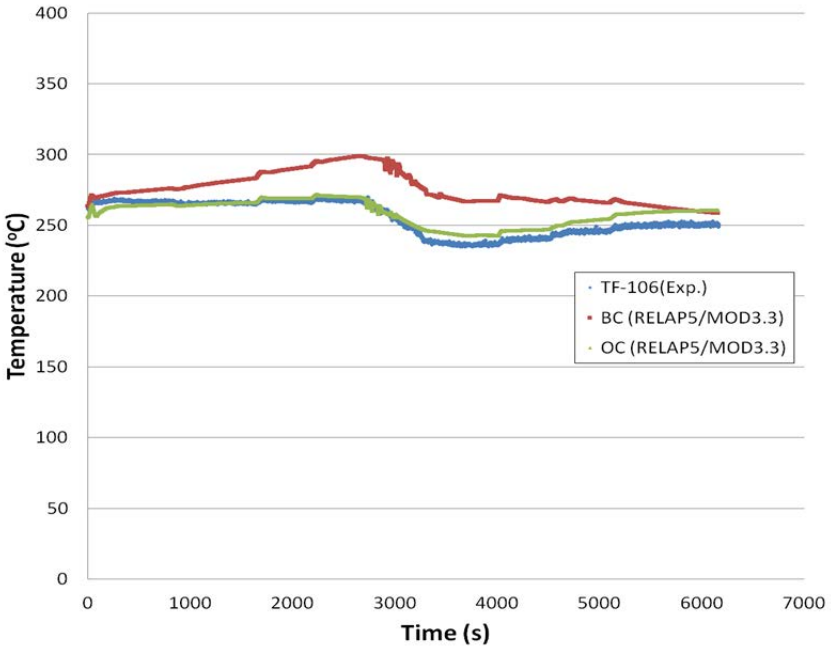

FIG. 4-304. Core exit temperature.

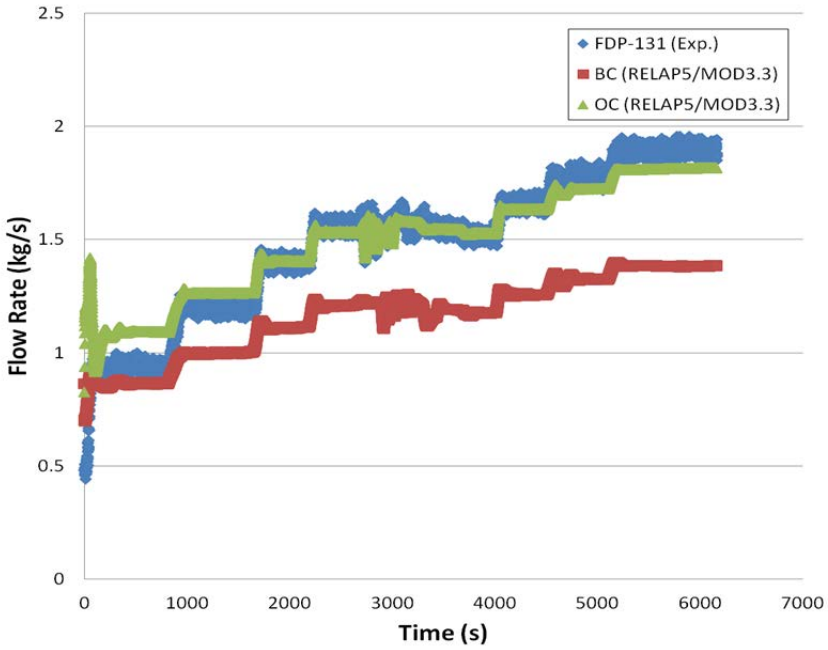

FIG. 4-305. Primary natural circulation flow rate.

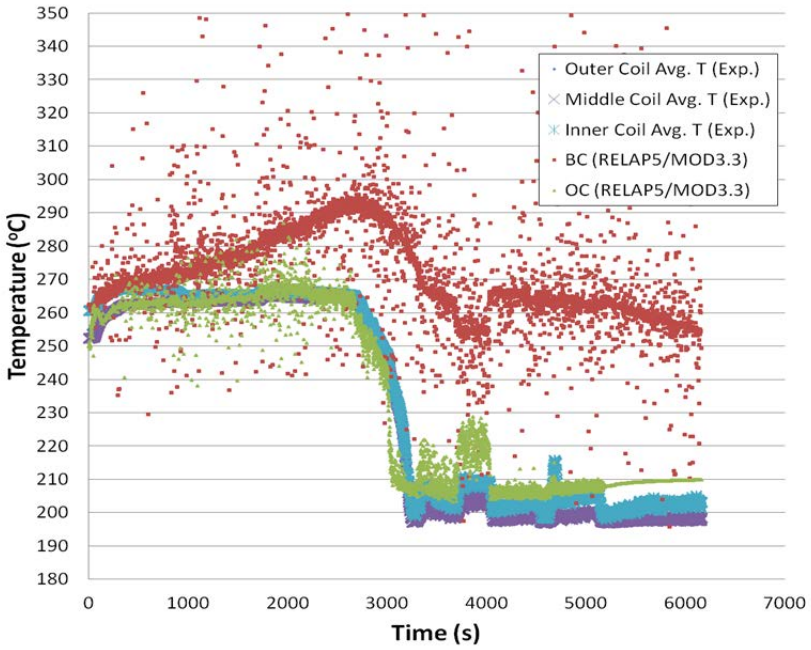

FIG. 4-306. Secondary steam temperature.

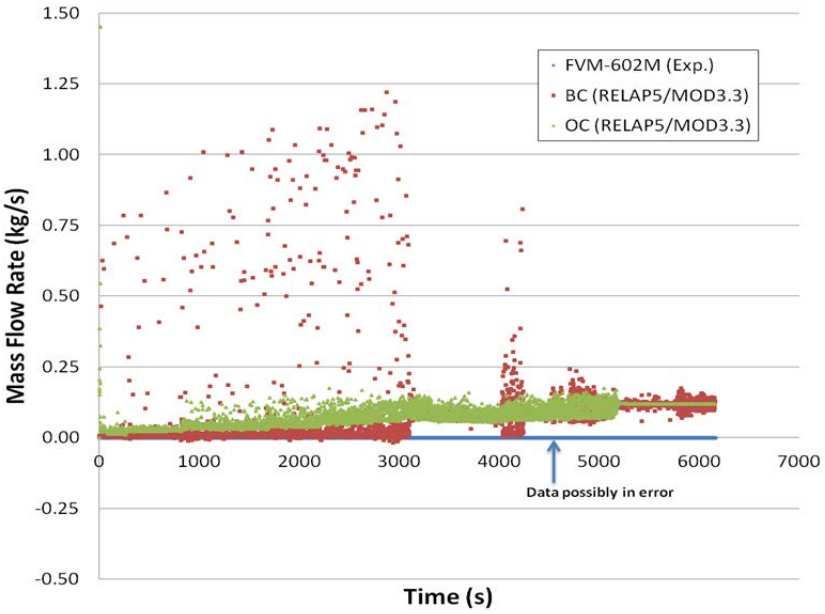

FIG. 4-307. Secondary steam mass flow.

4.12. BARC (CATHARE) - INDIA

4.12.1. Computer code

The calculations for IAEA ICSP on OSU MASLWR tests SP-2 and SP-3 have been carried out using computer code CATHARE (mod 2.1, version 25_1). CATHARE is extensively used for the safety analysis of PWRs.CATHARE2 was developed by CEA (Commissariat à l'énergie atomique**,** France), EDF (French Utility) and FRAMATOME (French vendor). The CATHARE code includes several independent modules that take into account the mechanical and thermal non-equilibrium, which can occur during reactor transients. CATHARE has six partial differential equations representing conservation of mass, energy and momentum for vapor and liquid phases. The code solves the equations using a completely implicit numerical solution method. In addition, models concerning the mass, energy and momentum exchanges between the liquid and vapor, and between the two phases and the pipe walls, have been added to the code [27].

4.12.2. System idealization

The CATHARE model for the test facility is shown in Figure 4-1. The detailed geometrical data used to develop the numerical model is compiled from the OSU MASLWR test facility description [4].

4.12.2.1. System Idealization for blind calculation

The different MASLWR regions are modeled with AXIAL and VOLUME type of elements in CATHARE. These are 1-D elements. The AXIAL element is specified with different scalar points along the length of element. The segment between two scalar points is further divided into number of volumes. The geometrical data (cross-sectional flow area, hydraulic diameter, orientation, etc.) is entered for each segment of the AXIAL. VOLUME type elements represent single vertically oriented volume and can have different flow area along the height. The geometrical data for VOLUME element is entered for the scalar points along the height of the volume. The Reactor Pressure Vessel (RPV) is modeled with circuit of AXIAL and VOLUME elements as shown in Figure 4-308. The lower plenum is modeled with VOLUME connected to two AXIAL elements at the top which represent the hot leg and cold leg. Lower plenum volume is connected to AXIAL element at the bottom representing the drain line. The drain line is used to transfer inventory from RPV to the atmosphere. The AXIAL elements representing hot leg and cold leg are connected to single volume at the top representing the upper plenum. The upper plenum volume is connected to pressurizer, modeled with AXIAL element at the top. The core heater is modeled as lumped 1-D AXIAL volumes; however 57 identical heat structures are modeled representing the heater rods. The High Pressure Containment (HPC) and Cooling Pool Vessel (CPV) are modeled with vertically oriented AXIAL elements (1-D). The hot leg of RPV and HPC are connected by six AXIAL elements representing the Automatic Depressurization System (ADS) vent line (2 nos.), blow down line (2 nos.) and sump return line (2 nos.).

The secondary side (helical coil steam generator) is modeled using circuit of AXIAL elements representing the three different coil groups (Inner, Middle and Outer) connected to flow line from pump and steam bustle. To simulate the cold water injection in the lower plenum a SOURCE component is used in the model and is connected to volume representing lower plenum.

The loss coefficients are calculated based on abrupt area change between the junctions/scalar points in the element. Loss coefficients based on the experimental measurements [19] are also considered. The details are given in Table 4-27.

The various valves in the system are modeled at the element junctions using VALVE directive in CATHARE. The VALVE directive modifies the loss coefficient at the specified junctions to simulate the closure and opening of the valve. For the valves in the ADS lines the closure is assumed to take place in duration of 1.0 s. The loss coefficient for fully open condition is 0.0.

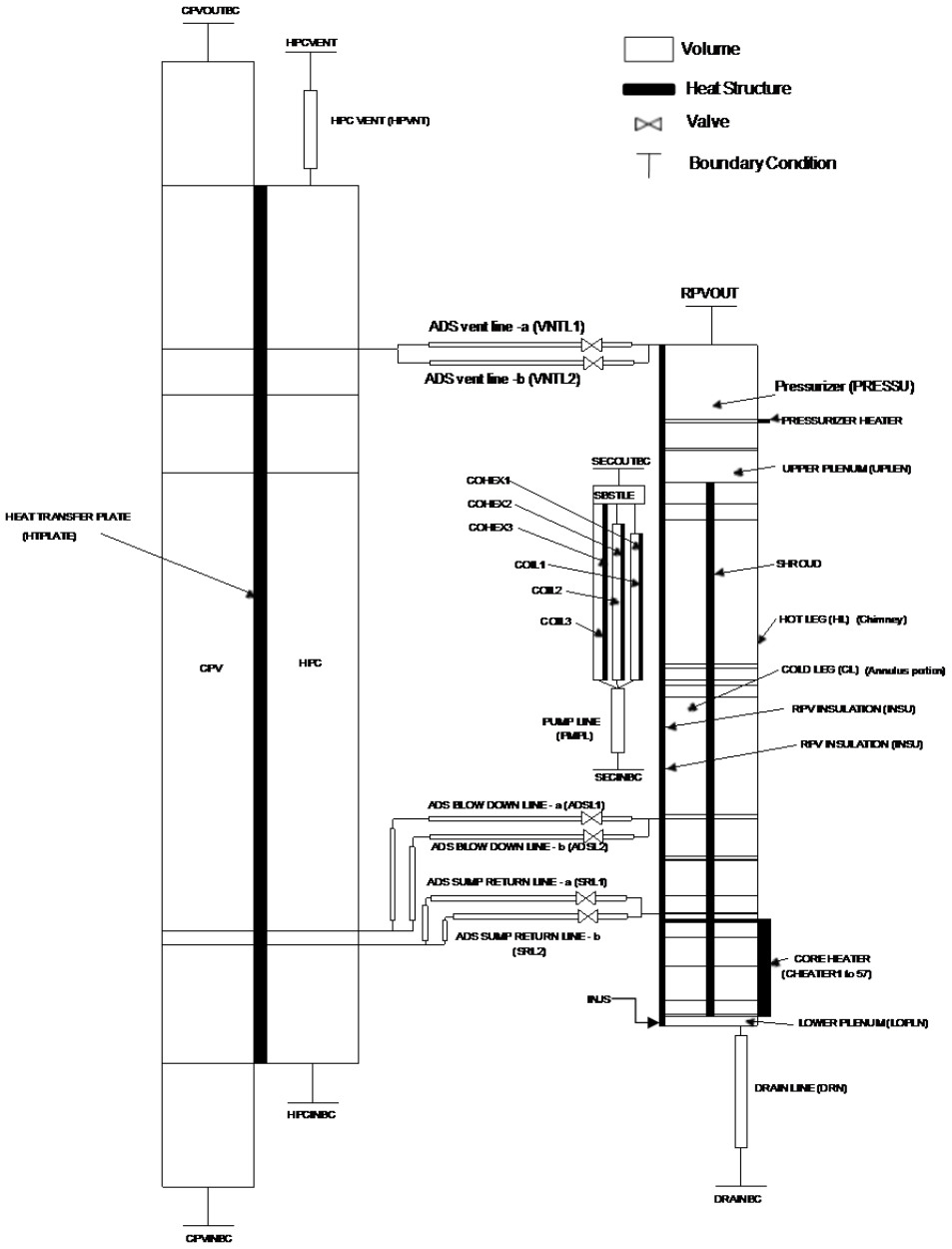

FIG. 4-308. OSU MASLWR facility nodalization.

The heat transfer from core heater to hot leg and hot leg to ambient is modeled using WALL directive. 57 heat structures are modeled simulating the heater rods. The power of each heater rod is manipulated using LAW directive of CATHARE. The pressurizer heater is modeled using WALL directive. The control logic of pressurizer heater is simple step input of 12kW power when RPV pressure falls below the desired test pressure. If RPV pressure is above the desired pressure level, PZR heaters are turned OFF instantaneously. Heat transfer from hot leg to helical coil steam generator, hot leg to cold leg of the RPV, and HPC to CPV is modeled using EXCHANGER directive of CATHARE. Heat loss from HPC and CPV and blowdown lines to atmosphere is not modeled. The material properties for heat structure with stainless steel are available in materials library of CATHARE, hence not entered explicitly. However, for Thermo-12 insulation the material properties were entered by modifying the CATHARE subroutine in FWMAXX.f.

Table 4-28 gives the detailed description of boundary conditions used in the model.

TABLE 4-27. LOSS COEFFICIENTS CONSIDERED IN THE MODEL

Section	Loss Coefficient	
	Blind	Open
Core inlet	171.1	171.1
Core to hot leg cone	3.2	3.2
Hot leg cone to chimney	21.5	21.5
Chimney outlet to SG shell	257.2	257.2
Downcomer to lower plenum	778.0	778.0

TABLE 4-28. BOUNDARY CONDITIONS

Name	Type	Description
DRAINBC	PIQBRK (OPEN and CLOSE)	This simulates a break in the pipe with specified downstream conditions.
RPVOUT	BLIND	Closed top end of RPV
HPCINBC	BLIND	Closed bottom end of HPC
HPCVENT	PIQBRK (OPEN and CLOSE)	To simulate the venting of HPC.
CPVINBC	BLIND	Closed bottom end of CPV
CPVOUTBC	BC5A (Pressure as a function of time)	Maintains constant pressure (atmospheric) at CPC.
SECINBC	BC3E (Inlet type condition with specified mass flow rate as a function of time)	Simulated constant mass flow rate at inlet of the secondary coils.
SECOUTBC	BC4C (Pressure as a function of time with void fraction 1.0 at connecting junction)	Simulates the constant steam pressure at the secondary outlet.

4.12.2.2. Modeling change for open calculation

The loss coefficients were modified for open calculations. The loss coefficients based on the abrupt area change were calculated and added in input deck for blind calculations. These loss coefficients were removed in open calculations. Loss coefficients given in Table 4-1 were retained in open calculations.

The heat loss from RPV was thought to be the parameter affecting this and heat loss from RPV was modified by increasing the conductivity of insulation from 0.058 to 0.4 W/m-K. The heat loss from RPV to ambient thus increased from 1 to 5 kW approximately at core power of 40 kW.

4.12.3. Analysis results for loss of feed water transient

These calculations were not performed due to failure of code at the time of opening of RPV vent valve for depressurization.

4.12.4. Analysis results for power maneuvering

To achieve the initial conditions for the transient the RPV pressure and temperature was set as 8.72 MPa(a) and 250°C at all volumes in RPV, zero flow at all junctions and zero power for core heaters. The core heater power was raised to 40 kW and pressurizer heater was made active to maintain RPV pressure. The calculation was terminated when core exit temperature reached 262.9°C, thus matching with initial conditions of temperatures as per experimental data. Subsequently the power maneuvering and feed water flow rate variation was simulated by restarting the calculations. The injection of inventory at RPV bottom was modeled as per the given experimental data. Following are the observations on the thermal-hydraulic behavior during transient.

4.12.4.1. RPV thermal-hydraulic behavior

Figures 4-309 to 4-315 shows the variation of various RPV parameters during the transient. The steady state flow rate is observed to increase with increase in power and has good agreement with experiments in the initial stages. The RPV pressure was observed to increase above the nominal value of 8.72 MPa in single blind calculation, but with open calculation the RPV pressure agrees very well with experiment. This is due to additional heat loss from RPV. During time t = 2000 to 4000 s, the core power is kept constant but the secondary side flow rate is varied and the heat removed through SG is higher than 200 kW. This is observed to result into the temperature drop in the RPV as indicated by core outlet temperature. The decrease in temperatures cause the increase in the density of RPV fluid and the level in pressurizer is observed to drop. To avoid the level dropping below the chimney top, water was injected in the lower plenum during experiments. The sequence of injection of water leads to the change in the lower plenum temperatures which are reflected in the change in core outlet temperature. In natural circulation these perturbations are reflected in terms of system oscillations. The open calculation results have captured these perturbations qualitatively very well for core flow rate, RPV level and temperatures as seen from the results.

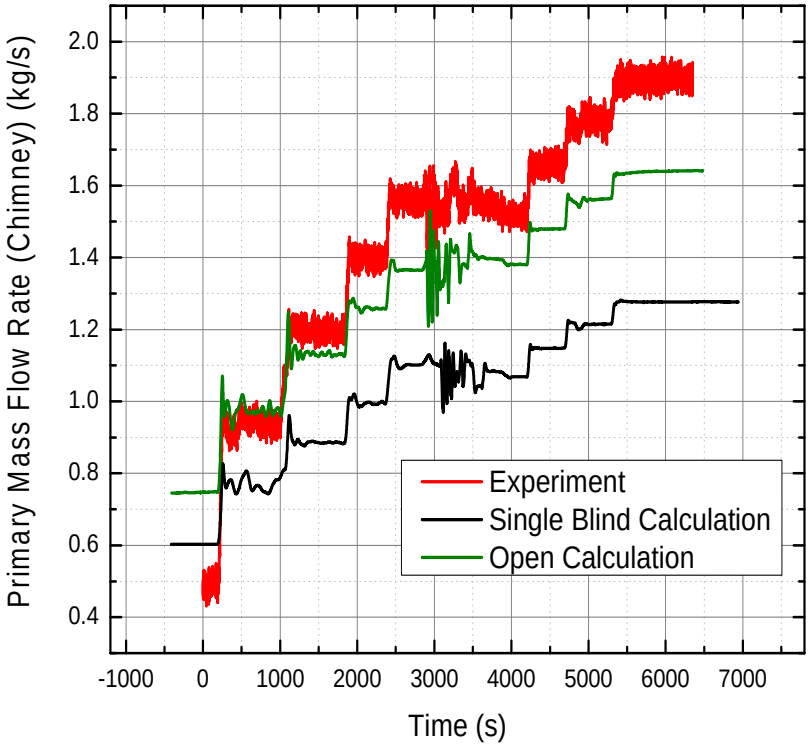

FIG. 4-309. Primary mass flow rate during power maneuvering transient.

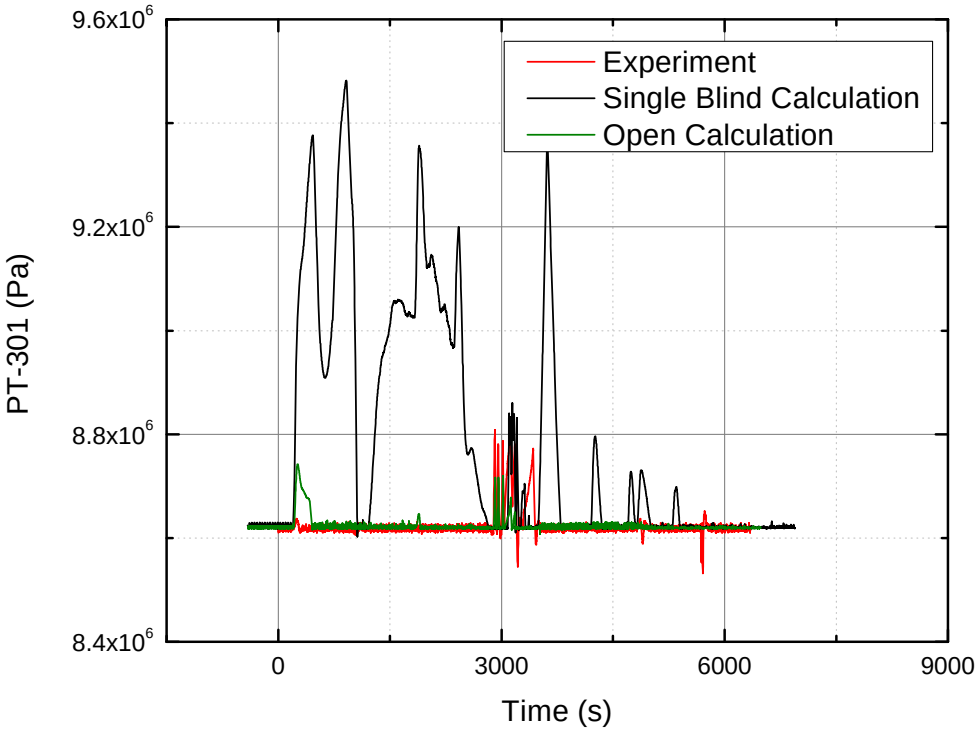

FIG. 4-310. RPV pressure during power maneuvering transient.

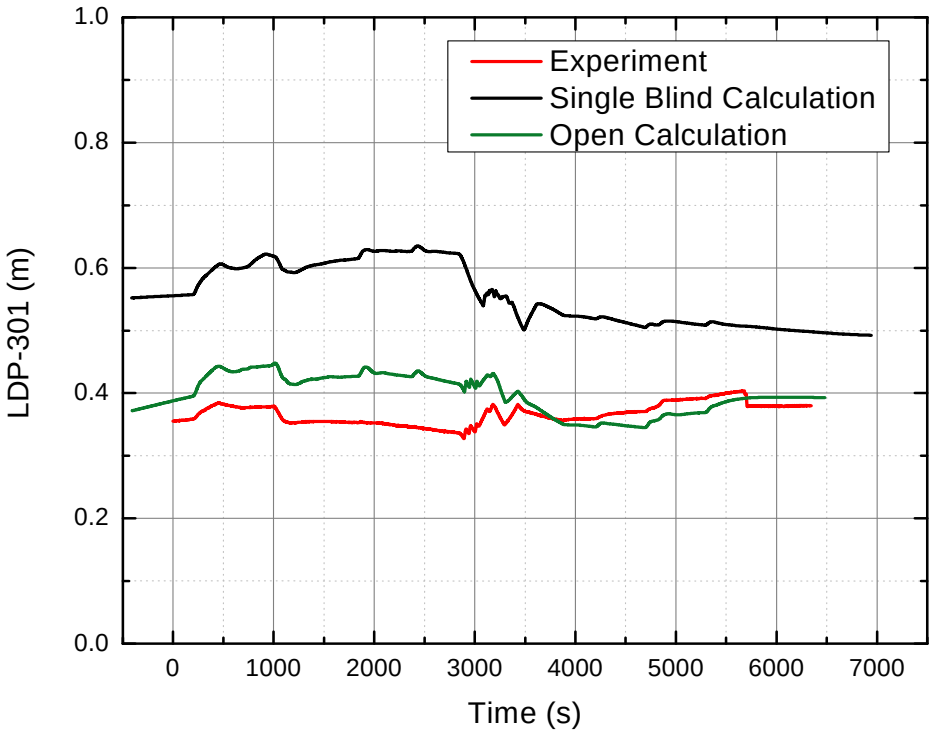

FIG. 4-311. RPV level during power maneuvering transient.

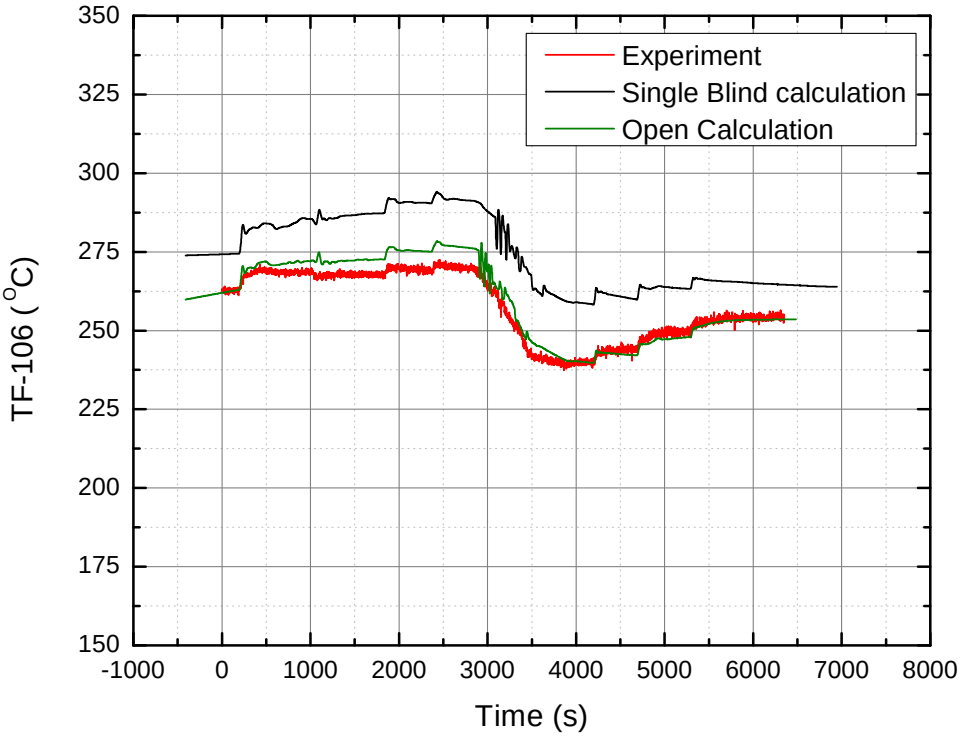

FIG. 4-312. Core outlet temperature during power maneuvering transient.

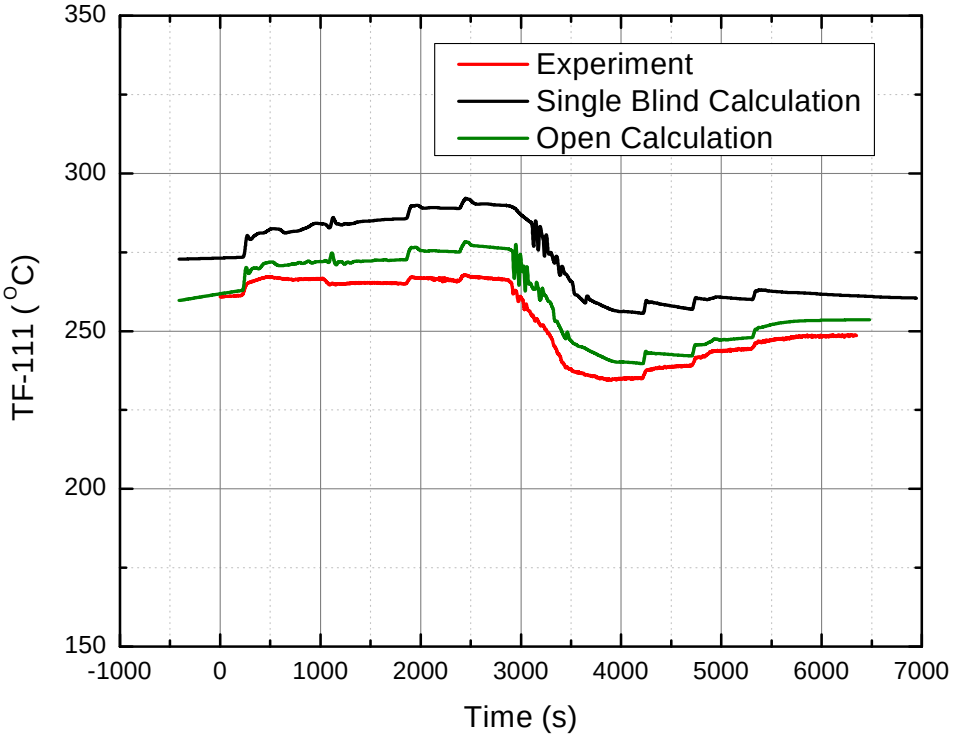

FIG. 4-313. Core inlet temperature during power maneuvering transient.

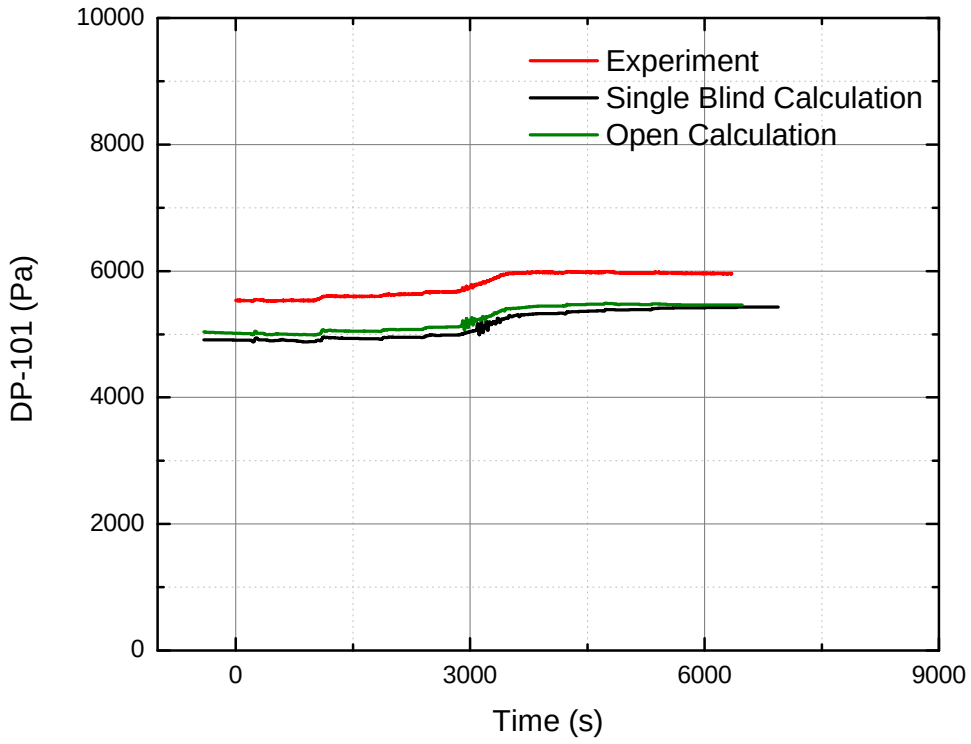

FIG. 4-314. Pressure loss in the core during power maneuvering transient.

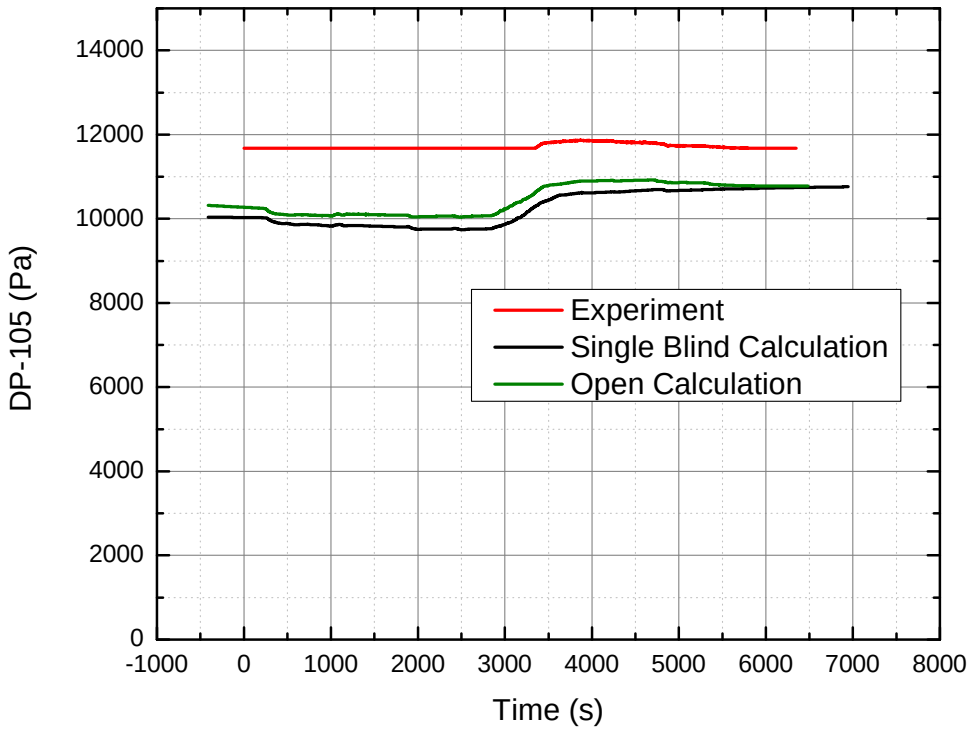

FIG. 4-315. Pressure loss in the steam generator coils during power maneuvering transient.

4.12.4.2. SG thermal-hydraulic behavior

Figure 4-316 and 4-317 show the variation of different SG parameters during the transient. The steam temperature at SG outlet depends directly on the feed water flow rate. The feed water is converted to steam completely i.e. flow quality of unity is achieved within short length of the SG coils (about 16% of the total length) and remaining length is used for superheating. The SG is modeled as three parallel coils representing the group of inner, outer and middle coils. The flow rate in individual groups is observed to be oscillatory. Though the sum of the flow rates remain positive, flow reversal is encountered by coils as shown by Figure 4-317. The Figure 4-318 shows the flow rate in individual coils, total feed water flow rate at the inlet and total steam flow rate at outlet (plotted over small interval between 1000 to 1040 s). It can be observed that the individual coil flow rates are oscillating out of phase with flow reversal, while the total steam flow rate and total feedwater flow rate are always positive. The three coils are having common inlet and outlet headers and the predicted behavior is typical of parallel channel instability. The predicted behavior might be purely numerical as experimental data do not show similar oscillations. It can be mentioned here that when the coils were lumped in to one channel, the flow was predicted to be stable and unidirectional. Further, in the present modeling no loss coefficients were assigned to the helical coils which could stabilize the flow.

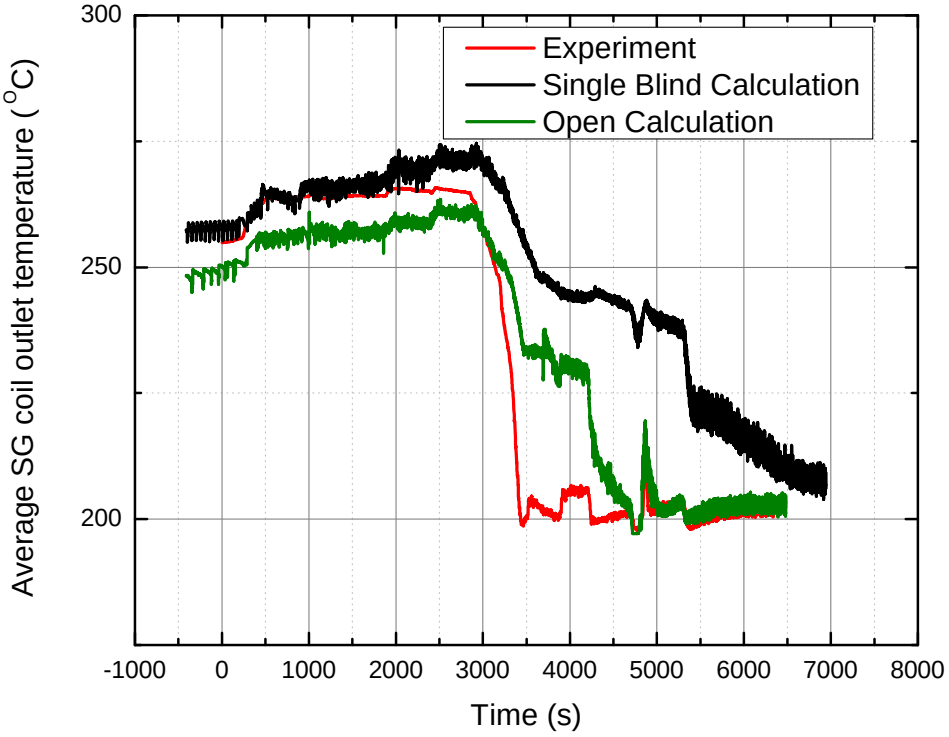

FIG. 4-316. Steam temperature during power maneuvering transient.

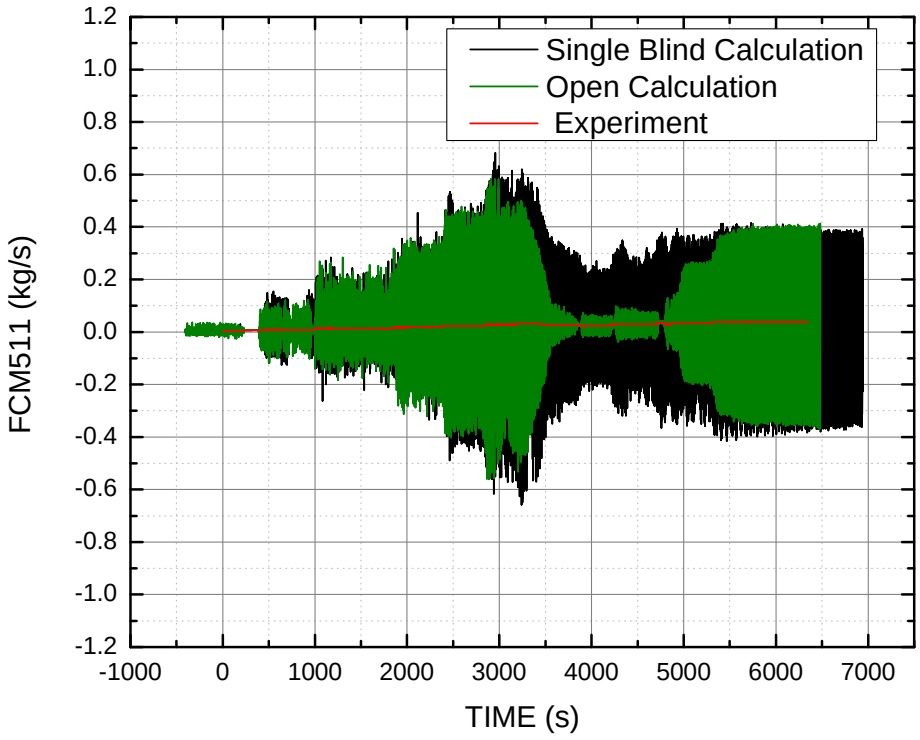

FIG. 4-317. Flow rate in steam generator coils during power maneuvering transient.

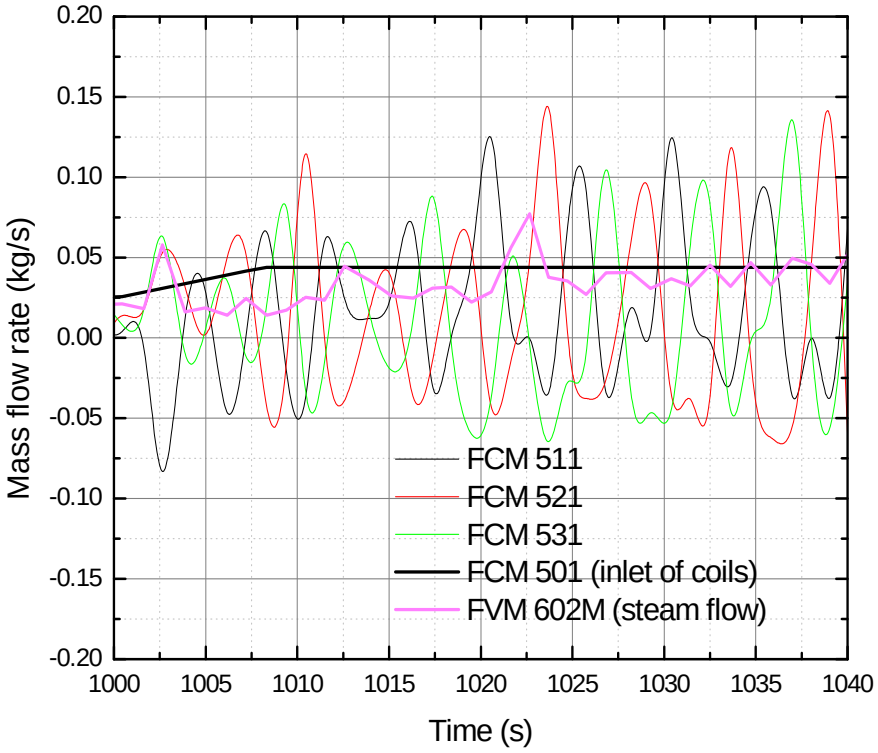

FIG. 4-318. Parallel channel instability in steam generator coils predicted by code

4.13. SJTU - CHINA

4.13.1. Computer codes

The RELAP5/MOD3.4 computer code is a light water reactor transient analysis code developed for the U.S. Nuclear Regulatory Commission (NRC) for use in rulemaking, licensing audit calculations, evaluation of operator guidelines, and as a basis for a nuclear plant analyzer. Specific applications of this capability have included simulations of transients in LWR systems, such as loss of coolant, anticipated transients without scram (ATWS), and operational transients such as loss of feedwater, loss of offsite power, station black-out, and turbine trip. RELAP5 is a highly generic code that is used for simulation of a wide variety of hydraulic and thermal transients in both nuclear and nonnuclear systems involving mixtures of steam, water, non-condensable gas, and solute.

4.13.2. System idealization

4.13.2.1. System idealization for blind calculation

Figure 4-319 shows the RELAP5 idealization for MASLWR test facility including RPV, SG coils, ADS lines, HPC and CPV.

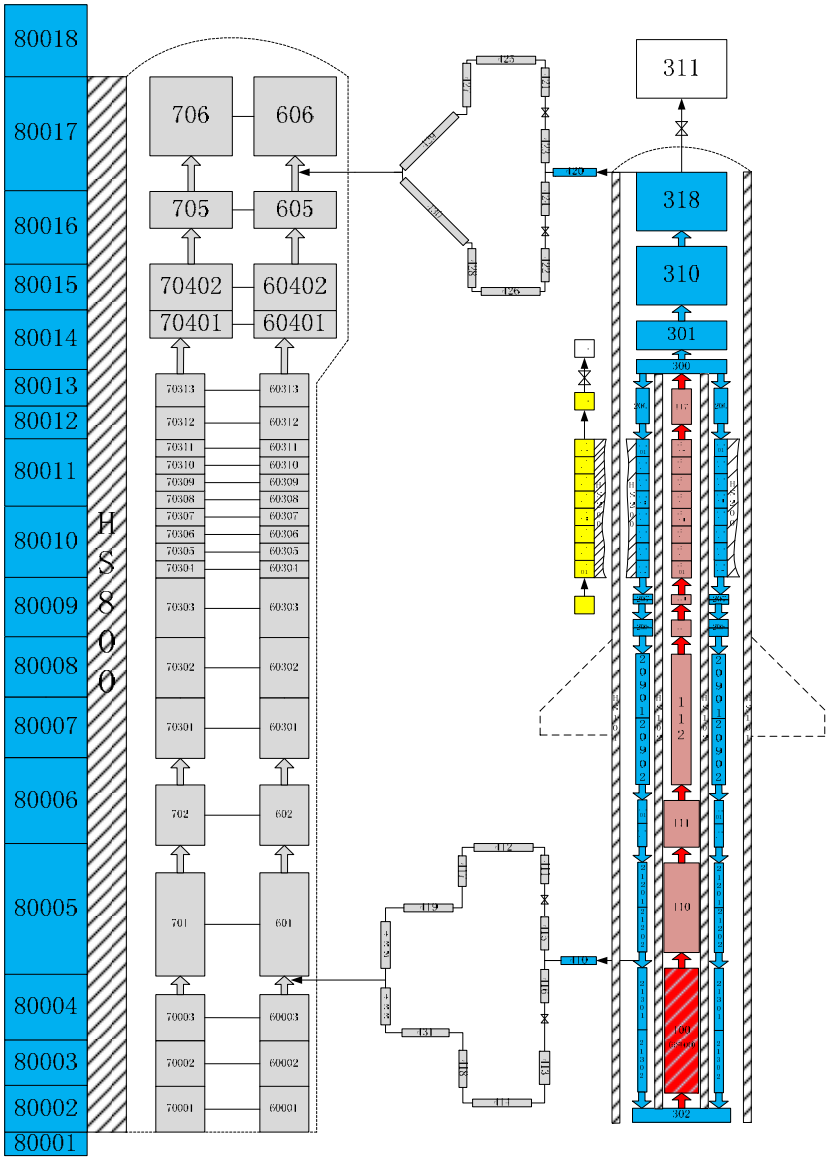

FIG. 4-319. RELAP5 idealization of MASLWR test facility

Chocking flow models are disabled for the blind calculation in junctions of ADS lines but used for the open calculation. Abrupt area changes in these junctions are used.

Pressurizer heaters are not simulated while a time dependent volume is used to simulate pressurizer during the steady state of simulation. Helical geometry of steam generator is ignored and is modelled as straight tube, the length and area of the heat structure between primary side and secondary side of SG is in accordance with the design data. Bypass heat transfer between hot and cold regions in RPV is considered.

4.13.2.2. Modelling change for open calculation

Several adjustments of modelling have been made for the open calculation since the results of blind calculation deviate to a certain degree from test results. The first and most important adjustment is the variation of decay power. For the blind calculation, an incorrect decay power programming:

$$P(t) = \frac{P_0}{(1 + A(t - t_0))^B}$$

with P_0 = 36, A = 0.013 and B = 0.236.

As shown in Figure 4-320, this mistake results in an overestimation of the decay power. A revised decay power input calculated with P_0 = 35.21, A =0.0031 and B =0.68 represented the experiment data very well in open calculation.

The comparison of the decay power variation between blind calculation, open calculation and test result is shown in Figure 4-320. Decay power progressing of open calculation is in accordance with test result and is significantly lower than the input for blind calculation.

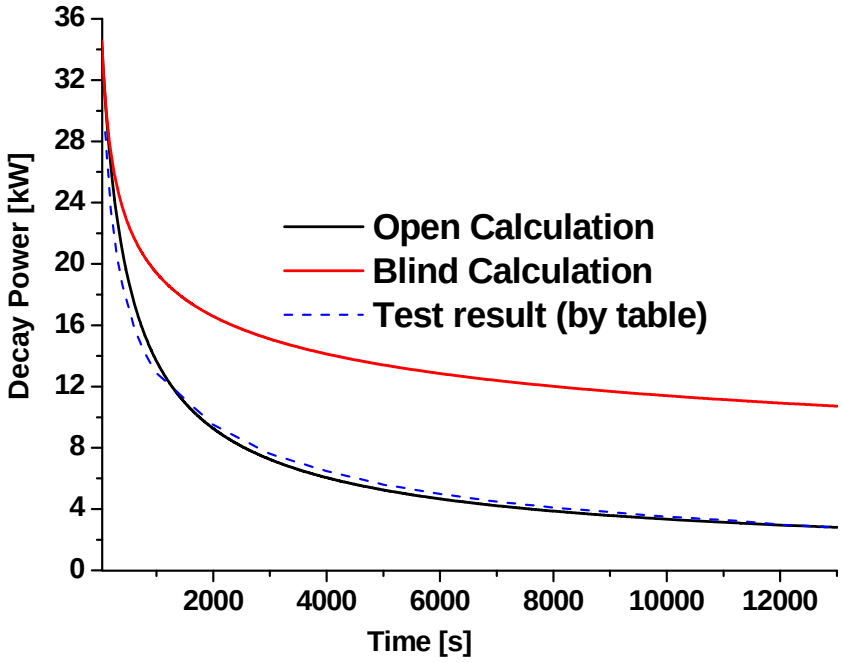

FIG. 4-320. Decay power comparison between open/blind calculation and test result.

Another change is related to the heat transfer area between HPC and CPV. The heat transfer area of the heat structure between HPC and CPV is revised according to the design data. However it's turned out that it's not the main reason of the deviation between the blind calculation and open calculation, compared to the incorrect input of the decay power.

Finally, initial physical properties and geometries of several control volumes of ADS lines are also adjusted, which are also believed that it may somehow result in a difference between blind and open calculation.

4.13.3. Analysis results for loss of feed-water transient

4.1.3.1. RPV thermal-hydraulic behaviour

Figure 4-321 shows the pressure variation of the upper plenum of reactor pressure vessel and the lower part of the high pressure containment. After the simulation reaches the steady state, then stop MFP at 0 s, close HPC vent valve SV-800 at 29 s, PZR pressure (PT-301) reaches 9.064 MPa(a), decay power mode is entered, 18s later, at 47 s, PZR is disabled and ADS vent valve (PCS-106A) is open. According to the control logic of PCS-106A, the valve repeats the open and close until about 5000s when pressure difference between primary system and HPC (PT-301 minus PT-801) becomes less than 5 psi (0.034 MPa). Then PCS-106A and PCS-106B, and PCS-108A and PCS-108B are open and remain open.

Figure 4-322 compares the pressure in RPV between blind, open and experiment. For the blind calculation, because of the overestimation of decay power, with the ADS system, the pressure of the primary system cannot be released adequately, this also leads to a bounce of pressure after ADS valves stay open, other incorrect inputs of blind calculation modelling may also contributes to the deviation but it's believed the main reason for the unrealistic phenomenon is the overestimation of decay power. The open calculation result is much closer to the test compare to the blind one, but for the open calculation, the time at which all ADS valves are opened and keep open is over 1000 s later than the experiment.

Figure 4-323 shows core outlet temperatures from blind/open calculations and experiment data. For the steady state the temperature difference between core inlet and outlet (compare with Figure 4-324) is about 35ºC, after opening of PCS-106A the temperature of core inlet and outlet become very close to each other and begin to decrease together. For the blind calculation, because of the overestimation of decay power, the temperature rebounded after the opening and stay opening status of the ADS valves. For the open calculation, the temperature in the primary system begins to decrease after the opening of the ADS valves. The test result indicated by the blue curve represents a similar trend of transient with the open simulation, except the starting time of long term cooling.

Figure 4-324 shows the comparison of core inlet temperature between experiment, open and blind calculation. For the test result, the temperature has a sharp decrease at about 4000 s, at which time the ADS valves start to keep open. However in the open simulation result, temperature also decreases after the opening of all the ADS valves, but this sharp decrease of temperature is not observed. The tendency of temperature decrease of open simulation is similar to the experiment, but temperature of open calculation is a little higher than the test result for most of the duration of the transient. For the blind calculation, there is a bounce of the temperature after about 4000 s, which deviates from test results. However, the blind calculation has a similar moment of opening of ADS valves with the experiment.

Figures 4-325 and 4-326 show the variation of primary mass flow rate, these curves indicate that after the opening of PCS-106A, the primary mass flow rate begins to decrease gradually and after about 6200 s, the mass flow rate oscillates around zero. The oscillation of primary mass flow for the open calculation is more drastic compare to blind simulation, before ADS system reaches the stay open status.

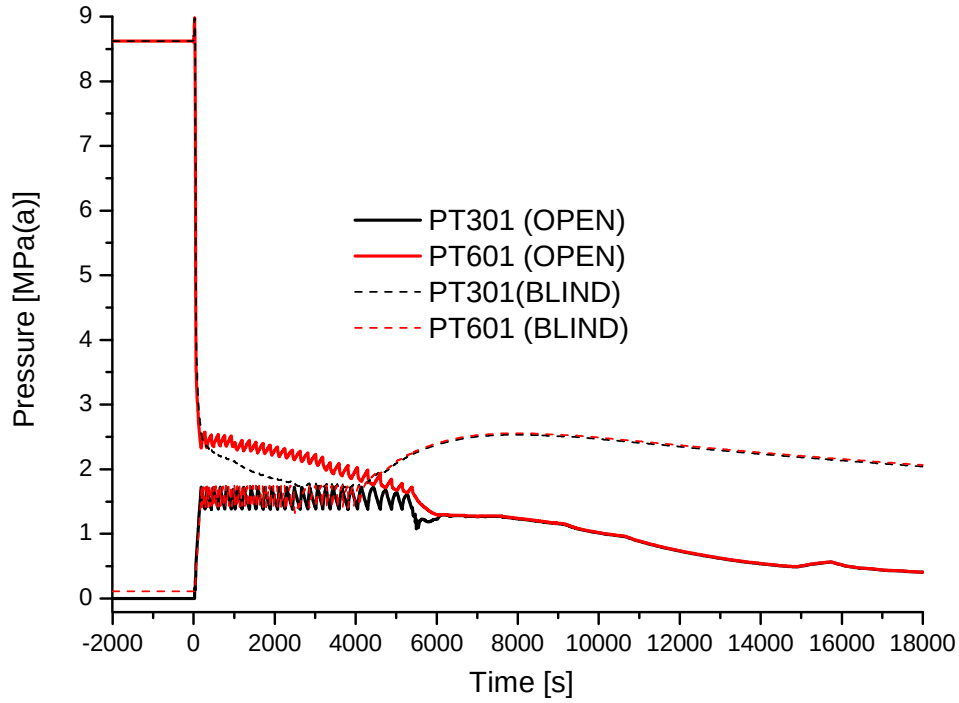

FIG. 4-321. Pressure in upper plenum of RPV and in lower part of the HPC.

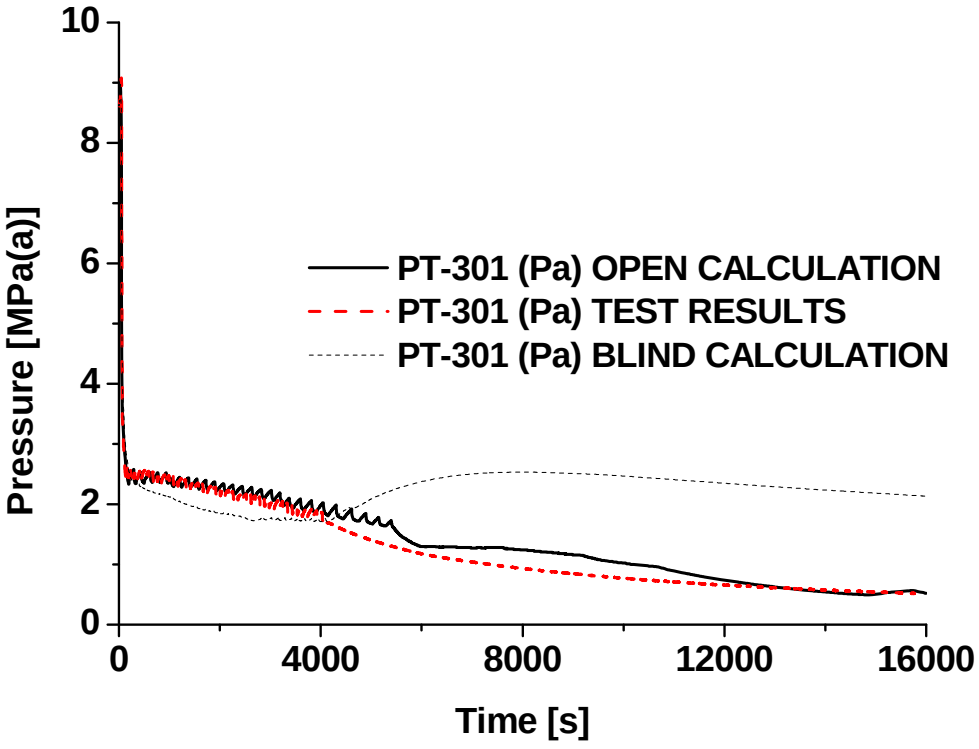

FIG. 4-322. Pressure in upper plenum of RPV.

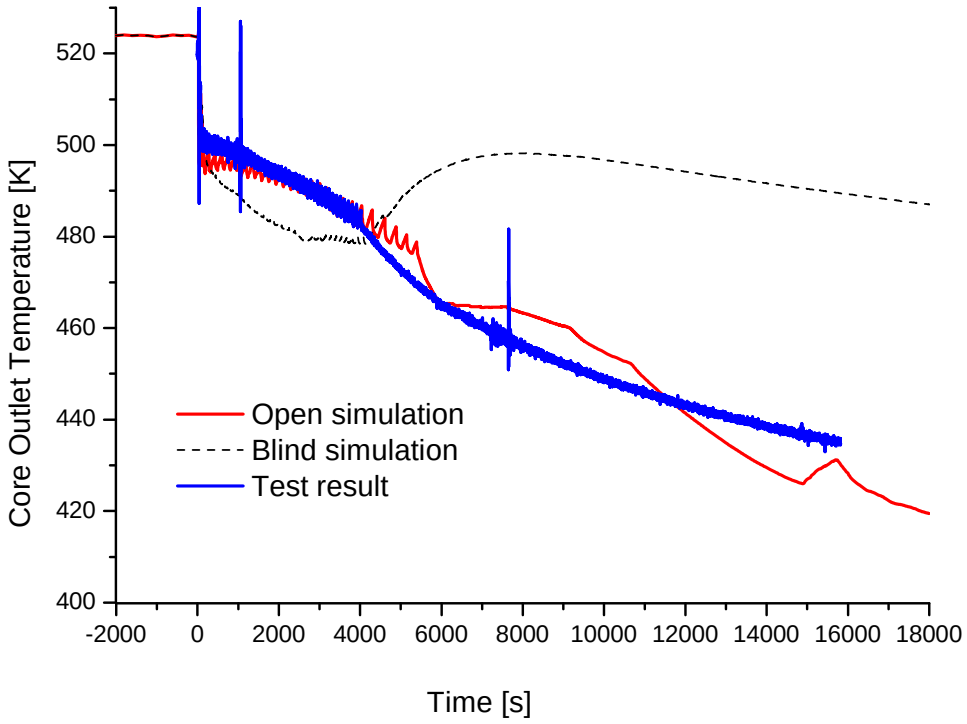

FIG. 4-323. Core outlet temperature.

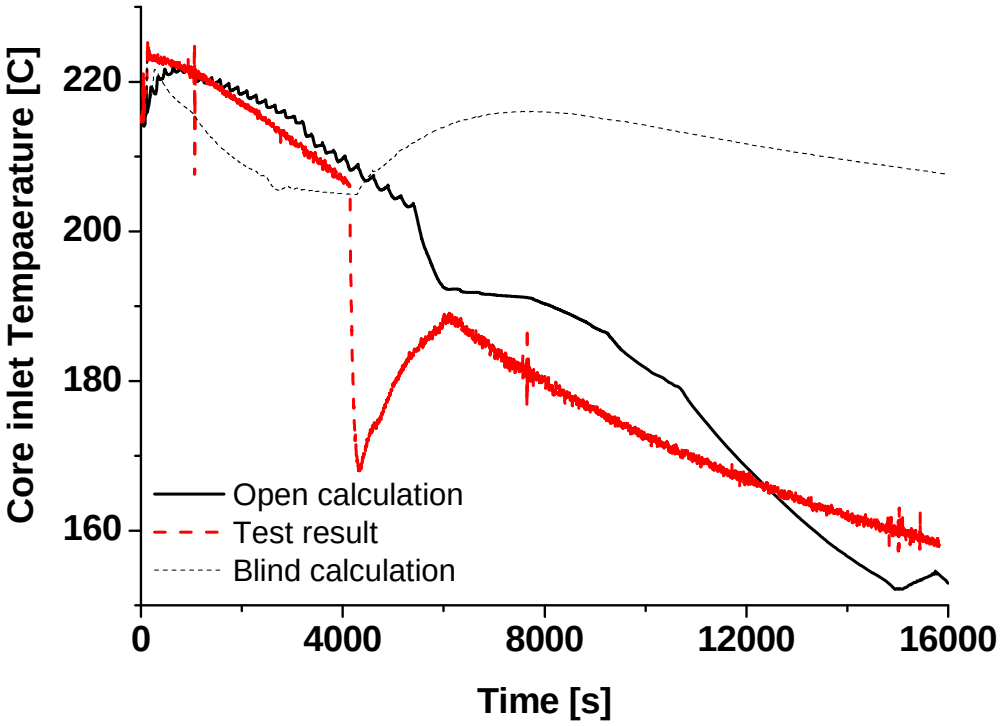

FIG. 4-324. Core inlet temperature.

4.13.3.2. HPC thermal-hydraulic behaviour

Figure 4-327 shows the temperature at different positions in the high pressure containment. For the open calculation results, all of these temperatures increase sharply after the opening of PCS-106A, from 350 to ~ 470°K, after about 4000 s for blind calculation and 5500 s for open calculation, pressure difference between primary system and HPC (PT-301 minus PT-801) becomes less than 5 psi (0.034 MPa), then all valves in ADS line (PCS-106A and PCS-106B, and PCS-108A and PCS-108B) open and remain open. For the blind calculation, because of the overestimation of decay power, there is a bounce of the temperature in the HPC after ADS system reaches the stay open status.

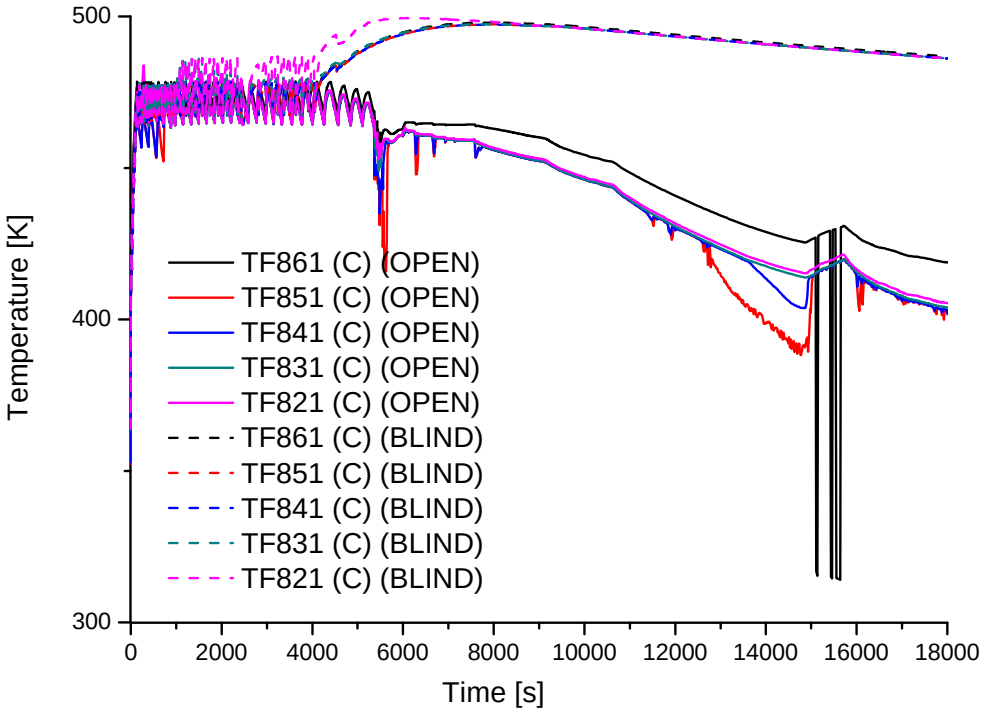

FIG. 4-327. Variation of temperature in HPC.

Solid lines of Figures 4-328 and 4-329 show the mass flow rate and cumulative discharge of PCS-106A, from the opening of PCS-106A to the time at which pressure difference between primary system and HPC (PT-301 minus PT-801) becomes less than 5 psi (0.034 MPa), the discharge rate of PCS-106A is large and after the opening of PCS-106B, PCS-108A and PCS-108B, the discharge rate becomes small and cumulative discharge increases slowly. The peak mass flow rate of PCS-106A for open simulation is higher than blind case, however the durations for the opening of PCS-106A are shorter. It's believed this difference is due to the adjustment of the geometries of ADS lines. For the cumulative discharge, blind calculation reaches a higher value, especially for the period of ADS discharge transient, compare to the open one. This is also due to the overestimation of the decay heat.

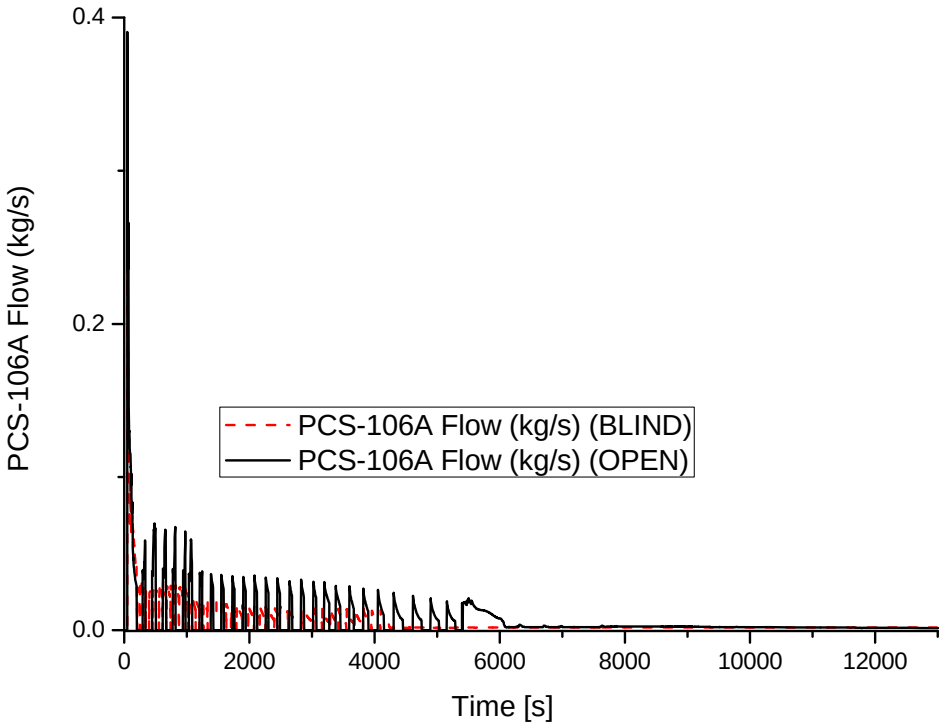

FIG. 4-328. Mass flow rate of PCS-106A.

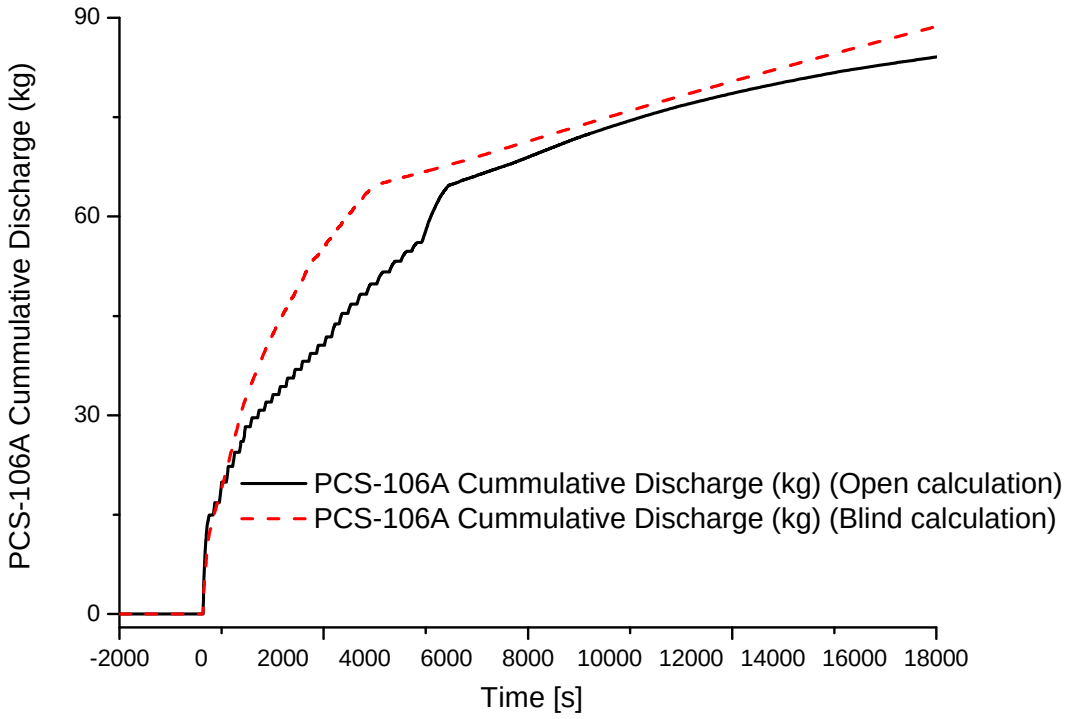

FIG. 4-329. Cumulative discharge of PCS-106A.

4.13.4. Analysis results for power maneuvering

4.13.4.1. RPV thermal-hydraulic behaviour

Figure 4-329 shows the power increase during the transient. According to test procedure, the core power has been increased gradually from 40 to 320 kW. The blue curve indicates the power input for blind calculation. For this input, one mistake has been made that it didn't follow the test boundary condition; the red line and black line indicate the test result and open calculation respectively. For the open calculation, the power input is the average values of every 70 s of test result. As a result, there is a slight discrepancy between test result and open calculation result.

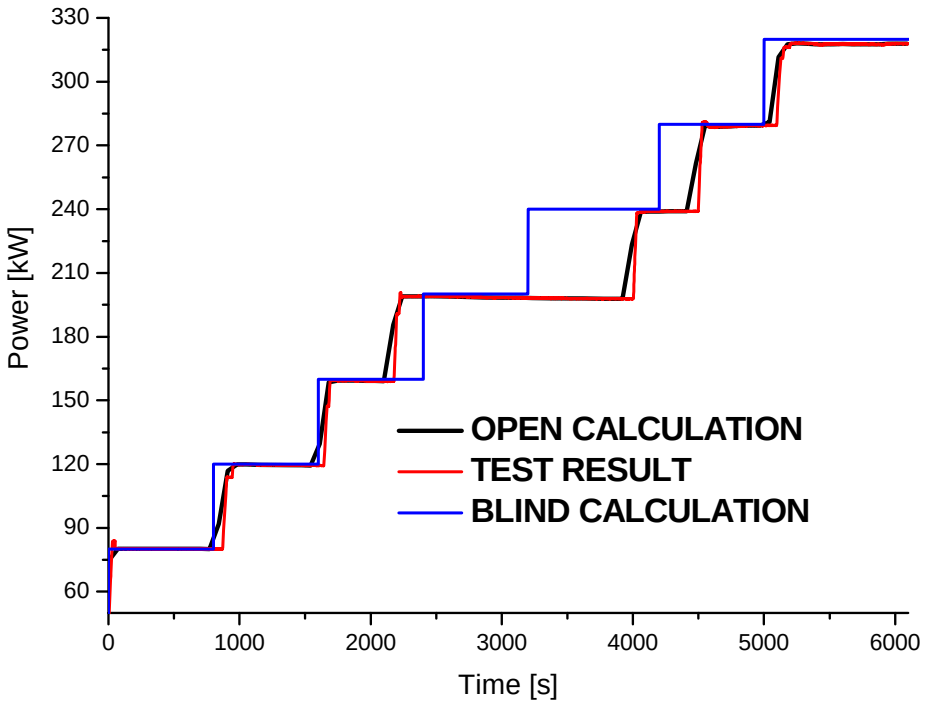

FIG. 4-330. Core power during the transient.

Figure 4-331 describes the variation of core inlet temperature and also outlet temperature, the temperature difference between these two temperatures is about 12°C and this difference is increased along with the increasing of the core power and the feed water flow rate, however at about 2500 s, both core inlet temperature and outlet temperature are decreased for the open calculation, and then rebound at about 4500 s. Dash curves are the result of blind calculation as the reference. Due to the difference of power change and feed water flow rate, the blind simulation deviates significantly from the open simulation.

Figure 4-332 shows the comparison between test result and open calculation result of core inlet temperature variation. For the test result, the temperature is remarkably lower than open simulation, the discrepancy is about 17°C, the phenomenon of overestimation of temperature for primary system is also observed in SP-2.

Figure 4-333 describes the variation of primary mass flow rate and it is increased in accordance with the power increasing step by step. Dash curves are the results of blind calculation as the reference. It’s obvious that the oscillation of primary mass flow rate for open calculation is more drastic than blind one. This is due to the change of the input of core power and feed water flow rate according to the experiment data.

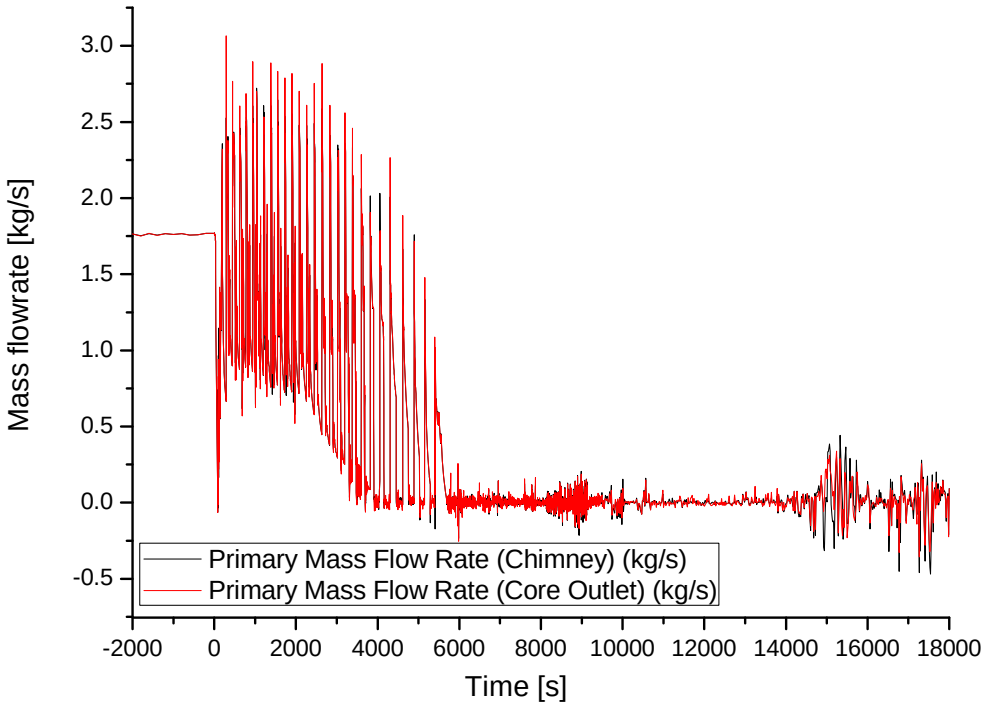

FIG. 4-325. Primary mass flow (open calculation).

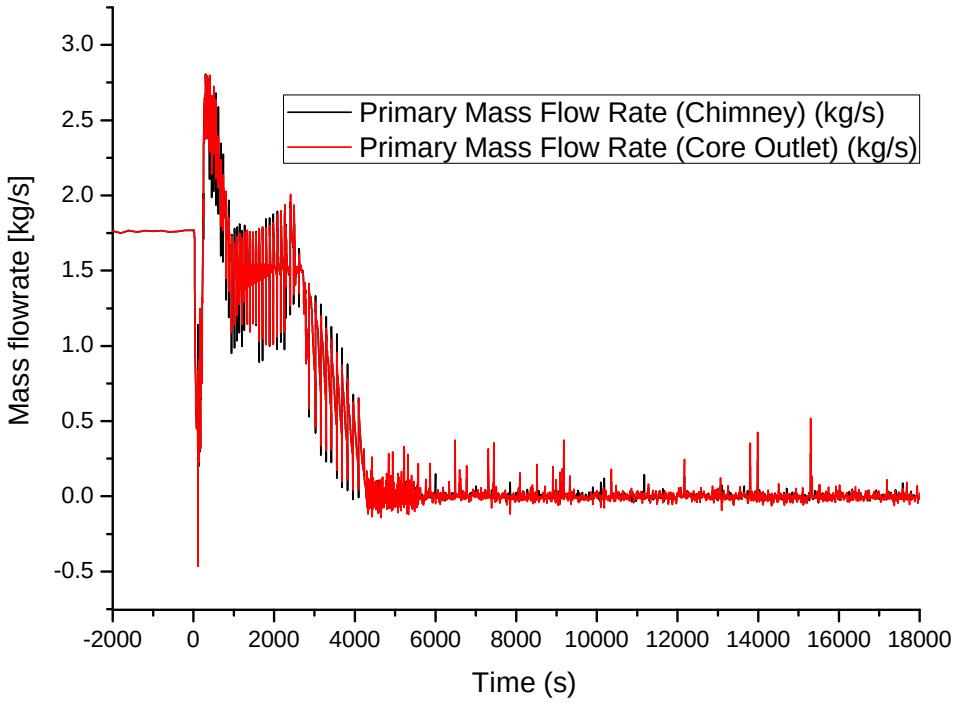

.

FIG. 4-326. Primary mass flow (blind calculation).

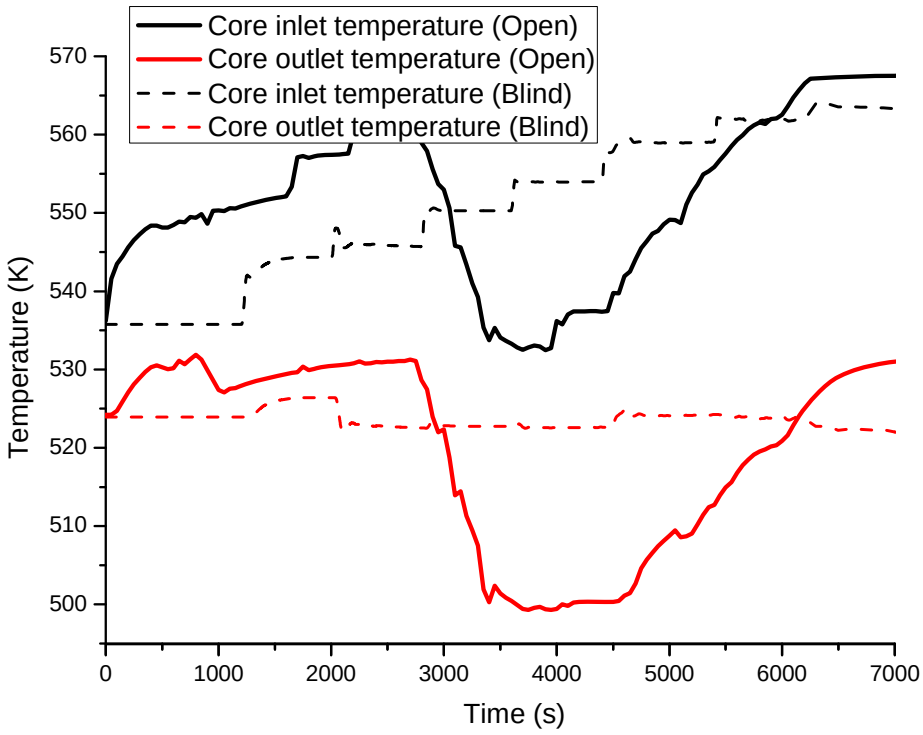

FIG. 4-331. Variation of core inlet/outlet temperature.

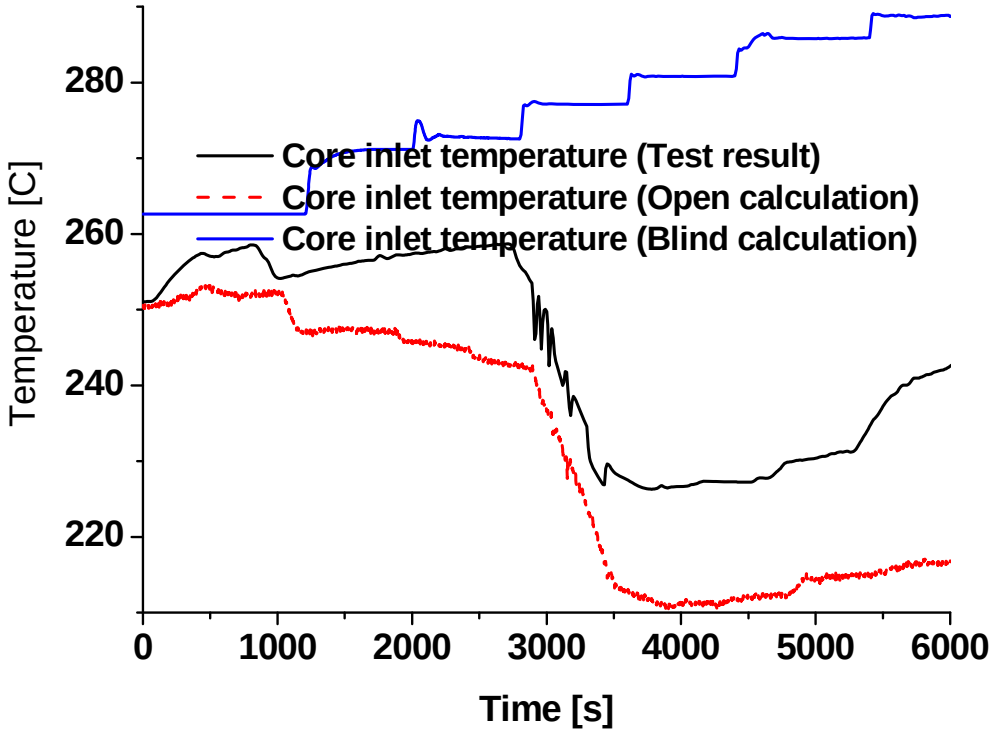

FIG. 4-332. Variation of core inlet/outlet temperature.

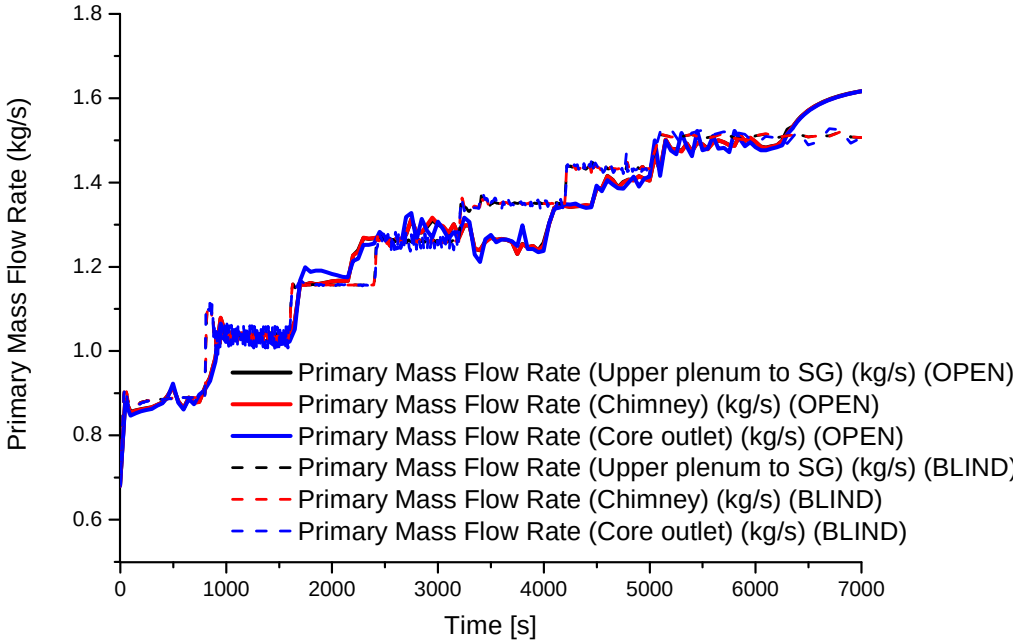

FIG. 4-333. Variation of primary mass flow rate (open calculation).

4.13.4.2. SG thermal-hydraulic behaviour

Figure 4-334 shows the comparison between test result and open/blind calculation result of feed water inlet flow rate. The feed water flow rate of blind calculation increases step by step and is without oscillation, and for the open simulation, the flow rate is revised according to experiment result.

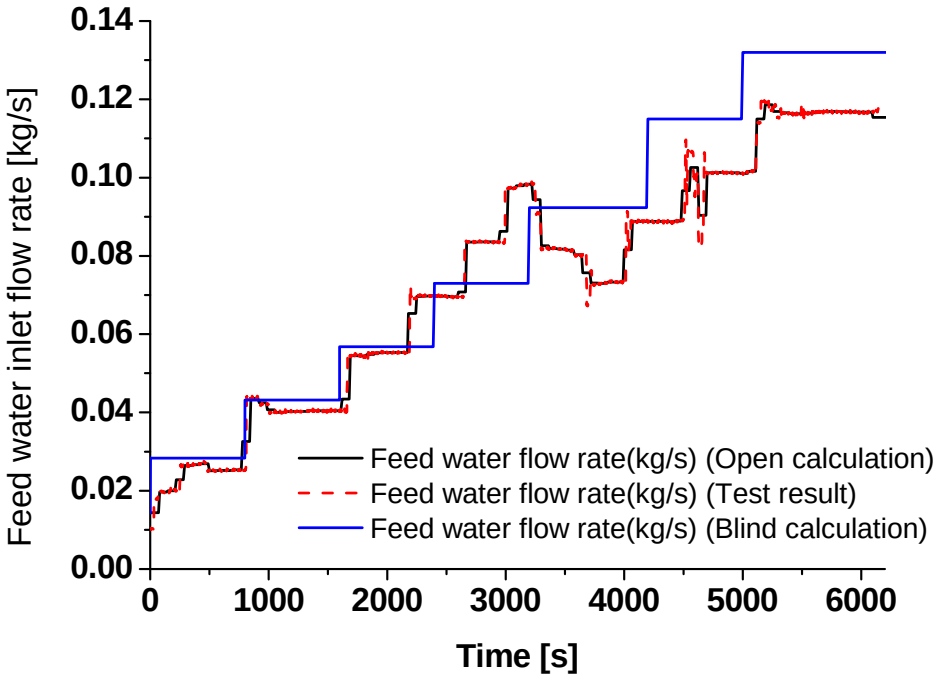

FIG. 4-334. Feed water inlet flow rate.

Figure 4-335 shows the comparison between test result and open/blind calculation result of feed water temperature. Figure 4-336 shows the blind and open calculation of steam flow rate.

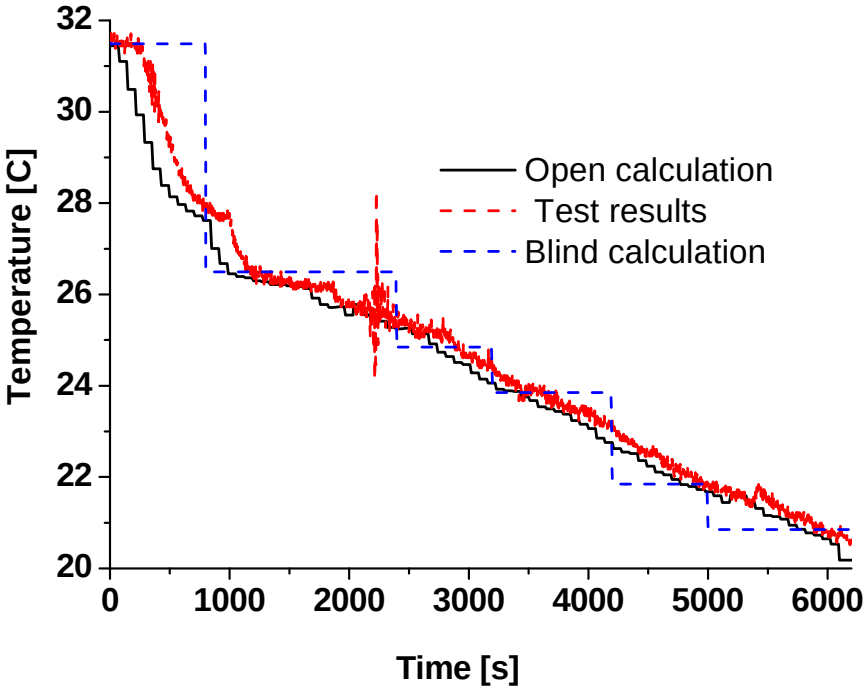

FIG. 4-335. Feed water temperature.

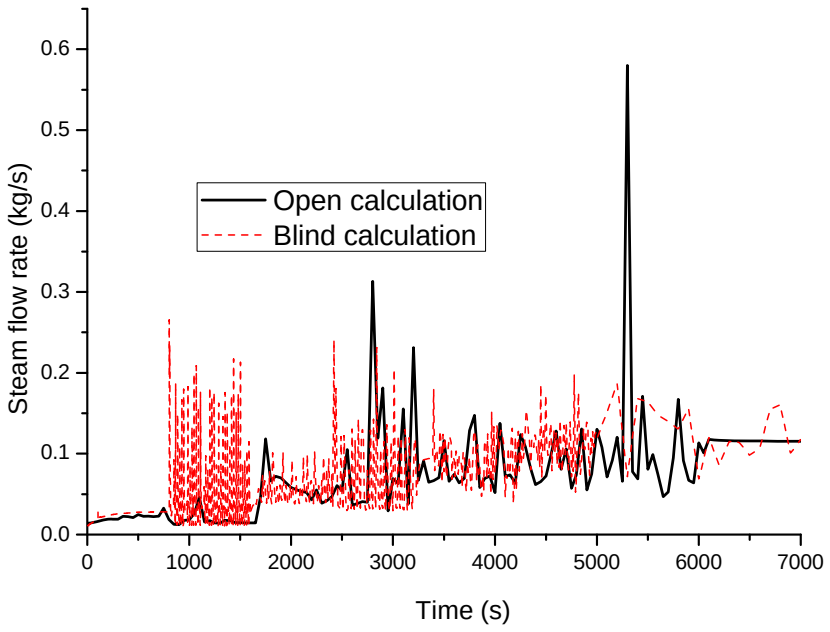

FIG. 4-336. SG steam flow rate.

Figure 4-337 shows the comparison between test result and open/blind calculation result of feed water outlet temperature. Open simulation has a similar temperature change for the feed water outlet, but oscillates more drastically. For the blind calculation, the temperature tends to be higher due to the higher input of core power after about 3000 s.

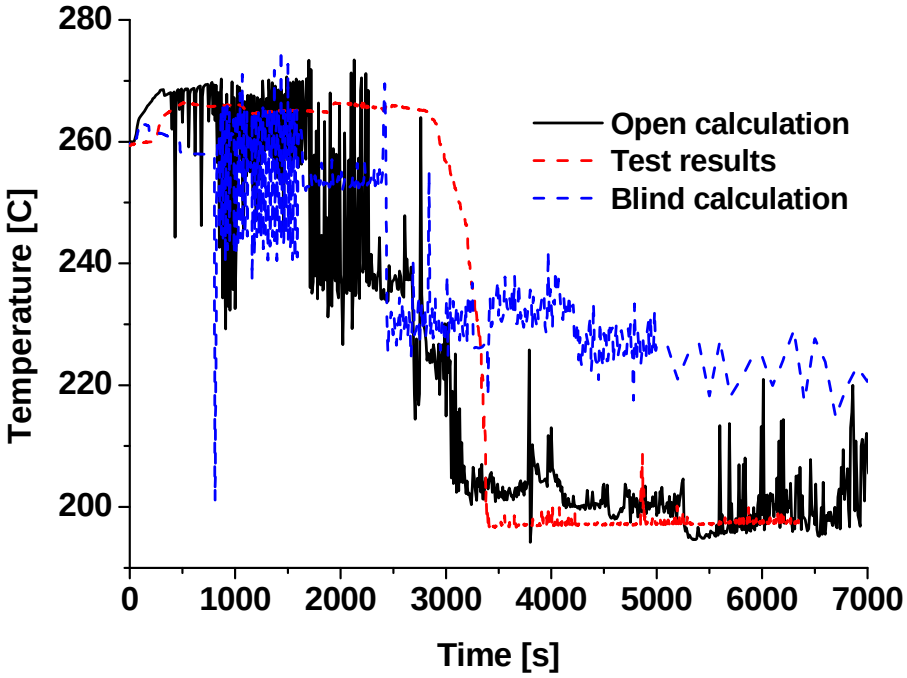

FIG. 4-337. SG steam temperature.

Figure 4-338 shows the comparison between test result and open/blind calculation results of steam outlet pressure. The figure indicates the steam outlet pressure of the test result is slightly smaller than the simulation. The oscillation of the test is also smaller than the simulation result.

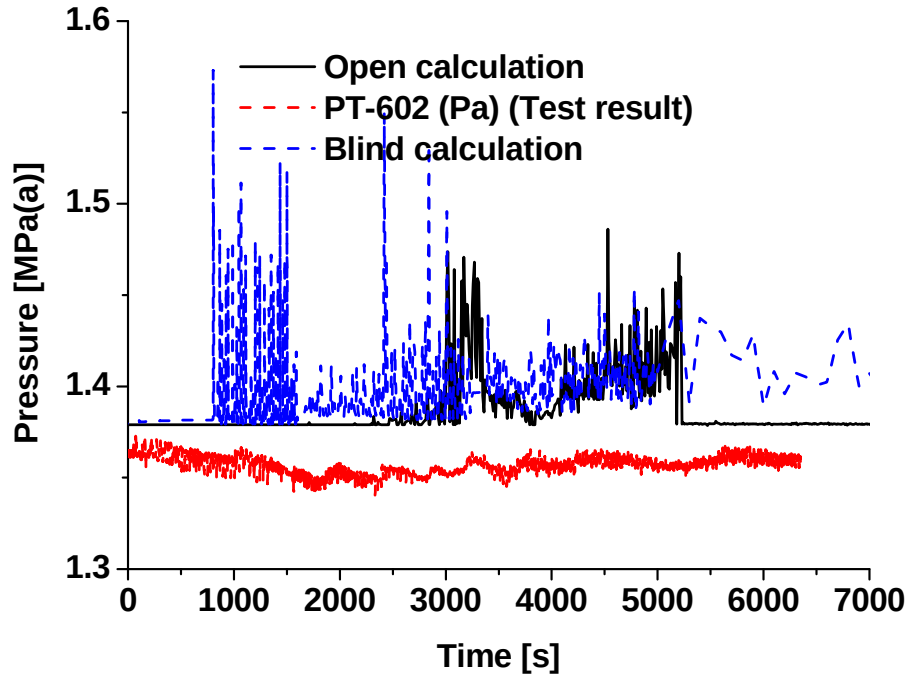

FIG. 4-338. Pressure variation of steam.

4.14. SNPTRD – CHINA

4.14.1. Computer codes

This work is an IAEA International Collaborative Standard Problem on Integral PWR Design Natural Circulation Flow Stability and Thermo-hydraulic Coupling of Containment and Primary System during Accidents. The double blind calculation of the experiments of MASLWR test facility is performed by the RELAP5/MOD3.4, the same as the open calculation, but different from the blind calculation version, which is RELAP5/MOD3.2.

4.14.2. System idealization

4.14.2.1. System idealization for blind calculation

The core channels were simulated as one pipe and the helical coil tubes are simulated into one set. The feed water and the steam lines are modeled by time dependent junction and time dependent volume. The PRZ heater was modeled but HPC heater was not simulated. The vent line and sump recirculation lines are modeled separately with two lines respectively. The CPV and the HPC was not divided into two parts based on the sensitivity that the division did not affect significantly the heat transfer.

The model of the facility for SP-2 and SP-3 tests is the same. The nodalization diagram is as follows when calculating the steady state in SP2. The CPV (500) and HPC are connected to the atmosphere by a valve respectively. The former is always open and the latter is controlled by the pressure according to the logic. There is no valve on the pressure vessel in both SP2 and SP3 problem.

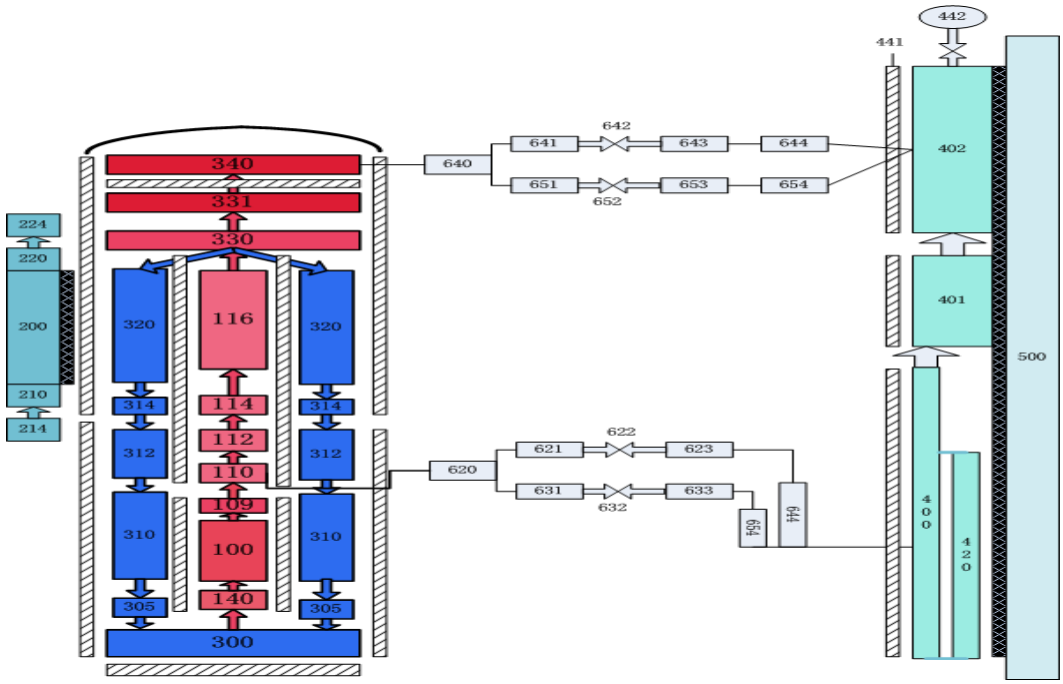

FIG. 4-339. Facility Nodalization

4.14.2.2. Modelling change for open calculation

The nodalization diagram of RPV is different for blind calculation and open calculation. The open calculation nodalization has the following differences from blind calculation:

- The re-nodalization of downcomer - length of some nodes were changed as well as loss coefficient.
- The SG tubes were nodalized into 3 sets in open calculation and only one straight pipe in blind calculation.
- The noncondensible gas portion in the upper part of the HPC.

Figure 4-340 shows the changed nodalization diagram.

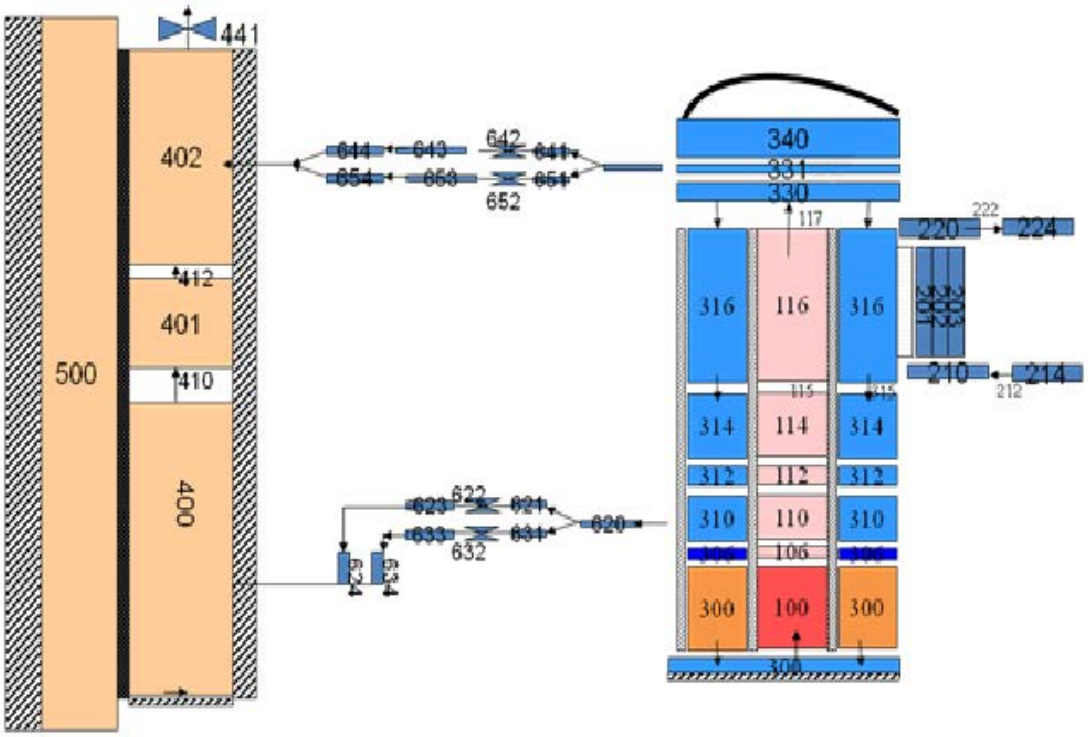

FIG. 4-340. Facility nodalization for open calculation.

4.14.3. Analysis results for loss of feed-water transient

The blind calculation is just calculated for 16,000 s. The core power in the blind calculation is used as the procedure rather than the experimental one, therefore, the system pressure rose after a short blowdown period and did not depressurized as expected.

4.14.3.1. RPV thermal-hydraulic behaviour

The calculated result is similar with the experiment with most of phenomenon. After loss of the feed water, the pressure rose quickly to about 9 MPa(a) at first and activates the ADS valve PCS-106 and trip the reactor. The pressure of the RPV decreases sharply to about 3 MPa(a), which is much higher than the experiment result. Several sensitivities were studied and found that it's difficult to decrease this near to the experiment one. The pressure of the HPC rises between 1.47 MPa(a) and 1.83 MPa(a) with the repeated open and close of the valve PCS-106. The RPV pressure goes down slowly after that and meet at the HPC pressure at about 3888 s (Fig. 4-342). At which the ADS valve and sump return valve (PCS-106B, PCS-108A/B) opens and large amount of water flow into the core from the return line. After that, the return flow reduces to near zero and fluctuates as well as the ADS flow rate (Fig. 4-341). During the transient, the temperature at the core outlet and chimney goes down, and the temperature in downcomer and inlet goes up and nearly the same. Both temperatures decrease slowly, after the open of return valve, there is a sharp drop of temperature (Fig. 4-344) at the downcomer and lower head, because large amount of water inject into the downcomer from the return line. But the calculated drop is much less than the experiment one. The reason may be interpreted as a small flow from the return line or because of the 3D effect of the experiment.

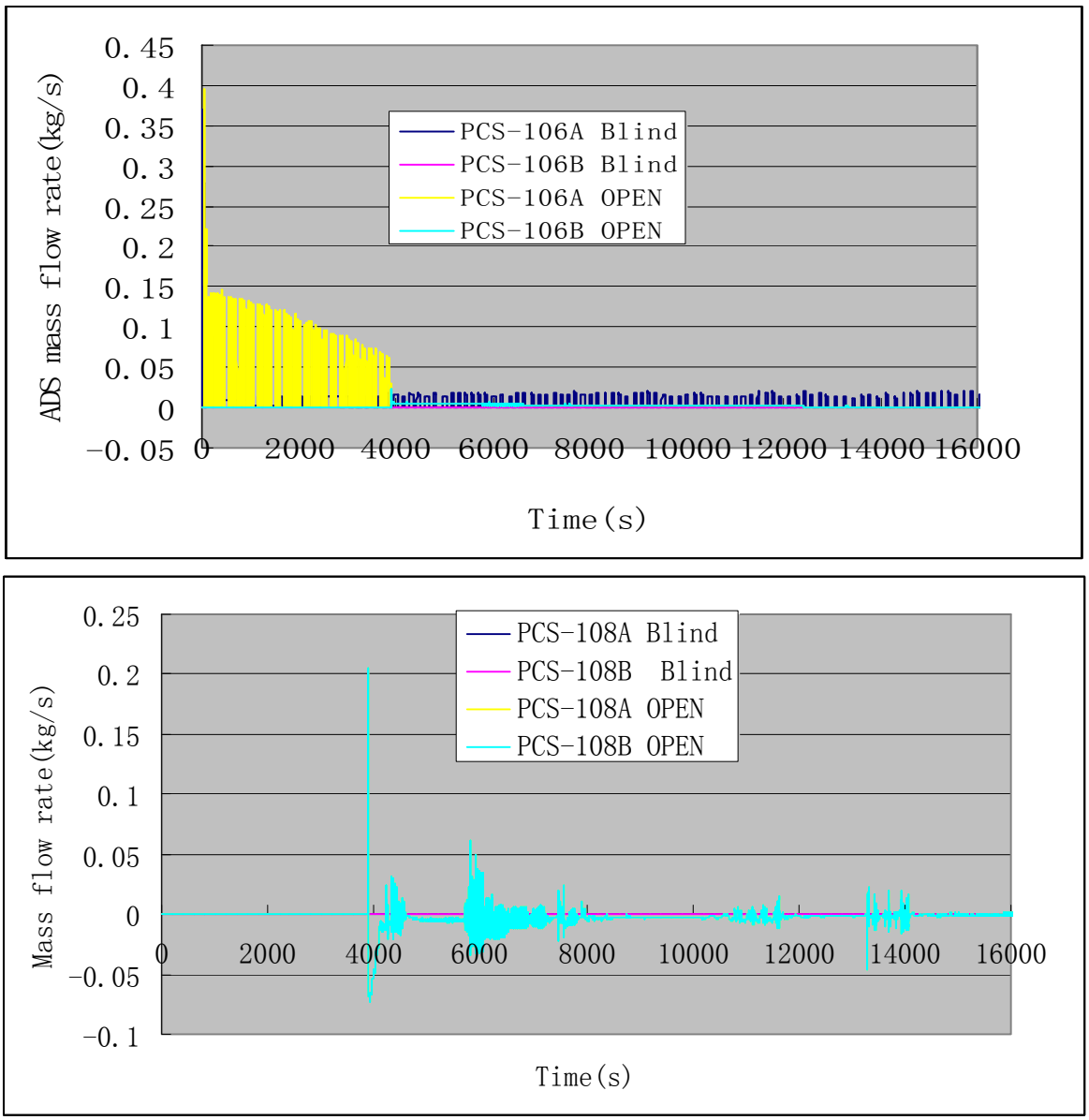

FIG. 4-341. ADS vent flow（PCS-106A and PCS-106B）and sump return line flow (PCS-108A and 108B).

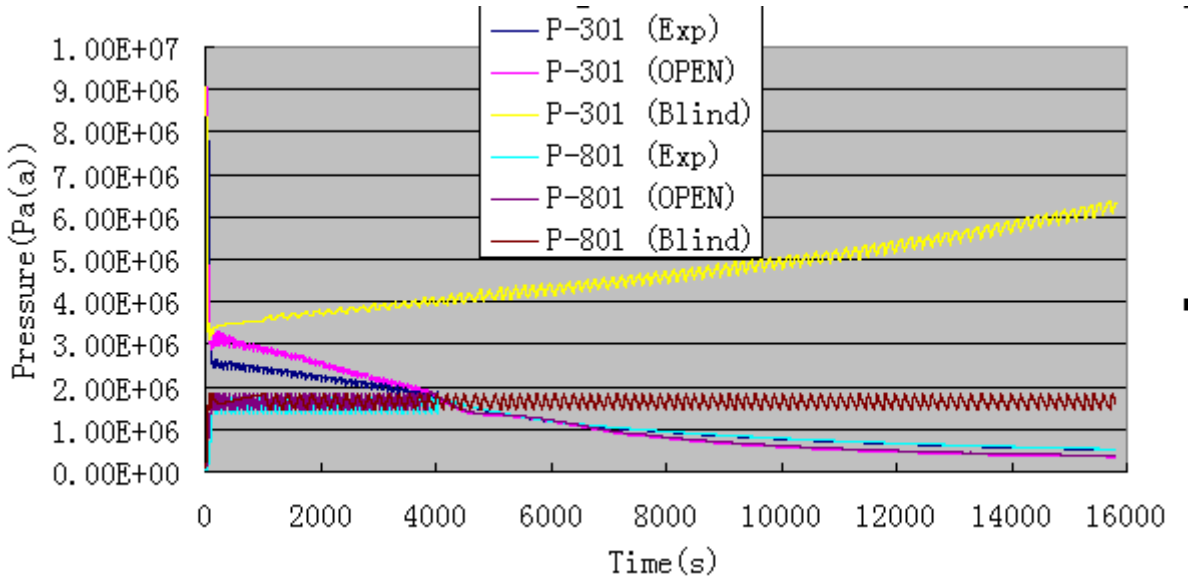

FIG. 4-342. Pressure at pressurizer (PT-301) and HPC bottom (PT801).

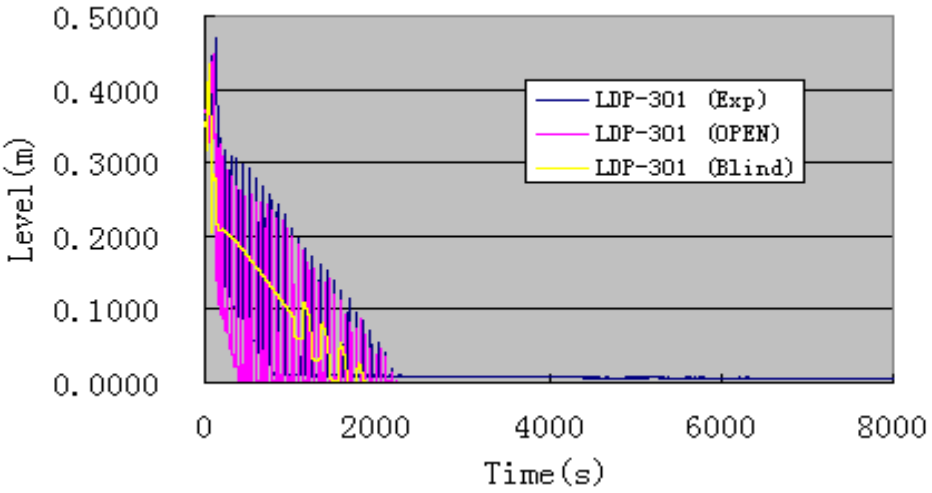

FIG. 4-343. Pressurizer water level (LDP-301).

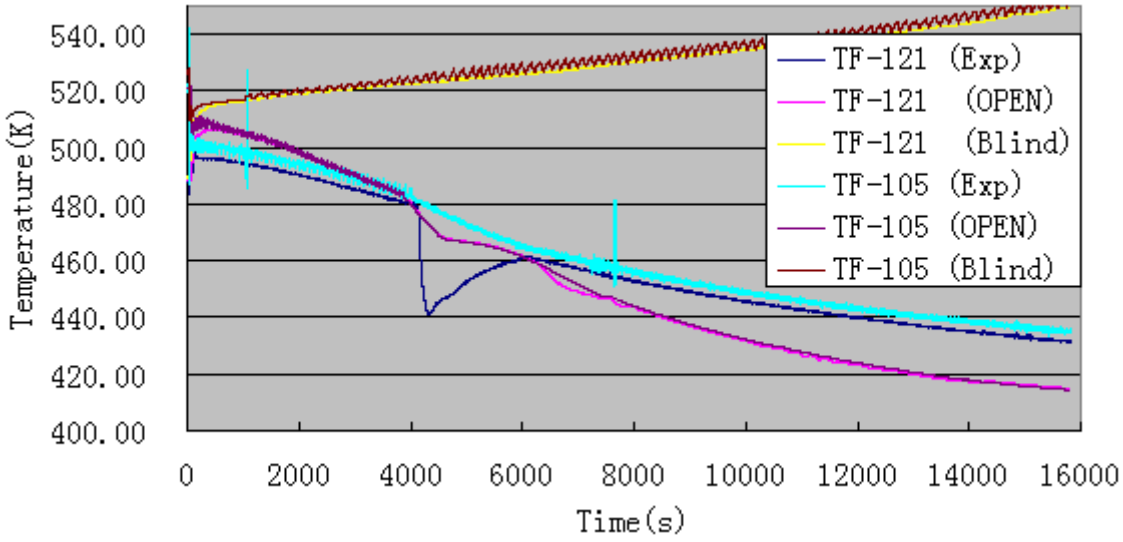

FIG. 4-344. Core inlet fluid temperature (TF-105) and outlet temperature (TF-121).

4.14.3.2. SG thermal-hydraulic behavior

The SG feedwater was lost and no attention was paid to the phenomena in SG.

4.14.3.3. HPC thermal-hydraulic behaviour

The pressure of HPC rises after the PCS-106A opened, and then maintained between the 1.47 MPa(a) and 1.83 MPa(a) and has oscillation because of the open and close of the PCA-106A periodically (Fig. 4-341). The SV-800 is never opened during the transient.

The upper part HPC temperature jumps and fluctuates till the open of the sump return line and then decreases slowly because of the condensation on the heat transfer plate. The calculated temperature in the HPC is much lower than the experiment's result except that the top one. This is hard to explain, but it might be because that the code calculated the average temperature. The water in the HPV is thermally stratified causing the heat is hard to be transferred to the lower part of the HPC (Fig. 4-346).

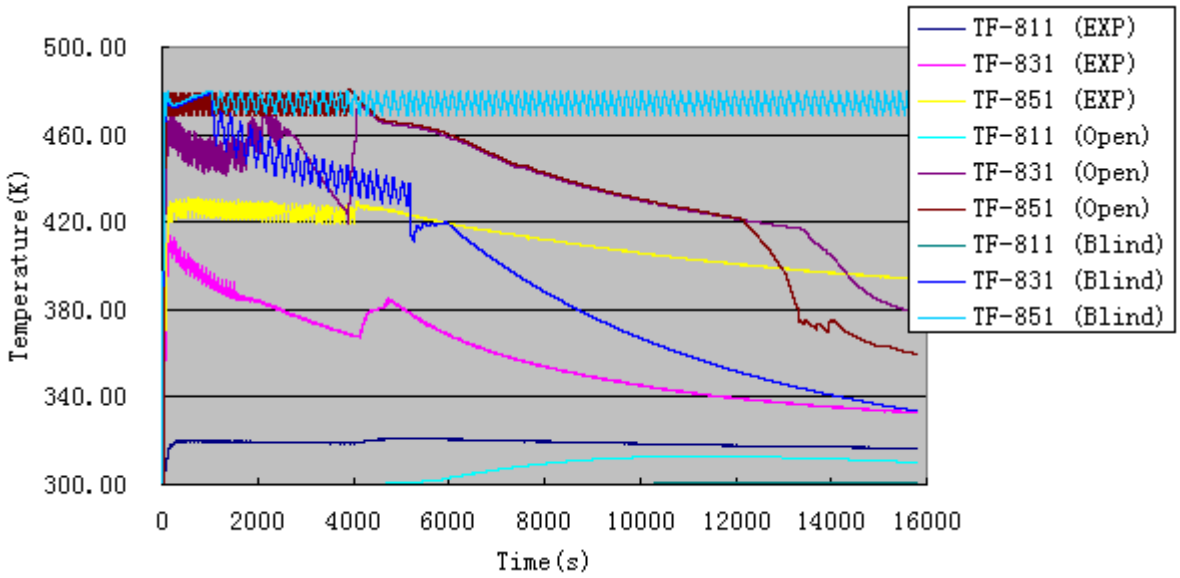

FIG. 4-345. Water temperature (for clearance only TF-811, 831, 851 were plotted).

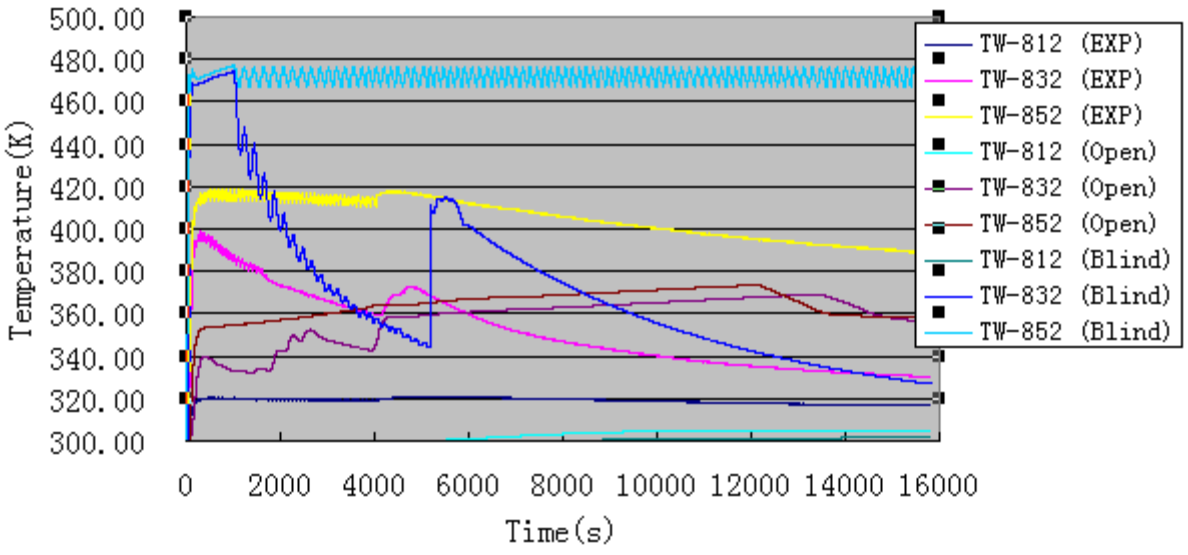

FIG. 4-346. HPC side wall temperature (TW-812,832 and 852).

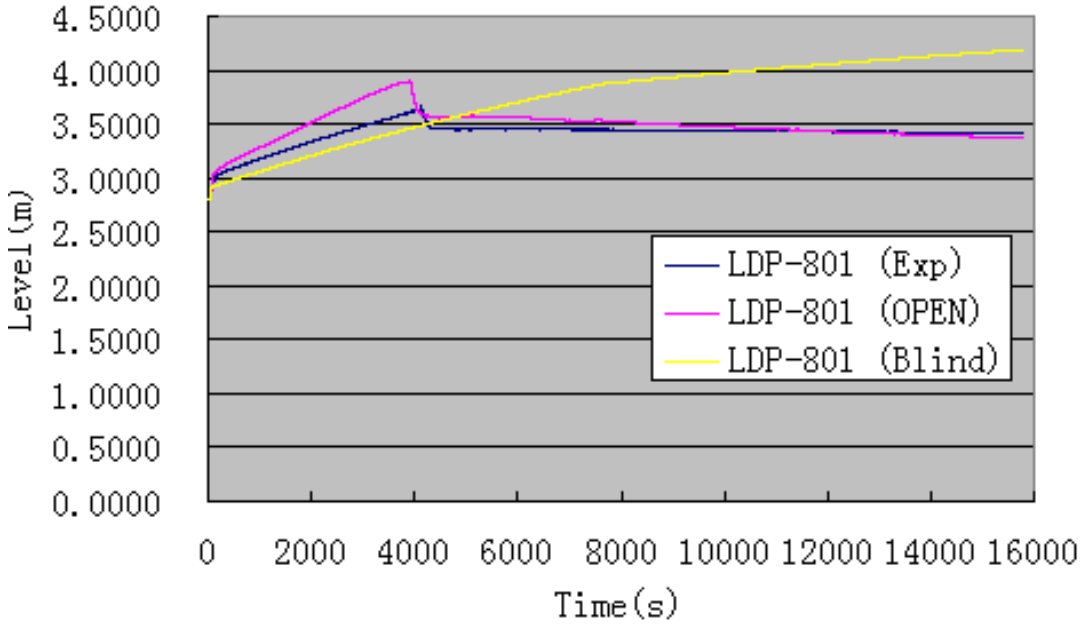

FIG. 4-347. HPC Water level (LDP-801).

4.14.3.4. CPV thermal-hydraulic behaviour

The upper part of the CPV temperature rise slowly because of the heat transfer through the heat transfer plate from HPC. The water in the CPV is thermally stratified highly. The temperature in lower part of the CPV keeps nearly the same except rises at about 10 degree after the return valve opens (Fig. 4-349). The calculated temperature is lower than the experiment result. The wall temperature of the heat transfer plate at the CPV side is a little higher than the water temperature in CPV.

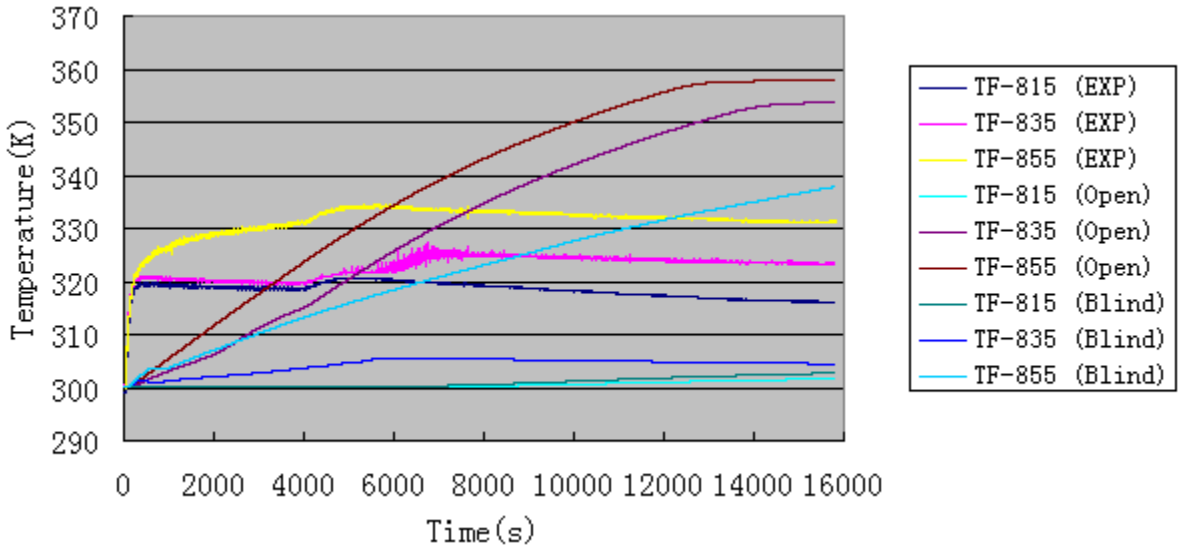

FIG. 4-348. CPV water temperature (TF-815, 835, 855).

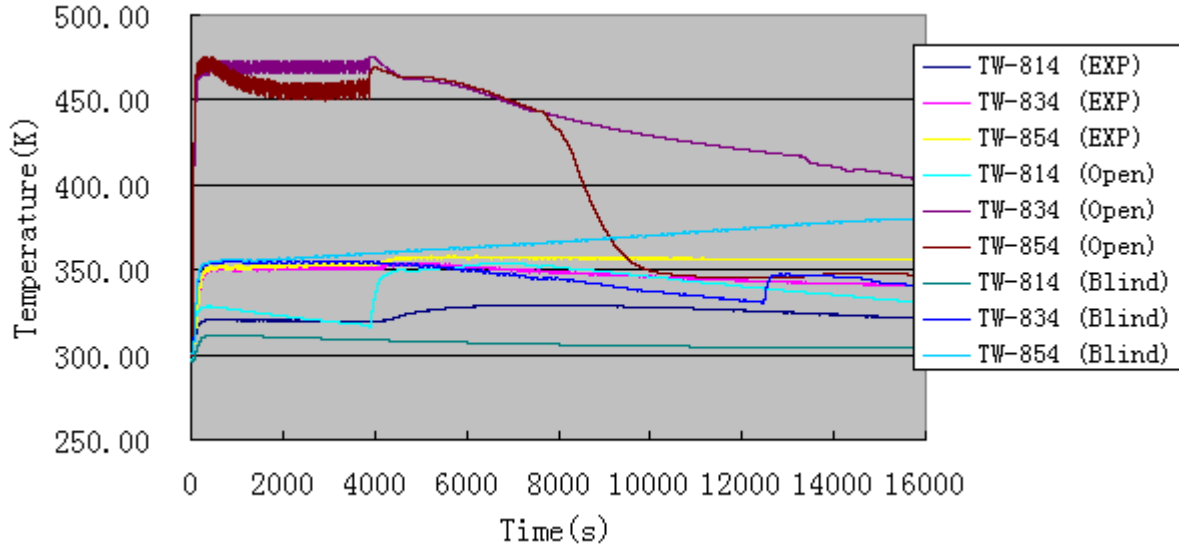

FIG. 4-349. CPV side wall temperature (TW-814,834 and 854).

4.14.4. Analysis results for power maneuvering

4.14.4.1. RPV thermal-hydraulic behavior

By given core power and feedwater mass flow rate, the pressure of the pressurizer calculated by RELAP5 fluctuated slightly and have 5 obviously waves (Fig. 4.-350).

The primary mass flow rate rises with the core power to take the heat generated by the heat rod. Figure 4-351 shows that the calculated flow rate is higher than the test, which might lead to the lower core temperature (Figs 4-352 and 4-353). After 5000 s, the mass flow difference is smaller, which causes the smaller core temperature difference.

Generally, the code results show that the inlet temperature decrease and outlet increases. The core outlet keeps subcooled in the whole process.

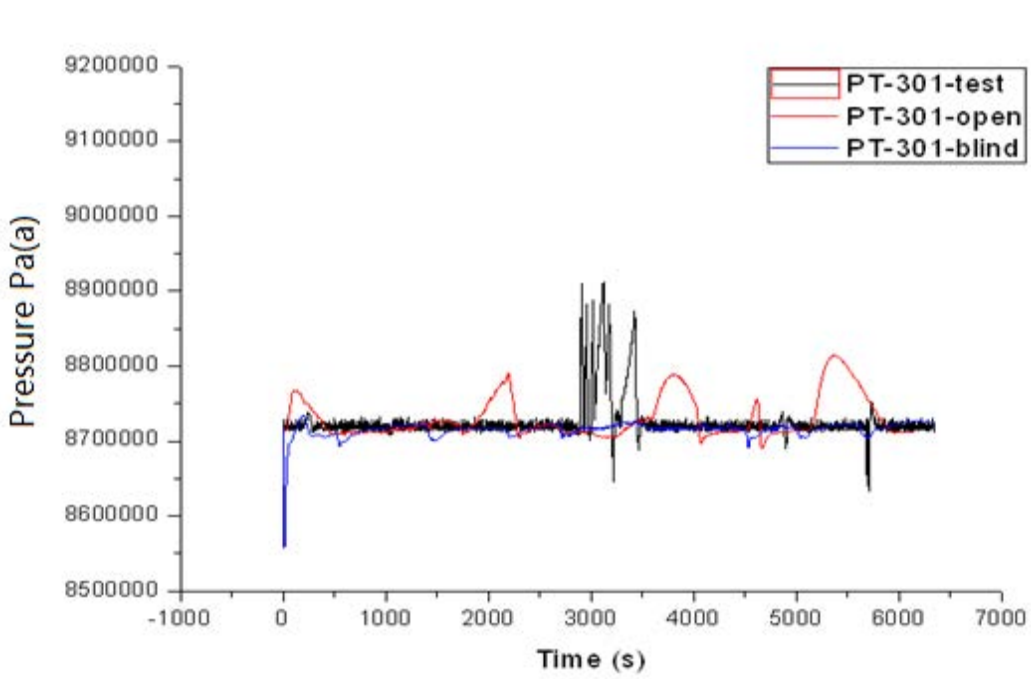

FIG. 4-350. Pressure PT-301 of pressurizer.

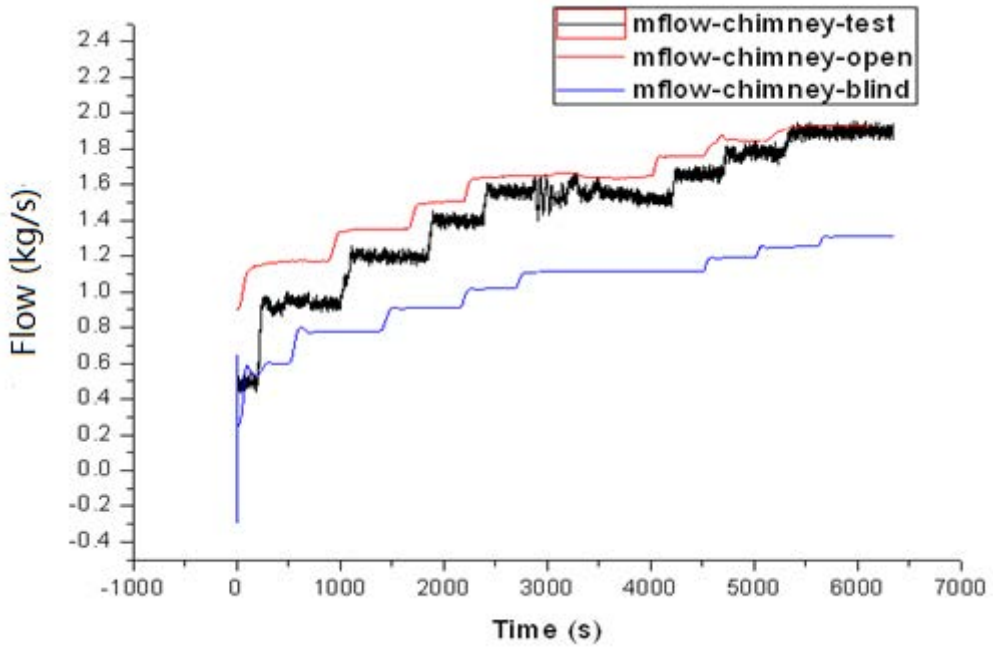

FIG. 4-351. Primary mass flow.

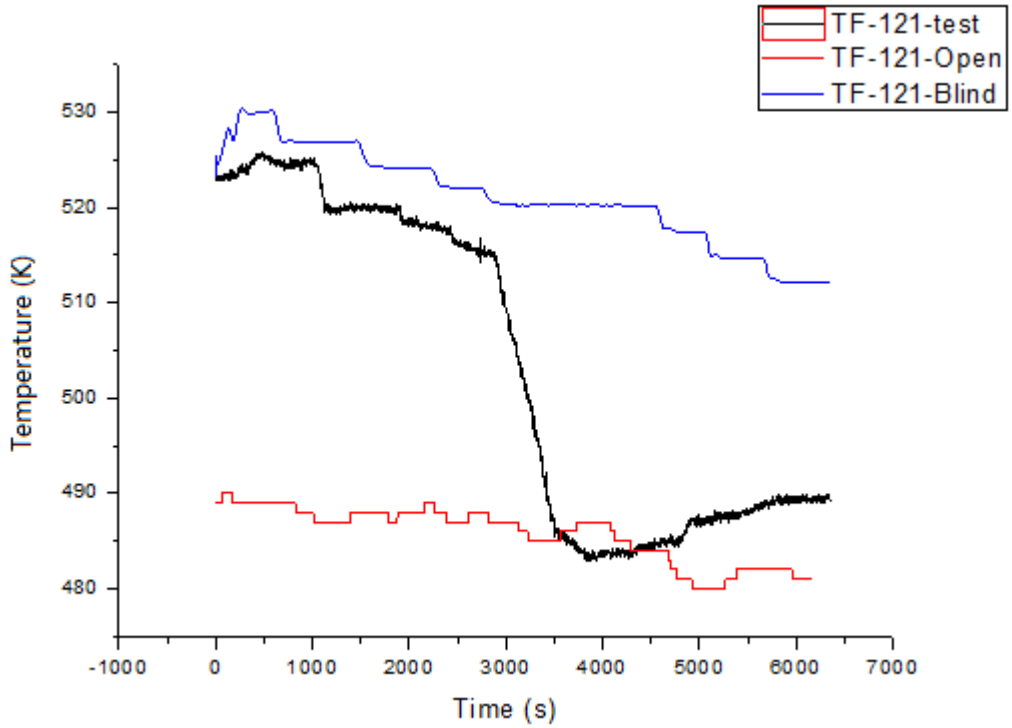

FIG. 4-352. Primary temperature of core inlet.

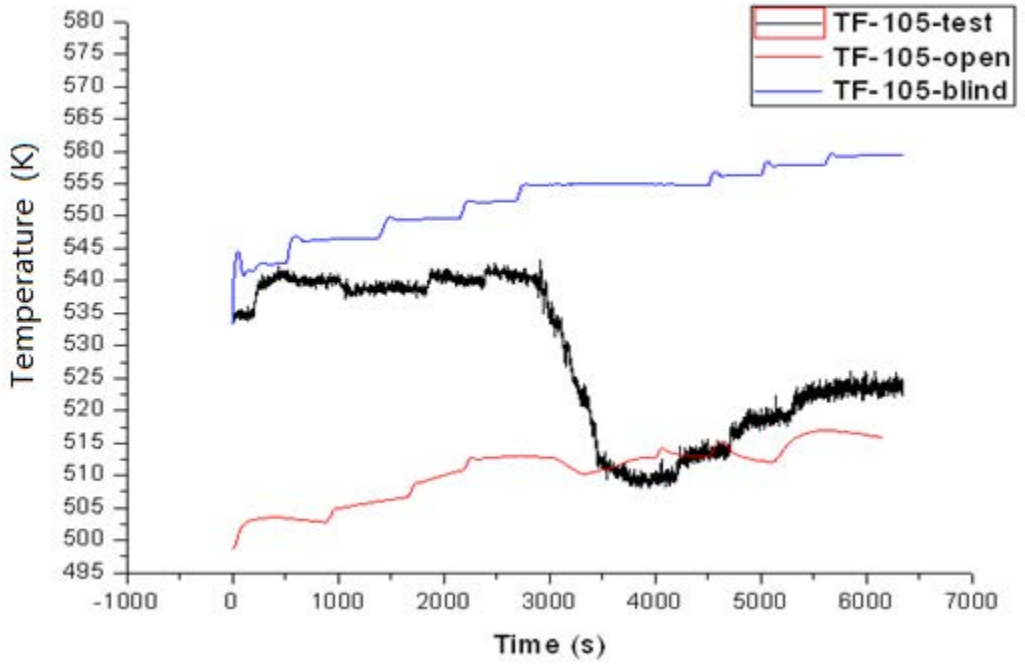

FIG. 4-353. Primary temperature of core outlet.

The primary water level is the same between the open calculaiton and the test (Fig. 4-354). The average pressurizer level by open calculation is higher and by blind calculation is lower than the experimental results (Fig. 4-355). It may be because the steady-state pressurizer level calculated by open code is higher and by blind code is lower than the test. The pressurizer level is always higher than 0.356 m in the open calculation results, so there is no charging flow during the whole process.

Figure 4-356 shows the surface temperature of core heater rod at core outlet. The surface temperature increases as the power increases. But the temperature calculated by code is lower than the test, which might be caused by the higher primary flow rate in the code calculation.

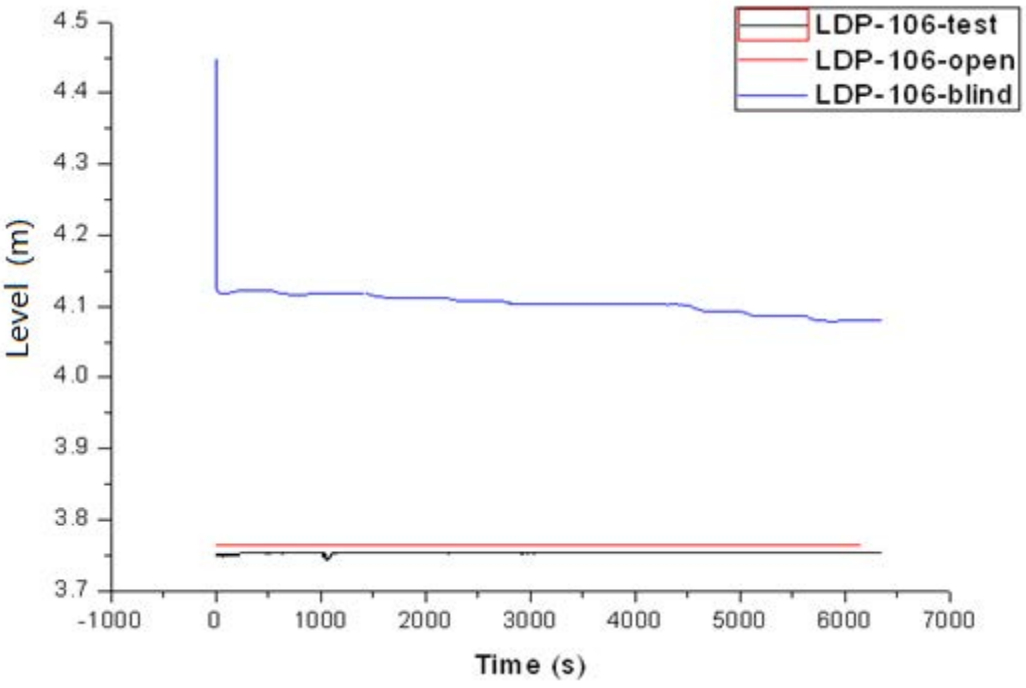

FIG. 4-354. Primary water level.

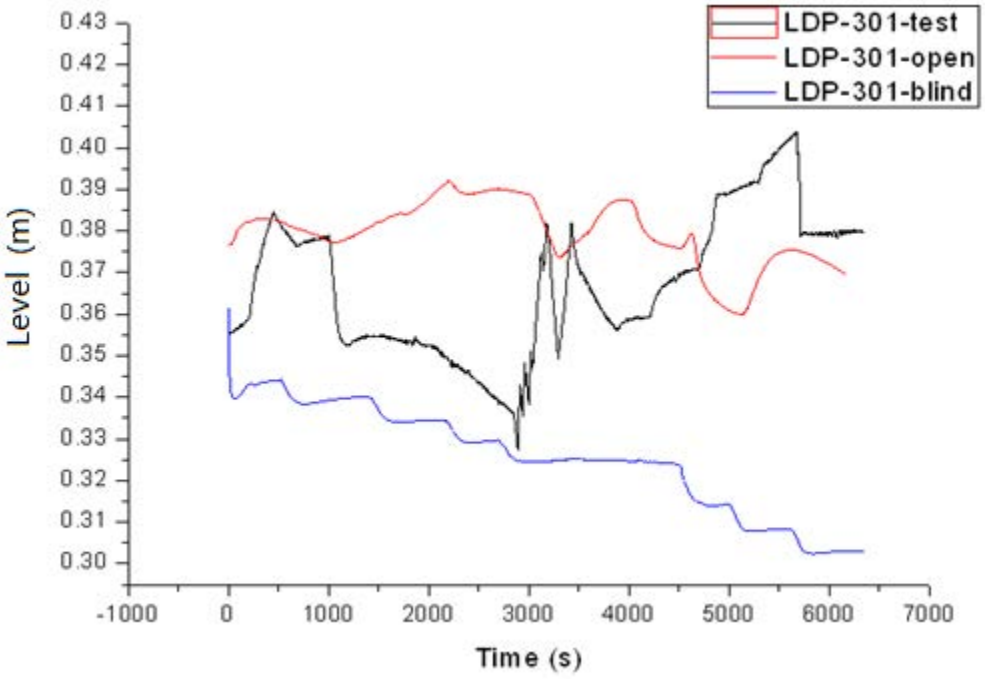

FIG. 4-355. Primary pressurizer level.

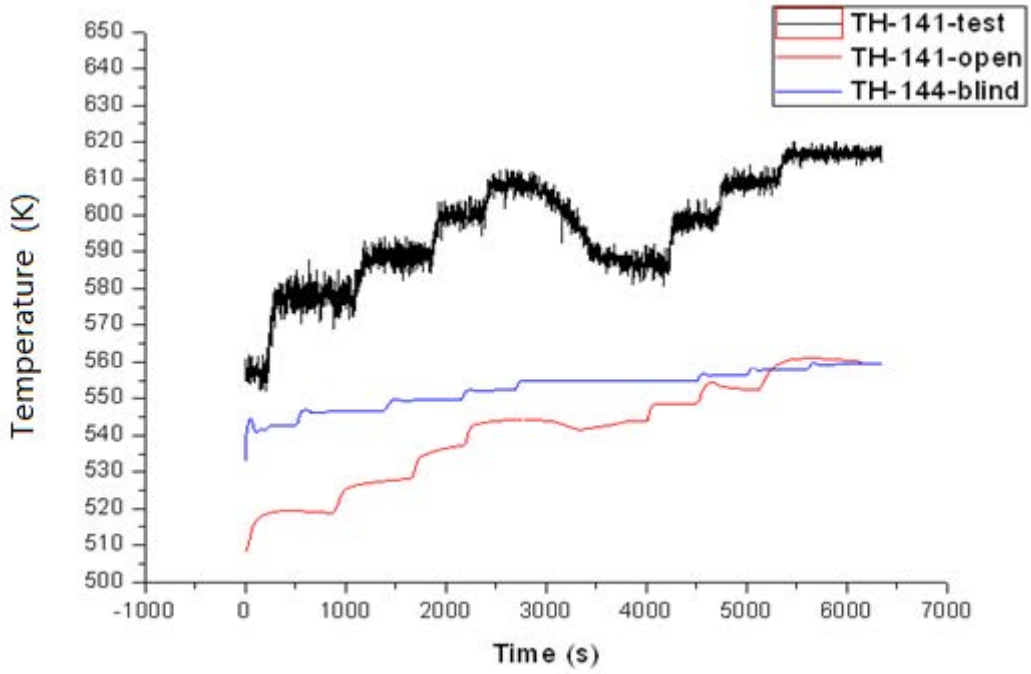

FIG. 4-356. Surface temperature of core heater rod at core outlet.

4.14.4.2. SG thermal-hydraulic behavior

The open calculation of steam temperature of the SG outlet is lower than the test, so is the pressure. However, the blind calculation is the opposite. The feed water flow rate in the code is nearly the same with the test in the first 4500 s, but grows larger to balance the pressure (Fig. 4-359).

The average steam mass flow rate calculated by code is nearly the same with the feedwater flow rate, but with large fluctuation. The steam mass flow rate in the test is very small, which may be caused by the inaccurate measurement of steam flow (Fig. 4-360)

The feed water temperature and the core power is the same with the value given by the OSU, while the little fluctuation is omitted (Fig. 4-361). Compared with the test results, the feed water pressure is higher in the blind calculation and lower in the open calculation, but the difference is small (Fig. 4-362).

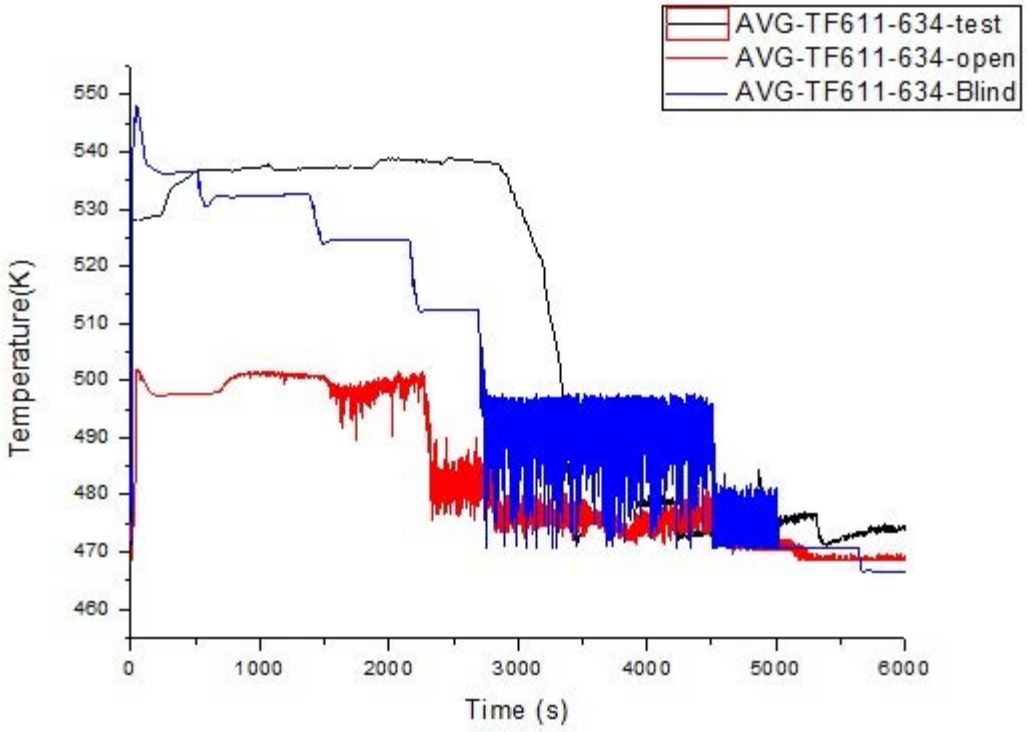

FIG. 4-357. SG outlet steam temperature.

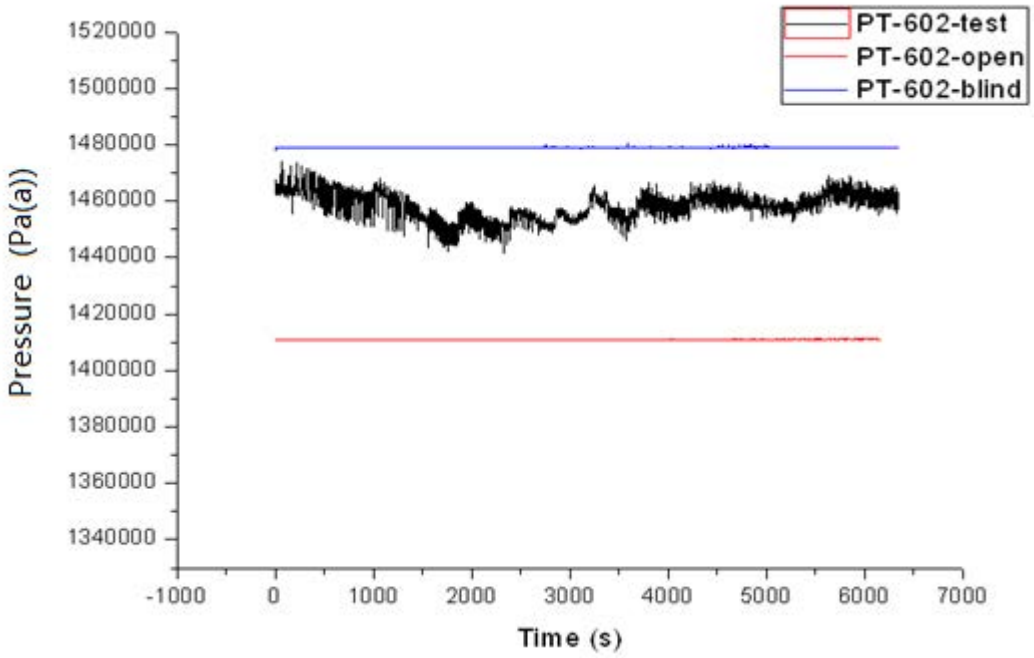

FIG. 4-358. SG outlet steam pressure.

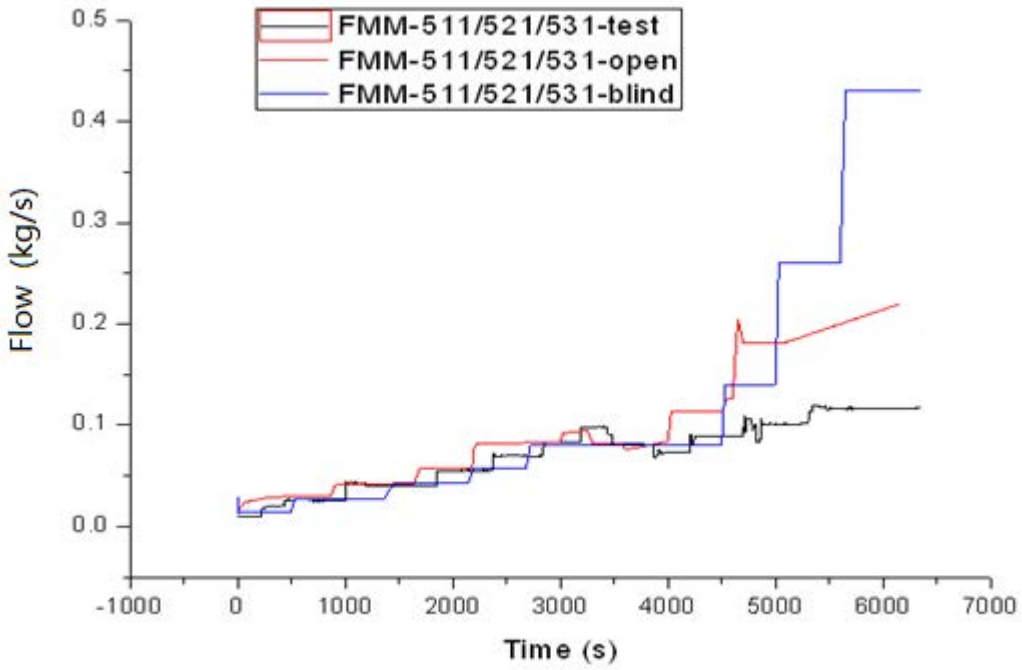

FIG. 4-359. Feed water flow rate.

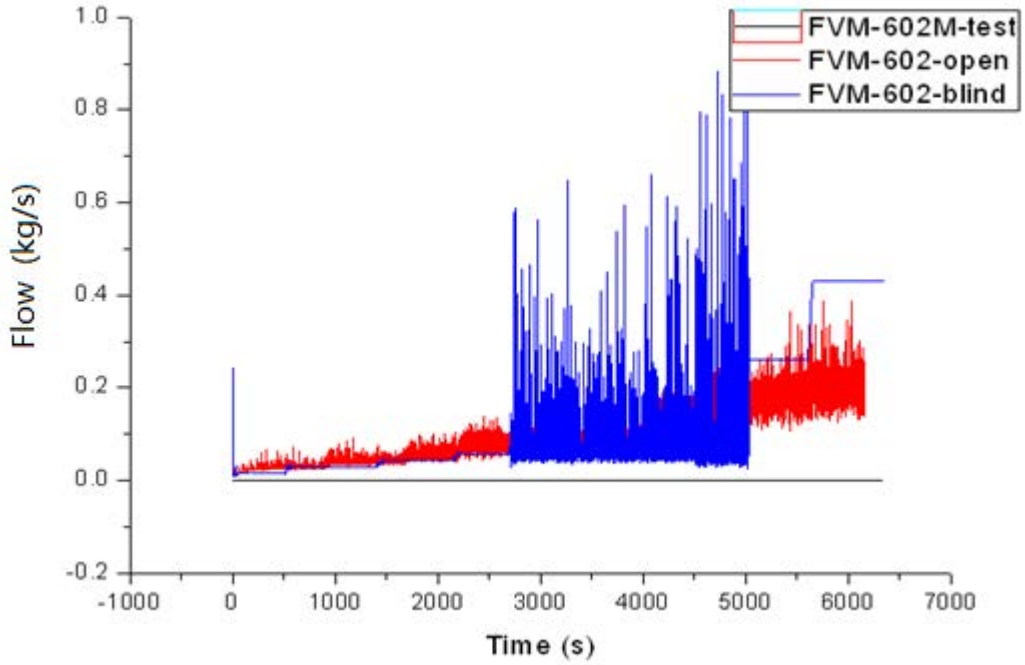

FIG. 4-360. SG steam flow rate.

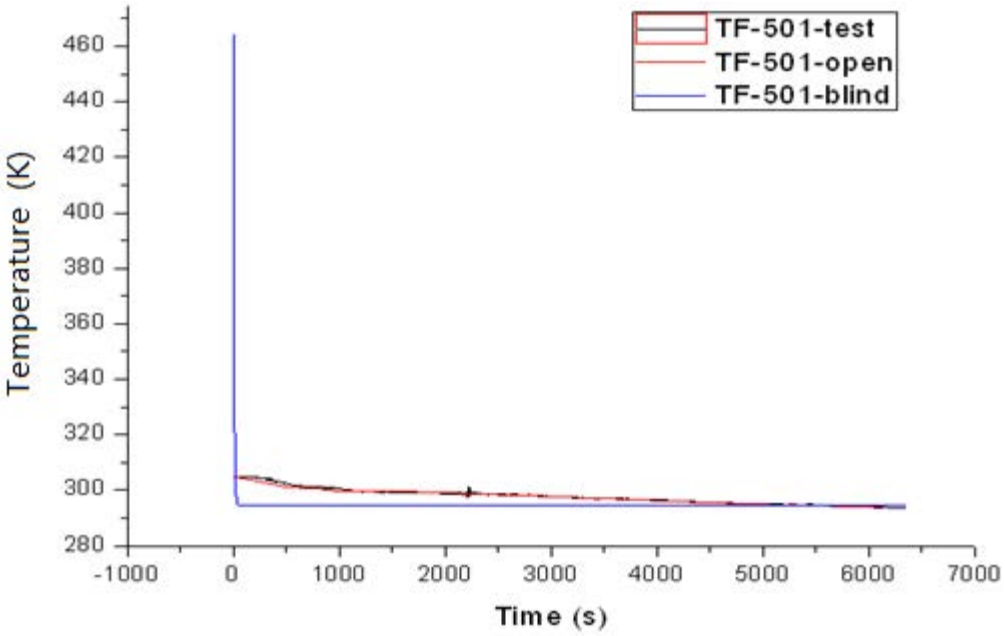

FIG. 4-361. Feed water temperature.

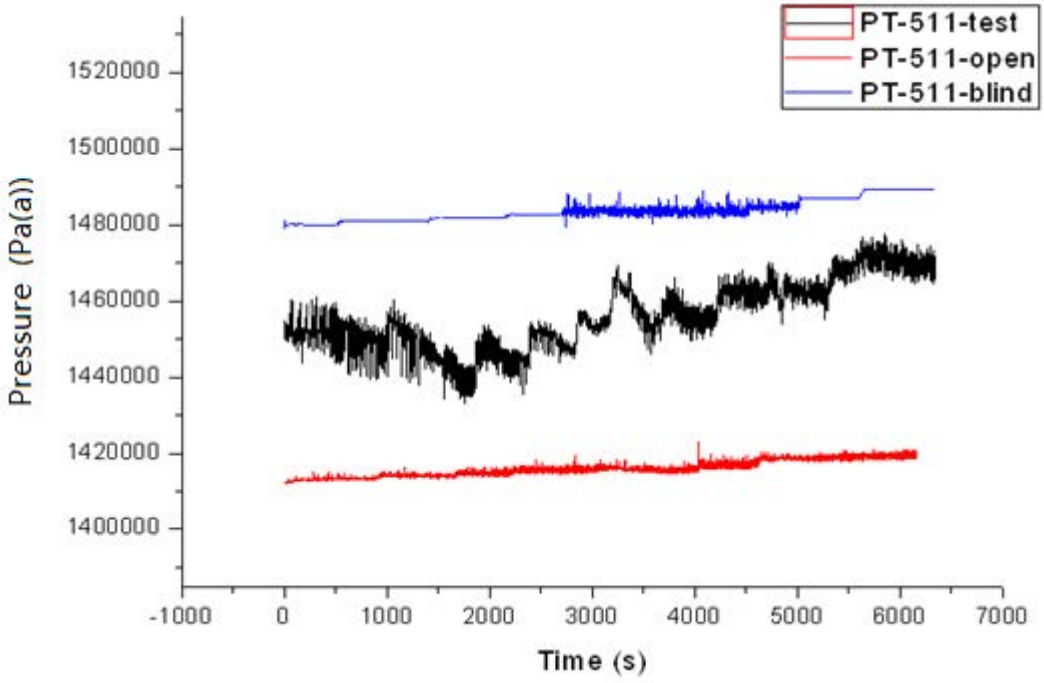

FIG. 4-362. Feed water pressure.

4.15. UNIPA - ITALY

4.15.1. Computer codes

TRACE code is used for ICSP analysis. Brief description on TRACE code is given in Section 4.10.1.

4.15.2. System idealization

The OSU-MASLWR TRACE nodalization [28], made by using SNAP [29] and shown in Figure 4-363, is developed in order to assess and validate the TRACE code [30] against the natural circulation database developed in the OSU-MASLWR test facility. The nodalization models the primary and the secondary circuit, the HPC, the heat transfer plate and the CPV. The ADS blow down lines, vent lines and sump return lines are modeled as well.

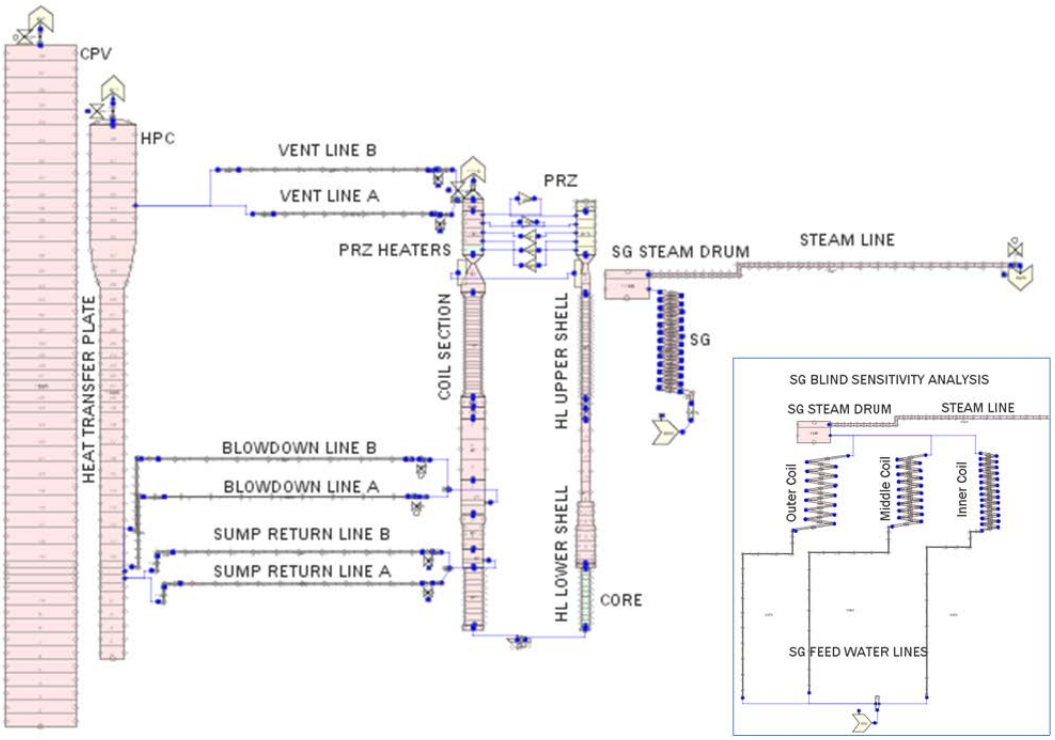

FIG. 4-363. OSU-MASLWR TRACE model [28].

The “slice nodalization” technique is adopted in order to improve the capability of the code to reproduce natural circulation phenomena. This technique consists in realizing the mesh cells of different nodalization zones, at the same elevation, with the same cell length. This is a way to avoid the error due to the position/elevation of the cell nodalization center that can influence the results of the calculated data when natural circulation regime is present.

The primary circuit of the TRACE model (Fig. 4-364) comprises the core, the Hot Leg (HL) riser, the Upper Plenum (UP), the Pressurizer (PRZ), the Steam Generator (SG) primary side, the Cold Leg (CL) down comer and the Lower Plenum (LP). After leaving the top of the HL riser, the flow enters the UP divided in two thermal hydraulic regions connected to the PRZ. After living the UP the flow continues downward through the SG primary section and into the CL down comer region.

The core is modeled with one hydraulic region thermally coupled with one equivalent active heat structure simulating the 56 electric heaters. The PRZ is modeled with two hydraulic regions, connected by different single junctions, in order to allow potential natural circulation/convection phenomena. The three different PRZ heater elements are modeled with one equivalent active heat structure. The thick baffle plate is modeled as well. The direct heat exchange by the internal shell between the hotter fluid in the ascending riser and the colder fluid in the descending annular down comer is modeled by heat structures thermally coupled with these two different hydraulic regions.

SG coils are modeled with only one “equivalent” vertical group of pipes thermally coupled, by an equivalent heat structure, with the SG primary side section. A model with three different equivalent oblique group of pipes has been implemented as well. Previous analyses, based on the TRACE simulation of the OSU-MASLWR-002 test, show that the instabilities of the superheat condition of the fluid at the outlet of the SG are also related to the equivalent SG model. Since in theses analyses a model with one equivalent vertical group of pipes shows a more stable fluid temperature at the SG outlet, this model is used as reference for the analysis of the ICSP test 2 and 3. A sensitivity study with three different equivalent oblique groups of pipe is considered for the BLIND analysis of the ICSP test 3 (Fig. 4-363). It is to underline that one of the outer coil is plugged; this is considered in both the models. In order to simulate the metal mass of this helical coil a passive equivalent heat structure is modeled. It is to underline that, in order to reach the initial conditions of the ICSP tests, the heat transfer area of the equivalent helical coil SG heat structure is incremented.

In order to simulate the ICSP test 2, the HPC is modelled with one hydraulic region connected by a heat structure, representing the heat transfer plate, to the CPV simulated with another hydraulic region. A sensitivity analysis, performed in the BLID calculation, considers the HPC region divided in two hydraulic regions, connected by single junctions, in order to allow possible natural circulation/convection phenomena. The ADS lines are modeled separately in order to simulate the ICSP test 2 logic. In the ADS lines are modeled the sparger (vent and blowdown ADS lines) the orifice (sump return, vent and blowdown lines) and the heat structure with related insulation. The heat losses of these lines are taken into account. The RPV, HPC and CPV shell and the connected insulation are modeled.

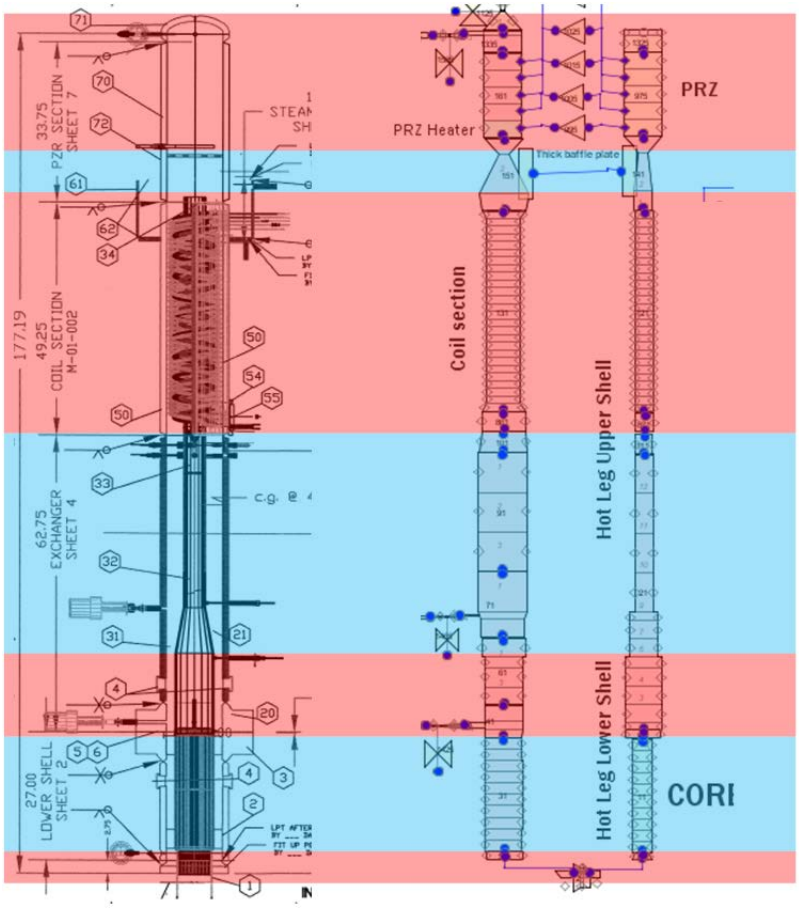

FIG. 4-364. Correspondence between the TRACE nodalization and the facility RPV.

The value of roughness used in the hydraulic component is 5.0 x 10^{-6} m. In order to estimate the k loss coefficient different options have been used [30].

4.15.2.1. System idealization for blind calculation

In order to reach the Boundary and Initial Conditions (BIC) of the ICSP test 2, an arbitrary pre-test phase is conducted during the simulation. At the end of this pre-test phase, Start of the Transient (SOT), the BIC of the test are stable for 10 minutes prior to the loss of feed water event.

At the beginning of the TRACE pre-test phase the core power is at about 298 kW, the PRZ pressure is controlled by using a break component coupled with a valve, the secondary feedwater is controlled in order to maintain the selected average SG outlet steam temperature, the secondary side outlet pressure is controlled in order to maintain ICSP specification value. After 500 s the PRZ pressure is not controlled and it starts to decrease for the energy removed by the secondary side and for the heat losses of the facility. The PRZ heaters are set up in order to control the primary side pressure at the ICSP specification value of 8.618 MPa(g). The PRZ heaters supply 0 to 12 kW following a pressure table. The length of the TRACE pre-test phase is 4000 s. The heat losses of the facility are evaluated by the code at about 1 kW. The initial conditions are in general stable in the 600 s of steady state analysis.

In order to reach the BIC of the ICSP test 3 an arbitrary pre-test phase is conducted during the simulation. At the end of this pre-test phase, SOT, the BIC of the test are stable for 10 minutes.

At the beginning of the TRACE pre-test phase the core power is about 40 kW, the PRZ pressure is controlled by using a break component coupled with a valve, the secondary feed water is controlled in order to maintain the selected average SG outlet steam temperature, the secondary side outlet pressure is controlled in order to maintain the ICSP specification value. After 500 s the PRZ pressure is not controlled and it starts to decrease for the energy removed by the secondary side and for the heat losses of the facility. The PRZ heaters are set up in order to control the primary side pressure at the ICSP specification value of 8.618 MPa(g). The length of the TRACE pre-test phase is 10,000 s. A value of heat losses of about 5 kW has been assumed considering the information distributed during the 3rd Workshop held on 27-30 March 2012 at KAERI in Daejeon, Rep. of Korea.

4.15.2.2. Modelling change for open calculation

In order to improve the results of the TRACE ICSP test 2 calculated data, few modifications have been implemented in the input deck. An increase of the heat losses, a revised increment of the SG equivalent heat transfer area and a better fitting of the SG secondary side outlet pressure, that is considered as a BIC, have been implemented. The control of the SG outlet temperature during the steady state phase has been implemented as well. The SG outlet pressure, the SG inlet pressure, the SG inlet temperature and the SG mass flow rate are imposed as BIC. Considering the availability of the experimental data, a revision of these BIC has been implemented during the ICSP OPEN case.

In order to improve the results of the TRACE ICSP test 3 calculated data, few modifications have been implemented in the input deck. An increase of the heat losses and a revised increment of the SG equivalent heat transfer area have been implemented. It is to underline that in order to have a better fitting of the RPV mass flow rate a Reynolds number - dependent loss coefficient is necessary. Since this option is not available in the TRACE V5.0 Patch 1 code version used for this ICSP, a fictitious valve with flow area dependent from the core power has been implemented at the core entrance. The Reynolds number - dependent loss coefficient is available in the new TRACE V5.0 Patch 3.

4.15.3. Analysis results for loss of feed-water transient

At the SOT, obtained by TRACE code, the primary system is filled with subcooled water, the primary system inventory is at 100% and the PRZ level is at about 0.35 m. When the core power is at about 298 kW, the PRZ heaters are ON in order to maintain the primary pressure set-point and the containment heaters are OFF. The primary pressure is around 8.7 MPa(a). The natural circulation is present in the facility primary side. The secondary side removes net primary power, core power less ambient losses, with a steam pressure of 1.414 MPa(a). The ADS blowdown line valves, the ADS vent line valves and the ADS sump return line valves are closed. The HPC vent valve SV-800 is open; during the transient it is closed. The boundary condition of the TRACE model during the simulation of the ICSP test 2 are reported in the Figure 4-365.

At the SOT a loss of feed water event takes place. Since the energy removing capacity of the secondary side tends to zero a primary pressure increase takes place. When the primary pressure reaches the value of 9.064 MPa(a) the core heaters are turned in decay mode following the experimental data disclosed in the BLIND ICSP phase specification (26 s after the SOT for the BLIND case). The valve PCS 106 A opens (44 s after the SOT) and a blowdown takes place. The primary and HPC pressure starts a process of equalization. Chocked flow phenomena take place in the vent line A. A rapid increase of the HPC pressure takes place. The volume of the HPC is filled with steam condensing in the containment wall transferring energy to the CPV.

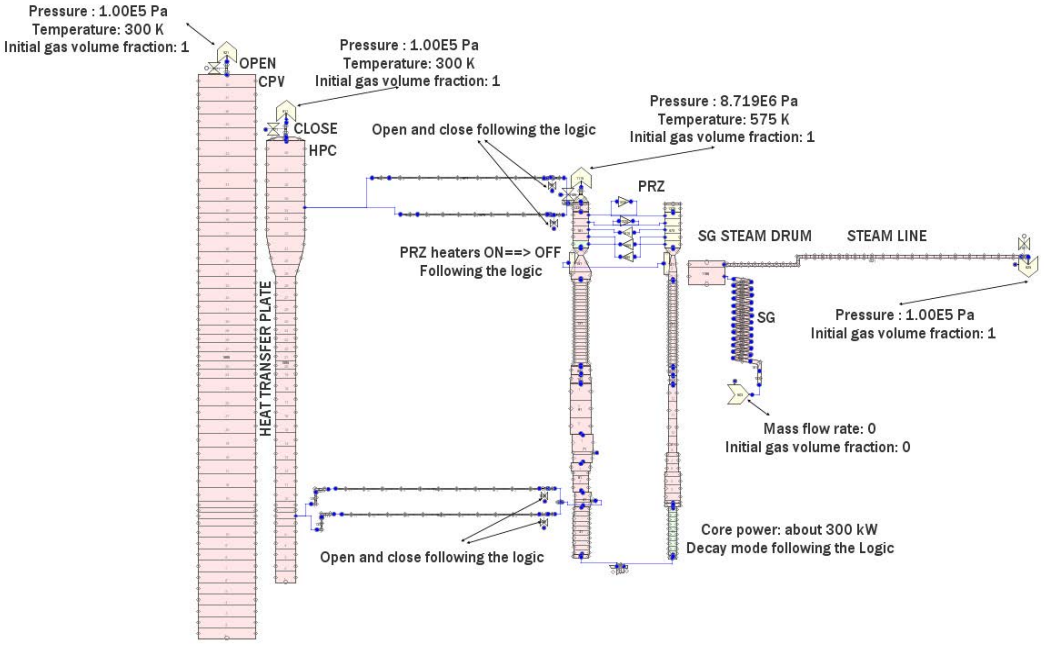

FIG. 4-365. Boundary condition of the TRACE model during the simulation of the ICSP test 2.

At 125 s after the SOT, the valve PCS 106 A starts to cycling following the ICSP logic actuation**.** In fact between 125 and 4062 s, the HPC pressure oscillates but never reaches the setpoint of 1.997 MPa(a).

At 4062 s after the SOT, the pressure differences between the primary side and the HPC is less than 0.034 MPa, therefore the valve PCS 106 A stays permanently open. The valves PCS 106 B (4152 s after the SOT), PCS 108 A (4154 s after the SOT) and B (4155 s after the SOT) stay permanently open permitting the refill of the primary side and the long term cooling phenomenology typical of the MASLWR design.

After the equalization of the HPC and primary pressure, the HPC pressure is in general higher than the primary side pressure in agreement with the experimental data. This is related to the position of the measurement instrument at the bottom of the HPC. A slow decrease of the primary and HPC pressure is predicted by the code.

During the long term cooling, the vapor produced in the core goes in the upper part of the facility and through the vent valves go to the HPC where it is condensed. At this point through the sump return lines the fluid go to the core again.

Thermal stratification in the HPC and in the CPV is observed. Some discrepancies are observed between experimental and calculated data, these could be related to the facility nodalization. However considering the increase of the CPV temperature, the study of the facility thermal hydraulic behavior, when the saturation condition is reached, is of interest for a safety point of view in relation to the long term cooling phenomenology.

At the end of the test (15822 s after the SOT) the primary pressure is at about 0.6 MPa(a).

Table 4-29 shows the ICSP test 2 event sequence and the related phenomena. The figures related to the BLIND and OPEN reference case are reported in the Figures 4-368 to 4-378. Figures 4-366 and 4-367

show animation models, developed by using SNAP, visualizing the facility configuration during selected instants in the BLIND case. The analyses of the thermal hydraulic phenomena of interest are reported in the following sections.

4.15.3.1. RPV thermal-hydraulic behavior

The main thermal hydraulic phenomena characterizing the RPV during this test are the single phase natural circulation, the two-phase natural circulation, the intermittent two phase natural circulation, the heat transfer in covered or uncovered core, the by-pass heat transfer between riser and downcomer and the primary containment coupling during blowdown and long term cooling [31].

In order to thermal hydraulically characterize these phenomena the core outlet flow (FDP-131), the core outlet fluid temperature (TF-106), the average core inlet fluid temperature (AVG(TF-121 to 124)), the delta T core, the pressure drop across SG (DP-105) and core (DP-101), the power to fluid in core, the RPV and PRZ water level (LDP-106 and LDP-301 respectively), the void fraction at core outlet and riser, the fluid temperature difference AVG(TF-131,133,134)-AVG(TF-121 to 124), the surface temperature of the core heater rod at the core outlet (TH-141 to 146), the sump return line flow (PCS-108A and 108B), the primary void fraction at SG inlet, the PRZ pressure (PT-301), the RPV heat losses, the ADS vent flow and the cumulative ADS flow are considered. A detailed analysis of these parameters is reported in the BLIND and OPEN calculation reports.

The PRZ pressure behavior, Figure 4-368, is well predicted by the TRACE code. In particular four different phases could be identify: primary pressure peak phase, blowdown phase, valve cycling phase and long term cooling phase. The primary pressure peak, related to the loss of feed water transient, and the rapid pressure decrease, related to the vent valve opening, are predicted by the code. The oscillation of the primary pressure is well predicted by the TRACE code; its length is in general depended from the steady state conditions before the SOT (for example the way to control the feed water mass flow rate before the SOT can influence the fluid condition of the facility before the SOT) and the heat losses of the facility as it is shown from the sensitivity analyses performed in the BLIND phase of the ICSP. During the long term cooling phase the vapor produced in the core, through the vent line, goes to the HPC where it is condensed; then the fluid, through the sump return lines, goes to the downcomer and then in the core again. This natural circulation flow path is well predicted by the TRACE code. The OPEN calculation results show a more accurate PRZ pressure behavior prediction; this is mainly related to an increase of the heat losses of the RPV TRACE model.

The mass flow rate behavior is characterized by flow oscillations during the valve cycling phase. The long term cooling phase is characterized by a liquid behavior oscillating between positive and negative small value and by a positive small gas mass flow rate.

In relation to the RPV and PRZ level, Figures 4-369 and 4-370 respectively, the results of the calculated data show a general agreement with the experimental data. The core, as in the experimental data, is never uncovered. The oscillation phase and the refill phase are predicted by the code. In both the simulations, BLIND and OPEN, an underestimation of the RPV refill level rise is observed, therefore an underestimation of the long term core cooling phase RPV level is observed.

The core outlet and the average core inlet fluid temperature**,** Figures 4-371 and 4-372 respectively**,** are predicted by the code. A decrease of the inlet core temperature is experimentally observed when the refill of the core takes place. During the simulation the decrease of the inlet temperature is not observed. This could be related to the mono dimensional model of the downcomer causing an average temperature of the water in the nodalization volumes. A fine three-dimensional model of the entire RPV could improve the quantitative prediction of this parameter. As it is expected, the BLIND sensitivity study show that the quantitative prediction of the inlet/outlet core fluid temperature is influenced by the steady state initial conditions and by the heat losses of the facility. The surface temperature of the core heater rod at the core outlet (TH-141 to 146) are predicted by the TRACE code.

The expected behavior of the vent and sump return valves is predicted by the code. The behavior of the PCS 106 A, is characterized by an oscillating mass flow rate due to the valve cycling and a long term cooling mass flow rate behavior. The PCS 106 B is characterized by a first mass flow rate peak,

when the valve is opened, and a long term cooling phase mass flow rate behavior; no oscillations are present for this valve. The PCS 108A/B are characterized by a first mass flow rate direction change with consequent mass flow rate peak and a long term cooling phase mass flow rate behavior.

4.15.3.2. SG thermal-hydraulic behavior

The main thermal hydraulic phenomena characterizing the SG are the transient of boiling in coil and the heat transfer to secondary.

In order to thermal hydraulically characterize these phenomena the steam temperature at the SG exit (AVG(TF-611 to 615, 621 to 625, 631 to 634)), the steam pressure (PT-602), the steam flow (FVM-602M), the average feedwater inlet pressure (AVG (PT-511, 521, 531)), the feedwater flow (SUM(FCM-511, 521, 531)), the feedwater temperature (TF-501) and the power removed at SG are considered. In order to have a direct visualization of the transient of boiling in coil, Figures 4-366 and 4-367 show animation models, developed by using SNAP, visualizing the facility configuration, in steady state and in selected transient instants, for the BLIND case. A detailed analysis of these parameters is reported in the BLIND and OPEN calculation reports.

It is to underline that during the steady state phase, before the SOT, the saturation condition is reached at the pipe 241 (1.63 m from the SG secondary inlet), and the superheat condition is reached at the pipe 401 (5.35 m from the SG secondary inlet). During the steady state phase, Figure 4-366, the SG secondary side subcooled saturated and superheated regions are predicted by the code and the steam will leave the SG superheated. During the transient, started from a loss of feed water event, the SG is not anymore the RPV heat sink. The calculated data show that the heat transfer through the SG is negligible. The SG is in superheated condition.

The steam temperature at the SG exit is in general qualitatively predicted by the code, Figure 4-373. During the BLIND calculation it is observed a general overestimation of the calculated data; in the OPEN calculation a general underestimation of the calculated data is observed during the long term core cooling phase. From the BLIND sensitivity study it is observed that the SG superheating behavior is depended from the steady state BIC and the heat losses of the facility.

The secondary SG outlet pressure, the SG inlet pressure, the SG inlet temperature and the SG mass flow rate are imposed as BIC. Considering the availability of the experimental trend a revision of these BIC has been implemented during the OPEN case.

4.15.3.3. HPC thermal-hydraulic behavior

The main thermal hydraulic phenomena characterizing HPC are the thermal stratification, the primary containment coupling during blowdown and long term cooling, the HPC/CPV thermal coupling through the heat transfer plate. This last phenomenon is considered in the CPV section.

The HPC thermal hydraulic behavior is characterized mainly by the pool pressure at the HPC bottom (PT-801), the air/steam pressure, the water level (LDP-801) and the SV-800 flow. In order to characterize its thermal stratification, the water temperatures located inside the HPC near the heat transfer plate (TF-811 to 861) and the temperatures within the walls of the HPC, between the heaters and the water, (TW-891 to 894) are considered. A detailed analysis of these parameters is reported in the BLIND and OPEN calculation reports.

The HPC pressure behavior, Figure 4-374, is predicted by the code. In particular, three different phases could be identified: a first pressure increase, an oscillation phase, and a long term cooling phase. As in the experimental data the HPC pressure oscillates between the setpoint values. The HPC pressure long term cooling phase is in general overestimated in comparison with the experimental data. A better quantitative prediction of the long term cooling phase is observed during the OPEN calculation, though and underestimation is observed in the last part of the transient. This is related to the better quantitative RPV pressure prediction of the OPEN calculations. It is to underline that, as it is shown from the BLIND sensitivity calculations, the slope of the HPC pressure increase is related to the PCS 106 A valve k loss coefficient. Considering the RPV/HPC coupling, it is to underline that the length of the HPC pressure oscillation is in general depended from the steady state conditions before

the SOT and the heat losses of the facility as it is shown from the sensitivity analyses performed in the BLIND phase of the ICSP.

The different phases of the HPC water level (Fig. 4-375) are predicted by the code. In particular the first rapid increase of level and the decrease of the HPC level slope are predicted by the code. When the sump return valves open, the decrease of the HPC level is well predicted by the TRACE code as the long term steady state level phase. In general during the simulations, though the long term level is in a quantitative agreement with the experimental data, it is underestimated the HPC level increase. From the BLIND sensitivity analyses it is observed that the maximum reached by the HPC level is dependent by the PCS 106 A k loss coefficient. The slope of the HPC level increase is in general depended from the heat losses of the facility.

As in the experimental data the SV 800 valve remains closed.

The thermal hydraulic experimental behavior of the HPC stratification is compared with the calculated data. Figure 4-376 shows the TF-821 and TF-861 behavior. The TF 811 and 821 are the lowest thermocouples. The TF-811 behavior is not predicted by the code. This is related to the mono dimensional model of the containment. In particular in the experimental data a general mixing of the primary vapor with the HPC water and an axial conduction along the heat transfer plate causes a rapid increase of the HPC water temperature. The calculated TF-821 temperature increases but with delay in comparison with the experimental data. In particular there isn't a temperature increase during the cycling phase. The TF-831, 841, 851, 861, are qualitatively but not quantitatively predicted by the code. A general overestimation of the calculated data is observed. This could be related to the position of the thermocouples; in fact they are located very close to the heat transfer plate, where the condensation takes place, therefore they could not represent the average fluid temperature; the temperature calculated by the code is the average temperature related to the nodalization volume. It is underline that the rapid increase of the HPC temperature is well predicted by the TRACE code.

In relation to the TW-891, 892, 893, 894 the comparison with the experimental data show that there is an agreement with the experimental data. Figure 4-377 shows the TW-891 and TW-893 behavior.

Blind sensitivity analyses show that a better prediction of the HPC temperature behavior could be reached by dividing the HPC volume in two hydraulic regions connected by single junctions. In this case the possible natural circulation/convection could be predicted by the code. A fine three-dimensional model could improve the code prediction.

4.15.3.4. CPV thermal-hydraulic behavior

The main thermal hydraulic phenomena characterizing the CPV are the thermal stratification and the HPC/CPV thermal coupling through the heat transfer plate.

The CPV thermal hydraulic behavior is characterized by water temperatures located inside the CPV near the heat transfer plate (TF-815 to 865) in order to analyse the thermal stratification, and the wall temperatures within the heat transfer plate, between the CPV and the HPC, nearest to the HPC (TW-812 to 862) and the wall temperatures within the heat transfer plate, between the CPV and the HPC, nearest to the CPV (TW-814 to 864) in order to analyse the heat transfer through the plate between HPC and CPV. A detailed analysis of these parameters is reported in the BLIND and OPEN calculation reports.

The experimental CPV thermal hydraulic behavior shows a first rapidly temperature increase, a change of slope during the cycling phase of the transient and a long term cooling behavior. The results of the calculated data show the discrepancies between experimental and calculated data; the code predicts a slowest temperature increase. This is could be related to the position of the thermocouples; in fact they are located very close to the heat transfer plate, therefore they could not represent the average water temperature; the temperature calculated by the code is the average temperature related to the nodalization volume. In agreement with the HPC behavior, a fine three-dimensional model could improve the code prediction of the CPV behavior. Figure 4-378 shows the TF-825 and TF 865 behavior.

TABLE 4-29. ICSP SP-2 EVENT SEQUENCE

Facility Operation	Time (s) EXP.	Time (s) Blind	Time (s) Open
Start of simulation – steady state (start of data collection)	0	-600	-600
Stop MFP Close HPC vent valve SV – 800	0	0	0
PZR pressure (PT-301) reaches 9.064 MPa(a) Enter decay power mode	30	26	42
PRZ pressure (PT-301) reaches 9.409 MPa(a) De-energize PZR heaters Open ADS vent valve (PCS-106A)	48	44	59
Start long-term cooling when pressure difference between primary system and HPC (PT-301 minus PT-801) becomes less than 5 psi (0.034 MPa) Open and remain open of PCS-106A	4024	4062	4039
Open and remain open of PCS-106B	4114	4152	4129
Open and remain open of PCS-108A	4116	4154	4131
Open and remain open of PCS-108B	4117	4155	4132
End of test when one of the following conditions is reached: -PZR pressure ≤ 0.135 MPa(a) -Primary coolant temperature (TF-132) ≤ 35 ºC -24 hours have elapsed	15822	15822	15822

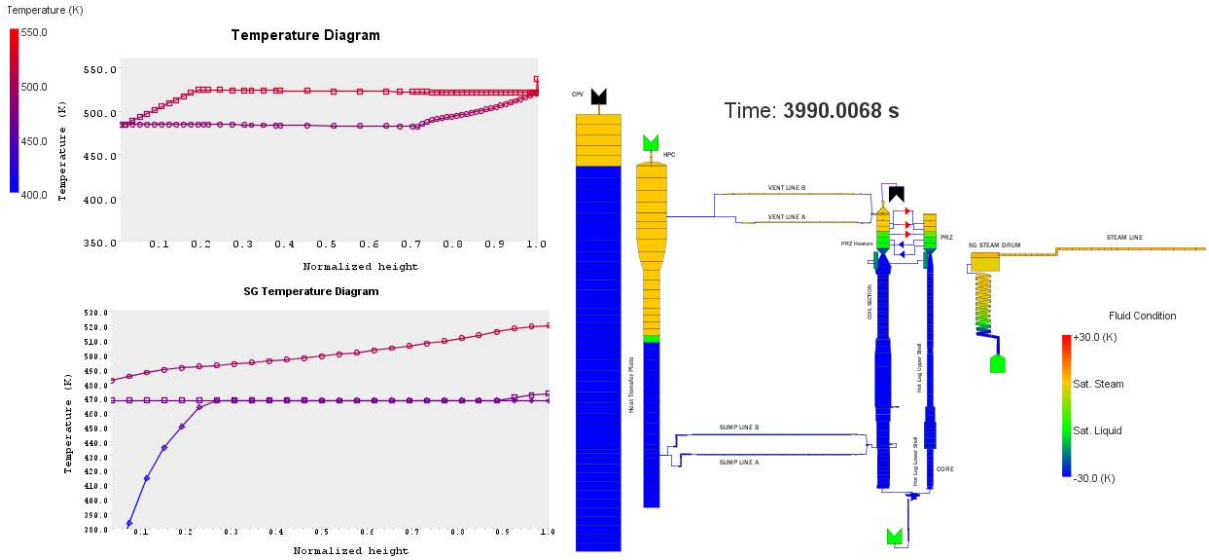

FIG. 4-366. SNAP animation model showing the steady state conditions of the TRACE model at the end of the steady state phase of the ICSP test 2 (BLIND case).

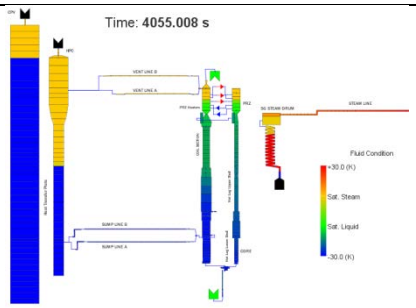

TRACE model condition 55 s after the SOT

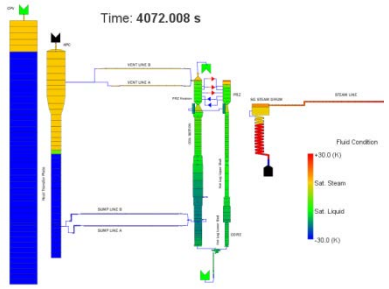

TRACE model condition 72 s after the SOT

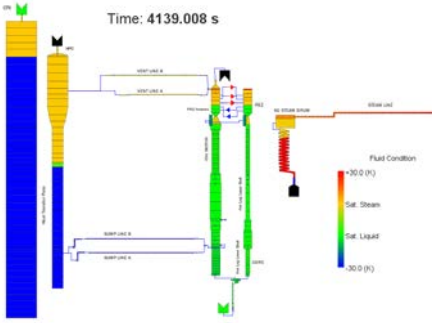

TRACE model condition 139 s after the SOT

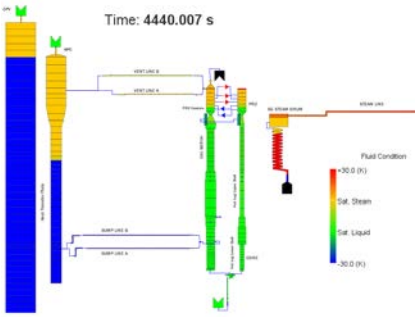

TRACE model condition 440 s after the SOT

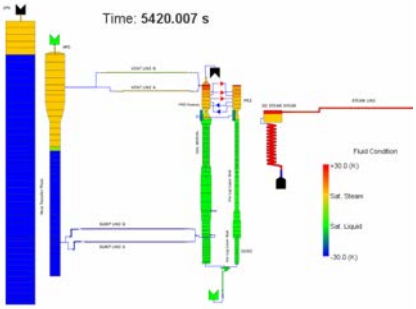

TRACE model condition 1420 s after the SOT

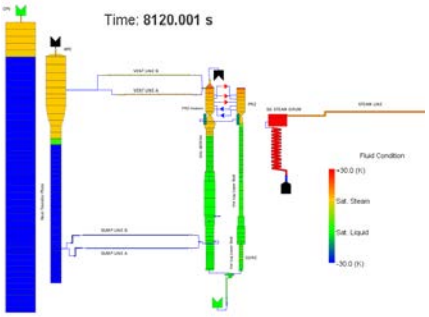

TRACE model condition 4120 s after the SOT

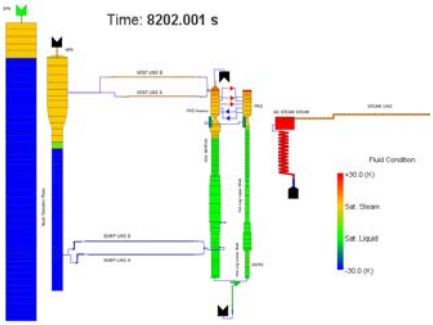

TRACE model condition 4202 s after the SOT

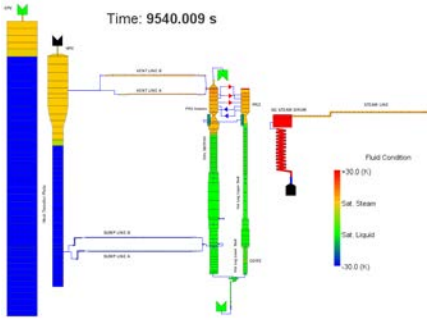

TRACE model condition 5540 s after the SOT

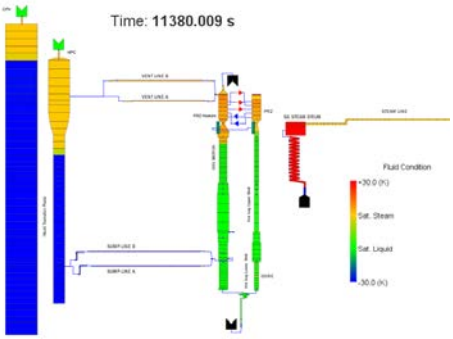

TRACE model condition 7380 s after the SOT

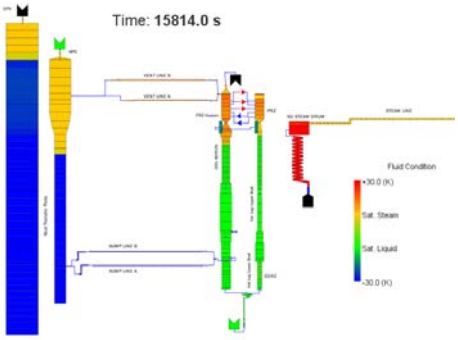

TRACE model condition 11814 s after the SOT

FIG. 4-367. SNAP visualization of selected instants during the ICSP test 2 transient.

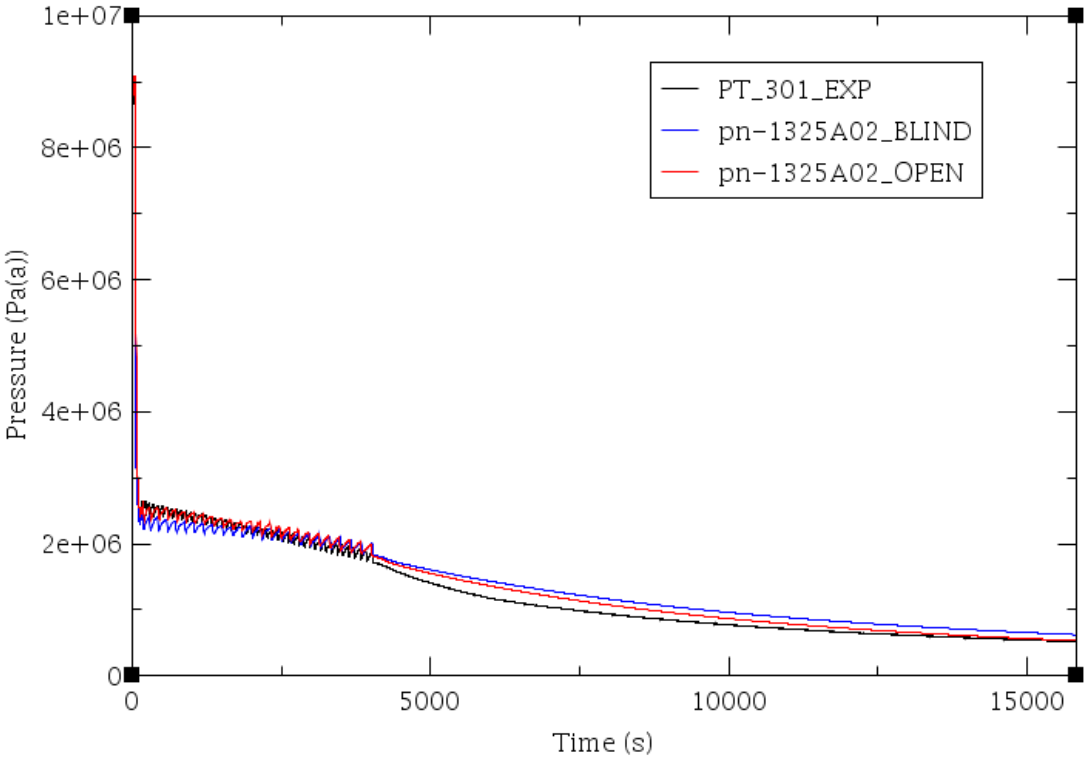

FIG. 4-368. PRZ pressure (PT-301).

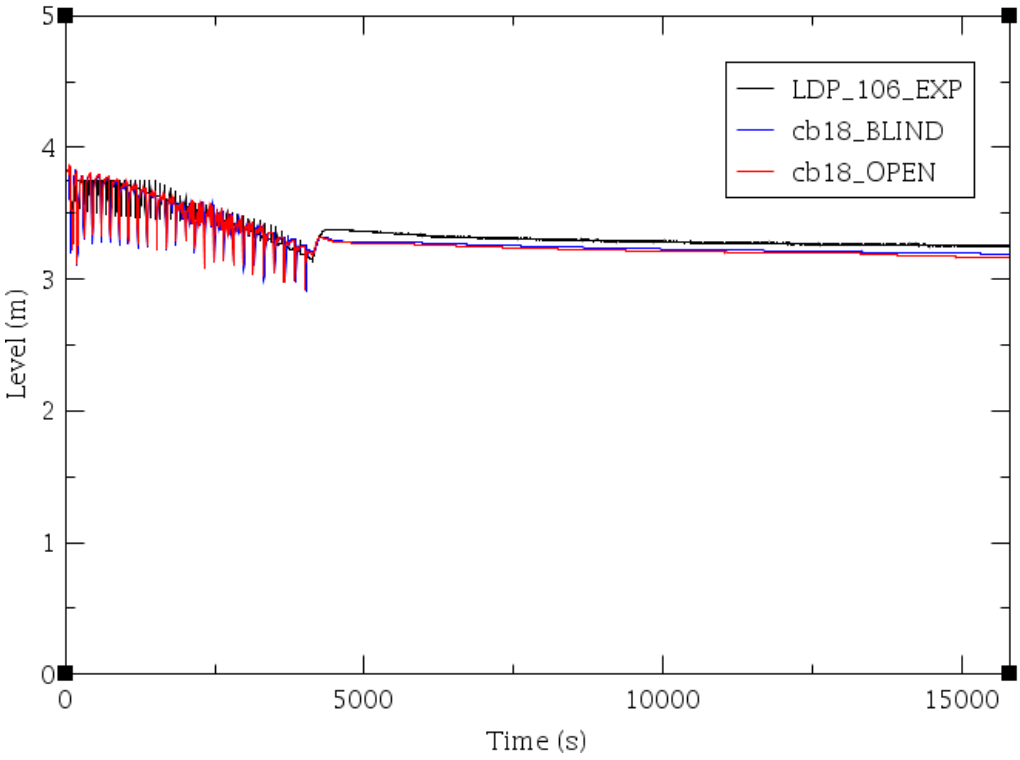

FIG. 4-369. RPV level (LDP-106).

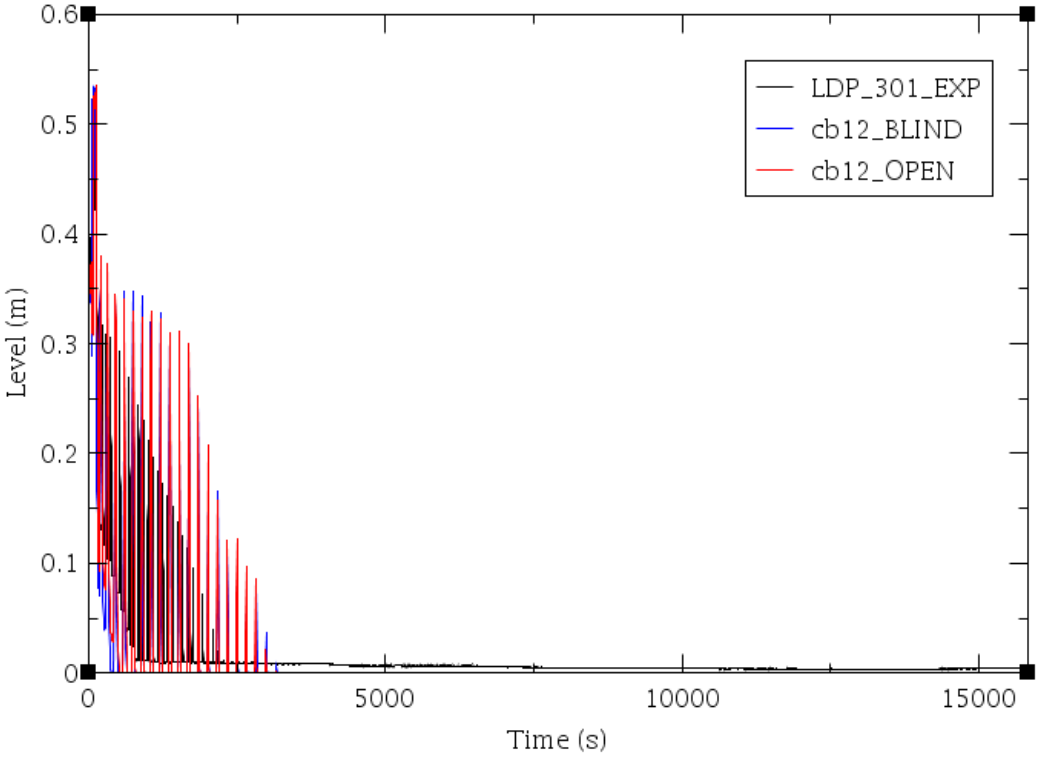

FIG. 4-370. PRZ level (LDP-301).

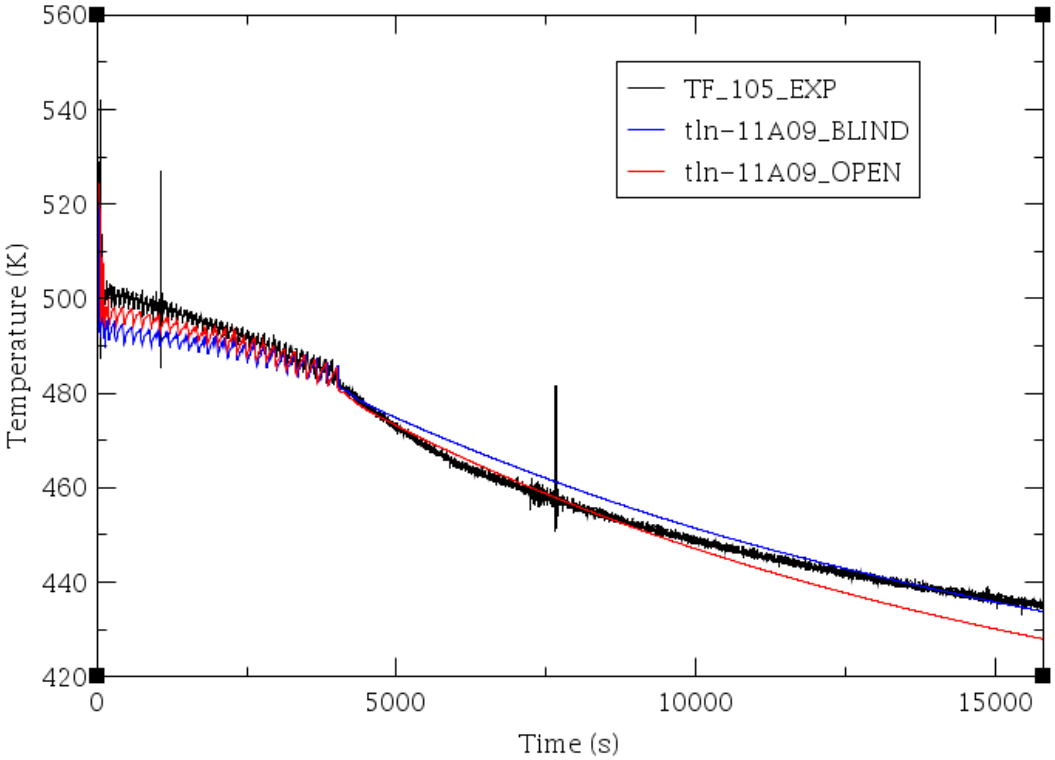

FIG. 4-371. Core outlet temperature (TF-105).

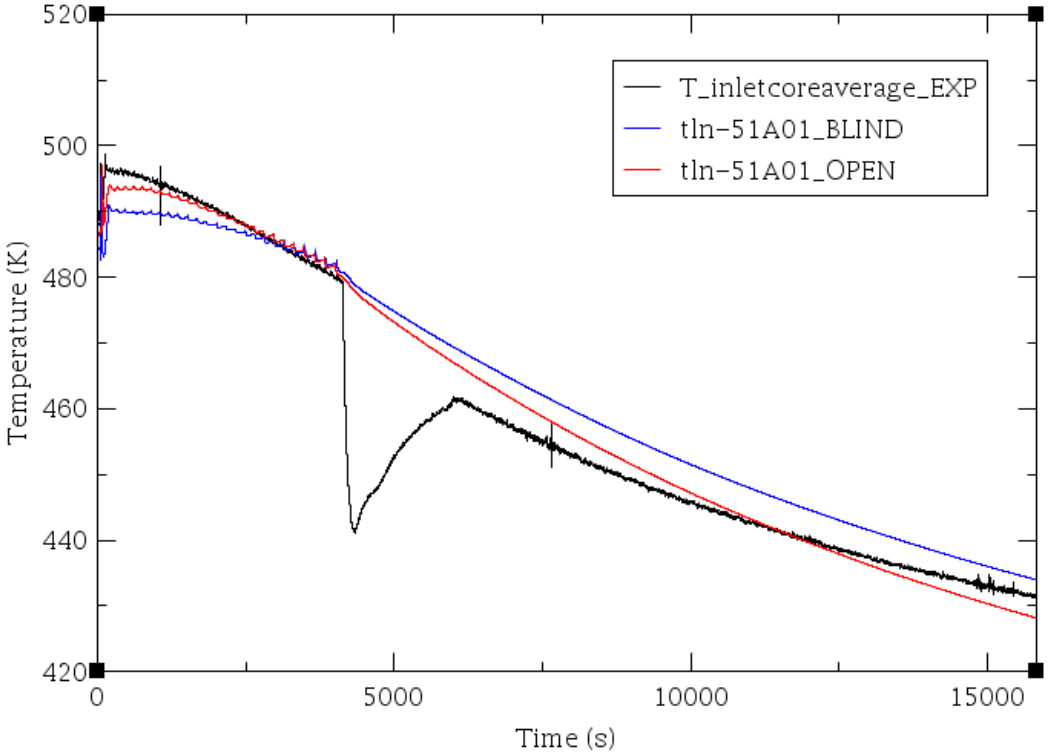

FIG. 4-372. Inlet core average temperature (AVG(TF-121,122,123,124)).

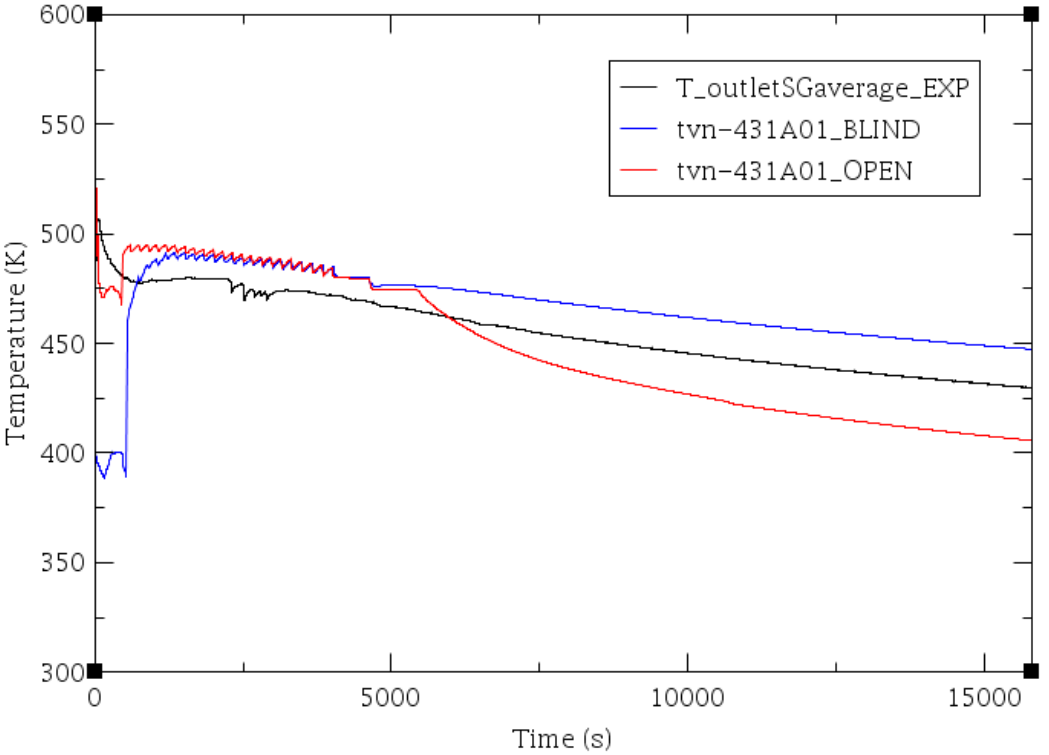

FIG. 4-373. Steam temperature at the SG exit (AVG(TF-611 to 615, 621 to 625, 631 to 634)).

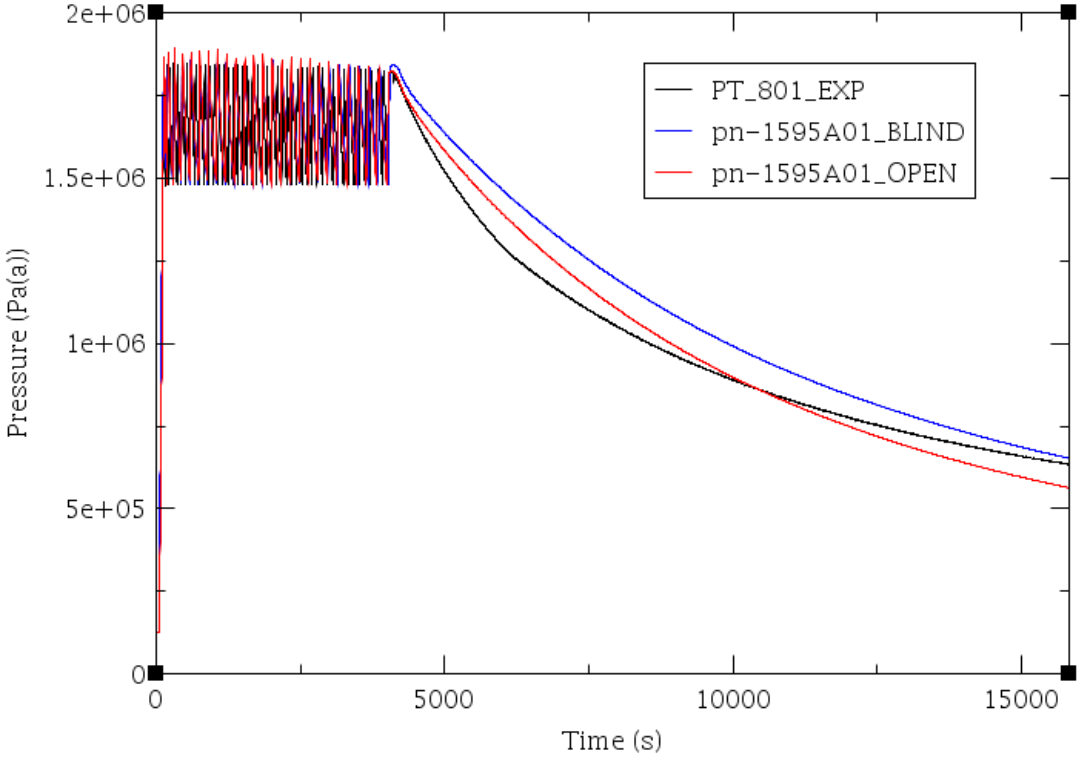

FIG. 4-374. HPC pressure (PT-801).

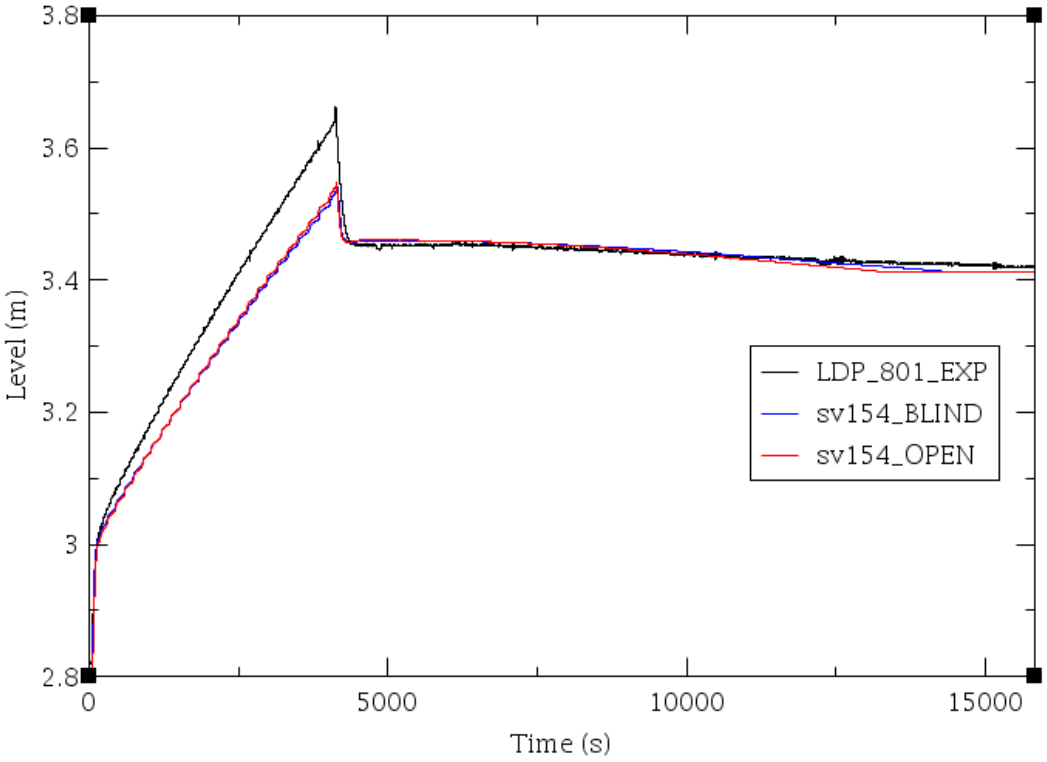

FIG. 4-375. HPC level (LDP-801).

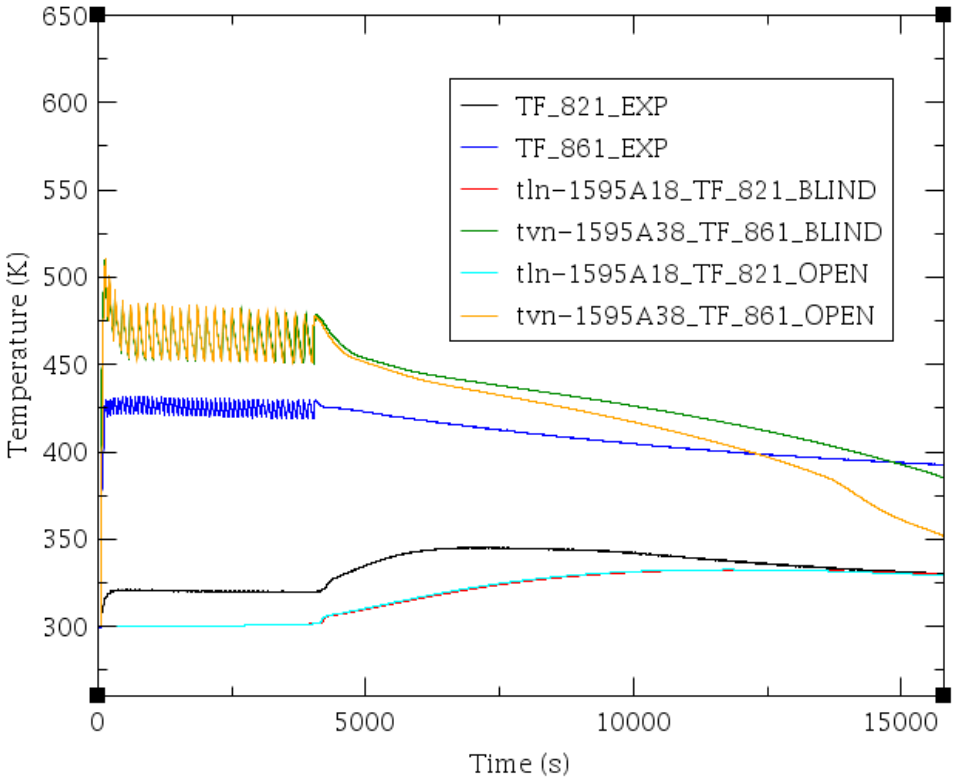

FIG. 4-376. HPC water temperature (TF-821, 861).

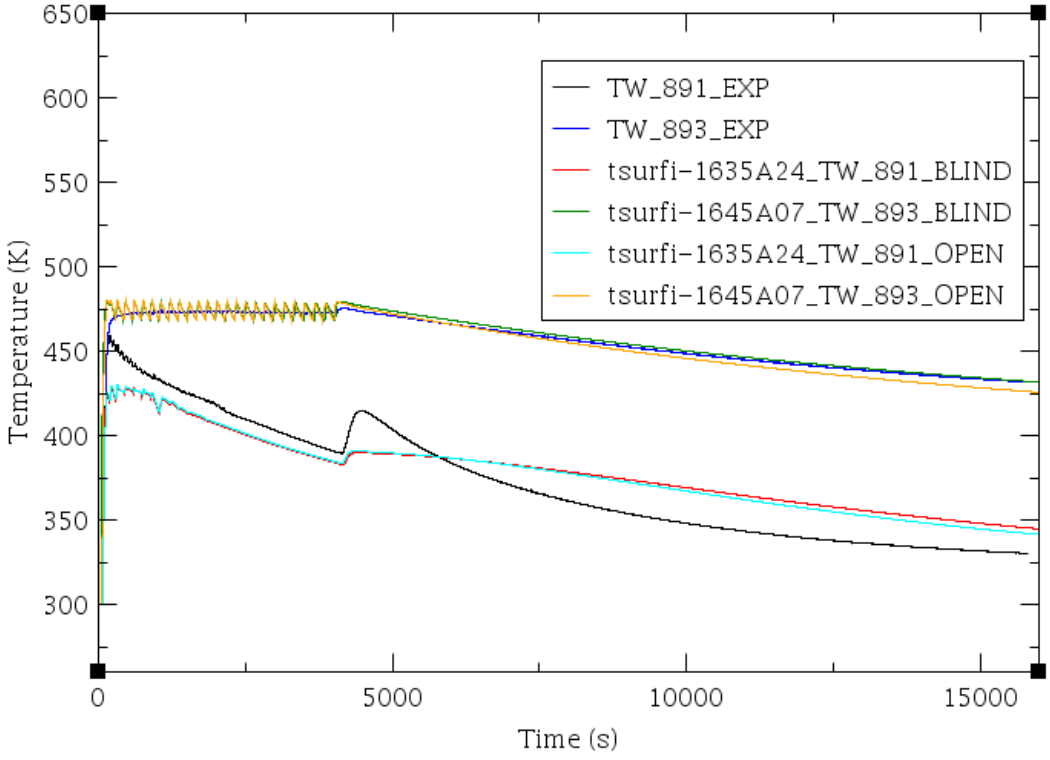

FIG. 4-377. HPC wall temperature (TW-891, TW-893).

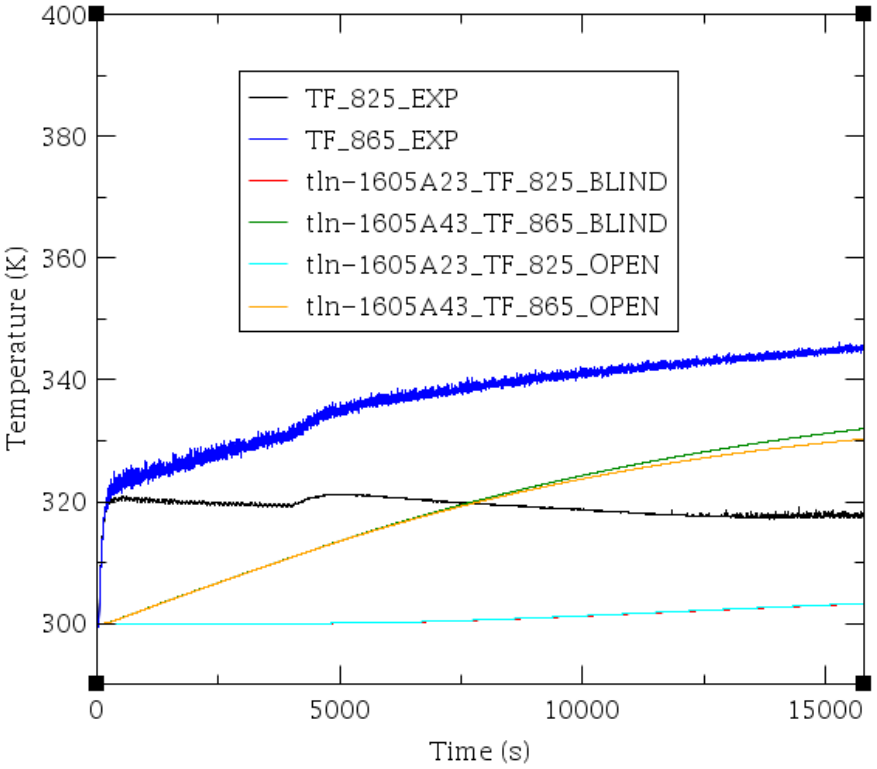

FIG. 4-378. CPV water temperature (TF-825, 865).

4.15.4. Analysis results for power maneuvering

The ICSP test 3 investigates the primary and secondary side thermal hydraulic behavior for a variety of core power levels and feed water flow rates. The simulation of this test is useful for evaluating the TRACE code capability in predicting natural circulation phenomena and heat exchange from primary to secondary side by helical SG in superheated condition.

The starting point for SP-3 is the achievement of steady state conditions, for two minutes, at the lowest power level in the test procedures, 40 kW. The HPC has no communication with the RPV during the entire test. The PRZ control follows the 8.618 MPa(g) setpoint during the entire SP-3 test. The ambient temperature during the testing was not measured but is estimated between 20 and 24 °C. The experimental primary power, the feedwater flow rate and the SG outlet pressure are assumed as boundary condition of the test at the SOT.

At the SOT, obtained by the TRACE code, the primary system is filled with subcooled water. The primary system inventory is at 100% and the PRZ level is at about 0.35 m. The core power is at about 40 kW, the PRZ heaters are on in order to maintain the primary pressure set-point and the containment heaters are off. The primary pressure is around 8.7 MPa(a) and the natural circulation is present in the facility primary side. The secondary side removes net primary power, core power less ambient losses, with a steam pressure of 1.446 MPa(a). The ADS blowdown line valves, the ADS vent line valves and the ADS sump return line valves are closed.

The analyses of the calculated data shows that the phenomena of interest ICSP-3 test are predicted by the code. Therefore the thermal hydraulic configuration of the primary and secondary side is collected by the TRACE analysis for a variety of core power levels and feed water flow rates.

Table 4-30 shows the ICSP test 3 event sequence. The figures related to the BLIND and OPEN cases are reported in the Figure 4-381 to 4-387. Figures 4-379 and 4-380 show animation models, developed by using SNAP, visualizing the facility configuration during selected instants.

4.15.4.1. RPV thermal-hydraulic behavior

The main thermal hydraulic phenomena characterizing the RPV during this test are the single phase natural circulation, the heat transfer in covered core and the by-pass heat transfer between riser and downcomer.

In order to thermal hydraulically characterize these phenomena, the core outlet flow (FDP-131), the core outlet fluid temperature (TF-106), the average core inlet fluid temperature AVG(TF-121, 122,123,124), the delta T core, the pressure drop across SG (DP-105) and core (DP-101), the power to fluid in core, the RPV and PRZ water level (LDP-106 and LDP-301 respectively), the PRZ pressure (PT-301), the subcooling at core outlet, the fluid temperature difference AVG(TF-131,133,134) and AVG(TF-121 to 124), the surface temperature of the core heater rod at the core outlet (TH-141 to 146), the heat losses and the comparison of core power (given BC) and the SG heat removal are considered. A detailed analysis of these parameters is reported in the BLIND and OPEN calculation reports.

The results of the blind calculated data show that the single phase natural circulation is qualitatively predicted by the TRACE code. As in the experimental data the primary fluid is in subcooled condition and the core power is removed by a single phase natural circulation. The BLIND data show a general overestimation of the primary side parameters. The outlet and inlet average core fluid temperature, the primary mass flow rate are shown in Figures 4-381 to 4-383. A general quantitative improvement of the calculated data is observed in the OPEN calculations. The analyses of the BLIND and OPEN calculations show that the pressure drop behavior is in general predicted by the TRACE code. The PRZ pressure and level, Figures 4-384 and 4-385 respectively, are qualitatively predicted by the TRACE code. During the test 3, a charging of the primary system is present. Considering the information's distributed in the ICSP specifications, this charging is simulated and a qualitative agreement with this phenomenology is obtained in the calculated data.

4.15.4.2. SG thermal-hydraulic behavior

The main thermal hydraulic phenomena characterizing the SG are the heat transfer to secondary and the boiling in coil.

In order to thermal hydraulically characterize the SG behavior the steam temperature exit (AVG(TF-611 to 615, 621 to 625, 631 to 634)), the steam pressure (PT-602), the steam flow (FVM-602M) the average feedwater pressure (AVG (PT-511, 521, 531)) the feedwater flow (SUM(FCM-511, 521, 531)), the feedwater temperature (TF-501) and the power removed at the SG are considered. In order to have a direct visualization of the boiling in coil in the calculated data, Figures 4-379 and 4-380 shows animation models, visualizing the facility configuration, in steady state and in selected transient instants, for the BLIND case. A detailed analysis of these parameters is reported in the BLIND and OPEN calculation reports attached with this TECDOC.

During the simulation the sub-cooled, saturated and superheated region of the SG secondary side are predicted and the steam will the SG superheated as in the experimental data.

The steam temperature at the SG exit (Fig. 4-386) is qualitatively predicted in the BLIND calculations though it shows a general overestimation in comparison with the experimental data. In the OPEN calculation it shows a first overestimation and a subsequent underestimation. Figure 4-387 shows the SG outlet pressure.

The results of the BLIND sensitivity studies show that if the SG is modelled with 3 equivalent oblique group of pipes, one each bank, more temperature oscillations at the outlet of the SG secondary side are predicted.

TABLE 4-30. ICSP SP-3 EVENT SEQUENCE

Facility Operation	Time (s) Experimental data	Time (s) Blind & Open calculations
Start of the simulation-steady state (start of data collection)	0	-600
Initiate Core power increase to 80 kW	0	0
Initiate Core power increase to 120 kW	870	870
Initiate Core power increase to 160 kW	1642	1642
Initiate Core power increase to 200 kW	2177	2177
Initiate Core power increase to 240 kW	4004	4004
Initiate Core power increase to 280 kW	4498	4498
Initiate Core power increase to 320 kW	5096	5096

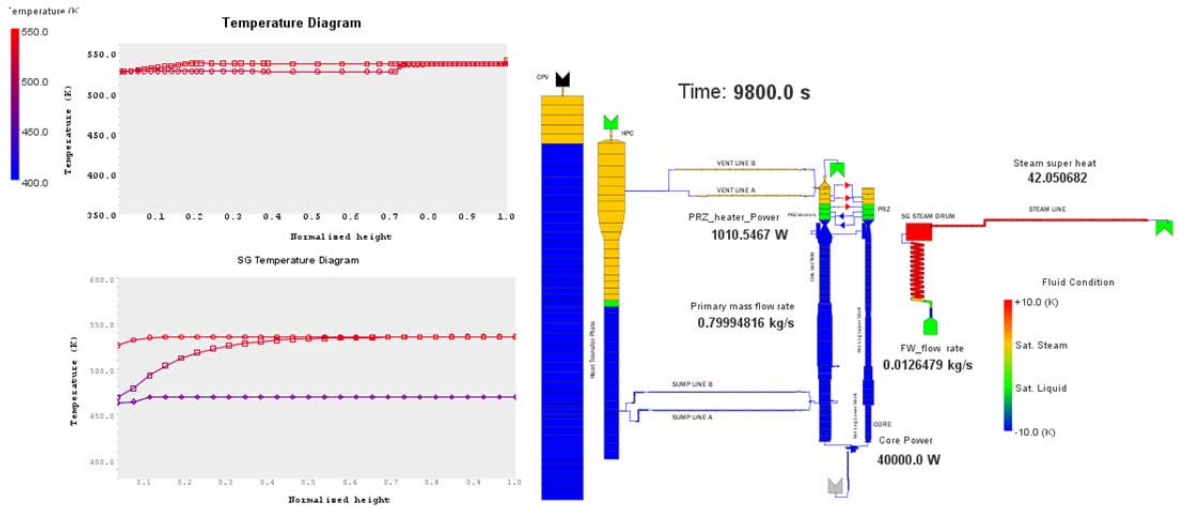

FIG. 4-379. SNAP animation model showing the steady state condition of the TRACE model at the end of the steady state phase of the ICSP test 3(BLIND case).

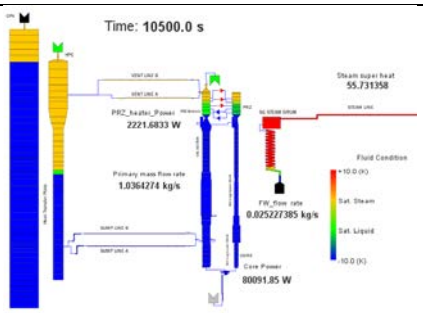

TRACE model condition 500 s after the SOT

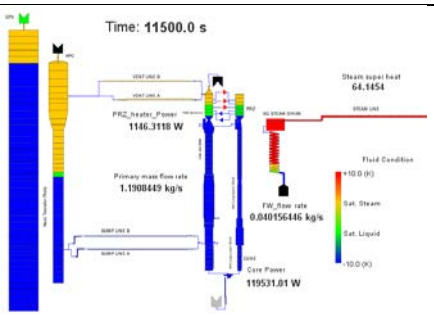

TRACE model condition 1500 s after the SOT

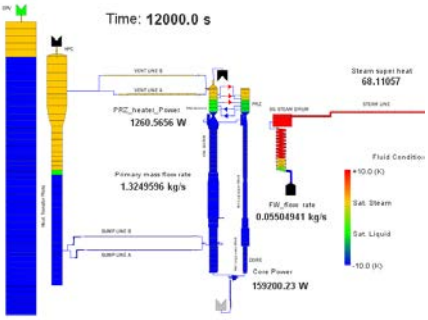

TRACE model condition 2000 s after the SOT

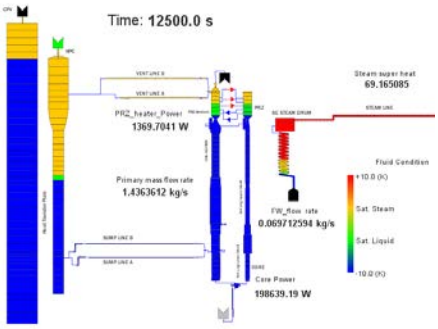

TRACE model condition 2500 s after the SOT

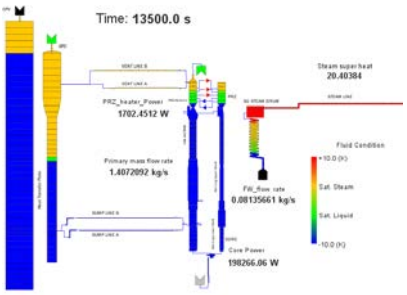

TRACE model condition 3500 s after the SOT

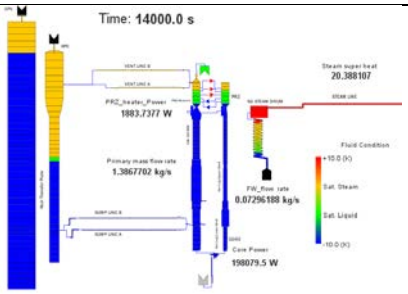

TRACE model condition 4000 s after the SOT

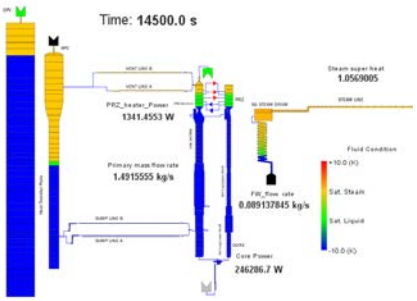

TRACE model condition 4500 s after the SOT

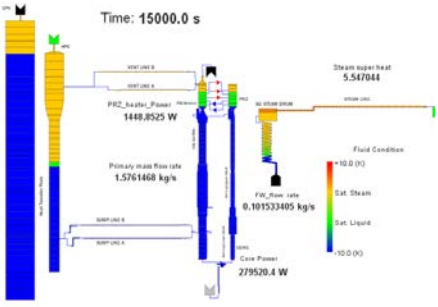

TRACE model condition 5000 s after the SOT

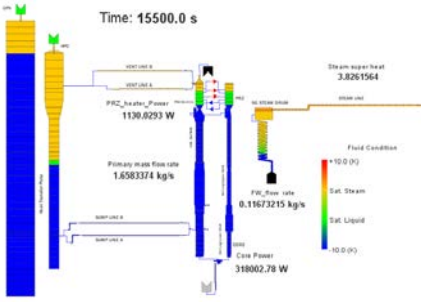

TRACE model condition 5500 s after the SOT

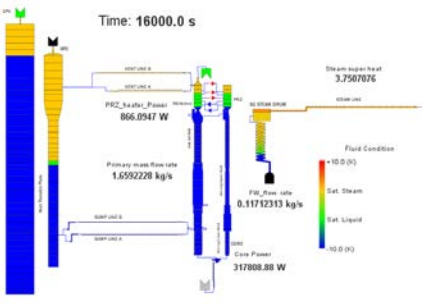

TRACE model condition 6000 s after the SOT

FIG. 4-380. SNAP visualization of selected instant during the ICSP test 3 transient.

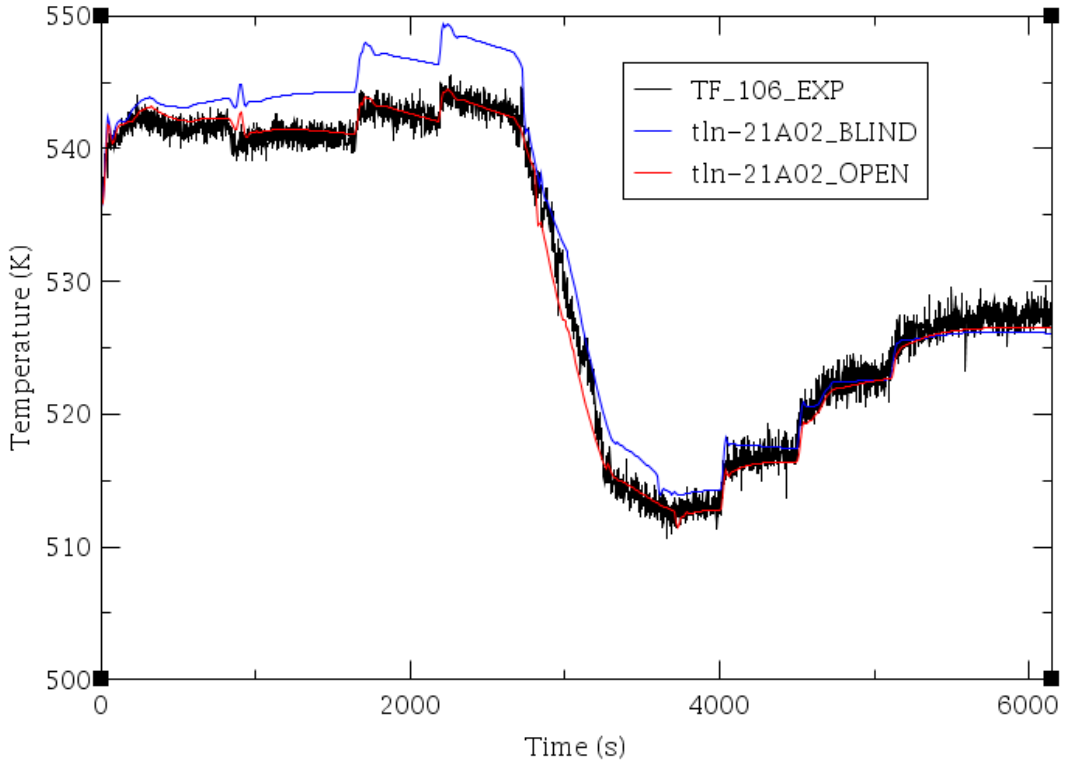

FIG. 4-381. Outlet core temperature (TF-106).

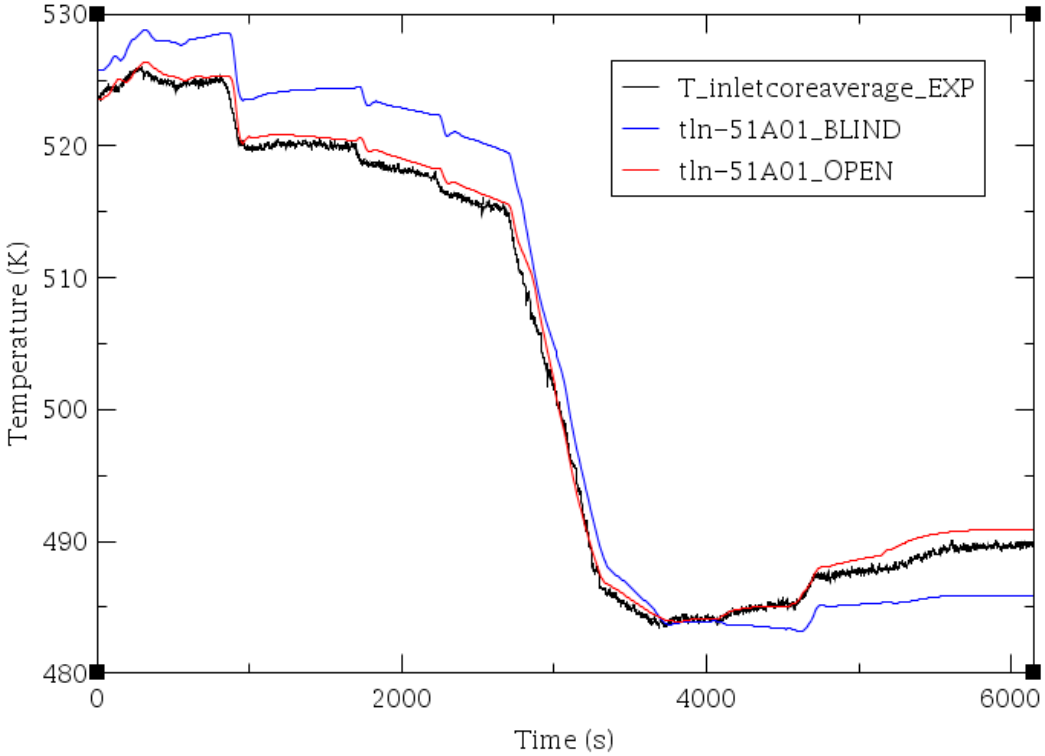

FIG. 4-382. Average inlet core temperature (AVG(TF-121, 122,123,124)).

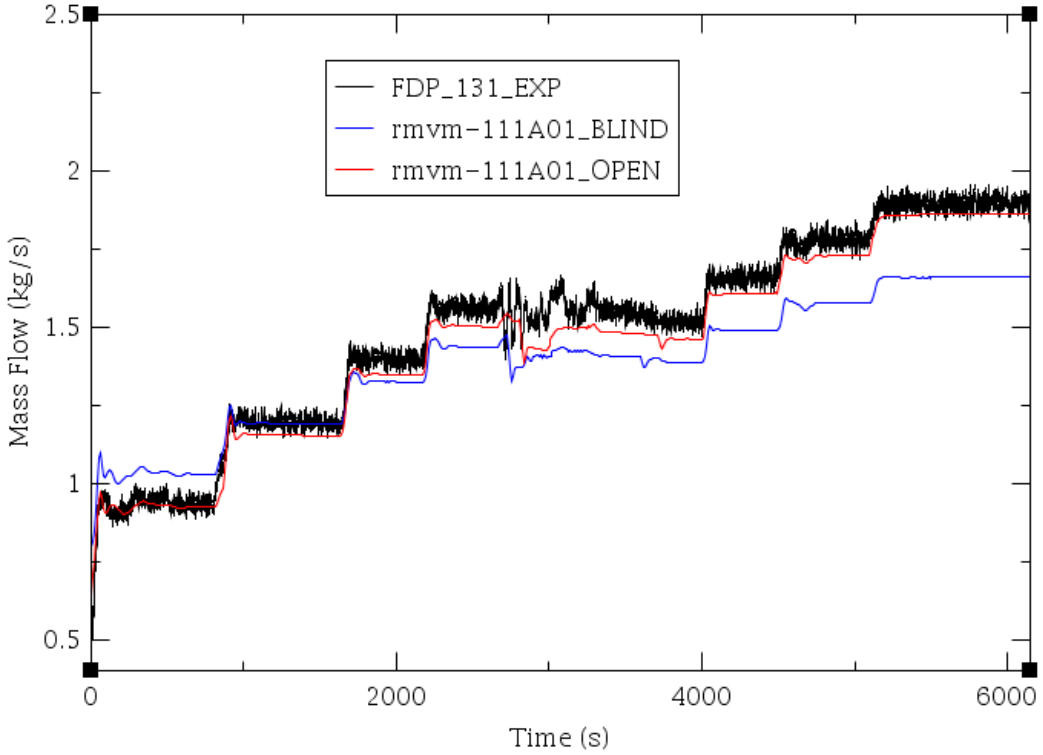

FIG. 4-383. Primary core mass flow rate (FDP-131).

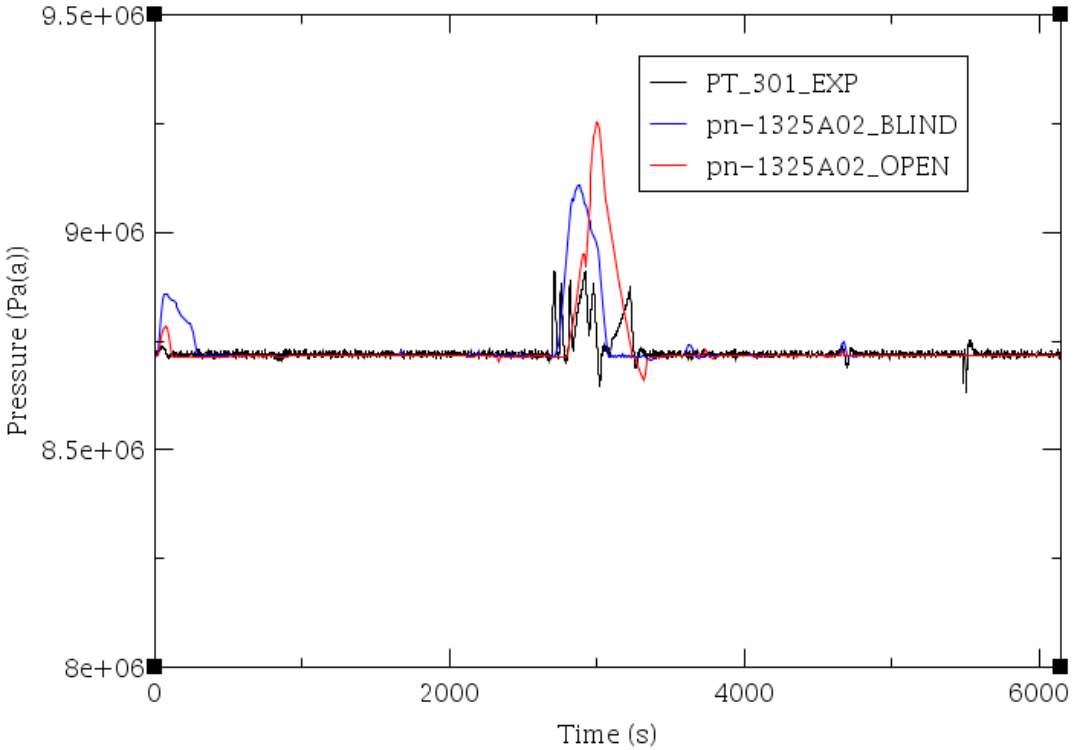

FIG. 4-384. Pressurizer pressure (PT-301).

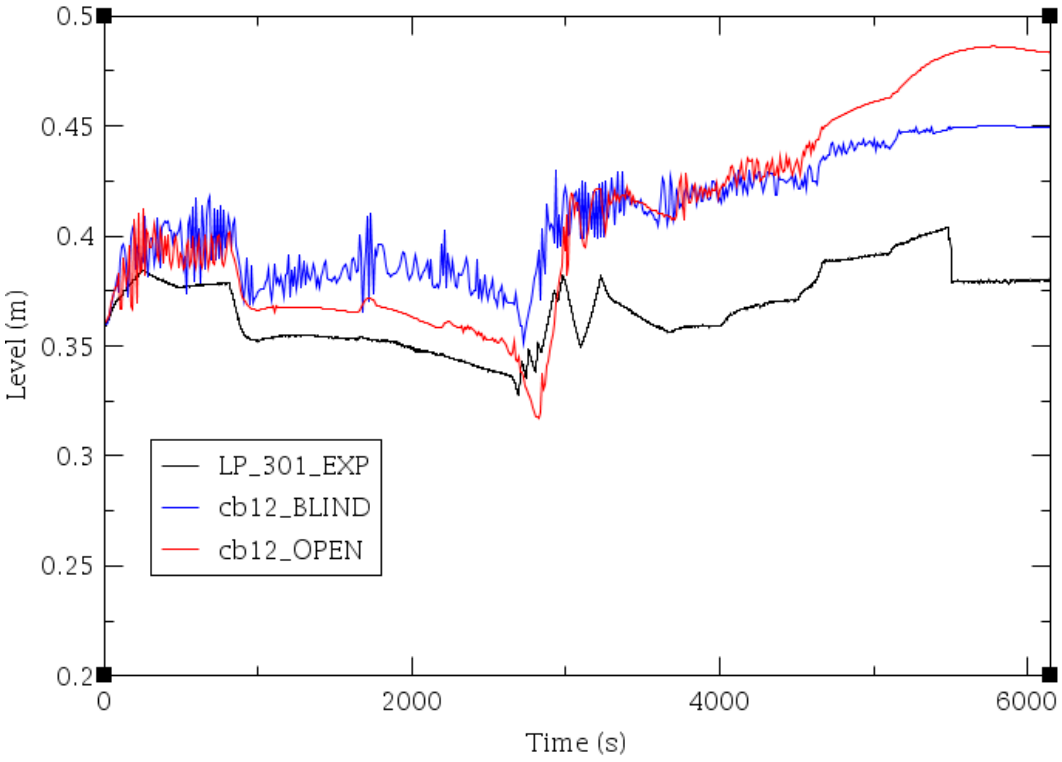

FIG. 4-385. Pressurizer level (LDP-301).

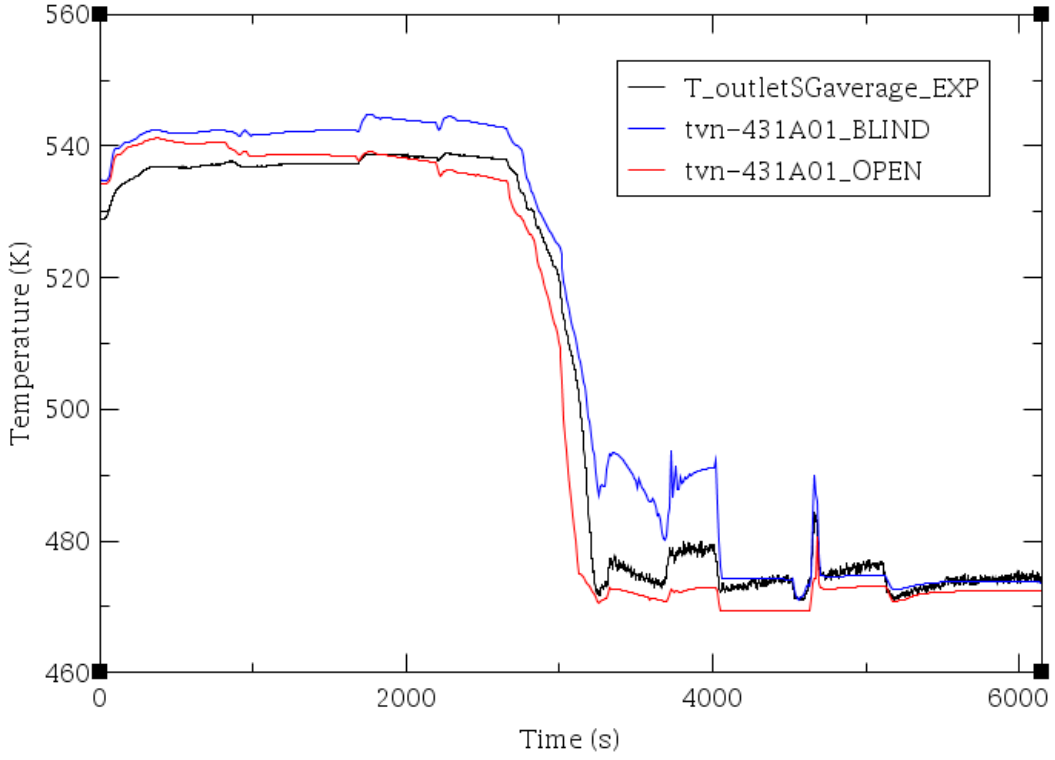

FIG. 4-386. Steam temperature exit (AVG(TF-611 to 615, 621 to 625, 631 to 634)).

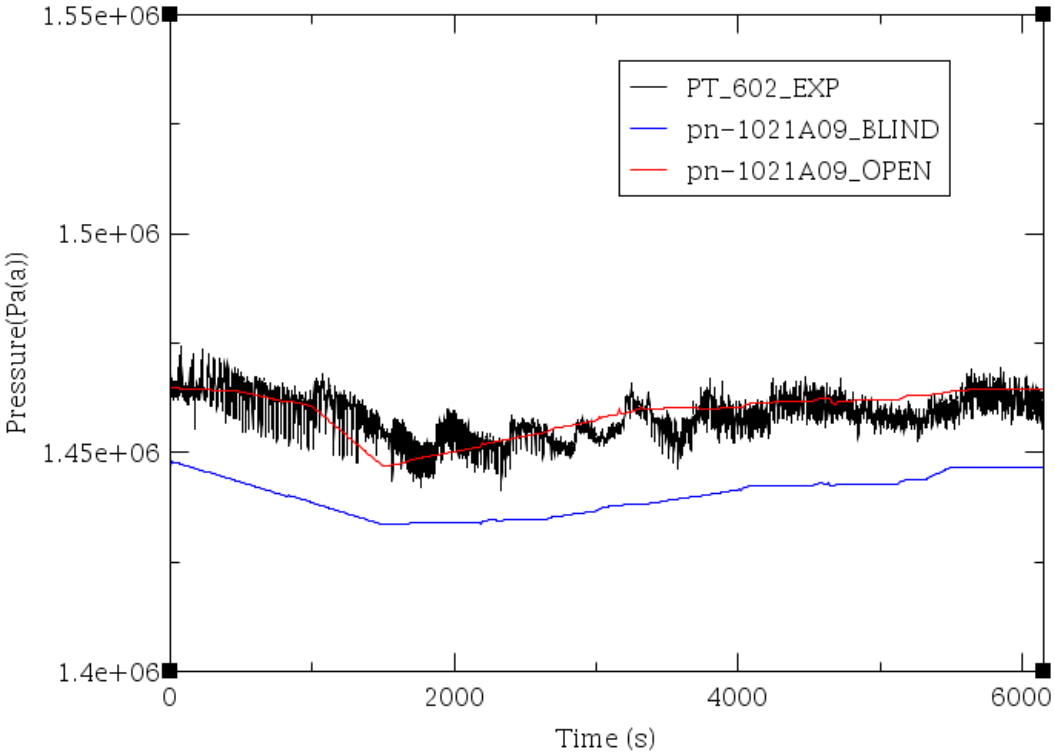

FIG. 4-387. SG outlet pressure (PT-602).

4.16. UNIPI – ITALY

4.16.1. Computer codes

The RELAP5-3D© code has been used by University of Pisa for simulation of MASLWR standard problems. The RELAP5-3D© code (http://www.inel.gov/relap5/) is an outgrowth of the one-dimensional RELAP5/Mod3 code developed at the Idaho National Laboratory (US). The most prominent attribute that distinguishes RELAP5-3D© from its predecessors is the fully integrated, multi-dimensional thermal-hydraulic and neutron kinetic modeling capability.

The code models the coupled behavior of the reactor coolant system and the core (point kinetic) for simulating accidents in LWR: such as loss of coolant, Anticipated Transients Without Scram (ATWS) and operational transients, such as loss of feed-water, loss of offsite power and turbine trip. A generic modeling approach is used that permits simulating a variety of thermal hydraulic systems such as turbines, condensers and secondary feed-water systems. The component models include also pumps, valves, pipes, heat releasing or absorbing structures, reactor point kinetics, electric heaters, jet pumps, etc.

This code is highly generic and can be used for simulation of a wide variety of hydraulic and thermal transients in both nuclear and non-nuclear systems involving mixtures of steam, water, non-condensable and solute. Based on one-dimensional, transient, and non-homogeneous and non-equilibrium hydrodynamic model for the steam and liquid phases, RELAP5-3D© code uses a set of six partial derivative balance equations and can treat a non-condensable component in the steam phase and a non-volatile component (boron) in the liquid phase. A choked-flow model developed by Ransom and Trapp is included primarily in RELAP5-3D© as the standard choked flow model for calculation of the mass discharge from the system at a pipe break or a nozzle. An optional choked flow model (modified Henry-Fauske) is also available.

A semi-implicit numeric scheme is used to solve the equations inside control volumes connected by junctions. The fluid scalar properties (pressure, energy, density and void fraction) are the average fluid condition in the volume and are viewed located at the control volume center. The fluid vector properties, i.e. velocities, are located at the junctions and are associated with mass and energy flows

between control volumes that are connected in series, using junctions to represents flow paths. The direction associated to the control volume is positive from the inlet to the outlet.

Heat flow paths are also modeled in a one-dimensional sense, using a staggered mesh to calculate temperatures and heat flux vectors. Heat structures and hydrodynamic control volumes are connected through heat flux, calculated using a boiling heat transfer formulation. These structures are used to simulate pipe walls, heater elements, nuclear fuel pins and heat exchanger surfaces.

RELAP5-3D© contains various correlation for simulating heat transfer in different geometrical configuration from convection in a straight pipe to heat transfer in bundles in the presence of crossflows. Nevertheless, no specific correlation for helical tubes geometry is available. Somewhat similar correlation is available for swirl tubes, based on experiments supporting fusion reactors, which takes into account the centrifugal effects inside the swirl tubes that are also present in helical geometry. Activating swirl tubes geometry at heat structure boundary gives use of alternate correlations for turbulent convection, nucleate boiling, transition boiling, and CHF.

4.16.2. System idealization

4.16.2.1. System idealization for blind calculation

The nodalization of the experimental facility for RELAP5-3D© code has been developed adopting 1D approach. The core, riser and downcomer sections of the reactor pressure vessel are simulated by pipe components, where the core part is represented by a single pipe. The lower and upper plena are modeled with branch components and the pressurizer part is represented by a pipe component. The nodalization sketch is shown on the Figure 4-388.

The nodalization use for the blind calculation phase has the following features:

- the elevations of the different part of the facility are maintained in the nodalization;
- the energy loss coefficients used in the junctions in the blind phase were evaluated on the basis of the geometry and further adjusted through calculation of characterization tests (002 and 003A);
- Surface roughness is set to 5×10^{-5} m through out the facility model except the core region, where it is set to 1×10^{-6} m;
- the node to node ratio is kept uniform with a maximum ratio of 1.2 between adjacent sub-volumes;
- the sliced approach is applied at all systems (i.e. primary, secondary, HPC, CPV and interfacing systems).

Pressure vessel and its internals are modeled by cylindrical heat structure components. Core heater rods are modeled as a single heat structure (with six axial heat structures) component with a power source specified with a general table (tabular data). Pressurizer heaters are simulated with single cylindrical heat structure as well.

The secondary side is modeled as a series of pipe and branch components. All the helical tubes (three coils) are modeled as a single pipe component, with a flow area equal to the total flow area of the tubes, hydraulic diameter of a single tube and a length of an average tube (in order to conserve the heat transfer area). The tapped SG tube is taken into account. The feedwater temperature and mass flowrate are imposed using the time-dependent volume and time-dependent junction components. The steam pressure is regulated by a time-dependent volume component at the outlet from the tubes.

The Automatic Depressurization System is represented by 6 separate lines using pipe, branch and valve components, thus, each line in the model represents one separate depressurization train of the experimental facility. The piping of the ADS is modeled with corresponding cylindrical heat structure components.

The HPC vessel is modeled with a two parallel vertical stacks of volumes using pipe and branch components: representing the “inner” (cylindrical) and “outer” (annular) part of the vessel internals. Such approach allows predicting of the internal circulation phenomena, which may be induced by heat exchange processes. The connection between the parallel volumes is modeled with cross-flow junctions. The vessel of the HPC is modeled with cylindrical heat structure components.

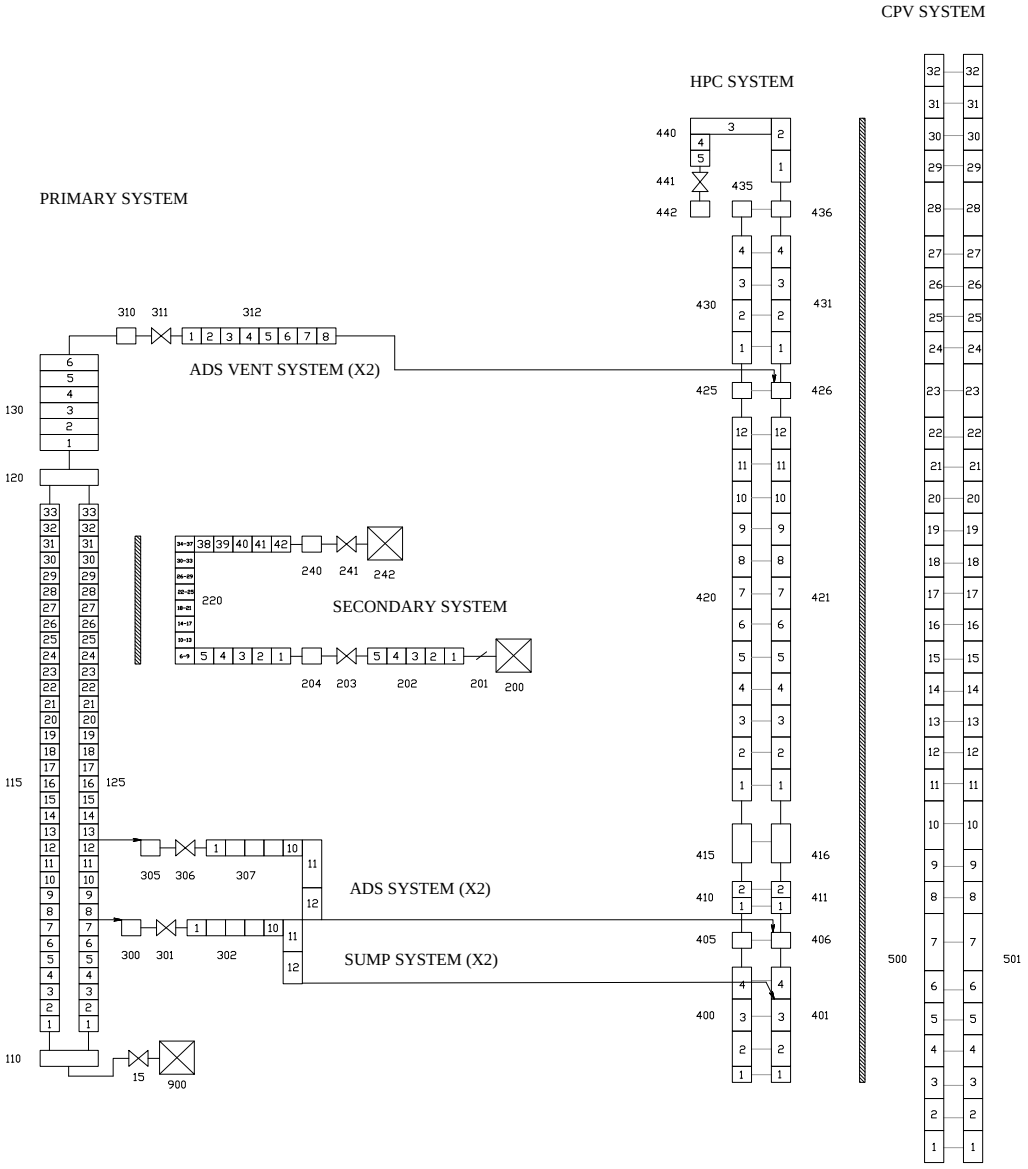

FIG. 4-388. UNIPI nodalization of MASLWR facility.

The Cooling Pool Vessel is modeled with a two parallel vertical stacks of volumes as well, based on the same engineering reasons. The approach is the same as for the HPC model.

The heat transfer plate is modeled as a plate-type heat structure with heat transfer area specified.

The default model options (all zeros) are used for the volumes and junctions of hydraulic components of the experimental facility model, except for the Henry-Fauske critical flow model activated at the valves of the ADS. Default coefficients are used for the Henry-Fauske model. Additionally, the abrupt area change flag is set at the junctions, where such type of geometry is observed.

For the most of the heat structure components the convective boundary condition type (certain set of heat transfer correlations) is set at the boundary with hydraulic components, representing the internals of the Primary Pressure Vessel, ADS piping, HPC vessel and CPV vessel. The exception constitute the heat structure representing the core heater rods, where “vertical bundle with cross-flow” condition type is set; and the external, “right”, side of the SG tubes heat structure, where “horizontal bundle” condition type is set for the lack of the correlations in RELAP specific for a helical geometry.

On the external, “right”, boundaries of the heat structure components, simulating the Primary Pressure Vessel, ADS piping, HPC vessel and CPV vessel, the heat transfer coefficients as a function of time or temperature is specified as a boundary condition type with the heat sink temperature specified by a

time-dependent volume set to air at an ambient temperature. The presence of insulation material is taken into account by assigning the provided in MASLWR facility description material properties (thermal conductivity and volumetric heat capacity) to the corresponding mesh intervals of the heat structure components.

The pressurizer heater “on-off” logic has been implemented using the hysteresis loop approach, where 2 setpoints, 8.70 MPa(a) and 8.72 MPa(a), define the operational range of the heaters. In the “on” mode the 12 kW power is applied as a power source to the corresponding heat structure component.

The operation logic of ADS valves is simulated by a set of variable and logical trips which implement the valves opening-closure according to the specifications provided in Initial and Boundary Conditions for SP-2. In such way the ADS vent valve 106-A operates as follows:

– OPEN: when HPC pressure (PT-801) is 1.479 MPa(a) (200 psig) and rising;
– CLOSE: when HPC pressure (PT-801) is 1.823 MPa(a) (250 psig) and lowering.

Once the pressure difference between Pressurizer (PT-301) and HPC (PT-801) is less than 0.034 MPa (5 psi), both ADS vent valves 106-A and 106-B and both Sump valves open and remain open until the end of transient calculation. The HPC vent valve remains closed during the transient.

The charging flow has been modeled in the SP-3 using the hysteresis loop approach, where 2 setpoints of pressurizer collapsed level, 35.6 cm and 40.6 cm, define the operational range of the charging system. When the system is in “ON” mode, water at 22.5°C is injected into the lower plenum at a constant mass flow rate 0.061 kg/s.

4.16.2.2. Modelling change for open calculation

Following the analysis of blind phase calculation results and comparison with available experimental data, certain minor modifications have been introduced to the model. The goals for the modifications were as follows:

– Correct revealed errors/imprecisions in simulation of logic and boundary conditions;
– Improve prediction of heat transfer across the helical tubes;
– Improve prediction of flow inside RPV at various power levels;
– Improve RPV-HPC pressure/level equalization process.

The model modifications are provided in Table 4-31.

TABLE 4-31. UNIPI OPEN PHASE MODEL MODIFICATIONS

Phenomena	Parameter	Blind phase model	Open phase model
RPV flow	Form losses at core inlet	--	decreased
ADS lines flow	Form losses in lines	--	decreased
Helical tubes heat transfer	HS “left” (inside) boundary condition type	convection	swirl tubes
SG behavior	Outlet pressure	constant	cooldown
Charging flow	Supplied mass flowrate	logic based on PRZ level setpoints	Exp. measured time trend imposed
Logic	First ADS valve opening	with SCRAM	at PRZ pressure of 9.181 MPa(a)
Logic	Sump valves opening	at ΔP (RPV-HPC) < 0.134 MPa	at ΔP (RPV-HPC) < 0.034 MPa

A sensitivity analysis performed during the blind phase showed great influence of predicted degree of mixing in HPC on RPV depressurization rate. In the present model, the magnitude of mixing processes in HPC model is regulated by form loss coefficients at cross-flow junctions between 2 parallel vertical channels representing the containment vessel. The value of K_{loss}=1000, chosen for the blind phase calculations, demonstrated satisfactory prediction of RPV depressurization rate and time of RPV and HPC pressure equalization. Therefore this value has been kept in the open phase calculations.

4.16.3. Analysis results for loss of feed-water transient

The initial conditions of the both blind and open calculations of SP-2 (Loss of feedwater transient) are reported in Table 4-32. They are achieved running the code for 3000 s with the 'TRANSNT' (transient) option.

Steady state and initial conditions are achieved accordingly with the specifications. Few minor deviations are observed in the primary pressure (i.e. 8.70 instead of 8.72 MPa(a)) due to the pressurizer heater imperfect operation logic and core inlet/outlet coolant temperature are slightly higher than specified ones due to the primary side heat-up at the initial stage of steady-state calculation. It should be noted that temperature difference across the core is predicted rather good in blind calculation while slightly underestimated in open calculation.

The transient is initiated by a decrease of feedwater mass flow rate until it is 0.0 kg/s (Fig. 4-389). As the pressure in the pressurizer reaches the setpoint of 9.063 MPa(a), the core power trip is activated and thereafter the core power decay is supplied in a form of the time-dependent tabular data. The pressurizer heaters are also deactivated immediately after high PRZ pressure setpoint is reached. The resulting sequence of events of test SP-2 is provided in Table 4-33.

The calculation is terminated on either of two conditions:

– Pressurizer pressure (PT-301) is less than 0.134 MPa(a);
– 16,000 s (as experimental data recorded) after the start of the transient.

TABLE 4-32. SP-2 STEADY-STATE RESULTS (UNIPI)

Parameter	MASLWR	Unit	Experimental Value	Blind calculation	Open calculation
Pressurizer pressure	PT-301	MPa(a)	8.719	8.70	8.70
Pressurizer level	LDP-301	m	0.3607	0.357	0.358
Power to core heater rods	KW-101/102	kW	297.4	297.4	297.4
Feedwater temperature	TF-501	ºC	21.39	21.39	21.39
Steam temperature	FVM-602-T	ºC	205.38	202.2	202.0
Steam pressure	FVM-602-P	MPa(a)	1.428	1.429	1.429
HPC pressure	PT-801	MPa(a)	0.125	0.141	0.141
HPC water temperature	TF-811	ºC	26.72	26.6	26.6
HPC water level	LDP-801	m	2.82	2.86	2.86
Flow at core outlet	--	kg/s	--	1.69	1.77
Primary coolant temperature at core inlet	TF-121/122/ 123/124	ºC	214.42 – 215.34	217.3	217.0
Primary coolant temperature at core outlet	TF-106	ºC	254.5	254.52	252.8
Feedwater flow	FMM-501	kg/s	0.106	0.125	0.125

TABLE 4-33: SP-2 TIME SEQUENCE OF EVENTS (UNIPI)

Event	System	Experiment	Blind calculation	Open calculation
Test SP 2 – LOFW Main FW pump stops	--	0.0	0.0	0.0
PRZ heaters off	PRZ heaters	--	36.0	36.0
SCRAM	Fuel rod simulator bundle	36.0	36.0	36.0
ADS Vent valve 106A first opening	PCS-106A	51.0	36.0	40.0
ADS Vent valve 106A first closure	PCS-106A	136.0	120.0	120.0
ADS Vent valve 106B and sump valves opening	PCS-106B PCS-108A/B	4046.0	3460.0	4006.0
End of test	--	15820	16000	16000

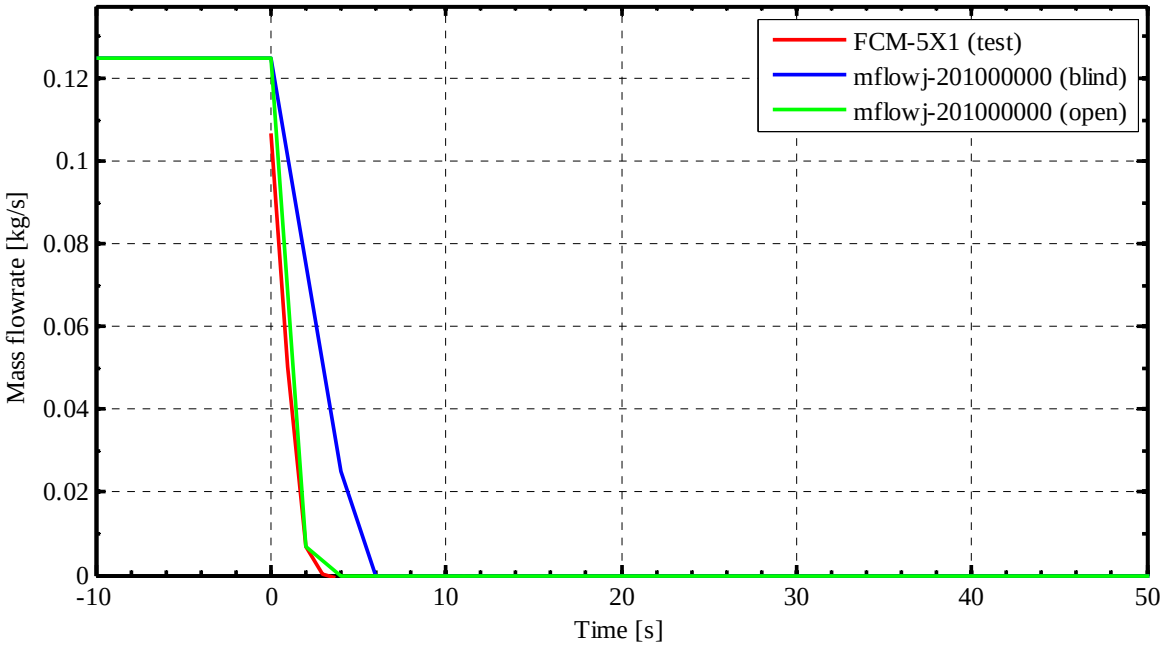

FIG. 4-389. SP-2 Feedwater mass flow rate.

4.16.3.1. RPV thermal-hydraulic behavior

As the supplied feedwater flow rate is rapidly diminishes (Fig. 4-389), the heat sink is lost and the primary side experiences an increase of pressure (Fig. 4-391). The scram is triggered on the high pressure signal and the decay heat curve is activated. The further increase in primary pressure results in of ADS valve opening, which causes a blowdown effect on the primary side. The blind phase calculation rather anticipated the ADS valve opening instant since the implemented logic triggered valve opening immediately after SCRAM. Correcting the valve opening signal in open phase calculation improved the timing of the start of blowdown.

The pressure undergoes a sharp decrease to experimentally measured ~2.6 MPa(a) (Fig. 4-391), causing flashing in the pressurizer and upper plenum (Fig. 4-395). Both blind and open calculation resulted in higher pressure and the end of blowdown (~3.2 MPa(a)). This is due to imperfect prediction of mixing (underestimated) during the blowdown which caused higher rate of pressure rise in HPC and, therefore, earlier closure of PCS-106A valve. Such underprediction may be due to inefficiency of the code and adopted nodalization to correctly predict complex turbulent vapor flow patterns and interaction with HPC water pool during the blowdown phase.

As the ADS valve continues further operation in cycling mode (in order not to exceed the 1.823 MPa(a) pressure in HPC) discharging the fluid from the primary side (Fig. 4-396), the primary side mass inventory and, therefore collapsed level diminishes (Fig. 4-392) and, consequently, the primary pressure decreases.

As the difference between RPV and HPC becomes less than 0.034 MPa at 4046 s, the second ADS valve and both SUMP valves are open, thus coupling both vessels. The blind phase analysis showed that the code predicted time of RPV and HPC pressure equalization depends on the prediction of mixing and stratification processes in HPC. In the present model these processes are mainly affected by the magnitude of form loss coefficients at the cross-flow junctions between the parallel vertical channels. Identical K_{loss} coefficients were used both in blind and open phases' calculations and resulted in reasonable prediction of RPV and HPC pressure equalization time in blind phase and excellent prediction in open phase.

The system cooldown continues until the 15,820 s of the transient with CPV as an ultimate heat sink. The experimentally measured pressurizer pressure reaches 0.62 MPa(a) by the end of transient (Fig. 4-390). Blind and open phase calculation reached 0.40 MPa(a) and 0.46 MPa(a) respectively. The discrepancy with experimental measurement is reasonable since long term cooling is affected by heat losses (experimentally unknown) from the RPV and HPC vessels and heat exchange with CPV which, in its turn is affected by the choices of the HPC and CPV nodalizations (see following paragraphs).

Due to flashing and subsequent loss of primary mass inventory from the primary side, the upper part of RPV, including riser, upper plenum and inlet to SG is significantly voided (Fig. 4-395). The calculated natural circulation however is not interrupted but continues in a two-phase mode (Fig. 4-393) until the 2500 s of the transient, when it seized and a boil-off mode is established. The spikes in the core mass flow rate in the period from 2500 to 4000 s are caused by opening-closing of the ADS valve.

After opening of the sump valves, the RPV mass inventory and level starts recovering (Fig. 4-392) and at the intermittent two-phase flow in the primary side is re-established (Fig. 4-393). At the absence of experimental mass flow measurement one can judge on water temperatures at the core inlet and outlet (Fig. 4-394). Open phase calculation provide more reasonable results while blind calculation shows delayed re-establishment of the natural circulation which is temporarily interrupted at around 10,000 s into the transient. This is due to the pressure increase in the HPC, which is affected by top-down mixing in HPC and pressure drops across the ADS vent and sump lines. Reducing form loss coefficients in these lines in open phase calculation improved the code predictions.

Throughout the transient the core remains covered (Fig. 4-392) although the water is boiling (Fig. 4-395) and no heater rods dryout is observed.

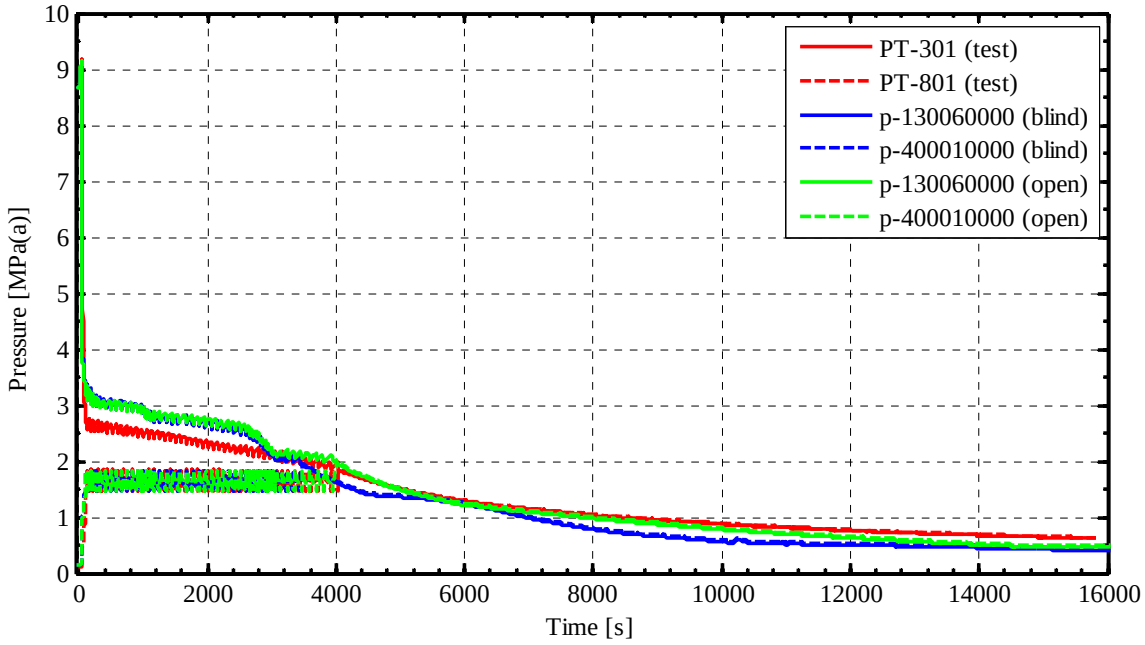

FIG. 4-390. SP-2 RPV and HPC pressure.

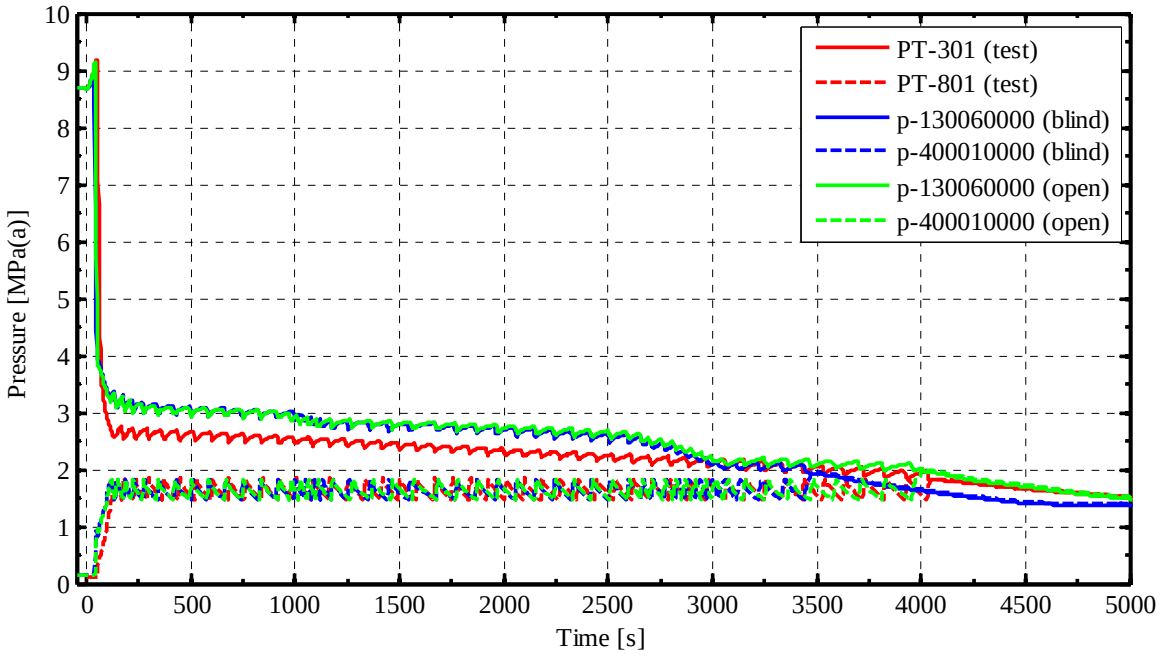

FIG. 4-391. SP-2 RPV and HPC pressure (before sump lines opening).

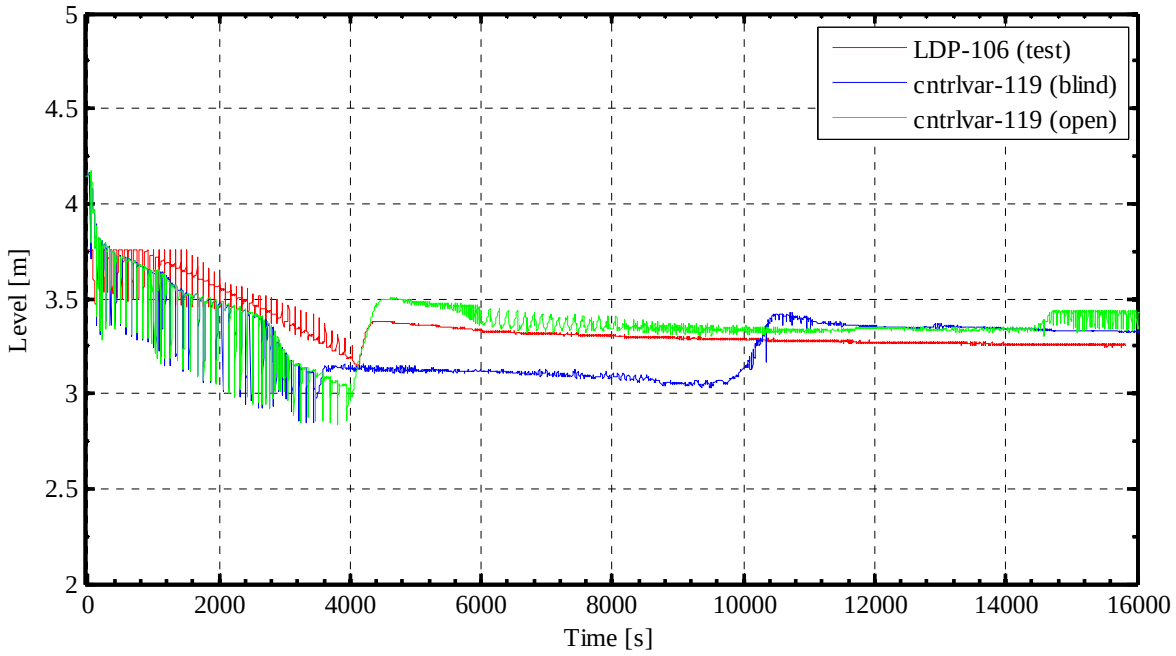

FIG. 4-392. SP-2 collapsed level in RPV.

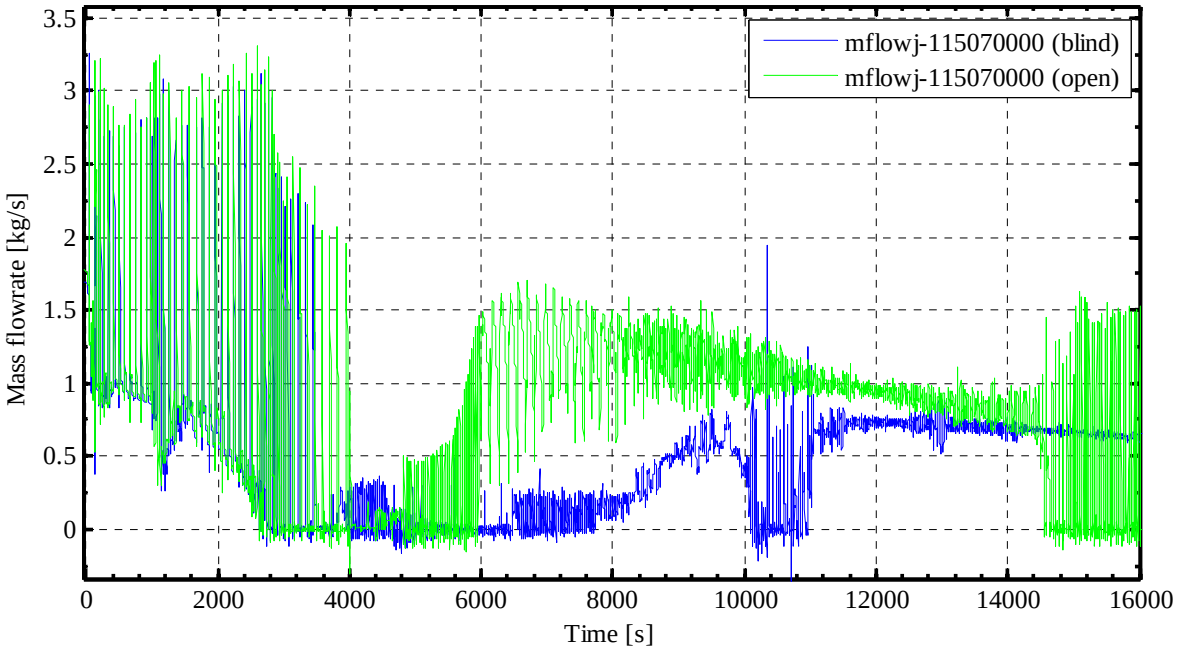

FIG. 4-393. SP-2 mass flow rate at core outlet.

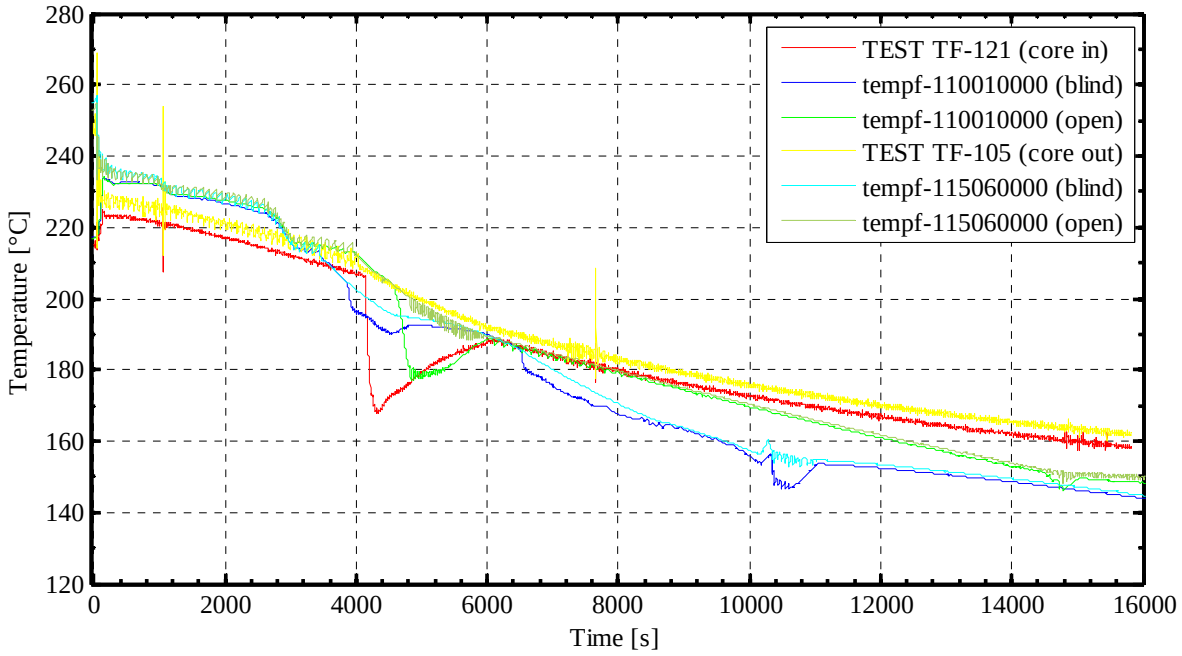

FIG. 4-394. SP-2 water temperature in RPV.

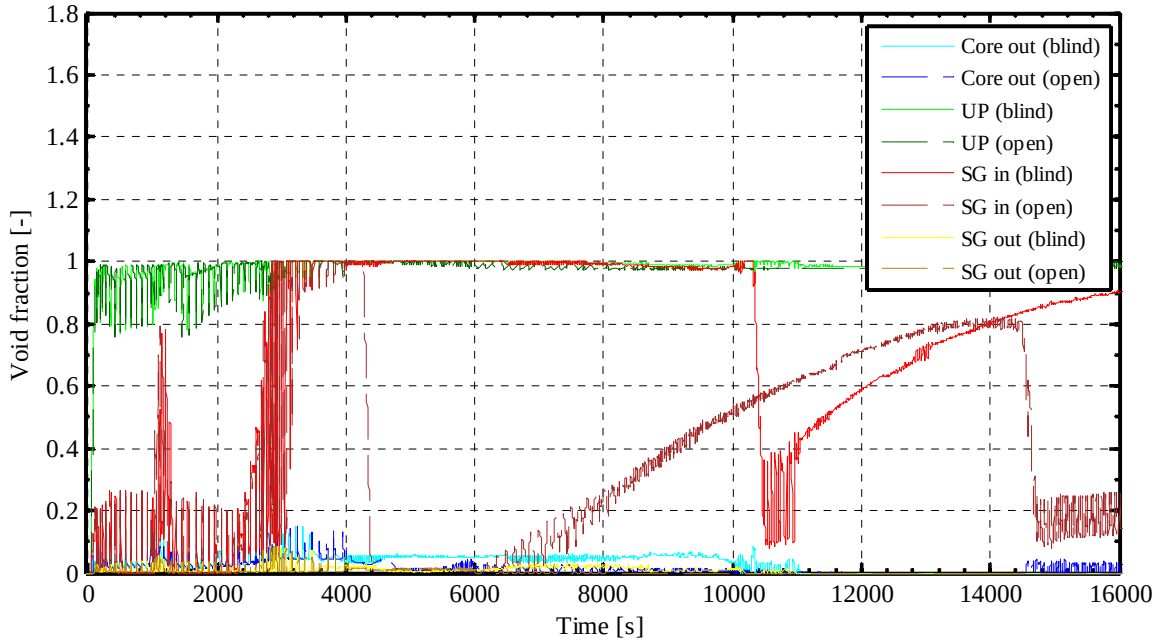

FIG. 4-395. SP-2 void fraction inside RPV.

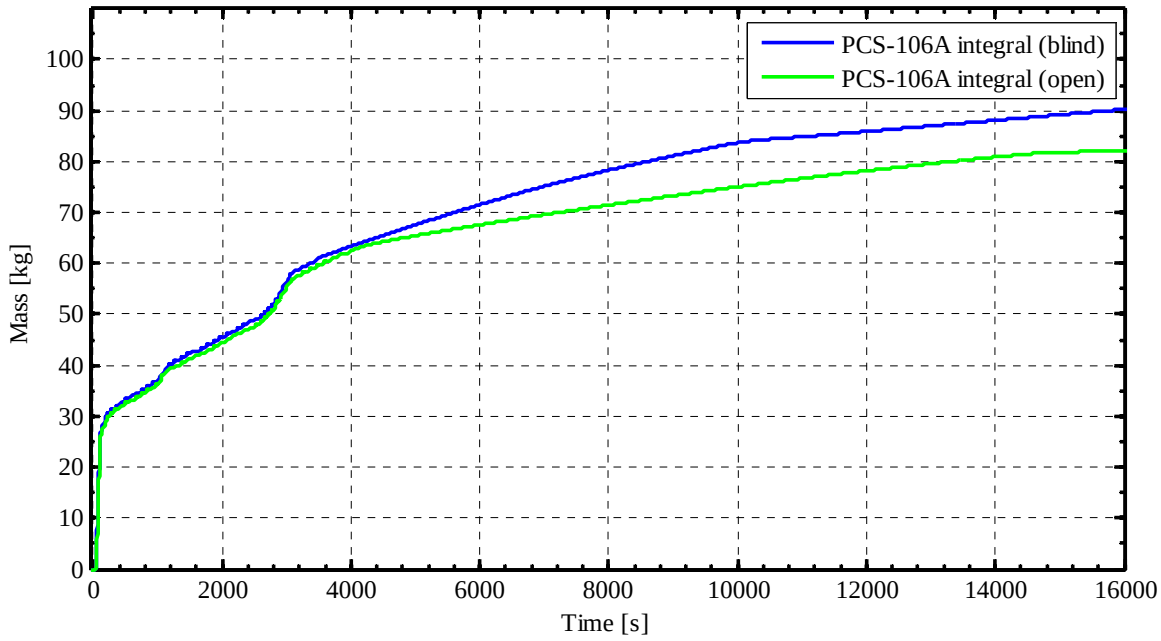

FIG. 4-396. SP-2 cumulative discharge through 106A valve.

4.16.3.2. SG thermal-hydraulic behavior

During the steady-state the subcooled water is supplied at the inlet of the helical tubes. It reaches saturation at about 2.2 m from the inlet to the heated part and the steam becomes superheated at about 5.5 m from the inlet (with 6.15 m total heated part). At the outlet from the tubes steam reaches 6.2°C superheat, which is under-predicted with respect to experimentally measured 9°C superheat. This is connected to the lack of interphase friction and heat transfer correlations adequate for helical tubes geometry. Nevertheless, the results may be considered satisfactory since the discrepancies at the secondary side resulted in acceptable errors in the predicted temperatures in the primary side.

As the feedwater switched off at the beginning of the transient, the heat transfer to SG quickly degrades and has no further effect on physical processes inside RPV.

4.16.3.3.HPC thermal-hydraulic behavior

After the first opening of ADS valve there is a steep pressure build-up in the HPC vessel (Fig. 4-391), stopped by the closing logic of the valve. Immediately a thermal stratification is formed along the elevation of the HPC (Fig. 4-397). Significant discrepancies may be noted between measured and calculated results both in the upper part (vapor) and lower part (water) of HPC. The measured temperature in the top part (TF-851) is well below the saturation temperature of about 195℃. While both blind and open calculation provide vapor temperature slightly superheated. On the contrary, a sharp increase in measured water temperature in the bottom part is observed (TF-811) while calculations predict gradual water heat-up. Similar discrepancy is noted in the HPC-CPV heat exchange plate temperatures on the HPC side (Fig. 4-398). There are several reasons for such a discrepancy identified:

- The code and adopted nodalization were not able to predict the initial strong vapor-water mixing at the beginning of blowdown which may be caused by strong and complex vapor turbulent flows;
- As the transient continues, the vertical heat conduction in HPC vessel and heat exchange plate adds to the top-down heat transfer. Such effect is not reproduced by the model since there is no axial heat conduction between heat structures;
- It should be noted that TF thermocouples are most probably located close to the heat exchange plate. Therefore it is quite probable that the measured values correspond to a limited layer along the wall while RELAP model provides the bulk water/vapor temperature. This observation is supported by the measured temperatures of the HPC vessel (Fig. 4-399) which are better predicted

by code and are similar to the vapor bulk temperatures. This effect may be addressed further by sensitivity analysis on nodalization of HPC vessel, namely different partitioning of the vessel volume into the vertical channels, with the purpose to simulate a formation of such near-wall layer.

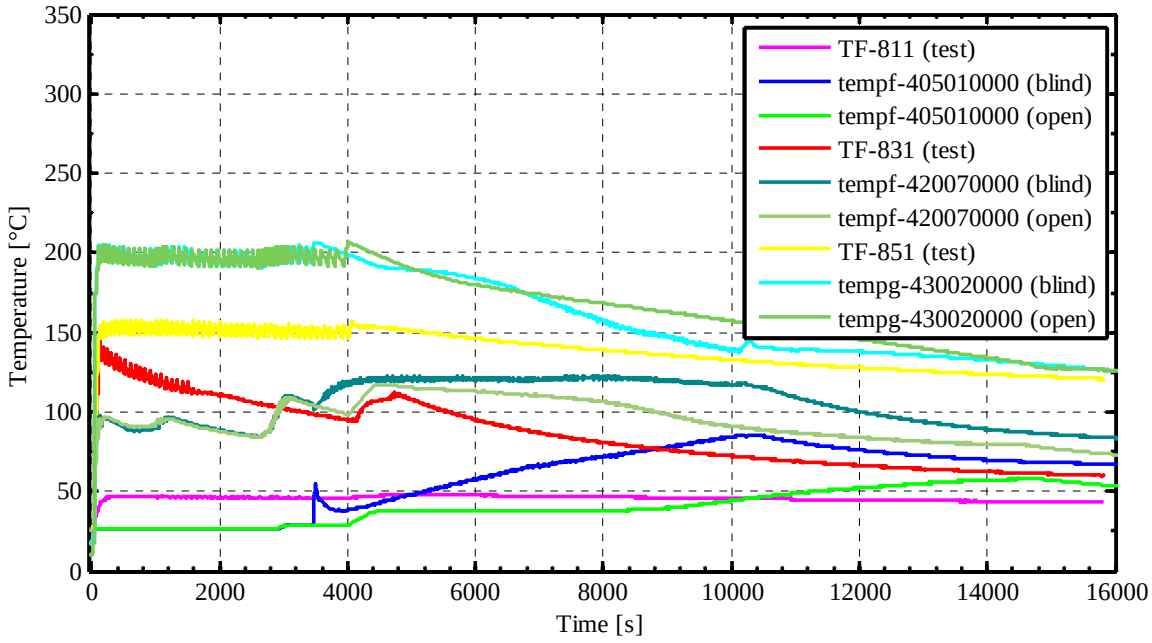

FIG. 4-397. SP-2 liquid and vapor temperatures in HPC.

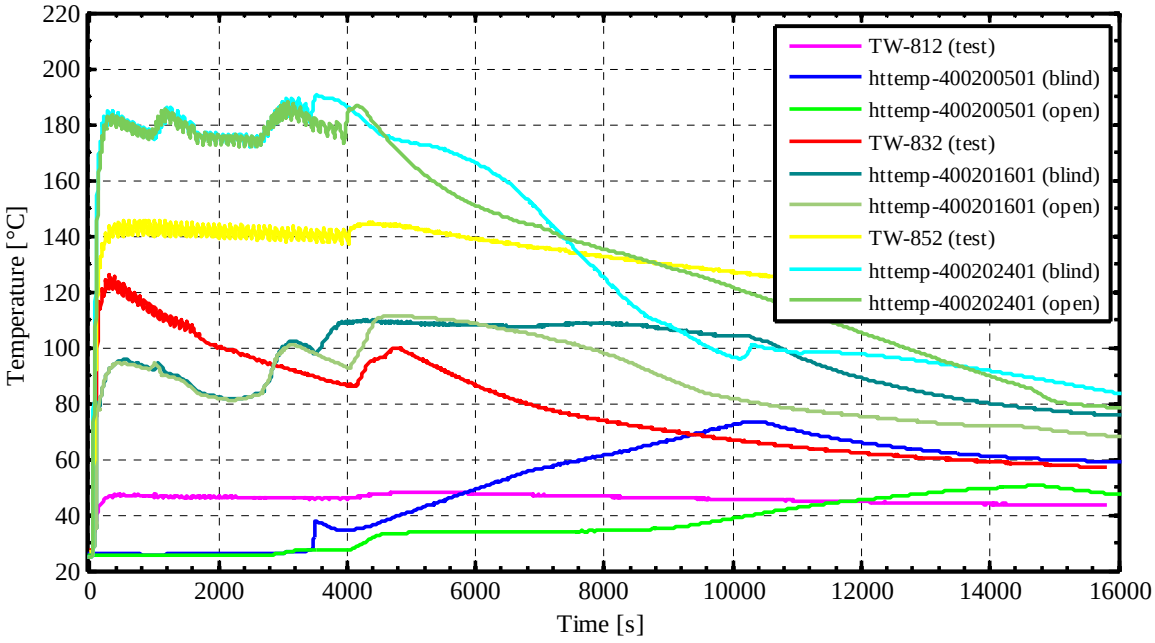

FIG. 4-398. SP-2 plate wall temperatures on HPC side.

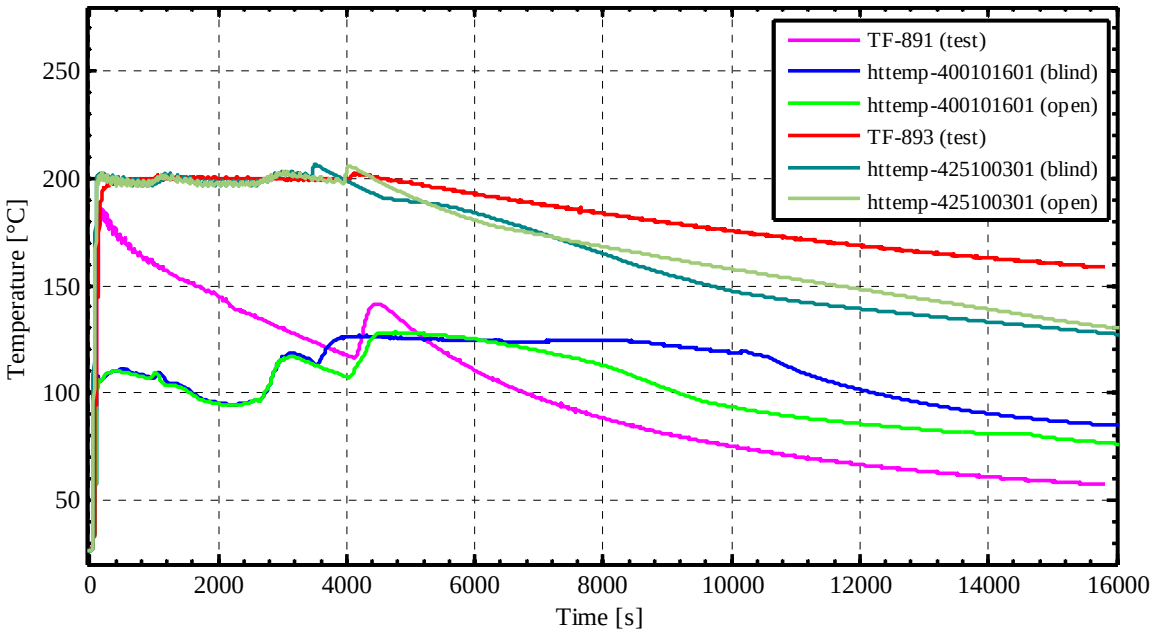

FIG. 4-399. SP-2 HPC vessel temperatures.

4.16.3.4. CPV thermal-hydraulic behavior

With the formation of thermally stratified hot steam-water pool in HPC, the heat transfer to CPV through the heat exchanging plate is intensified. For the major part of the transient it has been estimated at about 15 kW, slowly decreasing down to 5 kW by the end of the transient.

A fluid temperature discrepancy, similar to the one in HPC, is observed in CPV (Fig. 4-400). Instead of sharp water temperature increase, the gradual heat-up is predicted by the model. The discrepancies originate from the difference in water/steam temperature difference at the “hot” HPC side of the plate and the fact that thermocouples are probably located close to the plate while the code provides the bulk temperatures. Same considerations are applied for nodalization technique as for the HPC modeling.

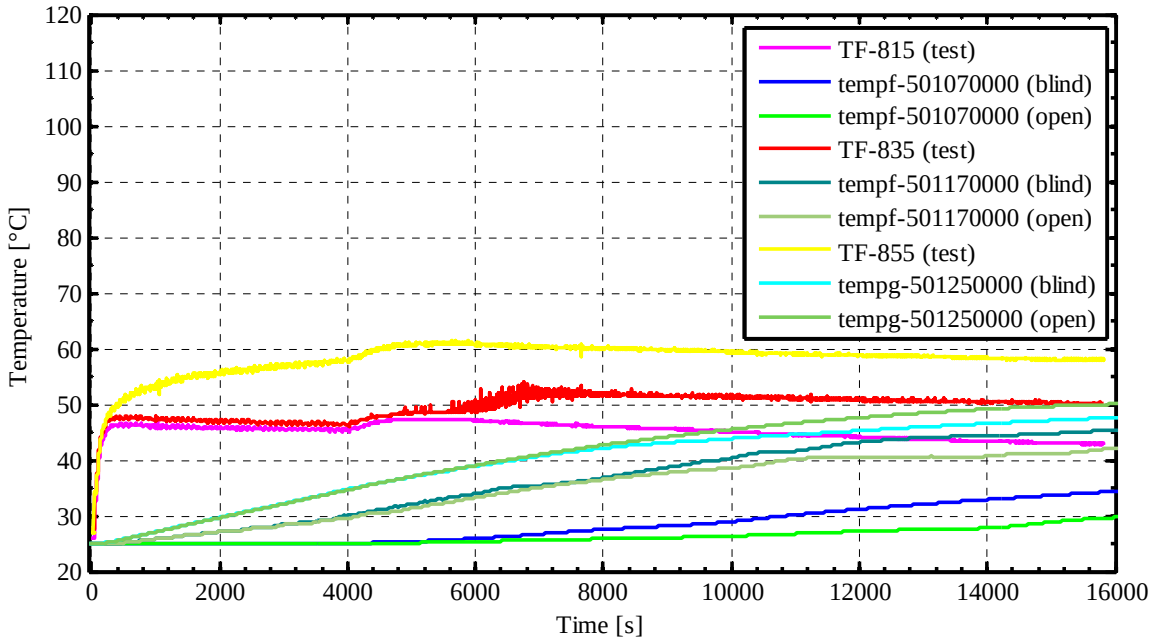

FIG. 4-400. SP-2 liquid and vapor temperatures in CPV.

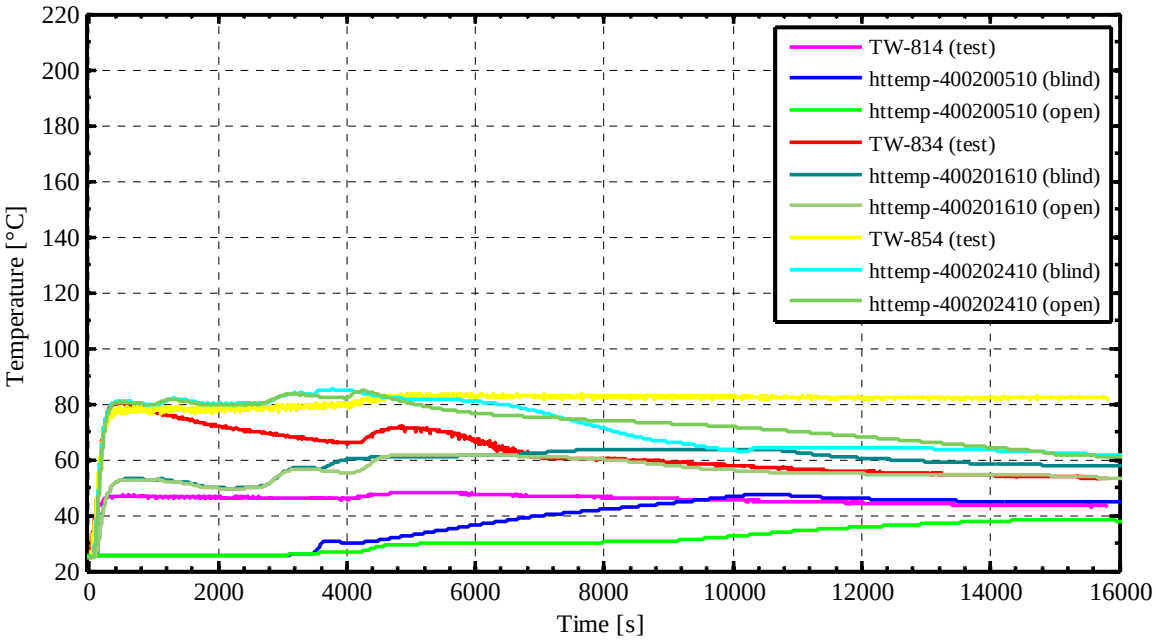

FIG. 4-401. SP-2 plate wall temperatures on CPV side.

4.16.4. Analysis results for power maneuvering

The initial conditions of the blind and open calculations of SP-3 (power maneuvering) are reported in Table 4-34. They are achieved running the code for 3000 s with the 'TRANSNT' (transient) option.

Steady state and initial conditions are achieved accordingly with the specifications. Few minor deviations are observed in the primary pressure due to the pressurizer heater imperfect operation logic and core inlet temperature is 1.5°C higher than specified value due to the imperfect set up of the form loss coefficients along the primary side circulation path.

It should be noted that FW mass flow rate at which the steady-state conditions are achieved is greatly overpredicted by the code. The reasons are the unsuitable heat transfer correlations applied by RELAP5 for the actual helical tube geometry and incorrectly predicted flow regime of the secondary side at the outlet from the tubes (annular mist instead of single-phase vapor).

The transient initiated by an increase of the core power heaters to 82 kW during 31 s. The core power provided from experimental measurements is supplied in a form of the time-dependent tabular data which implies 7 different levels of power simulated during the 6000 s of the transient (Fig. 4-402). The imposed time sequence of events is provided in Table 4-35 (identical for blind and open calculations).

The steam pressure and FW temperature time trends are taken from the experimental measurements and imposed by means of time-dependent volume components at the inlet and outlet of SG tubes while experimental FW mass flow rate is imposed at the inlet of SG tubes by means of time-dependent junction component (Fig. 4-403). Charging flow in blind calculation has been supplied into the bottom of RPV lower plenum by means of time-dependent junction component which operated according to the logic based on 2 setpoints of pressurizer collapsed level: 35.6 cm and 40.6 cm. In the open calculation the experimentally measured time-dependent charging flow has been is injected.

The PRZ heaters continue to maintain the pressure setpoint 8.719 MPa(a) through the entire transient simulation.

TABLE 4-34. SP-3 STEADY-STATE RESULTS (UNIPI)

Parameter	MASLWR	Unit	Experimental Value	Blind calculation	Open calculation
Pressurizer pressure	PT-301	MPa(a)	8.718	8.714	8.731
Pressurizer level	LDP-301	m	0.357	0.357	0.357
Power to core heater rods	KW-101/102	kW	42.0	42.0	42.0
Feedwater temperature	TF-501	ºC	31.49	31.49	31.49
Steam temperature	TF-611	ºC	260.0	260.5	260.2
Steam pressure	FVM-602-P	MPa(a)	1.464	1.465	1.465
Flow at core outlet	--	kg/s	0.47	0.83	0.89
Primary coolant temperature at core inlet	TF-121/122/ 123/124	ºC	250.2	251.9	251.9
Primary coolant temperature at core outlet	TF-106	ºC	261.5	262.1	261.5
Feedwater flow	FMM-501	kg/s	0.010	0.014	0.014

TABLE 4-35. SP-3 TIME SEQUENCE OF EVENTS (UNIPI)

Event	Time, s
Initiate core power increase to 80 kW	0.0
Initiate core power increase to 120 kW	845.0
Initiate core power increase to 160 kW	1619.0
Initiate core power increase to 200 kW	2135.0
Initiate core power increase to 240 kW	3990.0
Initiate core power increase to 280 kW	4465.0
Initiate core power increase to 320 kW	5184.0
End of test SP-3	SOT + 6000 s

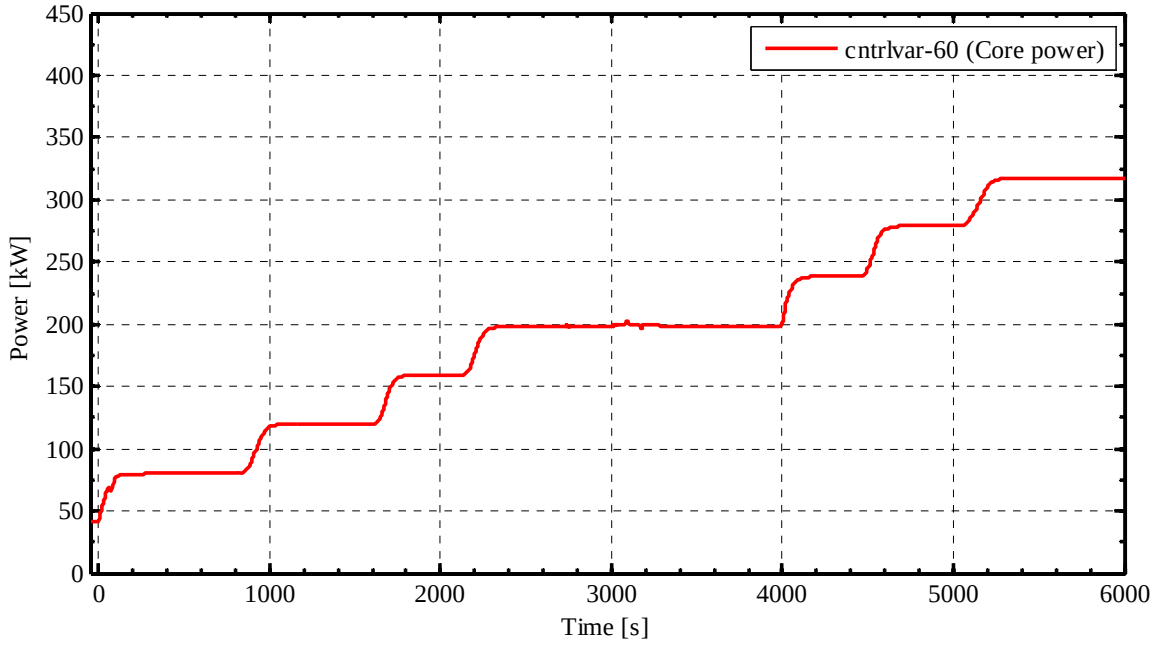

FIG. 4-402. SP-3 core power.

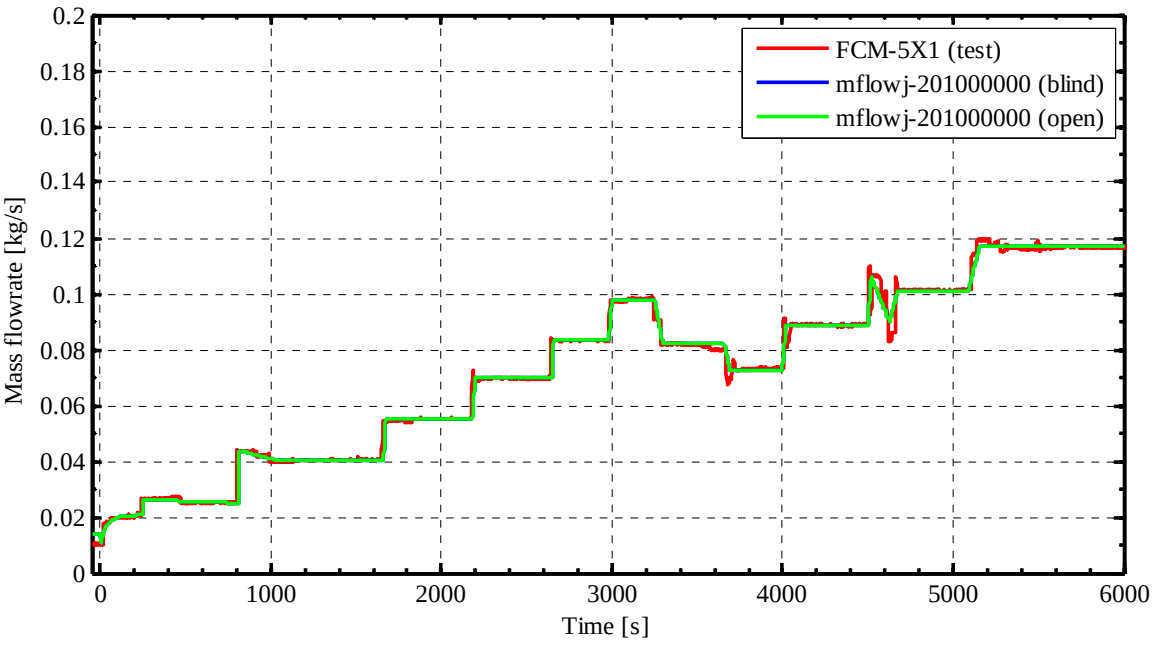

FIG. 4-403. SP-3 feedwater mass flow rate.

4.16.4.1. RPV thermal-hydraulic behavior

During entire transient the observed pressure in pressurizer remains rather constant (Fig. 4-404). Both calculations demonstrate some oscillation related to the imperfect setting of the PRZ heaters logic. Two strong pressure peaks (at the beginning and at about 3600 s) in blind phase calculation are caused by intervention of the charging flow system while in open phase calculation the experimental injection has been imposed. Hence, the absence of the strong peaks. Nevertheless, the pressure variations predicted by code are within irrelevant range and have negligible influence on heat transfer processes.

The predicted variations of the pressurizer level due to primary side heat-up and cooldown are in good agreement with experimental values (Fig. 4-405). Again, the correct modeling of charging flow results in better predictions in open calculations.

The single-phase natural circulation is sustained at all power levels. Model tends to overpredict mass flow in the primary side at the lower power levels and overpredict at higher (Fig. 4-406). The reason is imperfect setting of the form loss coefficients in the primary side. Both in blind and open calculations Re-independent loss coefficients were used. The differences in blind and open calculation results are due to reducing by 30% the K_{loss} coefficient at the core inlet. Use of Re-dependent form losses may significantly improve the code predictions.

The predicted coolant temperature trends at the core inlet and outlet locations (Fig. 4-407) are in good agreement. Two negative spikes in blind calculation are caused by the corresponding charging flow injections. Changing the boundary condition type in heat structure, representing the helical tubes, from "convective" to "swirl tubes" significantly improved the heat transfer prediction at higher power level resulting in better agreement of coolant temperatures with experimental data.

The estimated heat losses from the RPV remain about 3.5 kW through the entire transient. The power transferred across the chimney corresponds to 10 - 12% of generated power at all core power levels.

4.16.4.2. SG thermal-hydraulic behavior

The blind phase calculations resulted in very oscillatory behavior of the produced steam mass flow rate (Fig. 4-408). It is caused by rapid changing between the slug and horizontally stratified flow regimes in the boiling zone and between mist and horizontally stratified flow regimes in the steam zone. Such changes result in abrupt transition between different heat transfer modes and, consequently, in amount of steam produced. Specifying the "swirl tubes" heat transfer boundary type in the corresponding heat structure results in smooth transition between heat transfer modes and, consequently, non-oscillatory steam mass flow rate. Same smoothing effect in open phase calculation is observed in the power removed by SG (Fig. 4-409).

The degree of superheat predicted by code at lower power levels is in good agreement with experimental data (Fig. 4-410) for both blind and open phases. While at the higher power levels code overestimates slightly the steam temperature.

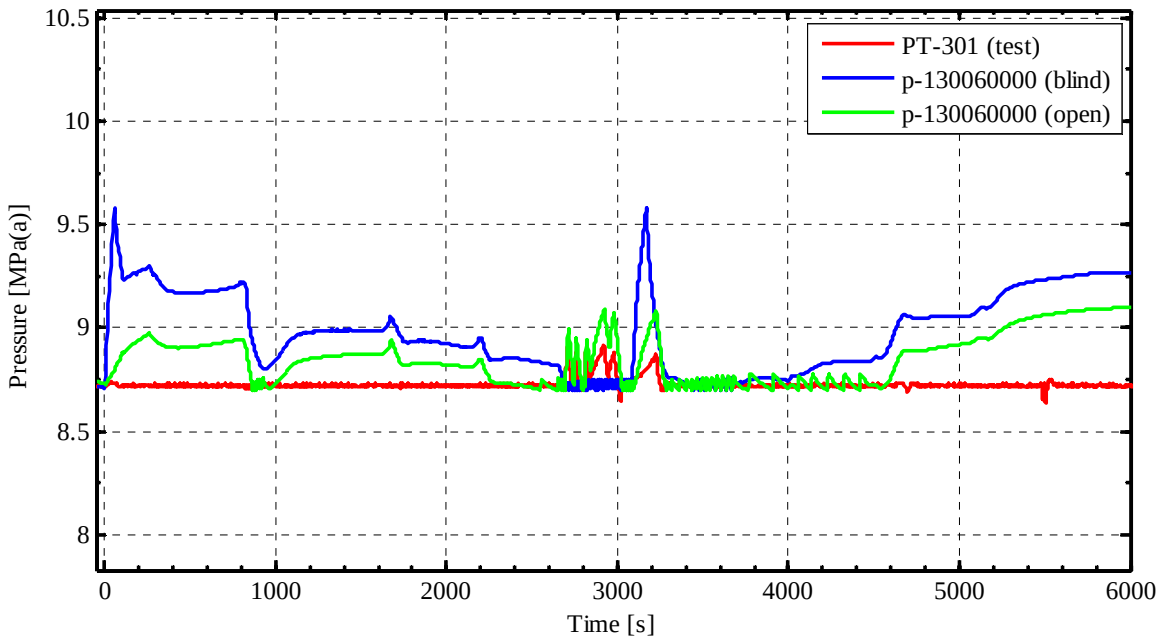

FIG. 4-404. SP-3 pressurizer pressure.

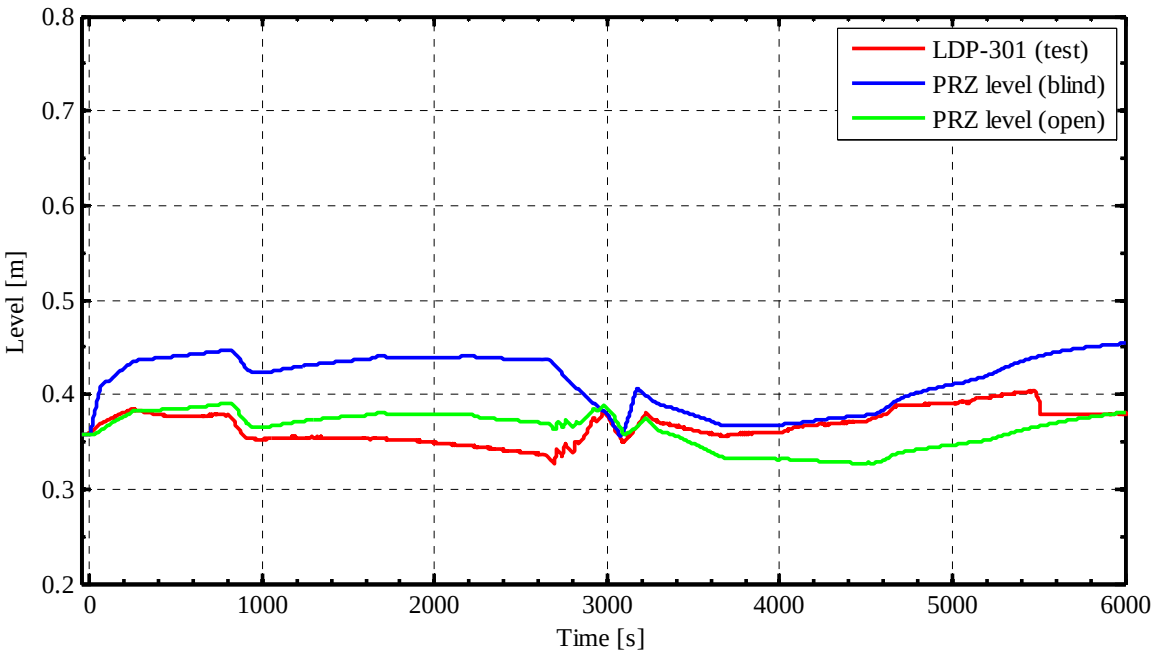

FIG. 4-405. SP-3 pressurizer level.

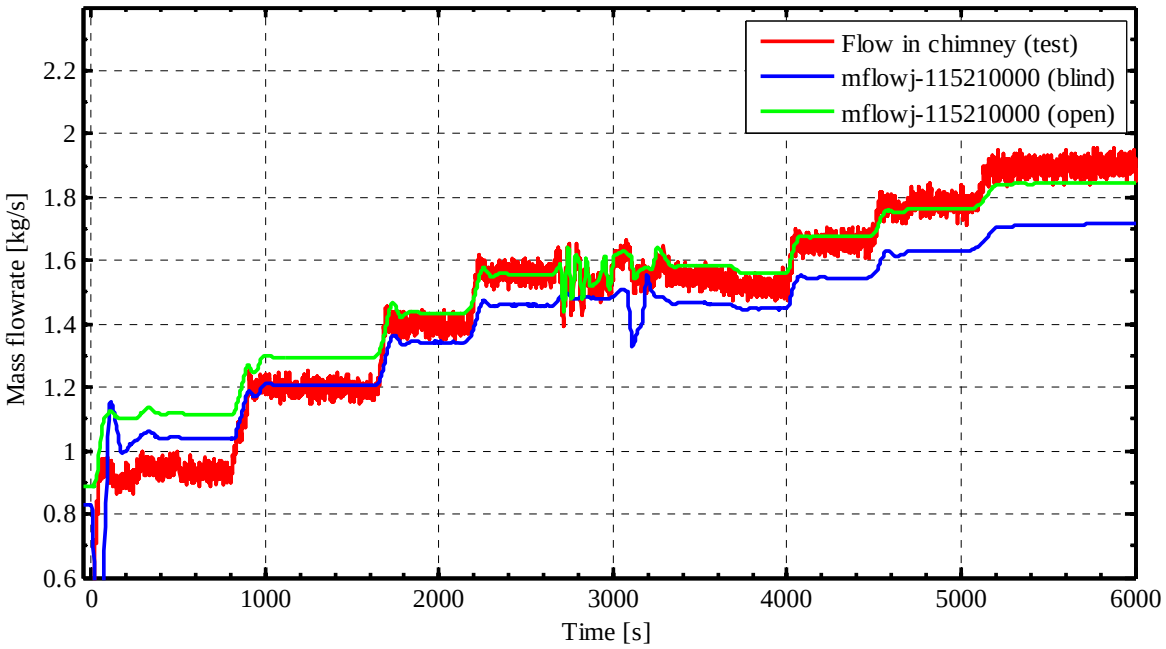

FIG. 4-406. SP-3 mass flow rate in RPV chimney.

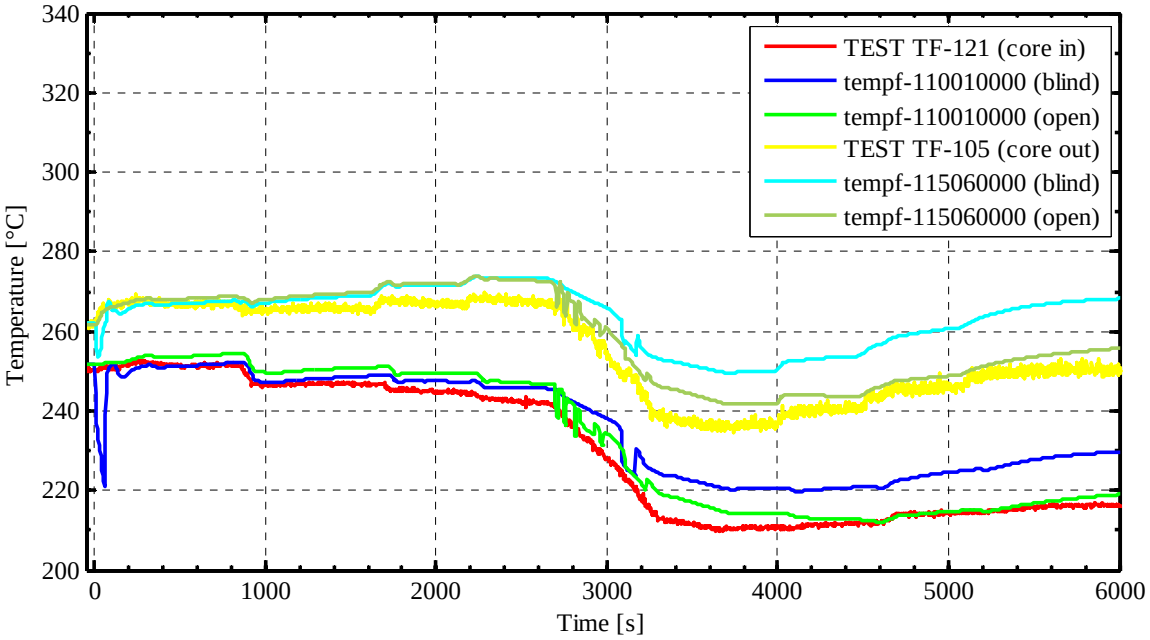

FIG. 4-407. SP-3 core inlet and outlet temperatures.

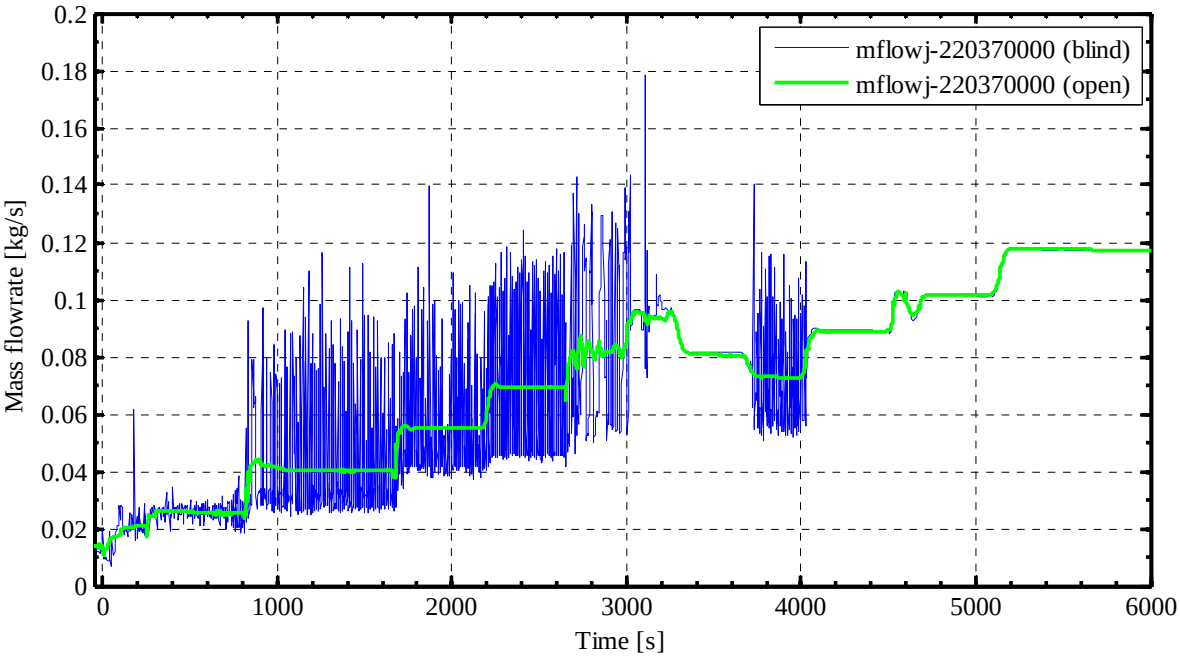

FIG. 4-408. SP-3 SG steam flow rate.

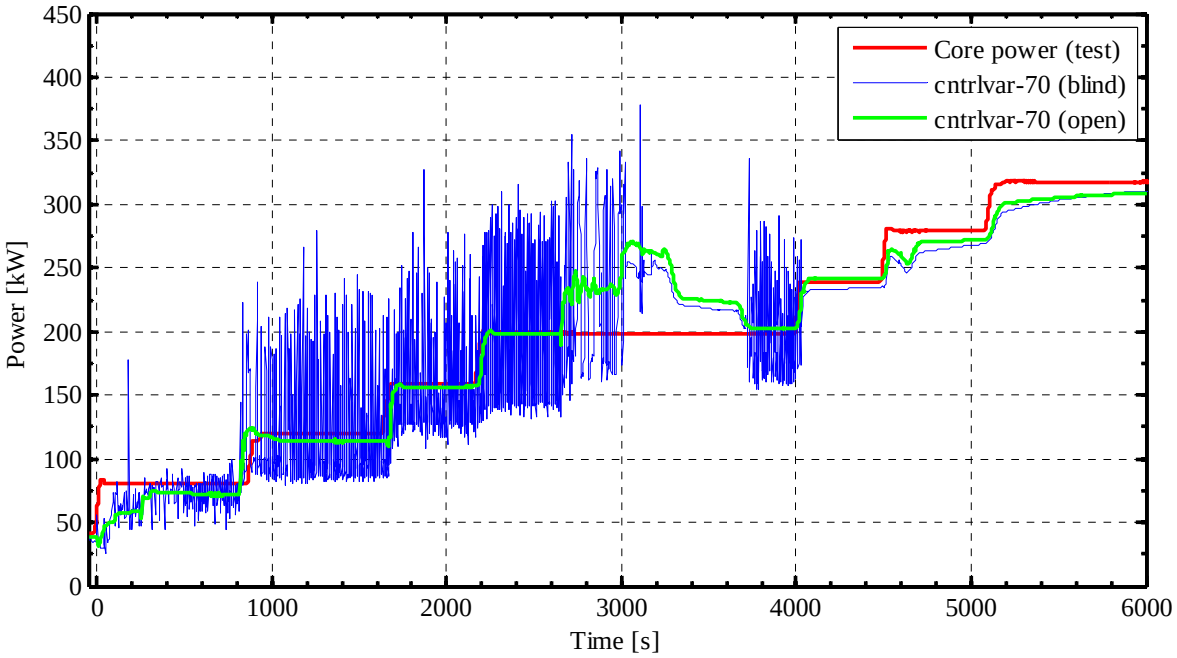

FIG. 4-409. SP-3 SG removed power.

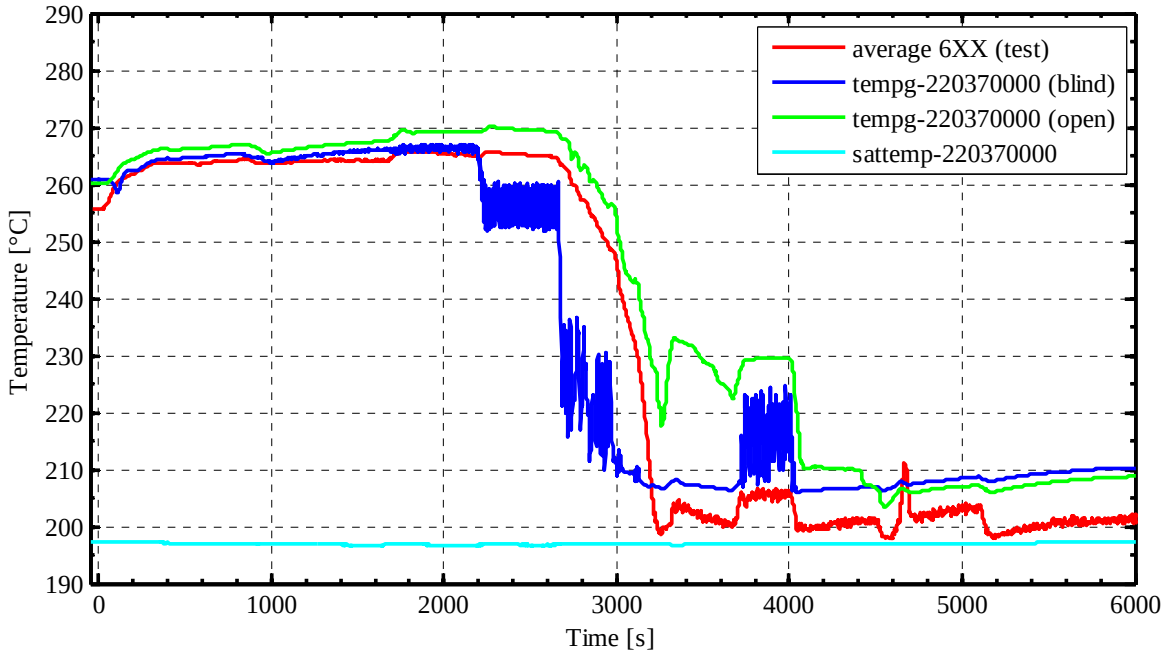

FIG. 4-410. SP-3 SG steam temperature.

5. COMPARISON OF BLIND CALCULATION RESULTS

5.1. LOSS OF FEEDWATER TRANSIENT

SP-2, the loss of feedwater transient, is initiated by a loss of the main feed water pump. The primary heat sink is lost with the loss of feed water as there is only a limited inventory of coolant in the steam generator coils. The loss of heat sink causes a rise in primary system pressure. As per procedure, once the system pressure reaches 9.064 MPa(a), the test facility will simulate a reactor trip by switching the core power controllers to decay heat mode. The pressure will continue to rise as the decay heat is still greater than the primary system's ability to remove the heat through heat loss from the primary vessel.

Once the system pressure reaches 9.409 MPa(a), the vent valve PCS-106A will open to signify a depressurization of the primary vessel. In the test facility, PCS-106A will cycle open and closed in order to prevent over pressurization in the high-pressure containment while at the same time depressurizing the primary vessel. Once the pressure difference between the primary vessel and the high-pressure containment is within 0.034 MPa all vent valves (PCS-106A/B) and sump recirculation valves (PCS-108A/B) open. At this point, the primary vessel and the high-pressure containment are at equal pressures and their subsequent cooldown and depressurization behavior is linked.

Table 5-1 compares the SP-2 sequence of events scheme for each of the participants. Note that all subsequent Figures have been adjusted so that time 0 represents the start of the transient.

5.1.1. RPV thermal hydraulic behavior

The core power decay during the transient is shown in Figure 5-1. In general, the initial decay is similar for all participants and matches the experimental core power very well. It can be noticed that a number of the participants overestimate the decay power after the initial decrease. It is likely that this change in the boundary condition will have a significant influence on the progress of the transient at later time.

Figure 5-2 shows the decrease in the system pressure following the initial increase. The oscillations in pressure are visible in the experimental data, which are caused by the opening and closing of vent valve PCS-106A up to time 4114 s. At that time the oscillations stop while the long-term pressure decrease continues due to the transfer of energy away from the system. Most of the participants were able to capture the general behavior of the pressure decrease although it appears as if a number of participants did not model the opening and closing of the vent valve as indicated by an absence of pressure oscillations.

Average core inlet and outlet temperatures are shown in Figures 5-3 and 5-4. On Figure 5-3, at time 4114 s, a temperature decrease can be seen at the core inlet. This is due to the opening of the sump recirculation valves and the inrush of cooler water from the high-pressure containment. This temperature decrease is not noticed significantly at the core outlet in the experiment. This inrush of water from the HPC as seen by the increase in primary coolant level is shown on Figure 5-5. Most of the participants were able to capture the general trend of core inlet temperature, core outlet temperature and core coolant level, but there is a considerable difference in both the temperature and water level values and the timing of the inrush of HPC coolant. This difference in timing of the sump recirculation valve opening is caused by differences in depressurization rate for the transient. Sump recirculation valve opening times are show in Table 5-1 for each of the participants which further highlights the differences between participants and the experiment. The core heater rod temperature is shown in Figure 5-6.

Figures 5-7, 5-8 and 5-9 show the core mass flow rate, void fractions in the core and void fractions in the chimney respectively. There are no experimental measurements for these values in SP-2. It is clear that there is a wide range of behavior for the participants as indicated by the variety between participants in these Figures. In general, the mass flow rate for each participant shows large fluctuations. This is expected since the flow rate through the chimney will be driven by a variety of phenomena including natural circulation and the influence of the flow paths between the HPC and the vessel. Most participants showed relatively little voiding in the core during the transient. Concerning voiding in the chimney region there was less agreement among the participants. For those that did

show considerable voiding, the void coincided with the drop in the liquid level in the vessel as a result of the blowdown.

The next four figures show the cumulative discharge through each of the four vents and sump recirculation lines. Again, there is no experimental measurement for these parameters. As is seen in Figure 5-10, there are significant differences among participants in reference to the discharge through vent valve PCS-106A. This will directly impact the rate of depressurization, with the high discharges resulting in a faster depressurization, although this is not obvious when one looks at the depressurization of the vessel in Figure 5-2. The discharge through PCS-106B, PCS-108A and PCS-108B are shown in Figures 5-11, 5-12 and 5-13 respectively. Again there are differences in the actual discharge amounts as well as the timing of flow start. Most of the participants did show flow through the sump recirculation valves from the HPC to the primary vessel.

5.1.2. SG thermal hydraulic behavior

The feed water flow is shown in Figure 5-14. As seen in this figure, the feed water is stopped at the start of the transient effectively eliminating the steam generator as a heat sink. This is also highlighted in Figure 5-15, which shows that the calculated heat transfer through the steam generator for the participants appears to be negligible.

5.1.3. HPC thermal hydraulic behavior

Figure 5.16 shows the pressure behavior inside of the high-pressure containment. This Figure shows the oscillatory behavior in pressure caused by the cycling of PCS-106A as well as the eventual decrease in pressure after the primary and HPC pressures equalize. Most, but not all, of the participants are able to capture this behavior qualitatively if not quantitatively.

The initial increase in HPC water level is shown in Figure 5-17. This is caused by the discharge of coolant from the primary through PCS-106A and the subsequent condensation of the steam that enters the HPC. At time 4114 s, this figure also shows the drop in HPC level as the sump recirculation valves open and coolant flows from the HPC to the primary vessel. This behavior was captured by most of the participants with differences in timing of HPC level drop noted previously caused by sump recirculation valve opening.

The next three Figures 5-18 through 5-20 show the water temperature inside of the HPC at a variety of levels. It is clear from these figures that the lowest temperature measurement remains well submerged in subcooled liquid while the upper thermocouples remain in a steam filled region. Mixing of coolants between HPC and the primary vessel can be seen in the lower thermocouples after time 4114 s. The middle elevation thermocouples appear to remain submerged in liquid but at temperatures closer to saturation which indicates that there is significant stratification of the liquid in the HPC during the transient. It is also of note that at 4114 s, the temperature of the middle elevation thermocouple increases significantly. This is likely caused by the dropping of the water level in the HPC when the sump recirculation valves are opened. As the water level drops, fluid higher in the HPC comes in contact with the middle elevation thermocouple due to the stratification of the coolant in the HPC. There was significant variation among the participants concerning the fluid temperatures in the HPC as shown in Figures 5-18 through 5-20.

5.1.4. CPV thermal hydraulic behavior

The water level in the CPV remains unchanged during the transient as shown in Figure 5-21.

Figures 5-22 through 5-24 show the water temperatures within the CPV at the same elevations for the fluid temperatures inside of the HPC shown in figures 5-18 through 5-20. Of note is the observation that the CPV water temperature increases very rapidly after the start of the transient, much faster than predicted by any of the participants. This is likely due to the positioning of the thermocouples very close to the heat transfer plate in the experimental facility. In addition, over the long-term operation of the transient, the water in the CPV becomes stratified as indicated by the water temperatures of the CPV fluid.

Figures 5-25 through 5-27 show the CPV heat transfer plate temperatures at the same levels as noted for the CPV and HPC fluid temperatures. These temperatures are measured halfway between the HPC and the CPV. The temperatures themselves measure between the temperatures in the CPV and the HPC as would be expected. The impact of the sump recirculation valve opening on the HPC coolant temperatures is also noted in the heat transfer plate albeit with less magnitude. As with the HPC fluid temperatures there is significant variation among the participants concerning the heat transfer plate temperatures.

TABLE 5-1. SP-2 SEQUENCE OF EVENTS

Event	Experimental Value (s)	AERB	BARC (RELAP)	CIAE	ENEA	GPRESS	IBRAE	KAERI	KINS
Start of simulation – steady state (start of data collection)	0	0	-600	-50	0	0	-600	0	-600
Stop MFP Close HPC vent valve SV-800	0	0	0	0	0	0	0	0	0
PZR pressure (PT-301) reaches 9.064 MPa(a) Enter decay power mode	30	30	20	9.6	37.4	17	25.5	28	29.6
PZR pressure (PT-301) reaches 9.409 MPa(a) De-energize PZR heaters Open ADS vent valve (PCS-106A)	48	48	48	28	54	53	30.5	48	47.6
Start long-term cooling when pressure difference between primary system and HPC (PT-301 minus PT-801) becomes less than 5 psi (0.034 MPa) Open and remain open of PCS-106A and PCS-106B Open and remain open of PCS-108A and PCS-108B	4024-4117	5500	4024 4114 4116 4117	4304	3882	4143	4052.9	4500	807
End of test when one of the following conditions is reached: - PZR pressure ≤ 0.135 MPa(a) - Primary coolant temperature (TF-132) ≤ 35ºC - 24 hours have elapsed	15822	24 h	30000	14300	21812	14000	15822		17400

TABLE 5-1. SP-2 SEQUENCE OF EVENTS (CONTINUED)

Event	Experimental Value (s)	NPCIL	NUSCALE	SJTU	SNPTRD	UNIPA	UNIPI	USNRC
Start of simulation – steady state (start of data collection)	0	0	0	0	0	-600	0	0
Stop MFP Close HPC vent valve SV-800	0	0	0	0	0	0	0	0
PZR pressure (PT-301) reaches 9.064 MPa(a) Enter decay power mode	30	28	28	29	17	26	36	37.1
PZR pressure (PT-301) reaches 9.409 MPa(a) De-energize PZR heaters Open ADS vent valve (PCS-106A)	48	48	46	47	20	44	37	55.1
Start long-term cooling when pressure difference between primary system and HPC (PT-301 minus PT-801) becomes less than 5 psi (0.034 MPa) Open and remain open of PCS-106A and PCS-106B Open and remain open of PCS-108A and PCS-108B	4024-4117	4780	552	5419	11132	4062-4155	3466	4717
End of test when one of the following conditions is reached: - PZR pressure ≤ 0.135 MPa(a) - Primary coolant temperature (TF-132) ≤ 35ºC - 24 hours have elapsed	15822	14360	NA (Simulation stop at 15184)	3 h		15822	18000	15000

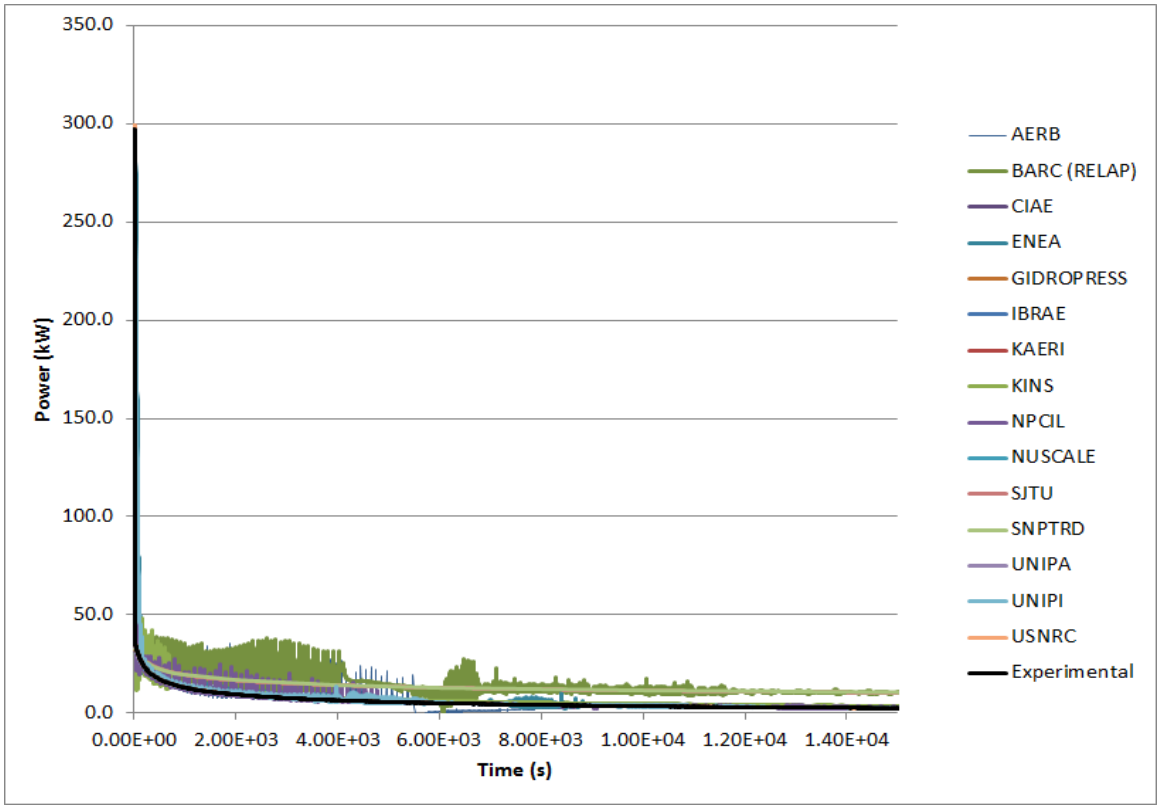

FIG. 5-1. SP-2 core power.

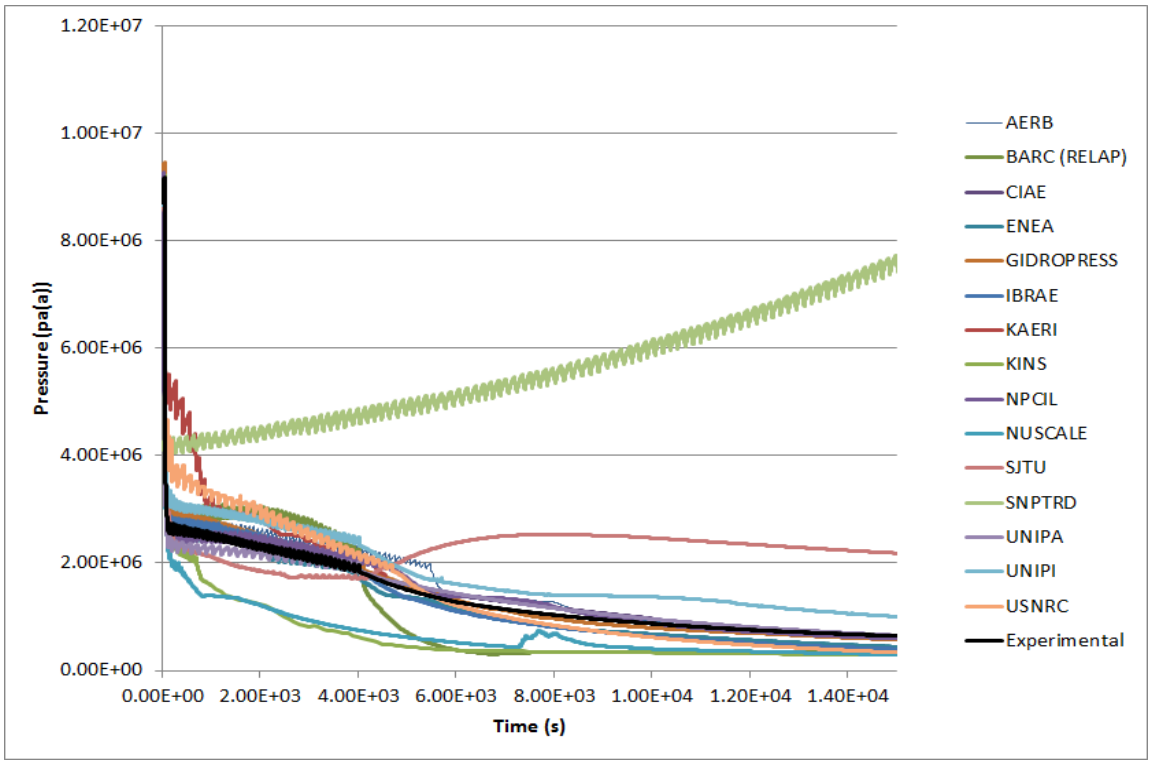

FIG. 5-2. SP-2 pressurizer pressure (PT-301).

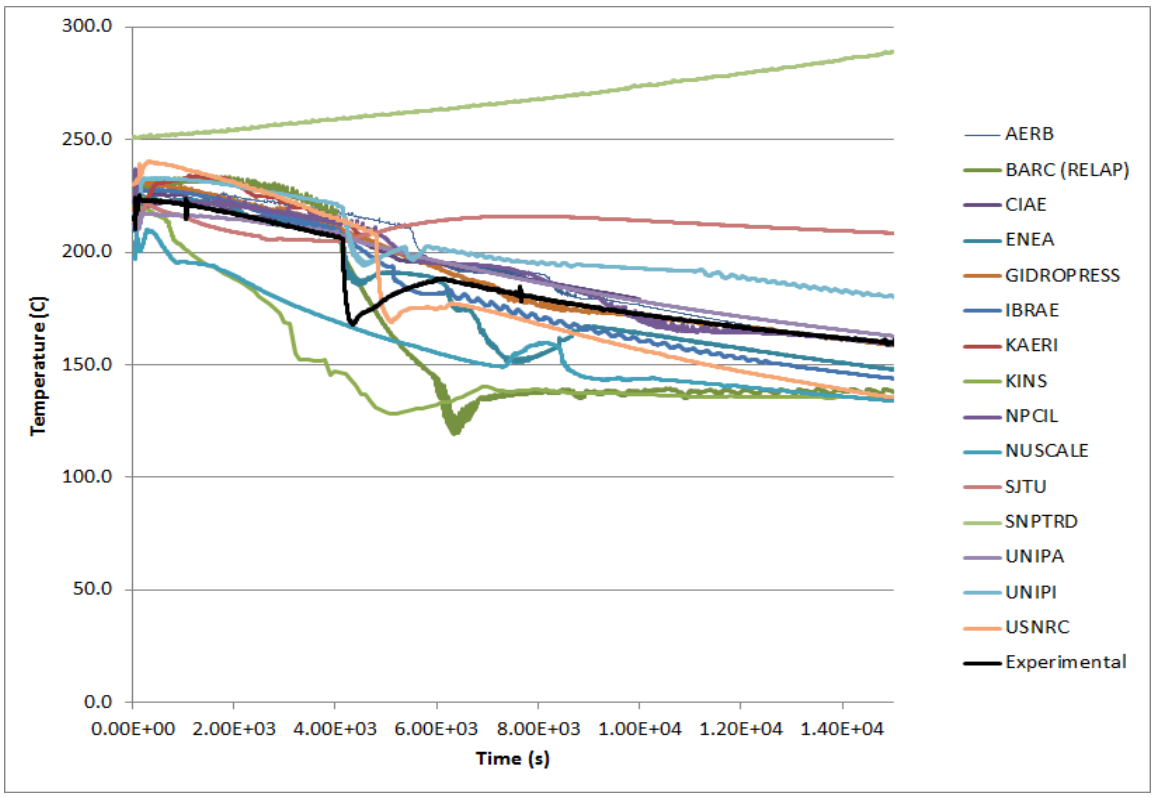

FIG. 5-3. SP-2 core inlet average temperature.

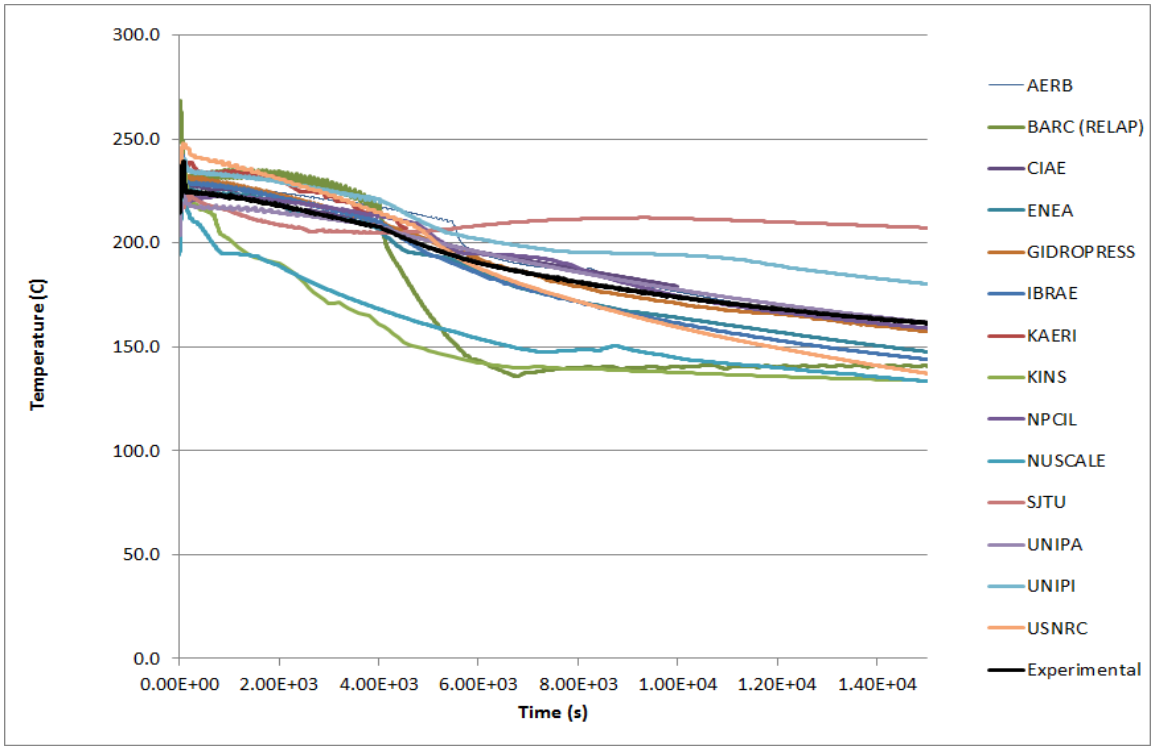

FIG. 5-4. SP-2 core outlet average temperature.

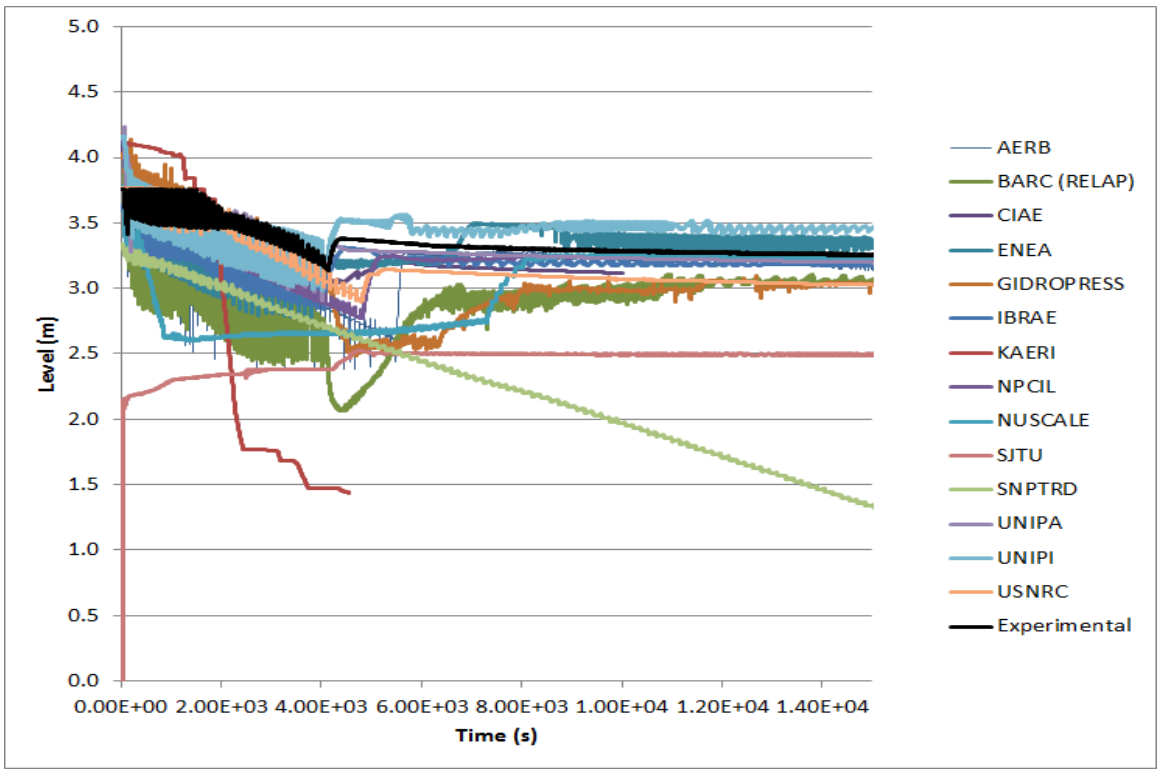

FIG. 5-5. SP-2 RPV water level (LDP-106).

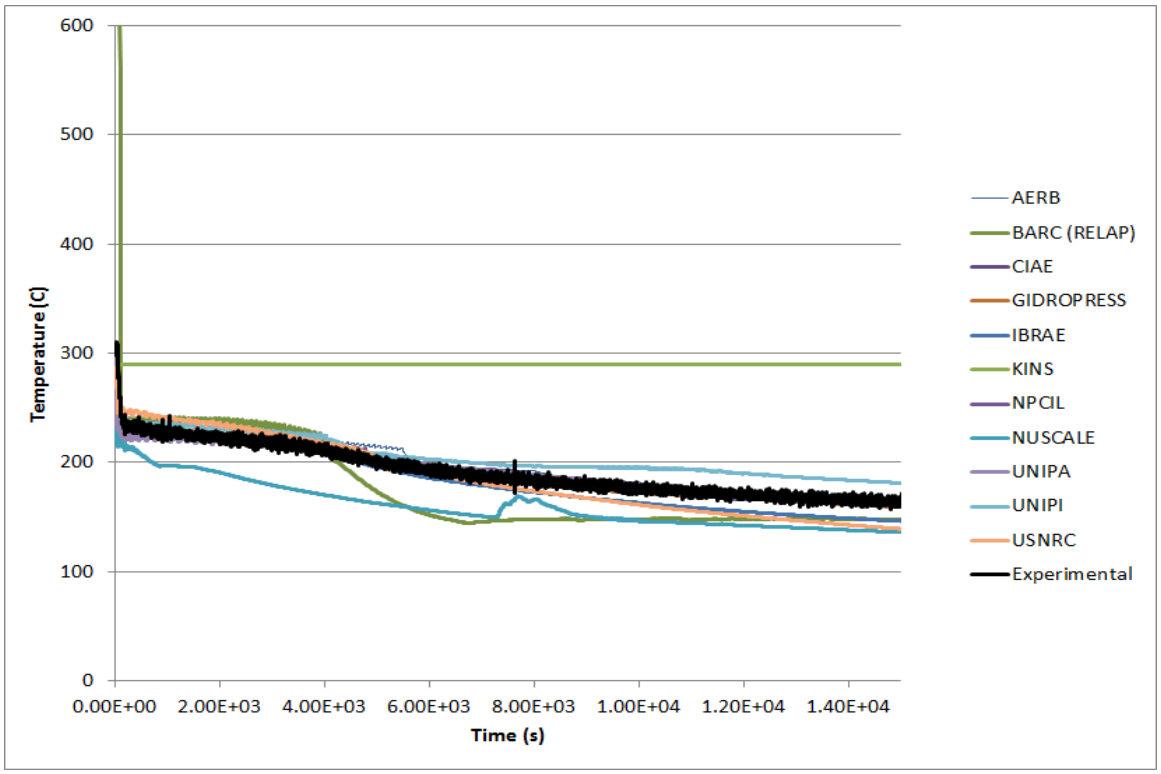

FIG 5-6. SP-2 heater rod temperature (TH-143).

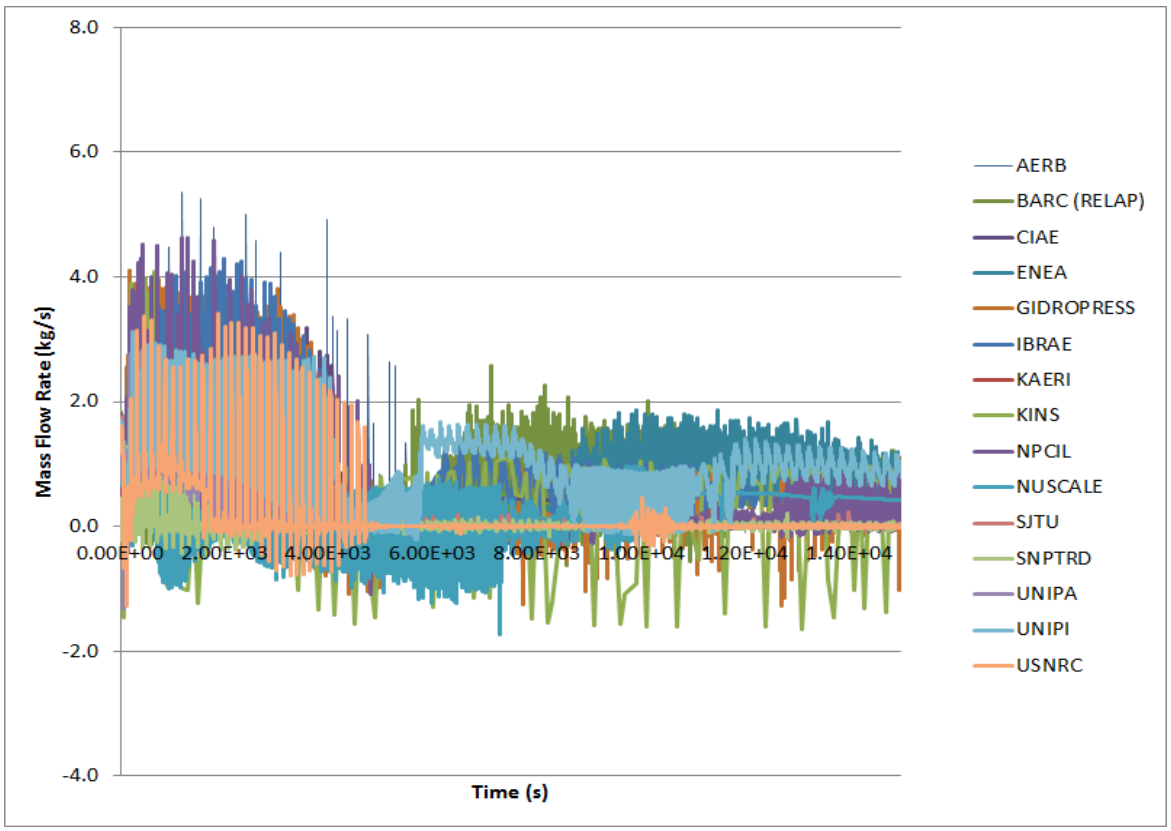

FIG. 5-7. SP-2 chimney mass flow rate.

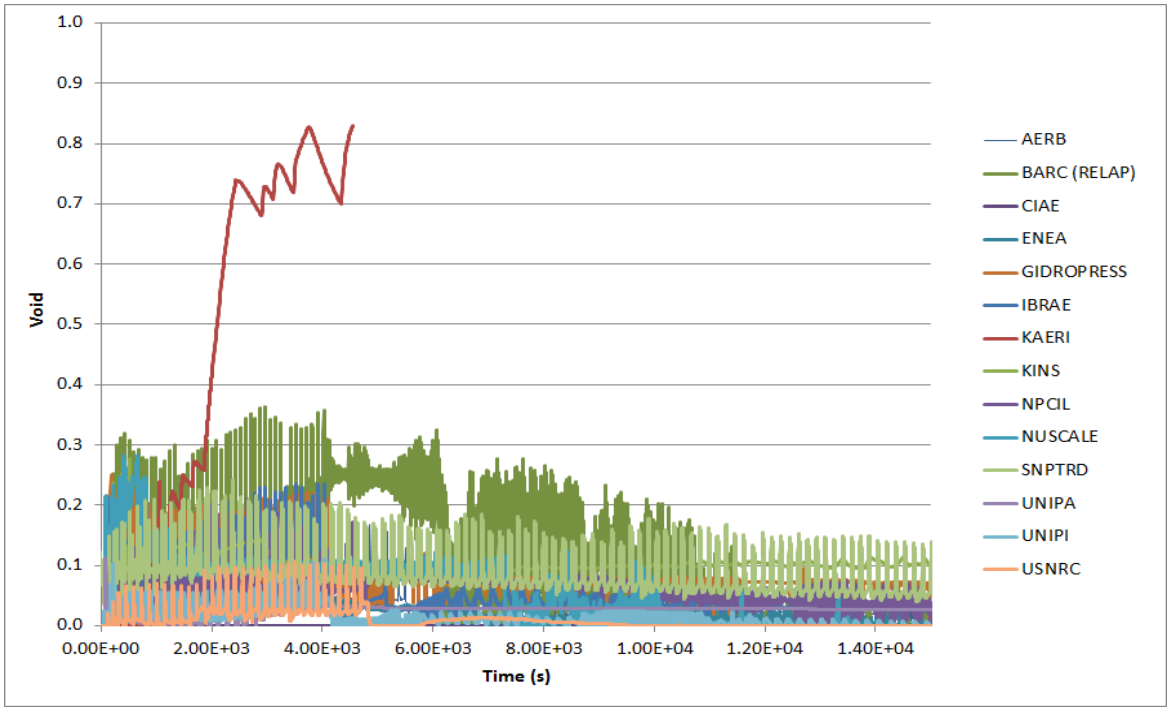

FIG. 5-8. SP-2 void fraction (core outlet).

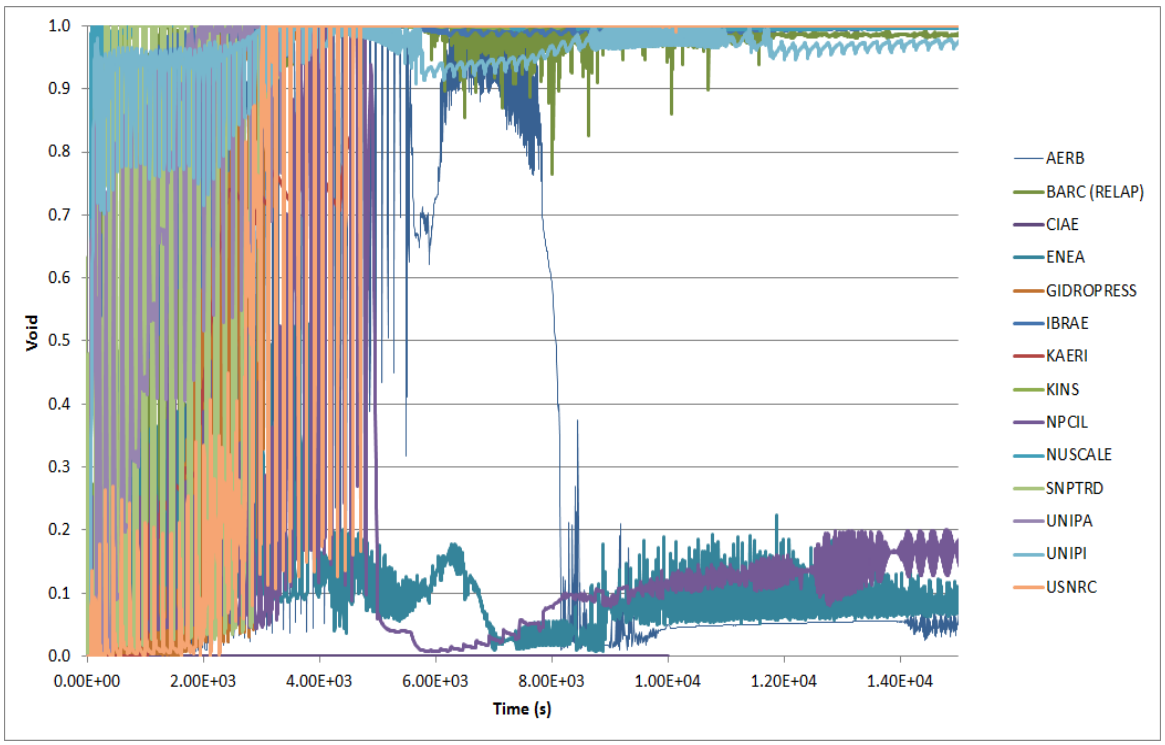

FIG. 5-9. SP-2 void fraction (chimney).

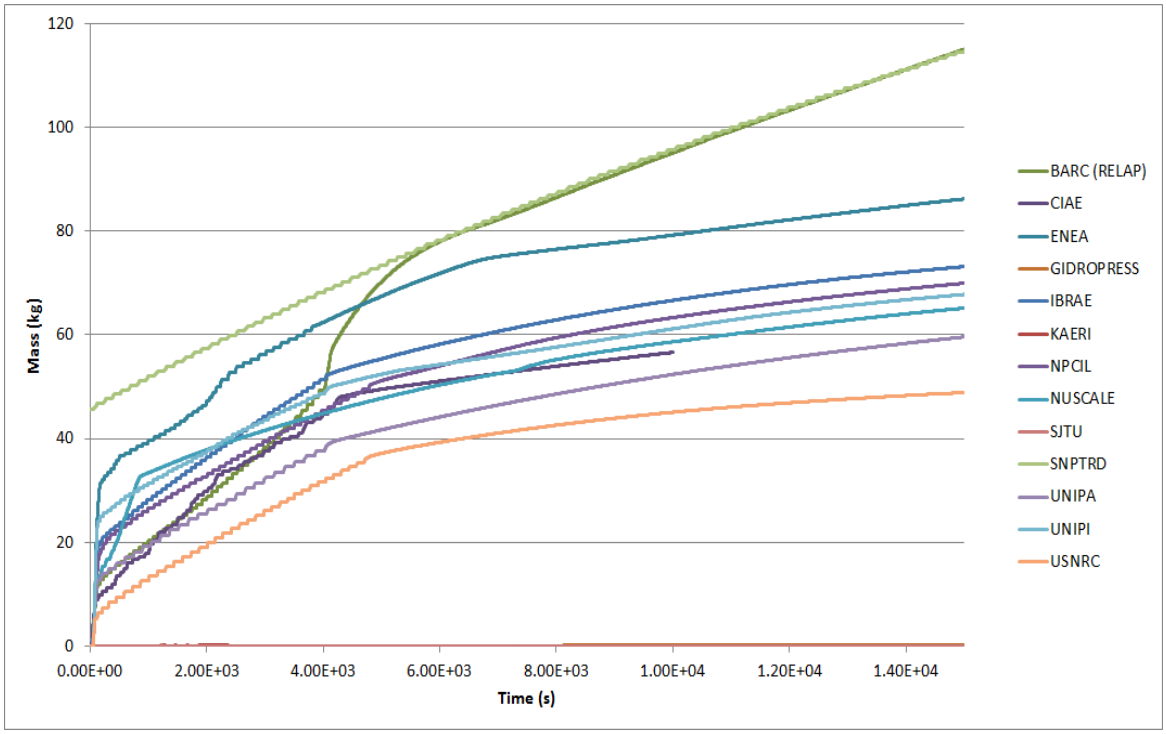

FIG. 5-10. SP-2 PCS-106A cumulative discharge.

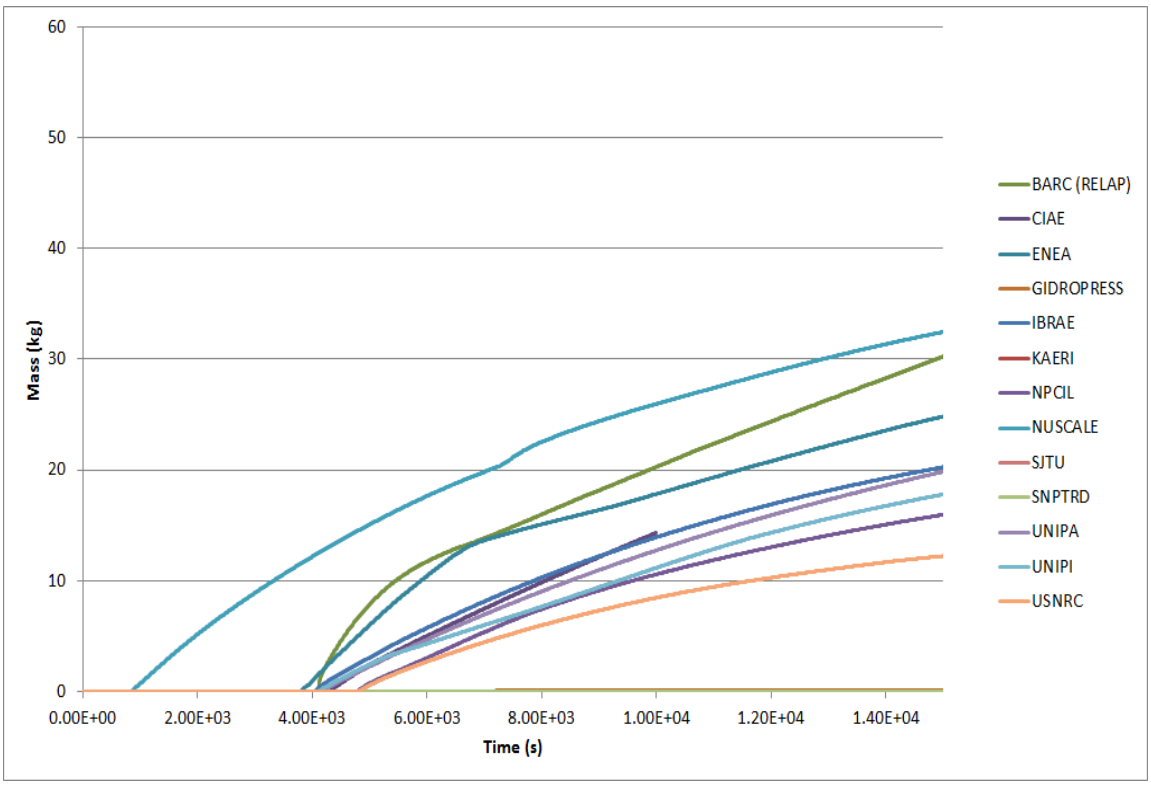

FIG. 5.11. SP-2 PCS-106B cumulative discharge.

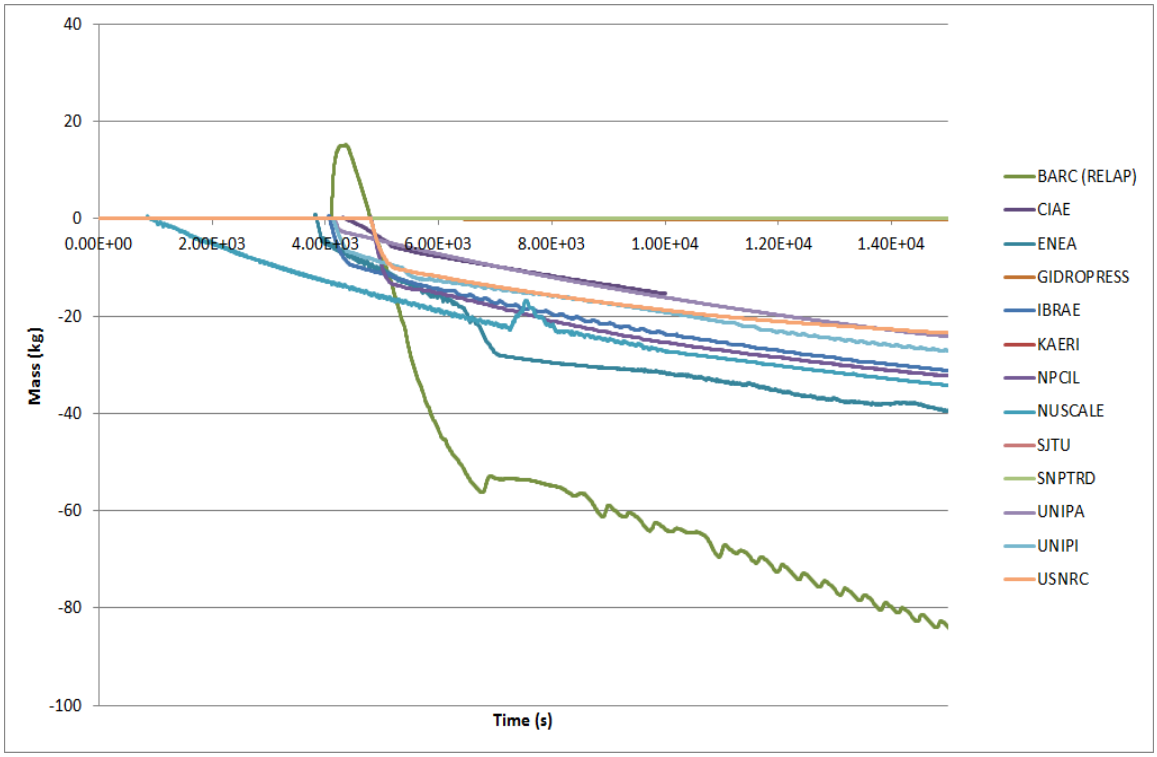

FIG. 5-12. SP-2 PCS-108A cumulative discharge.

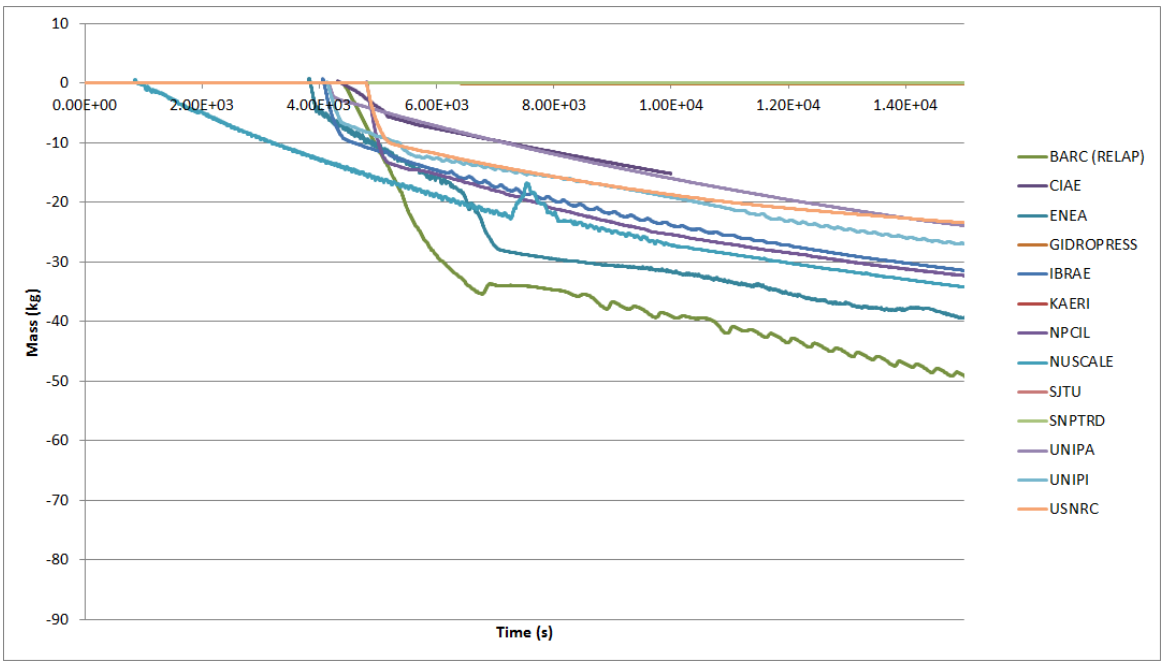

FIG. 5-13. SP-2 PCS-108B cumulative discharge.

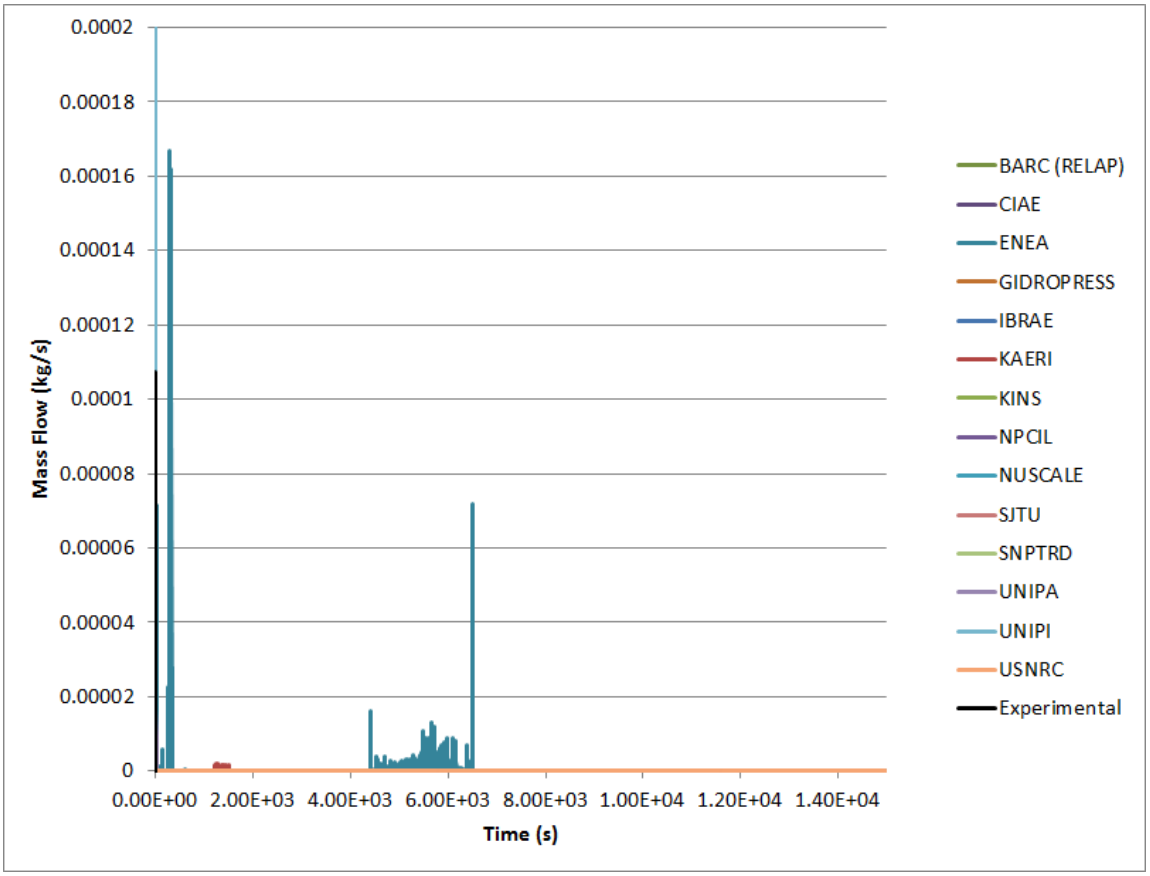

FIG. 5-14. SP-2 feed water mass flow rate (FMM-501).

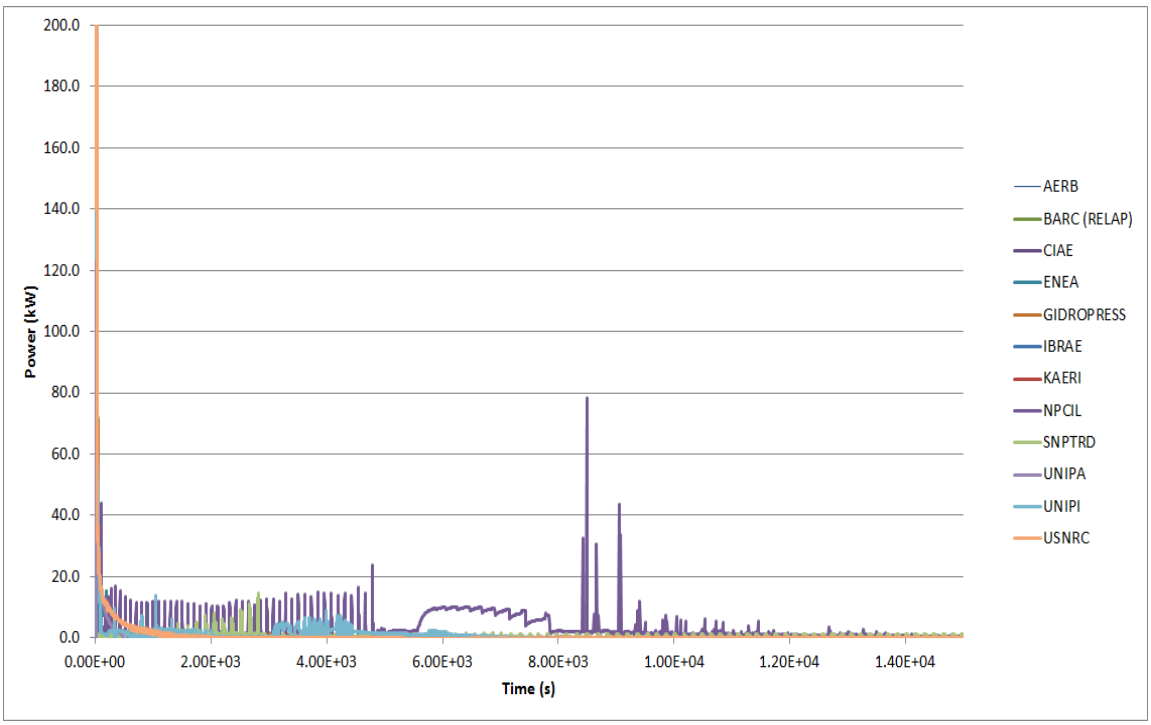

FIG. 5-15. SP-2 heat transfer (steam generator).

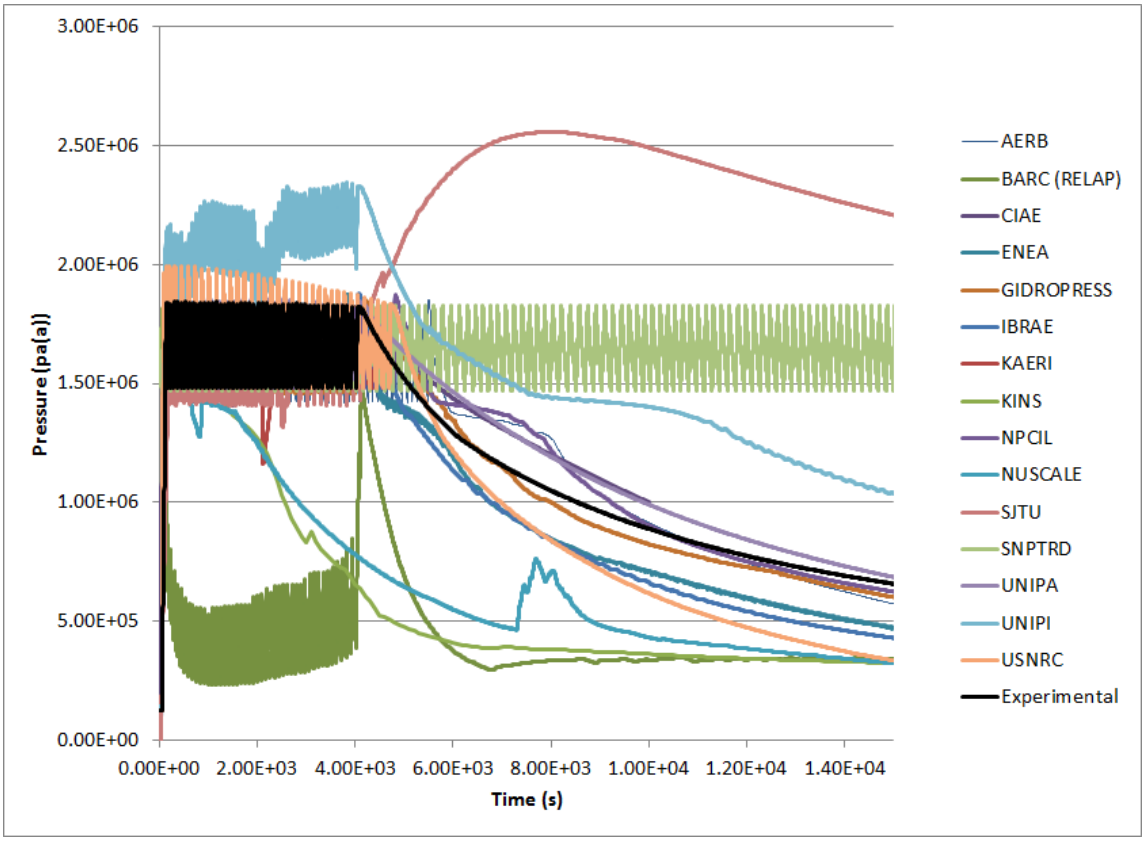

FIG. 5-16. SP-2 HPC pressure (PT-801).

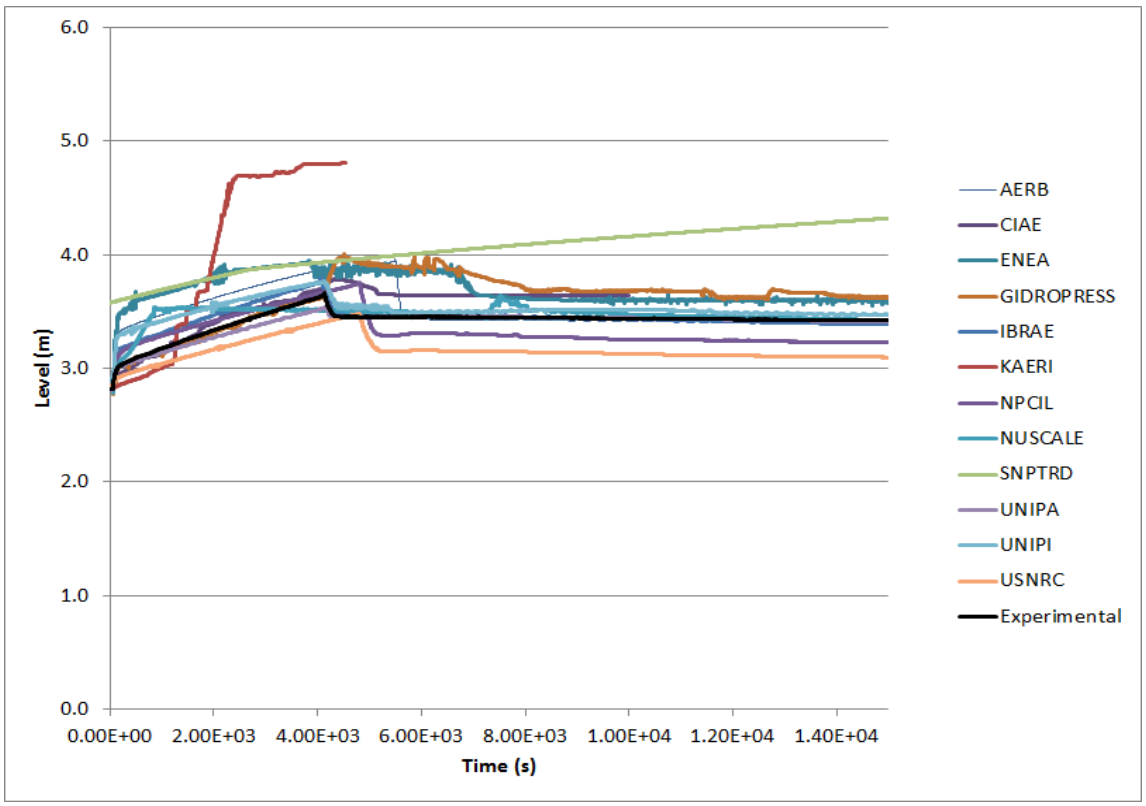

FIG. 5-17. SP-2 HPC water level (LDP-801).

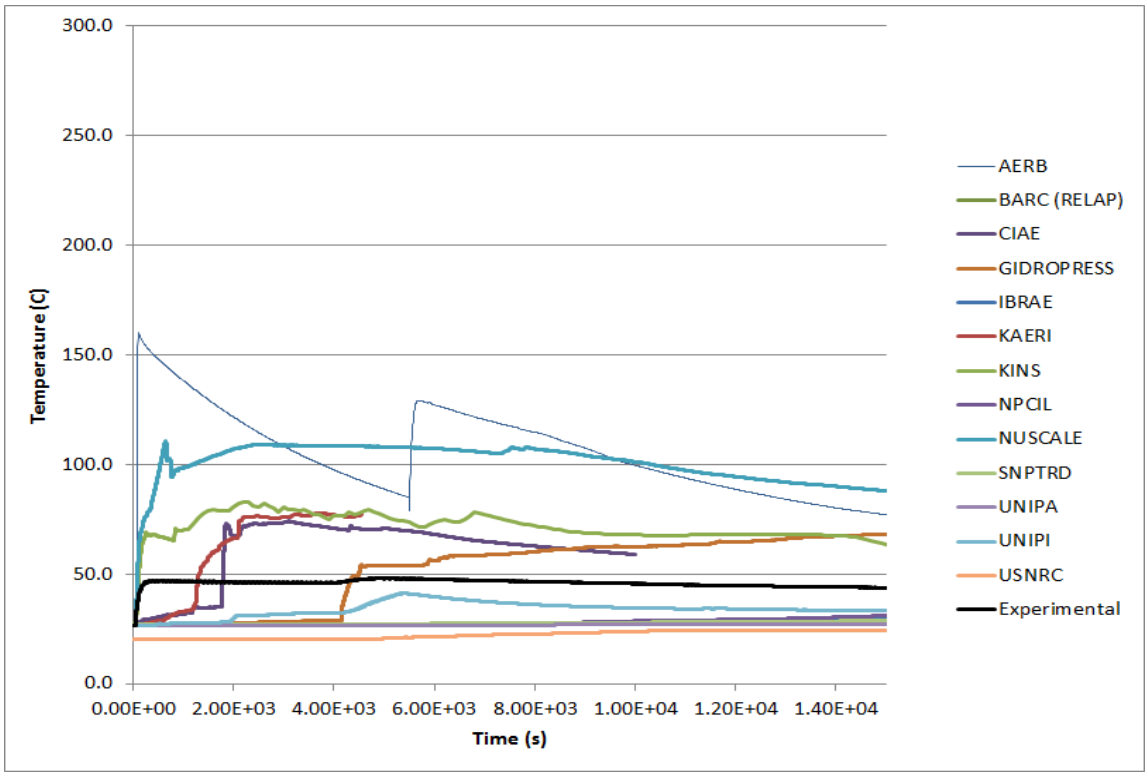

FIG. 5-18. SP-2 HPC fluid temperature (6.99 cm, TF-811).

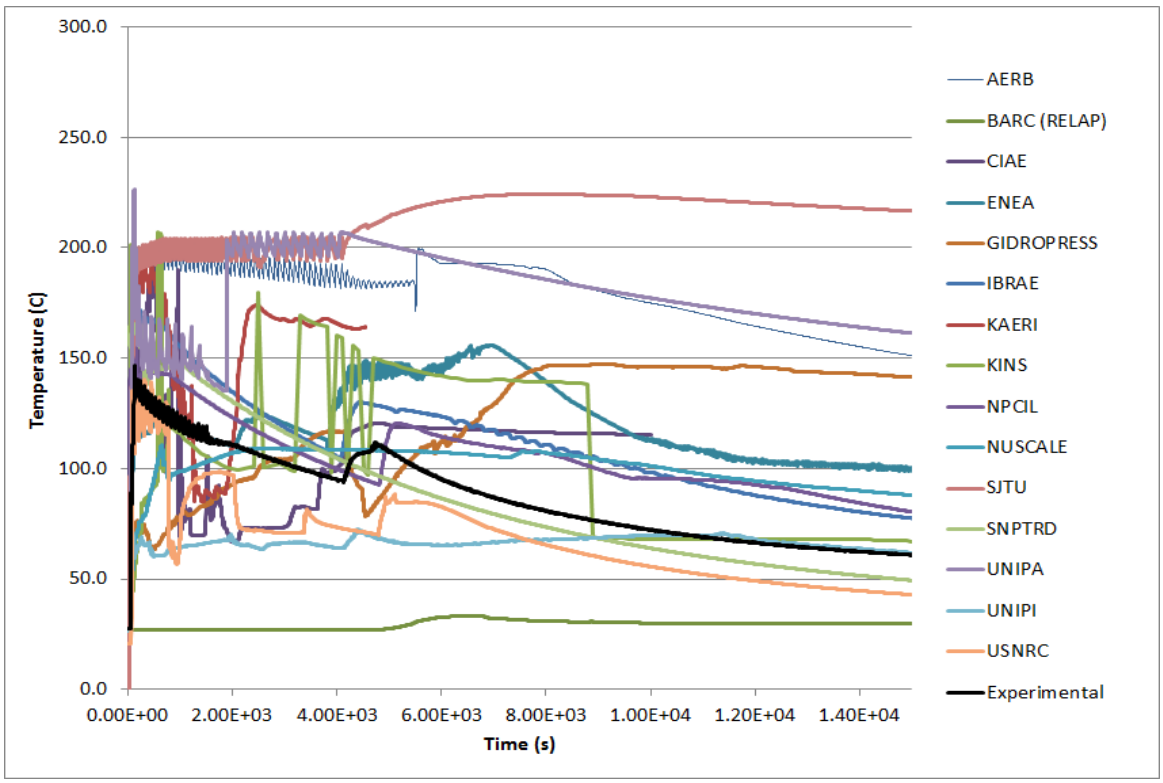

FIG. 5-19. SP-2 HPC fluid temperature (227.01 cm, TF-831).

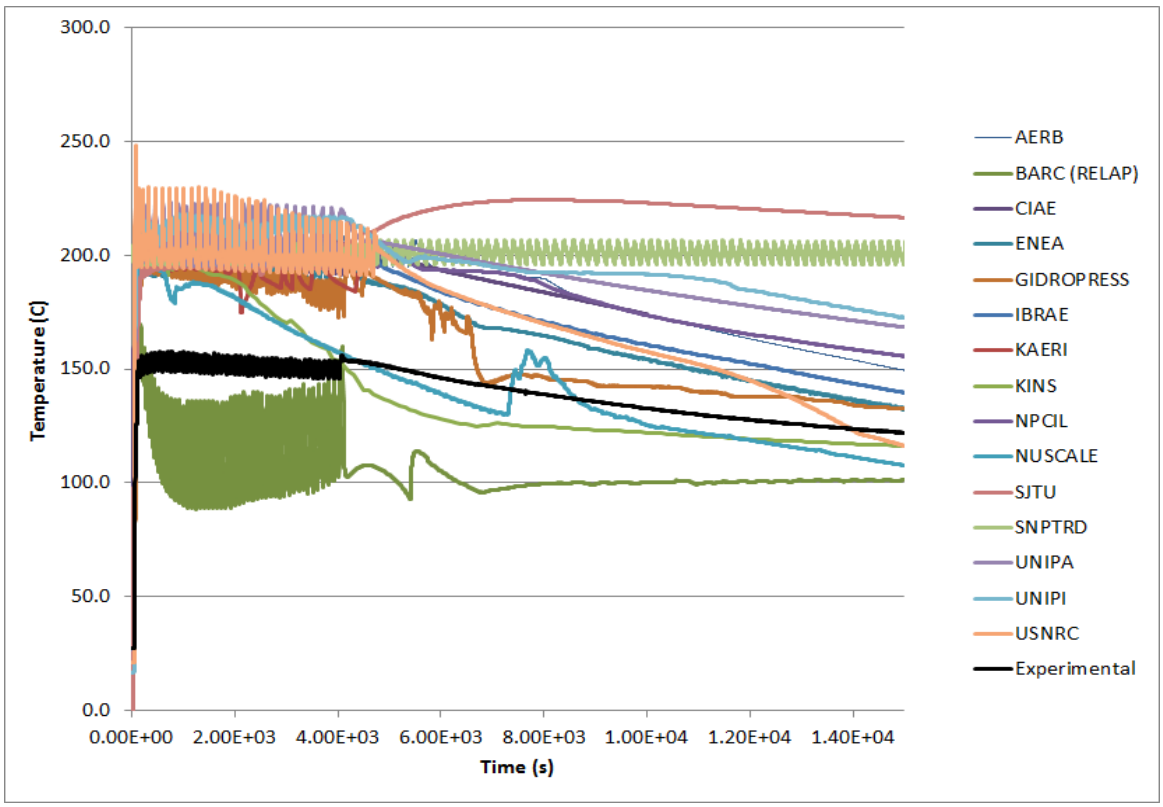

FIG. 5-20. SP-2 HPC fluid temperature (416.88 cm, TF-851).

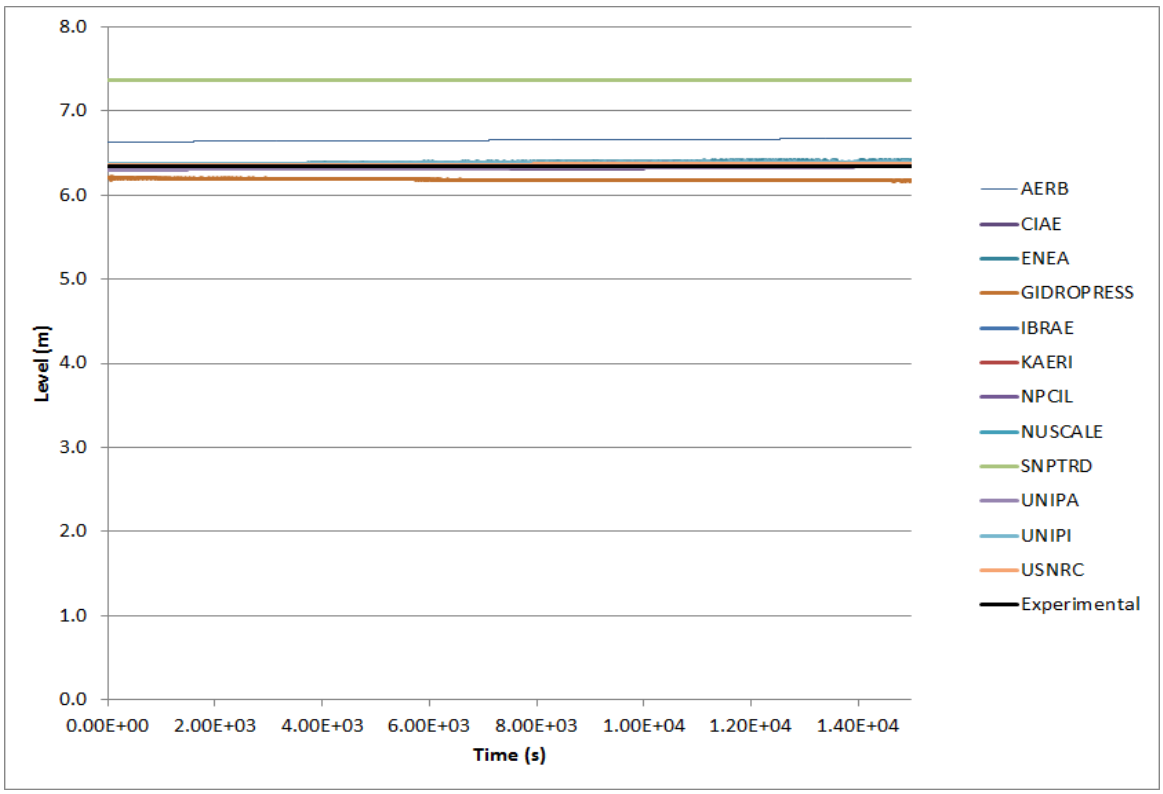

FIG. 5-21. SP-2 CPV level (LDP-901).

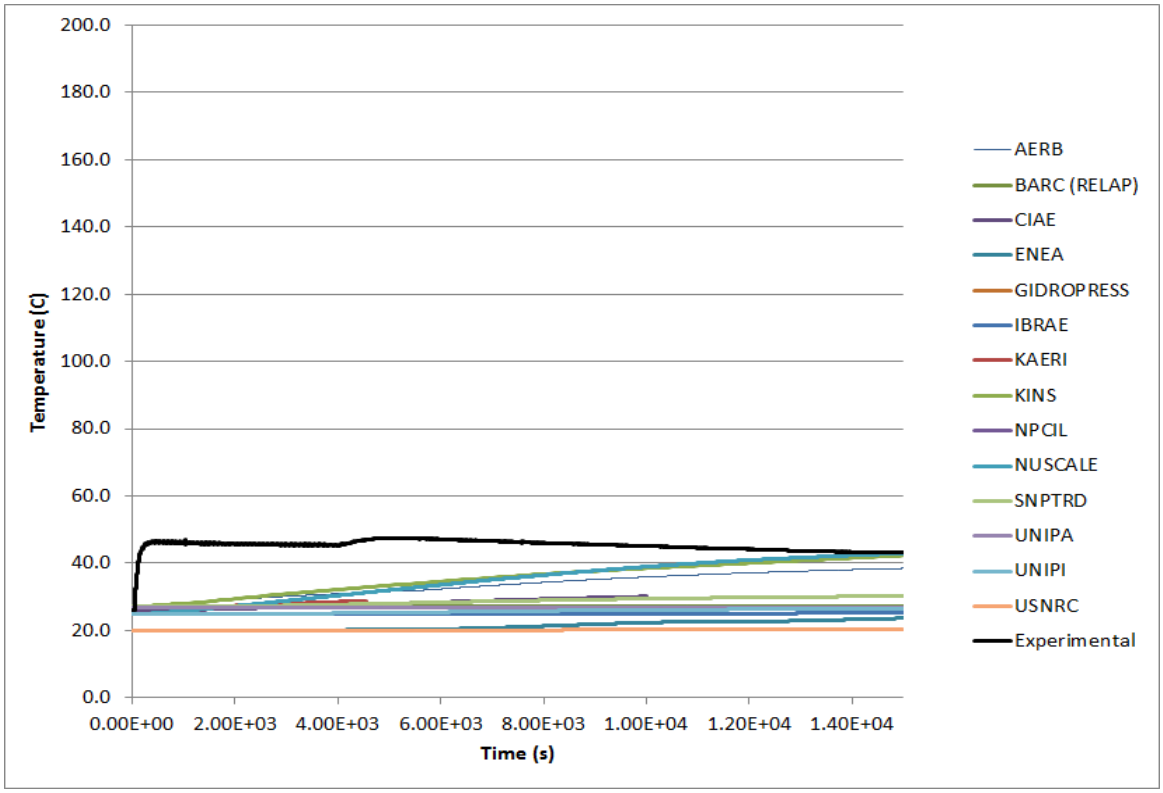

FIG. 5-22. SP-2 CPV water temperature (6.99 cm, TF-815).

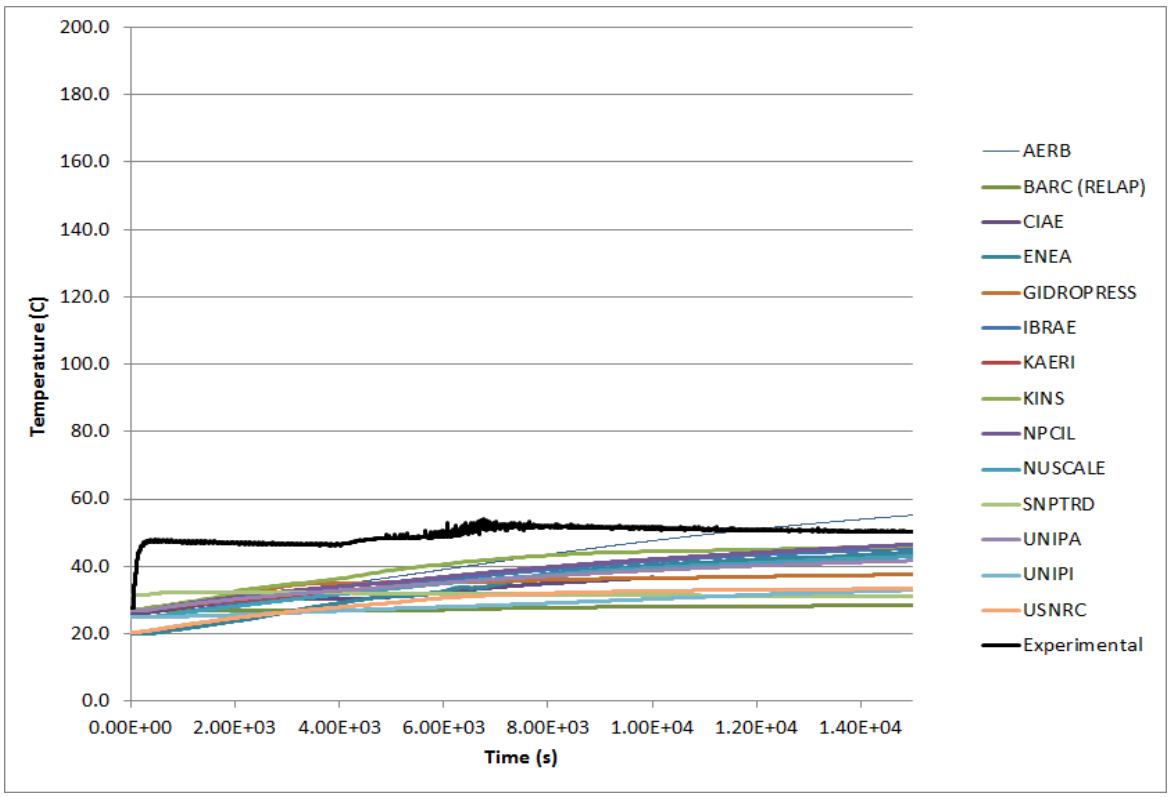

FIG. 5-23. SP-2 CPV water temperature (227.01 cm, TF-835).

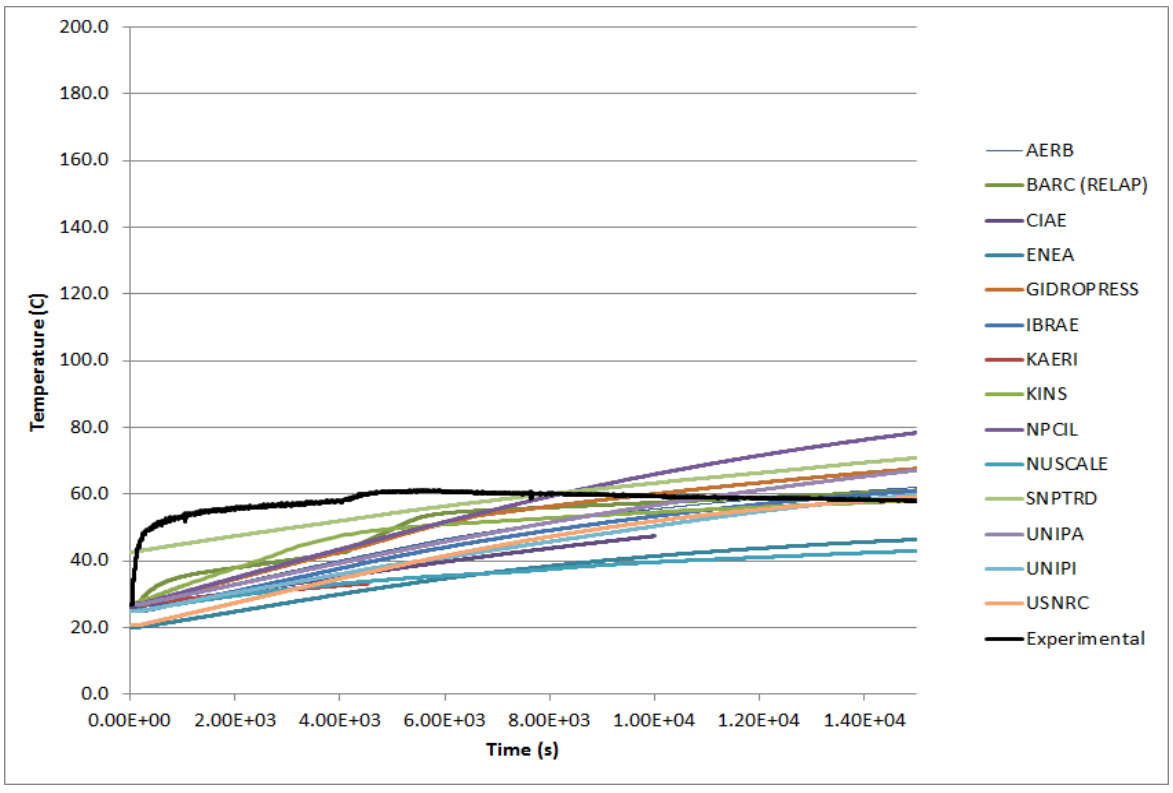

FIG. 5-24. SP-2 CPV water temperature (416.88 cm, TF-855).

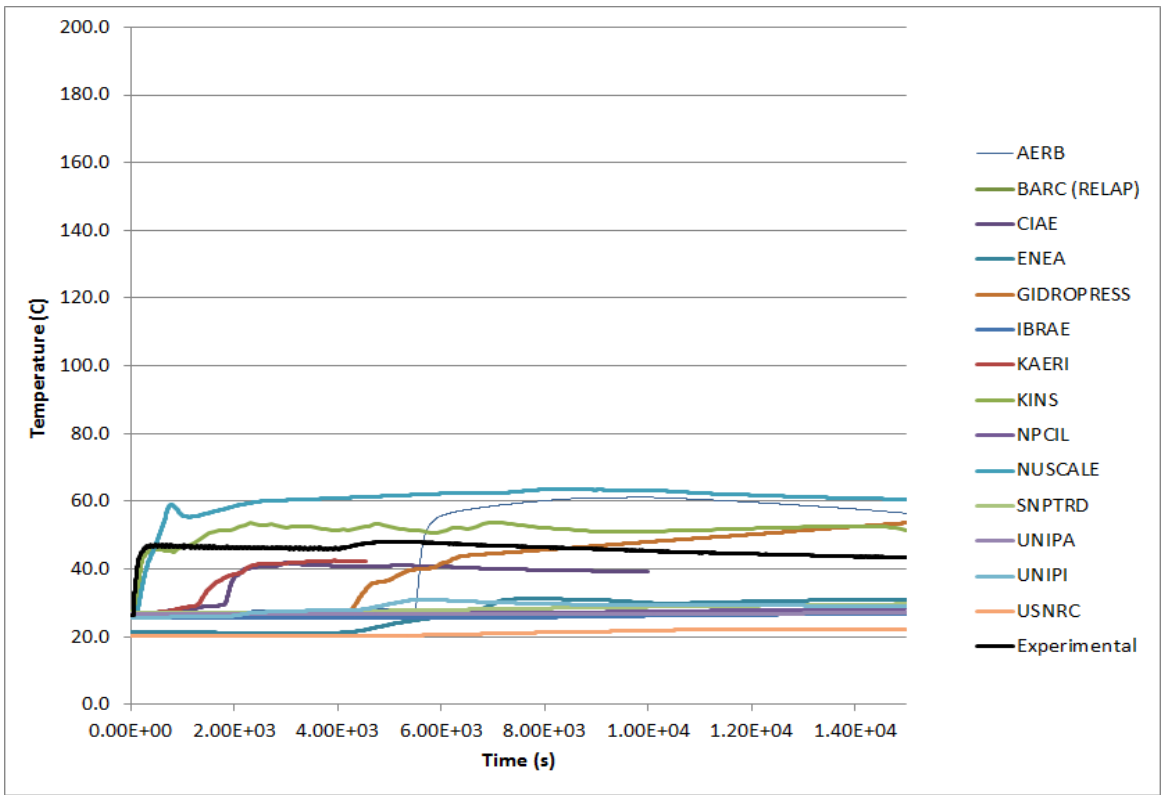

FIG. 5-25. SP-2 CPV heat transfer plate wall temperature (6.99 cm, TW-814).

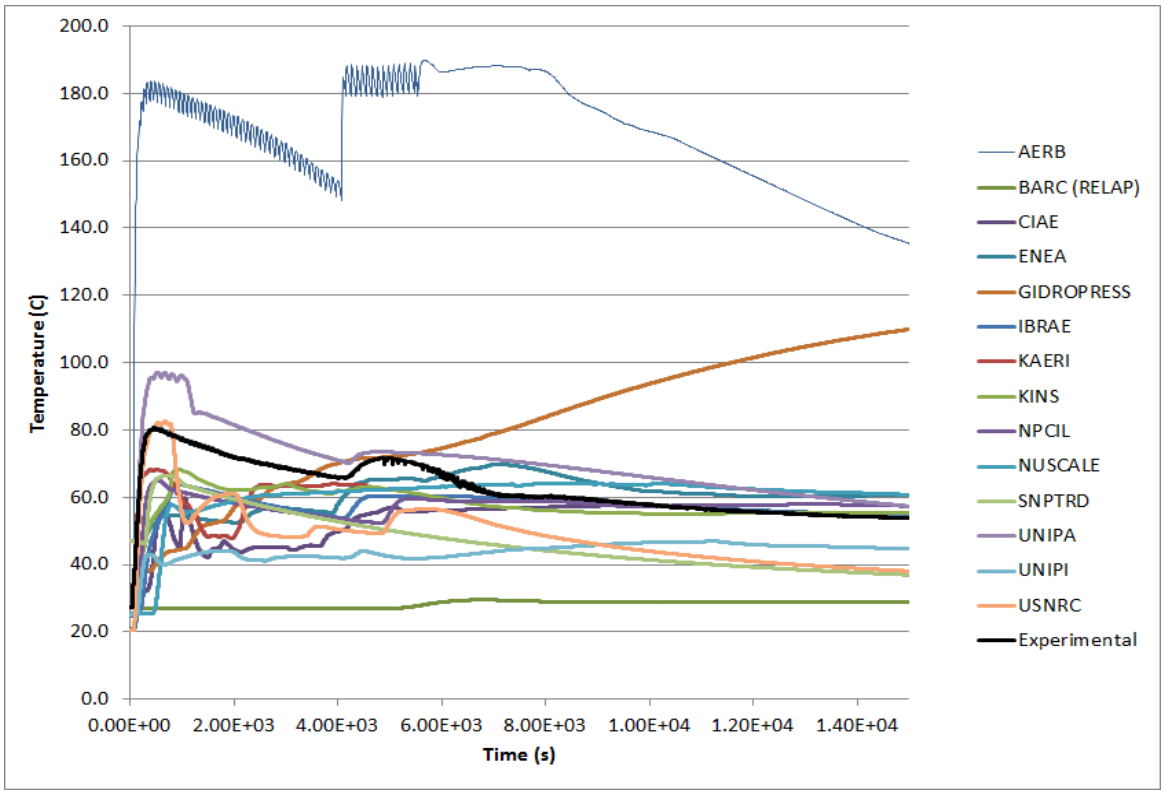

FIG. 5-26. SP-2 CPV heat transfer plate wall temperature (227.01 cm, TW-834).

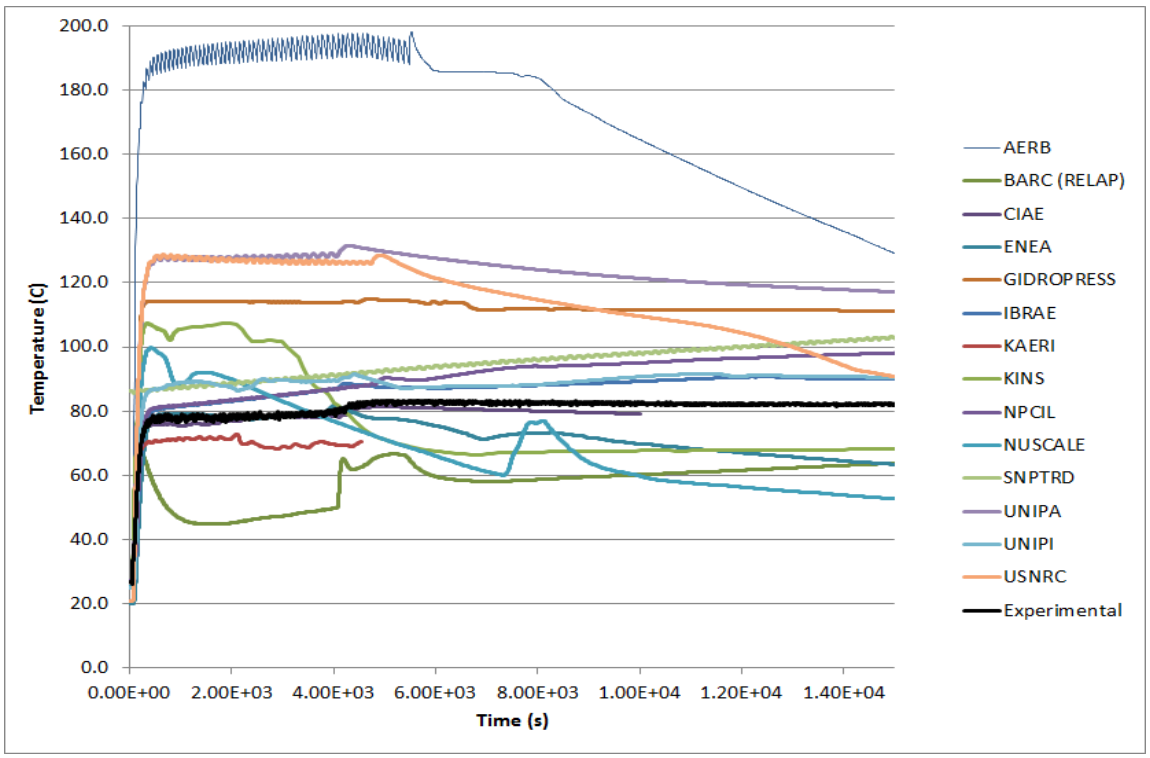

FIG. 5-27. SP-2 CPV heat transfer plate wall temperature (416.88 cm, TW-854).

5.2. POWER MANEUVERING

SP-3, power maneuvering is a test that examines the behavior of the MASLWR test facility at a number of steady-state steps. The boundary conditions for this test are the power level and the feed water flow rate. The test consists of 8 power levels, from 40 to 320 kW, 40 kW apart. Table 5-2 shows the test sequence of events for SP-3. During SP-3 there was a significant deviation from the original test procedures in that the charging pump was activated and water was pumped into the primary system.

5.2.1. RPV thermal hydraulic behavior

The core power boundary condition for SP-3 is shown in Figure 5-28. The 7 power steps following the initial power of 40 kW are clearly shown. In general, participants used power levels and timing very close to that of the actual experiment. Pressurizer pressure is shown in Figure 5-29. Experimentally, the pressure during SP-3 remains relatively constant. Most participants did capture this trend although there were several participants that showed significant pressure fluctuations during the test.

Figures 5-30 to 5-32 show the transient temperatures at the core inlet, core outlet and at the top of the chimney respectively. Most participants captured these transient temperatures very well. Note the drop in primary temperature that corresponds with the charging pump injection around 3000 s. The charging water was much cooler than the primary coolant and the injection of this charging flow reduced the overall temperature of the primary coolant. With the exception of the impact of the charging flow, the impact on the primary temperatures of the power level and feedwater flow tended to be of relatively small magnitudes.

The next two Figures 5-33 and 5-34 show the pressure drops across the primary system during the transient. The pressure drop across the steam generator (DP-105) was much higher than the pressure drop across the core. This is not unexpected due to the significant flow restriction represented by the helical coil steam generator. Note that DP-105 reached its maximum range of 11,675 Pa during the transient and thus there is no indication in the experiment above this value, but the pressure drop was at least this value. There was much better agreement between participants for the pressure drop across the core than across the steam generator. This can most likely be attributed to the difficulty in modeling the form loss across the steam generator coil bundle.

The primary mass flow rates are shown in Figure 5-35. In general each step is shown. However, it is clear that there is a disruption of the steady-state flow during the charging pump injection. All of the participants captured the stepped nature of this flow. During the early steps the participant average was close to the experimental values of the primary mass flow. However, by the final steps of the test, most participants were under predicting the primary mass flow rate as compared with the experimental data. This may be attributed to an influence of mass flow rate on loop form losses that is not captured by some of the models.

Figure 5-36 shows the primary system mass and the increase in mass with the charging pump injection. Figure 5-37 and 5-38 show heat transfer across the chimney and heat loss from the system. There are no experimental measurements for these parameters. The heat transfer across the chimney represents the heat transfer from the hot side to the cold side of the loop. In general, the participant's results show an increase in the heat transfer across the chimney with increasing core power with a minimum of close to zero and a maximum above 80 kW.

5.2.2. SG Thermal Hydraulic Behavior

Figure 5-39 shows the main feed water flow rate for the SP-3 test. This represents the total mass flow of the system feed water. Of notice is the stepped natured of the feed water flow which generally increases with core power in accordance with facility operating procedures. The addition of the colder fluid via the charging pump caused the facility operators to adjust feed water flow rates to maintain mass flow rates.

Figures 5-40 through 5-42 show the feed water mass flow rate through each of the steam generator coils. Not all participants used a three pipe model for the feed water flow and thus only the participants listed in the legend for these figures were able to report this data for their models. Again, the stepped nature of the feed water flow rate is shown from most participants although it looks like one participant had a highly oscillatory feed water flow rate into the steam generators.

Figures 5-43 through 5-46 show a variety of steam and feed water temperatures on the secondary side along with the steam mass flow rate and main steam pressure. It is shown that the injection of the charging coolant caused a significant disruption in the operation of the steam generator. The reduction in primary coolant temperature as a result of the charging pump injection caused a significant reduction in the main steam outlet temperature as less heat was transferred through the steam generator (Fig. 5-47). This caused a loss of most, if not all, of the steam superheat and thus there was likely a significant liquid fraction through most of the steam generator tubes. The reduction in feed water flow mentioned above was never able to recover the steam superheat lost during the charging pump injection.

TABLE 5-2. SP-3 SEQUENCE OF EVENTS

Event	Experimental Value (s)	AERB	BARC (CATHARE)	BARC (RELAP)	CIAE	ENEA	GPRESS	IBRAE	KAERI
Start of simulation – steady state (start of data collection)	0	0	-600	-600	-1	0	-1000	0	0
Initiate core power increase to 80 kW	0	0	0	0	0	5	0	0	0-30
Initiate core power increase to 120 kW	870	1000	869	869	890	875	870	870	870-950
Initiate core power increase to 160 kW	1642	2000	1642	1642	1630	1635	1642	1642	1640-1690
Initiate core power increase to 200 kW	2177	3000	2174	2174	2164	2175	2177	2177	2170-2220
Initiate core power increase to 240 kW	4004	4000	4006	4006	3972	4000	4004	4004	4000-4030
Initiate core power increase to 280 kW	4498	5000	4496	4496	4472	4500	4498	4498	4500-4530
Initiate core power increase to 320 kW	5096	6000	5100	5100	5092	5100	5096	5096	5100-5200

TABLE 5-2. SP-3 SEQUENCE OF EVENTS (CONTINUED)

Event	Experimental Value (s)	KINS	NPCIL	NUSCALE	SJTU	SNPTRD	UNIPA	UNIPI	USNRC
Start of simulation – steady state (start of data collection)	0	0	0	0	0	0	-600	0	0
Initiate core power increase to 80 kW	0	0	0	0	0	0-30	0	0	0
Initiate core power increase to 120 kW	870	881	872	600	800	870-950	870	774	809
Initiate core power increase to 160 kW	1642	1663	1642	1200	1600	1640-1690	1642	1290	1642
Initiate core power increase to 200 kW	2177	2194	2178	1800	2400	2180-2220	2177	3145	2176
Initiate core power increase to 240 kW	4004	4003	4005	2400	3200	4000-4030	4004	3620	4004
Initiate core power increase to 280 kW	4498	4500	4499	3000	4200	4500-4530	4498	4339	4498
Initiate core power increase to 320 kW	5096	5109	5096	3600	5000	5100-5130	5096	5155	5094

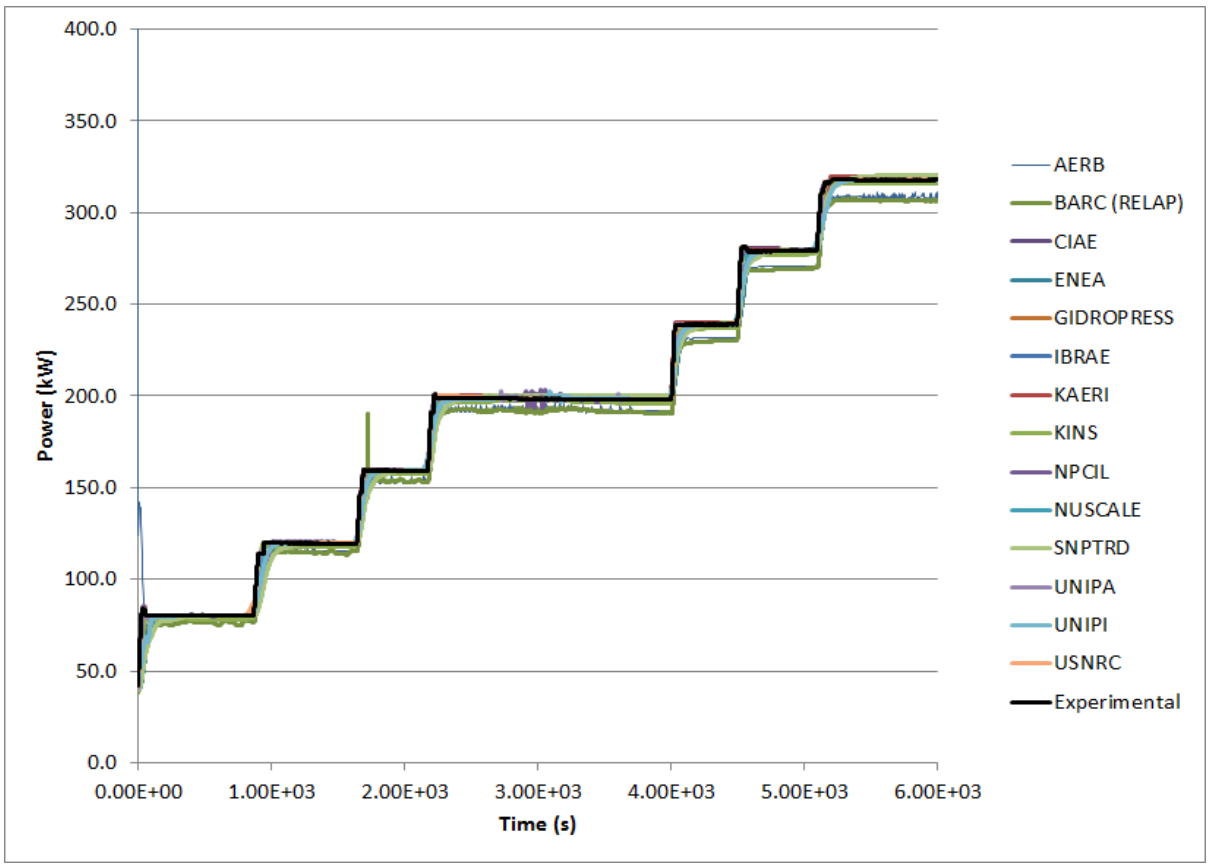

FIG. 5-28. SP-3 core power.

FIG. 5-29. SP-3 pressurizer pressure (PT-301).

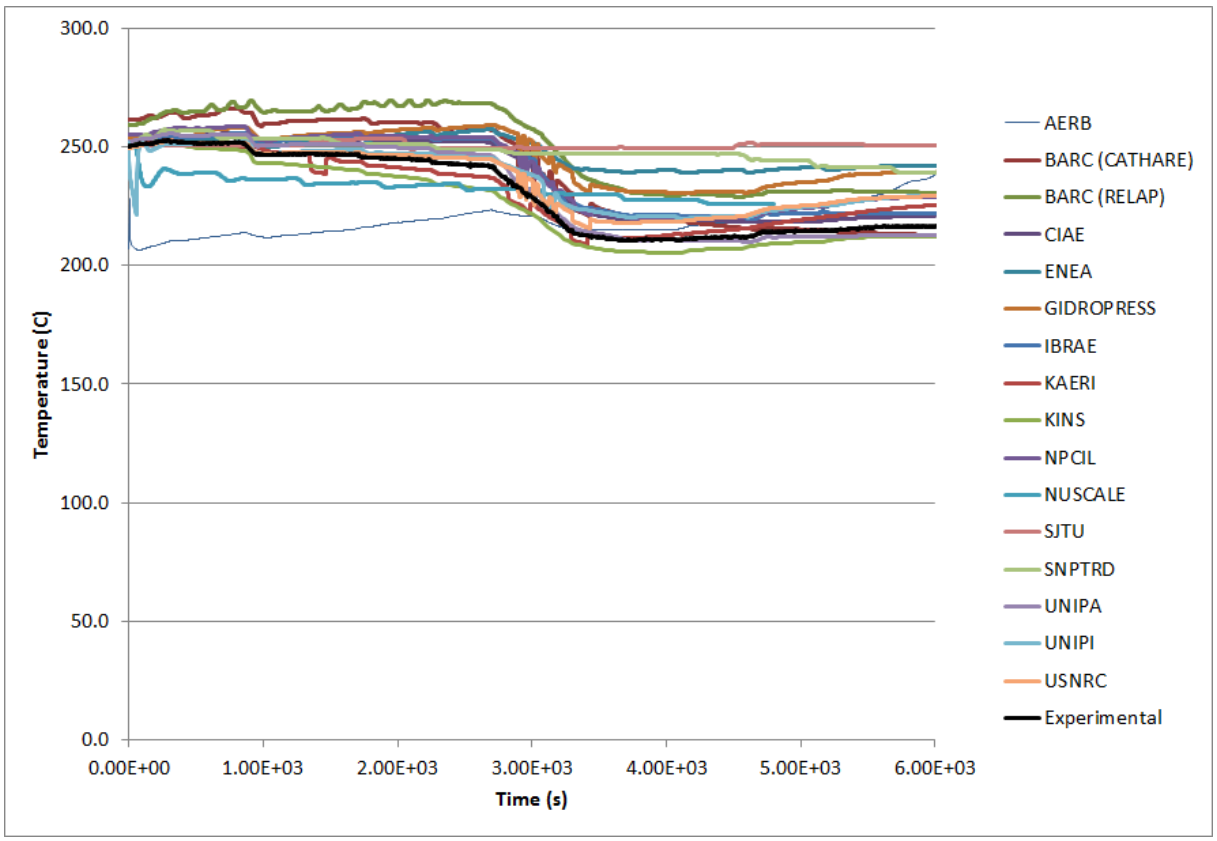

FIG. 5-30. SP-3 core inlet average temperature.

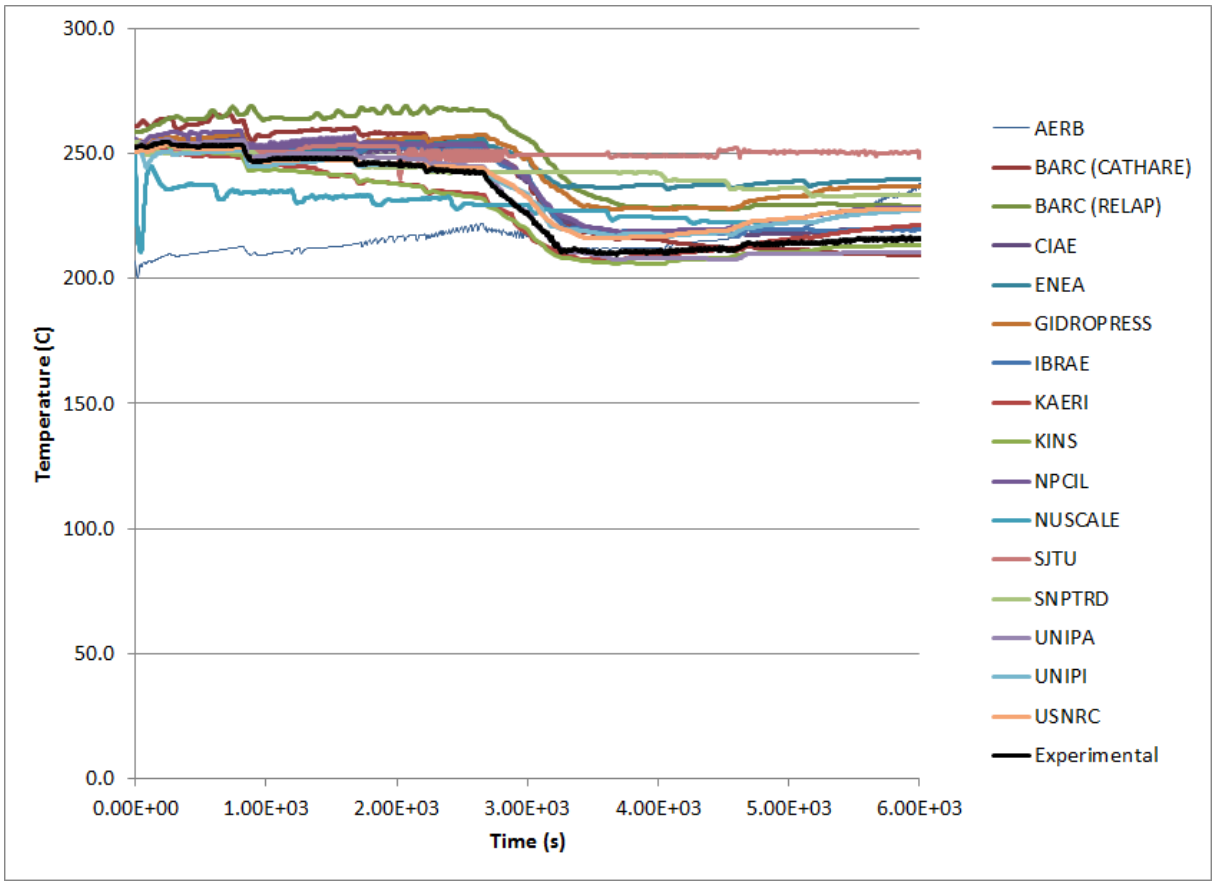

FIG. 5-31. SP-3 core outlet average temperature.

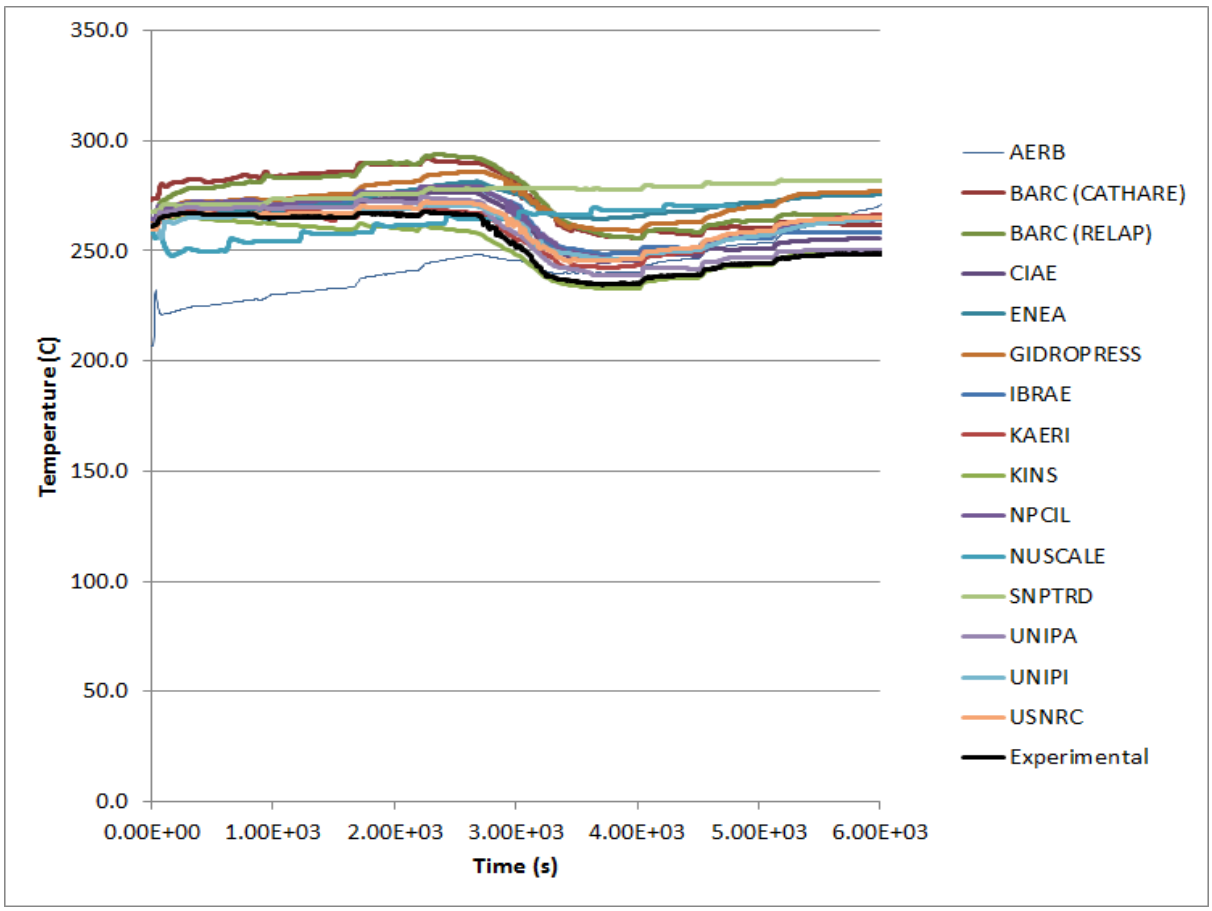

FIG. 5-32. SP-3 primary temperature at top of chimney (TF-111).

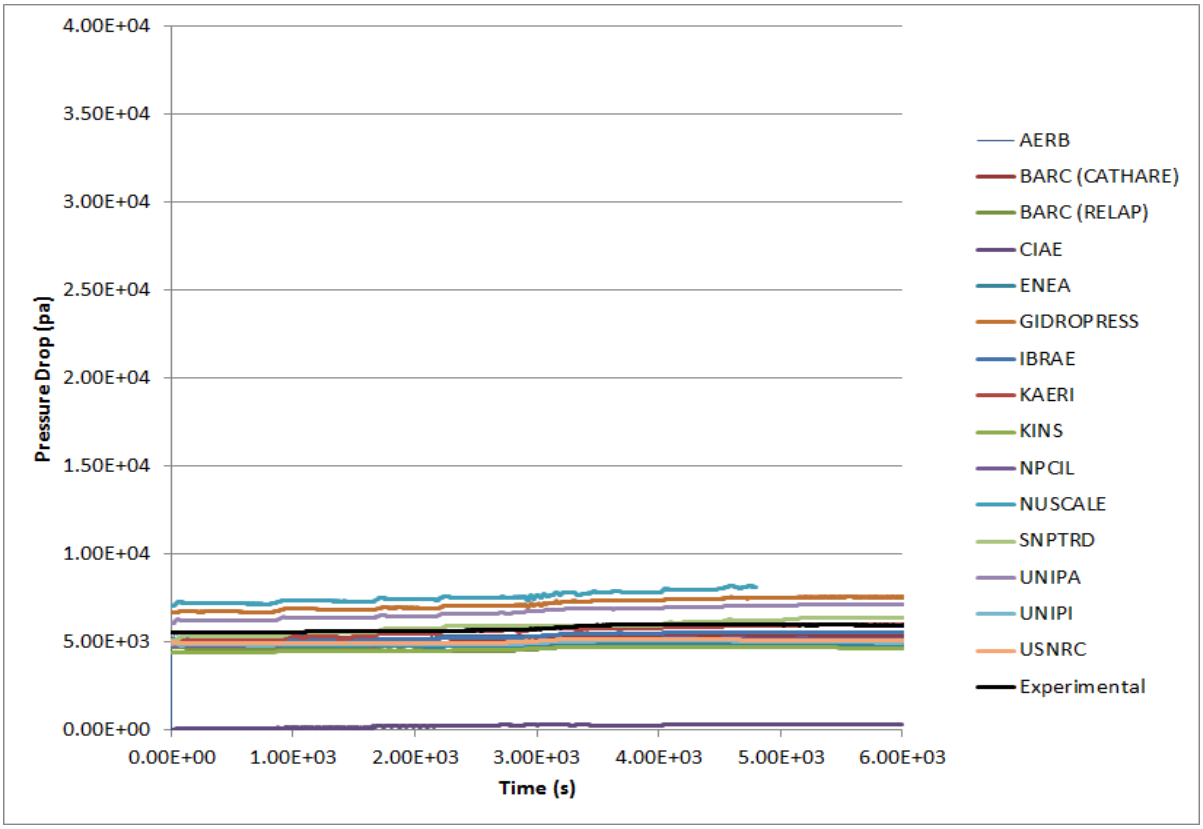

FIG. 5-33. SP-3 pressure drop across the core (DP-101).

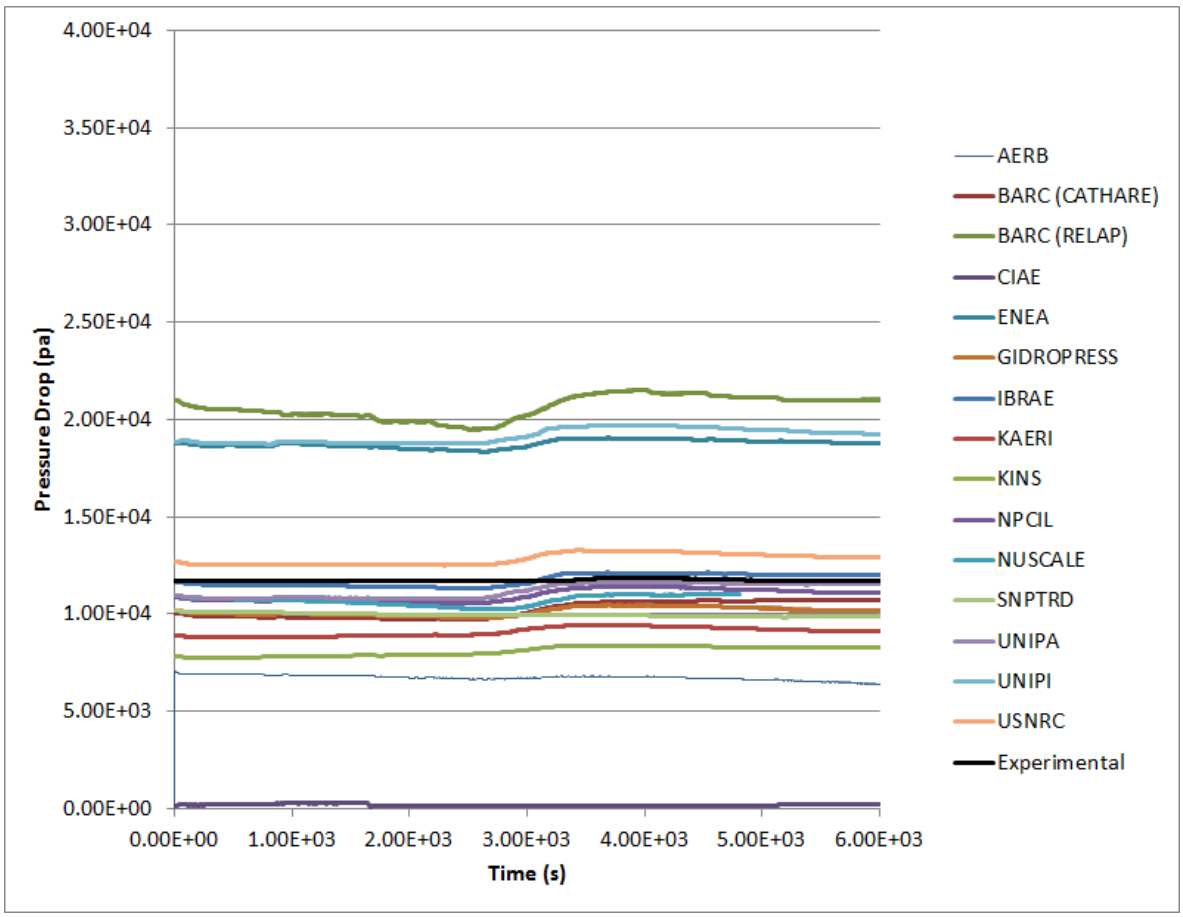

FIG. 5-34. SP-3 pressure drop across steam generator (DP-105).

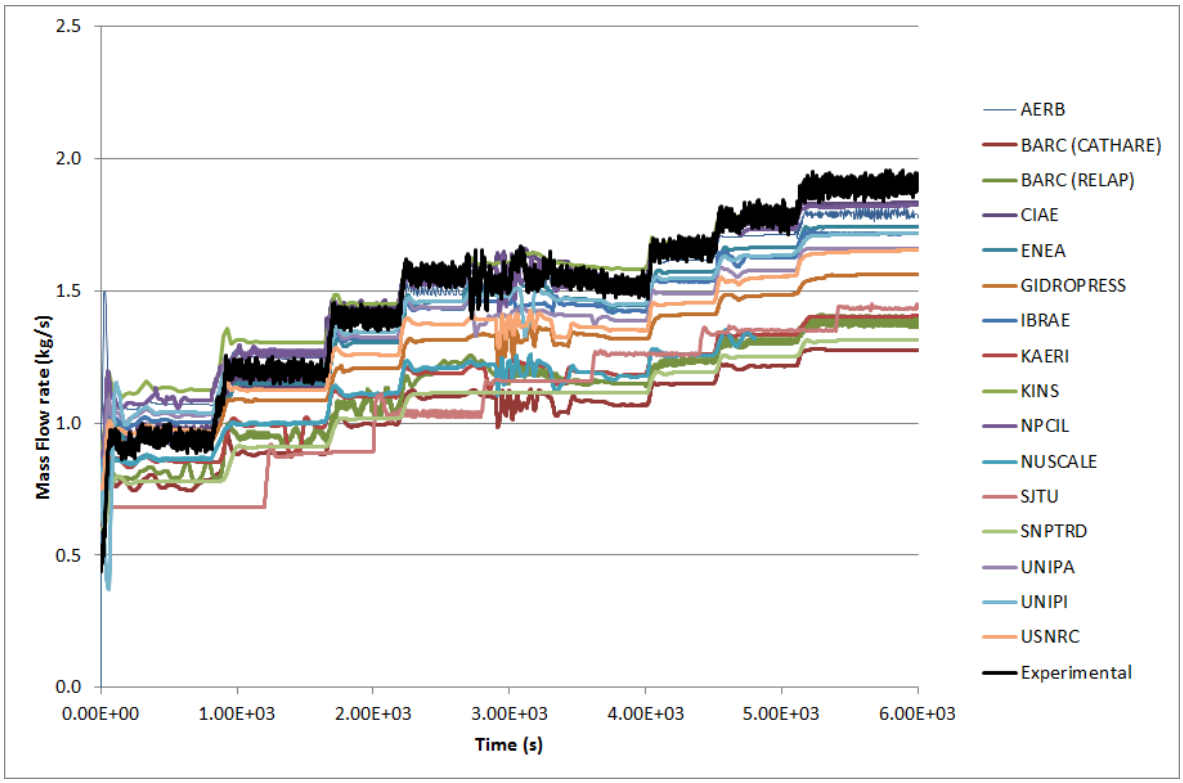

FIG. 5-35. SP-3 primary mass flow rate

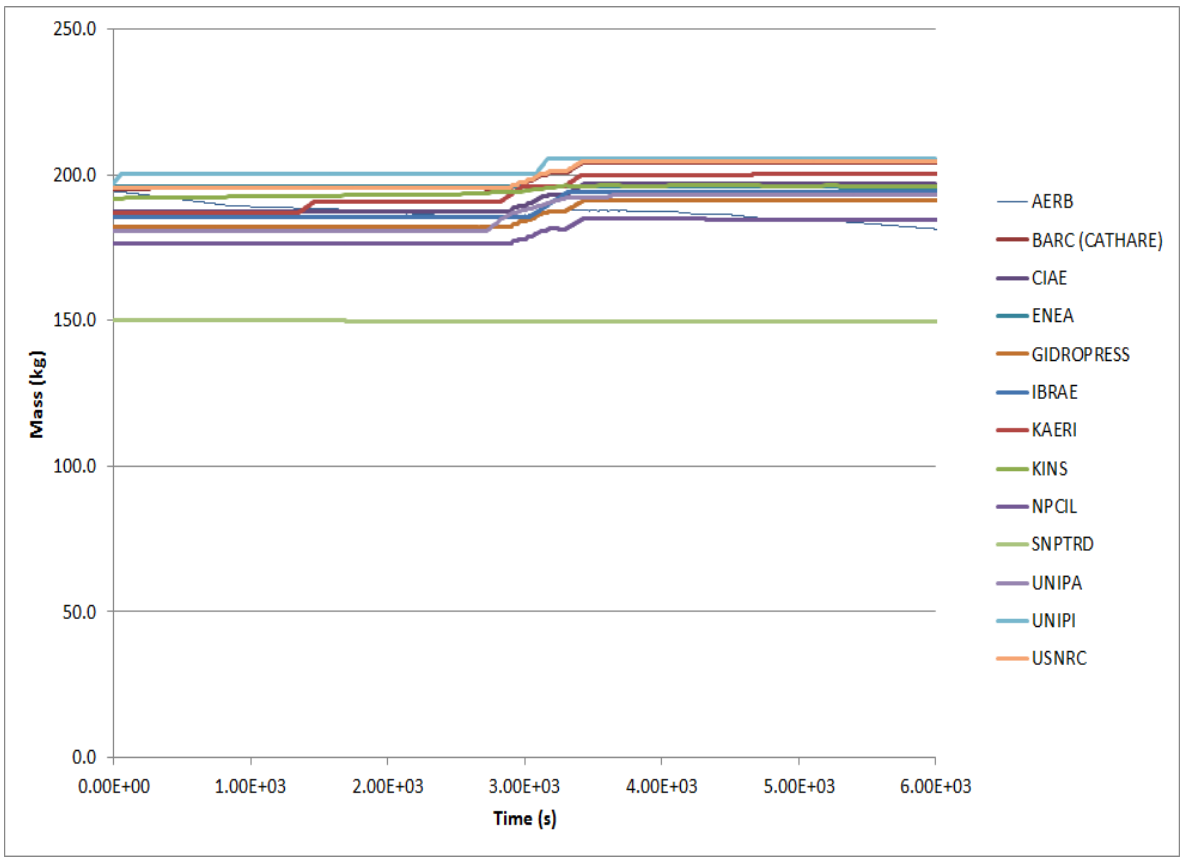

FIG. 5-36. SP-3 primary water mass

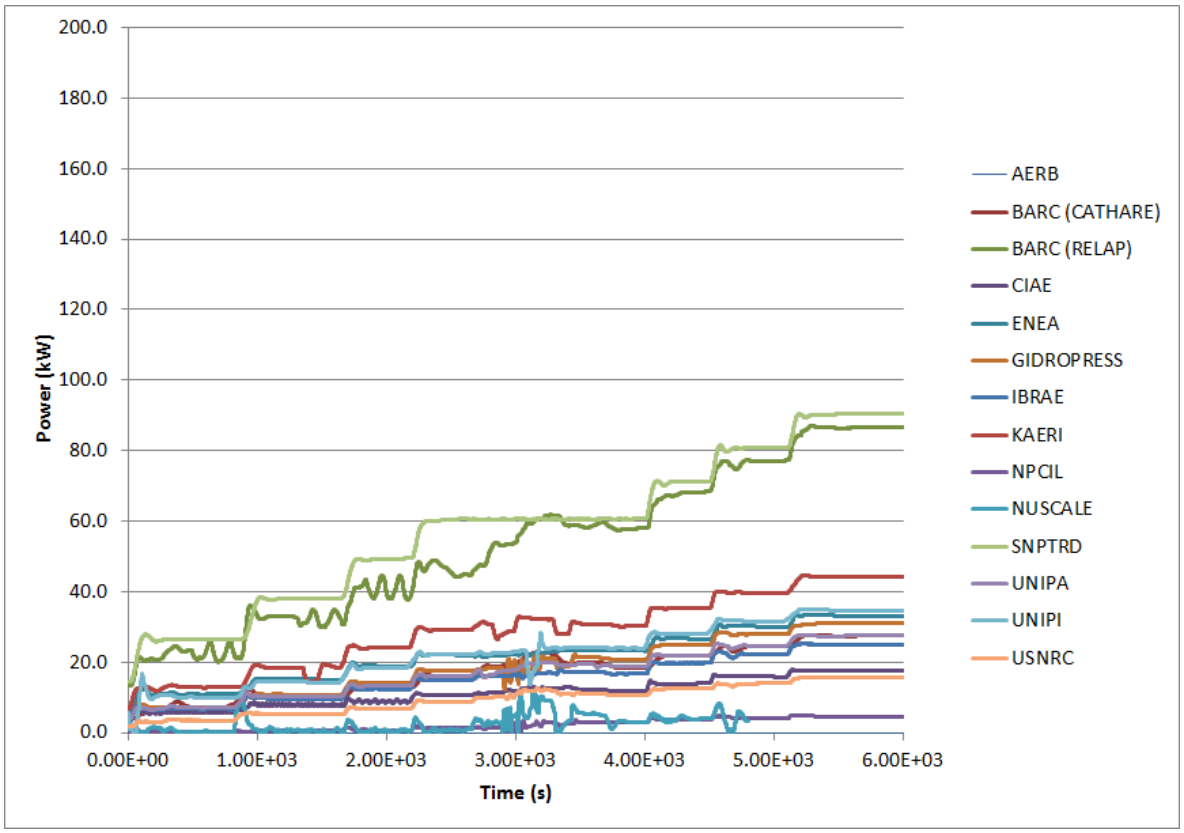

FIG. 5-37. SP-3 heat transfer across chimney

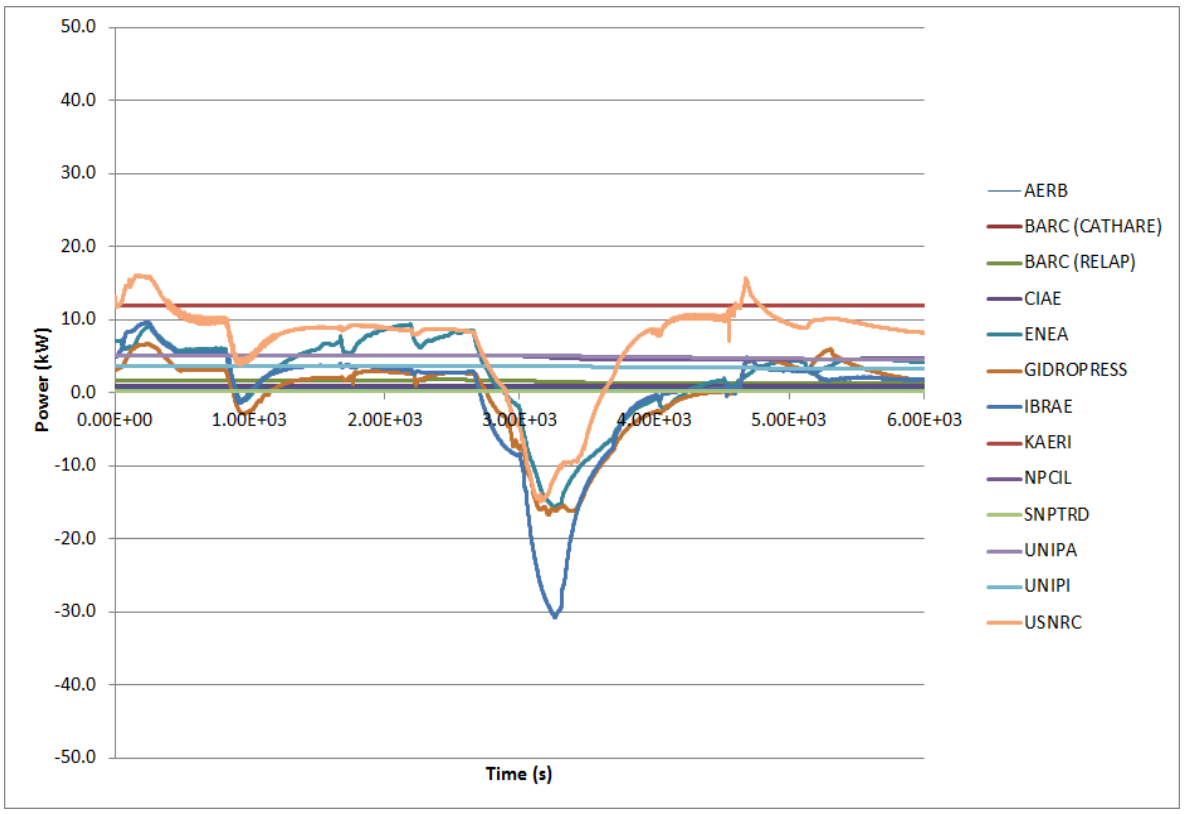

FIG. 5-38. SP-3 primary heat loss

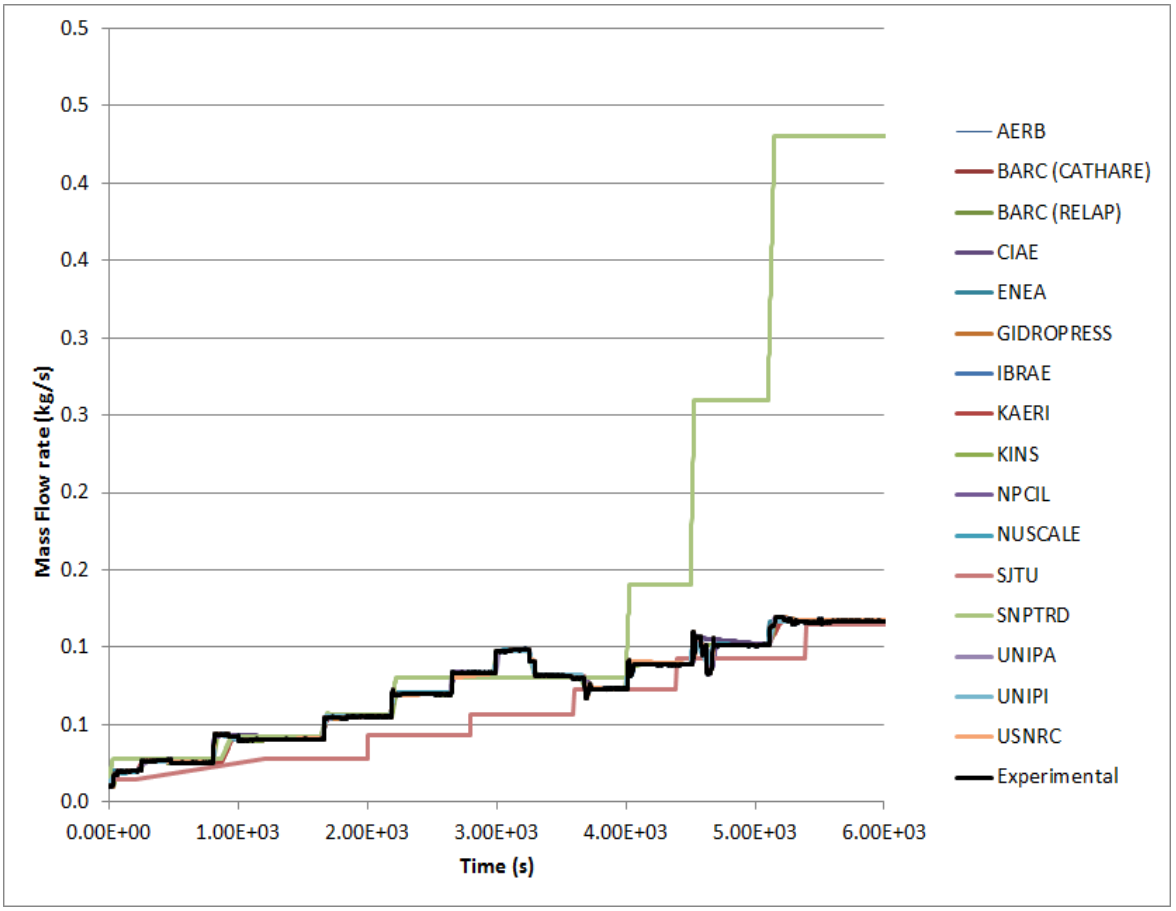

FIG. 5-39. SP-3 feed water mass flow rate (FMM-501).

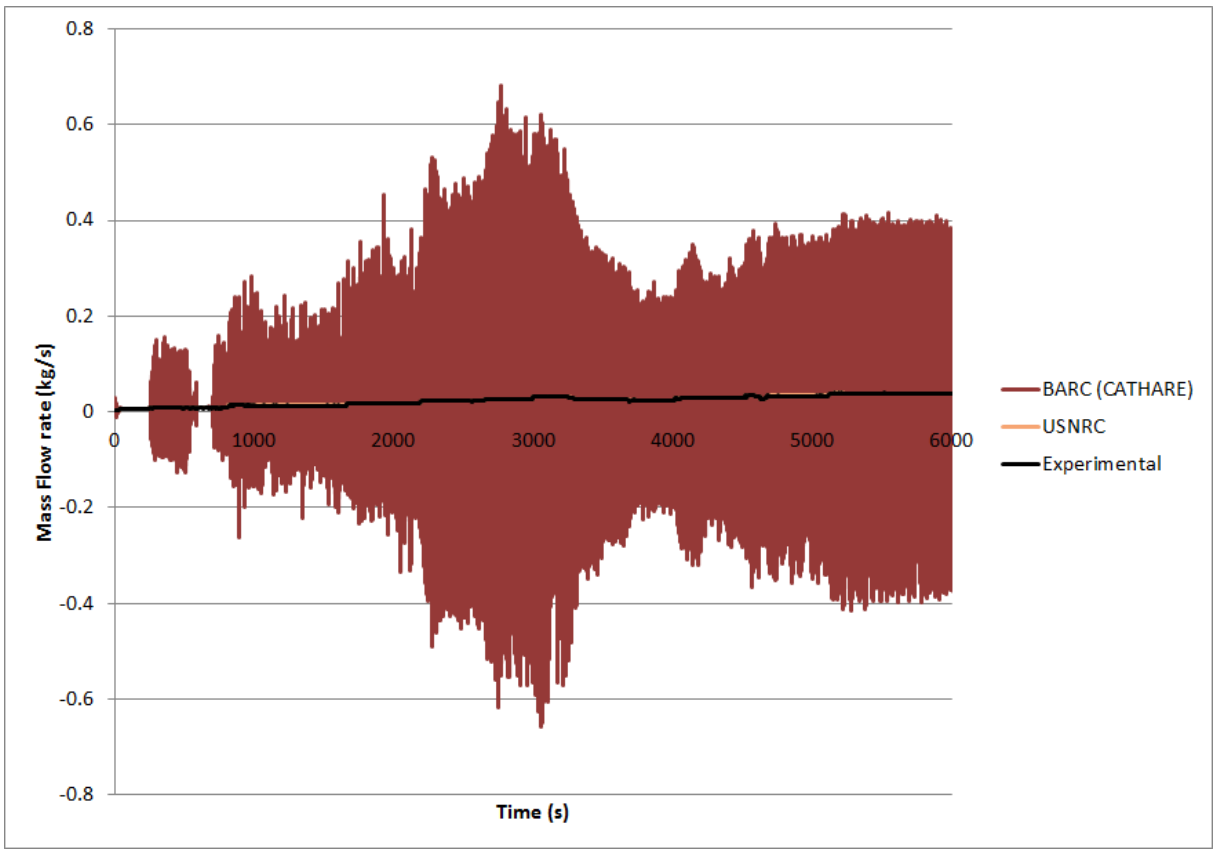

FIG. 5-40. SP-3 feed water mass flow rate (outer coil, FCM-511).

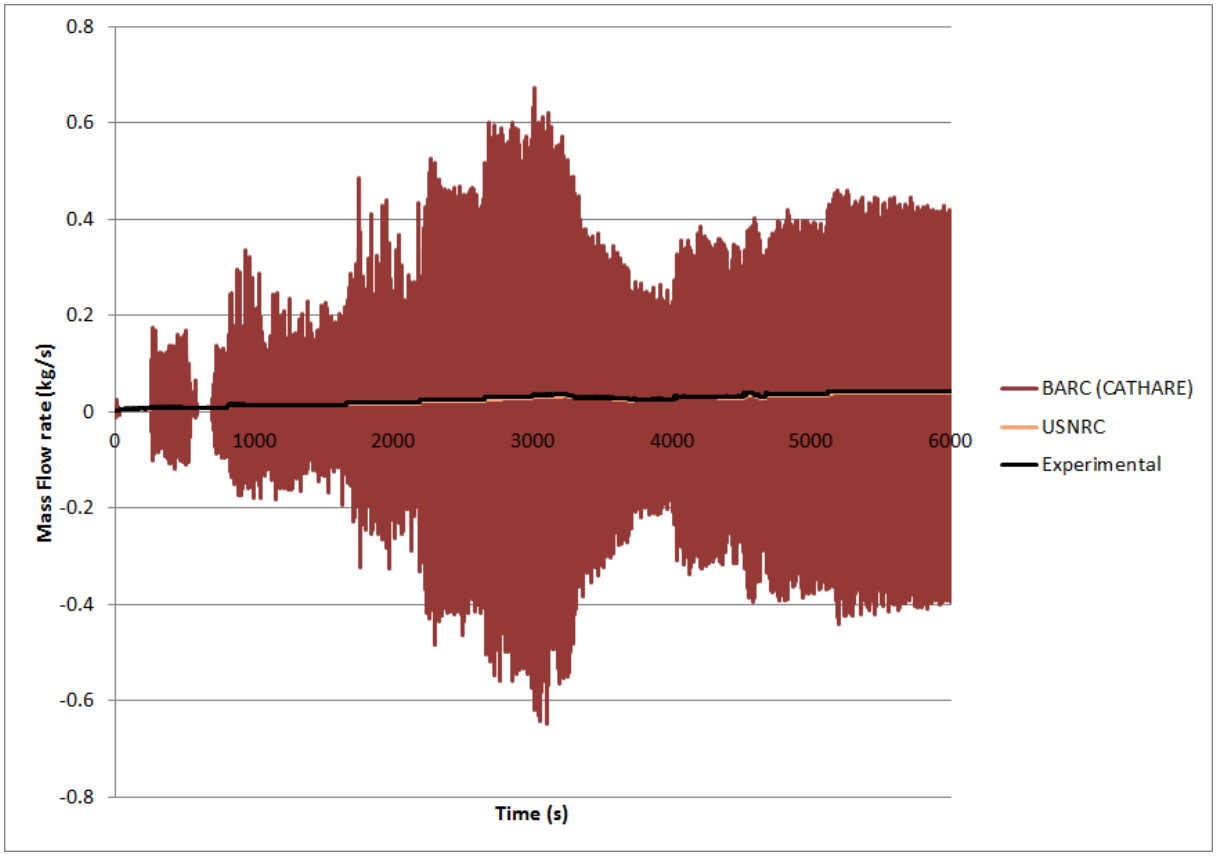

FIG. 5-41. SP-3 feed water mass flow rate (middle coil, FCM-521).

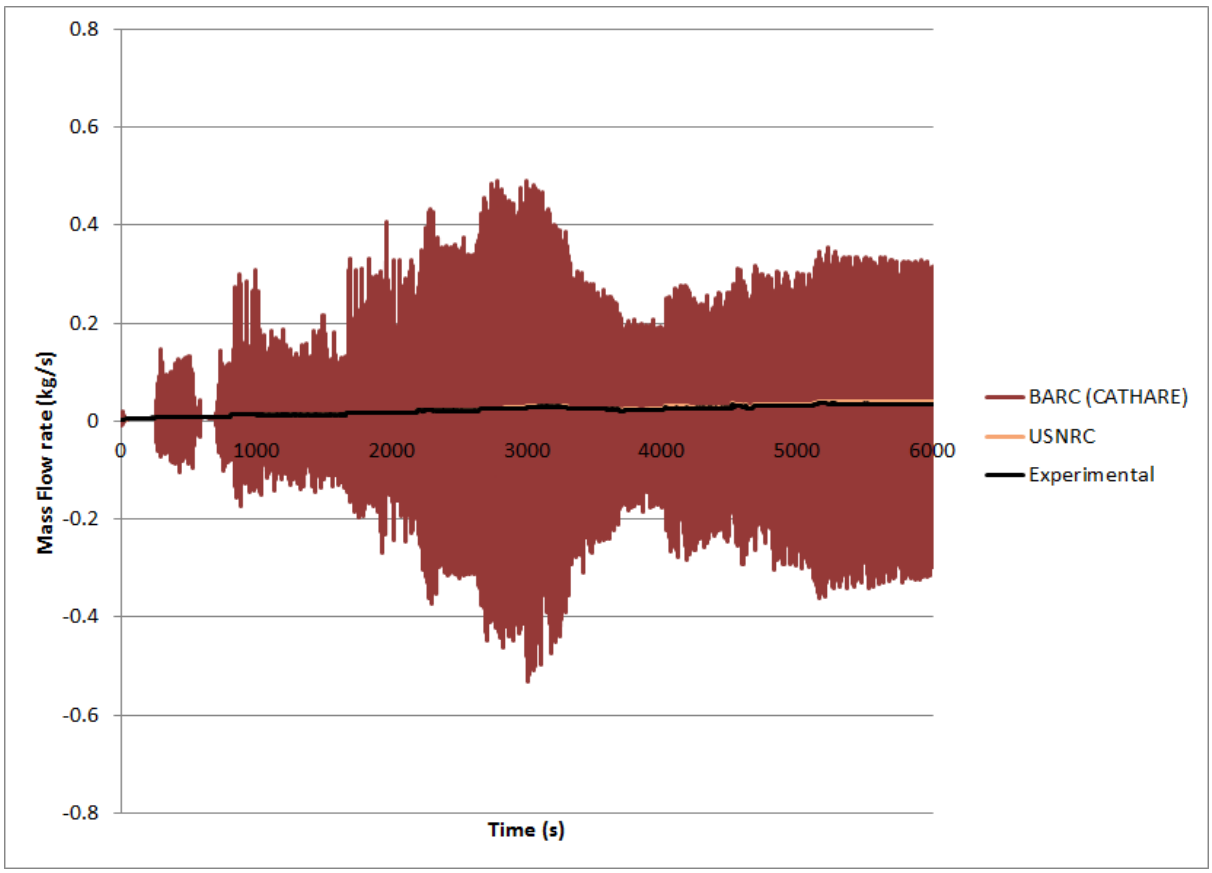

FIG. 5-42. SP-3 feed water mass flow rate (inner coil, FCM-531).

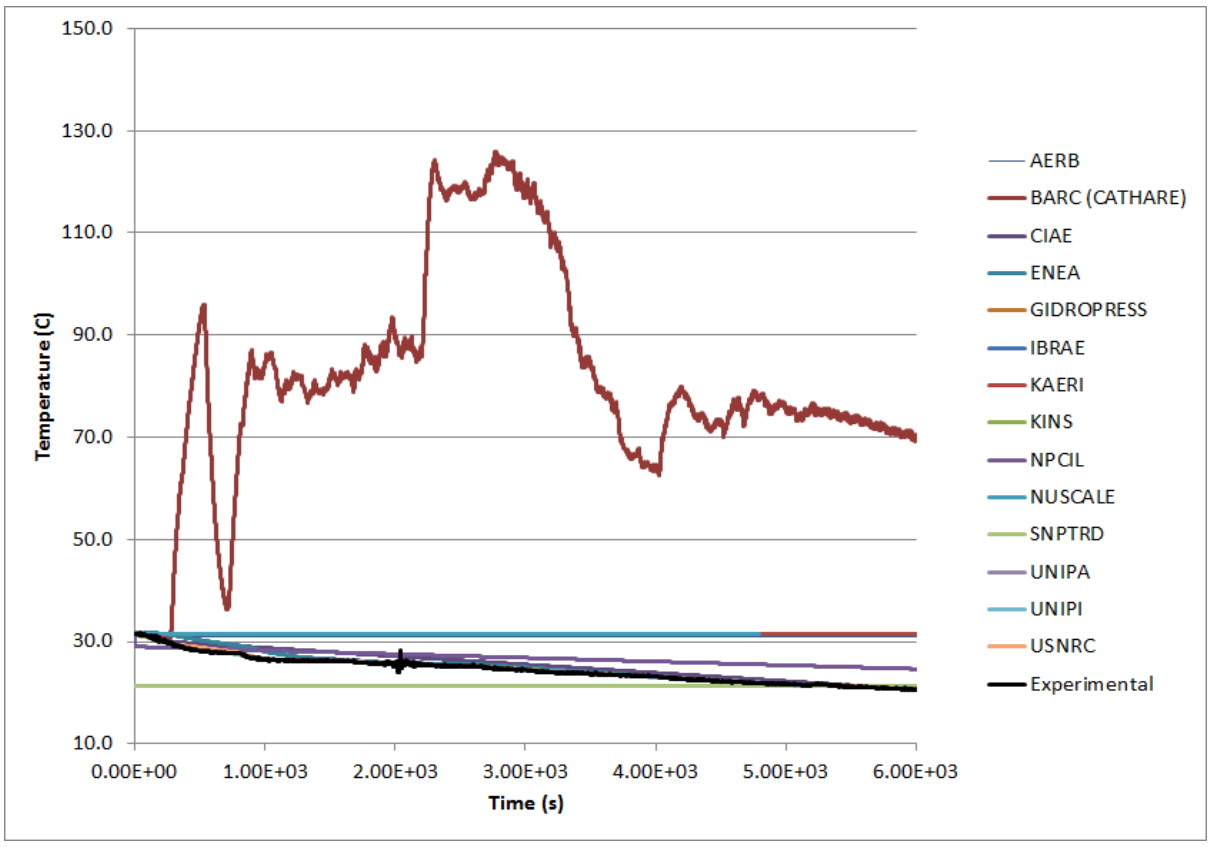

FIG. 5-43. SP-3 feed water temperature (TF-501).

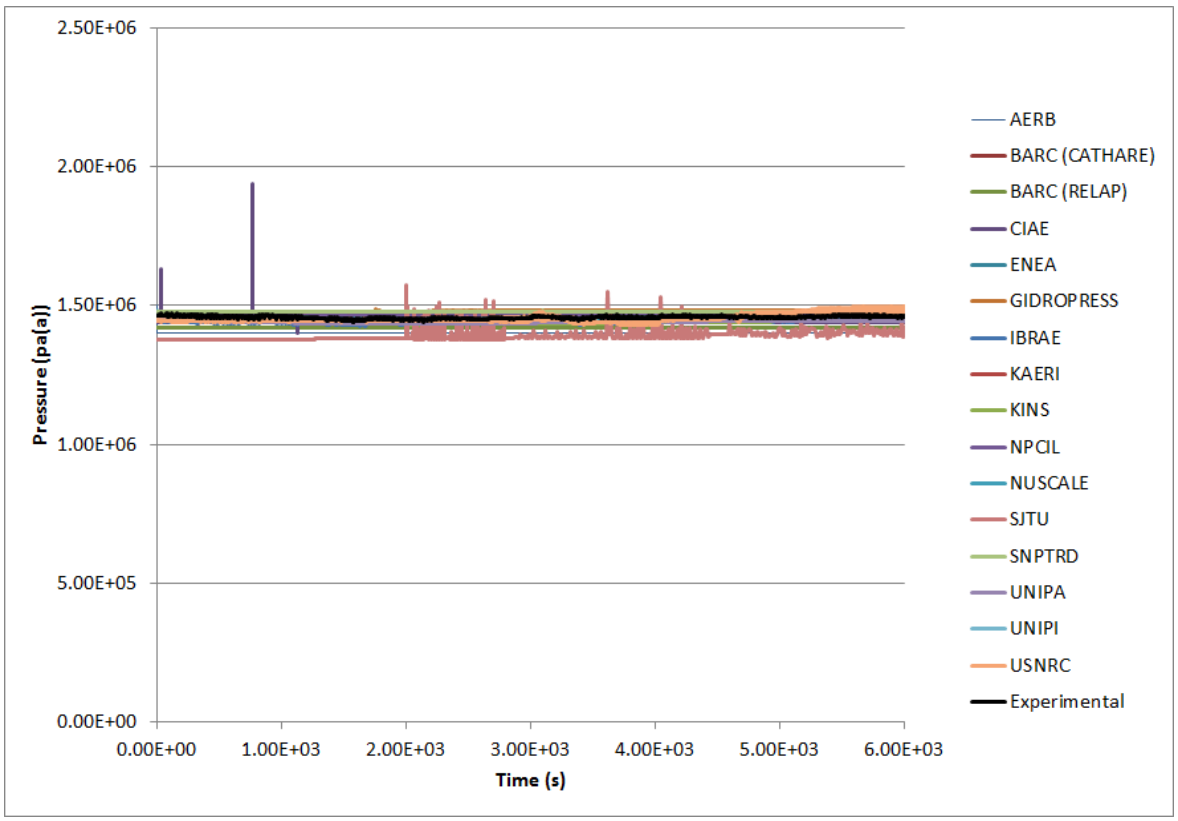

FIG. 5-44. SP-3 main steam pressure (PT-602).

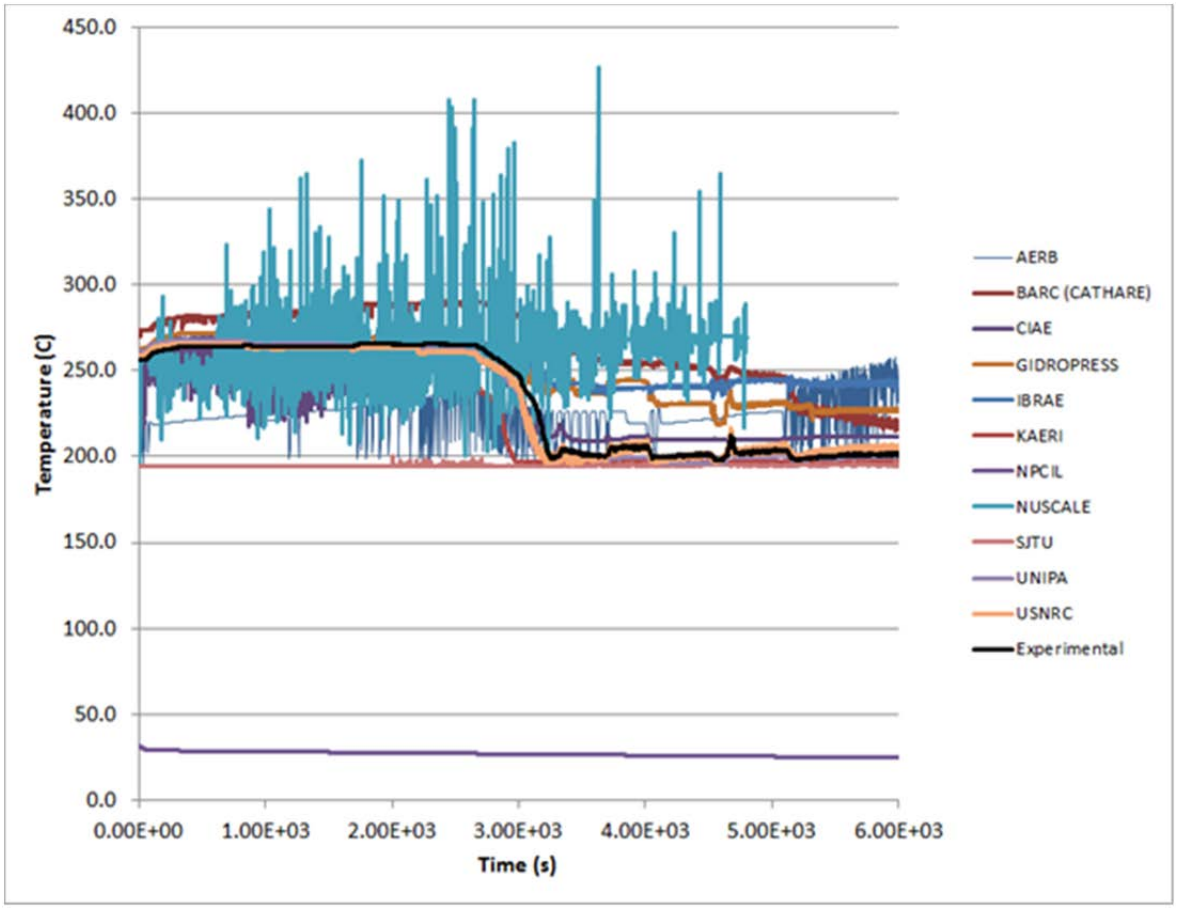

FIG. 5-45. SP-3 main steam temperature (average TF-611 to TF-63).

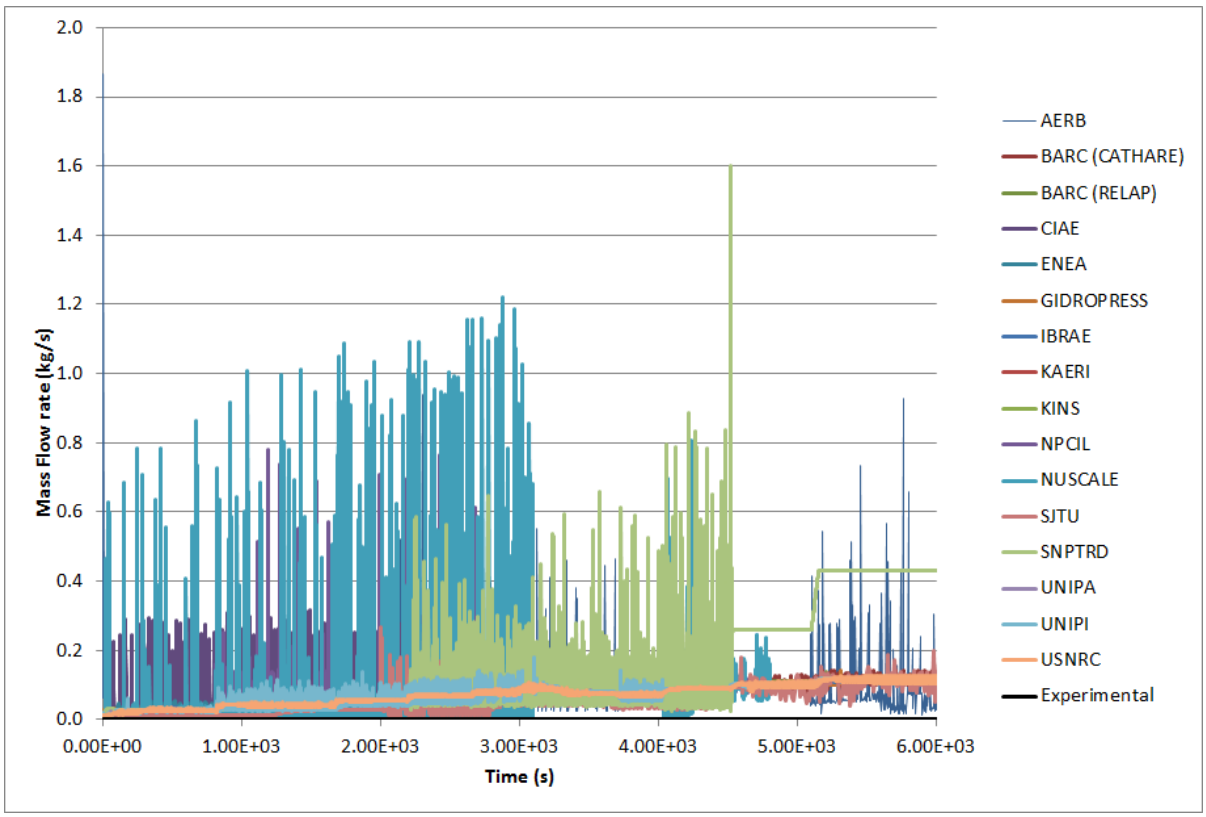

FIG. 5-46. SP-3 main steam mass flow rate (FVM-602-M).

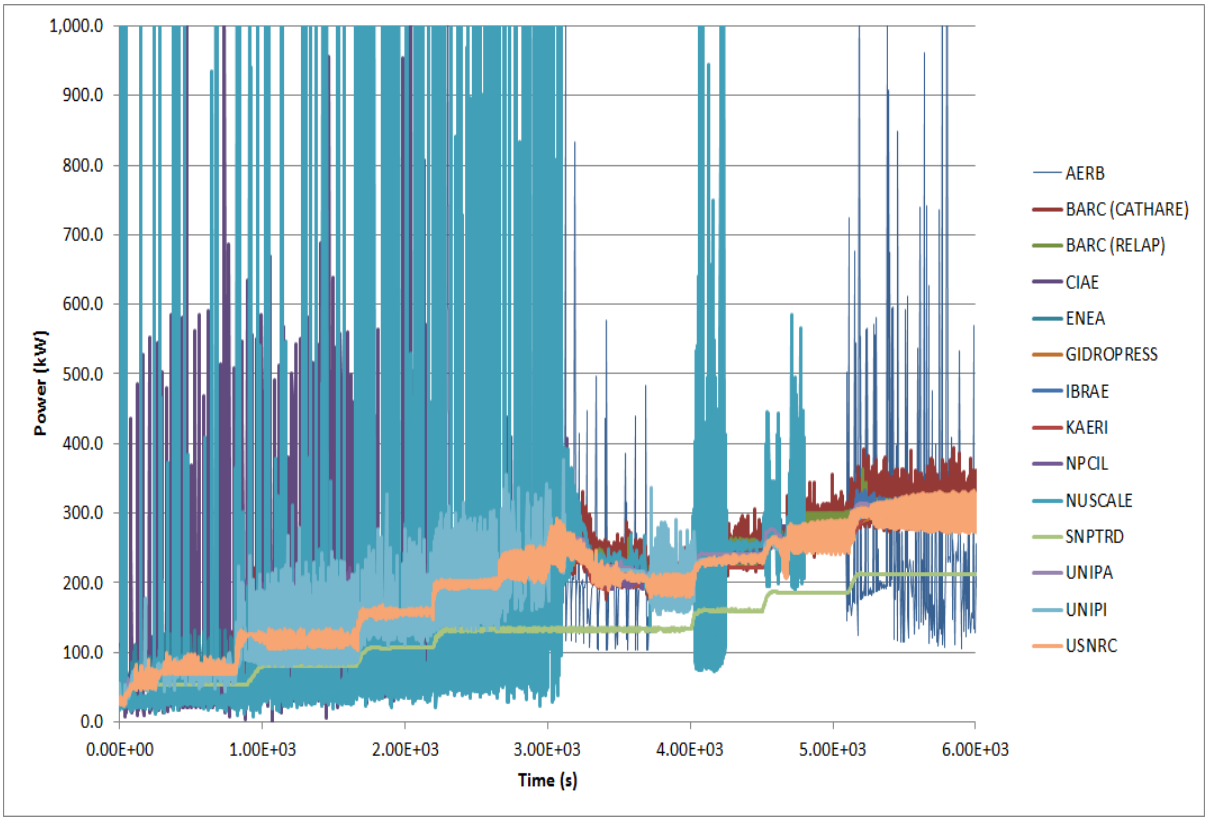

FIG. 5-47. SP-3 heat transfer through steam generator.

6. LESSONS LEARNED

The IAEA ICSP on Natural Circulation during Power Maneuvering and a Loss of Feed Water Transient in MASLWR has been conducted over a period of four years with eighteen participants. The complexities in such a project present a number of challenges. From this ICSP there are a number of lessons that can be learned and used by future IAEA ICSP participants to help make the ICSP process more efficient and effective.

6.1. PROCEDURAL CHALLENGES

One of the biggest problems that was encountered in this ICSP was a lack of discipline in completing the experimental test procedures. The MASLWR test procedures had originally been developed in the first two years of the ICSP. The ICSP participants had vetted the procedures during the 1st ICSP Workshop. All members, including the host organization, were in agreement that the procedures would produce valuable data for this ICSP.

When the tests were actually completed, the procedures were not followed to the letter especially in relation to test SP-3. For instance, for SP-3, between each step, the test procedure calls for the operators to adjust the position of MF-500 (feed water control) to achieve saturated conditions at the secondary side outlet. This step was not completed between each power increase during SP-3. Changes to the feed water control were not made during the test to control the secondary side outlet conditions, in violation of the approved procedure. In addition, around 3000 s of SP-3, the charging pump was turned on to raise the water level in the pressurizer. This injection of cool water into the system was not part of the procedure and introduces another complexity to the test that might be difficult to model.

There are several reasons for this lack of procedural discipline. More effective training of operators concerning adherence to procedures might be in order. In addition, it should be noted that due to the commercial nature of the MASLWR test facility, the organization planning the ICSP was not responsible for conducting the actual tests themselves. In the future, it would be more effective to have the testing organization more involved with the planning and conduct of the ICSP itself.

Because the group planning the ICSP test at the host organization was not the same group charged with completing the tests, the test procedures themselves were changed a number of times over the course of the ICSP. Originally, a test looking at natural circulation at reduced inventories was planned for the ICSP. After the test procedures were written and planned, the test organization decided that the test as designed did not have sufficient margin to run safely at the test facility. Therefore, this original test was cancelled and replaced with the power maneuvering test.

In addition, the procedures for SP-2 were changed just prior to the tests themselves based on input from the facility operators. For instance, the primary system venting logic as outlined in the procedure was changed. Since no flow measurement devices are installed at the MASLWR test facility that will track the mass lost through SV-800, it was determined that the pressure in the high-pressure containment would be controlled solely using PCS-106A. Thus SV-800 was closed for the duration of the transient while PCS-106A was opened at or below an HPC pressure of 1.480 MPa(a) and closed at or above an HPC pressure of 1.825 MPa(a). This cause cycling of PCS-106A for a large portion of the transient that is difficult to model.

During SP-3, it was also noted that steady-state as defined by procedure is likely not a very good indication of whether or not the system is at steady-state. By procedure, the MASLWR test facility should be allowed to reach steady state prior to increasing the core power and moving on to the next step. The following three parameters were used to determine whether the MASLWR test facility had reached steady state conditions or not:

- Constant hot leg temperature as indicated by TF-106 (±2.8°C);
- Constant cold leg temperature as indicated by TF-131 (±2.8°C);
- Constant primary mass flow rate as indicated by FDP-131 (±5%).

Following the completion of the test, during the data analysis phase, it became clear that although these three parameters may be steady state within the bounds of the procedure, many other parameters

within the test facility might not be. Thus, steady state conditions were not reached between steps during the completion of SP-3 as required by procedure.

Although, problems with the performance of a test, especially the first instance at a test facility, are likely to crop up, closer coordination between the host planning and testing groups might have identified procedural problems before test completion.

6.2. TECHNICAL LESSONS

The ICSP showed that the current heat transfer correlations applied for simulation of conventional U-tube bundle SG underestimates the heat transfer for the MASLWR helical coil SG. Most ICSP participants artificially increased heat transfer in the helical coil SG by 20 to 100% (by increasing heat transfer area, heat transfer coefficient or applying fouling factor greater than 1.0) to match the steady state results with experimental data. Some participants applied a helical coil heat transfer model without or minimum artificial adjustment. Those participants without special treatment for helical coil SG show the steady state with higher primary coolant temperature or lower secondary coolant temperature compared to experimental data.

The heat transfer and pressure drop in the helical coil are further complicated due to the fact that the inlet condition for the helical coil steam generator corresponds to single-phase flow while the outlet condition corresponds to superheated flow requiring not only the estimation of heat transfer and pressure drop under single- and two-phase flow conditions, but also the dryout and post dryout heat transfer. In addition, many geometric and operating parameters affect the helical coil heat transfer and pressure drop like diameter of the tube, diameter of helix, helical pitch, flow regime (laminar, transition and turbulent flow in single-phase fluid), orientation of the helical tube (vertical upward/downward, inclined or horizontal), flow patterns (bubbly, slug, annular, droplet flow), etc. Heat transfer performance of helical coil heat exchangers is significantly better compared to straight tubes. The increased heat transfer coefficient is a consequence of the curvature of the coil which induces centrifugal forces on the moving fluid resulting in secondary flows. Besides enhancing the heat transfer coefficient, the induced secondary flow also enhances the mixing and the frictional pressure drop especially in laminar flow.

The helical coil SG in the MASLWR test facility consists of 14 helical coils (4 inner, 5 middle and 5 outer coils). In general a lumped SG tube model showed more stable behaviour, however this did not allow for study of parallel channel instabilities which cannot be ruled out (SP-3).

Experiment (SP-2) shows an abrupt drop in core inlet temperature over a short duration when long-term cooling starts (PCS-108A/B open). Most ICSP participants could not predict this abrupt temperature drop even though they match the time and flow direction. It is concluded that it may be possible to capture this non-uniform temperature distribution using a more refined meshing/nodalization or multi-dimensional model.

For fluid temperature at high elevation above water (TF-841 through TF-861) in the HPC, most ICSP participants show significantly higher fluid temperature than experiment (SP-2). The difference may be attributed to the close proximity of the thermocouples to the heat transfer plate. But for low elevation in water (TF-811 and TF-821), all ICSP participants show significantly lower fluid temperature than experiment. Experiment data shows a very rapid initial temperature increase while the code simulation shows a gradual increase. The difference may be attributed to a number of physical phenomena including thermal mixing, axial conduction, and location of thermocouples. Multi-dimensional simulation may be required to improve predictions related to experimental observations.

All experiment data for CPV water temperature at high and low elevation (SP-2) shows very rapid initial temperature increase, but code simulations show a gradual increase. The difference may be attributed to the close proximity of the thermocouples to the heat transfer plate. Three-dimensional effect may be considered in future analysis related to thermal gradients and natural convection.

Predictions show a wide range of CPV side HTP temperatures (TW-864), higher and lower than experimental values. Differences in number of mesh nodes in the heat structures make it difficult to compare the results from different participants (SP-2).

Most ICSP participants show significantly higher steady state primary flow than experiment for SP-3. If they match the initial flow with experiment, they show lower primary flow than experiment according to the increase of power. If they have a significantly higher initial flow than experiment, they could match the primary flow with experiment in later phase. There is an evidence that the experimentally measured flow rate at low powers may be at the lower limit of the instruments valid range, leading to high error in reported values. Code predictions may be improved by applying a Reynolds number dependent form loss coefficient to accurately account for unrecoverable pressure losses.

User effects could be evaluated by comparing the results from the same computer code. Several versions of RELAP5 codes were used by 9 participants. The predictions from the same code show a wide range of spectrum. That means the results are quite sensitive to the nodalization, SG modeling, initial & boundary conditions, and etc.

Tables 6-1 and 6-2 show the summary on code deficiencies and capabilities for each phenomenon based on ICSP participant's blind and open calculations.

TABLE 6-1. SUMMARY ON CODE DEFICIENCIES AND CAPABILITIES FOR EACH PHENOMENON OF SP-2

Phenomena	Experiment		AERB	BARC (RELAP 5)	CIAE	ENEA	GIDRO PRESS	IBRAE	KAERI	KINS	NPCIL	NuScale	SJTU	SNPTRD	UNIPA	UNIPI	USNRC
	Phenomena	Measurement															
HPC Pool: Thermal stratification	+	+	+	NA	+	+	o	o	o	+	NA	NA	o	+	o	o	+
HPC Pool: Natural convection	+	NA	+	NA	+	NA	o	o	o	+	+	NA	+	NA	NA	o	o
HPC Pool: Steam condensation	+	NA	o	+	+	+	o	+	+	+	+	-	+	o	o	+	+
HPC: Effect of non-condensable gases on condensation heat transfer	+	NA	-	+	+	+	+	o	+	o	+	o	o	+	+	+	o
HPC: Condensation on containment structures	+	o	o	+	+	+	+	+	NA	-	+	+	o	+	+	+	o
Distribution of pressure drop through primary system	+	+	+	+	+	+	+	+	+	+	+	+	o	+	+	+	+
Break flow	+	o	+	+	o	+	+	+	+	+	+	+	+	+	+	+	+
Single phase NC	+	+	+	+	+	+	+	+	+	+	+	+	+	-	+	+	+
Two phase NC	+	NA	+	+	+	+	+	+	+	+	+	+	o	+	+	+	o
Intermittent two phase NC	o	NA	+	+	NA	+	+	o	o	+	o	+	-	+	+	o	-
Heat transfer in core	+	+	+	+	+	+	+	+	+	+	+	+	+	+	+	+	+
Heat transfer in SG	+	-	o	+	+	+	o	+	+	+	+	+	+	+	+	+	+
Primary-containment coupling during blowdown and long-term cooling	+	o	+	+	+	+	o	+	+	+	+	+	+	+	+	+	+

\+ Phenomenon occurred/predicted clearly

o Phenomenon occurred/predicted partially/indirectly

\- Phenomenon not occurred/predicted

NA Model is not appropriate to predict the phenomenon. No measurement in experiment.

TABLE 6-2. SUMMARY CODE DEFICIENCIES AND CAPABILITIES FOR EACH PHENOMENON OF SP-3

Phenomena	Experiment		AERB	BARC (RELAP5)	BARC (CATHARE)	CIAE	ENEA	GIDROPRESS	IBRAE	KAERI	KINS	NPCIL	NuScale	SJTU	SNPTRD	UNIPA	UNIPI	USNRC
	Phenomena	Measurement																
Distribution of pressure drop through primary system	+	+	+	+	+	+	+	+	+	+	+	+	+	o	+	+	+	+
NC: stability	+	+	+	+	+	+	NA	+	+	o	-	+	+	o	+	+	+	o
Bypass heat transfer from chimney to downcomer	+	+	+	+	+	+	+	+	+	+	-	+	+	+	+	+	+	+
Single phase NC	+	+	+	+	+	+	+	+	+	+	+	+	+	+	+	+	+	+
Two phase NC	NA		+	+	NA	+	NA	NA	-	-	-	-	-	o	-	-		NA
Intermittent two phase NC	NA		+	-	NA	NA	NA	NA	-	-	-	-	-	-	-	-		NA
Heat transfer in core	+	+	+	+	+	+	-	+	+	+	+	+	+	+	+	+	+	+
Heat transfer in SG	+	+	o	+	+	+	-	+	+	+	+	+	+	+	+	+	+	+
SG: superheating in secondary	+	+	+	+	+	+	-	+	o	+	+	+	+	+	+	+	+	+

+ Phenomenon occurred/predicted clearly

o Phenomenon occurred/predicted partially/indirectly

- Phenomenon not occurred/predicted

NA Model is not appropriate to predict the phenomenon. No measurement in experiment.

7. CONCLUSIONS

The content of this TECDOC is based on the work done during the IAEA International Collaborative Standard Problem on Natural Circulation. This ICSP was conducted from 2008 through 2013. Two tests were conducted at the OSU MASLWR test facility in support of the current ICSP.

- SP-2: loss of feedwater transient with subsequent ADS operation and long term cooling. The purpose of this test was to conduct a feedwater transient with subsequent automatic depressurization system (ADS) actuation and long term cooling to determine the progression of a loss of feedwater transient at the OSU MASLWR Test facility.
- SP-3: normal operating conditions at different power levels. The test was a substitute for the original test planned under this ICSP, "stepwise reduction in primary system volume at decay power." The substitution was made over concerns about the ability of the test facility to safely handle the reduction in primary system volume while at power.

Eighteen participants took part in this ICSP. Each participant used their thermal-hydraulic code of choice to model the two tests conducted at the OSU MASLWR test facility. The codes that were used in this ICSP include a number of the most advanced and widely used system level thermal-hydraulic codes including CATHARE, RELAP5, SOCRAT, TASS/SMR-S, and TRACE. RELAP5 was used by half of the participants, which included versions RELAP5/MOD3.2, RELAP5/MOD3.3, RELAP5/MOD3.4 and RELAP5-3D.

All ICSP participants were given the opportunity to conduct three phases of simulation analysis for the ICSP test: pre-test, blind and open.. The goal of this ICSP was to evaluate each of the codes for their capability to simulate the thermal-hydraulic transients in integral type reactor including helical coil steam generator. The IAEA ICSP provided all participants with a chance to evaluate the strength and weakness of their system codes in the transient analysis for integral reactor.

For the loss of feedwater event, the core was never uncovered during the entire test period in the experiment. Single-phase natural circulation and intermittent two-phase natural circulation flow are seen in the experiment. The thermal-hydraulic coupling between the RPV and HPC and between the HPC and CPV are seen in the experiment as well and shown to be effective cooling mechanisms.

The thermal-hydraulic codes used show ability to predict major phenomena and trends in RPV well. The HPC predictions are consistent between codes and participants, however there is disagreement with experimental data, which may be explained by instrumentation location uncertainty and multi-dimensional phenomena and effects.

A Helical coil steam generator is used for many integral type reactors. It is well known and also found in this ICSP that a helical coil heat exchanger improves the heat transfer significantly compared to a conventional U-tube bundle steam generator. Most existing thermal-hydraulic codes do not have appropriate heat transfer models for helical coil steam generators and thus ICSP participants were forced to add artificial heat transfer contributions in order to effectively simulate the tests conducted at the test facility. The method used to add this artificial heat transfer contribution varied by participant and included increasing the heat transfer area of the steam generator, increasing the heat transfer coefficient or using a fouling factor greater than 1.0. Further study on heat transfer in helical coil heat exchangers and the incorporation of improved helical coil steam generator heat transfer models into the system codes is recommended from this ICSP.

For the normal operating conditions test at various power levels, the primary phenomena observed was single-phase natural circulation and the impact of core power and feedwater flow on the magnitude of the natural circulation flow rate. During this test, no natural circulation flow instabilities were noted. Heat transfer through the helical coil steam generator was the principal method of heat removal in this test and any improvements in the modeling of heat transfer through helical coil heat exchangers mentioned above would be beneficial to this normal operations simulation as well.

This second test was also characterized by significantly higher natural circulation flow rates through the primary as compared against the first test. The modeling of the form losses across the geometric discontinuities and internal vessel structures thus becomes very important for this test. The participants had challenges in accurately simulating the primary natural circulation flow rate over the entire range

of flow rates experienced during this test. Models that accurately predicted flow rates at low flow rate conditions had trouble predicting flow rates at high flow rate conditions and vise versa. In the future, experimenters should rule out flow rate measurement uncertainty a low flow rates as a cause for this discrepancy. The use of Reynolds number dependent form losses should also be examined for the improvement of these predictions over the full range of expected natural circulation flow rates.

APPENDIX I: TEST PROCEDURES

I.1 SP-2: LOSS OF FEEDWATER TRANSIENT WITH SUBSEQUENT ADS OPERATION AND LONG TERM COOLING

Purpose

Conduct a loss of feedwater transient with subsequent automatic depressurization system (ADS) actuation and long term cooling to determine the progression of a loss of feedwater transient in the Oregon State University (OSU) Multi-Application Small Light Water Reactor (MASLWR) test facility.

Initial Conditions

OSU MASLWR test facility in steady state with the following conditions established:

- Core power level at 299 ± 2 kW (≈50% of 598 kW). Core heaters in constant power mode.
- Primary coolant subcooled at the core outlet.
- Pressurizer (PZR) pressure P_{pzr} = 1250 psig (8.618 MPa gage), PZR heaters in automatic mode.
- PZR level L_{pzr} = 14 ± 1 inches (35.56 cm).
- Feedwater is supplied by the main feed water pump (MFP).
- Secondary system operating to remove net primary power (core power less ambient losses), with steam pressure P_{stm} = 200 psig (1.379 MPa gage) and steam superheat $\Delta T_{stm,sh}$ = 15ºF (8.33°C).
- Feed water regulating valve (FRV) manually set to match specified setpoint.
- High pressure containment (HPC) level L_{hpc} = 110 ± 1 inches (279.4 cm).
- HPC vent valve SV-800 is closed.
- Cooling pool vessel (CPV) level L_{cpv} = 250 ± 1 inches (635 cm).
- Data acquisition and control system (DACS) is operating and test facility is being controlled from the Operator Control Console (OCC).

Procedure

1. At the OCC, start recording data by performing the following:
    1.a. Navigate to the Main Control Screen.
    1.b. Click the Start Test button. A pop-up window will open.
    1.c. Verify green bar (OK) status for remote input/output on the right side of the pop-up window.
    1.d. Enter the following on the pop-up window:
        1.d.i. In the Test Name field, enter “IAEA ICSP SP-2”.
        1.d.ii. Enter the Test Engineer name(s) in the Test Engineer field.
        1.d.iii. In the Test Description field, enter “Loss of Feedwater Transient with Subsequent ADS Operation and Long Term Cooling”.
        1.d.iv. In the Root Filename field, enter “IAEASP2”.
    1.e. Press Start! button at bottom of pop-up window.

2. At the OCC, perform the following:
    2.a. Navigate to the Core Operation Screen.
    2.b. Enter the following decay power values:
        2.b.i. P_o=36
        2.b.ii. T_o=0
        2.b.iii. A=0.013
        2.b.iv. B=0.236

NOTE

36 kW is approximately 6% of 598 kW.

NOTE

Decay power is programmed as:

$$P(t) = \frac{P_o}{(1 + A(t - T_o))^B}$$

3. Wait approximately 10 minutes before proceeding to Step 11.

NOTE

This wait allows collecting steady state data prior to initiating the transient.

4. Disable PCS-103 Auto Mode at the OCC.

5. At the OCC, click on the ‘Safetylimit-2’ screen tab.

6. Disable the core relay trip for the Pressurizer Low Limit and Low Low Limit alarms. This will enable the core heaters to stay on once the level drops below the pressurizer heaters.

7. At the OCC, navigate back to the main control screen by clicking on the ‘Main Control’ button in the lower left of the screen.

8. Enter “200” in the “PT801 Lower Pressure Setpoint” field on the left hand side of the OCC main screen.

9. Enter “250” in the “PT801 Upper Pressure Setpoint” field on the left hand side of the OCC main screen. The last two steps are for the PCS-106A Auto Mode.

10. Take an ambient temperature measurement in the ATHRL building and record in the test log.

NOTE

Blank space below is intentional to start the instructions for the transient at the top of the following page.

WARNING

Once the MFP is stopped, pressure in the primary vessel is expected to rise quickly. Be prepared to perform Step 12.

11. At the OCC, perform the following:

    11.a. Stop the MFP.

    11.b. Shut feedwater isolation valve MF-508.

12. When PZR pressure as indicated by PT-301 reaches 1300 psig (8.963 MPa gage), on the Core Operation Screen click the Decay P button to place the core in decay power mode.

CAUTION

The maximum HPC operating pressure is 300 psig. Do not exceed 300 psig HPC pressure or HPC overpressurization and structural damage may result.

CAUTION

Ensure PZR heaters are deenergized prior to performing Step 13.b. Operating the PZR heaters when not covered with water could lead to heater overheating and burnout.

13. After Decay Power has been activated,

    13.a. Deenergize PZR heaters.

    13.b. Click “PCS-106A Auto Mode” button or open ADS vent valve PCS-106A manually.

WARNING

The operator is still responsible for opening SV-800 in accordance with the table below.

    13.c. If operating manually, take action in accordance with the table below until the difference between reactor pressure vessel (RPV) pressure and HPC pressure (PT-301 minus PT-801) is ≤ 5 psi (0.034 MPa):

PT-801 Indicated HPC Pressure	PCS-106A	SV-800
250 psig and rising	SHUT	SHUT
275 psig and rising	SHUT	OPEN
200 psig and lowering	OPEN	SHUT

14. When the difference between RPV pressure and HPC pressure (PT-301 minus PT-801) is ≤ 5 psi (0.034 MPa),

14.a. Check open or open PCS-106A.

14.b. Open PCS-106B.

14.c. Open PCS-108A.

14.d. Open PCS-108B.

15. Take an ambient temperature measurement in the ATHRL building and record measurement and temperature in test. Repeat every hour until test has been terminated.

16. Monitor test facility cooldown until the one of the following conditions is reached:

- P_{pzr}(PT-301) ≤ 75 psig (0.034 MPa gage), or
- 5 hours have elapsed since commencing this procedure.

17. At the OCC, stop recording data by performing the following:

17.a. Navigate to the Main Control Screen.

17.b. Click the Stop Test button.

18. At the OCC, deenergize the core heaters.

19. Shutdown and cooldown the test facility in accordance with *OP-3, Test Facility Depressurization and Cooldown.*

I.2 SP-3: POWER MANEUVERING

Purpose

Run the Oregon State University (OSU) Multi-Application Small Light Water Reactor (MASLWR) facility at normal operating conditions as a substitute for SP-1, Stepwise Reduction in Primary System Volume at Decay Power.

Initial Conditions

OSU MASLWR test facility in steady state with the following conditions established:

- Core power level at 40 kW. Core heaters in constant power mode.
- Primary coolant subcooled at the core outlet.
- Pressurizer (PZR) pressure P_{pzr} = 1250 psig (8.618 MPa gage), PZR heaters in automatic mode.
- PZR level L_{pzr} = 14 ± 2 inches (35.56 cm). PZR level automatically controlled at the Operator Control Console (OCC).
- Feedwater is supplied by the main feed water pump (MFP).
- Secondary system operating to remove net primary power (core power less ambient losses), with steam pressure P_{stm} = 200 psig (1.379 MPa gage).
- Feed water regulating valve (FRV) is manually operated and set to achieve saturated condi-tions at secondary side outlet.
- Data acquisition and control system (DACS) is operating and test facility is being controlled from the OCC.

Procedure

1. At the OCC, start recording data by performing the following:

    1.a. Navigate to the Main Control Screen.

    1.b. Click the Start Test button. A pop-up window will open.

    1.c. Verify green bar (OK) status for remote input/output on the right side of the pop-up window.

    1.d. Enter the following on the pop-up window:

        1.d.i. In the Test Name field, enter “IAEA ICSP SP-3”.

        1.d.ii. Enter the Test Engineer name(s) in the Test Engineer field.

        1.d.iii. In the Test Description field, enter “Normal Operating Conditions at Different Power Levels”.

        1.d.iv. In the Root Filename field, enter “IAEASP3”.

    1.e. Press Start! button at bottom of pop-up window.

2. Wait 2 min to take steady state data at 10% core power (≈40 kW) before proceeding.

3. At the OCC manually set core power to 20% and proceed as follows:

    3.a. If the core subcooled margin begins to degrade below 20ºF, at the OCC decrease the core heater setpoint by 20 kW. Take further actions as necessary to decrease core power if subcooled margin continues to degrade below 15ºF.

    NOTE

    The goal of the following operator actions is to achieve steady state at 20% power with saturated conditions at the secondary side outlet while maintaining at least a 15ºF subcooled margin with the expectation of achieving a much larger margin.

    3.b. Adjust the position of MF-500 to achieve saturated conditions at secondary side outlet. Saturation temperature and secondary exit temperature are shown on OCC main screen.

    3.c. When subcooled margin has been established at 20% power with saturated conditions at secondary side outlet, monitor for indications that the system is in steady state. Steady state is indicated by ALL of the following

        3.c.i.

        - Constant hot leg temperature as indicated by TF-106 (±5ºF)
        - Constant cold leg temperature as indicated by TF-131 (±5ºF)
        - Constant primary mass flow rate as indicated by FDP-131 (±5%)

    3.d. Record time of Steady State Indication: _____

    3.e. Adjust MF-500 as necessary to achieve steady state.

    3.f. Wait 2 min to take steady state data at 20% core power before proceeding.

4. At the OCC manually set core power to 30% and proceed as follows:

    4.a. If the core subcooled margin begins to degrade below 20ºF, at the OCC decrease the core heater setpoint by 20 kW. Take further actions as necessary to decrease core power if subcooled margin continues to degrade below 15ºF.

NOTE

The goal of the following operator actions is to achieve steady state at 30% power with saturated conditions at the secondary side outlet while maintaining at least a 15º F subcooled margin with the expectation of achieving a much larger margin.

4.b. Adjust the position of MF-500 to achieve saturated conditions at secondary side outlet. Saturation temperature and secondary exit temperature are shown on OCC main screen.

4.c. When subcooled margin has been established at 30% power with saturated conditions at secondary side outlet, monitor for indications that the system is in steady state. Steady state is indicated by ALL of the following:

4.c.i.

- Constant hot leg temperature as indicated by TF-106 (±5ºF)
- Constant cold leg temperature as indicated by TF-131 (±5ºF)
- Constant primary mass flow rate as indicated by FDP-131 (±5%)

4.d. Record time of Steady State Indication:_____

4.e. Adjust MF-500 as necessary to achieve steady state.

4.f. Wait 2 min to take steady state data at 30% core power before proceeding.

5. At the OCC manually set core power to 40% and proceed as follows:

5.a. If the core subcooled margin begins to degrade below 20ºF, at the OCC decrease the core heater setpoint by 20 kW. Take further actions as necessary to decrease core power if subcooled margin continues to degrade below 15ºF.

NOTE

The goal of the following operator actions is to achieve steady state at 40% power with saturated conditions at the secondary side outlet while maintaining at least a 15ºF subcooled margin with the expectation of achieving a much larger margin.

5.b. Adjust the position of MF-500 to achieve saturated conditions at secondary side outlet. Saturation temperature and secondary exit temperature are shown on OCC main screen.

5.c. When subcooled margin has been established at 40% power with saturated condi-tions at secondary side outlet, monitor for indications that the system is in steady state. Steady state is indicated by ALL of the following:

5.c.i.

- Constant hot leg temperature as indicated by TF-106 (±5ºF)
- Constant cold leg temperature as indicated by TF-131 (±5ºF)
- Constant primary mass flow rate as indicated by FDP-131 (±5%)

5.d. Record time of Steady State Indication:_____

5.e. Adjust MF-500 as necessary to achieve steady state.

5.f. Wait 2 min to take steady state data at 40% core power before proceeding.

6. At the OCC manually set core power to 50% and proceed as follows:

6.a. If the core subcooled margin begins to degrade below 20ºF, at the OCC decrease the core heater setpoint by 20 kW. Take further actions as necessary to decrease core power if subcooled margin continues to degrade below 15ºF.

NOTE

The goal of the following operator actions is to achieve steady state at 50% power with saturated conditions at the secondary side outlet while maintaining at least a 15ºF subcooled margin with the expectation of achieving a much larger margin.

6.b. Adjust the position of MF-500 to achieve saturated conditions at secondary side outlet. Saturation temperature and secondary exit temperature are shown on OCC main screen.

6.c. When subcooled margin has been established at 50% power with saturated condi-tions at secondary side outlet, monitor for indications that the system is in steady state. Steady state is indicated by ALL of the following:

6.c.i.

- Constant hot leg temperature as indicated by TF-106 (±5ºF)
- Constant cold leg temperature as indicated by TF-131 (±5ºF)
- Constant primary mass flow rate as indicated by FDP-131 (±5%)

6.d. Record time of Steady State Indication: _____

6.e. Adjust MF-500 as necessary to achieve steady state.

6.f. Wait 2 min to take steady state data at 50% core power before proceeding.

7. At the OCC manually set core power to 60% and proceed as follows:

7.a. If the core subcooled margin begins to degrade below 20ºF, at the OCC decrease the core heater setpoint by 20 kW. Take further actions as necessary to decrease core power if subcooled margin continues to degrade below 15ºF.

NOTE

The goal of the following operator actions is to achieve steady state at 60% power with saturated conditions at the secondary side outlet while maintaining at least a 15ºF subcooled margin with the expectation of achieving a much larger margin.

7.b. Adjust the position of MF-500 to achieve saturated conditions at secondary side outlet. Saturation temperature and secondary exit temperature are shown on OCC main screen.

7.c. When subcooled margin has been established at 60% power with saturated condi-tions at secondary side outlet, monitor for indications that the system is in steady state. Steady state is indicated by ALL of the following:

7.c.i.

- Constant hot leg temperature as indicated by TF-106 (±5ºF)
- Constant cold leg temperature as indicated by TF-131 (±5ºF)
- Constant primary mass flow rate as indicated by FDP-131 (±5%)

7.d. Record time of Steady State Indication: _____

7.e. Adjust MF-500 as necessary to achieve steady state.

7.f. Wait 2 min to take steady state data at 60% core power before proceeding.

8. At the OCC manually set core power to 70% and proceed as follows:

8.a. If the core subcooled margin begins to degrade below 20ºF, at the OCC decrease the core heater setpoint by 20 kW. Take further actions as necessary to decrease core power if subcooled margin continues to degrade below 15ºF.

NOTE

The goal of the following operator actions is to achieve steady state at 70% power with saturated conditions at the secondary side outlet while maintaining at least a 15ºF subcooled margin with the expectation of achieving a much larger margin.

8.b. Adjust the position of MF-500 to achieve saturated conditions at secondary side outlet. Saturation temperature and secondary exit temperature are shown on OCC main screen.

8.c. When subcooled margin has been established at 70% power with saturated conditions at secondary side outlet, monitor for indications that the system is in steady state. Steady state is indicated by ALL of the following:

8.c.i.

- Constant hot leg temperature as indicated by TF-106 (±5ºF)
- Constant cold leg temperature as indicated by TF-131 (±5ºF)
- Constant primary mass flow rate as indicated by FDP-131 (±5%)

8.d. Record time of Steady State Indication:

8.e. Adjust MF-500 as necessary to achieve steady state.

8.f. Wait 2 min to take steady state data at 70% core power before proceeding.

9. At the OCC manually set core power to 80% and proceed as follows:

9.a. If the core subcooled margin begins to degrade below 20ºF, at the OCC decrease the core heater setpoint by 20 kW. Take further actions as necessary to decrease core power if subcooled margin continues to degrade below 15ºF.

NOTE

The goal of the following operator actions is to achieve steady state at 80% power with saturated conditions at the secondary side outlet while maintaining at least a 15ºF subcooled margin with the expectation of achieving a much larger margin.

9.b. Adjust the position of MF-500 to achieve saturated conditions at secondary side outlet. Saturation temperature and secondary exit temperature are shown on OCC main screen.

9.c. When subcooled margin has been established at 80% power with saturated conditions at secondary side outlet, monitor for indications that the system is in steady state. Steady state is indicated by ALL of the following:

9.c.i.

- Constant hot leg temperature as indicated by TF-106 (±5ºF)
- Constant cold leg temperature as indicated by TF-131 (±5ºF)
- Constant primary mass flow rate as indicated by FDP-131 (±5%)

9.d. Record time of Steady State Indication: _____

9.e. Adjust MF-500 as necessary to achieve steady state.

9.f. Wait 2 min to take steady state data at 80% core power before proceeding.

10. At the OCC, stop recording data by performing the following:

10.a. Navigate to the Main Control Screen.

10.b. Click the Stop Test button.

11. At the OCC, perform the following:

11.a. Deenergize core heaters.

11.b. Wait 10 min before stopping the MFP to let the heat stored in the MASLWR metal mass dissipate and avoid a pressure spike.

11.c. Stop the MFP.

11.d. Wait approximately 2 min for the MFP to coast down.

11.e. Shut feedwater isolation valve MF-508.

12. Shutdown and cooldown the test facility in accordance with OP-3, *Test Facility Depressurization and Cooldown.*

APPENDIX II: SUMMARY ON HEAT TRANSFER AND PRESSURE DROP IN HELICAL COIL STEAM GENERATOR

MASLWR as well as the OSU-MASLWR test facility, in which the ICSP tests were conducted, have a helical coil steam generator. Most of the present day computer codes used for thermal-hydraulic analysis does not contain appropriate heat transfer and pressure drop correlations for the inside and outside surfaces of the helical coil. The problem is further complicated due to the fact that the inlet condition for the helical coil steam generator corresponds to single-phase flow while the outlet condition corresponds to superheated flow requiring not only the estimation of heat transfer and pressure drop under single- and two-phase flow conditions, but also the dryout and post dryout heat transfer. In addition, many geometric and operating parameters affect the helical coil heat transfer and pressure drop like diameter of the tube, diameter of helix, helical pitch, flow regime (laminar, transition and turbulent flow in single-phase fluid), orientation of the helical tube (vertical upward/downward, inclined or horizontal), flow patterns (bubbly, slug, annular, droplet flow), etc. More over the entrance effect also needs to be considered for both heat transfer and pressure drop. This note gives a brief review on the inside and outside heat transfer coefficients and pressure drops.

Inside heat transfer coefficient

In general, heat transfer performance of helical coil heat exchangers is significantly better compared to straight tubes. The increased heat transfer coefficient is a consequence of the curvature of the coil which induces centrifugal forces on the moving fluid resulting in secondary flows. Besides enhancing the heat transfer coefficient, the induced secondary flow also enhances the mixing and the frictional pressure drop especially in laminar flow. Several correlations are reported in literature [32, 33, 34] for the laminar flow heat transfer coefficient with the general the functional dependence of the Nusselt number (Nu) in terms of the Dean number (De) and the Prandtl number (Pr). Depending on the value of the Dean number, the Nuratio of helical coil over that of straight tube can be as high as 5 at Dean number of 2000 (see Fig. AII-1). For turbulent flow [35, 36, 37, 38] the Nu number for helical coils is generally expressed in terms of the Reynolds and Prandtl numbers. The ratio of Nu for helical tube over that of straight tubes decreases from a value of ~ 2.5 at Reynolds number of 3000 to an asymptotic value of ~1.2 beyond a Reynolds number of about 50000 (see Fig. AII-2).

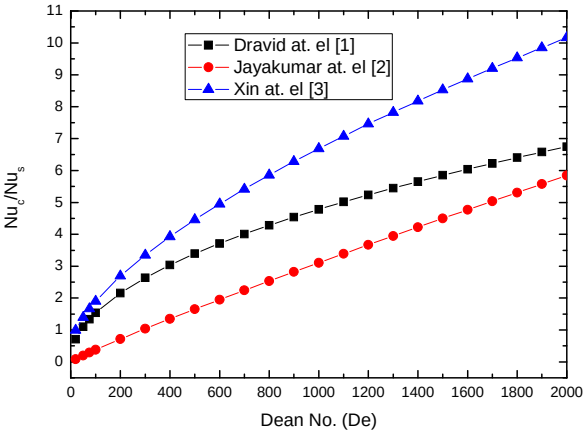

FIG. AII-1. Variation of ratio of Nusselt number for helical coil and straight tube with Dean number.

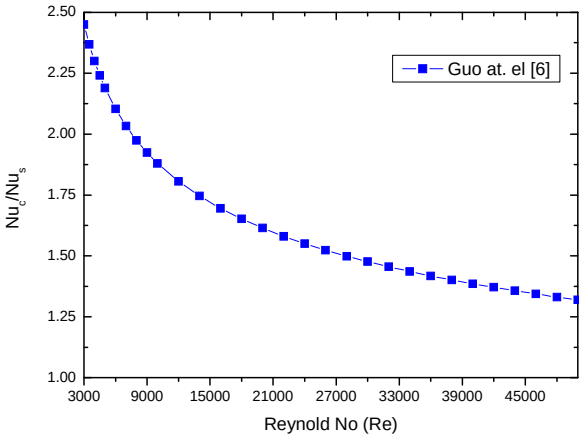

FIG. AII-2. Variation of ratio of Nusselt number for helical coil and straight tube with Re number.

Outside Heat Transfer Coefficient

The reported data in literature [39] show that the outside heat transfer coefficient variation from coiled tube surfaces in cross-flow is similar to that in shell and tube heat exchangers.

Two-phase flow heat transfer coefficient

Two phase flow heat transfer could be boiling or condensation. As compared to single-phase heat transfer, reported work on the two-phase heat transfer characteristics in helically coiled tubes is very few. An exhaustive review is required to arrive at general conclusions with respect to straight tubes.

Pressure dropfor single-phase flow in helical coils

As mentioned earlier, secondary flow is induced due to the difference in the centrifugal force caused by fluid elements moving with different axial velocities. Due to this, the pressure drop for flow in helical tube is higher than that for straight tube at the same flow rate and tube length. Several equations for laminar flow friction factor are reported in the literature [40, 41] for different values of Dean number. For De<11.6, the friction factor ratio of the helical tube over the straight tube is unity. Ju et al. [40] studied the hydraulic performance of small bending radius helical pipes. They showed that the critical Reynolds number of helical pipe is a function of the Dean number and were much greater than that of a straight pipe. There are indications that the friction factor is also affected by the size of the vortex formed inside the helical tube. Besides the friction factor is also a function of Reynolds number and the ratio of the tube diameter to the helix diameter (see Fig. AII-3 and 4). Mathematically this can be expressed as:

$$For\ De < 11.6, it\ is\ laminar\ flow; f_s = \frac{64}{Re};\ \frac{f_c}{f_s} = 1$$

$$For\ De < 11.6, it\ is\ laminar\ flow;$$

$$For\ De > 11.6, Re < Re_{cr}\ it\ is\ laminar\ with\ large\ vortex;$$

$$f_s = \frac{64}{Re};\ \frac{f_c}{f_s} = 1 + 0.015Re^{0.75}\left(\frac{d}{D}\right)^{0.4}$$

$$For\ De > 11.6, Re > Re_{cr}\ It\ is\ turbulent\ flow; f_s = \frac{0.316}{Re^{0.25}} for\ smooth\ pipe$$

$$f_s = 0.1\left(1.46\frac{\Delta}{d} + \frac{100}{Re}\right)^{0.25}\ (\Delta: roughness\ of\ pipe)$$

$$\frac{f_c}{f_s} = 1 + 0.11Re^{0.23}\left(\frac{d}{D}\right)^{0.14}$$

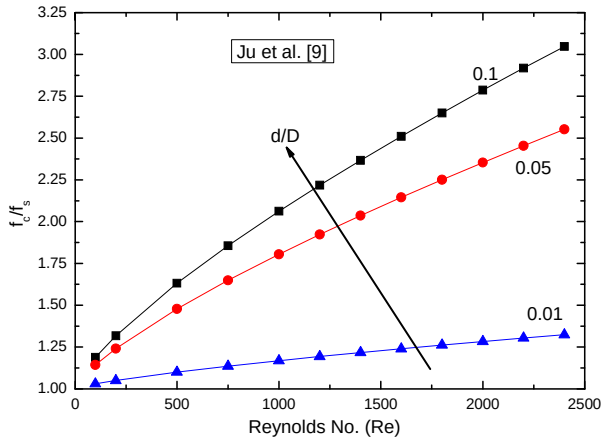

FIG. AII-3. Variation of friction factor ratio for helical coil and straight tube with Re (Re < 2500).

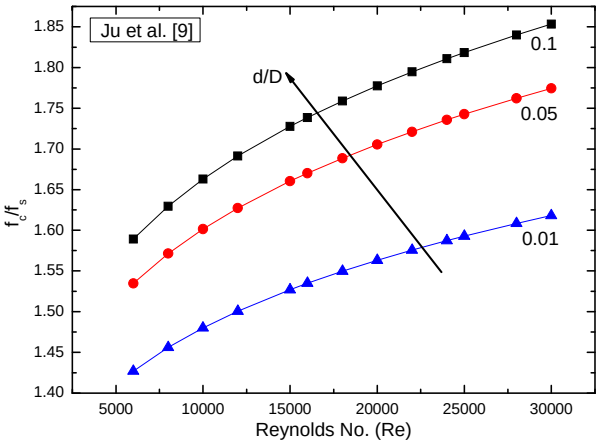

FIG. AII-4. Variation of friction factor ratio for helical coil and straight tube with Re (Re > 2500).

Tarbell and Samuels [41] solved the equations of motion and energy to study flow characteristics in helical coils by using the alternating direction implicit technique. A correlation of friction factor representing the data within 3% was proposed:

$$For\ 20 < De < 500, 3 < \lambda < 30$$

$$\frac{f_c}{f_s} = 1.0 + \left[8.279 \times 10^{-4} + \frac{7.964 \times 10^{-3}}{\lambda}\right] Re - 2.096 \times 10^{-7} Re^2$$

Pressure drop for two-phase flow in helical coils

Frictional pressure drop for two phase flow in helical tubes are obtained by multiplying the single phase pressure drop using the two phase friction factor multiplier concept. The Lockhart-Martinelli model is generally used [42, 43, 44].

NOMENCLATURE:

d	Diameter of tube
D	Diameter of helix
De	Dean number $\left(Re\sqrt{\frac{d}{D}}\right)$
f	Friction factor
Nu	Nusselt number (hd/k)
Re	Reynolds number (Duρ/μ)
u	Velocity of fluid
Greek symbols	
λ	Aspect ratio (D/d)
μ	viscosity
ρ	Density
Subscripts	
c	Coil
s	Straight tube

REFERENCES

[1] MODRO, S. M., FISHER, J. E., WEAVER, K. D., REYES, J. N., GROOME, J. T., BABKA, P., and CARLSON, T. M., Multi-Application Small Light Water Reactor Final Report, DOE Nuclear Energy Research Initiative Final Report, Idaho National Engineering and Environmental Laboratory (2003).

[2] MAI, A. T., and ASCHERL, G., OSU MASLWR Test Facility Quick Look Report, OSU-MASLWR-QLR-SP2 (2011).

[3] MAI, A. T., and LUO, H., OSU MASLWR Test Facility Quick Look Report, OSU-MASLWR-QLR-SP3 (2011).

[4] WOODS, B. G., GALVIN, M. R., JORDAN, B. C., Problem specification for the IAEA ICSP on integral PWR design natural circulation flow stability and TH coupling of containment and primary system during accidents, OSU-MASLWR-10005-R, Oregon State University (2011).

[5] INFORMATION SYSTEMS LABORATORIES, RELAP5/Mod3.3 code manual volume I: code structure, system models, and solution methods (2003).

[6] INFORMATION SYSTEMS LABORATORIES, RELAP5/Mod3.3 code manual volume II: user's guide and input requirements (2003).

[7] INFORMATION SYSTEMS LABORATORIES, RELAP5/Mod3.3 code manual volume II: appendix A input requirements (2004).

[8] INFORMATION SYSTEMS LABORATORIES, RELAP5/Mod3.3 code manual volume VII: summaries and reviews of independent code assessment reports (2001).

[9] INFORMATION SYSTEMS LABORATORIES, RELAP5/Mod3.3 code manual volume IV: models and correlations (2001).

[10] DEL NEVO, A., MANFREDINI, A., ORIANI, L., ORIOLO, F., PACI, S., Integrated Analysis for a Small Break LOCA in the IRIS Reactor Using MELCOR and RELAP5 Codes, Nuclear Option in Countries with Small and Medium Electricity Grids, vol. CD, Dubrovnik (HR) (2004) pp. 1-17.

[11] DEMICK, N. T., GALVIN, M. R., GROOME, J. T. and WOODS B. G., OSU MASLWR Test Facility Description Report, OSU-MASLWR-07001 (Revision NC) (2007).

[12] IDELCHIK, I.E., Handbook of Hydraulic Resistance, 3rd Edition, Begell House (1996).

[13] DEL NEVO, A., IAEA ICSP on Integral PWR Design Natural Circulation Flow Stability and TH Coupling of Containment and Primary System during Accident, Blind Calculation Results, Rev. 2 (2012).

[14] DEL NEVO, A., ROZZIA, D., AGOSTINI, P., Investigation of RELAP5 code capability in predicting phenomena in a SMR system, Proc. of 21st Int. Conf. NENE, Ljubljana (2012).

[15] DEL NEVO, A., IAEA ICSP on Integral PWR Design Natural Circulation Flow Stability and TH Coupling of Containment and Primary System during Accident, Open Calculation Results, Rev. 0, (2012).

[16] DEL NEVO, A., COSCARELLI, E., KOVTONYUK, A., and D'AURIA, F., Analytical Exercise on OECD/NEA/CSNI PKL-2 Project Test G3.1: Main Steam Line Break Transient in PKL-III Facility Phase 2: Post-Test Calculations, OECD/NEA/CSNI PKL-2 Project, TH/PKL-2/02(10) Rev. 1, Pisa (2011).

[17] AKSAN, N., D'AURIA, F., GLAESER, H., POCHARD, R., RICHARDS, C., and SJOBERG, A., Separate effects test matrix for thermal-hydraulic code validation Vol.I: phenomena characterization and selection of facilities and tests, OECD/GD(94)82, Paris, France (1994).

[18] CHOI, J.H., Summary of 3rd Workshop IAEA ICSP on Natural Circulation during Power Maneuvering and Loss of Feedwater Transient in Integral PWR Design MASLWR, Daejeon, Rep. of Korea (2012) 27-30.

[19] OREGON STATE UNIVERSITY, Analysis of RELAP5-3D Modeling Techniques for Natural Circulation Small Integral Light Water Reactors, OSU-MASLWR-08002 (Draft).

[20] The data spreadsheets for SP-2 and SP-3. http://people.oregonstate.edu/~woodsb/MASLWR/ICSP/

[21] GALVIN, M.R., BOWSER, C.J., OSU MASLWR Test Facility Modification Description Report, IAEA Contract Number USA-13386, OSU-MASLWR-07002 (2010).

[22] ZHUKAUSKAS, A.A., Heat Transfer from Tubes in Cross-Flow, in: T.F. Irvine, J.P. Hartnett (Eds.), Advances In Heat Transfer, Academic Press, New York (1987) pp. 87–159.
[23] CHUNH, Y.J, JUN, I.S., KIM, S.H., YANG, S.H., KIM, H.R., LEE, W.J., Development and assessment of system analysis code, TASS/SMR for integral reactor, SMART, Nuclear Engineering and Design 244 (2012) 52-60.
[24] KOREA ATOMIC ENERGY RESEARCH INSTITUTE, MARS code manual volume I: code structure, system models, and solution method, KAERI/TR-2812/2004 (2009).
[25] MORI, Y. and NAKAYAMA, W., Study on Forced Convective Heat transfer in Curved Pipes, Int. J. Heat and Mass Transfer, Vol. 10 (1967) pp. 37-59.
[26] ZUKAUSKAS, A. A., Heat transfer from tubes in cross flow, Adv. Heat Transfer Academic, Vol. 8 (1972) pp. 93-106.
[27] BESTION, D., The physical closure laws in the CATHARE code, Nuclear Engineering and Design 124 (1990) 229-245.
[28] MASCARI, F., VELLA, G., WOODS, B. G., TRACE Code Analyses For The IAEA ICSP On Integral PWR Design Natural Circulation Flow Stability And Thermo-Hydraulic Coupling Of Containment And Primary System During Accidents. Proceedings of the ASME 2011 Small Modular Reactors Symposium, Washington DC, USA (2011).
[29] Symbolic Nuclear Analysis Package (SNAP), Users Manual, Applied Programming Technology, Inc., Bloomsburg, PA (2007).
[30] U.S. NUCLEAR REGULATORY COMMISSION, TRACE V5.0, Theory and User's Manuals. Division of System Analysis, Office of Nuclear Regulatory Research, U.S. NRC, Washington, DC (2008).
[31] INTERNATIONAL ATOMIC ENERGY AGENCY, Natural Circulation Phenomena and Modelling for Advanced Water Cooled Reactors, IAEA-TECDOC-1677, IAEA, Vienna (2012).
[32] DRAVID, A. N., SMITH, K. A., MERRILL, E. W., BRAIN, P. L .T., Effect of secondary fluid on laminar flow heat transfer in helically coiled tubes. AIChE J (1971) 17:1114–22.
[33] JAYAKUMAR, J.S., MAHAJANI, S.M., MANDAL, J.C., VIJAYAN, P.K., ROHIDAS, B., Experimental and CFD estimation of heat transfer in helically coiled heat exchangers,Chemical Engineering Research and Design 86 (2008) 221–232.
[34] XIN, R. C., EBADIAN, M. A., The effects of Prandtl numbers on local and average convective heat transfer characteristics in helical pipes, J Heat Transfer (1997) 119:463–7.
[35] YANG, G., EBADIAN, M. A., Turbulent forced convection in a helicoidal pipe with substantial pitch, Int J Heat Mass Transfer (1996) 39, 2015–22.
[36] LIN, C. X., EBADIAN, M. A., Developing turbulent convective heat transfer in helical pipes, Int J Heat Mass Transfer (1997) 40:3861–73.
[37] GUO, L., CHEN, X., FENG, C. Z., BAI, B., Transient convective heat transfer in a helical coiled tube with pulsatile fully developed turbulent flow, Int J Heat Mass Transfer (1998) 41:2867–75.
[38] ROGER, G. F. C., MAYHEW, Y. R., Heat transfer and pressure loss in helically coiled tubes with turbulent flow, Int. J Heat Mass Transfer (1964) 7:1207–16.
[39] RAHUL, S., GUPTA, S. K., SUBBARAO, P. M. V., An experimental study for estimating heat transfer coefficient from coiled tube surfaces in cross-flow of air, Proceedings of the third ISHMT-ASME heat and mass transfer conference and fourth national heat and mass transfer conference (1997) p. 381–5.
[40] JU, H., HUANG, Z., XU, Y., DUAN, B., YU, Y., Hydraulic performance of small bending radius helical coil-pipe, J Nucl. Sci. Technol (2001) 18:826–31.
[41] TARBELL, J. M., SAMUELS, M. R., Momentum and heat transfer in helical coils, Chem Eng J (1973) 5:117–27.
[42] AWWAD, A., XIN, R. C., DONG, Z. F., EBADIAN, M. A., SOLIMAN, H. M., Measurement and correlation of the pressure drop in air–water two-phase flow in horizontal helicoidal pipes, Int. J. Multiphase Flow (1995) 21:607–19.

[43] XIN, R. C., AWWAD, A., DONG, Z. F., EBADIAN, M. A., An investigation and comparative study of the pressure drop in air–water two-phase flow in vertical helicoidal pipes, Int J Heat Mass Transfer (1996) 39:735–43.
[44] XIN, R. C., AWWAD, A., DONG, Z. F., EBADIAN, M. A., An experimental study of single-phase and two-phase flowpressure drops in annular helicoidal pipes, Int J Heat Fluid Flow (1997) 18:482–8.

ABBREVIATIONS

ADS	Automatic Depressurization System
ATWS	Anticipated Transients Without Scram
BIC	Boundary and Initial Conditions
CHF	Critical Heat Flux
CL	Cold Leg
CPV	Cooling Pool Vessel
DP	Differential Pressure meter
FCM	Coriolis Flow Meter
FDP	Flow Differential Pressure meter
FMM	Magnetic Flow Meter
FVM	Vortex Flow Meter
FW	Feed Water
HEM	Homogeneous Equilibrium Model
HL	Hot Leg
HPC	High-Pressure Containment
HTC	Heat Transfer Coefficient
HTP	Heat Transfer Plate
ICSP	International Collaborative Standard Problem
LDP	Level Differential Pressure meter
LOCA	Loss-Of-Coolant Accident
LOFW	Loss-Of-Feed Water
LOOP	Loos-Of-Offsite Power
LP	Lower Plenum
LWR	Light Water Reactor
MASLWR	Multi-Application Small Light Water Reactor
MFP	Main Feed Pump
MFW	Main Feed Water
NC	Natural Circulation
NPCIL	Nuclear Power Corporation of India Limited
NPP	Nuclear Power Plant
NRC	Nuclear Regulatory Commission
NSSS	Nuclear steam supply steam
OSU	Oregon State University
PS	Primary System
PT	Pressure Transducer
PWR	Pressurized Water Reactor
PZR	Pressurizer
RCP	Reactor Coolant Pump

RELAP	Reactor Excursion and Leak Analysis Program
RPV	Reactor Pressure Vessel
SG	Steam Generator
SMART	System-integrated Modular Advanced ReacTor
SNAP	Symbolic Nuclear Analysis Package
SOCRAT	System Of Codes for Realistic AssessmenT of severe accidents
SOT	Start Of the Transient
SP	Standard Problem
SS	Secondary System or Stainless Steel
TDJ	Time Dependent Junction
TDV	Time Dependent Volume
TH	Thermal-Hydraulic
TRACE	TRAC/RELAP Advanced Computational Engine
UNIPA	Università degli Studi di Palermo
UNIPI	Università di Pisa
UP	Upper Plenum
VVER	Russian version of the Pressurized Water Reactor

CONTRIBUTORS TO DRAFTING AND REVIEW

Chen, Y.	China Institute of Atomic Energy, China
Choi, J.-H.	International Atomic Energy Agency
Chung, Y.-J.	Korea Atomic Energy Research Institute, Rep. of Korea
Del Nevo, A.	ENEA, Italy
Dolganov, K.	IBRAE, Russian Federation
Fang, F.	State Nuclear Power Technology Research & Development Center, China
Khan, T.A.	Nuclear Power Corporation of India Limited, India
Kovtonyuk, A.	University of Pisa, Italy
Lakshmanan, S.P.	Atomic Energy Regulatory Board, India
Lien, P.	U.S. Nuclear Regulatory Commission, USA
Liu, X.	Shanghai Jiao Tong University, China
Mascari, F.	University of Palermo, Italy
Park, J.-Y.	Korea Institute of Nuclear Safety, Rep. of Korea
Sorokin, Y.	JSC OKB “Gidropress”, Russian Federation
Tomaschik, D.	IBRAE, Russian Federation
Vijayan, P.K.	Bhabha Atomic Research Center, India
Woods, B.	Oregon State University, USA
Wolf, B.	NuScale Power, LLC, USA
Wu, Q.	Oregon State University, USA

Technical Meetings

Vienna, Austria: 21 – 23 March 2011,
Daejeon, Rep. of Korea: 27 – 30 March 2012,
Pisa, Italy: 25 – 28 February 2013

Consultants Meeting

Corvallis, Oregon, USA: 16 – 19 March 2010

IAEA
International Atomic Energy Agency

No. 23

ORDERING LOCALLY

In the following countries, IAEA priced publications may be purchased from the sources listed below or from major local booksellers.

Orders for unpriced publications should be made directly to the IAEA. The contact details are given at the end of this list.

AUSTRALIA
DA Information Services
648 Whitehorse Road, Mitcham, VIC 3132, AUSTRALIA
Telephone: +61 3 9210 7777 • Fax: +61 3 9210 7788
Email: books@dadirect.com.au • Web site: http://www.dadirect.com.au

BELGIUM
Jean de Lannoy
Avenue du Roi 202, 1190 Brussels, BELGIUM
Telephone: +32 2 5384 308 • Fax: +32 2 5380 841
Email: jean.de.lannoy@euronet.be • Web site: http://www.jean-de-lannoy.be

CANADA
Renouf Publishing Co. Ltd.
5369 Canotek Road, Ottawa, ON K1J 9J3, CANADA
Telephone: +1 613 745 2665 • Fax: +1 643 745 7660
Email: order@renoufbooks.com • Web site: http://www.renoufbooks.com

Bernan Associates
4501 Forbes Blvd., Suite 200, Lanham, MD 20706-4391, USA
Telephone: +1 800 865 3457 • Fax: +1 800 865 3450
Email: orders@bernan.com • Web site: http://www.bernan.com

CZECH REPUBLIC
Suweco CZ, spol. S.r.o.
Klecakova 347, 180 21 Prague 9, CZECH REPUBLIC
Telephone: +420 242 459 202 • Fax: +420 242 459 203
Email: nakup@suweco.cz • Web site: http://www.suweco.cz

FINLAND
Akateeminen Kirjakauppa
PO Box 128 (Keskuskatu 1), 00101 Helsinki, FINLAND
Telephone: +358 9 121 41 • Fax: +358 9 121 4450
Email: akatilaus@akateeminen.com • Web site: http://www.akateeminen.com

FRANCE
Form-Edit
5 rue Janssen, PO Box 25, 75921 Paris CEDEX, FRANCE
Telephone: +33 1 42 01 49 49 • Fax: +33 1 42 01 90 90
Email: fabien.boucard@formedit.fr • Web site: http://www.formedit.fr

Lavoisier SAS
14 rue de Provigny, 94236 Cachan CEDEX, FRANCE
Telephone: +33 1 47 40 67 00 • Fax: +33 1 47 40 67 02
Email: livres@lavoisier.fr • Web site: http://www.lavoisier.fr

L'Appel du livre
99 rue de Charonne, 75011 Paris, FRANCE
Telephone: +33 1 43 07 50 80 • Fax: +33 1 43 07 50 80
Email: livres@appeldulivre.fr • Web site: http://www.appeldulivre.fr

GERMANY
Goethe Buchhandlung Teubig GmbH
Schweitzer Fachinformationen
Willstätterstrasse 15, 40549 Düsseldorf, GERMANY
Telephone: +49 (0) 211 49 8740 • Fax: +49 (0) 211 49 87428
Email: s.dehaan@schweitzer-online.de • Web site: http://www.goethebuch.de

HUNGARY
Librotade Ltd., Book Import
PF 126, 1656 Budapest, HUNGARY
Telephone: +36 1 257 7777 • Fax: +36 1 257 7472
Email: books@librotade.hu • Web site: http://www.librotade.hu

INDIA
Allied Publishers
1st Floor, Dubash House, 15, J.N. Heredi Marg, Ballard Estate, Mumbai 400001, INDIA
Telephone: +91 22 2261 7926/27 • Fax: +91 22 2261 7928
Email: alliedpl@vsnl.com • Web site: http://www.alliedpublishers.com

Bookwell
3/79 Nirankari, Delhi 110009, INDIA
Telephone: +91 11 2760 1283/4536
Email: bkwell@nde.vsnl.net.in • Web site: http://www.bookwellindia.com

ITALY
Libreria Scientifica "AEIOU"
Via Vincenzo Maria Coronelli 6, 20146 Milan, ITALY
Telephone: +39 02 48 95 45 52 • Fax: +39 02 48 95 45 48
Email: info@libreriaaeiou.eu • Web site: http://www.libreriaaeiou.eu

JAPAN
Maruzen Co., Ltd.
1-9-18 Kaigan, Minato-ku, Tokyo 105-0022, JAPAN
Telephone: +81 3 6367 6047 • Fax: +81 3 6367 6160
Email: journal@maruzen.co.jp • Web site: http://maruzen.co.jp

NETHERLANDS
Martinus Nijhoff International
Koraalrood 50, Postbus 1853, 2700 CZ Zoetermeer, NETHERLANDS
Telephone: +31 793 684 400 • Fax: +31 793 615 698
Email: info@nijhoff.nl • Web site: http://www.nijhoff.nl

Swets Information Services Ltd.
PO Box 26, 2300 AA Leiden
Dellaertweg 9b, 2316 WZ Leiden, NETHERLANDS
Telephone: +31 88 4679 387 • Fax: +31 88 4679 388
Email: tbeysens@nl.swets.com • Web site: http://www.swets.com

SLOVENIA
Cankarjeva Zalozba dd
Kopitarjeva 2, 1515 Ljubljana, SLOVENIA
Telephone: +386 1 432 31 44 • Fax: +386 1 230 14 35
Email: import.books@cankarjeva-z.si • Web site: http://www.mladinska.com/cankarjeva_zalozba

SPAIN
Diaz de Santos, S.A.
Librerias Bookshop • Departamento de pedidos
Calle Albasanz 2, esquina Hermanos Garcia Noblejas 21, 28037 Madrid, SPAIN
Telephone: +34 917 43 48 90 • Fax: +34 917 43 4023
Email: compras@diazdesantos.es • Web site: http://www.diazdesantos.es

UNITED KINGDOM
The Stationery Office Ltd. (TSO)
PO Box 29, Norwich, Norfolk, NR3 1PD, UNITED KINGDOM
Telephone: +44 870 600 5552
Email (orders): books.orders@tso.co.uk • (enquiries): book.enquiries@tso.co.uk • Web site: http://www.tso.co.uk

UNITED STATES OF AMERICA
Bernan Associates
4501 Forbes Blvd., Suite 200, Lanham, MD 20706-4391, USA
Telephone: +1 800 865 3457 • Fax: +1 800 865 3450
Email: orders@bernan.com • Web site: http://www.bernan.com

Renouf Publishing Co. Ltd.
812 Proctor Avenue, Ogdensburg, NY 13669, USA
Telephone: +1 888 551 7470 • Fax: +1 888 551 7471
Email: orders@renoufbooks.com • Web site: http://www.renoufbooks.com

United Nations
300 East 42nd Street, IN-919J, New York, NY 1001, USA
Telephone: +1 212 963 8302 • Fax: 1 212 963 3489
Email: publications@un.org • Web site: http://www.unp.un.org

Orders for both priced and unpriced publications may be addressed directly to:

IAEA Publishing Section, Marketing and Sales Unit, International Atomic Energy Agency
Vienna International Centre, PO Box 100, 1400 Vienna, Austria
Telephone: +43 1 2600 22529 or 22488 • Fax: +43 1 2600 29302
Email: sales.publications@iaea.org • Web site: http://www.iaea.org/books

14-01881

International Atomic Energy Agency
Vienna
ISBN 978–92–0–100314–0
ISSN 1011–4289